FINAL REPORT

Task 6: Radiation Doses and Risk to Residents from FMPC Operations from 1951–1988
Volume II Appendices

The Fernald Dosimetry Reconstruction Project

Centers for Disease Control and Prevention
Department of Health and Human Services

September 1998

Contributing Authors

George G. Killough, Hendecagon Corporation
Marilyn J. Case, Eagle Rock Scientific, Inc.
Kathleen R. Meyer, Ph.D., Keystone Scientific, Inc.
Robert E. Moore, Ph.D., Moore Technical Associates, Inc.
Susan K. Rope, Environmental Perspectives, Inc.
Duane W. Schmidt, Health Physics Applications
Bernard Shleien, Ph.D., Scinta, Inc.
Warren K. Sinclair, Ph.D., Warren K. Sinclair, Ph.D, Inc.
Paul G. Voillequé, MJP Risk Assessment, Inc.
John E. Till, Ph.D., *Radiological Assessments Corporation*

Submitted to the Centers for Disease Control and Prevention
in Partial Fulfillment of Contract No. 200-90-08037

Radiological Assessments Corporation
417 Till Road, Neeses, SC 29107
Phone 803.536.4883 Fax 803.534.1995

RADIATION DOSES AND RISK TO RESIDENTS FROM FMPC OPERATIONS FROM 1951–1988

VOLUME II
TABLE OF CONTENTS

APPENDIX A—THE GARDEN MODEL FOR PRODUCE AND ANIMAL PRODUCTS A-1
INTRODUCTION A-1
STRUCTURE OF GARDEN A-1
System of Equations A-3
Vegetable Crops, Pasture Grass A-4
Calculations for Radioactivity in the Muscle of Beef and Poultry A-5
Calculations for Milk A-6
Intakes for Beef Cattle A-7
Intakes for Milk Cattle A-8
Intakes for Poultry and Eggs A-8
Concentrations in Freshwater Fish A-9
PARAMETERS FOR GARDEN A-9
UNCERTAINTIES A-10
SOME NORMALIZED RESULTS OF CALCULATIONS WITH GARDEN A-12
REFERENCES A-14

APPENDIX B—A MODEL OF URANIUM, THORIUM, AND DECAY PRODUCTS IN SOIL B-1
INTRODUCTION B-1
STRUCTURE OF THE MODEL B-1
CALIBRATION B-3
DISCUSSION B-4
REFERENCES B-4

APPENDIX C—USE OF SOIL DATA TO CONFIRM THE MAGNITUDE OF AIRBORNE RELEASES AND DEPOSITION OF URANIUM OVER TIME C-1
INTRODUCTION C-1
QUALITATIVE OVERVIEW C-2
DATA AND PARAMETERS C-10
MATHEMATICAL DETAILS C-13
The Dynamic Mass-Balance Model and Nonlinear Regression C-13
Deposition Based on the 1986 Excess Inventory C-14
UNCERTAINTY ANALYSIS C-15
CONCLUSIONS C-18
REFERENCES C-20

APPENDIX D—VARIATION IN CONCENTRATION OF AIRBORNE PARTICULATES OVER TIME D-1
INTRODUCTION D-1
ESTIMATING DUST LOADING D-2
REFERENCES D-5

APPENDIX E—RADIONUCLIDE CONCENTRATIONS FOR WATER PATHWAYS E-1
REFERENCES E-2

APPENDIX F—ESTIMATES OF CONCENTRATIONS OF URANIUM AND DECAY PRODUCTS IN SOUTH PLUME WELLS F-1
INTRODUCTION F-1
URANIUM LEVELS F-1
OTHER RADIONUCLIDES F-2
REFERENCES F-4

APPENDIX G—GAMMA RADIATION DOSES FROM WASTE STORAGE SILOS G-1
INTRODUCTION G-1
LOCATIONS OF THE SILOS G-1
CALCULATED EXPOSURE RATES VERSUS DISTANCE FROM K-65 SILOS G-1
CONVERSION OF EXPOSURE RATE TO DOSE RATE G-5
REFERENCES G-9

APPENDIX H—PARTICLE SIZE DISTRIBUTIONS FOR DUST COLLECTORS H-1
INTRODUCTION H-1
PARTICLE SIZE SAMPLING AND REPRESENTATION OF DISTRIBUTIONS H-2
DEPENDENCE OF DOSE ON PARTICLE SIZE DISTRIBUTION H-4
RELATIONSHIP OF A DISTRIBUTION TO ITS CASCADE IMPACTOR DATA H-6
RESULTS H-11
CONCLUSIONS H-11
REFERENCES H-13

APPENDIX I—DOSIMETRIC METHODS I-1
INTRODUCTION I-1
DECAY CHAINS I-2
URANIUM, THORIUM, AND THEIR DECAY PRODUCTS I-4
Internal Dose I-4
External Dose I-17
Dose to the Embryo/Fetus I-18
PHYSIOLOGICAL PARAMETERS RELATED TO DOSE ESTIMATION I-19
RADON-222 AND ITS DECAY PRODUCTS I-21
The Radon-222 Decay Chain I-22
Unattached RaA I-27
Indoor and Outdoor Concentrations of Radon-222 and Decay Products I-28
The NCRP Radon Dose Model I-29
Sensitivity of Estimates of Dose to Parameter Values and Initial State I-30
Final Example of Dose Calculation for Radon Decay Products I-34
REFERENCES I-36

APPENDIX J—SPECIFICATIONS OF THE NINE EXPOSURE SCENARIOS J-1
REFERENCES J-3

APPENDIX K—DOSE ESTIMATES FOR MEMBERS OF THE PUBLIC RESIDING NEAR THE FEED MATERIALS PRODUCTION CENTER K-1
INTRODUCTION K-1
EXPOSURE SCENARIOS K-2
DOSE ESTIMATES FOR THE NINE SCENARIOS K-5
DOSE TO THE EMBRYO/FETUS K-14
REFERENCES K-14

APPENDIX L—DETERMINATION OF AIR SAMPLER COLLECTION EFFICIENCY ... L-1
INTRODUCTION L-1
QUANTITATIVE ASSESSMENT OF COLLECTION EFFICIENCY L-1
RESULTS OF ASSESSMENT OF COLLECTION EFFICIENCY L-3
APPLICATION OF COLLECTION EFFICIENCY ESTIMATES L-5
REFERENCES L-5

APPENDIX M—AIR DISPERSION MODELS FOR THE PRODUCTION AREA AND THE K-65 SILOS M-1
INTRODUCTION M-1
SOME PRELIMINARY MATTERS M-3
The Model Equations M-4
Remarks about Uncertainty Distributions M-7
THE GAUSSIAN MODEL FOR A CIRCULAR AREA SOURCE REGION M-8
AIRBORNE RELEASES FROM THE PRODUCTION AREA M-11
Deposition M-11
Calibration of the Air Dispersion Model to Uranium Data M-13
DISPERSION OF RADON FROM THE K-65 SILOS M-24
Overview M-25
Daytime vs. Nighttime Releases M-27
Calibration of the Air Dispersion Model to the Mound and FMPC Radon Data M-30
Interpretations of the Fitted Air Dispersion Models M-34
MEASURED RADON CONCENTRATIONS AND UNCERTAINTIES M-37
Overview M-37
FMPC Routine Monitoring M-38
Mound Monitoring M-46
METEOROLOGICAL DATA M-51
Concerns about the FMPC Datasets M-51
Monte Carlo Estimation of Uncertainty Using Five-Year Composite Dataset M-54
OTHER UNCERTAINTIES M-57
RECAPITULATION OF UNCERTAINTIES M-60
Calibration M-63
Predictions M-63
DISCUSSION M-69
REFERENCES M-70

APPENDIX N—DETAILED VALIDATION RESULTS N-1
INTRODUCTION N-1

RADON VALIDATION DATA N-1
Measurements of Radon Flux on K-65 Silo Domes N-2
Hourly Measurements of Radon in Air Near K-65 Silos N-5
Time-Integrated Measurements of Radon in Air at Boundary Station BS–6. N-11
Measurements of Radon Daughters in Air at Boundary Station BS-6 ..... N-15
URANIUM VALIDATION RESULTS N-16
Data Completeness and Average Concentrations of Uranium in Air N-16
Uranium in Air at Perimeter and Boundary Monitoring Stations N-25
Deposition of Uranium on Gummed-Film N-36
Uranium in Soil N-37
Summary of Validation Results for Uranium N-48
REFERENCES N-48

APPENDIX O—INVESTIGATION OF RELATIVELY HIGH BACKGROUND URANIUM MEASUREMENTS AT DISTANT ENVIRONMENTAL MONITORING STATIONS ... O-1
PREFACE O-1
INTRODUCTION O-1
SUMMARY OF THE PROBLEM O-2
SUMMARY OF APPROACH TO INVESTIGATION OF THE PROBLEM O-8
NON-FMPC SOURCES OF URANIUM AND INDEPENDENT MEASUREMENTS O-9
Natural Background Uranium in Soil and Air O-9
Contributors to Measured Depositions O-12
Resuspension and Redistribution of Uranium Released from the FMPC before 1959 ..... O-13
Other Facilities Handling Large Amounts of Uranium O-15
Fallout of Uranium from Nuclear Weapons Testing O-19
Summary of Contributions from Various Sources O-22
DATA QUALITY AND INTERPRETATION ISSUES O-23
IMPLICATIONS FOR USE OF THE ENVIRONMENTAL DATA O-25
REFERENCES O-26

APPENDIX P—PREVIOUS STUDIES OF URANIUM AND RADON RELEASES P-1
PREVIOUS AIRBORNE URANIUM RELEASE ESTIMATES CALCULATIONS P-1
Site-based Estimates P-1
Independent Contractor-based Estimate P-3
Estimates from Other Organizations P-3
PREVIOUS RADIATION DOSE ESTIMATES TO THE PUBLIC FROM URANIUM RELEASED TO AIR FROM THE FMPC P-3
EVALUATION OF PREVIOUS ESTIMATES OF RADON RELEASES FROM THE K-65 SILOS P-8
SUMMARY AND CONCLUSIONS P-9
REFERENCES P-11

APPENDIX Q—FOLLOWUP OF ISSUES RELATED TO RADON SOURCE TERM Q-1
INTRODUCTION Q-1
EVALUATION OF ADDITIONAL INFORMATION AND DOCUMENTS RELATED TO RADON SOURCE TERM Q-1
Additional Document Searches Q-2

Discussions with Personnel with Knowledge of K-65 Silos or Radon Monitoring Q-3
Evaluation of Additional Documents of Interest Q-4
Conclusions Q-13
ADJUSTMENT OF RADON SOURCE TERM FOR 1988 ..... Q-14
Revised Methodology for Radon Source Term for 1988 ..... Q-14
Results Q-18
REVISITING THE ALTERNATIVE SOURCE TERM CALCULATIONS Q-19
Review of Equations Used for Alternative Source Term Calculations Q-19
Revisions to Parameter Distributions and Calculation Results Q-21
Minimum Radon Production to Support Radon Concentration in Head Spaces Q-22
Comparison of Results from Preferred Method and Alternative Method Q-25
UPDATED ESTIMATE OF RADIUM-226 CONTENT OF THE K-65 SILOS Q-27
ASSESSMENT OF A POSSIBLE BIAS IN PREFERRED-METHOD CALCULATIONS OF RADON RELEASES FOR 1959–1979 ..... Q-27
SUMMARY DESCRIPTION OF RELEASE MODEL FOR RADON IN K-65 SILOS ... Q-30
REVISION OF EQUILIBRIUM RATIOS OF RADON DECAY.. ..... Q-36
EXPANSION OF THE UNCERTAINTY FOR RADON RELEASES DURING 1959–1979 ..... Q-37
EFFECT OF RAPID TURNOVER DURING 1959–1979 ON DECAY PRODUCT EQUILIBRIUM AND GAMMA-FIELD MEASUREMENTS ON THE SILO DOMES . Q-40
REFERENCES Q-44

APPENDIX R—TOXICITY TO THE KIDNEYS FROM NATURAL URANIUM R-1
URANIUM CONCENTRATIONS IN THE KIDNEY R-1
Introduction R-1
Retention Function for Uranium in the Kidneys R-1
Intake and Retention Estimates R-5
Uncertainty Distributions for Maximum Concentrations R-8
A Method for Estimating Uncertainty for Scenario 3 ..... R-10
THE CHEMICAL TOXICITY OF NATURAL URANIUM R-13
THE NEPHROTOXICITY OF URANIUM FOR THE NINE EXPOSURE SCENARIOS R-16
DISCUSSION OF URANIUM TOXICITY R-16
CONCLUSIONS R-17
REFERENCES R-17

APPENDIX S—LIFETIME RISKS OF FATAL CANCER FOR INDIVIDUAL SCENARIOS AT THE FEED MATERIALS PRODUCTION CENTER S-1
INTRODUCTION S-1
EVALUATIONS OF THE RISK OF RADIATION-INDUCED CANCER S-2
Lifetime Risk Estimates S-2
Risk to the Kidney S-4
Radon Dosimetry and Risk S-5
Epidemiological Experience with Uranium S-7
EXPOSURES AND DOSIMETRY AT FERNALD S-9
Individual Exposure Scenarios S-9
Exposure and Dosimetry S-9
The Most Important Organs Exposed to the Releases at Fernald S-12
ADJUSTMENTS TO THE RISK FOR AGE AND SEX OF THE REPRESENTATIVE

INDIVIDUALS IN THE NINE SCENARIOS S-14
Lung Cancer Risk S-15
Bone Cancer Risk S-16
Liver Tumor Risk S-16
Bone Marrow Cancer Risk S-17
Kidney Tumor Risk S-18
Summary of Age and Sex Corrections for Different Tumor Sites S-18
Procedure for Correction of Bone Tumor Risks for Age and Sex S-18
Summary of Risks of Cancer Derived for Each Scenario S-22
LIFETIME RISKS FOR THE INDIVIDUAL EXPOSURE SCENARIOS S-19
UNCERTAINTIES IN ESTIMATES OF FATAL CANCER RISKS FOR THE EXPOSURE SCENARIOS AT FERNALD S-27
Uranium and Thorium Radionuclides S-28
Radon S-30
Risk and Uncertainty for All Sources at Fernald S-32
The Effect of Smoking on Radiation Risk to the Lung S-33
RISK ESTIMATES FOR CANCER AND COMPARISONS WITH HUMAN EXPERIENCE S-34
Natural Background Radiation S-34
Scenarios for Radiation Exposure from Fernald Sources S-35
DETERMINISTIC EFFECTS S-36
REFERENCES S-37

APPENDIX T—EPISODIC RELEASES T-1
INTRODUCTION T-1
CRITERIA FOR TREATMENT AS EPISODIC RELEASE T-1
SUMMARY OF EPISODIC RELEASES T-2
EVALUATION OF DOSE CONSEQUENCES OF EPISODIC RELEASES T-3
Uranium Hexafluoride Gas Releases from Pilot Plant (11/7/53 and 2/14/66) T-4
Episodic Releases Identified Using Ambient Air Monitoring Data T-9
Chemical Toxicity Considerations for Uranium Episodic Releases T-12
Radon Release (April 25, 1986) T-16
REFERENCES T-20

APPENDIX A

THE GARDEN MODEL FOR PRODUCE AND ANIMAL PRODUCTS

INTRODUCTION

The GARDEN model, which we have applied to estimates of internal dose by consumption of radioactively contaminated produce and animal products, was designed specifically to meet the conceptual needs and computational constraints of the Feed Materials Production Center (FMPC) dose reconstruction. The model is similar in some respects to the RAGTIME model (Pleasant et al. 1980; Killough et al. 1993), but it incorporates numerous simplifications. The features of GARDEN include the following: (1) GARDEN explicitly treats radioactive decay chains; (2) GARDEN has a radionuclide-specific database that is restricted to data for only those radionuclides that are considered in connection with the FMPC dose reconstruction; (3) GARDEN considers kinetics of uptake of radionuclides and their removal from the muscle of beef cattle and poultry in calculations with radionuclides and decay chains; and (4) GARDEN estimates radionuclide concentrations in the food types that it considers but does not provide estimates of dose (dose estimates are derived by other models that use the GARDEN concentrations). The food types that GARDEN considers are leafy vegetables, root vegetables, milk, beef, fish, poultry, and eggs.

STRUCTURE OF GARDEN

Like most food chain models, GARDEN is based on the kinetics of simple arrangements of compartments. Figure A-1 illustrates the simulated partitioning of radioactivity. The model was designed to operate within the context of the methodology developed for implementing the estimates of exposure and dose for the FMPC domain, and this fact imposes some constraints. The model interprets the deposition rate of each radionuclide in the airborne release as an annual average, and the concentrations of radionuclides in the soil that are available for uptake through the roots of plants are available to GARDEN at the same annual time resolution. Similar constraints apply to the contaminated forage and drinking water of animals. Intake rates for a beef or dairy animal throughout a given year are estimated as the annual average contamination on pasture grass multiplied by the animal's annual consumption of pasture grass. Using this constant intake rate, radioactivity levels in muscle and milk are dynamically calculated, using decay-chain kinetics and derived parameters for the rates of removal of the elements from the animal. The time for accumulation of radioactivity in an animal's tissues does not exceed one year (i.e., animals are not carried over from year to year); to model more realistic life cycles for cattle would entail added complexity and information about herd dynamics that are not available to this study, although such models have been proposed (Pleasant et al. 1982). The assumption made in GARDEN is that of a one-year life cycle for beef and milk cattle and that these animals are on pasture for the entire year (this level of exposure tends to compensate for the lack of accumulation over a period longer than a year). Poultry are assumed to consume commercially-produced uncontaminated grain for nine months of the year before

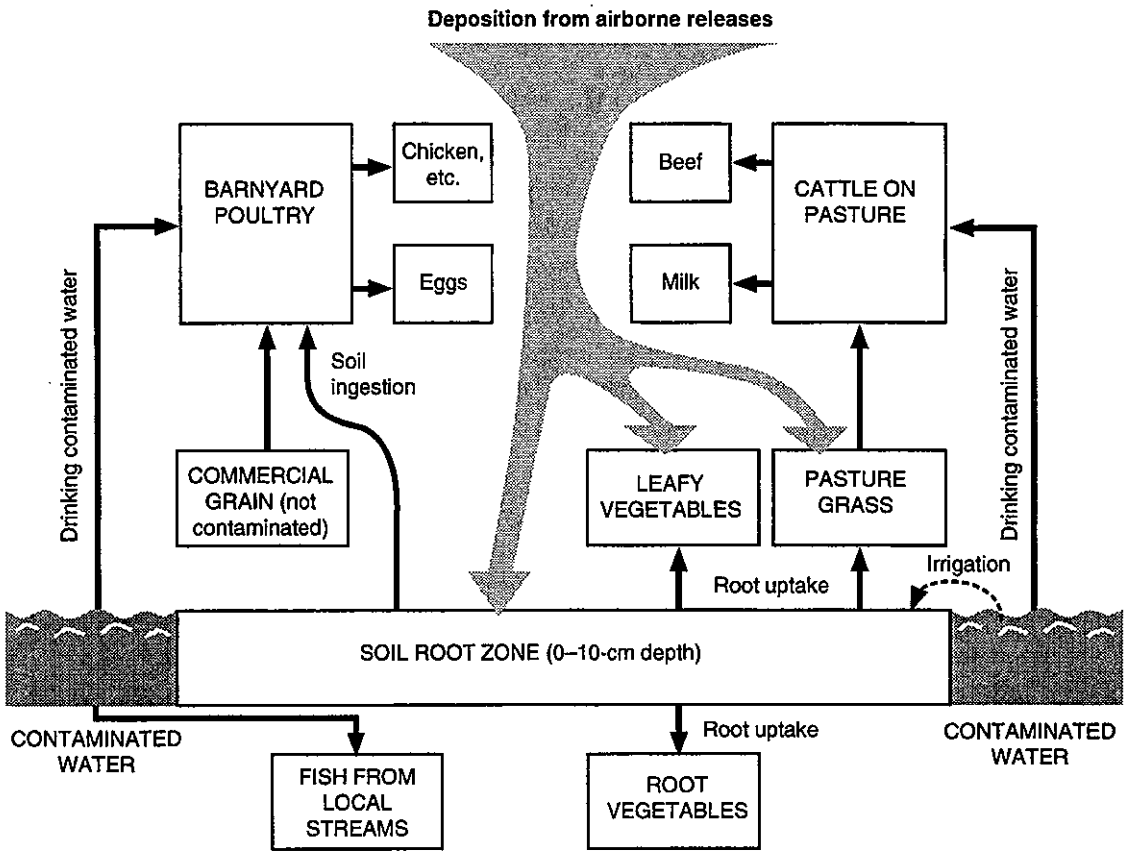

Figure A-1. The GARDEN model for transfer of radioactivity into crops and animal products.

being slaughtered; their only intake of radioactivity is assumed to be from the ingestion of contaminated soil in the barnyard. These assumptions are not intended to apply to commercial farms or dairies, from which the products would likely be sold outside the assessment domain, but rather to smaller farms and backyard gardens with a few animals available for home consumption.

Contaminated water pathways are treated conservatively. If crops are irrigated from a contaminated source, as in Scenarios 2, 6, and 7 (Appendix J), the amounts of radionuclides in the water are added to deposition on crops and pasture, rather than being introduced by way of the root uptake pathway. Moreover, animals are assumed to get their drinking water from the same contaminated source. This cautious approach primarily affects Scenario 2, in which the irrigation source is unrealistically assumed to be Paddy's Run Creek. In Scenarios 6 and 7, the Great Miami River is assumed to be the source of irrigation.

System of Equations

The equations that describe a compartment's input and removal of radioactive species in a decay chain, together with decay and decay-chain dynamics, are extensions of the Bateman equations, expressed in units of radioactivity (e.g., Bq):

$$\frac{dY_i}{dt} = -(\lambda_i^{\mathrm{R}} + \lambda^{\mathrm{E}})Y_i + \lambda_i^{\mathrm{R}} \sum_{j=1}^{i-1} \beta_{i,j} Y_j + P_i\,, \quad Y_i|_{t=0} = Y_i^0\,, \quad i = 1, \ldots, N \tag{A-1}$$

where

Y_i = radioactivity (Bq) of species i in the compartment at time t

λ_i^{R} = radiological decay rate coefficient for species i (units of reciprocal time)

λ^{E} = "environmental" removal rate coefficient for the compartment (e.g., for radioactivity deposited on a plant surface, this coefficient would characterize the rate of loss by weathering; units of reciprocal time)

$\beta_{i,j}$ = branching fraction, indicating the proportion of species j decays to species i (dimensionless)

$P_i(t)$ = rate of input of radioactivity of species i to the compartment at time t (e.g., rate of deposition of a radionuclide onto the surface of a plant; units of Bq per unit time)

Y_i^0 = initial value of Y_i (Bq)

N = number of radionuclide species in the decay chain.

For applications of Equation A-1 to GARDEN, the exogenous terms P_i are constant rates during each year (i.e., P_i is constant during the year i but may have different constant values for subsequent years $i + 1, i + 2, \ldots$).

It will be useful to introduce vector notations for the solution of the system of differential equations of Equation A-1. For a specified decay chain, abbreviated by the symbol C, we express the solution vector $\mathbf{Y}$ in terms of the operator $\mathbf{Act}_C()$ (for "activity") that "solves" the system given the necessary parametric quantities:

$$\mathbf{Y}(t) = \mathbf{Act}_C(t, \lambda^{\mathrm{E}}, \mathbf{P}, \mathbf{Y}^0) \tag{A-2}$$

where

C = decay chain specification and parameters, including decay-rate coefficients $\lambda_1^{\mathrm{R}}, \ldots, \lambda_N^{\mathrm{R}}$ and the matrix of branching ratios $\beta_{i,j}$

$\mathbf{Y}(t) = [Y_1(t), \ldots, Y_N(t)]^{\mathrm{T}}$ = solution vector at time t

$\mathbf{P} = [P_1, \ldots, P_N]^{\mathrm{T}}$

$\mathbf{Y}^0 = [Y_1^0, \ldots, Y_N^0]^{\mathrm{T}}$.

(NOTE: The superscript T in the vector definitions just given denotes the matrix transpose operator, which converts the conveniently-written row vectors into column vectors that are compatible with matrix multiplication conventions.) Most radionuclide concentrations calculated by GARDEN can be expressed conveniently in terms of the operator $\mathbf{Act}_C()$.

Vegetable Crops, Pasture Grass

The concentration of each radionuclide of a decay chain C deposited on a growing vegetable crop is computed as

$$C_i^{\text{crop}} = [\mathbf{Act}_C(t_{\text{grow}}, \lambda^{\text{E}}, \mathbf{P}^{\text{dep}}, \mathbf{0})]_i + k_{\text{v}} B_{i\text{v}}^{\text{crop}} A_i^{\text{soil}}/S \tag{A-3a}$$

$$C_i^{\text{grass}} = M^{-1} \sum_{j=0}^{M-1} [\mathbf{Act}_C((j+1/2)M^{-1}t_{\text{graze}}, \lambda^{\text{E}}, \mathbf{P}^{\text{dep}}, \mathbf{0})]_i + k_{\text{v}} B_{i\text{v}}^{\text{grass}} A_i^{\text{soil}}/S \tag{A-3b}$$

where

$$[\mathbf{P}^{\text{dep}}]_i = r\omega_i/Y_{\text{v}} \tag{A-4}$$

and

C_i^{crop} = concentration of radionuclide i (Bq kg^{-1}) in a food crop at the time of harvest

C_i^{grass} = concentration of radionuclide i (Bq kg^{-1}) in pasture grass, averaged over the grazing season

t_{grow} = length of the growing season for a food crop (units of time compatible with the reciprocal time units of the rate coefficients λ_i^{R} and λ^{E})

t_{graze} = period within the year that cattle are assumed to be on pasture (units of time compatible with the reciprocal time units of the rate coefficients λ_i^{R} and λ^{E})

M = number of terms chosen to represent an average of contamination from deposition on pasture grass (taken as 10 in our calculations)

r = interception fraction for the plant, averaged for the growing season

ω_i = deposition rate of radionuclide i (Bq m^{-2} per unit time)

Y_{v} = yield of the crop (kg m^{-2})

$B_{i\text{v}}$ = soil-to-plant concentration factor for radionuclide i (tabulated, for food crops, as Bq kg^{-1} wet weight of plant per Bq kg^{-1} dry soil, and for pasture grass as Bq kg^{-1} dry weight of plant per Bq kg^{-1} dry soil)

k_{v} = conversion factor for wet vs. dry weight in the units of $B_{i\text{v}}$, with value 1 for food crops and 0.2 for pasture grass (Till and Meyer 1983)

A_i^{soil} = radioactivity (Bq) of radionuclide i per m^2 of soil; this quantity is based on the dynamic inventory predicted by the soil model for each year of FMPC operation

S = effective surface density of dry soil (kg m^{-2}).

The first term on the right side of each of Equations A-3 accounts for deposition of the airborne radionuclides on the plant (through the vector $\mathbf{P}^{\text{dep}}$), and the second term represents uptake of radioactivity from the soil through the roots. The estimates for a food crop are computed for the end of the growing season (time t_{grow} if time 0 represents the beginning of the growing season), but for pasture grass (Equation A-3b) the concentration on the plant due to deposition is averaged over the grazing season. Deposition is treated as a continuous constant source in the first terms, whereas uptake by plants is simulated by a concentration factor relative to the level of radioactivity in the soil root zone. Pleasant et al. (1980) gave explicit treatment to radionuclide decay chains in crops and pasture grass, in ways similar to those expressed in Equations A-3 and A-4.

As noted previously, irrigation with contaminated water is not conventionally treated in the model. This radioactivity flux is added to the deposition term, rather than being made available to root uptake.

The model permits a delay time between the harvest and the consumption of the crop, during which loss of radioactivity by decay is calculated. Table A-7 indicates the generic values used in our calculations.

Calculations for Radioactivity in the Muscle of Beef and Poultry

When radioactive decay chains are considered in estimating concentrations of radionuclides in beef and poultry, it is not possible to give a satisfactory account of the resultant concentrations in muscle without considering the stable-element retention dynamics for each radionuclide and incorporating appropriate terms into the differential equations. Pleasant et al (1982) developed such an approach. The retention of radionuclide i in the muscle is modeled by means of a function

$$R_i(t) = \sum_{j=1}^{J} c_{ij} \exp(-\lambda_{ij}^{B} t) \qquad \text{(A-5)}$$

where the fractional coefficients c_{ij} sum to 1 over j (i.e., $R_i(0) = 1$) and the removal rate coefficients λ_{ij}^{B} are associated with biological processes. The function $R_i(t)$ represents theoretically the fraction of one mass unit of the stable element of radionuclide i that would remain in the muscle at an elapsed time t after its acute introduction there. Such data are not well known for the animals in question, and we have provisionally substituted corresponding stable-element parameters for human beings. The terms of Equation A-5 are often said to correspond to "compartments"; this usage is convenient, and we employ it in the discussion, but we note that the parameters c_{ij} and λ_{ij}^{B} are more likely empirical than physiological.

Because of the assumed parallelism of the compartments, we express the differential equations for the components of concentration as follows:

$$\frac{dC_{ij}^{B}}{dt} = -(\lambda_{1j}^{B} + \lambda_i^{R})C_{ij}^{B} + Q_{ij} + \lambda_i^{R} \sum_{k=1}^{i-1} \beta_{ik} C_{kj}^{B}, \quad i = 1, \ldots, N, \quad j = 1, \ldots, J \qquad \text{(A-6a)}$$

where the rate of uptake for component j is

$$Q_{ij} = \begin{cases} c_{ij} f_{ui} I_i m_B^{-1} (1 + \lambda_i^{R}/\lambda_u)^{-1} & \text{if } i = 1; \\ 0 & \text{otherwise} \end{cases} \qquad \text{(A-6b)}$$

and

J = number of compartments that represent the retention function of radionuclide $i = 1$

C_{ij}^{B} = component j of concentration of radionuclide i in muscle (Bq kg^{-1}). The sum of the C_{ij}^{B} for $j = 1, \ldots, J$, multiplied by the mass of the muscle, is the total level of radioactivity in the muscle

I_i = rate of intake of radionuclide i by the animal (Bq per unit time)

m_B = mass of the muscle (kg)

f_{ui} = fractional incorporation of ingested radionuclide i into muscle

$(1 + \lambda_i^R/\lambda_u)^{-1}$ = a factor to adjust the amount of a short-lived radionuclide i taken up by the muscle for loss due to radioactive decay during the process of translocation to muscle through the blood. The transfer rate coefficient λ_u was given a value equivalent to 4.0 day^{-1}.

Note that in Equation A-6a the biological rate coefficient λ_{1j}^B is used rather than λ_{ij}^B; this usage is required by our assumption, discussed below, that for a radionuclide taken into the muscle, all decay products that form within the muscle are governed by the retention parameters of the parent species, here indexed as $i = 1$.

It is useful to eliminate the parameters m_B and f_{ui} by relating them to the transfer ratios F_{iA} of the model's database. It is possible to show that the input term Q_{ij} of Equation A-6b can be expressed as

$$Q_{ij} = \begin{cases} c_{ij}F_{iA}I_i\left(\sum_{k=1}^{J} c_{ik}/\lambda_{ik}^B\right)^{-1}(1 + \lambda_i^R/\lambda_u)^{-1} & \text{if } i = 1 \\ 0 & \text{otherwise} \end{cases} \qquad \text{(A-6c)}$$

where F_{iA} has units day kg^{-1} and the parameters c_{ij} and λ_{ij}^B were defined in connection with Equation A-5. Thus the unknown uptake parameter f_{ui} and the mass of the muscle are replaced by the stable-element equilibrium parameters F_{iA} that have been measured for many elements and several animal products.

Equations A-6a and A-6b represent only the amount of radionuclide $i = 1$ (the parent) and radioactive progeny that are descended from the intake and decay of that species. To account for other radionuclides in the decay chain that are ingested with feed, we must apply the equations repeatedly, first where radionuclide $i = 2$ (the first daughter) becomes the parent and each subsequent radionuclide is reindexed, and so on until the chain is exhausted (Figure A-2). After each repetition, the newly calculated increment of concentration of each radionuclide is added to the previously calculated values, and the totals account for intake and decay of all the radionuclides in the chain.

Subjecting all radioactive decay products of a radionuclide taken into the animal's muscle to the same retention function suggests the hypothesis that the decay products remain bound in such a way as to move with the parent species. The contrary hypothesis that each radioactive decay product obeys its own retention parameters has been applied to similar calculations (e.g., Killough et al. 1978) and perhaps possesses a greater intuitive appeal, but it requires a more difficult calculation, one that is more prone to numeric loss-of-significance errors, and one that we have passed over in favor of the computationally simpler approach outlined above. We note that the International Commission on Radiological Protection incorporated an assumption similar to the one we have made in its metabolic methodology for the dose estimates of ICRP Publication 30 (ICRP 1979).

Calculations for Milk

Estimates of concentrations of radionuclides in milk are based on a special case of the methodology discussed in the previous section. Rather than a characterization of biological turnover in muscle by a multicompartment retention function of the form of Equation A-5, this function is adapted to attribute characteristic removal to two milkings per day. Thus, we set $J = 1$, $c_{i1} = 1$, and $\lambda_{i1}^B = 2$ day^{-1} (or the equivalent in units compatible with other time constants).

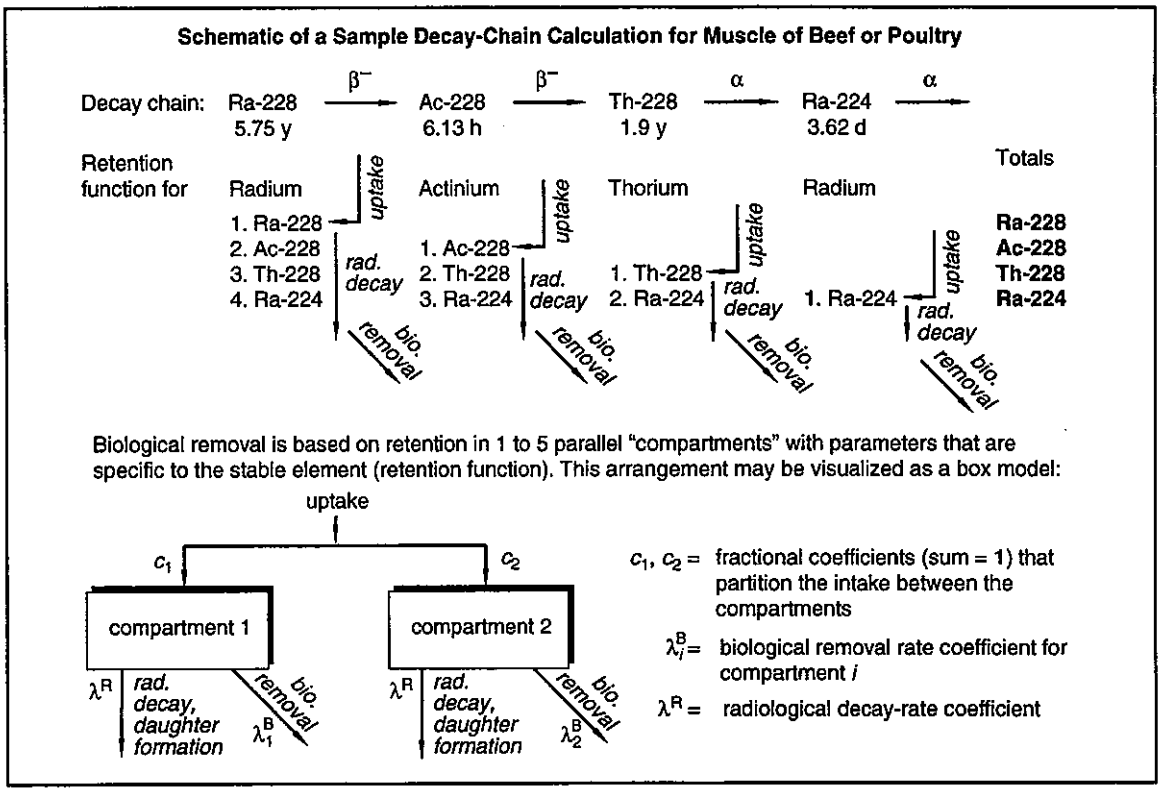

Figure A-2. Schematic presentation of decay-chain calculations for radionuclides in the muscle of beef and poultry.

Intakes for Beef Cattle

Concentrations of radionuclides in beef are based on those in pasture grass and contaminated drinking water consumed by the animal. The calculations use Equations A-6a and A-6c, where the intake I_i is given by

$$I_i = Q_F C_i^{grass} + Q_{Aw} C_i^{water} \quad \text{(A-7)}$$

where

I_i = intake rate of radionuclide i by the animal (Bq day^{-1})

C_i^{grass} = concentration of radionuclide i in the animal's feed (Bq kg^{-1})

C_i^{water} = concentration of radionuclide i in the animal's drinking water (Bq L^{-1})

Q_F = consumption rate of contaminated feed by an animal (kg day^{-1} wet weight)

Q_{Aw} = consumption rate of contaminated drinking water by an animal (L day^{-1}).

The foregoing approach bases the estimate of radionuclide concentrations in beef on concentrations in feed and drinking water for the year in which the beef is consumed, and it does not incorporate refinements that account for differences between levels of contamination in stored feed and pasture grass. The assumption that the animal was fed on freshly contaminated

pasture grass for twelve months of the year tends to overestimate the concentration of radioactivity in beef. The assumption that the levels of radioactivity in beef depend only on feed and drinking water for the current year of consumption also introduces some time distortion into the calculation if one assumes that the mean lifetime of the beef cattle is eighteen months to two years, but the total estimate of dose to the consumer of the beef over a period of years would not be seriously affected.

Intakes for Milk Cattle

As is the case for beef, concentrations of radionuclides in milk are based on those in pasture grass and contaminated drinking water consumed by the animal. The analogous equation for intake is

$$I_i = Q_F C_i^{grass} + Q_{Aw} C_i^{water} \quad \text{(A-8)}$$

where

I_i = intake rate of radionuclide i by milk cow (Bq day^{-1})

C_i^{grass} = concentration of radionuclide i in the animal's feed (Bq kg^{-1})

C_i^{water} = concentration of radionuclide i in the animal's drinking water (Bq L^{-1})

Q_F = consumption rate of contaminated feed by an animal (kg day^{-1} wet weight)

Q_{Aw} = consumption rate of contaminated drinking water by an animal (L day^{-1}).

The remarks made above concerning the simplified assumption of nine-month feeding of the animal on pasture grass also applies to estimates of radionuclide concentrations in milk and would tend similarly to overestimate these concentrations.

Intakes for Poultry and Eggs

Concentrations of radionuclides in poultry and eggs are based on those in contaminated water and contaminated soil consumed by the animal. The equation is

$$I_i = Q_{Aw} C_i^{water} + Q_{soil} C_i^{soil} \quad \text{(A-9)}$$

where

I_i = intake of radionuclide i by bird (Bq day^{-1})

C_i^{water} = concentration of radionuclide i in the animal's drinking water (Bq L^{-1})

C_i^{soil} = concentration of radionuclide i in soil ingested by bird (Bq kg^{-1})

Q_{Aw} = consumption rate of contaminated drinking water by an animal (L day^{-1})

Q_{soil} = consumption rate of contaminated soil by bird (taken as 0.008 kg day^{-1}).

Feed for poultry is assumed to be uncontaminated commercial grain, and consequently, this component does not appear in Equation A-9. Ingestion of soil in barnyard foraging is assumed to be the primary pathway of contamination for poultry flesh and eggs, although the drinking water pathway takes into account the possible watering of animals from contaminated sources.

Concentrations in Freshwater Fish

Consumption of fish caught from the Great Miami River is considered in the nine scenarios. Estimation of initial concentrations of the radionuclides of interest in the fish is accomplished by the equation

$$C_i^{fish} = B_i^{fish} C_i^{water} \quad \text{(A-10)}$$

where

C_i^{fish} = concentration of radionuclide i in the flesh of freshwater fish (Bq kg^{-1})

B_i^{fish} = stable-element bioaccumulation factor for transfer of radionuclide i from water to freshwater fish (L kg^{-1})

C_i^{water} = concentration of radionuclide i in water from which fish were caught (Bq L^{-1}).

Values of the bioaccumulation factors B_i^{fish} from Equation A-10 are given in Table A-6.

PARAMETERS FOR GARDEN

The element-specific parameters used in GARDEN for the FMPC dose reconstruction are given only for uranium, thorium, radium, actinium, protactinium, and plutonium, of which some radioactive isotopes affect the assessment. Table A-1 shows the soil-to-plant concentration factors B_{iv} for food crops and pasture grass. Miscellaneous parameters for these plant types are collected in Table A-2.

Table A-3 gives the radionuclide-specific transfer coefficients from daily intake in feed to concentrations in animal products (F_{iA}). These coefficients apply to the basic food types beef, milk, poultry, and eggs.

Assumptions about intakes of feed and drinking water for cattle and poultry are summarized in Table A-4.

Bioaccumulation factors for the radionuclides of interest in freshwater fish are shown in Table A-5.

The parameters used for stable-element turnover in the muscle of beef and poultry are shown in Table A-6 (for notations refer to Equations A-6a and A-6b). The use of retention functions given for human beings is a crude approximation, but one that nonetheless seems preferable to attempting a reformulation of the models in order to avoid consideration of biological removal of radionuclides from animal tissue.

Finally, the interval after harvesting of crops, milking, collection of eggs, and slaughter of animals, and before the consumption of the product results in changes of radioactivity levels because of decay-chain kinetics. Delay times generically assumed for the various products are given in Table A-7.

The surfaces of vegetables were assumed to be washed to the extent of reducing the radioactivity on them by a factor of two. No explicit assumptions about peeling or loss of radioactivity through cooking were incorporated. Home-grown fruits were not included in the diets of the subjects of exposure scenarios 1–9 (Appendix A-J), although the methodology provides the capability. In our discussions with agricultural officials for Butler and Hamilton Counties, locally grown fruit other than apples did not emerge as being important. Bakery products were considered an unlikely source of ingested contamination from the FMPC site, because few householders would have milled their own grain for baking.

Table A-1. Concentration Factors for Soil-to-Plant Uptake (B_{iv})

Element	Pasture grass[a]	Leafy and root vegetables[b]
U	8.5×10^{-3}	1.7×10^{-3}
Th	8.5×10^{-4}	3.6×10^{-5}
Ra	1.5×10^{-2}	6.4×10^{-4}
Pa	2.5×10^{-3}	1.1×10^{-4}
Ac	1.5×10^{-2}	6.4×10^{-4}
Pu	4.5×10^{-4}	1.9×10^{-5}

[a] Killough et al. (1993). Factor is relative to dry weight of pasture grass.

[b] Killough et al. (1993). Factor is relative to wet weight of edible parts of leafy vegetables.

Table A-2. Miscellaneous Parameters for Food and Forage Crops

Parameter	Pasture grass	Leafy vegetables	Root vegetables
Interception fraction (r)	0.20[a]	0.15[b]	0
Growing season (days)	365[c]	50	115[b]
Yield (Y_v) (kg wet m^{-2})	0.7[b]	2.0[b]	2.0[a]

[a] USNRC (1977).

[b] Killough et al. (1993).

[c] A twelve-month grazing season is assumed for beef and milk cattle.

UNCERTAINTIES

Because of the dosimetric dominance of the inhalation pathway over the ingestion pathway for FMPC releases, we have treated the uncertainties associated with the Garden model in a simple way. Lognormal uncertainties are applied to transfer factors for root uptake for food crops, root uptake for pasture grass, feed-to-beef, feed-to-milk, poultry, feed-to-eggs, and water-to-fish. Factors in these distinct categories are assumed independent, but the same uncertainty is multiplied by same-category factors for all elements (the same uncertainty factor would be multiplied by the feed-to-beef transfer factors for uranium, thorium, and plutonium, for example). We have used a common geometric standard deviation for all categories of GSD = 1.52, which corresponds to $v_{95}/v_{50} = 2$, where v_{50} and v_{90} are the 50th and 95th percentiles,

Table A-3. Stable-Element Transfer Coefficients (F_{iA}) Relating Intake by Animals to Food Products[a]

Element	Beef	Milk	Poultry	Eggs
U	2×10^{-4}	6×10^{-4}	1.2	9.9×10^{-1}
Th	5×10^{-3}	2.5×10^{-6}	4×10^{-3}	2×10^{-3}
Ra	9×10^{-4}	2×10^{-4}	9.9×10^{-4}	2×10^{-5}
Pa	5×10^{-3}	2.5×10^{-6}	4×10^{-3}	2×10^{-3}
Ac	4×10^{-4}	2×10^{-5}	4×10^{-3}	2×10^{-3}
Pu	2×10^{-6}	1×10^{-7}	1.5×10^{-4}	8×10^{-3}

[a] Schreckhise et al. (1993).

Table A-4. Consumption Rates for Animals[a]

	Feed (kg day^{-1})	Drinking water (L day^{-1})
Beef cattle	68	50
Dairy cattle	55	60
Poultry	0.12	0.30

[a] Schreckhise et al. (1993).

Table A-5. Concentration Factors for Freshwater Fish[a]

Element	L kg^{-1}
U	50
Th	100
Ra	50
Pa	30
Ac	330
Pu	250

[a] Schreckhise et al. (1993).

respectively, of the lognormal distribution. Thus, a 90% confidence interval places the unknown parameter within a factor of two of the assumed geometric mean.

Table A-6. Retention Parameters for Stable Elements in Beef and Poultry[a]

Element	Retention function parameters c_j, λ_j^B				
Uranium					
c_j	0.996	0.004			
λ_j^B	42.2	0.169			
Thorium					
c_j	1.0				
λ_j^B	0.361				
Radium					
c_j	0.291	0.545	0.109	0.046	0.009
λ_j^B	5.06×10^3	2.53×10^2	7.23	1.26	0.181
Protactinium					
c_j	0.7	0.3			
λ_j^B	25.3	4.22			
Actinium					
c_j	0.239	0.761			
λ_j^B	0	0			
Plutonium					
c_j	1.0				
λ_j^B	0.017				

[a] Based on retention parameters for human soft tissue from ICRP Publication 30 (ICRP 1979). See Equation A-5. Rate coefficients λ_j^B are in units of reciprocal years.

Table A-7. Delay Times Before Consumption of Food Products

Product	Beef	Milk	Poultry	Eggs	L. Veg.	R. Veg.	Fish
Delay (days)	20	4	20	4	14	14	7

SOME NORMALIZED RESULTS OF CALCULATIONS WITH GARDEN

It is useful to provide results of the GARDEN model normalized to a unit exposure. Table A-8 estimates the concentration of each each radionuclide of each decay chain in each of the eight food types resulting from the radioactivity on surfaces of crops and pasture grass; a year's cumulative deposition of 1 Bq m^{-2} of each parent radionuclide is assumed (the interception fraction of each plant is taken into account), and no contamination of the soil is considered. Note that the results for root vegetables, poultry, and eggs are all zero. Root vegetables are assumed to receive all contamination of edible parts from the soil. Poultry are assumed to be fed uncontaminated grain and to ingest radioactivity only with contaminated soil from the barnyard, and contamination of eggs is also calculated from the levels ingested by the

Table A-8. Concentrations of Decay Chains in Food Products from Direct Deposition of Parent Radionuclides on Crops and Pasture (1 Bq m^{-2} $year^{-1}$)

	Pasture (Bq kg^{-1})	L. Veg. (Bq kg^{-1})	R. Veg. (Bq kg^{-1})	Beef (Bq kg^{-1})	Milk (Bq L^{-1})	Grain (Bq kg^{-1})	Poultry (Bq kg^{-1})	Eggs (Bq kg^{-1})
U-234	1.5×10^{-2}	1.9×10^{-3}	0	1.1×10^{-4}	4.8×10^{-4}	1.2×10^{-2}	0	0
Th-230	6.7×10^{-9}	1.4×10^{-9}	0	6.5×10^{-10}	5.5×10^{-11}	9.5×10^{-9}	0	0
U-235	1.5×10^{-2}	1.9×10^{-3}	0	1.1×10^{-4}	4.8×10^{-4}	1.2×10^{-2}	0	0
Th-231	3.7×10^{-14}	7.6×10^{-15}	0	3.5×10^{-15}	3.0×10^{-16}	5.2×10^{-14}	0	0
U-238	1.5×10^{-2}	1.9×10^{-3}	0	1.1×10^{-4}	4.8×10^{-4}	1.2×10^{-2}	0	0
Th-234	5.1×10^{-3}	1.0×10^{-3}	0	9.6×10^{-5}	5.9×10^{-5}	6.6×10^{-3}	0	0
Pa-234m	5.1×10^{-3}	1.0×10^{-3}	0	9.6×10^{-5}	5.9×10^{-5}	6.6×10^{-3}	0	0
Pa-234	8.1×10^{-6}	1.6×10^{-6}	0	1.5×10^{-7}	8.7×10^{-8}	1.1×10^{-5}	0	0
Th-228	1.4×10^{-2}	1.8×10^{-3}	0	1.0×10^{-3}	2.0×10^{-6}	1.1×10^{-2}	0	0
Ra-224	1.1×10^{-2}	1.8×10^{-3}	0	1.0×10^{-3}	5.1×10^{-5}	1.1×10^{-2}	0	0
Th-230	1.5×10^{-2}	1.9×10^{-3}	0	1.2×10^{-3}	2.0×10^{-6}	1.2×10^{-2}	0	0
Th-231	1.5×10^{-2}	1.9×10^{-3}	0	1.2×10^{-3}	2.0×10^{-6}	1.2×10^{-2}	0	0
Th-232	1.5×10^{-2}	1.9×10^{-3}	0	1.2×10^{-3}	2.0×10^{-6}	1.2×10^{-2}	0	0
Ra-228	8.9×10^{-5}	1.8×10^{-5}	0	5.8×10^{-5}	9.8×10^{-7}	1.3×10^{-4}	0	0
Ac-228	8.7×10^{-5}	1.8×10^{-5}	0	5.8×10^{-5}	9.8×10^{-7}	1.2×10^{-4}	0	0
Th-228	1.7×10^{-6}	3.1×10^{-7}	0	5.3×10^{-6}	4.2×10^{-9}	2.6×10^{-6}	0	0
Ra-224	1.3×10^{-6}	2.3×10^{-7}	0	5.0×10^{-6}	6.8×10^{-9}	2.0×10^{-6}	0	0
Th-234	9.6×10^{-3}	8.6×10^{-4}	0	6.1×10^{-5}	1.2×10^{-6}	5.0×10^{-3}	0	0
Pa-234m	9.6×10^{-3}	8.6×10^{-4}	0	6.1×10^{-5}	1.2×10^{-6}	5.0×10^{-3}	0	0
Pa-234	1.5×10^{-5}	1.4×10^{-6}	0	9.8×10^{-8}	1.9×10^{-9}	8.0×10^{-6}	0	0
Ra-224	3.2×10^{-3}	2.9×10^{-5}	0	1.6×10^{-7}	1.4×10^{-5}	1.7×10^{-4}	0	0
Ra-226	1.5×10^{-2}	1.9×10^{-3}	0	4.0×10^{-4}	1.6×10^{-4}	1.2×10^{-2}	0	0
Ra-228	1.5×10^{-2}	1.9×10^{-3}	0	3.8×10^{-4}	1.6×10^{-4}	1.1×10^{-2}	0	0
Ac-228	1.4×10^{-2}	1.9×10^{-3}	0	3.8×10^{-4}	1.6×10^{-4}	1.1×10^{-2}	0	0
Th-228	2.6×10^{-4}	5.4×10^{-5}	0	5.6×10^{-5}	7.0×10^{-7}	3.7×10^{-4}	0	0
Ra-224	2.0×10^{-4}	4.4×10^{-5}	0	5.5×10^{-5}	1.1×10^{-6}	3.1×10^{-4}	0	0
Pa-234m	9.2×10^{-7}	0	0	0	0	0	0	0
Pa-234	1.4×10^{-9}	1.5×10^{-25}	0	8.9×10^{-34}	2.6×10^{-18}	8.6×10^{-25}	0	0
Pa-234	3.1×10^{-4}	3.2×10^{-20}	0	1.9×10^{-28}	5.7×10^{-13}	1.8×10^{-19}	0	0
Ac-228	2.8×10^{-4}	1.2×10^{-21}	0	1.2×10^{-62}	1.5×10^{-12}	6.7×10^{-21}	0	0
Th-228	5.2×10^{-6}	6.7×10^{-7}	0	3.6×10^{-7}	7.8×10^{-10}	4.1×10^{-6}	0	0
Ra-224	4.0×10^{-6}	6.7×10^{-7}	0	3.6×10^{-7}	1.8×10^{-8}	4.1×10^{-6}	0	0
Pu-239	1.5×10^{-2}	1.9×10^{-3}	0	2.5×10^{-8}	8.1×10^{-8}	1.2×10^{-2}	0	0

birds. Thus, assuming uncontaminated soil implies that these three food types would be uncontaminated.

Table A-9 considers only the contaminated soil pathway resulting from a year's cumulative deposition of 1 Bq m^{-2} of each parent radionuclide (the interception fraction is used to compute the component that would deposit on the plant, and that much is neglected). This pathway feeds radioactivity into roots of pasture grass and food crops and to poultry through ingestion of soil (ingestion of soil by beef and dairy cattle has been neglected because of the conservatism of the assumptions about pasturing of the animals).

Table A-10 shows estimates of levels of radioactivity in the flesh of fish after one year in water contaminated with 1 Bq L^{-1} of the parent radionuclide.

Table A-9. Concentrations of Decay Chains from Root Uptake due to Soil Contamination of 1 Bq m^{-2} $year^{-1}$ of the Parent Radionuclides

	Pasture (Bq kg^{-1})	L. Veg. (Bq kg^{-1})	R. Veg. (Bq kg^{-1})	Beef (Bq kg^{-1})	Milk (Bq L^{-1})	Grain (Bq kg^{-1})	Poultry (Bq kg^{-1})	Eggs (Bq kg^{-1})
U-234	8.8×10^{-9}	4.1×10^{-7}	8.2×10^{-8}	5.2×10^{-8}	2.3×10^{-7}	1.8×10^{-8}	2.2×10^{-5}	3.3×10^{-5}
Th-230	2.9×10^{-14}	4.0×10^{-13}	1.5×10^{-13}	1.9×10^{-12}	2.9×10^{-14}	2.6×10^{-14}	2.3×10^{-11}	4.1×10^{-12}
U-235	8.8×10^{-9}	4.1×10^{-7}	8.2×10^{-8}	5.2×10^{-8}	2.3×10^{-7}	1.8×10^{-8}	2.2×10^{-5}	3.3×10^{-5}
Th-231	1.6×10^{-19}	2.2×10^{-18}	8.0×10^{-19}	1.1×10^{-17}	1.6×10^{-19}	1.4×10^{-19}	1.3×10^{-16}	2.2×10^{-17}
U-238	8.8×10^{-9}	4.1×10^{-7}	8.2×10^{-8}	5.2×10^{-8}	2.3×10^{-7}	1.8×10^{-8}	2.2×10^{-5}	3.3×10^{-5}
Th-234	8.6×10^{-9}	2.8×10^{-7}	7.2×10^{-8}	7.5×10^{-8}	2.9×10^{-8}	1.5×10^{-8}	1.3×10^{-5}	4.4×10^{-6}
Pa-234m	8.6×10^{-9}	2.8×10^{-7}	7.2×10^{-8}	7.5×10^{-8}	2.9×10^{-8}	1.5×10^{-8}	1.3×10^{-5}	4.4×10^{-6}
Pa-234	1.4×10^{-11}	4.4×10^{-10}	1.1×10^{-10}	1.2×10^{-10}	4.3×10^{-11}	2.3×10^{-11}	2.0×10^{-8}	6.5×10^{-9}
Th-228	7.7×10^{-10}	8.4×10^{-9}	1.6×10^{-9}	4.3×10^{-8}	8.5×10^{-11}	3.4×10^{-8}	2.7×10^{-8}	6.6×10^{-8}
Ra-224	7.7×10^{-10}	8.5×10^{-9}	1.6×10^{-9}	4.3×10^{-8}	2.8×10^{-9}	3.4×10^{-8}	2.7×10^{-8}	4.1×10^{-8}
Th-230	8.8×10^{-10}	8.8×10^{-9}	1.8×10^{-9}	5.6×10^{-8}	9.7×10^{-11}	3.6×10^{-8}	3.2×10^{-8}	6.7×10^{-8}
Th-231	8.8×10^{-10}	8.8×10^{-9}	1.8×10^{-9}	5.6×10^{-8}	9.7×10^{-11}	3.6×10^{-8}	3.2×10^{-8}	6.7×10^{-8}
Th-232	8.8×10^{-10}	8.8×10^{-9}	1.8×10^{-9}	5.6×10^{-8}	9.7×10^{-11}	3.6×10^{-8}	3.2×10^{-8}	6.7×10^{-8}
Ra-228	3.8×10^{-11}	1.1×10^{-10}	4.1×10^{-11}	3.5×10^{-9}	3.4×10^{-10}	6.9×10^{-10}	1.5×10^{-9}	1.1×10^{-10}
Ac-228	3.8×10^{-11}	1.1×10^{-10}	4.1×10^{-11}	3.5×10^{-9}	3.4×10^{-10}	6.9×10^{-10}	1.5×10^{-9}	1.0×10^{-10}
Th-228	2.5×10^{-12}	2.1×10^{-12}	1.4×10^{-12}	4.6×10^{-10}	1.7×10^{-12}	2.0×10^{-11}	1.4×10^{-10}	2.5×10^{-13}
Ra-224	2.3×10^{-12}	1.6×10^{-12}	1.2×10^{-12}	4.4×10^{-10}	8.8×10^{-12}	1.6×10^{-11}	1.3×10^{-10}	6.4×10^{-14}
Th-234	1.8×10^{-11}	2.9×10^{-9}	2.2×10^{-10}	9.2×10^{-11}	1.7×10^{-12}	6.6×10^{-9}	2.5×10^{-9}	5.7×10^{-8}
Pa-234m	1.8×10^{-11}	2.9×10^{-9}	2.2×10^{-10}	9.2×10^{-11}	1.7×10^{-12}	6.6×10^{-9}	2.5×10^{-9}	5.7×10^{-8}
Pa-234	2.9×10^{-14}	4.6×10^{-12}	3.6×10^{-13}	1.5×10^{-13}	2.8×10^{-15}	1.1×10^{-11}	4.0×10^{-12}	9.3×10^{-11}
Ra-224	9.2×10^{-20}	8.8×10^{-11}	3.5×10^{-14}	3.6×10^{-21}	3.3×10^{-19}	1.1×10^{-11}	2.6×10^{-11}	2.5×10^{-10}
Ra-226	1.5×10^{-8}	1.5×10^{-7}	3.1×10^{-8}	3.4×10^{-7}	1.4×10^{-7}	8.9×10^{-7}	1.5×10^{-8}	6.7×10^{-10}
Ra-228	1.5×10^{-8}	1.5×10^{-7}	3.0×10^{-8}	3.1×10^{-7}	1.3×10^{-7}	8.8×10^{-7}	1.4×10^{-8}	6.7×10^{-10}
Ac-228	1.5×10^{-8}	1.5×10^{-7}	3.0×10^{-8}	3.1×10^{-7}	1.3×10^{-7}	8.8×10^{-7}	1.4×10^{-8}	6.7×10^{-10}
Th-228	1.9×10^{-9}	5.8×10^{-9}	2.1×10^{-9}	1.4×10^{-7}	7.5×10^{-10}	5.0×10^{-8}	1.4×10^{-9}	3.1×10^{-12}
Ra-224	1.8×10^{-9}	5.0×10^{-9}	1.9×10^{-9}	1.4×10^{-7}	6.9×10^{-9}	4.6×10^{-8}	1.4×10^{-9}	1.1×10^{-12}
Pa-234m	0	0	0	0	0	0	0	0
Pa-234	$< 10^{-99}$	1.1×10^{-55}	1.9×10^{-91}	$< 10^{-99}$	$< 10^{-99}$	2.0×10^{-75}	8.6×10^{-39}	2.0×10^{-20}
Pa-234	$< 10^{-99}$	2.3×10^{-50}	4.1×10^{-86}	$< 10^{-99}$	$< 10^{-99}$	4.3×10^{-70}	2.4×10^{-31}	5.7×10^{-13}
Ac-228	$< 10^{-99}$	1.7×10^{-53}	1.7×10^{-92}	$< 10^{-99}$	$< 10^{-99}$	7.8×10^{-78}	2.2×10^{-64}	2.1×10^{-13}
Th-228	5.0×10^{-12}	5.5×10^{-11}	1.1×10^{-11}	2.8×10^{-10}	5.5×10^{-13}	9.3×10^{-12}	1.9×10^{-41}	1.4×10^{-11}
Ra-224	5.0×10^{-12}	5.5×10^{-11}	1.1×10^{-11}	2.8×10^{-10}	1.8×10^{-11}	9.3×10^{-12}	1.9×10^{-41}	8.4×10^{-12}
Pu-239	4.6×10^{-10}	4.7×10^{-9}	9.3×10^{-10}	6.5×10^{-13}	2.1×10^{-12}	3.6×10^{-9}	6.5×10^{-11}	2.7×10^{-7}

REFERENCES

International Commission on Radiological Protection (ICRP). 1979. *Limits for Intakes of Radionuclides by Workers.* ICRP Publication 30 Part 1, *Ann. ICRP* **2(3/4)**.

Killough G.G., M.J. Case, K.R. Meyer, R.E. Moore, J.F. Rogers, S.K. Rope, D.W. Schmidt, B. Shleien, J.E. Till, and P.G. Voillequé. 1993. *The Fernald Dosimetry Reconstruction Project — Task 4: Environmental Pathways — Models and Validation.* Report RAC Report No. CDC-3, Radiological Assessments Corp., Neeses, South Carolina.

Table A-10. Concentrations in Fish (Bq kg^{-1}) Resulting from a Steady-State Level of 1 Bq L^{-1} of Parent Radionuclide in Water

U-234	5.0×10^{1}
Th-230	2.3×10^{-4}
U-235	5.0×10^{1}
Th-231	1.3×10^{-9}
U-238	5.0×10^{1}
Th-234	5.0×10^{1}
Pa-234m	5.0×10^{1}
Pa-234	8.0×10^{-2}
Th-228	8.3×10^{1}
Ra-224	8.3×10^{1}
Th-230	1.0×10^{2}
Th-231	1.0×10^{2}
Th-232	1.0×10^{2}
Ra-228	6.1×10^{0}
Ac-228	6.1×10^{0}
Th-228	5.4×10^{-1}
Ra-224	5.1×10^{-1}
Th-234	4.3×10^{-1}
Pa-234m	4.3×10^{-1}
Pa-234	6.9×10^{-4}
Ra-224	8.7×10^{-15}
Ra-226	5.0×10^{1}
Ra-228	4.7×10^{1}
Ac-228	4.7×10^{1}
Th-228	8.3×10^{0}
Ra-224	8.1×10^{0}
Pa-234m	0
Pa-234	$< 10^{-99}$
Pa-234	$< 10^{-99}$
Ac-228	$< 10^{-99}$
Th-228	1.0×10^{-1}
Ra-224	1.0×10^{-1}
Pu-239	2.5×10^{2}

Killough G.G., D.E. Dunning, Jr., and J.C. Pleasant. 1978. *INREM II: A Computer Implementation of Recent Models for Estimating the Dose Equivalent to Organs of Man from an Inhaled or Ingested Radionuclide.* Report NUREG/CR-0114, ORNL/NUREG/TM-84, Oak Ridge National Laboratory, Oak Ridge, Tennessee.

Pleasant J.C., L.M. McDowell-Boyer, and G.G. Killough. 1982. *RAGBEEF: A FORTRAN IV Implementation of a Time-Dependent Model for Radionuclide Contamination of Beef.* Report NUREG/CR-2610, ORNL/TM-8011, Oak Ridge National Laboratory, Oak Ridge, Tennessee.

Pleasant J.C., L.M. McDowell-Boyer, and G.G. Killough. 1980. *RAGTIME: A FORTRAN IV Implementation of a Time-Dependent Model for Radionuclides in Agricultural Systems.* Report NUREG/CR-1196, ORNL/NUREG/TM-371, Oak Ridge National Laboratory, Oak Ridge, Tennessee.

Schreckhise R.G., K. Rhoads, J.S. Davis, B.A. Napier, and J.V. Ramsdell. 1993. *Recommended Environmental Dose Calculation Methods and Hanford-Specific Parameters.* Report PNL-3777 Rev. 2. Pacific Northwest Laboratory, Richland, Washington.

Till J.E. and H.R. Meyer (editors). 1983. *Radiological Assessment — A Textbook on Environmental Dose Analysis.* U.S. Nuclear Regulatory Commission, Washington, D.C.

U.S. Nuclear Regulatory Commission (USNRC). 1977. *Calculation of Annual Doses to Man from Routine Releases of Reactor Effluents for the Purpose of Evaluating Compliance with 10 CFR Part 50, Appendix I.* Regulatory Guide 1.109, Revision 1 (October 1977). Washington, D.C.

APPENDIX B

A MODEL OF URANIUM, THORIUM, AND DECAY PRODUCTS IN SOIL

INTRODUCTION

In modeling the movement of radionuclides released from the Feed Materials Production Center (FMPC), it is necessary to quantify certain assumptions about the rates of removal of radionuclides from surface soils and the formation of decay products during the period 1951–1988. We sought the simplest model that would be compatible with our requirements for dose estimation and that would give reasonable agreement with the measurements that are available.

Movement in soil of the radionuclides of concern in this study is a very complex process that depends on variables whose values over space and time are poorly known. The model that we have adopted is empirical rather than process-level, with parameters for relatively insoluble compounds calibrated to measurements at the FMPC boundary stations and with parameters for soluble compounds based on results reported for a nuclear facility that released primarily soluble uranium.

This model assumes that all radionuclides considered in the calculation — including the relatively small amounts of processed thorium and trace amounts of transuranics from recycled uranium that occurred in the source term for airborne releases — have the same environmental rate coefficient (λ_E in the text that follows) as uranium. Such data as exist for other radionuclides in soil around the FMPC are not time series and would be essentially useless in calibrating separate soil-removal coefficients for concomitant radionuclides.

STRUCTURE OF THE MODEL

The soil model structure consists of a single compartment replicated over two factors: solubility and mixing depth. Each factor is implemented with two levels. Radionuclides are considered soluble or insoluble. Mixing depths are 0.5 cm or 10 cm, according to the particular transport or dose calculation that depends on the concentration of a radionuclide in the soil. Figure B-1 illustrates the breakdown by mixing depth; the table in the figure gives the mean transit times for the four possible combinations of factors and levels. The mechanisms of removal of deposited radioactivity from the soil compartment are runoff and migration into deeper soil. Decay-chain kinetics are also considered as the radionuclides pass through the compartment.

The two mixing depths are appropriate for different calculations. We chose the 10-cm depth for the root zone of food crops and pasture grasses and for validations, because most time series data for uranium near the FMPC are based on soil samples of that depth. Some calculations (such as resuspension) should be based on the soil concentration of radioactivity near the surface; for calculations of this kind, we chose to use a 0.5-cm layer. In general, this layer contains recently-deposited radioactivity in higher concentration than the 10-cm layer, which represents an average over a deeper profile.

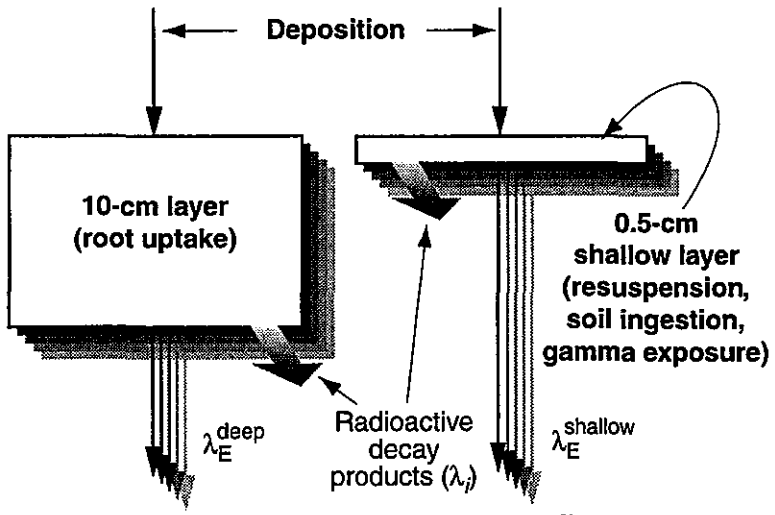

Mean transit (residence) times $1/\lambda_E$

	Deep	Shallow
Insoluble	14 years	9 months
Soluble	1 month	2 days

Figure B-1. Schematic representation of the dynamic soil model. Each year's deposition enters a compartment with environmental removal kinetics governed by a first-order rate coefficient λ_E. Environmental mean transit time of radioactivity in the compartment depends on solubility and mixing depth, as indicated by the table. Radioactive decay and the formation of decay products are represented by the drop-shadow boxes. Losses of primary radionuclides and decay products are by runoff and migration into deeper soil.

After deposition, the formation of radioactive decay products is calculated for each of the model's compartments (i.e., for each combination of solubility and mixing depth). Decay-chain kinetics are applied a year at a time and the process consists of two steps: (1) incorporation of the newly-deposited material, and (2) decay of each radioactive species in the chain for one year and simultaneous formation of the decay products.

Loss from the compartment is regulated by a first-order rate coefficient λ_E, which depends on the combination of factors represented by the compartment (table in Figure B-1). Material leaving the compartment migrates into deeper soil or is lost by runoff. No distinction between the two fates is made in the calculation. There is no immobile residue in any compartment: given sufficient time and a cessation of deposition, residual amounts (even in the absence of radioactive decay) will drop below any arbitrary level. The natural background level of uranium in the soil is considered constant and is not simulated directly by the model.

Deposition of each airborne radionuclide is treated as insoluble or soluble according to the chemical compound of the material, as indicated below:

Insoluble	U_3O_8, UO_2, thorium, plutonium
Soluble	UF_4, UO_3

We now give the equations that quantify the process. Each airborne radionuclide, as it is deposited on the soil, is treated as the parent in a decay chain in the model compartment, and levels of the parent and each decay product are calculated over time at one-year intervals. For year s (= 1951, ..., 1988), the differential equations of a compartment are

$$\frac{dY_i}{dt} = -(\lambda_i^R + \lambda_E)Y_i + \lambda_i^R \sum_{j=1}^{i-1} \beta_{ij} Y_j + P_i(t), \quad s \le t < s+1, \quad i = 1, \ldots, N \tag{B-1a}$$

where

$$P_i(t) = \begin{cases} \text{parent deposition rate for year } s & \text{if } i = 1 \\ 0 & \text{otherwise} \end{cases} \tag{B-1b}$$

and the initial values are given by

$$Y_i(s) = \begin{cases} \lim_{t \to s-} Y_i(t) & \text{if } s > 1951 \\ 0 & \text{if } s = 1951 \end{cases} \tag{B-1c}$$

The remaining symbols are

$Y_i(t)$ = radioactivity (Bq) of decay-chain species i at time t

λ_i^R = radiological decay-rate constant for species i (year^{-1})

λ_E = removal rate coefficient from surface soil layer for all radionuclides considered (year^{-1})

β_{ij} = fraction of species j that decays to species i.

The meaning of the initial condition of Eq. B-1c is that the model carries forward all radioactivity of each species that remains in the compartment at the end of a year to the beginning of the next year. The deposition rate for the parent species is constant within each year but varies from year to year, as it is driven by the airborne source term and estimated by the wet and dry deposition models (Appendix M).

Equations B-1a through B-1c are for total levels of radioactivity (Bq) in one square meter of soil down to depth Δz. Conversion to concentrations is based on the bulk density ρ of the soil. As a generic value of the bulk density, we have used 1.4 g cm^{-3}.

CALIBRATION

Our estimate of the parameter λ_E for insoluble uranium is based on measurements of uranium in 10-cm depth samples of soil at the FMPC boundary stations. The value 0.069 year^{-1} is the average of the values that were estimated for the six time series that we evaluated (Appendix C), and this value gave a geometric mean of 1.0 for the predicted/observed ratios for the years 1986–1988. The corresponding rate coefficient for the 0.5-cm shallow compartment is 1.4 year^{-1}.

Because of the preponderance of relatively insoluble uranium in the releases from the FMPC to the atmosphere (about 65% by mass over the 38 years of plant operation), it is highly unlikely that an analysis of the kind described in Appendix C could furnish an estimate of the parameter λ_E for soluble forms of uranium. For this purpose, we have examined results from a 1950s survey from the Harshaw Chemical Company in Cleveland Ohio, which released primarily the soluble compound UO_2F_2 (Weinstein 1958). The rainfall for the Cleveland area (38 in. year^{-1}) was comparable to that of the Fernald area. On the basis of the survey data, we estimated $\lambda_E^{sol}\Delta z \approx 120$ cm year^{-1} near the soil surface. Thus, for the 10-cm compartment we have $\lambda_E^{sol} = 12$ year^{-1}; the corresponding value for the 0.5-cm layer is 240 year^{-1}.

DISCUSSION

In judging the adequacy of the foregoing model for retention of radionuclides in surface soil, it is appropriate to consider the uses to which it is put. This model serves the following purposes in our simulations of radionuclide transport and dose:

1. Uptake of radionuclides from the soil by food crops and pasture grass in the GARDEN model (Appendix A) is based on the dynamic levels simulated by this soil model (10-cm layer).
2. Ingestion of radionuclides with soil is calculated from results given by the soil model (0.5-cm layer).
3. Irradiation of individuals outdoors by gamma-emitting radionuclides in surface soil is based on the levels simulated by the soil model (0.5-cm layer).
4. Breathing of resuspended radionuclides depends on concentrations of radionuclides in soil that were provided by the soil model (0.5-cm layer).

The model validations have included considerations of measurements in soil (Appendix N), and the results have indicated that the soil model gives good qualitative agreement with measurements of uranium in soil.

One may criticize the application of the same removal coefficient to elements that are known to show distinct mobilities in soil, particularly uranium and plutonium. But releases of plutonium and other transuranics were very low relative to those of uranium, and the minor distortion created by applying the rate coefficient for insoluble radionuclides both to insoluble compounds of uranium and to plutonium was judged unimportant in relation to the added complexity of introducing a different coefficient for each species. Moreover, our calibration depended on long-term site-specific measurements, which were available only for uranium.

REFERENCES

Weinstein M.S. 1958. "Environmental Contamination." In *Symposium on Occupational Health Experience and Practices in the Uranium Industry,* held in New York City, October 15–17, 1958, sponsored by the U.S. Atomic Energy Commission Division of Biology and Medicine and the Health and Safety Laboratory, Report HASL-58, Health and Safety Laboratory, New York, pp. 180–185.

APPENDIX C

USE OF SOIL DATA TO CONFIRM THE MAGNITUDE OF AIRBORNE RELEASES AND DEPOSITION OF URANIUM OVER TIME

INTRODUCTION

The purpose of this appendix is to use the results of soil sampling to estimate the deposition of airborne releases of uranium from the Feed Materials Production Center (FMPC). By a process of back calculation, using models and data, we infer an estimate of the total airborne release from the facility, together with parametric uncertainty. This estimate is compared with the direct estimate based on historical records that was reported in the Task 2/3 report (Voillequé et al. 1995). The estimate developed in this appendix involves some relatively crude assumptions. It is not intended to supersede the Task 2/3 estimate, but rather to provide a different approach for purposes of comparison.

In connection with litigation concerning releases of radioactivity from the FMPC, the Department of Energy (DOE) commissioned the gathering of numerous samples of soil within about a 9-km radius of the facility. A preliminary sampling was carried out in 1984, and a more extensive effort followed in 1986. The samples were analyzed for uranium content and in some cases for thorium. Sediments and vegetation were also included in the sampling. IT Corporation carried out the sampling and much of the subsequent analysis under contract to DOE.

In 1990, the Centers for Disease Control and Prevention (CDC) transmitted to *Radiological Assessments Corporation (RAC)* an undocumented file, named SOIL13, which contained a database that included results of the 1984 and 1986 sampling and analysis projects. In preparing Appendix N of the Task 4 report (Killough et al. 1993), we made use of the SOIL13 data together with other soil data to estimate ranges of deposition of released airborne uranium on the soil.

Our first examination of the SOIL13 file revealed numerous entries that were substantially below the natural background level (approximately 2 pCi total uranium per gram of soil). We learned from representatives of DOE and IT Corporation that an independent reanalysis of a selection of the samples by two DOE laboratories [Environmental Measurements Laboratory (EML) and Radiological and Environmental Sciences Laboratory (RESL)] had confirmed a trend of low-biased IT estimates for uranium activities less than about 2.7 pCi g^{-1}, but that the IT analysis, on average, was accurate or slightly high for samples above this radioactivity concentration level.

In September of 1993, six months after the Task 4 draft report was issued, a paper appeared in *Health Physics* that discussed the reanalysis of a subset of the 1986 dataset by the IT laboratory and EML and RESL (Stevenson and Hardy 1993). The authors of the paper also used the original observations, together with information from the reanalyses, to estimate the uranium soil inventory near the FMPC (i.e., excess over natural background) that is presumably attributable to releases from the facility. Their estimate, based on the reanalyzed samples of

Table C-1. Parameters and Results from Paper of Stevenson and Hardy (1993)

Description	Value and units
Natural background for total uranium in soil	2.2 pCi $(g\ soil)^{-1}$
Bulk density of soil	1.0 g cm^{-3}
Sampling depth	5 cm
Excess total uranium within about 2–3 km from center of FMPC production area (excluding the FMPC site)	2,130–6,140 kg

the top 5 cm of soil, was that in 1986, the excess uranium in soil within 2–3 km of the FMPC (excluding the site itself) was in the range 2,130–6,140 kg.

The National Research Council (NRC) review of the Fernald Dosimetry Reconstruction Project (Schull et al. 1994) raised several questions about the relationship between our previous estimates of release and deposition and the excess inventory for 1986 given in the Stevenson and Hardy paper. The matter was pursued primarily in connection with the review of the Task 4 report (Killough et al. 1993). Most of these questions focus on Appendix N of the Task 4 report. We have subsequently reanalyzed some of the data with different mathematical tools and without reference to the soil-water partition coefficient (K_d) that was drawn into the discussion in Appendix N of the Task 4 report. In the present appendix, we give the results of the new analysis and describe the models used to carry it out.

Inasmuch as the Stevenson and Hardy paper appeared months after the release of the Task 4 report, that report obviously could not respond to any questions that the paper might have appeared to raise. Some of the review comments of the Task 4 report, however, seemed to indicate that the reviewers were not aware of the sequence of the documents and that they believed the Task 4 report presented estimates that were in conflict with the results of the Stevenson and Hardy paper. In fact, there is no such conflict. We believe that the results of the Stevenson and Hardy paper have been misinterpreted, and an important part of our purpose in this appendix is to clarify the relationship between (1) the 1986 soil inventory of excess uranium near the FMPC and (2) the cumulative deposition of airborne uranium from the FMPC from 1951 through 1988 (the period of the facility's operation). These two quantities have very different magnitudes. The first is what Stevenson and Hardy estimated from the reanalyzed data. The second is what we estimated in Appendix N of the Task 4 report and what we recalculate in this appendix.

QUALITATIVE OVERVIEW

An estimate of offsite excess total uranium from the FMPC remaining in the soil near the facility in 1986 was recently published by Stevenson and Hardy (1993). Table C-1 summarizes the key parameters and numeric results from that paper.

We will use the term *inventory* to denote the excess total uranium residue in the soil at a specific time. As a nominal value of the 1986 inventory, for convenience in this discussion, we assign the midrange value 4,140 kg based on the last line of Table C-1. Remember that this value is based on samples of the top 5 cm of soil. Our model is based primarily on time-series data from the top 10 cm of soil at six of the FMPC boundary stations, and we need to make the 1986 inventory estimate of Stevenson and Hardy (1993) compatible with the model's predictions. In the middle 1980s, the boundary station samples were separated into 0–5 cm and 5–10 cm layers. A comparison of the layers indicated that assuming equal amounts of uranium in the 0–5 cm and 5–10 cm layers was reasonable (although this assumption might not be reasonable for locations inside the boundary). We are going to apply this assumption to extend the Stevenson and Hardy offsite inventory to a 10 cm layer by doubling the estimated inventory. Thus, we will take the 1986 inventory in the top 10 cm of the region to be $2 \times 4{,}140 = 8{,}280$ kg of total uranium.

The region over which this quantity of uranium is distributed (and to which it is confined), according to Stevenson and Hardy (1993), is bounded by an irregular ovoid shape with principal axis oriented southwest to northeast. The length of this axis is roughly 5 km, and the perpendicular minor axis is about 3.3 km. Uranium deposited in the subregion belonging to the plant site (about 4 km^2) is excluded. Outside of the ovoid region, the 1986 levels are considered to be at natural background. Stevenson and Hardy estimated the total area of the oval (excluding the plant site) as 8.0 ± 0.9 km^2. We call this the 1986 region, or sometimes the small region. If, as we contend, excess uranium levels in soil had been declining since 1971, this region is a 1986 snapshot of an area that was larger in past years (our calculations suggest 1964 as the year when it was largest). Figure C-1 shows the concentration isopleths estimated by Stevenson and Hardy (1993) superimposed on a map of the FMPC site and regional roads and waterways.

It is *not* reasonable to assume that the 1986 excess uranium inventory in this region is approximately equal to the cumulative deposition of uranium from airborne releases from the FMPC since operations began in 1951. There are several flaws in such an assumption:

1. It is well documented that a fraction of the airborne release was in a soluble form, which would leach rapidly into deeper soil and run off into the waterways with rainfall (Voillequé et al. 1995). Essentially none of this component would remain in 1986 from the period of maximum releases (1950s and early 1960s).
2. There is evidence from the FMPC and other facilities to show that even relatively insoluble uranium compounds, such as U_3O_8, are removed from the top layer of soil over time, although much more slowly than the soluble compounds.
3. The outer boundary of the 1986 region defined by Stevenson and Hardy (Figure C-1) is determined by the point at which one would reach background level in proceeding outward from the plant site in 1986. But if the levels of uranium within the 1986 region were somewhat higher in earlier years (as items 1 and 2 imply that they must have been), then the outer boundary of the above-background region must have enclosed more area in earlier years (an abrupt discontinuity at the boundary does not make physical sense).

We emphasize that Stevenson and Hardy (1993) neither state nor suggest the assumption that we are criticizing. In their paper, they draw no conclusions beyond the direct evidence that they present, and we have no reason to dispute that evidence.

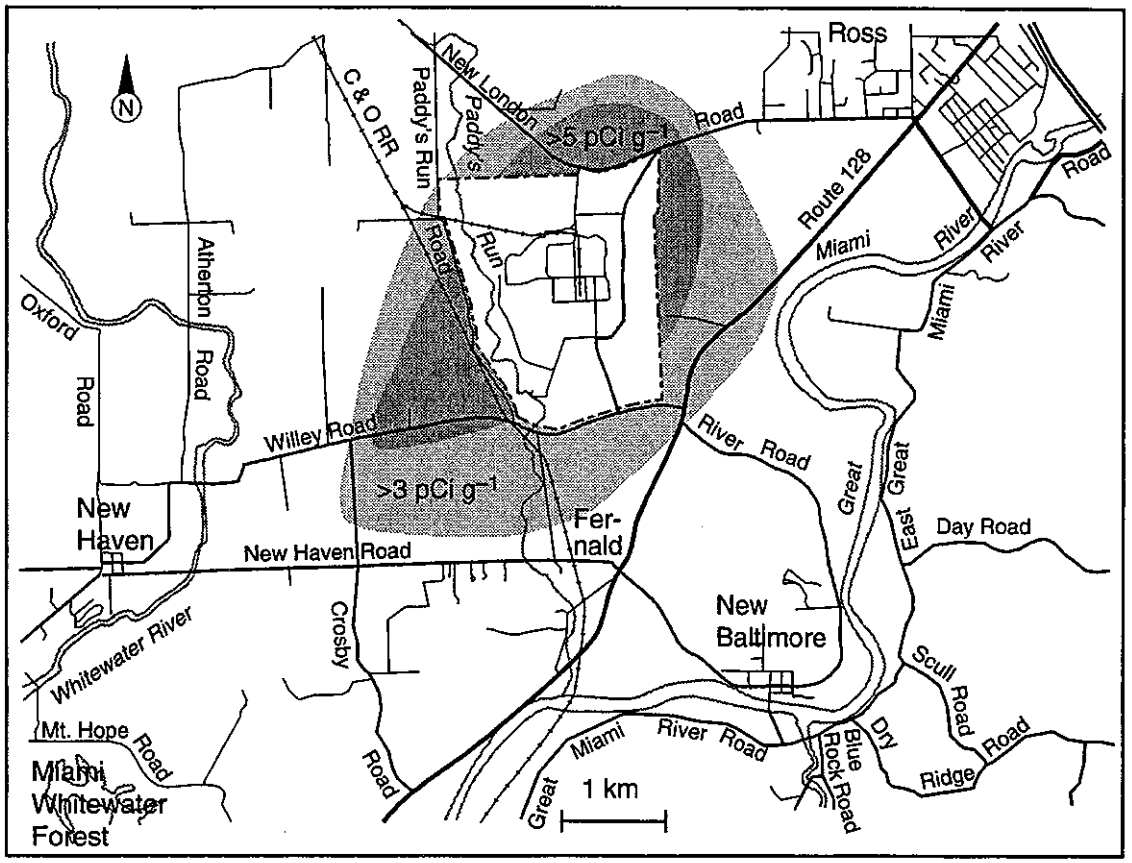

Figure C-1. Isopleths for concentration of total excess uranium in soil in 1986, redrawn from Stevenson and Hardy (1993). The outer boundary of the lighter region approximates the locus at which the concentration reaches background level (2.2 pCi U g^{-1} soil), according to the estimate of these authors, which was based on their examination of reanalyzed samples. The roads and waterways are based on a USGS topographic map.

Estimating the deposition over time that would be consistent with the 1986 Stevenson and Hardy scaled inventory (i.e., to a 10-cm depth) requires a dynamic mass-balance model of deposition, retention, and removal. Figure C-2 illustrates the model we have used and its parameters. Table C-2 gives values and ranges of the parameters and lists the deposition curve in terms of annual percentages. In a later section of this appendix, we present mathematical details of the model. For the purpose of this overview section, however, it is sufficient to know the following things about the model:

a. The model predicts, for each year, the inventory of uranium and calculates the cumulative deposition from previous years. Thus, the cumulative deposition at the end of 1988 is the total deposition over all years of plant operation, which equals the parameter $\mathcal{M}$. The inventory for 1988 is what remains in the surface soil at that time.

b. The model uses weathering rates that depend on two coefficients, λ_{insol} (for insoluble uranium, generically U_3O_8) and λ_{sol} (for soluble forms of uranium), given in units of $year^{-1}$.

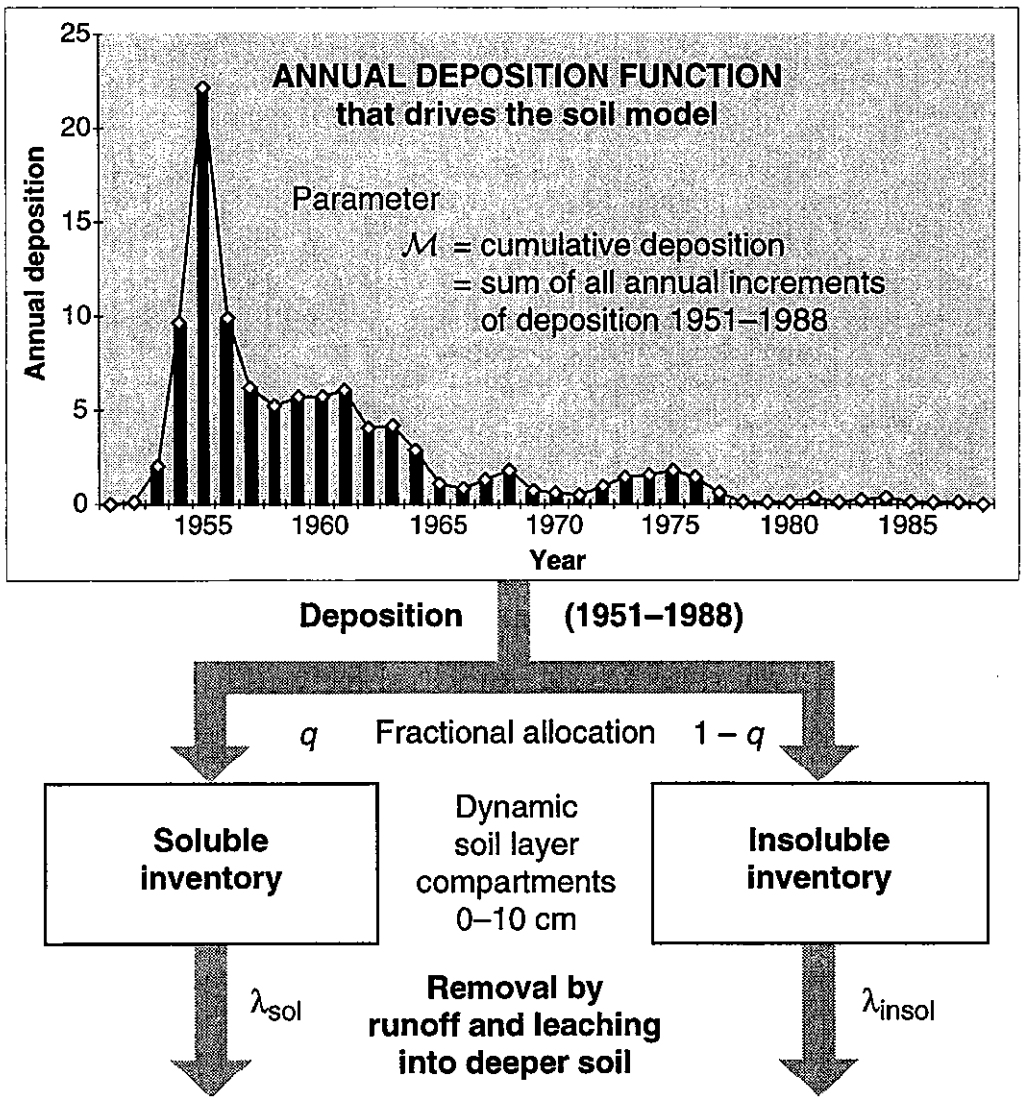

Figure C-2. Mass balance model of uranium in surface soil used for back calculation. The model is driven by a deposition function controlled by a single parameter, $\mathcal{M}$, which is the total deposition from 1951 through 1988. The shape of the curve is determined by the normalized airborne releases given as annual percentages in Table C-2. A fixed fraction q of annual deposition is assumed to be in soluble form. Runoff and migration into deeper soil from the dynamic soil compartments are determined by the first-order parameters λ_{sol} (soluble) and λ_{insol} (insoluble), in units year^{-1}. Given the values of the parameters $\mathcal{M}$, q, λ_{sol}, and λ_{insol}, the model will calculate the inventory of uranium in the soil for each of the years 1951 through 1988. It will also give the cumulative deposition for each of those years. It can also back calculate: if we know q, λ_{sol}, and λ_{insol}, and we are given the inventory of uranium in the soil in a particular year, the model can calculate the value of $\mathcal{M}$ and hence the inventory and cumulative deposition for every year.

Table C-2. Parameters Used by Mass Balance Model

Quantity	Description and units	Nominal Value	Range
λ_{insol}	removal rate coefficient for insoluble uranium ($year^{-1}$)	0.069	0.054 – 0.089
λ_{sol}	removal rate coefficient for soluble uranium ($year^{-1}$)	12	8 – 16
q	fraction of airborne release of uranium that is in a soluble form (dimensionless)	0.35	0.30 – 0.40

Annual deposition fraction	Year	%	Year	%	Year	%	Year	%
	1951	0.01	1961	6.07	1971	0.50	1981	0.33
	1952	0.10	1962	4.00	1972	0.96	1982	0.16
	1953	2.08	1963	4.18	1973	1.37	1983	0.19
	1954	9.61	1964	2.84	1974	1.50	1984	0.37
	1955	22.1	1965	1.13	1975	1.76	1985	0.11
	1956	9.83	1966	0.84	1976	1.44	1986	0.11
	1957	6.15	1967	1.29	1977	0.62	1987	0.09
	1958	5.21	1968	1.77	1978	0.08	1988	0.05
	1959	5.76	1969	0.76	1979	0.13		
	1960	5.71	1970	0.56	1980	0.16		

c. The model requires a parameter q that estimates, on average, the fraction of the cumulative deposition of uranium that is in soluble form.

d. The model relies on a function that gives each year's fraction of the cumulative 38-year deposition (Figure C-2 and Table C-2). This function does not tell how much uranium was deposited in any given year, but only that year's fraction of the 38-year cumulative amount. When a year's fractional deposition is multiplied by the model parameter M, the result is the deposition for that year.

e. The model can back calculate. If we specify any year of plant operation and the uranium inventory in soil during that year (e.g., 1986 and the 8,280 kg of uranium based on the scaled Stevenson and Hardy estimate), the model (if it has values of the parameters M, q, λ_{sol}, and λ_{insol}) will estimate the entire history of inventory and cumulative deposition. In other words, the inventory for any year determines the corresponding inventory and cumulative deposition for all years. This point is very important.

Figure C-3 illustrates the properties of the mass-balance model. The inventory curve rises from the early 1950s to a maximum in 1964 and declines subsequently. The curve was determined by the 1986 estimate of 8,280 kg of uranium (midrange of our adjustment to a 10 cm depth of the Stevenson and Hardy estimate for the 1986 region). The cumulative deposition curve increases to 66,700 kg at the end of 1988. But it is very important to realize that this estimate would apply only to uranium deposited within the 1986 region shown in Figure C-1. The cumulative deposition value of 66,700 kg would underestimate the total offsite deposition, because the region defined by the above-background distribution of uranium in 1986 would

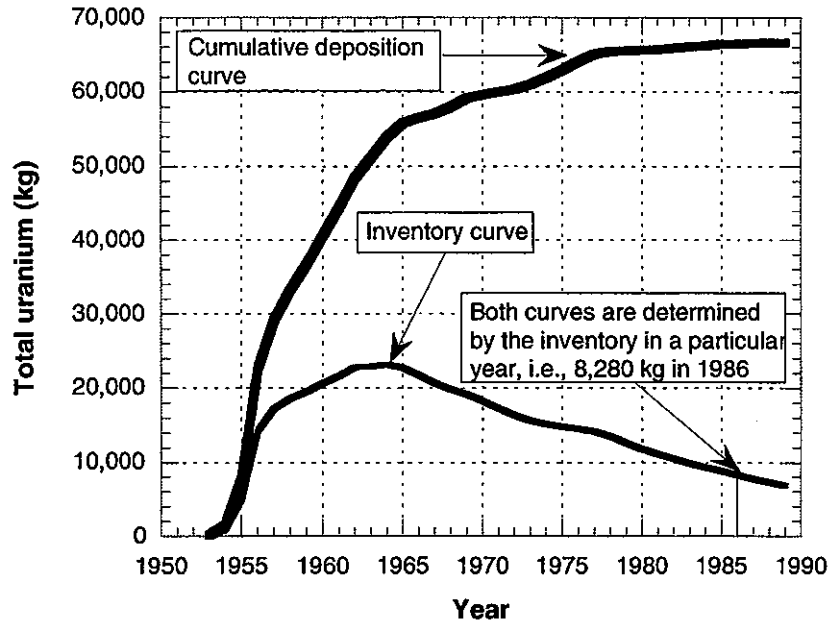

Figure C-3. Soil inventory and corresponding cumulative deposition calculated by the mass-balance model. The curves are determined by the requirement that the 1986 inventory is 8,280 kg of uranium. The cumulative curve applies only to uranium deposited in the 1986 small region. Other parameter values are discussed in the text.

have been larger in the past. Our task is to extend the calculation to a more realistic view of what took place over time.

The following steps, illustrated in Figures C-4 and C-5, describe the back calculation that estimates the total deposition over a larger region:

1. We use the SOIL13 data (suitably adjusted for the bias discussed in the introduction) with a regression procedure to estimate uranium concentration in soil (pCi g^{-1}) vs. distance from the center of the facility. We use those data in the range 900–3,000 m and fit a power function of the form $y = ax^b$, where x is distance (m), y is uranium concentration (pCi g^{-1}), and a and b are parameters to be determined. This procedure gives a down-sloping straight line on a logarithmic plot (the solid line in Figure C-4).
2. Now we use the mass-balance model with the value of 8,280 kg in 1986 to see what the soil inventory of the small region would have been when it was maximum. This turns out to have occurred in 1964, and the value was 23,100 kg (Figure C-5).
3. Using the 1964 inventory calculated in step 2, we move the regression line upward, keeping it parallel to its original direction, until it is located where the integral over the small region agrees with the 1964 inventory (Figure C-4).
4. Now we extend the line representing the 1964 function until it reaches natural background level (2.2 pCi g^{-1}). This occurs at 5,290 m, which, according to this calculation, would be the outer boundary of the region if the measurements had been made in 1964 rather than in 1986. We call this 1964 space the large region (1,150–5,290 m). Note that this region still excludes the FMPC site (Figure C-4).

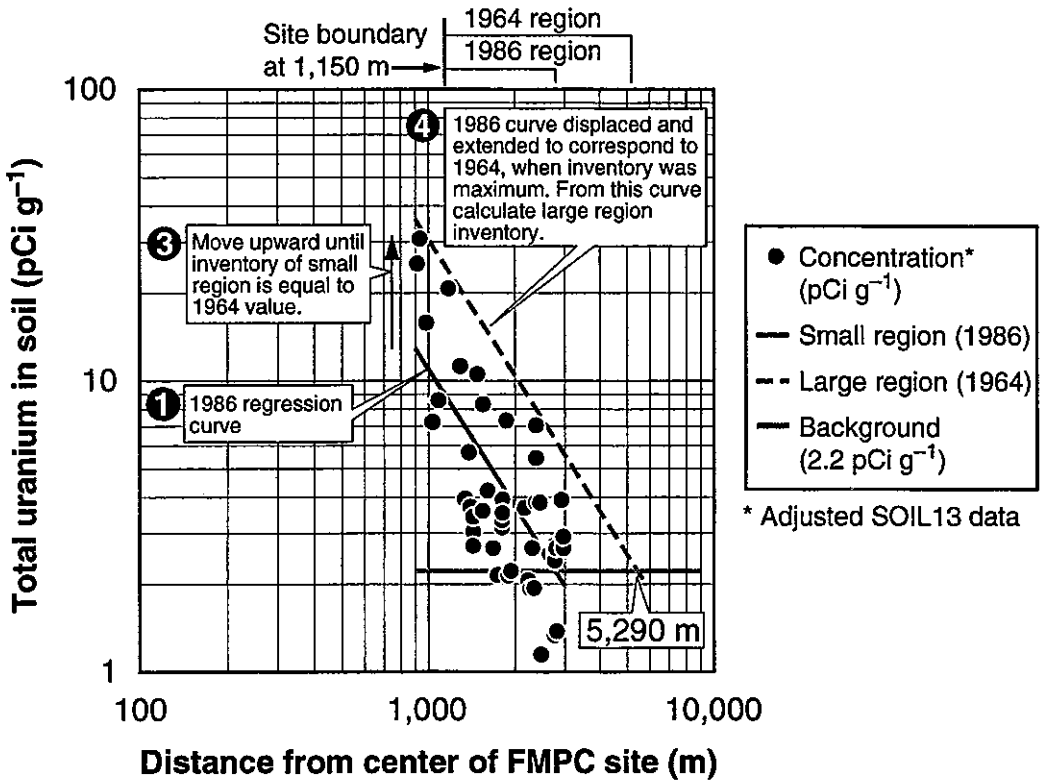

Figure C-4. The 1986 small region (lower solid line) and the 1964 large region (upper dashed line). The plotted points are from the SOIL13 file for the appropriate range of distances, adjusted for underestimation of low activities, and the lower line is a regression curve based on these data. The upper line is consistent with the mass-balance model's estimate of inventory for 1964, and the extension of this line defines the large region. Integration of the latter function leads to the estimate of total cumulative deposition (Figure C-5). The reversed numerals in the figure refer to steps 1–6 in the text.

5. We integrate the deposition given by the 1964 extended line to estimate the 1964 inventory of the large region. This leads to an excess of 33,700 kg (Figure C-5).

6. Finally, we use the mass-balance model once more, this time with the inventory 33,700 kg in 1964 obtained in step 5. The model predicts that the corresponding cumulative deposition over the period of plant operation (i.e., through 1988) would be 97,000 kg of uranium. This is the estimate that we are looking for.

The estimate of approximately 97,000 kg of total uranium deposited from 1951 through 1988 accounts for deposition in the region between 1,150 and 5,290 m from the center of the site. Calculations with the power function model (i.e., the lines in Figure C-4) indicate that about 35% of the cumulative release would deposit in that annular region. Thus we calculate 97,000/0.35 = 277,000 kg. This number is about 89% of the median estimate of 310,000 kg given in the Task 2/3 report (Voillequé et al. 1995). The 5th, 50th, and 95th percentiles of uncertainty for our estimate of airborne releases are 130,000, 284,000, and 720,000 kg, respectively. These percentiles correspond to parametric uncertainties based on (a) the adjusted

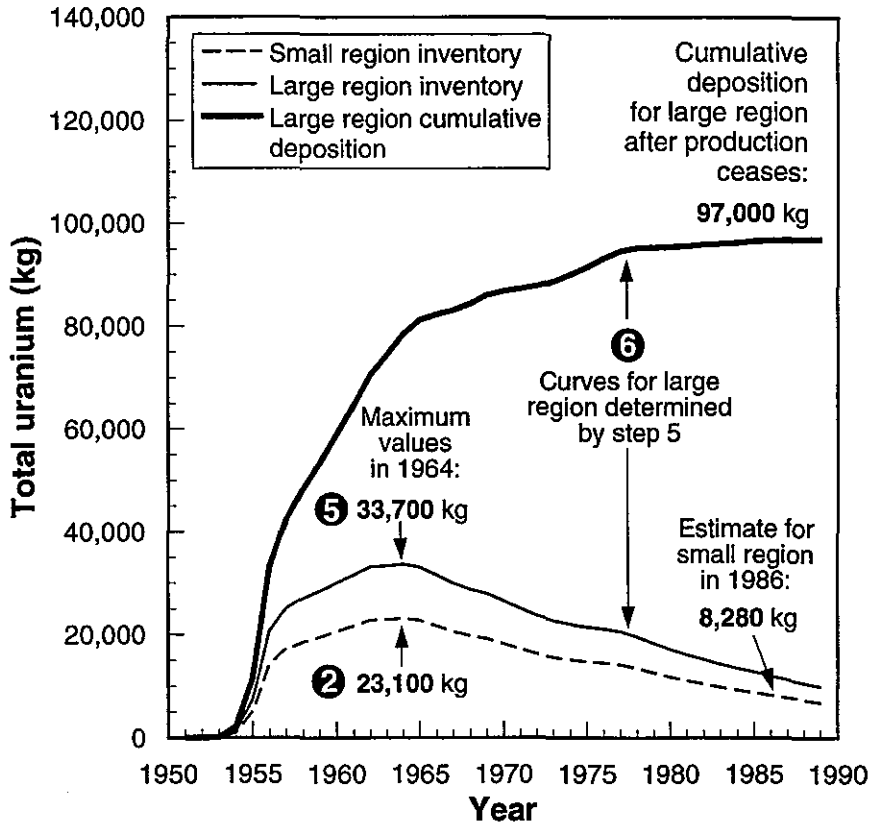

Figure C-5. Use of the mass-balance model to estimate total deposition within the large region (1,150–5,290 m). The lower curve is based on the Stevenson and Hardy 1986 midrange inventory estimate, adjusted to 8,280 kg excess uranium in the top 10 cm of soil. The maximum of this curve indicates a 1964 inventory for the small region of 23,100 kg. Extending this to the large region by integrating the deposition given by the upper curve of Figure C-4 gives a 1964 inventory of 33,700 kg (upper inventory curve of this figure). The cumulative deposition through 1988 corresponding to this large-region scenario is 97,000 kg of excess uranium. One might expect the small and large regions to have the same inventory in 1986, but the latter region shows a larger inventory. The surplus can be interpreted as material dispersed outside the small region that cannot be distinguished from background. The reversed numerals in the figure refer to steps 1–6 in the text.

range of excess uranium in the top 10 cm in 1986 (4,260–12,300 kg), (b) uncertainty ranges for of the removal rate coefficients λ_{sol} and λ_{insol} used in the model (Table C-2), (c) the range 0.3–0.4 for the fraction q of the release that was soluble (Table C-2), and (d) the residual uncertainty in the regression line derived from the adjusted SOIL13 data (which influences the estimated fractional deposition). The resultant uncertainty range includes the median and the uncertainty range given in the Task 2/3 report (Figure C-6). The parametric uncertainty distributions are discussed in the next section.

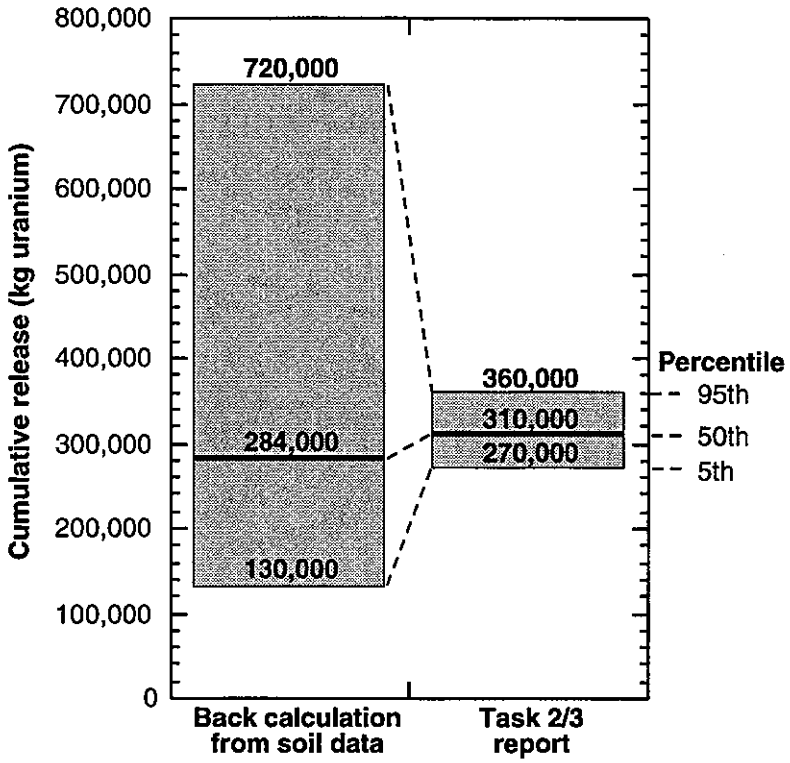

Figure C-6. Cumulative airborne release of uranium: estimates of parametric uncertainty ranges based on the back calculation described in this appendix and the Task 2/3 estimate. The sources of uncertainty for the back calculation are the range of the excess uranium estimated for 1986, the removal rate coefficients, the fraction of the release that was soluble, and the regression line derived from the adjusted SOIL13 data.

DATA AND PARAMETERS

The mass-balance model and other aspects of the calculation depend on certain parameters that must be estimated from the data that are available. We review these parameters and the related datasets. Table C-2 provides a list, which we summarize.

It probably is impossible to estimate the removal-rate parameter λ_{sol} for soluble uranium directly from the FMPC boundary station data because of the predominance of the insoluble portion in the data. Instead, we have estimated λ_{insol} with time-series data measured at the boundary stations, using a value of λ_{sol} based on data from another facility. The Harshaw Chemical Company in Cleveland, Ohio, released a soluble form of uranium almost exclusively (Weinstein 1958). The survey provided both levels in soil and release estimates. Using this information, we estimated λ_{sol} = 12 year^{-1} (Table C-2). The uncertainty range in λ_{sol} was developed from assumptions about uncertainties in the release from Harshaw. This range was propagated in the regressions used to estimate λ_{insol}.

The removal rate coefficient λ_{insol} is estimated from time-series data based on annual soil samples taken at six of the seven FMPC boundary stations beginning in 1971. The data, including natural background, are shown in Table C-3. From 1971 through 1982, the samples

Table C-3. Total Uranium in Soil (pCi g^{-1} dry) at FMPC Boundary Stations 1–7[a]

Year	BS1	BS2	BS3	BS4	BS5	BS6	BS7
1971	6.7	13.5	64.6	6.0	11.4	12.1	
1972	1.8[d]	8.1	29.6	3.0	4.6[d]	5.0	
1973	14.1	18.2	92.2	10.1	9.4	10.1	
1974	10.1	12.1	63.3	3.0	8.1	9.4	
1975	17.5	17.5	78.8	8.1	13.5	14.8	
1976	12.1	14.8	78.8	6.3	10.1	11.4	
1977	14.8	14.8	89.5	6.3	10.8	10.8	
1978	15.5	14.1	68.7	7.4	10.8	7.4	
1979	8.1	11.4	74.1	7.4	7.4	9.4	
1980	9.4	14.1	41.7	6.1	10.1	12.8	
1981	11.4	15.5	90.2	4.0	16.2		2.0
1982	7.4	7.4	43.1	3.4	5.4	6.1	2.7
1983[b]	8.7	11.6	47.2	4.7	5.5	7.9	2.5
1984[b]	8.5	8.0	48.3	7.4	8.2	4.0	3.2
1985[b]	4.0	1.8[d]	32.0	3.0	2.6	1.1[d]	0.39[d]
1986[c]	4.0	8.1	38.8	5.9	5.1	5.4	2.9
1987[c]	4.0	9.0	35.0	4.1	6.5	8.7	3.6
1988[c]	4.0	9.7	60.0	5.6	5.5	7.1	4.4

[a] No subtraction of background uranium has been applied. Except as noted, sampling depth was 10 cm, and tabular entries were converted from μg g^{-1} (natural uranium was assumed for the conversion).

[b] Sampling depth was 5 cm in 1983–1985. The observations have been adjusted using the vertical distributions observed in 1986–1988, when core profiles were taken at 0–5 cm and 5–10 cm. Tabular entries were converted from μCi g^{-1}.

[c] Sampling depth was 10 cm, and the core profile was analyzed for layers 0–5 cm and 5–10 cm. The tabulated values are averages of the data for the individual layers. After 1985, a different laboratory analyzed the samples, but no adjustment for this change has been made. Tabular entries were converted from μCi g^{-1}.

[d] Outlier. An observation was treated as an outlier if its residual ε_j satisfied the inequality $|\varepsilon_j - \text{median}_i(\varepsilon_i)| / (\text{median}_i(|\varepsilon_i - \text{median}_k(\varepsilon_k)|)) > 5.2$ (Huber 1977).

for each location and year represented composites of six cores, 2 cm in diameter, and drilled to a depth of 10 cm. The cores were taken about 1.5 m apart. In 1983–1985, the depth was reduced to 5 cm. In 1986, the number of cores was increased to 10, and the 10-cm depth was resumed with reporting of concentrations for layers 0–5 cm and 5–10 cm. An additional complication was introduced in 1986 when samples were sent to a different laboratory from the one that had performed the analysis in previous years. The annual monitoring report for 1986 cited this change as a possible explanation for increases in the levels of uranium from the 1986 values. In performing the regressions for λ_{insol}, we used the data through 1985. We have had to make some adjustments, which are indicated in the footnotes of Table C-3.

The remainder of the information in Table C-2 is based on the direct analysis of the FMPC airborne source term that was reconstructed in Task 2, though the quantities shown in the

table do not depend on the absolute magnitude of the airborne uranium release from the plant. The fraction q of the release that is soluble is based on ratios of release magnitudes for different chemical forms of uranium. It is likely that these ratios would vary relatively little even if the estimate of the total magnitude of the release changed. The parameter q is interpreted as an average over the 38 years of plant operation. The uncertainty range for q is a judgment based on the experience of the source-term reconstruction given in the Task 2/3 report.

The mass-balance model also requires that some assumption be made about the annual deposition as a function of time, which we estimate by using the corresponding annual fraction of the total airborne release given by the Task 2 reconstruction. Every attempt to quantify the FMPC airborne uranium source term has reached the conclusion that the release rate peaked sharply in the middle 1950s, and all release curves are similar in their general shape. Deterministic calculations using annual release fractions based on the source terms of Clark et al. (1989) show a reduction of more than 20% in the release predicted by the normalized deposition curve based on the Task 2 source term. The difference results from the respective estimates of relative magnitudes of releases during different periods of plant operation, primarily differences between the period of the 1950s through the early 1960s (when releases were highest) and the period consisting of all subsequent years. The back calculation is sensitive to the relative magnitude of the early releases, because of the deterministic nature of the mass balance model. Thus, to this extent the back calculation is tied quantitatively to the Task 2/3 source term reconstruction.

Despite the obvious scatter in the data in Table C-3, they do contain trend information for the period 1971–1988, and we have used that information as a basis for estimating the removal coefficient λ_{insol} for insoluble uranium. We discount data from boundary station 7 because of the brevity of the record at that location.

To dispose of possible doubts that the data show a trend, we performed a linear regression on the log-transformed concentrations for boundary stations 1–6 and performed a test of hypothesis for a negative slope on the semilogarithmic plot. This amounts to a regression of the form

$$\ln y \approx A + Bt, \tag{C-1}$$

where $t = 1971, 1972, \ldots, 1988$, and A and B are parameters to be estimated. We are interested in (1) estimating the slope B and (2) testing the null hypothesis H_0: $B \geq 0$ (i.e., the curve is either flat or has an uptrend). This is a standard one-sided test with the t-distribution and a statistic computed from the regression (Snedecor and Cochran 1967). The results are as follows:

(1) For all boundary stations 1–6, the regression estimate of slope B is negative.

(2) For all boundary stations except 4, the null hypothesis H_0 is rejected at the 5% level.

Thus, it would be difficult to sustain an argument that these data contain no trend information, unless one could present evidence of some systematic effect that would introduce an artificial trend. We know of no such evidence. If one assumes a global null hypothesis of no downtrend for boundary stations 1–6, the probability of the outcome we obtained is about 2 in one million.

The linear regressions described above were not intended to provide the desired estimates of the removal parameter λ_{insol}. For such estimates, we have performed nonlinear regressions, using the mass balance model with the data from Table C-3 (1971 through 1985).

MATHEMATICAL DETAILS

This section provides details and additional information about the calculations described in the previous sections.

The Dynamic Mass-Balance Model and Nonlinear Regression

The dynamic mass-balance model of excess uranium in a soil compartment is essentially the soil model described in Appendix B of this Task 6 report, except that the deposition curve is always a constant multiple of the annual deposition fractions shown in Table C-2. Also, this model does not calculate radioactive decay products. The excess inventory f (kg) predicted by the model at time t is

$$f(t, \lambda_{sol}, \lambda_{insol}, \mathcal{M}) = \mathcal{M} \sum_{j=1}^{N} \left[q g_j(t, \lambda_{sol}) + (1 - q) g_j(t, \lambda_{insol}) \right] \tag{C-2}$$

where

$$\begin{aligned} g_j(t, \lambda) &= 0 \quad \text{if } t < \tau_j \\ &= (p_j/\lambda)\left(1 - \exp(-\lambda(t - \tau_j))\right) \quad \text{if } \tau_j \le t < \tau_{j+1} \\ &= (p_j/\lambda)\left(1 - \exp(-\lambda(\tau_{j+1} - \tau_j))\right) \exp(-\lambda(t - \tau_{j+1})) \quad \text{if } \tau_{j+1} \le t \end{aligned} \tag{C-3}$$

and

$\mathcal{M}$ = total magnitude of the deposition over all years of plant operation (kg)

N = the number of years of plant operation (38)

τ_j = 1951, 1952, ..., 1989 for $j = 1, 2, \ldots, N + 1$

q = fraction of the deposited uranium that is soluble

p_j = annual fraction of deposition for year τ_j ($\sum_{j=1}^{N} p_j = 1$).

The cumulative deposition through year τ_i is $\mathcal{M} \sum_{j=1}^{i} p_j$.

In the beginning the total deposition $\mathcal{M}$ that we want to estimate is unknown. If we are given an estimate Y_j (kg) of the excess uranium at the beginning of year τ_j, the corresponding value of $\mathcal{M}$ is

$$\mathcal{M} = Y_j / f(\tau_j, \lambda_{sol}, \lambda_{insol}, 1) \tag{C-4}$$

and from this value of $\mathcal{M}$ we can now estimate the inventory and the cumulative deposition for any year from the formulas of Equations C-2 and C-3 just discussed. One must be aware that if the given level of uranium in the soil includes background $\mathcal{B}$ (in the same units as Y_j), then in Equation C-4, the quantity Y_j must be replaced by $Y_j - \mathcal{B}$ (or 0 if $Y_j < \mathcal{B}$). The word "excess" that we used in defining Y_j for Equation C-4 implied that we were considering only the component of uranium above background.

This model can have various interpretations. It can be applied to estimate deposition per unit area if $\mathcal{M}$ has units such as mg m^{-2}. Or, as illustrated above, with $\mathcal{M}$ in kg, it can represent the total deposition over a large area. The latter interpretation is the one we are mostly concerned with in this appendix, but the former interpretation is appropriate to the nonlinear regression, which we summarize next.

Table C-4. Estimates of Removal and Deposition for Six Boundary Stations

Station	λ_{insol} (year^{-1})				$\mathcal{M}$ (mg cm^{-2})
	5%	50%	95%	Nominal	
BS1	0.083	0.142	0.221	0.141	1.54
BS2	0.022	0.050	0.079	0.050	0.57
BS3	0.013	0.041	0.078	0.043	2.89
BS4	0	0.028	0.107	0.031	0.13
BS5	0.032	0.073	0.139	0.076	0.52
BS6	0.043	0.074	0.115	0.073	0.59
Average[a]	0.054	0.070	0.089	0.069	—

[a] Values in the Percentile columns correspond to the distribution of the sample average $\bar{\lambda} = \sum_{i=1}^{6}(\lambda_{insol})_i$. The boundary stations were assumed stochastically independent. The value in the nominal column is the average of the column entries.

For each of the boundary stations 1–6, we solve the nonlinear least squares problem

$$\sum_{j=0}^{N} \left[Y_j - \left(k \cdot f(\tau_j, \lambda_{sol}, \lambda_{insol}, \mathcal{M}) + \mathcal{B}\right)\right]^2 = \text{minimum} \qquad \text{(C-5)}$$

for the parameters λ_{insol} and $\mathcal{M}$, where $\mathcal{B}$ denotes natural uranium in soil (pCi g^{-1}). The parameter k, which depends on soil bulk density and natural uranium specific activity, converts the excess inventory (expressed as mg m^{-2}) to pCi of natural uranium g^{-1}. The regression is repeated a large number of times in a bootstrap procedure (Efron 1982), with Monte Carlo sampling from the residuals with replacement, to generate a distribution of λ_{sol}. For each Monte Carlo iteration, each of the parameters λ_{insol} and q is sampled from its distribution. Table C-4 gives percentiles of λ_{insol} and nominal (deterministic) values of λ_{insol} and local deposition $\mathcal{M}$.

Deposition Based on the 1986 Excess Inventory

As we noted earlier, a regression procedure is applied to a subset of the SOIL13 data to estimate a trend of total uranium concentration (pCi g^{-1}) vs. distance from the center of the FMPC production area. We used the data measured at distances in the range 900–3,000 m; data taken at greater distances were near or below background (2.2 pCi g^{-1}). It was necessary to make adjustments to values that fell below 2.7 pCi g^{-1} because of the difficulties in the laboratory analyses that we mentioned earlier. We estimated an approximate adjustment from Figure 3 of Stevenson and Hardy (1993): $x' = 1.53x^{0.574}$, where x is the raw measurement and x' is the adjusted value. The plotted points in Figure C-4 include the adjustment.

We represent the trend suggested by the subset of the SOIL13 data by the power curve

$$y = ax^b \qquad \text{(C-6)}$$

where y is the soil concentration of total uranium (pCi g^{-1}) and x is the distance from the center of the FMPC production area (m). The nominal values of the parameters a and b are

determined by applying a linear least-squares algorithm to the transformed equation

$$\ln y = \ln a + b \ln x . \tag{C-7}$$

We have also applied a bootstrap procedure to estimate a joint distribution of the parameters a and b corresponding to the variability expressed by the residuals of the regression (Efron 1982). The distribution of the coefficients is needed for the uncertainty analysis.

The trend function determined by the parameters a and b enables us to estimate the total excess uranium in the soil in the annular region between two radial distances x_1 and x_2. The formula is

$$\text{Excess U} = C \int_{x_1}^{x_2} 2\pi x(ax^b - \mathcal{B})\,dx \qquad \text{(kg)} \tag{C-8}$$

where $C = 7.46 \times 10^{-5}$ kg m^{-2} per pCi g^{-1} and $\mathcal{B} = 2.2$ pCi g^{-1} (natural background). The power curve reaches the background level at the distance

$$x_2 = (\mathcal{B}/a)^{1/b} . \tag{C-9}$$

When the mass-balance model has been used to estimate the earlier maximum inventory I_{max} for the small region, we use I_{max} and the value of x_2 from Equation C-9 to calculate a new coefficient a' of the power curve corresponding to the maximum inventory:

$$a' = \frac{(I_{max}/(2\pi C) + \mathcal{B}(x_2^2 - x_1^2)/2)(b+2)}{x_2^{b+2} - x_1^{b+2}} . \tag{C-10}$$

Using the expression $a'x^b$ in Equation C-8 would give the maximum (1964) excess uranium for the small region; this amounts to displacing the original power curve upward parallel to itself (step 3; also see Figure C-4). Now we recalculate the upper limit of integration x_2 from Equation C-9 by using a' in place of a. Using the larger of the values x_2 and the coefficient a' in the upper integration limit in Equation C-8, we obtain the maximum (1964) inventory of the large region (step 5). Finally, using the maximum inventory of the large region for the year 1964 in the mass-balance model (Equations C-2 and C-3), we determine the inventory and cumulative deposition for all years, and the most recent cumulative deposition value is the total deposition estimate that we are seeking (step 6).

UNCERTAINTY ANALYSIS

Possible parametric sources of uncertainty in the calculation outlined in the overview section are

1. The 1986 estimate of the uranium soil inventory near the FMPC
2. The removal-rate coefficients λ_{sol} and λ_{insol}
3. The fraction q of deposited uranium that was in soluble form
4. The normalized deposition curve (percentages in Table C-2)
5. The coefficients of the power curve used to extrapolate the concentration trend with distances from the FMPC (Figure C-4).

We have not included an uncertainty term for the annual deposition fractions (item 4) explicitly in the Monte Carlo calculations. We pointed out in a previous section that the back calculation is sensitive to the fraction of the total release that is assumed to be released in the early years. Calculations using a normalized curve based on the estimates of Clark et al. (1989) in place of the normalized Task 2 curve yielded a reduction of more than 20% in the 50th percentile estimates. Although this is not a dependence on the absolute magnitude of the release as such, it does introduce the ratio of early to recent magnitudes as an implicit parameter. We believe the Task 2 work argues persuasively that the normalized Task 2 curve should be preferred, but the dependence on this ratio of magnitudes needs to be kept in mind.

For the 1986 value of the excess uranium inventory (item 1), the uncertainty estimate is based on the range given by Stevenson and Hardy (1993). This range, scaled to a 10-cm depth, is 4,260–12,300 kg. We have used these values as the limits of a triangular distribution with mode at the midrange.

The uncertainty distribution of the removal-rate coefficient λ_{insol} (year^{-1}) is derived from the nonlinear parameter estimation (regression) procedure that we carried out for the data from each of the FMPC boundary stations BS1 through BS6 (the data from BS7 were too brief to be used in this way). The result for each boundary station is an estimate of the distribution of the soil removal coefficient λ_{insol}. The six distributions are sampled independently, and the distribution of the arithmetic average of the six random variables so generated is used to represent the regional soil. The result is the median value 0.070 year^{-1} (50th percentile of the distribution of the average) and the range 0.054–0.089 year^{-1} (5th–95th percentile) shown in Table C-2.

A joint uncertainty distribution for the coefficients a and b of the power curve is based on a bootstrap procedure applied to the residuals of the linear equation for the transformed data (Equation C-6).

Once the uncertain parameters are represented by appropriate sampling distributions, the analysis is carried out by Monte-Carlo repetitions of the calculation outlined for the nominal case, but with each affected parameter replaced at each trial by a value sampled from the corresponding distribution. A resultant distribution of inventory, cumulative deposition, and estimated airborne release is accumulated for each year. We used 100 trials, which gave adequate definition in the tails. Figure C-6 gives the parametric uncertainty distribution of the back calculated cumulative airborne release at the end of 1988, contrasted with the airborne release range estimated for the Task 2/3 report (Voillequé et al. 1995). Deposition estimates were converted to release estimates by dividing by the estimated fractional deposition (0.35 in the deterministic case), which is the proportion of the simulated release that the power function model of Equation C-8 predicts in the annular region between 1,250 m and the outer boundary of the large region (the total release is estimated by evaluating the integral of Equation C-8 between zero and the radius of the outer boundary).

Figures C-7 and C-8 show the distribution through time of the inventory and the cumulative deposition, respectively.

It can be argued that substituting the trend of a normalized airborne release curve for annual fractional deposition ignores factors that might interfere with the correspondence. For example, the tendency of large particles to deposit nearer the point of release than smaller particles introduces a spatial distortion. In years when the scrubbers operated, the very large

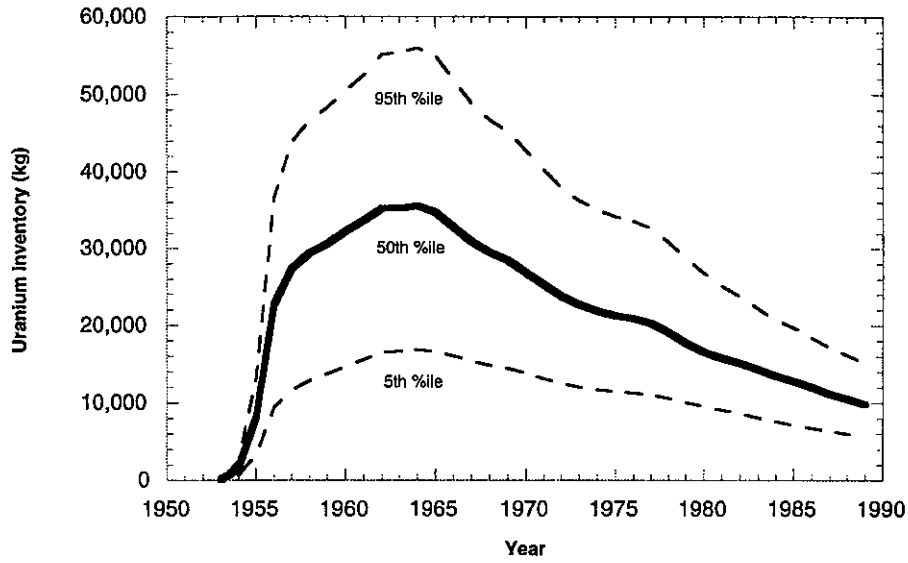

Figure C-7. Annual uncertainty distribution for the uranium inventory calculated for the annular region which would have extended from 1,150 to 5,290 m from the center of the site in 1964. The region would have shrunk to 1,150–2,700 m in 1986. This region does not include the area within the FMPC site boundary.

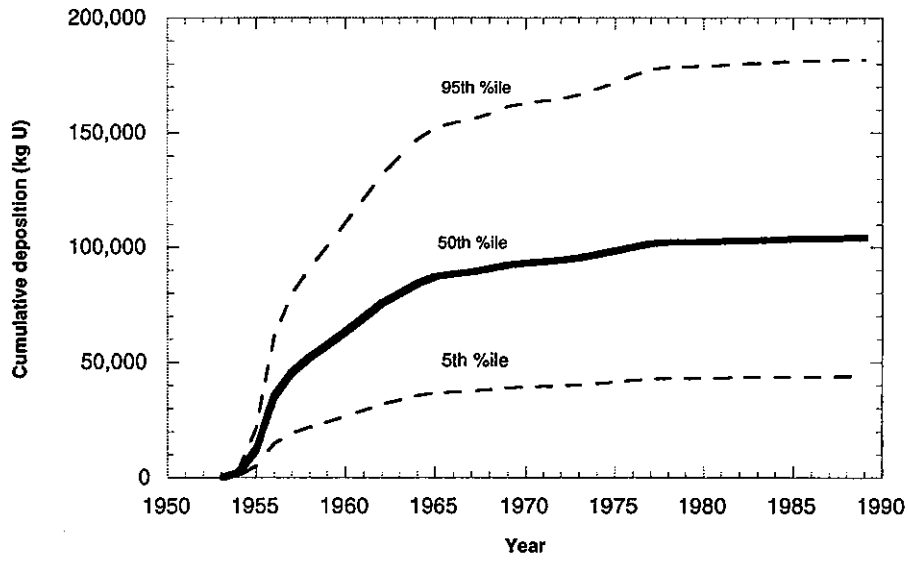

Figure C-8. Annual uncertainty distribution for the cumulative deposition of uranium on the soil in the vicinity of the FMPC. The annular region would have extended from 1,150 to 5,290 m from the center of the site in 1964 and would have shrunk to 1,150–2,700 m in 1986. This region does not include the area within the FMPC site boundary.

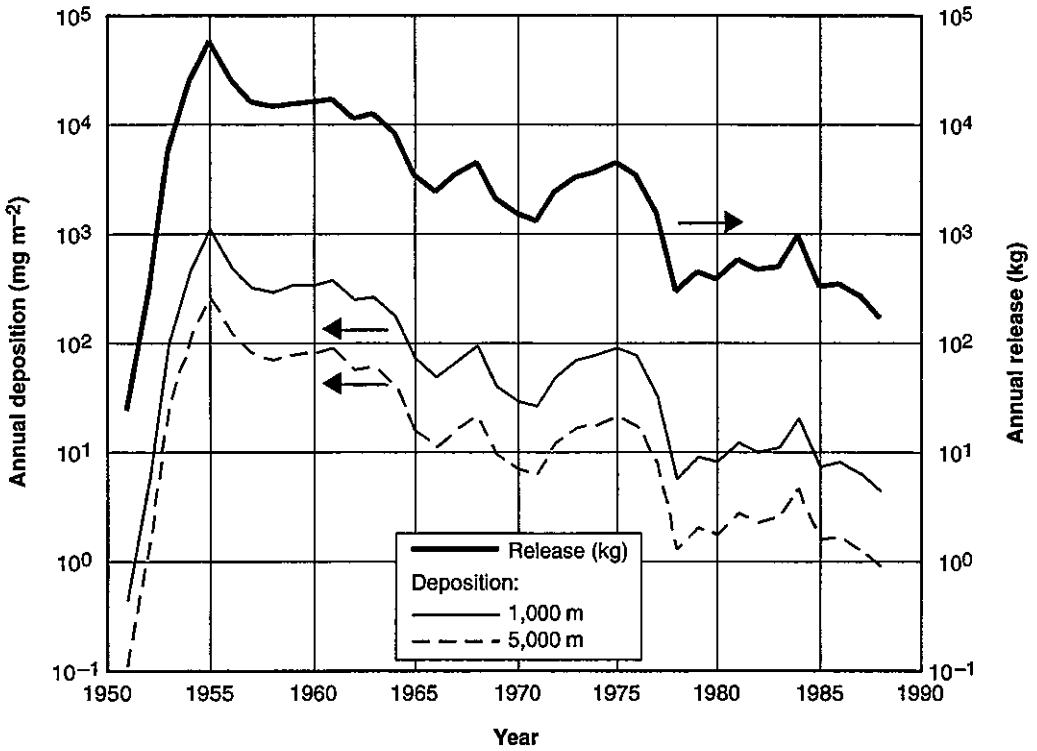

Figure C-9. Uranium annual airborne release from the FMPC and annual deposition at locations 1,000 and 5,000 m northeast of the center of the site. The deposition curves are based on simulations with the air transport and deposition models used for calculations in this Task 6 report (Appendix M). The nearly identical shapes of the curves indicate very strong correlation and support the use of the normalized release curve for deposition in the back calculation.

particles that resulted from reentrainment would accentuate the spatial distortion, and the fact that the scrubbers did not operate during some years of the period under study produces a temporal distortion as well. However, in our atmospheric modeling approach, the release and deposition curves are highly correlated. Figure C-9 shows the annual releases on the same semilogarithmic plot with annual deposition curves for locations 1,000 and 5,000 m northeast of the center of the site. The curves are virtually copies of each other, except for vertical displacement.

CONCLUSIONS

This appendix describes a calculation that makes use of a recent estimate of excess total uranium inventory in the top 5 cm of soil near the FMPC (Stevenson and Hardy 1993), a dynamic mass-balance model of uranium in soil, and other parametric information to estimate total deposition of uranium on the soil in the vicinity of the facility throughout the 38 years of its operation. The principal result is the median estimate of the cumulative airborne release of uranium (284,000 kg), together with the 5th- and 95th-percentile uncertainty bounds shown in Figure C-6. Figures C-7 and C-8 give a sense of how this distribution evolves over the time of the FMPC's operations.

We note that the median estimate of cumulative release is 34 times the depth-adjusted midrange (8,280 kg) of the 1986 inventory estimate of Stevenson and Hardy (1993). When the factors that we have discussed are taken into account, a difference of this magnitude in the two quantities should not be surprising. Even so, questions have arisen that implied a belief that most of the deposited uranium incorporated into the surface soil should have remained there in 1986. This conclusion is highly unlikely, as both our work and the surveys from the 1950s reported by Weinstein (1958) indicate.

One purpose of this investigation is to provide corroboration (or contradiction) for the nearly-independent estimate of airborne releases of uranium from the FMPC reported in the Task 2/3 report (Voillequé et al. 1995). After examining Figure C-6, a casual reader might interpret the 26,000-kg discrepancy between the 50th percentiles of the two estimates to be a repudiation of the Task 2/3 estimate, but such a conclusion is unwarranted. The back calculation described in this appendix depends critically on estimates of the removal parameter λ_{insol} from data that statistically imply a downtrend but that offer less potential for quantifying the trend with precision. An uncertainty band of a factor of more than five is the result. We must also recognize that some of the assumptions are crude, such as the circular symmetry and the related use of a power function to represent the concentration of uranium in soil as a function of distance from the site. It is also possible that the use of first-order kinetics to model relatively insoluble uranium in the 0–10-cm soil layer may have a distorting effect. Other approaches can give different results, but their application here would be more difficult to explain and defend.

We close this discussion with a reminder of several major points:

1. The 1986 inventory of uranium estimated by Stevenson and Hardy (1993) is not an estimate of the total amount of uranium from FMPC releases that was deposited offsite in the vicinity of the facility. Estimates of the latter quantity inevitably depend on the application of models to the data supporting the inventory calculation, as well as to data related to the removal of excess uranium from surface soil by weathering processes.

2. The deterministic estimate of cumulative deposition reported in this appendix (97,000 kg) applies only to the region from the site boundary out to a distance of about 5,290 m from the center of the production area. The power function model that represents excess uranium in the soil indicates that this region accounts for about 35% of what was released. Thus, the estimated release is 277,000 kg of uranium.

3. The simple foundations of the calculation reported in this appendix should not be allowed to obscure the fact that the estimates it produces are uncertain. The 5th and 95th percentiles of the distribution of cumulative release span a factor of more than five. This range includes the 5th- to 95th-percentile uncertainty range of the Task 2 reconstruction of the airborne uranium source term (Figure C-6). This level of consistency seems adequate for a confirmatory result.

REFERENCES

Clark T.R., L. Elikan, C.A. Hill, and B.L. Speicher. 1989. *History of FMPC Radionuclide Discharges — Revised Estimates of Uranium and Thorium Air Emissions from 1951–1987.* Report Addendum to FMPC-2082 Special, Westinghouse Materials Company of Ohio, Cincinnati, Ohio.

Efron B. 1982. *The Jackknife, the Bootstrap and Other Resampling Plans.* CBMS 38. Society for Industrial and Applied Mathematics, Philadelphia, Pennsylvania.

Huber P.J. 1977. *Robust Statistical Procedures.* CBMS 27. Society for Industrial and Applied Mathematics, Philadelphia, Pennsylvania.

Killough G.G., M.J. Case, K.R. Meyer, R.E. Moore, J.F. Rogers, S.K. Rope, D.W. Schmidt, B. Shleien, J.E. Till, and P.G. Voillequé. 1993. *The Fernald Dosimetry Reconstruction Project, Task 4: Environmental Pathways — Models and Validation.* Draft Report CDC-3, Radiological Assessments Corporation, Neeses, South Carolina.

Schull W.J. (chairman), Benjamin S.A., Bouville A., Eichholz G.G., Kheifets L.I., Martin J.E., Nelson C.B., Royal H.D., Shore R.E., Thomas R.G., Wagner H.N., Jr., and Wall J.M. 1994. *Dose Reconstruction for the Fernald Nuclear Facility — A Review of Task 4.* Committee on an an Assessment of CDC Radiation Studies, Board on Radiation Effects Research, Commission on Life Sciences, National Research Council. National Academy Press, Washington, D.C.

Snedecor G.W. and W.G. Cochran. 1967. *Statistical Methods.* Sixth Edition. Iowa State University Press, Ames, Iowa.

Stevenson K.A. and E.P. Hardy. 1993. "Estimate of Excess Uranium in Surface Soil Surrounding the Feed Materials Production Center Using a Requalified Data Base." *Health Phys.* **65**(3): 283–287.

Voillequé P.G., K.R. Meyer, D.W. Schmidt, S.K. Rope, G.G. Killough, M. Case, R.E. Moore, B. Shleien, and J.E. Till. 1995. *The Fernald Dosimetry Reconstruction Project, Tasks 2 and 3: Radionuclide Source Terms and Uncertainties.* Report CDC-5, Radiological Assessments Corporation, Neeses, South Carolina.

Weinstein M.S. 1958. "Environmental Contamination." In *Symposium on Occupational Health Experience and Practices in the Uranium Industry.* Report HASL-58, U.S. Atomic Energy Commission, Health and Safety Laboratory, New York, New York.

APPENDIX D

VARIATION IN CONCENTRATION OF AIRBORNE PARTICULATES OVER TIME

INTRODUCTION

Appendix D documents a refinement of the method used to evaluate resuspension of particulates (defined below), which was developed and described in Killough et al. (1993), Appendix O. This refinement investigates how concentrations of airborne particulates have varied over time. This appendix develops and tabulates the parameter values used in the dose calculations presented in this report.

During the time period of interest for the dose reconstruction project, the resuspension pathway was a relatively minor contributor to exposure of the public from airborne releases of uranium from the Feed Materials Production Center (FMPC). We estimate that direct inhalation of airborne uranium was 100 times more important than inhalation of resuspended material (see Appendix K). In addition, dose to the public from past releases of radon is much more important than dose from releases of uranium. For these reasons, investigation of three additional modifying factors in the resuspension equation described in Killough et al. (1993) has not been pursued further.

Airborne releases of uranium from the FMPC were eventually deposited on the ground surface through gravitational settling and wet and dry deposition processes. One subsequent transport process for this deposited material was resuspension, which refers to the reentry of previously deposited particles into the air. There are a number of approaches to estimating the magnitude of resuspension. Healy (1980) groups the approaches into three basic types: (1) resuspension factor approach, (2) resuspension rate approach, and (3) mass loading approach. We chose the mass loading approach to reconstruct the exposure of the public to resuspended uranium from the ground surrounding the FMPC.

The mass loading concept is attractive for this purpose because of its empirical nature and its lack of dependence on detailed knowledge of soil characteristics and the resuspension process, which have not been extensively studied in this area. Two parameters, the mass loading of dust in surface air (ML, in grams of soil per cubic meter of air) and the concentration of the contaminant in the surface layer of soil (C_s, in curies per gram of soil), are needed to provide an estimate of the air concentration of the contaminant (C_a, in curies per cubic meter of air), which is due to resuspension. That is,

$$C_a = C_s \times ML \quad . \tag{D-1}$$

For the FMPC dose reconstruction, the environmental transport model provided estimates of the uranium concentrations in surface soil (C_s) over time. The model was constructed so that a shallow layer of soil, 0.5 cm (0.2 in.), was the compartment from which resuspension could occur. Airborne uranium from FMPC releases was deposited into this compartment annually and removed to deeper soil layers by weathering (see Appendix B). The other variable in equation D-1, mass loading in air (ML), is discussed in this appendix. Another term that is used synonymously with mass loading is *dust loading*.

ESTIMATING DUST LOADING

To characterize the variations in dust loading around the Fernald facility, we examined weekly measurements for 3 years (1989–1991), which were available in electronic spreadsheet format from Westinghouse Environmental Management Company of Ohio (Byrne 1992). These spreadsheets contained a copy of the Radiological Environmental Monitoring group's raw data files. The particulates were collected by 8 × 10-in. Whatman EPM-2000 glass fiber filters in high-volume air samplers, which were located within 6 km (4 mi) of the production area center (Figure D-1). The distant air monitoring stations in Cincinnati were excluded from our analysis, because they are influenced by urban sources of particulates (urban areas typically have higher concentrations) and would not represent resuspension within the area of greatest uranium deposition. The analytical and sample collection procedures for airborne particulate matter are described in Grant (1992) and Kraps (1991), respectively.

For each location and week during 1989–1991, we computed the micrograms of particulate per cubic meter ($\mu g\ m^{-3}$) of air from the measured total suspended particulate per sample and the volume of air sampled. Data for all locations were pooled into a monthly average and standard deviation. Originally, a monthly time scale was chosen to be consistent with that being used for initial validation work (Killough et al. 1993). Tables O-1, O-2, and O-3 of Killough et al. (1993) presented the monthly averages and standard deviations for 1991, 1990, and 1989, respectively. Table O-4 from Killough et al. (1993), reprinted here as Table D-1, presents the 3-year average and uncertainty.

Table D-1. Summary of Total Suspended Particulates in Air ($\mu g\ m^{-3}$) Surrounding the FMPC by Month, 1989–1991

Month	1989	1990	1991	3–year average	Standard error
January	27.7	25.6	25.4	26.2	0.7
February	30.0	21.3	26.8	26.0	2.5
March	43.5	26.5	23.6	31.2	6.2
April	27.5	23.0	25.0	25.2	1.3
May	35.0	32.9	43.6	37.2	3.3
June	46.4	34.6	50.8	43.9	4.8
July	41.5	38.8	44.8	41.7	1.7
August	43.5	41.4	41.1	42.0	0.8
September	32.0	33.5	45.4	37.0	4.2
October	34.0	27.6	37.0	32.9	2.8
November	25.4	31.1	33.2	29.9	2.3
December	39.3	22.2	22.9	28.1	5.6
All	35.4	30.0	35.1	33.5	1.8

The data for these 3 years show a factor of 2 variation between the minimum monthly average dust loading and the maximum monthly average. The annual averages are quite consistent and in good agreement with the 1966 National Air Surveillance Network, which

showed a mean for all nonurban locations of 38 μg m^{-3} (Healy 1980). The average for urban stations ranged from 33 to 254 μg m^{-3}. In the final validations and dose calculations in this project, a time resolution of 1 year is used. Therefore, annual averages of dust loading measurements were obtained or were estimated for other years.

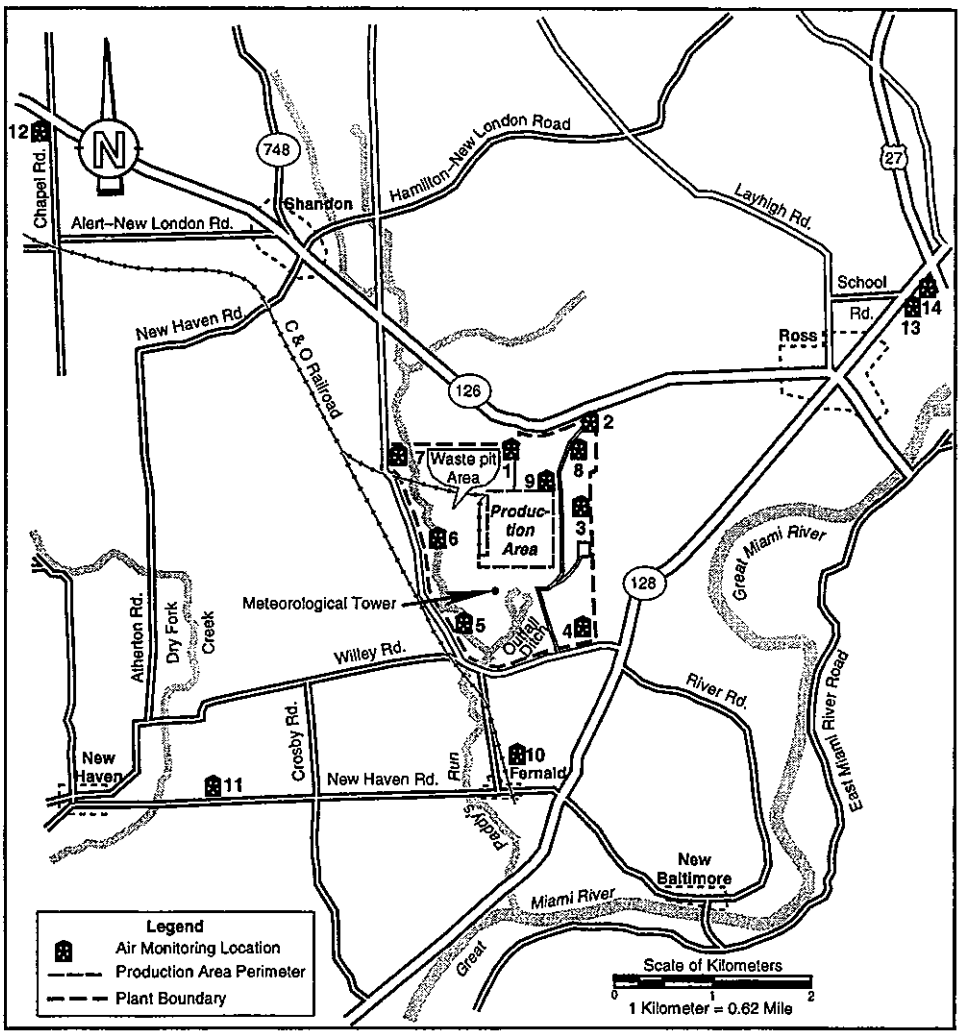

Figure D-1. Locations of high-volume air samplers.

The reporting of particulate concentrations in ambient air around the FMPC began in 1971, when the air monitoring was still conducted at the perimeter stations at the corners of the production area. In 1972, the stations were moved to the boundary, where shed-roof air samplers were used, and which remained substantially unchanged throughout the succeeding years. In 1986, the designation of the air monitoring stations changed from "BS-#" to "AMS–#," and some additional locations were added.

The available data for particulates in air around Fernald were compiled from 1971 through 1988 from the annual environmental reports from the FMPC contractor. This was necessary to apply the methodology developed in Killough et al. (1993) to the entire time

period of interest for the dose reconstruction. The average measurements at each station and the all-station average for each year are included in Table D-3 at the end of this appendix. The minima and maxima for each station are also reported in the monitoring reports, but they are not shown in Table D-3. A 95% confidence limit on the station averages was stated as ±5% between 1971 and 1983. A geometric standard deviation, which ranged from 0.6 to 1.1, was given for 1985 and 1986. No uncertainty was reported in 1987 and 1988. The standard error of our annual mean of all stations is also given in Table D-3. The variation among stations in any given year is small.

A somewhat unexpected observation was that the dust loading showed a rather definite upward trend as one goes back in time (Figure D-2). Thus, for years before 1971, we were faced with the need to decide how to project back another 15 years. There was a possibility that the dust loading trend did not truly represent reality but was a sampling and/or analysis artifact. However, that conclusion could not be supported based on the descriptions of the air samplers. Thus, we were left with the distinct possibility that dust loading had decreased during the years, perhaps because of a smaller contribution from agricultural and industrial sources (including the FMPC).

Figure D-2 shows an approximately linear projection into the previous two decades that does not extend into implausible ranges. As stated previously, Healy (1980) reports annual average particulate concentrations in air at urban stations around the U.S. in 1966 ranging from 33–254 $\mu g\ m^{-3}$ and nonurban stations ranging from 9–79 $\mu g\ m^{-3}$ (mean = 38 $\mu g\ m^{-3}$).

For the dose reconstruction project, we used the values in Table D-2 for assessing the magnitude of the resuspension pathway for the general population. Real measurement data were used when available (1971 and later), and the observed temporal trend was extended to obtain estimates for earlier years (Figure D-2). The annual average for 1984 was not included in the annual environmental report, so there is no data point for that year. Therefore, we used a value that fell along the general observed trend (Table D-2) for that year.

Table D-2. Dust Loading Values Used in Dose Calculations for Exposure of the Public from Resuspension of Previously Deposited Uranium

Year	Dust loading ($\mu g\ m^{-3}$)	Year	Dust loading ($\mu g\ m^{-3}$)
1951–1959	80	1979	43
1960–1970	60	1980	39
1971	55	1981	44
1972	59	1982	43
1973	53	1983	39
1974	53	1984	40
1975	53	1985	35
1976	51	1986	35
1977	48	1987	36
1978	50	1988	39

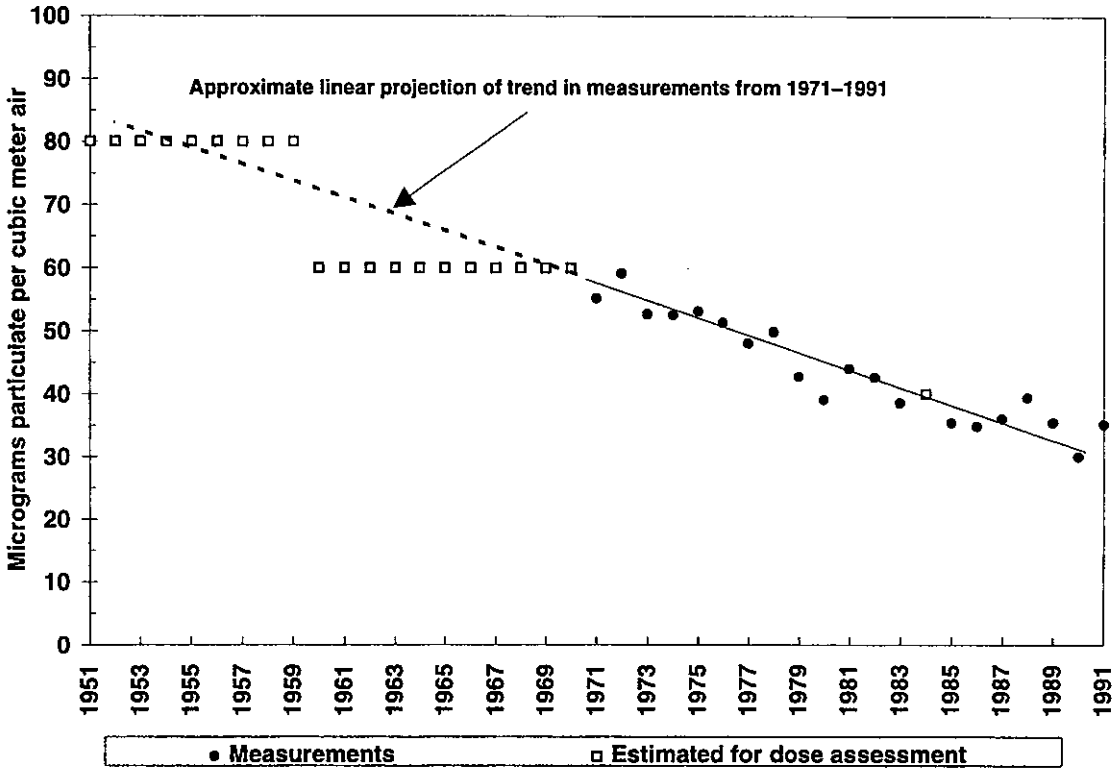

Figure D-2. Back-projection of dust loading in air around the FMPC. Solid dots represent annual average measurements for all air monitoring stations around the FMPC. The dotted line indicates an approximately linear projection before 1971 when these data began to be reported. Open squares indicate estimated values that were used in the dose assessment calculations (Table D-2).

The scope of this appendix has been the reconstruction of exposures of the public to releases of uranium particulates from the FMPC. In their review of a previous draft of this report, the National Research Council (NRC) Committee on Assessment of CDC Radiation Studies suggested that radon daughter products would be removed from the airborne plume by attachment to dust particles, which would have been abundant near the site due to plant operations and construction. An analysis of this effect was conducted and the impact on individual doses to nearby residents was found to be minor (see Appendix I).

REFERENCES

Byrne J.M. 1992. "1991 Particulate Data." Letter and disk transmission to S. K. Rope, dated July 24, 1992. Westinghouse Environmental Management Company of Ohio, Cincinnati, Ohio.

Grant D.L. circa 1992. "Determination of Airborne Particulates." Procedure ESH-P-30-068. Westinghouse Environmental Management Company of Ohio, Cincinnati, Ohio.

Healy J.W. 1980. "Review of Resuspension Models." In: *Transuranic Elements in the Environment*, pp. 209-235, W. C. Hanson, ed. DOE/TIC-22800. National Technical Information Service, Springfield, Virginia.

Killough G.G., M.J. Case, K.R. Meyer, R.E. Moore, J.F. Rogers, S.K. Rope, D.W. Schmidt, B. Shleien, J.E. Till, and P.G. Voillequé. 1993. *The Fernald Dosimetry Reconstruction Project. Task 4. Environmental Pathways — Models and Validation.* RAC Report CDC-3. Radiological Assessments Corporation, Neeses, South Carolina.

Kraps P. 1991. "REMP Air Monitoring." Environmental Monitoring Section Procedure No. EM–RM–001. Westinghouse Materials Company of Ohio, Cincinnati, Ohio.

Table D-3. Annual Average Concentration of Particulates in Air ($\mu g\ m^{-3}$) Around the FMPC, 1971–1988

	Location								
Year	SW	NW	NE	SE	STP	E		All-station average	Std. error
1971	46	57	64	55	55	54		55	2
	BS–1	BS–2	BS–3	BS–4	BS–5	BS–6	BS–7		
1972	58	56	50	65	62	64		59	2
1973	48	52	52	58	54	52		53	1
1974	52	53	46	58	54	52		53	2
1975	48	55	52	53	60	51		53	2
1976	48	49	48	59	51	53		51	2
1977	46	45	47	53	49	48		48	1
1978	47	52	47	52	48	53		50	1
1979	48	42	34	47	42	43		43	2
1980	38	42	31	48	37	38		39	2
1981	40	44	37	49	56	43	39	44	2
1982	42	38	44	45	46	43	40	43	1
1983	36	37	38	42	37	41	39	39	1
1984	Data not reported in annual report.								
1985	31	32	35	40	37	37	36	35	1

	Year		
Location	1986	1987	1988
AMS–1	33	29	32
AMS–2	34	32	38
AMS–3	37	32	36
AMS–4	39	35	39
AMS–5	32	31	37
AMS–6	36	34	37
AMS–7	32	35	37
AMS–8	34	35	40
AMS–9	37	38	41
AMS–10		47	51
AMS–11		42	41
AMS–12		35	38
AMS–13		45	49
AMS–14			37
All-station average	35	36	39
Standard error	1	2	1

APPENDIX E

RADIONUCLIDE CONCENTRATIONS FOR WATER PATHWAYS

This appendix presents tables of concentrations of radionuclides in the Great Miami River (Table E-1) and Paddy's Run Creek (Table E-2) that are used as inputs to the dose calculations. These radionuclides were released during operations at the Fernald Feed Materials Production Center (FMPC) during the years 1951–1988. The methods used in reconstructing releases of the radionuclides have been described in detail previously (Voillequé et al. 1995).

Uranium was the primary material processed at the FMPC, with some thorium processing occurring at various times. Most of the feed material had previously been separated chemically from the naturally occurring decay products. Consequently, effluents from the facility consisted primarily of uranium and, when it was being processed, thorium. The isotopes of radium, ^{228}Ra and ^{224}Ra, are decay products of ^{232}Th, and ^{226}Ra is a decay product of ^{238}U. Other radionuclides, like ^{239,240}Pu, were released during FMPC operations from the processing of recycled uranium, that is, uranium that was not completely separated from fission and activation products before it was returned to the FMPC as feed material. Recycled uranium was processed at the FMPC beginning in the fall of 1962 (Voillequé et al. 1995).

Early in the project, we found that the radium isotopes ^{228}Ra and ^{226}Ra were important potential contributors to offsite dose relative to the other radionuclides released to water (Voillequé et al. 1995). Uranium and thorium isotopes were important contributors also, but their contribution depended on the particular exposure pathway under consideration. Other radionuclides, like ^{99}Tc and ^{90}Sr, were relatively minor contributors to offsite dose, according to the methodology of the National Council on Radiation Protection and Measurements (NCRP 1995).

Because only certain radionuclides were measured in liquid effluents at the FMPC during various periods of operation, we used different approaches for calculating concentrations of the radionuclides listed in Tables E-1 (Great Miami River) and E-2 (Paddy's Run Creek). As shown in Table E-3, the concentrations of some radionuclides are based on actual measurements, while the concentrations of others are based on calculations with decay chain kinetics and assumptions indicated in the footnotes of Tables E-1 and E-2.

The concentrations of uranium, thorium, radium, and some fission and activation products were measured in liquid effluents discharged from the FMPC, but the extent of those measurements varied significantly. The concentrations of ^{226}Ra, ^{228}Ra, ^{232}Th, and ^{239,240}Pu are based on our release or source term estimates described previously (Appendix L, Voillequé et al. 1995).

Concentrations of the other radionuclides listed in the tabulations are based on decay chain dynamics (Appendix D, Voillequé et al. 1995). The radionuclides ^{234}Th, ^{234m}Pa, ^{234}Pa, and ^{230}Th are decay products of ^{238}U, while ^{228}Th, ^{228}Ac, and ^{224}Ra are decay products of ^{232}Th. The first product in the decay chain for ^{235}U is ^{231}Th.

For all radionuclides, we used a simple dilution model to calculate the radionuclide concentrations in the Great Miami River and Paddy's Run Creek, using site-specific liquid effluent and river flow rates, which had been measured routinely. This approach is outlined in Appendix R, Task 4 (Killough et al. 1993) and requires that we account for dilution and transport

of the material in the receiving body of water, i.e., either the Great Miami River or Paddy's Run Creek. The aquatic transport calculations assume that the radionuclide concentrations at the downstream receptor point of interest (Tables E-1 and E-2) are equal to the radionuclide concentrations at the discharge point divided by the dilution factor. These values can be found in our earlier reports. For example,

- The uranium concentration at the discharge point is determined from the estimated quantity of uranium released from the site to the Great Miami River (Table L-5, Voillequé et al. 1995) and to Paddy's Run Creek (Table L-8, Voillequé et al. 1995), and the annual flow rate of the effluent discharged to the river or stream (Table L1-36, Voillequé et al. 1996).
- The dilution factor is based on the river flow characteristics of the Great Miami River and Paddy's Run Creek, and FMPC discharge volumes for the site. An example of the dilution factor determination for the Great Miami River for 1960–1962 is shown in Table RS-1, Task 4 (Killough et al. 1993).

The radionuclide concentrations in Tables E-1 and E-2 are the basis for calculating radiation doses via surface water exposure pathways for all years of operation.

REFERENCES

Killough G.G., M.J. Case, K.R. Meyer, R.E. Moore, J.F. Rogers, S.K. Rope, D.W. Schmidt, B. Shleien, J.E. Till, and P.G. Voillequé. 1993. *The Fernald Dosimetry Reconstruction Project, Task 4: Environmental Pathways — Models and Validation.* Report CDC-3, Radiological Assessments Corporation, Neeses, South Carolina.

National Council on Radiation Protection and Measurements (NCRP). 1996. *Screening Models for Releases of Radionuclides to the Atmosphere, Surface Water, and Ground.* NCRP Report No. 123 (Vol. I and II), NCRP, Bethesda, Maryland.

Voillequé P.G., K.R. Meyer, D.W. Schmidt, S.K. Rope, G.G. Killough, M.J. Case, R.E. Moore, B. Shleien, and J.E. Till. 1995. *The Fernald Dosimetry Reconstruction Project, Tasks 2 and 3: Radionuclide Source Terms and Uncertainties.* Report CDC-5, Radiological Assessments Corporation, Neeses, South Carolina.

Table E-1. Radionuclide Concentrations in the Great Miami River (Bq L^{-1})[a]

Year	U-234	U-235	U-238	Th-228	Th-230	Th-231	Th-232	Th-234
1951	0	0	0	0	0	0	0	0
1952	5.60×10^{-2}	2.60×10^{-3}	5.33×10^{-2}	0	9.53×10^{-3}	2.60×10^{-3}	0	5.33×10^{-2}
1953	9.19×10^{-2}	4.30×10^{-3}	8.92×10^{-2}	0	1.56×10^{-2}	4.30×10^{-3}	0	8.92×10^{-2}
1954	8.60×10^{-2}	4.06×10^{-3}	8.41×10^{-2}	2.76×10^{-4}	1.46×10^{-2}	4.06×10^{-3}	1.45×10^{-2}	8.41×10^{-2}
1955	6.16×10^{-2}	2.92×10^{-3}	6.04×10^{-2}	1.97×10^{-4}	1.05×10^{-2}	2.92×10^{-3}	1.03×10^{-2}	6.04×10^{-2}
1956	7.93×10^{-2}	3.62×10^{-3}	7.52×10^{-2}	2.18×10^{-4}	1.35×10^{-2}	3.62×10^{-3}	1.15×10^{-2}	7.52×10^{-2}
1957	7.87×10^{-2}	3.64×10^{-3}	7.59×10^{-2}	2.18×10^{-4}	1.34×10^{-2}	3.64×10^{-3}	1.15×10^{-2}	7.59×10^{-2}
1958	4.49×10^{-2}	2.08×10^{-3}	4.36×10^{-2}	0	7.62×10^{-3}	2.08×10^{-3}	0	4.36×10^{-2}
1959	6.31×10^{-2}	2.95×10^{-3}	6.17×10^{-2}	0	1.07×10^{-2}	2.95×10^{-3}	0	6.17×10^{-2}
1960	2.19×10^{-1}	1.03×10^{-2}	2.13×10^{-1}	0	3.73×10^{-2}	1.03×10^{-2}	0	2.13×10^{-1}
1961	1.86×10^{-1}	8.62×10^{-3}	1.75×10^{-1}	0	3.16×10^{-2}	8.62×10^{-3}	0	1.75×10^{-1}
1962	1.55×10^{-1}	7.24×10^{-3}	1.50×10^{-1}	0	2.63×10^{-2}	7.24×10^{-3}	0	1.50×10^{-1}
1963	2.14×10^{-1}	9.83×10^{-3}	2.09×10^{-1}	0	3.64×10^{-2}	9.83×10^{-3}	0	2.09×10^{-1}
1964	2.22×10^{-1}	1.04×10^{-2}	2.11×10^{-1}	1.57×10^{-5}	3.78×10^{-2}	1.04×10^{-2}	8.24×10^{-4}	2.11×10^{-1}
1965	1.21×10^{-1}	5.62×10^{-3}	1.17×10^{-1}	7.34×10^{-6}	2.06×10^{-2}	5.62×10^{-3}	3.86×10^{-4}	1.17×10^{-1}
1966	9.58×10^{-2}	4.54×10^{-3}	9.17×10^{-2}	5.71×10^{-6}	1.63×10^{-2}	4.54×10^{-3}	3.00×10^{-4}	9.17×10^{-2}
1967	4.86×10^{-2}	2.29×10^{-3}	4.70×10^{-2}	3.58×10^{-6}	8.26×10^{-3}	2.29×10^{-3}	1.88×10^{-4}	4.70×10^{-2}
1968	5.04×10^{-2}	2.32×10^{-3}	4.84×10^{-2}	3.15×10^{-6}	8.56×10^{-3}	2.32×10^{-3}	1.66×10^{-4}	4.84×10^{-2}
1969	4.41×10^{-2}	2.06×10^{-3}	4.21×10^{-2}	2.62×10^{-6}	7.50×10^{-3}	2.06×10^{-3}	1.38×10^{-4}	4.21×10^{-2}
1970	3.22×10^{-2}	1.49×10^{-3}	3.11×10^{-2}	1.92×10^{-6}	5.47×10^{-3}	1.49×10^{-3}	1.01×10^{-4}	3.11×10^{-2}
1971	5.37×10^{-2}	2.52×10^{-3}	5.15×10^{-2}	3.63×10^{-6}	9.13×10^{-3}	2.52×10^{-3}	1.91×10^{-4}	5.15×10^{-2}
1972	2.13×10^{-2}	9.78×10^{-4}	2.05×10^{-2}	1.56×10^{-6}	3.62×10^{-3}	9.78×10^{-4}	8.24×10^{-5}	2.05×10^{-2}
1973	1.80×10^{-2}	8.46×10^{-4}	1.74×10^{-2}	1.05×10^{-6}	3.05×10^{-3}	8.46×10^{-4}	5.53×10^{-5}	1.74×10^{-2}
1974	1.13×10^{-2}	5.18×10^{-4}	1.07×10^{-2}	1.02×10^{-6}	1.92×10^{-3}	5.18×10^{-4}	5.36×10^{-5}	1.07×10^{-2}
1975	1.18×10^{-2}	5.50×10^{-4}	1.12×10^{-2}	7.52×10^{-7}	2.01×10^{-3}	5.50×10^{-4}	3.96×10^{-5}	1.12×10^{-2}
1976	1.70×10^{-2}	7.98×10^{-4}	1.64×10^{-2}	1.27×10^{-6}	2.89×10^{-3}	7.98×10^{-4}	6.67×10^{-5}	1.64×10^{-2}
1977	2.97×10^{-2}	1.35×10^{-3}	2.87×10^{-2}	1.88×10^{-6}	5.05×10^{-3}	1.35×10^{-3}	9.87×10^{-5}	2.87×10^{-2}
1978	1.07×10^{-2}	4.94×10^{-4}	1.03×10^{-2}	6.23×10^{-7}	1.82×10^{-3}	4.94×10^{-4}	3.28×10^{-5}	1.03×10^{-2}
1979	6.67×10^{-3}	3.10×10^{-4}	6.40×10^{-3}	3.81×10^{-7}	1.13×10^{-3}	3.10×10^{-4}	2.01×10^{-5}	6.40×10^{-3}
1980	8.23×10^{-3}	3.75×10^{-4}	7.72×10^{-3}	4.75×10^{-7}	1.40×10^{-3}	3.75×10^{-4}	2.50×10^{-5}	7.72×10^{-3}
1981	9.11×10^{-3}	4.20×10^{-4}	8.70×10^{-3}	4.67×10^{-7}	1.55×10^{-3}	4.20×10^{-4}	2.46×10^{-5}	8.70×10^{-3}
1982	1.57×10^{-2}	7.31×10^{-4}	1.51×10^{-2}	8.57×10^{-7}	2.67×10^{-3}	7.31×10^{-4}	4.51×10^{-5}	1.51×10^{-2}
1983	1.82×10^{-2}	8.56×10^{-4}	1.76×10^{-2}	1.14×10^{-6}	3.10×10^{-3}	8.56×10^{-4}	5.98×10^{-5}	1.76×10^{-2}
1984	1.70×10^{-2}	7.88×10^{-4}	1.65×10^{-2}	9.43×10^{-7}	2.89×10^{-3}	7.88×10^{-4}	4.96×10^{-5}	1.65×10^{-2}
1985	1.64×10^{-2}	7.57×10^{-4}	1.54×10^{-2}	9.74×10^{-7}	2.79×10^{-3}	7.57×10^{-4}	5.13×10^{-5}	1.54×10^{-2}
1986	7.09×10^{-3}	3.32×10^{-4}	6.89×10^{-3}	4.21×10^{-7}	1.21×10^{-3}	3.32×10^{-4}	2.21×10^{-5}	6.89×10^{-3}
1987	2.16×10^{-2}	1.01×10^{-3}	2.14×10^{-2}	1.19×10^{-6}	3.68×10^{-3}	1.01×10^{-3}	6.24×10^{-5}	2.14×10^{-2}
1988	2.91×10^{-2}	1.35×10^{-3}	2.75×10^{-2}	1.53×10^{-6}	4.94×10^{-3}	1.35×10^{-3}	8.05×10^{-5}	2.75×10^{-2}

Table E-1. Radionuclide Concentrations in the Great Miami River (Bq L^{-1})[a] (continued)

Year	Ra-224	Ra-226	Ra-228	Pa-234m	Pa-234	Ac-228	Pu-239
1951	0	0	0	0	0	0	0
1952	0	8.41×10^{-3}	0	5.33×10^{-2}	8.53×10^{-5}	0	0
1953	0	1.38×10^{-2}	0	8.92×10^{-2}	1.43×10^{-4}	0	0
1954	2.62×10^{-4}	1.29×10^{-2}	1.35×10^{-2}	8.41×10^{-2}	1.34×10^{-4}	1.60×10^{-3}	0
1955	1.86×10^{-4}	9.25×10^{-3}	8.93×10^{-3}	6.04×10^{-2}	9.66×10^{-5}	1.14×10^{-3}	0
1956	2.06×10^{-4}	1.19×10^{-2}	1.19×10^{-2}	7.52×10^{-2}	1.20×10^{-4}	1.26×10^{-3}	0
1957	2.07×10^{-4}	1.18×10^{-2}	1.16×10^{-2}	7.59×10^{-2}	1.21×10^{-4}	1.26×10^{-3}	0
1958	0	6.73×10^{-3}	0	4.36×10^{-2}	6.98×10^{-5}	0	0
1959	0	9.46×10^{-3}	0	6.17×10^{-2}	9.87×10^{-5}	0	0
1960	0	3.29×10^{-2}	0	2.13×10^{-1}	3.42×10^{-4}	0	0
1961	0	2.79×10^{-2}	0	1.75×10^{-1}	2.80×10^{-4}	0	0
1962	0	2.32×10^{-2}	0	1.50×10^{-1}	2.39×10^{-4}	0	2.94×10^{-5}
1963	0	3.22×10^{-2}	0	2.09×10^{-1}	3.34×10^{-4}	0	1.91×10^{-4}
1964	1.48×10^{-5}	2.31×10^{-2}	3.22×10^{-2}	2.11×10^{-1}	3.37×10^{-4}	9.06×10^{-5}	1.59×10^{-4}
1965	6.95×10^{-6}	1.09×10^{-2}	1.79×10^{-2}	1.17×10^{-1}	1.87×10^{-4}	4.25×10^{-5}	9.02×10^{-5}
1966	5.41×10^{-6}	8.51×10^{-3}	1.31×10^{-2}	9.17×10^{-2}	1.47×10^{-4}	3.30×10^{-5}	8.61×10^{-5}
1967	3.39×10^{-6}	5.58×10^{-3}	7.25×10^{-3}	4.70×10^{-2}	7.52×10^{-5}	2.07×10^{-5}	4.35×10^{-5}
1968	2.98×10^{-6}	4.30×10^{-3}	7.66×10^{-3}	4.84×10^{-2}	7.74×10^{-5}	1.82×10^{-5}	4.46×10^{-5}
1969	2.48×10^{-6}	3.87×10^{-3}	6.01×10^{-3}	4.21×10^{-2}	6.74×10^{-5}	1.52×10^{-5}	3.92×10^{-5}
1970	1.82×10^{-6}	3.21×10^{-3}	4.68×10^{-3}	3.11×10^{-2}	4.98×10^{-5}	1.11×10^{-5}	2.87×10^{-5}
1971	3.44×10^{-6}	5.25×10^{-3}	6.85×10^{-3}	5.15×10^{-2}	8.24×10^{-5}	2.10×10^{-5}	4.80×10^{-5}
1972	1.48×10^{-6}	2.09×10^{-3}	3.04×10^{-3}	2.05×10^{-2}	3.28×10^{-5}	9.06×10^{-6}	1.90×10^{-5}
1973	9.96×10^{-7}	1.57×10^{-3}	2.60×10^{-3}	1.74×10^{-2}	2.78×10^{-5}	6.09×10^{-6}	1.63×10^{-5}
1974	9.64×10^{-7}	1.47×10^{-3}	1.77×10^{-3}	1.07×10^{-2}	1.71×10^{-5}	5.89×10^{-6}	9.84×10^{-6}
1975	7.13×10^{-7}	1.09×10^{-3}	1.66×10^{-3}	1.12×10^{-2}	1.79×10^{-5}	4.36×10^{-6}	1.05×10^{-5}
1976	1.20×10^{-6}	1.79×10^{-3}	2.41×10^{-3}	1.64×10^{-2}	2.62×10^{-5}	7.34×10^{-6}	1.54×10^{-5}
1977	1.78×10^{-6}	2.87×10^{-3}	4.60×10^{-3}	2.87×10^{-2}	4.59×10^{-5}	1.09×10^{-5}	2.63×10^{-5}
1978	5.90×10^{-7}	9.60×10^{-4}	1.62×10^{-3}	1.03×10^{-2}	1.64×10^{-5}	3.61×10^{-6}	9.61×10^{-6}
1979	3.61×10^{-7}	5.51×10^{-4}	1.14×10^{-3}	6.40×10^{-3}	1.02×10^{-5}	2.21×10^{-6}	5.68×10^{-6}
1980	4.50×10^{-7}	6.35×10^{-4}	1.24×10^{-3}	7.72×10^{-3}	1.23×10^{-5}	2.75×10^{-6}	7.24×10^{-6}
1981	4.42×10^{-7}	6.94×10^{-4}	1.30×10^{-3}	8.70×10^{-3}	1.39×10^{-5}	2.70×10^{-6}	8.11×10^{-6}
1982	8.12×10^{-7}	1.26×10^{-3}	2.05×10^{-3}	1.51×10^{-2}	2.41×10^{-5}	4.96×10^{-6}	1.41×10^{-5}
1983	1.08×10^{-6}	1.69×10^{-3}	2.63×10^{-3}	1.76×10^{-2}	2.82×10^{-5}	6.57×10^{-6}	1.63×10^{-5}
1984	8.94×10^{-7}	1.52×10^{-3}	2.33×10^{-3}	1.65×10^{-2}	2.64×10^{-5}	5.46×10^{-6}	1.53×10^{-5}
1985	9.23×10^{-7}	1.36×10^{-3}	2.59×10^{-3}	1.54×10^{-2}	2.46×10^{-5}	5.64×10^{-6}	1.32×10^{-5}
1986	3.99×10^{-7}	5.74×10^{-4}	9.57×10^{-4}	6.89×10^{-3}	1.10×10^{-5}	2.44×10^{-6}	5.68×10^{-6}
1987	1.12×10^{-6}	1.97×10^{-3}	3.40×10^{-3}	2.14×10^{-2}	3.42×10^{-5}	6.87×10^{-6}	1.78×10^{-5}
1988	1.45×10^{-6}	2.25×10^{-3}	3.99×10^{-3}	2.75×10^{-2}	4.40×10^{-5}	8.85×10^{-6}	2.36×10^{-5}

[a] Data for ^{234}U, ^{235}U, and ^{238}U were given for 1952–1988. Data for ^{232}Th were given for 1954–1958 and 1964–1988. Missing ^{232}Th data were assumed to correspond to no thorium production. Radium-226 data were given for 1952–1988, ^{228}Ra data were given for 1954–1988, and $^{239,240}Pu$ data were given for 1962–1988. Otherwise, levels of radionuclides were inferred from decay chain kinetics. A decay time of 20,000 years gives the ratio $^{234}U : {}^{230}Th : {}^{226}Ra = 0.945 : 0.160 : 0.143$, which gives $^{226}Ra : {}^{234}U = 0.15$, about the value for measurements from 1964 onward. Radium-226 values before 1964 were calculated from this ratio. The ratio $^{230}Th : {}^{234}U = 0.17$ was used to estimate the ^{230}Th values for all years. Data for ^{228}Ra and ^{232}Th give ratios $^{228}Ra : {}^{232}Th = 46$, which cannot be if the thorium is the source of the radium. In consideration of other possibilities, however, we have left the data in place. For other nuclides in the ^{232}Th chain, we have used the ratios $^{232}Th : {}^{228}Ra : {}^{228}Ac : {}^{228}Th : {}^{224}Ra = 1 : 0.11 : 0.11 : 0.019 : 0.018$ (corresponding to 1 year's decay) to estimate the levels of ^{228}Ac, ^{228}Th, and ^{224}Ra (using ^{232}Th as the basis and ignoring the anomalous ^{228}Ra).

Table E-2. Radionuclides in Paddy's Run (Bq L^{-1})[a]

Year	U-234	U-235	U-238	Th-228	Th-230	Th-231	Th-232	Th-234
1951	0	0	0	0	0	0	0	0
1952	2.06	9.54×10^{-2}	1.97	0	3.50×10^{-1}	9.54×10^{-2}	0	1.97
1953	2.06	9.54×10^{-2}	1.97	0	3.50×10^{-1}	9.54×10^{-2}	0	1.97
1954	2.06	9.54×10^{-2}	1.97	1.25×10^{-4}	3.50×10^{-1}	9.54×10^{-2}	6.60×10^{-3}	1.97
1955	2.06	9.54×10^{-2}	1.97	1.25×10^{-4}	3.50×10^{-1}	9.54×10^{-2}	6.60×10^{-3}	1.97
1956	1.05	4.85×10^{-2}	1.00	6.37×10^{-5}	1.78×10^{-1}	4.85×10^{-2}	3.35×10^{-3}	1.00
1957	1.35	6.26×10^{-2}	1.29	8.23×10^{-5}	2.29×10^{-1}	6.26×10^{-2}	4.33×10^{-3}	1.29
1958	2.48	1.15×10^{-1}	2.38	0	4.22×10^{-1}	1.15×10^{-1}	0	2.38
1959	3.23	1.50×10^{-1}	3.10	0	5.50×10^{-1}	1.50×10^{-1}	0	3.10
1960	5.13	2.38×10^{-1}	4.92	0	8.72×10^{-1}	2.38×10^{-1}	0	4.92
1961	5.52	2.56×10^{-1}	5.30	0	9.39×10^{-1}	2.56×10^{-1}	0	5.30
1962	5.92	2.74×10^{-1}	5.67	0	1.01	2.74×10^{-1}	0	5.67
1963	3.56	1.65×10^{-1}	3.41	0	6.04×10^{-1}	1.65×10^{-1}	0	3.41
1964	6.79	3.15×10^{-1}	6.51	4.14×10^{-4}	1.15	3.15×10^{-1}	2.18×10^{-2}	6.51
1965	2.45	1.14×10^{-1}	2.35	1.50×10^{-4}	4.17×10^{-1}	1.14×10^{-1}	7.87×10^{-3}	2.35
1966	3.04	1.41×10^{-1}	2.92	1.85×10^{-4}	5.17×10^{-1}	1.41×10^{-1}	9.76×10^{-3}	2.92
1967	2.97	1.38×10^{-1}	2.85	1.81×10^{-4}	5.05×10^{-1}	1.38×10^{-1}	9.53×10^{-3}	2.85
1968	1.41	6.55×10^{-2}	1.36	8.61×10^{-5}	2.40×10^{-1}	6.55×10^{-2}	4.53×10^{-3}	1.36
1969	1.14	5.31×10^{-2}	1.10	6.98×10^{-5}	1.95×10^{-1}	5.31×10^{-2}	3.67×10^{-3}	1.10
1970	1.38	6.39×10^{-2}	1.32	8.40×10^{-5}	2.34×10^{-1}	6.39×10^{-2}	4.42×10^{-3}	1.32
1971	1.97	9.12×10^{-2}	1.89	1.20×10^{-4}	3.34×10^{-1}	9.12×10^{-2}	6.31×10^{-3}	1.89
1972	1.27	5.89×10^{-2}	1.22	7.74×10^{-5}	2.16×10^{-1}	5.89×10^{-2}	4.07×10^{-3}	1.22
1973	9.12×10^{-1}	4.23×10^{-2}	8.75×10^{-1}	5.56×10^{-5}	1.55×10^{-1}	4.23×10^{-2}	2.93×10^{-3}	8.75×10^{-1}
1974	2.22	1.03×10^{-1}	2.13	1.35×10^{-4}	3.77×10^{-1}	1.03×10^{-1}	7.12×10^{-3}	2.13
1975	9.66×10^{-1}	4.48×10^{-2}	9.26×10^{-1}	5.89×10^{-5}	1.64×10^{-1}	4.48×10^{-2}	3.10×10^{-3}	9.26×10^{-1}
1976	1.07	4.98×10^{-2}	1.03	6.54×10^{-5}	1.82×10^{-1}	4.98×10^{-2}	3.44×10^{-3}	1.03
1977	8.05×10^{-1}	3.73×10^{-2}	7.72×10^{-1}	4.91×10^{-5}	1.37×10^{-1}	3.73×10^{-2}	2.58×10^{-3}	7.72×10^{-1}
1978	2.68×10^{-1}	1.24×10^{-2}	2.57×10^{-1}	1.64×10^{-5}	4.56×10^{-2}	1.24×10^{-2}	8.61×10^{-4}	2.57×10^{-1}
1979	3.31×10^{-1}	1.53×10^{-2}	3.17×10^{-1}	2.02×10^{-5}	5.62×10^{-2}	1.53×10^{-2}	1.06×10^{-3}	3.17×10^{-1}
1980	1.97×10^{-1}	9.12×10^{-3}	1.89×10^{-1}	1.20×10^{-5}	3.34×10^{-2}	9.12×10^{-3}	6.31×10^{-4}	1.89×10^{-1}
1981	7.69×10^{-2}	3.57×10^{-3}	7.38×10^{-2}	4.69×10^{-6}	1.31×10^{-2}	3.57×10^{-3}	2.47×10^{-4}	7.38×10^{-2}
1982	7.69×10^{-2}	3.57×10^{-3}	7.38×10^{-2}	4.69×10^{-6}	1.31×10^{-2}	3.57×10^{-3}	2.47×10^{-4}	7.38×10^{-2}
1983	2.15×10^{-1}	9.95×10^{-3}	2.06×10^{-1}	1.31×10^{-5}	3.65×10^{-2}	9.95×10^{-3}	6.89×10^{-4}	2.06×10^{-1}
1984	2.24×10^{-1}	1.04×10^{-2}	2.14×10^{-1}	1.36×10^{-5}	3.80×10^{-2}	1.04×10^{-2}	7.17×10^{-4}	2.14×10^{-1}
1985	1.54×10^{-1}	7.12×10^{-3}	1.47×10^{-1}	9.37×10^{-6}	2.61×10^{-2}	7.12×10^{-3}	4.93×10^{-4}	1.47×10^{-1}
1986	6.70×10^{-2}	3.11×10^{-3}	6.42×10^{-2}	4.08×10^{-6}	1.14×10^{-2}	3.11×10^{-3}	2.15×10^{-4}	6.42×10^{-2}
1987	3.94×10^{-3}	1.83×10^{-4}	3.78×10^{-3}	2.40×10^{-7}	6.70×10^{-4}	1.83×10^{-4}	1.26×10^{-5}	3.78×10^{-3}
1988	3.94×10^{-3}	1.83×10^{-4}	3.78×10^{-3}	2.40×10^{-7}	6.70×10^{-4}	1.83×10^{-4}	1.26×10^{-5}	3.78×10^{-3}

Table E-2. Radionuclides in Paddy's Run (Bq L^{-1})[a] (continued)

Year	Ra-224	Ra-226	Ra-228	Pa-234m	Pa-234	Ac228	Pu-239,240
1951	0	0	0	0	0	0	0
1952	0	3.09×10^{-1}	0	1.97	3.16×10^{-3}	0	0
1953	0	3.09×10^{-1}	0	1.97	3.16×10^{-3}	0	0
1954	1.19×10^{-4}	3.09×10^{-1}	7.26×10^{-4}	1.97	3.16×10^{-3}	7.26×10^{-4}	0
1955	1.19×10^{-4}	3.09×10^{-1}	7.26×10^{-4}	1.97	3.16×10^{-3}	7.26×10^{-4}	0
1956	6.04×10^{-5}	1.57×10^{-1}	3.69×10^{-4}	1.00	1.60×10^{-3}	3.69×10^{-4}	0
1957	7.80×10^{-5}	2.02×10^{-1}	4.76×10^{-4}	1.29	2.07×10^{-3}	4.76×10^{-4}	0
1958	0	3.72×10^{-1}	0	2.38	3.81×10^{-3}	0	0
1959	0	4.85×10^{-1}	0	3.10	4.96×10^{-3}	0	0
1960	0	7.69×10^{-1}	0	4.92	7.87×10^{-3}	0	0
1961	0	8.28×10^{-1}	0	5.30	8.47×10^{-3}	0	0
1962	0	8.87×10^{-1}	0	5.67	9.08×10^{-3}	0	3.99×10^{-3}
1963	0	5.33×10^{-1}	0	3.41	5.46×10^{-3}	0	4.36×10^{-3}
1964	3.92×10^{-4}	1.02	2.40×10^{-3}	6.51	1.04×10^{-2}	2.40×10^{-3}	3.89×10^{-3}
1965	1.42×10^{-4}	3.68×10^{-1}	8.66×10^{-4}	2.35	3.77×10^{-3}	8.66×10^{-4}	2.31×10^{-3}
1966	1.76×10^{-4}	4.56×10^{-1}	1.07×10^{-3}	2.92	4.67×10^{-3}	1.07×10^{-3}	2.53×10^{-3}
1967	1.71×10^{-4}	4.45×10^{-1}	1.05×10^{-3}	2.85	4.56×10^{-3}	1.05×10^{-3}	1.85×10^{-3}
1968	8.16×10^{-5}	2.12×10^{-1}	4.99×10^{-4}	1.36	2.17×10^{-3}	4.99×10^{-4}	1.08×10^{-3}
1969	6.61×10^{-5}	1.72×10^{-1}	4.04×10^{-4}	1.10	1.76×10^{-3}	4.04×10^{-4}	1.06×10^{-3}
1970	7.95×10^{-5}	2.07×10^{-1}	4.86×10^{-4}	1.32	2.11×10^{-3}	4.86×10^{-4}	1.41×10^{-3}
1971	1.14×10^{-4}	2.95×10^{-1}	6.94×10^{-4}	1.89	3.02×10^{-3}	6.94×10^{-4}	1.36×10^{-3}
1972	7.33×10^{-5}	1.90×10^{-1}	4.48×10^{-4}	1.22	1.95×10^{-3}	4.48×10^{-4}	9.19×10^{-4}
1973	5.27×10^{-5}	1.37×10^{-1}	3.22×10^{-4}	8.75×10^{-1}	1.40×10^{-3}	3.22×10^{-4}	1.32×10^{-3}
1974	1.28×10^{-4}	3.33×10^{-1}	7.83×10^{-4}	2.13	3.40×10^{-3}	7.83×10^{-4}	1.34×10^{-3}
1975	5.58×10^{-5}	1.45×10^{-1}	3.41×10^{-4}	9.26×10^{-1}	1.48×10^{-3}	3.41×10^{-4}	8.59×10^{-4}
1976	6.20×10^{-5}	1.61×10^{-1}	3.79×10^{-4}	1.03	1.65×10^{-3}	3.79×10^{-4}	7.91×10^{-4}
1977	4.65×10^{-5}	1.21×10^{-1}	2.84×10^{-4}	7.72×10^{-1}	1.24×10^{-3}	2.84×10^{-4}	4.52×10^{-4}
1978	1.55×10^{-5}	4.02×10^{-2}	9.47×10^{-5}	2.57×10^{-1}	4.12×10^{-4}	9.47×10^{-5}	2.52×10^{-4}
1979	1.91×10^{-5}	4.96×10^{-2}	1.17×10^{-4}	3.17×10^{-1}	5.08×10^{-4}	1.17×10^{-4}	2.22×10^{-4}
1980	1.14×10^{-5}	2.95×10^{-2}	6.94×10^{-5}	1.89×10^{-1}	3.02×10^{-4}	6.94×10^{-5}	1.15×10^{-4}
1981	4.44×10^{-6}	1.15×10^{-2}	2.71×10^{-5}	7.38×10^{-2}	1.18×10^{-4}	2.71×10^{-5}	6.48×10^{-5}
1982	4.44×10^{-6}	1.15×10^{-2}	2.71×10^{-5}	7.38×10^{-2}	1.18×10^{-4}	2.71×10^{-5}	1.23×10^{-4}
1983	1.24×10^{-5}	3.22×10^{-2}	7.58×10^{-5}	2.06×10^{-1}	3.29×10^{-4}	7.58×10^{-5}	1.85×10^{-4}
1984	1.29×10^{-5}	3.35×10^{-2}	7.89×10^{-5}	2.14×10^{-1}	3.43×10^{-4}	7.89×10^{-5}	1.59×10^{-4}
1985	8.87×10^{-6}	2.30×10^{-2}	5.42×10^{-5}	1.47×10^{-1}	2.36×10^{-4}	5.42×10^{-5}	9.29×10^{-5}
1986	3.87×10^{-6}	1.00×10^{-2}	2.36×10^{-5}	6.42×10^{-2}	1.03×10^{-4}	2.36×10^{-5}	2.99×10^{-5}
1987	2.27×10^{-7}	5.91×10^{-4}	1.39×10^{-6}	3.78×10^{-3}	6.04×10^{-6}	1.39×10^{-6}	3.32×10^{-6}
1988	2.27×10^{-7}	5.91×10^{-4}	1.39×10^{-6}	3.78×10^{-3}	6.04×10^{-6}	1.39×10^{-6}	1.66×10^{-6}

[a] Thorium-232 and $^{239,240}Pu$ are based on the respective ratios to total uranium in the Great Miami River. Thorium-230 and ^{226}Ra are based on the ^{226}Ra : ^{234}U ratio observed in the river effluent. Radium-228, ^{228}Ac, ^{228}Th, and ^{224}Ra are based on the calculated decay of ^{232}Th for one year.

Table E-3. Radionuclides Listed by Estimation Method

Measurements	Decay chain
^{234}U	^{238}Th
^{235}U	^{230}Th
^{238}U	^{231}Th
^{232}Th	^{234}Th
^{226}Ra	^{224}Ra
^{228}Ra	^{234m}Pa
$^{239,240}Pu$	^{234}Pa
	^{228}Ac

APPENDIX F

ESTIMATES OF CONCENTRATIONS OF URANIUM AND DECAY PRODUCTS IN SOUTH PLUME WELLS

INTRODUCTION

Uranium concentrations in contaminated wells in the South Plume area were estimated in our Task 2/3 report (Voillequé et al. 1995). This appendix summarizes those estimates and tabulates levels of isotopes of uranium and calculated levels of other radionuclides in Well 15. We have used the reconstructed radionuclide concentrations in this well, beginning in the late 1960s when the plume first reached the well and continuing forward to the 1980s when monitoring began, for estimating doses from drinking water to the subject of scenario 3 (see Appendix J). The measured levels of uranium in Well 15 exceeded those in other private wells, and we have used the data and calculated values for this well to construct an extreme exposure case for scenario 3 with respect to drinking water.

The dose estimates for scenario 3 account not only for uranium, but also for radioactive decay products in the well water, which we have calculated from decay-chain kinetics. We also assumed the presence of thorium and plutonium in concentrations similar to those of the Great Miami River water and ^{226}Ra in the same ^{226}Ra : ^{234}U ratio measured in releases to surface water. Inclusion of these radionuclides in calculated concentrations supplements the incomplete reporting of measurements of radionuclides other than uranium in groundwater. This appendix presents results of these calculations as a table of concentrations over time for Well 15 (Table F-1).

URANIUM LEVELS

Monitoring of the three contaminated private wells (Wells 12, 15, and 17) was initiated in late 1981. Routine monitoring of these and other private wells has been performed by the Feed Materials Production Center (FMPC) since 1982. We obtained results of monthly measurements of uranium concentration in well water for the three contaminated wells for late 1981 through 1992. Annual average uranium concentrations for these wells are shown in Table M-1, Appendix M, of the Task 2/3 report (Voillequé et al. 1995). We used the annual average concentrations for 1982–1988 as the basis for dose calculations for these years.

For the period 1963–1981, for which well monitoring was not performed, we used models to estimate concentrations of uranium that might have existed in well water of the South Plume. We first developed an estimated upper bound on the annual average uranium concentration that could have existed in Wells 12, 15, and 17. The primary source of uranium contamination of the South Plume is uranium-bearing waters released into Paddy's Run and the storm sewer outfall ditch (SSOD). Thus, uranium concentrations in the groundwater are expected to be less than or equal to concentrations in Paddy's Run and the SSOD. We used uranium concentration data for Paddy's Run and the SSOD and compiled the data in Appendices L and M of the Task 2/3 report. Uranium concentrations were higher in the SSOD than in Paddy's Run. In

the SSOD, the maximum annual average concentration was 8,300 pCi L^{-1} for the year 1960. Thus, this value is an upper bound of the annual average uranium concentration that might have existed in the contaminated wells during 1963–1981.

We recognized that this upper bound is an extremely conservative estimate of the uranium concentrations in the three contaminated wells for 1963–1981 (conservative in the sense that the estimate is too high). The conservatism results from the following factors: (1) the maximum annual average concentration was used to represent the concentrations for the complete period, (2) dilution of the uranium with water from Paddy's Run (which had lower uranium concentrations than the water from the SSOD) was ignored, and (3) dilution in the groundwater (from other groundwater sources) was also ignored. For the dose calculations, we believe the use of the upper bound uranium concentration of 8,300 pCi L^{-1} to represent concentrations in private wells of the South Plume area for 1963–1981 is unrealistically conservative.

For this reason, we developed an empirical model to estimate uranium concentrations in the contaminated wells. An empirical model is based primarily on measurement data, rather than on theory, to explain particular conditions. In this case, we used the annual-average measured uranium concentrations in the contaminated wells, for 1982–1992, and the calculated quantities of uranium released to Paddy's Run and the SSOD, for 1952–1988. These releases are discussed in Appendix L of the Task 2/3 report. Details of the model are described in Appendix M of the Task 2/3 report, and results of the calculations are given in Table M–7 of that appendix. We believe the use of this model provides more realistic, though still somewhat conservative, estimates of uranium concentrations that might have existed in the contaminated wells for 1963–1981. Figure F-1 shows the predicted annual median and 5th and 95th percentiles of uranium concentration in Well 15, compared with plotted measurements from that well. The figure also shows the annual uranium release to the SSOD.

Concentrations of total uranium were partitioned into concentrations of the isotopes ^{234}U, ^{235}U, and ^{238}U on the basis of the isotopic activity ratios 1 : 0.0475 : 1 for natural uranium (Killough et al. 1993, Appendix N, Table N-6).

OTHER RADIONUCLIDES

The radioelement of primary concern in the South Plume has been uranium (see, for example, DOE 1990a; Dames and Moore 1985; Byrne et al. 1991). However, other radionuclides were also released into surface waters, and thus the potential exists for other radionuclides to be present in the South Plume groundwater. Appendix D of the Task 2/3 report discusses releases of radionuclides other than uranium from the FMPC to air and to surface waters. Appendix D reports the results of a screening-level assessment of the relative importance of radionuclide releases to surface waters, based primarily on information about releases to the Great Miami River. From this assessment, the radium isotopes ^{226}Ra and ^{228}Ra were determined to be of primary importance.

This determination applies, however, only to radionuclides in surface waters. For radionuclides in groundwater, the environmental transport is different, and different exposure pathways may be pertinent. Because large quantities of these two radium isotopes were released to surface waters, they would be of concern in the groundwater if they migrated into the South Plume along with the uranium.

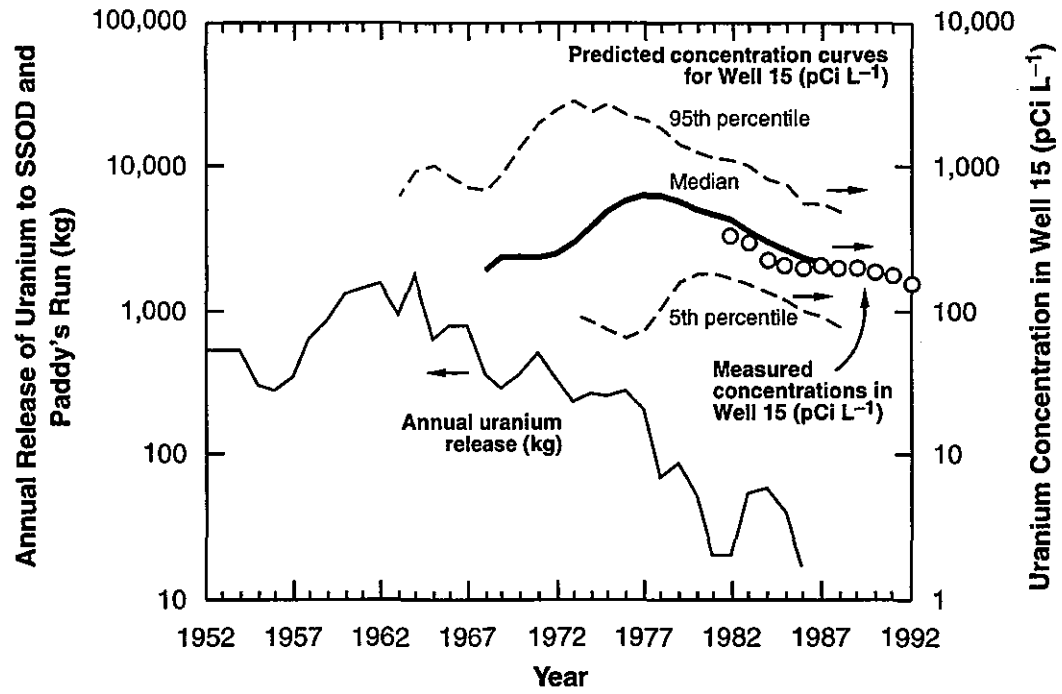

Figure F-1. Measured and model-predicted annual concentrations of uranium in Well 15. Details of the model are discussed in Appendix L of the Task 2/3 report (Voillequé et al. 1995). Annual releases of uranium to the SSOD are shown for comparison of time scales.

From recent environmental monitoring reports for the FMPC, it appears that the private offsite wells have not been routinely monitored for radionuclides other than uranium (Dugan et al. 1990; Byrne et al. 1991; WEMCO 1992; FERMCO 1993). In the 1989 environmental monitoring report, radionuclides other than uranium are not discussed (Dugan et al. 1990). The 1990 report summarizes results from the comprehensive groundwater program (which involves wells in addition to the routine monitoring wells), which monitored for ^{90}Sr, ^{99}Tc, ^{226}Ra, ^{228}Ra, and ^{232}Th (Byrne et al. 1991). This report provides only those results that were above the U.S. Department of Energy concentration guidelines for drinking water. For these other radionuclides, none of the wells in the South Plume area exceeded the guidelines. In the 1991 and 1992 reports, no results for other radionuclides are presented because of problems with data validation (WEMCO 1992; FERMCO 1993).

As part of the Remedial Investigation/Feasibility Study (RI/FS) of the environmental restoration work at the FMPC, a study of the South Plume groundwater included installation of additional groundwater monitoring wells, followed by sampling and analysis of these new wells and the existing monitoring wells in the late 1980s and 1990 (DOE 1990a). The radionuclide analyses of the well samples included total uranium, total thorium, isotopic uranium, isotopic thorium, isotopic plutonium, ^{226}Ra, ^{228}Ra, ^{237}Np, ^{99}Tc, ^{90}Sr, and gamma-emitting radionuclides by gamma spectroscopy. Except for uranium, none of these radionuclides were found at concentrations above natural background (DOE 1990a).

Another report prepared for the RI/FS work included a comprehensive compilation of

groundwater contamination monitoring data from August 1987 through April 1990, as well as descriptions of the nature and extent of groundwater contamination at the FMPC (DOE 1990b). Some results from that report are summarized here. Outside the FMPC boundary, the only recurrent detections of radionuclides other than uranium were for ^{226}Ra and ^{228}Ra, both at a monitoring well (not one of the private wells) near the town of Fernald, south of New Haven Road. These measured concentrations were low and were spatially isolated. It was concluded that the presence of radium in this well probably was not due to the South Plume. No radionuclides other than uranium and radium were recurrently detected in the wells of the South Plume area. Thus, for all radionuclides other than uranium, it was concluded that the FMPC was not contributing significant quantities to the South Plume.

These studies do not indicate the presence of other radionuclides in offsite groundwater in concentrations above background. In modeling the levels of radionuclides in the wells over time, however, we have estimated concentrations of radionuclides other than uranium that might have been present in the South Plume groundwater because (1) measurement results for other radionuclides have not been obtained for the private wells; (2) the sampling for other radionuclides was limited to only a few recent years, when earlier higher levels may have subsided; (3) no analyses of other radionuclides in private wells were available for the 1970s, which included the years of estimated highest uranium concentrations in private wells; and (4) the contamination reaching the wells is clearly old enough to permit the formation of certain decay products, which although short-lived, would, in the presence of their precursors, add to the dose (e.g., ^{234}Th, half-life 24 days, would be in secular equilibrium with its precursor, ^{238}U). It is for these reasons that we have made calculations of other radionuclides in Well 15 on the basis of decay-chain analyses and estimates of source ratios (Table F-1). The footnote below the table indicates the methods. Well 15 had the highest levels of uranium concentrations of the three private wells represented by our data, and we have used the data and estimates for this well as a generic source for exposure scenario 3 (Appendix J).

REFERENCES

Byrne J.M., T.A. Dugan, and J.S. Oberjohn. 1991. *Feed Materials Production Center Annual Environmental Report for Calendar Year 1990.* Report FMPC-2245, Westinghouse Materials Company of Ohio, Cincinnati, Ohio.

Dames and Moore. 1985. *Department of Energy, Feed Materials Production Center, Groundwater Study, Task C Report.* Dames and Moore, White Plains, New York.

Dugan T.A., G.L. Gels, J.S. Oberjohn, and L.K. Rogers. 1990. *Feed Materials Production Center Annual Environmental Report for Calendar Year 1989.* Westinghouse Materials Company of Ohio, Cincinnati, Ohio.

Fernald Environmental Restoration Management Corporation (FERMCO). 1993. *1992 Fernald Environmental Management Project Site Environmental Report.* Report FEMP-2290, FERMCO.

Table F-1. Estimated Radionuclide Concentrations in Contaminated Water from Well 15 (Bq L^{-1})[a]

Year	U-234	U-235	U-238	Th-228	Th-230	Th-231	Th-232	Th-234
1951–1967	0	0	0	0	0	0	0	0
1968	3.25	1.55×10^{-1}	3.25	1.86×10^{-2}	5.53×10^{-1}	1.55×10^{-1}	1.86×10^{-2}	3.25
1969	4.16	1.97×10^{-1}	4.16	2.38×10^{-2}	7.07×10^{-1}	1.97×10^{-1}	2.38×10^{-2}	4.16
1970	4.16	1.97×10^{-1}	4.16	2.38×10^{-2}	7.07×10^{-1}	1.97×10^{-1}	2.38×10^{-2}	4.16
1971	4.16	1.97×10^{-1}	4.16	2.38×10^{-2}	7.07×10^{-1}	1.97×10^{-1}	2.38×10^{-2}	4.16
1972	4.34	2.06×10^{-1}	4.34	2.49×10^{-2}	7.37×10^{-1}	2.06×10^{-1}	2.49×10^{-2}	4.34
1973	5.24	2.49×10^{-1}	5.24	3.00×10^{-2}	8.91×10^{-1}	2.49×10^{-1}	3.00×10^{-2}	5.24
1974	6.69	3.18×10^{-1}	6.69	3.83×10^{-2}	1.14	3.18×10^{-1}	3.83×10^{-2}	6.69
1975	8.85	4.21×10^{-1}	8.85	5.08×10^{-2}	1.51	4.21×10^{-1}	5.08×10^{-2}	8.85
1976	$1.05\times10^{+1}$	4.98×10^{-1}	$1.05\times10^{+1}$	6.01×10^{-2}	1.78	4.98×10^{-1}	6.01×10^{-2}	$1.05\times10^{+1}$
1977	$1.12\times10^{+1}$	5.32×10^{-1}	$1.12\times10^{+1}$	6.42×10^{-2}	1.90	5.32×10^{-1}	6.42×10^{-2}	$1.12\times10^{+1}$
1978	$1.12\times10^{+1}$	5.32×10^{-1}	$1.12\times10^{+1}$	6.42×10^{-2}	1.90	5.32×10^{-1}	6.42×10^{-2}	$1.12\times10^{+1}$
1979	$1.03\times10^{+1}$	4.89×10^{-1}	$1.03\times10^{+1}$	5.91×10^{-2}	1.75	4.89×10^{-1}	5.91×10^{-2}	$1.03\times10^{+1}$
1980	9.22	4.38×10^{-1}	9.22	5.28×10^{-2}	1.57	4.38×10^{-1}	5.28×10^{-2}	9.22
1981	8.31	3.95×10^{-1}	8.31	4.77×10^{-2}	1.41	3.95×10^{-1}	4.77×10^{-2}	8.31
1982	5.78	2.75×10^{-1}	5.78	3.32×10^{-2}	9.83×10^{-1}	2.75×10^{-1}	3.32×10^{-2}	5.78
1983	5.24	2.49×10^{-1}	5.24	3.00×10^{-2}	8.91×10^{-1}	2.49×10^{-1}	3.00×10^{-2}	5.24
1984	3.98	1.89×10^{-1}	3.98	2.28×10^{-2}	6.76×10^{-1}	1.89×10^{-1}	2.28×10^{-2}	3.98
1985	3.61	1.72×10^{-1}	3.61	2.07×10^{-2}	6.14×10^{-1}	1.72×10^{-1}	2.07×10^{-2}	3.61
1986	3.43	1.63×10^{-1}	3.43	1.97×10^{-2}	5.84×10^{-1}	1.63×10^{-1}	1.97×10^{-2}	3.43
1987	3.61	1.72×10^{-1}	3.61	2.07×10^{-2}	6.14×10^{-1}	1.72×10^{-1}	2.07×10^{-2}	3.61
1988	3.43	1.63×10^{-1}	3.43	1.97×10^{-2}	5.84×10^{-1}	1.63×10^{-1}	1.97×10^{-2}	3.43

Year	Ra-224	Ra-226	Ra-228	Pa-234m	Pa-234	Ac-228	Pu-239
1951–1967	0	0	0	0	0	0	0
1968	1.86×10^{-2}	4.88×10^{-1}	1.86×10^{-2}	3.25	5.20×10^{-3}	1.86×10^{-2}	1.40×10^{-3}
1969	2.38×10^{-2}	6.23×10^{-1}	2.38×10^{-2}	4.16	6.65×10^{-3}	2.38×10^{-2}	1.79×10^{-3}
1970	2.38×10^{-2}	6.23×10^{-1}	2.38×10^{-2}	4.16	6.65×10^{-3}	2.38×10^{-2}	1.79×10^{-3}
1971	2.38×10^{-2}	6.23×10^{-1}	2.38×10^{-2}	4.16	6.65×10^{-3}	2.38×10^{-2}	1.79×10^{-3}
1972	2.49×10^{-2}	6.51×10^{-1}	2.49×10^{-2}	4.34	6.94×10^{-3}	2.49×10^{-2}	1.86×10^{-3}
1973	3.00×10^{-2}	7.86×10^{-1}	3.00×10^{-2}	5.24	8.38×10^{-3}	3.00×10^{-2}	2.25×10^{-3}
1974	3.83×10^{-2}	1.00	3.83×10^{-2}	6.69	1.07×10^{-2}	3.83×10^{-2}	2.87×10^{-3}
1975	5.08×10^{-2}	1.33	5.08×10^{-2}	8.85	1.42×10^{-2}	5.08×10^{-2}	3.81×10^{-3}
1976	6.01×10^{-2}	1.57	6.01×10^{-2}	$1.05\times10^{+1}$	1.68×10^{-2}	6.01×10^{-2}	4.51×10^{-3}
1977	6.42×10^{-2}	1.68	6.42×10^{-2}	$1.12\times10^{+1}$	1.79×10^{-2}	6.42×10^{-2}	4.82×10^{-3}
1978	6.42×10^{-2}	1.68	6.42×10^{-2}	$1.12\times10^{+1}$	1.79×10^{-2}	6.42×10^{-2}	4.82×10^{-3}
1979	5.91×10^{-2}	1.55	5.91×10^{-2}	$1.03\times10^{+1}$	1.65×10^{-2}	5.91×10^{-2}	4.43×10^{-3}
1980	5.28×10^{-2}	1.38	5.28×10^{-2}	9.22	1.47×10^{-2}	5.28×10^{-2}	3.96×10^{-3}
1981	4.77×10^{-2}	1.25	4.77×10^{-2}	8.31	1.33×10^{-2}	4.77×10^{-2}	3.57×10^{-3}
1982	3.32×10^{-2}	8.67×10^{-1}	3.32×10^{-2}	5.78	9.25×10^{-3}	3.32×10^{-2}	2.49×10^{-3}
1983	3.00×10^{-2}	7.86×10^{-1}	3.00×10^{-2}	5.24	8.38×10^{-3}	3.00×10^{-2}	2.25×10^{-3}
1984	2.28×10^{-2}	5.96×10^{-1}	2.28×10^{-2}	3.98	6.36×10^{-3}	2.28×10^{-2}	1.71×10^{-3}
1985	2.07×10^{-2}	5.42×10^{-1}	2.07×10^{-2}	3.61	5.78×10^{-3}	2.07×10^{-2}	1.55×10^{-3}
1986	1.97×10^{-2}	5.15×10^{-1}	1.97×10^{-2}	3.43	5.49×10^{-3}	1.97×10^{-2}	1.48×10^{-3}
1987	2.07×10^{-2}	5.42×10^{-1}	2.07×10^{-2}	3.61	5.78×10^{-3}	2.07×10^{-2}	1.55×10^{-3}
1988	1.97×10^{-2}	5.15×10^{-1}	1.97×10^{-2}	3.43	5.49×10^{-3}	1.97×10^{-2}	1.48×10^{-3}

[a] Data for 1982–1988 were given as total uranium in Appendix M of the Task 2/3 report (Voillequé et al. 1995); estimates of total uranium for previous years are discussed in the main text of the present report. Total uranium was partitioned into the isotopes U-234, -235, -238 in the ratios 1:0.0475:1. Thorium-232 is assumed to be primarily from thorium production; because it is present in river water, it is prudent to assume groundwater infiltration in a similar Th:U ratio, for which the value was estimated to be 0.0028 (geometric mean of river values). The ratio U-234 : Th-230 : Ra-226 was assumed to be 0.945 : 0.160 : 0.143, which gives the approximate observed U-234 : Ra-226 ratio in releases to surface water. Plutonium values are based on the ratio Pu : U = 2.1×10^{-4} estimated for the Great Miami River.

Killough G.G., M.J. Case, K.R. Meyer, R.E. Moore, J.F. Rogers, S.K. Rope, D.W. Schmidt, B. Shleien, J.E. Till, and P.G. Voillequé. 1993. *The Fernald Dosimetry Reconstruction Project Task 4: Environmental Pathways — Models and Validation.* RAC Report No. CDC-3, Radiological Assessments Corporation, Neeses, South Carolina.

U.S. Department of Energy (DOE). 1990a. *Engineering Evaluation / Cost Analysis, South Plume, Feed Materials Production Center, Fernald, Ohio.* Report FMPC-0003-6, U.S. Department of Energy, Oak Ridge Operations Office, Oak Ridge, Tennessee.

U.S. Department of Energy (DOE). 1990b. *Groundwater Report, Feed Materials Production Center, Fernald, Ohio, Remedial Investigation and Feasibility Study.* Volume 1, Volume 2, and Volume 1 and Volume 2 Supplement (abbreviated appendices). Draft report, U.S. Department of Energy, Oak Ridge Operations Office, Oak Ridge, Tennessee.

Voillequé P.G., K.R. Meyer, D.W. Schmidt, S.K. Rope, G.G. Killough, M. Case, R.E. Moore, B. Shleien, and J.E. Till. 1995. *The Fernald Dosimetry Reconstruction Project Tasks 2 and 3 — Radionuclide Source Terms and Uncertainties.* RAC Report No. CDC-5. Radiological Assessments Corporation, Neeses, South Carolina.

Westinghouse Environmental Management Company of Ohio (WEMCO). 1992. *Fernald Environmental Management Project, Annual Site Environmental Report for Calendar Year 1991.* Report FEMP-2275, WEMCO.

APPENDIX G

GAMMA RADIATION DOSES FROM WASTE STORAGE SILOS

INTRODUCTION

Waste materials stored in the K-65 silos (Silos 1 and 2) and the metal oxide silo (Silo 3) emit gamma radiation, which is a source of direct radiation exposure of people around the Feed Materials Production Center (FMPC). Direct radiation exposure means exposures of people outside the FMPC boundary to radiation from radioactive sources remaining on the FMPC site. In the Task 2/3 report (Voillequé et al. 1995) we determined that these three silos were the only significant sources of such direct radiation exposures. Because the exposure pathway is different from those for particulate and radon releases from the site, doses from direct gamma radiation from the silos are discussed separately in this appendix. The doses from this pathway are tabulated and summed with doses from other sources in Appendix K of this report.

LOCATIONS OF THE SILOS

The K-65 and metal oxide silos are on the west side of the FMPC (Figure G-1). Coordinate locations are needed to determine distances to receptor points, which are used in the direct exposure calculations. Coordinates of the silos were given in Appendix J of the Task 2/3 report (Voillequé et al. 1995). Coordinates for the K-65 silos and the metal oxide silo are shown in Table G-1. Of these three silos, the K-65 silos are the major contributors to the total calculated exposure rates. For the exposure rate calculations, we assumed that the three silos of concern (Silos 1, 2, and 3) are all located at the point centered between Silos 1 and 2. This assumption greatly simplifies calculations of exposure rates for specific receptor points, and calculations have shown that this assumption introduces insignificant errors into the results. Table G-1 thus also includes coordinates for the center between the two K-65 silos. For compatibility with the rest of the transport and dose calculations, these coordinates were converted from Ohio State Plane (OSP) coordinates to universal transverse mercator (UTM) coordinates using the PLANE-PC software (USGS 1985).

CALCULATED EXPOSURE RATES VERSUS DISTANCE FROM K-65 SILOS

The methodology for calculating exposure rates due to gamma radiation emissions from the K-65 and metal oxide silos is described in the Task 4 report (Killough et al. 1993). As described in that report, the MicroShield computer software (Negin and Worku 1992) is used to perform the calculations. The sources of gamma radiation emissions are modeled as cylinders (thick disks), as shown in Figure G-2. Parameter values to be used in the calculations are described in the reports of Task 2/3, Task 4, and Task 5 of this project (Voillequé et al. 1995, Killough et al. 1993, Shleien et al. 1995). The Task 2/3 report (Voillequé et al. 1995) is considered the primary source of parameter values.

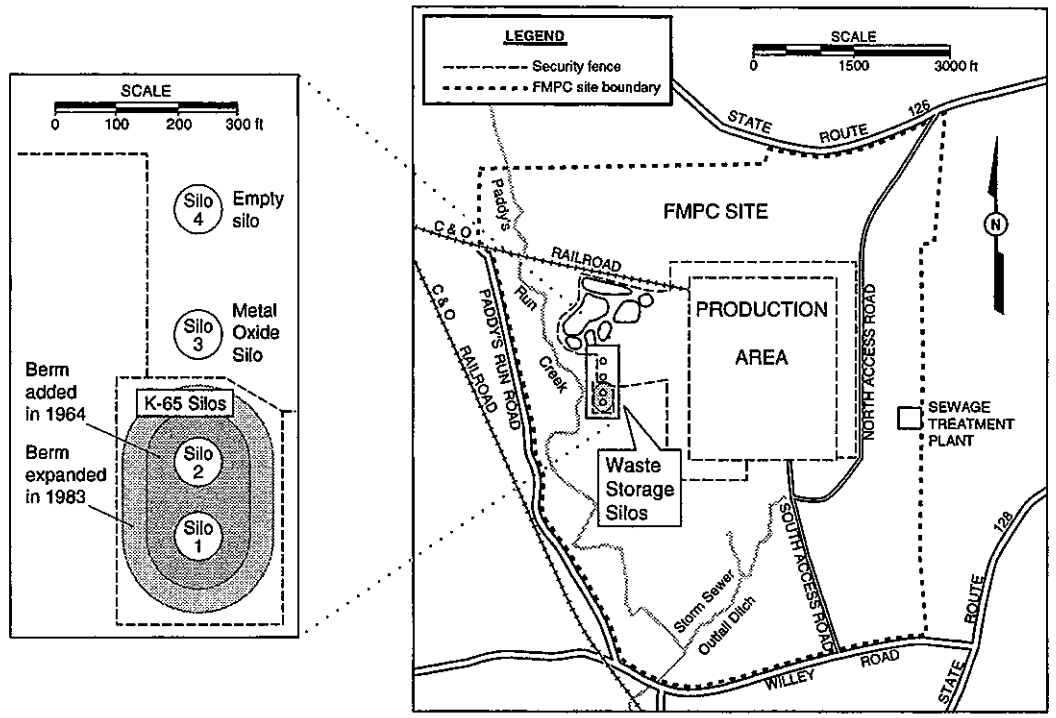

Figure G-1. Locations of the K-65 and metal oxide silos on the FMPC site.

Table G-1. Coordinate Locations of the Waste Storage Silos

	OSP coordinates (ft)		UTM coordinates (m)	
Silo	East	North	East	North
Silo 1 (K-65)	1,378,484	480,400		
Silo 2 (K-65)	1,378,486	480,522		
Center between Silos 1 and 2	1,378,485	480,461	698,648	4,352,217
Silo 3 (metal oxide)	1,378,492	480,730		

Based on changes to the K-65 silos that have occurred over the years, the exposure rate calculations were broken into four major periods: 1952–1958, 1959–April 1964, May 1964–June 1979, and July 1979–1988. The first was an operational period, during which material was being added to the K-65 silos. Thus, for 1952–1958, the quantities of K-65 material in the silos changed each year, and exposure rates were calculated separately for each year. For each of the latter three periods, there were no changes that would significantly impact exposure rates, so calculated exposure rates apply to each year within the period (they differ between periods). The second period (1959–April 1964) was post-operational, but before the berms were added around the K-65 silos. The third (May 1964–June 1979) was a period with the berms in place but before silo dome penetrations were sealed. The last period (July 1979–1988) was after the sealing of dome penetrations.

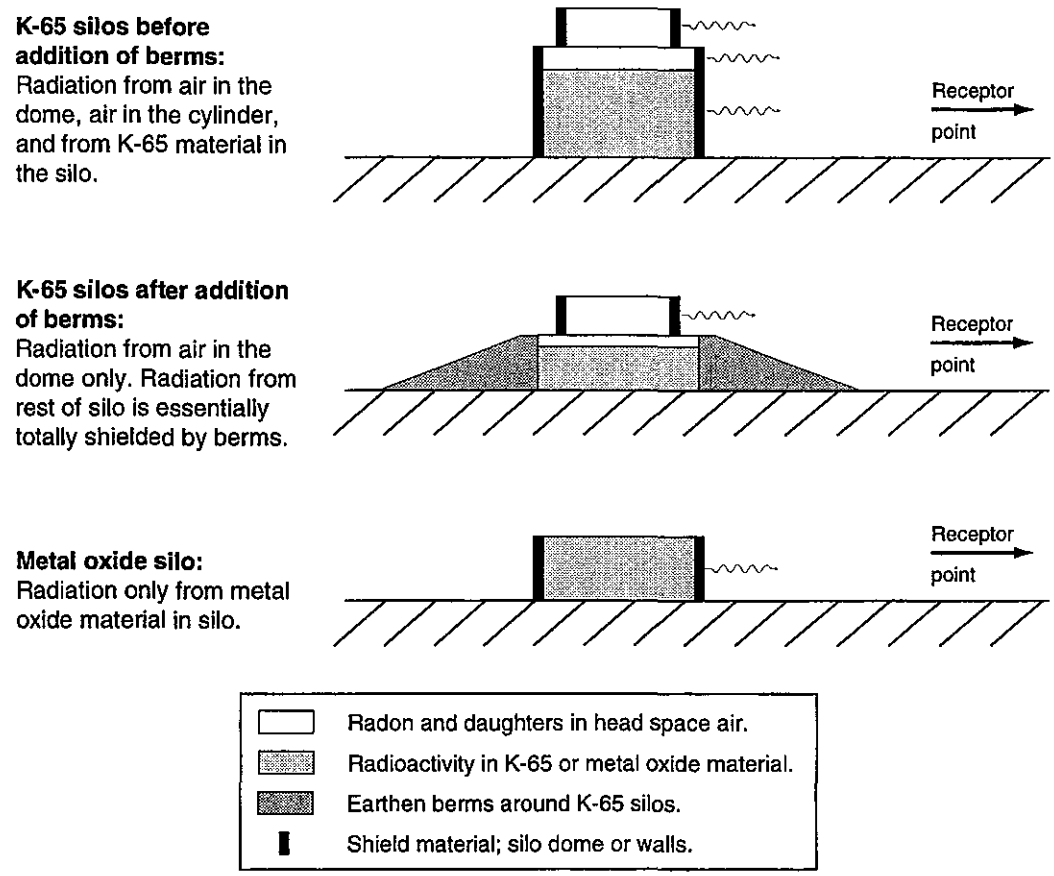

Figure G-2. Source and shield geometry models used to estimate direct exposures from the K-65 and metal oxide silos. As described in the Task 4 report (Killough et al. 1993), we model the two K-65 silos as a single silo, with twice the actual height.

Calculations were first performed for 1959–April 1964, May 1964–June 1979, and July 1979–1988. For each of these periods, calculations were performed separately for the K-65 silos and the metal oxide silo. For 1959–April 1964, the calculations for the K-65 silos were broken into three sources: (1) the K-65 material, (2) ^{222}Rn and daughters in air in the cylinder part of the head space, and (3) ^{222}Rn and daughters in air in the dome part of the head space. For May 1964–June 1979 and July 1979–1988, the calculations for the K-65 silos only required a single source (^{222}Rn and daughters in the dome part of the head space), since the earthen berms (thickness 8 ft and greater) provide essentially total shielding against emissions from the other sources.

For 1952–1958, the general configuration of sources was the same, and radionuclide concentrations were assumed to be the same, as those of 1959–April 1964. The only differences in calculations between these periods were the model heights, and thus total source strengths, used to represent each of the three K-65 silo sources and the Silo 3 source. Thus, exposure rates for each of the years in 1952–1958 were calculated from the exposure rates for 1959–April 1964 along with factors to account for the relative heights of the sources.

The assumption that radionuclide concentrations for 1952–1958 are the same as those for 1959–April 1964 is a simplification. For 1959–April 1964 we used the average concentrations because both Silos 1 and 2 were full. But, for earlier years, Silo 2 would not have been totally full, so the effective concentrations would be closer to those of Silo 1. As an example, the concentrations of ^{226}Ra (the source of the ^{222}Rn) in Silos 1 and 2 deviated from the average ^{226}Ra concentration by less than 30%. Doses to people from the direct radiation from the silos contribute a small fraction of the total doses from FMPC releases. Since the difference in ^{226}Ra concentrations is small, it is reasonable to assume the concentrations for 1959–April 1964 also apply to 1952–1958.

In Appendix J of the Task 2/3 report (Voillequé et al. 1995), we determined source strengths to be used for the three K-65 silo sources for 1952–1958. We assumed the diameters of the sources were constant and calculated model heights, which are proportional to the source strength. These model heights, and relative heights normalized to the heights of 1959–April 1964, are shown in Table G-2. The normalized heights are called $f_{i,j}$, where the indices i and j correspond to the year, from 1952 to 1958, and the different sources, respectively. The filling of Silo 3 was discussed in Appendix J of the Task 2/3 report (Voillequé et al. 1995). In that report, we decided to assume that Silo 3 was full at the time construction was completed in July 1953. Based on this assumption, the values of $f_{i,j}$ for Silo 3 were easily determined and are also shown in Table G-2.

Table G-2. Annual Average Heights Used to Model K-65 Silo Sources and Relative Heights, $f_{i,j}$, of K-65 Silo and Silo 3 Sources

	Heights (ft) of K-65 silo sources[a]			Heights relative to those of 1959 ($f_{i,j}$)			
Year	(j = 1) K-65 material	(j = 2) Air in cylinder	(j = 3) Air in dome	(j = 1) K-65 material	(j = 2) Air in cylinder	(j = 3)Air in dome	(j = 4) Silo 3
1952[b]	4.88	21.8	9.33	0.115	2.02	0.500	0.000
1953	19.5	22.8	14.8	0.457	2.11	0.792	0.500
1954	25.5	27.9	18.66	0.599	2.58	1.00	1.00
1955	29.6	23.8	18.66	0.694	2.21	1.00	1.00
1956	33.6	19.8	18.66	0.790	1.83	1.00	1.00
1957	37.7	15.7	18.66	0.885	1.45	1.00	1.00
1958	41.6	11.8	18.66	0.976	1.09	1.00	1.00
1959	42.6	10.8	18.66	1.00	1.00	1.00	1.00

[a] The K-65 material cylinder represents the K-65 material in the silos. The air in cylinder represents that part of the head space that is in the cylindrical part of the silos. The air in dome represents that part of the head space in the dome part of the silos.

[b] Values for 1952 are not annual averages. They apply only to the period July through December, which is the period of emissions after filling of Silo 1 began.

At the distances from the silos where members of the public might have been exposed, the exposure rate from a given source (of the four: K-65 material, air in cylinder, air in dome, and Silo 3) varies linearly with the source strength. With our model of the sources, the model

height is proportional to the source strength, so the exposure rate from a given source is proportional to the model height. Thus, we calculated the exposure rates for the years 1952–1958 by:

$$\dot{X}_{i,k} = \sum_j f_{i,j} \dot{X}_{1959,j,k} \qquad \text{(G-1)}$$

where the indices i and j are as before, and

k = an index corresponding to distance from the silos

$\dot{X}_{i,k}$ = the total (from the four sources), average exposure rate for year i at distance k from the silos

$\dot{X}_{1959,j,k}$ = the exposure rate for 1959–April 1964 (previously calculated), from source j, at distance k from the silos.

From a map of the FMPC site (WMCO 1989), the minimum distance from the K-65 silos to the site boundary was estimated to be about 330 m. This minimum distance is consistent with the distance from the K-65 silos to the air monitoring station AMS-6, as estimated in the Task 5 report (Shleien et al. 1995). Based on this minimum distance to the site boundary, the exposure rate calculations were performed for distances of 300 to 1000 m, at 25-m intervals. Calculations were also performed for the 330-m distance.

The results of the initial, base calculations for each of the four sources are provided in Table G-3. Table G-4 summarizes results of the calculations for the ten time periods, as exposure rates versus distance from the K-65 silos. The total exposure rates (Table G-4) are sums of the exposure rates for the K-65 silos and Silo 3. The summary results have been rounded to two significant figures. Figure G-3 is a plot of the exposure rates versus distance, for some of the periods. To a distance of 1000 m, the exposure rate curves are close to straight lines on a semi-log plot. Thus, exposure rates for distances greater than 1000 m are calculated using an exponential extrapolation from the data of Table G-4 and Figure G-3. This approach is considered adequate for the very low exposure rates predicted at these greater distances.

CONVERSION OF EXPOSURE RATE TO DOSE RATE

The calculation of dose from gamma exposure is often accomplished using conversion factors to relate exposure to "whole body" dose. However, when these calculations were initiated, the significance of doses from this pathway (direct gamma exposure) was unknown; therefore we desired to calculate organ doses. Our preference would be to proceed directly from exposure rate to organ dose rate, but such conversion factors were not available for the exposure geometry of the scenarios considered. Related conversion factors, for organ dose and effective dose per unit concentration of gamma emissions from the ground surface, were readily available. To use these conversion factors, we first had to convert exposure into effective dose. In addition to this complication, organ doses are dependent not only on the organ, but also on the photon energy. We used reference energy levels, E_l, to represent ranges of photon energies. Thus, the following equation was used to account for organ and energy dependencies in calculating organ dose rates:

$$\dot{H}_T(E_l) = \dot{X}(E_l)\, DCF \left[\frac{H_T}{H_E}\right]_{E_l} \quad \text{(G-2)}$$

where

$\dot{H}_T(E_l)$ = dose rate to organ T (Sv), for photon energy range E_l

$\dot{X}(E_l)$ = exposure rate in air (R h^{-1}), from photons in energy range E_l

DCF = dose conversion factor, to convert from exposure rate in air to effective dose equivalent (Sv R^{-1})

$\left[\frac{H_T}{H_E}\right]_{E_l}$ = ratio of organ dose to effective dose equivalent, from tabulated values.

The total dose rate to an organ (for all photon energies) was then calculated as:

$$\dot{H}_T = \sum_{E_l} \dot{H}_T(E_l) \quad \text{(G-3)}$$

The total organ doses for a scenario are obtained by summing the products of the organ dose rates by the occupancy times and summing over the different periods. The occupancy times are given in the description of the scenarios (Appendix J of this report).

The exposure rates for different photon energies were extracted from the MicroShield results (not shown here). The factor to convert exposure into dose, *DCF*, was taken to be 0.008 Sv R^{-1}, obtained from a report of the International Commission on Radiation Units and Measurements (ICRU 1988). The ratios of organ dose to effective dose equivalent were obtained from Table II.6 (which tabulates organ doses and effective dose from monoenergetic plane sources at the air-ground interface) of the Environmental Protection Agency's *Federal Guidance Report No. 12* (Eckerman and Ryman 1993).

It is acknowledged that the contaminated ground surface geometry differs from the geometry for exposure from the silos. However, it is thought to be a reasonable approximation. For scenario 2, direct exposures from the silos constitute the major source of *external* radiation doses. For all scenarios, the doses from the direct exposures from the silos are much less than doses from inhalation of radon daughters or inhalation of uranium and other particulates. Because the doses from the direct exposures from the silos are relatively small compared to other pathways, we have chosen not to revise the calculational method described above.

Table G-3. Details of Calculated Initial, Base Exposure Rates ($\mu R\ h^{-1}$) from K-65 and Metal Oxide Silo Sources, Versus Distance from the K-65 Silos [a]

	K-65 silos [b]					
Distance (m)	1959–1964 K-65 material	1959–1964 Air in cylinder	1959–1964 Air in dome	1964–1979	1979–1988	Silo 3
300	7.667	1.562	0.8367	0.8367	8.798	0.1048
325	5.699	1.164	0.6236	0.6236	6.556	0.07868
330	5.380	1.099	0.5889	0.5889	6.191	0.07441
350	4.290	0.8773	0.4704	0.4704	4.944	0.05983
375	3.263	0.6683	0.3585	0.3585	3.768	0.04599
400	2.505	0.5137	0.2757	0.2757	2.897	0.03569
425	1.939	0.3980	0.2137	0.2137	2.245	0.02793
450	1.512	0.3105	0.1668	0.1668	1.752	0.02202
475	1.186	0.2438	0.1310	0.1310	1.376	0.01748
500	0.9363	0.1925	0.1035	0.1035	1.087	0.01396
525	0.7427	0.1528	0.08215	0.08215	0.8628	0.01120
550	0.5920	0.1218	0.06552	0.06552	0.6881	0.009038
575	0.4739	0.09753	0.05248	0.05248	0.5511	0.007324
600	0.3809	0.07839	0.04220	0.04220	0.4431	0.005960
625	0.3072	0.06323	0.03405	0.03405	0.3576	0.004869
650	0.2486	0.05118	0.02757	0.02757	0.2895	0.003992
675	0.2018	0.04155	0.02239	0.02239	0.2351	0.003283
700	0.1643	0.03382	0.01823	0.01823	0.1914	0.002709
725	0.1341	0.02761	0.01489	0.01489	0.1563	0.002241
750	0.1097	0.02259	0.01218	0.01218	0.1279	0.001859
775	0.08996	0.01853	0.009994	0.009994	0.1049	0.001546
800	0.07393	0.01523	0.008215	0.008215	0.08625	0.001289
825	0.06087	0.01254	0.006766	0.006766	0.07103	0.001077
850	0.05021	0.01035	0.005583	0.005583	0.05861	0.0009016
875	0.04149	0.008555	0.004614	0.004614	0.04844	0.0007563
900	0.03434	0.007083	0.003820	0.003820	0.04010	0.0006356
925	0.02847	0.005873	0.003167	0.003167	0.03325	0.0005351
950	0.02363	0.004877	0.002629	0.002629	0.02760	0.0004513
975	0.01964	0.004055	0.002186	0.002186	0.02295	0.0003812
1000	0.01635	0.003376	0.001820	0.001820	0.01910	0.0003224

[a] The individual results shown are taken directly from the MicroShield computations. The significant figures shown in the total values are only used for intermediate calculations and do not imply this degree of certainty in the results.

[b] For 1959–1964, the three sources for the K-65 silos are the K-65 material, ^{222}Rn and daughters in the cylindrical part of the silo head space (air in cylinder), and ^{222}Rn and daughters in the dome part of the silo head space (air in dome). The time periods given are nominal only; exact periods are given in the text.

Table G-4. Calculated Average Exposure Rates from Direct Radiation from K-65 and Metal Oxide Silos, Versus Distance from K-65 Silos

Distance (m)	Exposure rate ($\mu R\ h^{-1}$) for period									
	Jul–Dec 1952	1953	1954	1955	1956	1957	1958	1959–Apr 1964	May 1964–Jun 1979	Jul 1979–1988
300	4.5	7.5	9.6	9.7	9.9	10.	10.	10.	0.94	8.9
325	3.3	5.6	7.1	7.2	7.3	7.4	7.5	7.6	0.70	6.6
330	3.1	5.3	6.7	6.8	6.9	7.0	7.1	7.1	0.66	6.3
350	2.5	4.2	5.4	5.4	5.5	5.6	5.7	5.7	0.53	5.0
375	1.9	3.2	4.1	4.1	4.2	4.3	4.3	4.3	0.40	3.8
400	1.5	2.5	3.1	3.2	3.2	3.3	3.3	3.3	0.31	2.9
425	1.1	1.9	2.4	2.5	2.5	2.5	2.6	2.6	0.24	2.3
450	0.88	1.5	1.9	1.9	2.0	2.0	2.0	2.0	0.19	1.8
475	0.69	1.2	1.5	1.5	1.5	1.6	1.6	1.6	0.15	1.4
500	0.55	0.92	1.2	1.2	1.2	1.2	1.2	1.2	0.12	1.1
525	0.43	0.73	0.93	0.95	0.96	0.97	0.99	0.99	0.093	0.87
550	0.35	0.58	0.74	0.75	0.76	0.78	0.79	0.79	0.075	0.70
575	0.28	0.47	0.60	0.60	0.61	0.62	0.63	0.63	0.060	0.56
600	0.22	0.38	0.48	0.49	0.49	0.50	0.51	0.51	0.048	0.45
625	0.18	0.30	0.39	0.39	0.40	0.40	0.41	0.41	0.039	0.36
650	0.15	0.25	0.31	0.32	0.32	0.33	0.33	0.33	0.032	0.29
675	0.12	0.20	0.25	0.26	0.26	0.26	0.27	0.27	0.026	0.24
700	0.096	0.16	0.21	0.21	0.21	0.22	0.22	0.22	0.021	0.19
725	0.079	0.13	0.17	0.17	0.17	0.18	0.18	0.18	0.017	0.16
750	0.064	0.11	0.14	0.14	0.14	0.14	0.15	0.15	0.014	0.13
775	0.053	0.089	0.11	0.11	0.12	0.12	0.12	0.12	0.012	0.11
800	0.043	0.073	0.093	0.094	0.096	0.097	0.098	0.099	0.0095	0.088
825	0.036	0.060	0.077	0.078	0.079	0.080	0.081	0.081	0.0078	0.072
850	0.029	0.050	0.063	0.064	0.065	0.066	0.067	0.067	0.0065	0.060
875	0.024	0.041	0.052	0.053	0.054	0.055	0.055	0.055	0.0054	0.049
900	0.020	0.034	0.043	0.044	0.045	0.045	0.046	0.046	0.0045	0.041
925	0.017	0.028	0.036	0.036	0.037	0.037	0.038	0.038	0.0037	0.034
950	0.014	0.023	0.030	0.030	0.031	0.031	0.031	0.032	0.0031	0.028
975	0.012	0.019	0.025	0.025	0.025	0.026	0.026	0.026	0.0026	0.023
1000	0.0096	0.016	0.021	0.021	0.021	0.022	0.022	0.022	0.0021	0.019

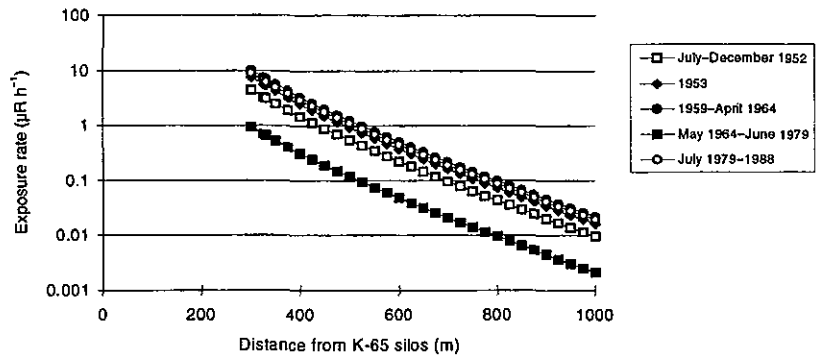

Figure G-3. Calculated exposure rates from direct radiation from the K-65 and metal oxide silos, for some periods of interest, versus distance from the K-65 silos.

REFERENCES

Eckerman K.F. and J.C. Ryman. 1993. *Federal Guidance Report No. 12, External Exposure to Radionuclides in Air, Water, and Soil, Exposure-to-Dose Coefficients for General Application, Based on the 1987 Federal Radiation Protection Guidance*. Report EPA 402-R-93-081, Oak Ridge National Laboratory, Oak Ridge, Tennessee.

ICRU (International Commission on Radiation Units and Measurements). 1988. *Determination of Dose from External Radiation Sources—Part 2*. ICRU Report 43, ICRU, Bethesda, Maryland.

Killough G.G., M.J. Case, K.R. Meyer, R.E. Moore, J.F. Rogers, S.K. Rope, D.W. Schmidt, B. Shleien, J.E. Till, and P.G. Voillequé. 1993. *The Fernald Dosimetry Reconstruction Project, Task 4, Environmental Pathways — Models and Validation*. Draft report for comment, dated March 1993. RAC Report CDC-3, Radiological Assessments Corporation, Neeses, South Carolina.

Negin C.A. and G. Worku. 1992. *MicroShield, Version 4, User's Manual*. Report Grove 92-2, Grove Engineering, Inc., 15215 Shady Grove Road, Suite 200, Rockville, Maryland 20850.

Shleien B., S.K. Rope, M.J. Case, G.G. Killough, K.R. Meyer, R.E. Moore, D.W. Schmidt, J.E. Till, and P.G. Voillequé. 1995. *The Fernald Dosimetry Reconstruction Project, Task 5. Review of Historic Data and Assessments for the FMPC*. RAC Report CDC-4, Radiological Assessments Corporation, Neeses, South Carolina.

USGS (U.S. Geological Survey). 1985. *PLANE-PC Interactive Grid Coordinate Conversion for Personal Computers, Users Manual*. USGS, National Mapping Division, Reston, Virginia.

Voillequé P.G., K.R. Meyer, D.W. Schmidt, S.K. Rope, G.G. Killough, M. Case, R.E. Moore, B. Shleien, and J.E. Till. 1995. *The Fernald Dosimetry Reconstruction Project, Tasks 2 and 3, Radionuclide Source Terms And Uncertainties*. RAC Report CDC-5, Radiological Assessments Corporation, Neeses, South Carolina.

WMCO (Westinghouse Materials Company of Ohio). 1989. *Feed Materials Production Center*. Map of the FMPC site and immediate surroundings, dated June 27, 1989, WMCO, Cincinnati, Ohio.

APPENDIX H

PARTICLE SIZE DISTRIBUTIONS FOR DUST COLLECTORS

INTRODUCTION

The distributions of particle size in releases of particulate radioactive material from the Feed Materials Production Center (FMPC) are important in two respects for estimating transport and radiation dose. First, atmospheric deposition processes are sensitive to particle aerodynamic properties determined by size, shape, and density, and thus successful estimation of the rate of depletion of the plume depends on making reasonable assumptions about these distributions. Second, our use of the respiratory model of the International Commission on Radiological Protection (ICRP) requires the assumption of a distribution of aerodynamic diameters appropriate to the material.

In 1985, FMPC and subcontractor Northern Kentucky Environmental Services (NKES) performed sampling operations on the inlet and outlet ducts of 16 dust collectors. Uranium particle-size distributions and isotopic fractions for these samples are presented by Boback et al. (1987), by NKES in an unpublished report (Reed 1985), and in the original data sheets. These data provide essentially all of the usable information on distributions of particle size in FMPC stacks fitted with dust collectors that has come to light, and this information has been taken as the basis of generic representations of particle size in the source term for purposes of transport simulation and dose reconstruction.

For dust collectors that were sampled in the 1985 study, we assumed that the particle size distribution determined from the sample was representative of that emission source over time. For unsampled dust collectors, generic estimates were assembled from averages of distributions from sampled dust collectors.

The Task 2/3 report (Voillequé et al. 1995) shows data and plots of particle size distributions that were based directly on the data from the eight-stage Andersen Mark III cascade impactor that was used in the 1985 study. Rather than making the prior assumption that all particle size distributions were lognormal, we fitted cubic polynomials to the log-probability–transformed cumulative sampler data in order to represent the distributions by continuous functions for further calculations. This approach accommodates reasonably-behaved curvilinear (including bimodal) distributions, as well as lognormal distributions. Similar procedures for fitting particle size data have been used since the 1950s (DallaValle et al. 1951). We also accepted the sampler data at face value, which is to say that we did not consider possible distortion of the distribution of particles that entered the sampler.

In the peer review process for the Task 2/3 and the Task 4 (Killough et al. 1993) reports, questions were raised about this approach. It was suggested that (1) all of the particle size distributions should be assumed lognormal, and therefore the curvilinear representations of the distributions should be abandoned in favor of linear fits, and (2) the question of possible distortion of the input distribution by the sampler should be investigated.

Each of these questions has been considered carefully. We have examined the properties of the Andersen Mark III cascade impactor, and we have developed a simulation of the instrument

to study its potential for distorting the sampled distribution. We have found no reason to alter our approach to representing particle size distributions. This appendix first summarizes the method of representation of the particle size distributions, which is reported in detail in Appendix F of the Task 2/3 report. Then it provides some perspective for the dependence of dose on particle size distributions. Finally, it describes the computer simulation of the sampler and shows examples of the results.

PARTICLE SIZE SAMPLING AND REPRESENTATION OF DISTRIBUTIONS

A particle is treated mathematically as a sphere that has the mass and density of the particle. The equivalent diameter of the particle is the diameter of its representative sphere. Each measured diameter is expressed as an (equivalent) aerodynamic diameter, which by definition is the diameter of a sphere of unit density (ρ = 1 g cm^{-3}) that has the same gravitational settling velocity as the particle. Physical diameter is approximately equal to equivalent aerodynamic diameter divided by the square root of the density (expressed in units of g cm^{-3}) of the particular compound of uranium. This approximation is adequate for diameters in the ranges considered in this study. By using aerodynamic diameters, one may eliminate the particle density as a parameter in the particle size distribution.

Sixteen dust collectors were sampled in the 1985 NKES study, in both the inlet and outlet ducts, giving two distributions per dust collector. The result of each sampling operation can be represented as a table of eight aerodynamic diameters with corresponding cumulative mass fractions. A complete presentation of the curves and data is given in Appendix F of the Task 2/3 report. As an example, we show the two distributions for dust collector G4-5 in Figure H-1 and the numeric data in Table H-1. In the log-probability plot of Figure H-1, the plotted points represent the sampler data. The curves are mass distributions that were fitted to the sampler data by methods described in detail in Appendix F of the Task 2/3 report.

The fitted curves are cubic polynomials, and the data to which they are fitted have been transformed to log-probability space. The fitting process has to be constrained to ensure that the resulting curves are monotonically increasing, as cumulative distributions must be. Otherwise, in a few cases, the solution does not provide a distribution function. The constraint makes the formulation nonlinear, and an iterative method is used for determining the polynomial coefficients. The details are given in Appendix F of the Task 2/3 report. The analytic form of these distribution functions makes it possible to compute various quantities needed in transport and dose calculations, such as how much uranium from a particular dust collector was in aerodynamic diameters between 1 and 5 μm, or what particle diameter is the 95th percentile of the distribution. It is usually necessary to partition a distribution into ranges of particle size and compute a representative dose conversion factor for each size range (see Appendix I, Figure I-6). Similar ranges of particle sizes are used in estimating representative deposition velocities for removal of uranium particles from an airborne plume (Appendix G of the Task 4 report).

If the points in the sample tend to lie on a straight line in a log-probability plot, the cubic polynomial will simplify to linear form (or nearly so). In such cases, the fitted straight-line distribution is lognormal. The suggestion has been made that many, if not all, of the fitted distributions could be adequately represented by lognormal distributions for purposes of dose

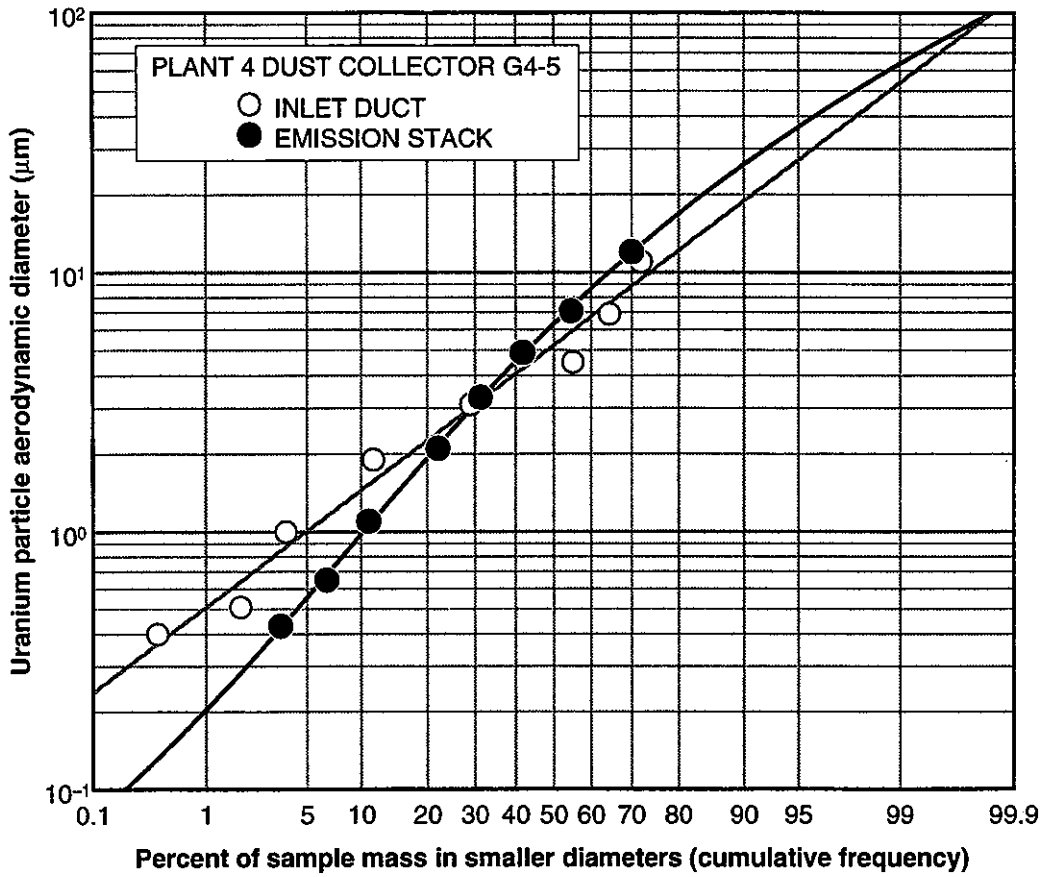

Figure H-1. Cascade impactor data and fitted mass distributions for dust collector G4-5. The curves are constrained cubic polynomials fitted to log-probability data. In this case, both distributions are nearly lognormal.

Table H-1. Cascade Impactor Data for Dust Collector G4-5

Inlet duct		Emission stack	
Aerodynamic Diameter (μm)	Cumulative mass fraction	Aerodynamic Diameter (μm)	Cumulative mass fraction
11.	0.722	12.	0.700
6.9	0.646	7.1	0.546
4.5	0.551	4.9	0.418
3.1	0.290	3.3	0.313
1.9	0.115	2.1	0.220
1	0.037	1.1	0.109
0.51	0.018	0.65	0.065
0.4	0.004	0.43	0.034

estimation. This may be true, provided the lognormal distribution approximates the middle part and upper tail of the curve, but one first has to determine the curve before such an approximation can be made. The plots in Appendix F of the Task 2/3 report show that the impactor data give little or no information above the 50th percentile of the mass. We see no particular reason to prefer the lognormal distribution in these calculations involving particle sizes.

When we first examined the sampler data from the 1985 NKES study, we fitted lognormal distributions to the data as a matter of course, but a critical examination of the plots revealed some cases in which the lognormal distribution was obviously not an appropriate representation of the data (whether the data were properly representative of the distribution taken in by the sampler is a separate question). Figure H-2 shows the most extreme example, the emission stack of dust collector G5-249, but there were others for which the data showed a strong curvilinear trend in the log-probability plots. Such poor representation of the data by lognormal distributions for some of the samples led to our formulation of the constrained cubic polynomial procedure for fitting the cascade impactor data. Figure H-2 displays a constrained cubic polynomial fit to the same impactor data.

Knutson and Lioy (1989) discourage the routine assumption of lognormality for particle size data: "The authors are of the opinion that the lognormal distribution has been overused. The availability of log probability graph paper, the shortcut method of finding the geometric mean and standard deviation, and the Hatch-Choate equations add up to a powerful incentive to force data into a lognormal mold. This is acceptable for a cursory, first-cut look at data, but in many cases, a second look will show that there are significant departures from lognormality." Such departures are quite obvious in the FMPC cascade impactor data.

DEPENDENCE OF DOSE ON PARTICLE SIZE DISTRIBUTION

It is easy to attatch too much significance to the exact form of particle size distributions and its effect on radiation dose from the inhaled particles. Early in this study we made some calculations for natural uranium of respiratory solubility class Y, i.e., a relatively insoluble form that would be cleared from the lungs over a period of years (Appendix I).

The calculations are best summarized by Figure H-3, which shows annual dose in an environment with a constant concentration of 1 mg U m^{-3} plotted against median particle aerodynamic diameter (μm). Each plotted point represents the annual dose for a distribution having the median aerodynamic diameter given by the point's horizontal coordinate. The points represent the particle size distributions for the inlet ducts of the 16 sampled dust collectors. Vertical variation of points with the same median is due to the effects of different forms of particle size distribution.

The curves in Figure H-3 are for two extremes of the lognormal distribution. A monodisperse aerosol has all particles of the same size, and its median is that common size. This is a degenerate form of the lognormal distribution with geometric standard deviation (GSD) equal to 1. The other extreme (as far as dosimetry is usually concerned) is given by lognormal distributions with GSD = 5, which is greater than the maximum (4.5) normally considered by the lung model of the International Commission on Radiological Protection (ICRP 1979).

The lognormal curves in Figure H-3 indicate a strong decreasing dependence of dose on

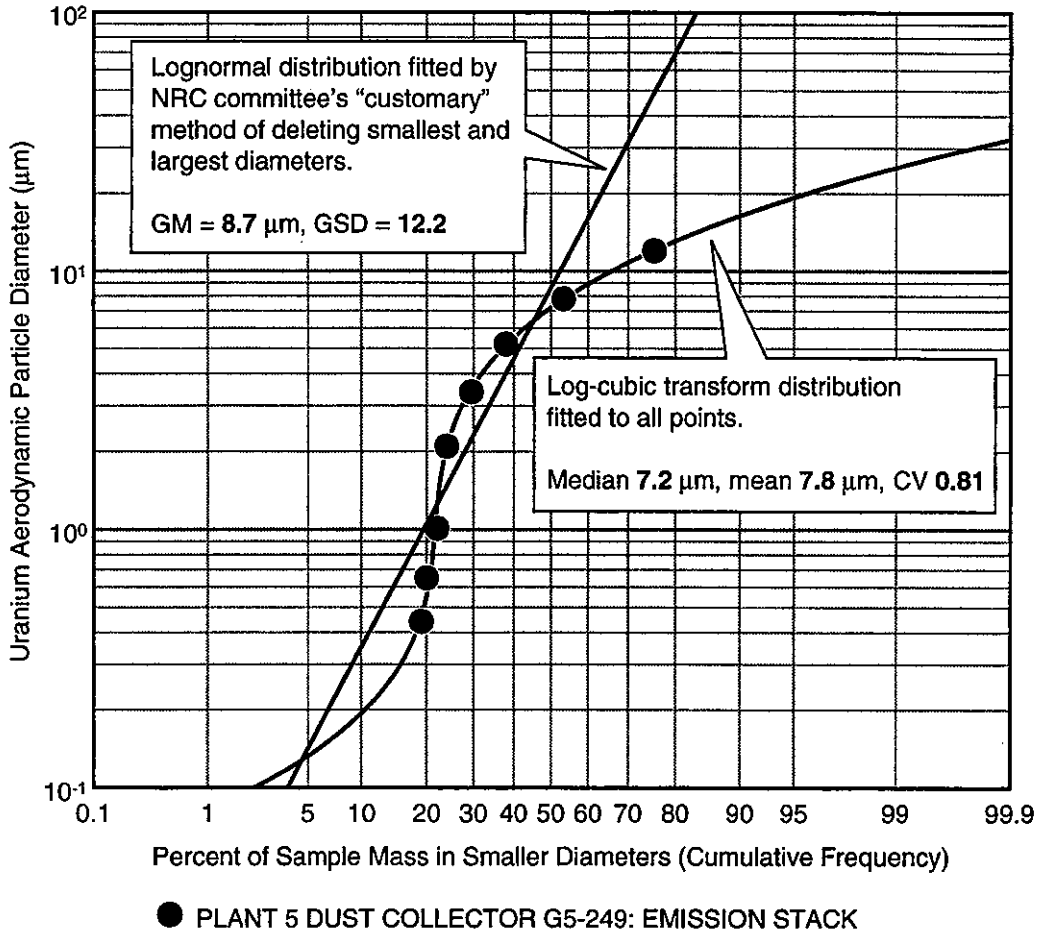

Figure H-2. An extreme example of a lognormal distribution fitted to cascade impactor sampler data from dust collector G5-249 (emission stack). The lognormal line was fitted by a standard handbook method that recommends disregarding the data for the first and last stages and fitting the best straight line (in the sense of least squares) to the remaining points (Cheremisinoff and Morresi 1978). For comparison, a constrained cubic polynomial is fitted to the same log-probability data.

increasing aerodynamic diameter, with nearly an order of magnitude of dose discrepancy between the dust collectors with the smallest and largest median aerodynamic diameters. But for any given median aerodynamic diameter, the vertical extent of variation is less impressive — about a factor of two for the largest of the observed medians (i.e., the vertical discrepancy between the monodisperse and lognormal curves for those medians). But the component of dose for these large particles is much lower than for smaller particles. And most of the release was in median aerodynamic diameters between 5 and 15 μm (clustered points).

Figure H-3 is a fairly comprehensive summary of the importance of not only median particle aerodynamic diameter, but also the form of the distribution, for releases of uranium from the FMPC. This figure lends some perspective about the extent to which the subject needs to be pursued.

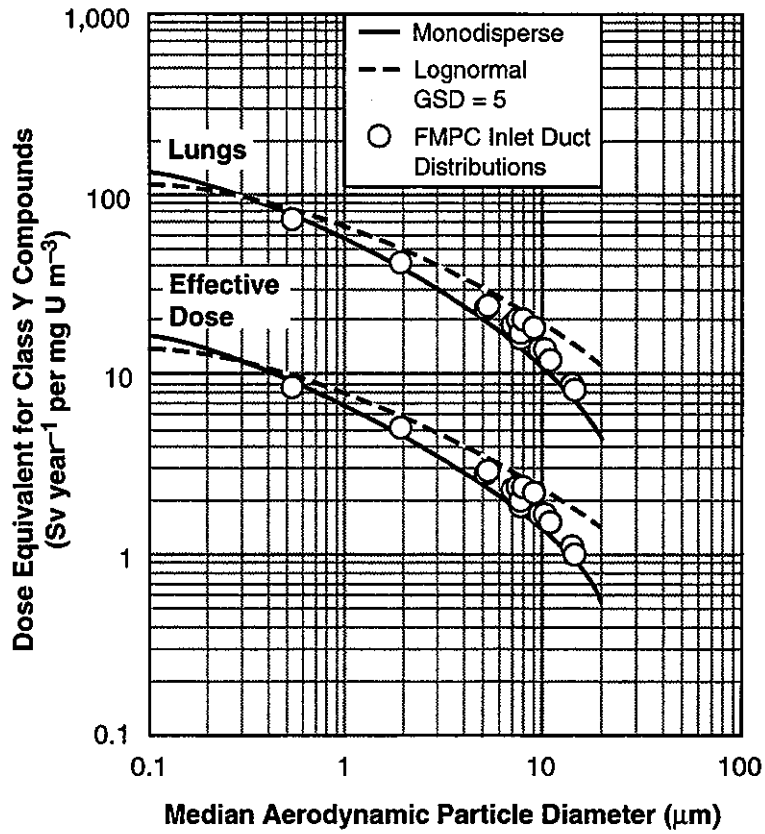

Figure H-3. Annual inhalation dose for the lungs and effective dose for class Y natural uranium. The plotted points represent the measured distributions of particle aerodynamic diameter in the inlet ducts of the FMPC dust collectors. The measured distributions were, in general, not lognormal. The curves represent a monodisperse aerosol (degenerate lognormal distribution with GSD = 1) and a lognormal distribution with GSD = 5.

RELATIONSHIP OF A DISTRIBUTION TO ITS CASCADE IMPACTOR DATA

In the introduction, we alluded to the question of the adequacy of the impactor data for representing the sampled distribution. It is obvious that an essentially continuous mass distribution of particle aerodynamic diameters loses much of its information when it is transformed by a cascade impactor into eight data points, such as the datasets we have shown in Table H-1. But if reasonably smooth distributions were consistently found to be transformed into discrete points that lay near the distribution curves, we would be encouraged by the representation, and the displacement of the points from the distribution curve that produced them would be a measure of the instrument's distortion (Figure H-4).

The inverse calculation — i.e., given the eight points, calculating the distribution curve that would produce them when sampled by the cascade impactor — is a currently active area of research. Its solution is not unique until certain constraints are imposed. The classical algorithm is due to Twomey (1975). Adaptations of the method have been developed by Markowski (1987) and Winklmayr et al. (1990). Crump and Seinfeld (1982) apply functional analysis to

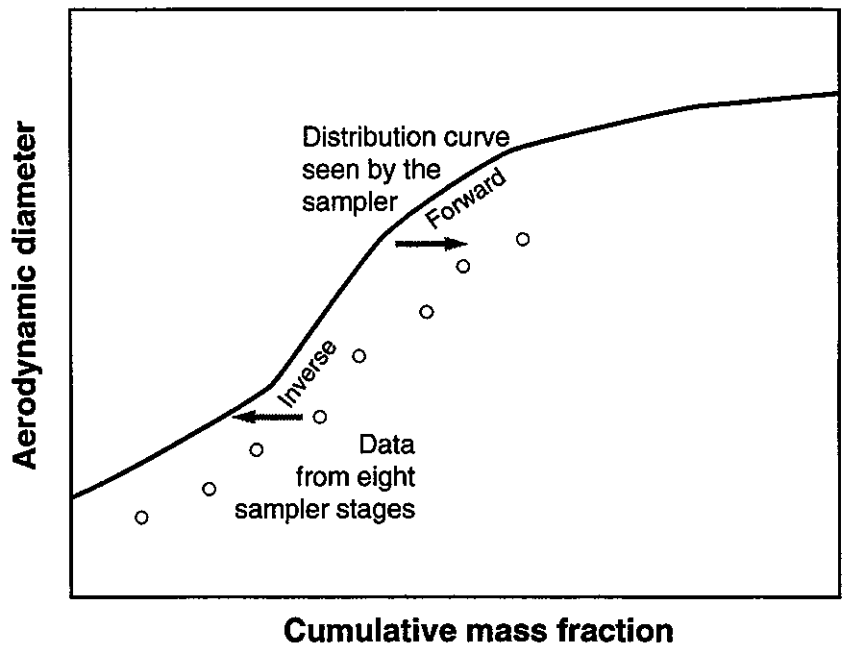

Figure H-4. Schematic portrayal of the relationship of a particle size distribution curve and the data that result from sampling the distribution with an eight-stage cascade impactor. Sampling the distribution constitutes a forward transformation. Inferring the distribution curve from the eight data points is an inverse transformation. The displacement of the points from the curve is a measure of distortion by the instrument.

constrain solutions. These citations represent only a sampling of the relatively recent activity in this field.

If significant distortion were found to exist in the discrete representation of the sampled distribution (i.e., the eight data points), then an appropriate course of action would be to apply the inverse calculation to each set of impactor data. If there is no significant distortion, however, an acceptable distribution fitted to the data is all that is required.

To investigate this question, we have developed a computer simulation of the eight-stage Andersen Mark III cascade impactor, using literature from the manufacturer, efficiency curves from the literature, and basic aerosol physics. Using the simulation program with the fitted inlet duct curves from Appendix F of the Task 2/3 report, we have produced graphical estimates of the displacement of the estimated data points (which we plotted along with the actual data). Sample results are shown in the next section. We devote the remainder of this section to a summary of the simulation program.

In each of the eight sequentially arranged stages of the impactor, the airstream carrying the particles is forced through jets and against collection plates that are perpendicular to the direction of flow. The airstream is forced around each plate, and particles either are able to follow the sharp turn in the airflow or are captured by the plate, according to the inertial properties of the particles and characteristics of the airflow. Larger particles tend to be forced out of the airstream and deposit on the plates. The particles that escape one plate are carried on to the next stage, or to a backup filter after the last stage (Figure H-5). The instrument

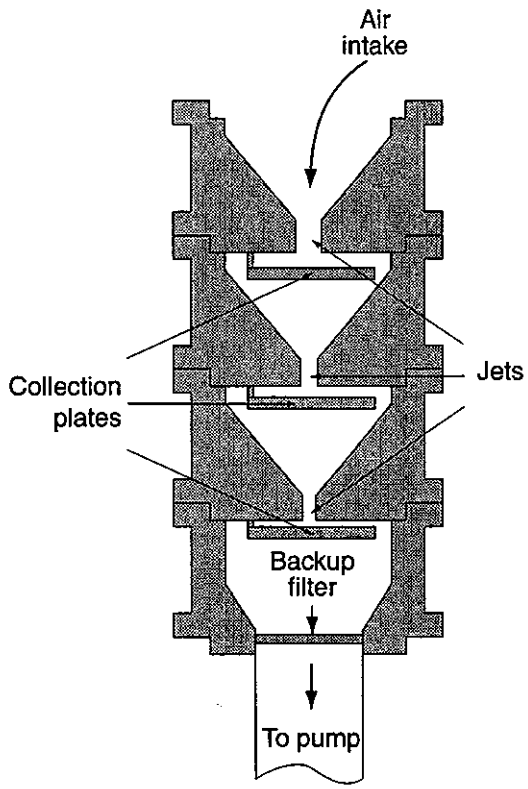

Figure H-5. Schematic of a hypothetical three-stage cascade impactor. At each stage, the particle-bearing airstream is forced through a jet and deflected by a collection plate. Larger particles are forced out of the airstream by their inertia and are captured. Smaller particles move around the plate with the airflow and to the next stage or to the backup filter after the last stage. The largest particles are captured by the earliest stages. The smaller diameters of the jets of later stages produce higher velocities, which increase the probability of capturing smaller particles. The Andersen Mark III cascade impactor differs from this illustrative schematic in two ways: it has eight stages rather than three, and each stage has multiple jets.

is designed in such a way that the characteristics of the airflow are different at each stage, with earlier stages trapping the largest particles and the last stages collecting the smallest particles. The efficiency of each stage for trapping particles of different aerodynamic diameters is represented by a curve showing the cumulative percentage as a function of aerodynamic diameter. The eight efficiency curves characterize the sampler. The efficiency curves change in response to the jet velocities, which depend on the airflow rate through the sampler. The curves also depend to a lesser extent on air viscosity, density, temperature, and pressure.

The aerodynamic diameter corresponding to 50% efficiency for a stage is the cutpoint diameter D_{50}. This is the diameter that is associated with the data point for the stage. The design ideal would be an efficiency curve that captures all particles of aerodynamic diameter greater than D_{50} and passes all smaller particles. Such a design, however, is unattainable, and the real efficiency curves are of sigmoid shape (Figure H-6), implying that some particles larger than the cutpoint diameter will pass the stage and (less frequently) some smaller particles will be trapped by the stage's collection plate.

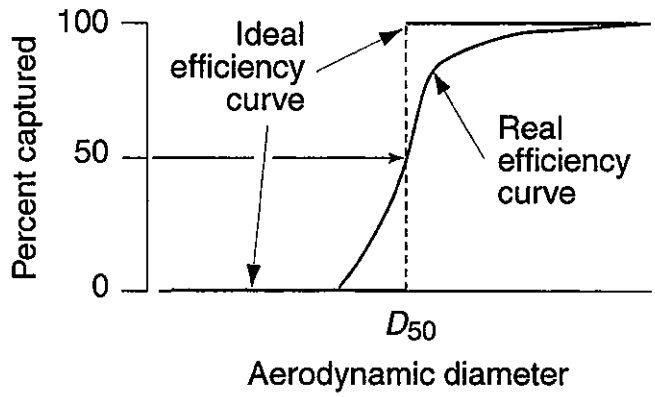

Figure H-6. Real and ideal efficiency curves for a cascade impactor stage. Each curve represents a function of aerodynamic diameter, and its value is the probability of capture of a particle of the given aerodynamic diameter. The most accurate measurement would be provided by a stage that would capture all particles larger than cut diameter D_{50} and pass all smaller particles through to the next stage. Real efficiency curves have a sigmoid shape.

When the efficiency curves are known for a given airflow, it is simple in principle to use the efficiency curves to estimate the proportions of particles of a given aerodynamic diameter that would be captured by each stage. When this calculation is repeated for particles of different aerodynamic diameters and the partitioning for each aerodynamic diameter D is weighted in proportion to the abundance of size-D particles in the input distribution, the result is a simulation of the sampler. The proportion of size-D particles captured by stage s of the sampler is

$$\alpha(D) \cdot p_s(D) = \alpha(D) \cdot E_s(D)\big(1 - E_{s-1}(D)\big) \cdots \big(1 - E_1(D)\big) \qquad \text{(H-1)}$$

where $\alpha(D)$ is the relative abundance of size-D particles in the input to the sampler, $p_s(D)$ is the fraction of size-D particles reaching the sampler that are trapped by stage s, and $E_s(D)$ is the fractional efficiency of stage s for size-D particles (taken from the efficiency curve for stage s). Summing or integrating Equation H-1 over all particle aerodynamic diameters D gives (for this application) the fractional mass of uranium captured by stage s of the simulated sampler. The sum of the eight fractions is generally less than 1, and the remainder is assigned to the backup filter. A table of cumulative fractions and the corresponding 50% cut aerodynamic diameters for the simulated airflow is the result (such tables for the real sampler are shown in Table H-1; the differences in aerodynamic diameters for the inlet duct and the emission stack are due to differences in the airflow through the sampler).

To program the simulation, we digitized theoretical efficiency curves from Figure 7 of Marple and Liu (1974). These curves were given for different flow regimes characterized by different values of the Reynolds number Re. We interpolated between curves corresponding to different Reynolds numbers to obtain appropriate efficiencies for the flow regime we were simulating. The Reynolds number is defined as

$$\mathrm{Re} = \rho_{\mathrm{air}} V W / \mu, \qquad \text{(H-2)}$$

where ρ_{air} is the density of the air (g cm^{-3}), V is the mean velocity of air in the jet (cm s^{-1}), W

is the jet diameter (cm), and μ is the viscosity of the air (g cm^{-1} s^{-1}). The efficiency curves are steeper for higher Reynolds numbers, corresponding to improved collection efficiency.

Descriptive literature from Andersen Samplers, Incorporated, provided jet dimensions and jet velocities for a standard volume airflow rate (from which the Reynolds number for a particular flow rate could be calculated) and a table of cutpoint diameters for all stages for airflows ranging from 0.1 to 0.75 ft^3 min^{-1}. Recorded cutpoint diameters from the 1985 NKES study at the FMPC varied slightly, in inconsistent ways, from the tabulated values. We assume that these small discrepancies resulted from an alternative method of estimating the cutpoint diameters. In any case, we believe the correlation of those calculated cutpoint diameters with the tabulated values that we used is adequate for our present purpose.

A point of concern in an analysis of this kind is particle bounce, which occurs when some of the particles that strike a collection plate do not adhere but are reentrained into the airflow. It is possible that some of these particles will be captured by a subsequent stage. Otherwise, they are trapped by the backup filter, and the cumulative fractions for all stages are increased. When particle bounce occurs, distorted efficiency curves are effectively being substituted for the theoretical curves on which the analysis is based.

Particle bounce is affected by the type of collection surface presented by the collection plates. A notation in the report of Reed (1985) indicates that dried fiberglass filters were employed as collection substrates. This type of medium is said to diminish particle bounce, but not to eliminate it altogether. Hering (1989) reprints a figure that indicates a maximum of about 75% efficiency (compared with 100% for the theoretical curve) for collection of solid polystyrene latex particles on fiber filter media in a single-jet impactor experiment. In addition, a fraction of the airstream flows through this type of substrate and is filtered by it; the result is that the efficiency curves derived from impactor theory no longer govern the process. The effect of this phenomenon would be some apparent shifting of the mass distribution toward smaller particles, as some of the larger ones that are preferentially affected are trapped on later stages of the device or by the backup filter. The result would tend toward underestimation of median particle diameters and overestimation of dose to the lungs for insoluble materials. We do not know the extent to which particle bounce might have influenced the results of the FMPC sampling, but we are not inclined to assume the worst case. It is possible that the sampled particles had better adhesion properties than the latex particles used in the experiment. It is also possible (although we are unable to verify it) that experimental calibration was used in the NKES study at the FMPC; such calibration would tend to compensate for the effects of particle bounce. Nonetheless, the reader must keep in mind that our results assume a sampler that is governed by the theoretical efficiency curves.

Another question comes up in connection with discontinuous particle size distributions. An extreme example is a mixture of two monodisperse aerosols having different aerodynamic diameters (the cumulative distribution function of such a distribution is discontinuous at each of the two diameters). If the aerosol aerodynamic diameters are within the range of cutpoint aerodynamic diameters of the sampler and are separated by at least one cutpoint diameter, our method would lead to an approximating continuous bimodal distribution whose cumulative distribution function would show sharp increases at the two discontinuities. The consequences for dose estimation would be minor. The case of more than two discontinuities in the sampled distribution (e.g., a mixture of three or more monodisperse aerosols) is less easily analyzed,

because the constrained polynomials cannot represent a frequency function with three or more modes (relative maximum points). We see no anomalies in the impactor data that lead us to suspect peculiar distributions of the latter sort, but we cannot rule them out unequivocally. Even so, it is not obvious to us that physically possible examples can be constructed of distributions for which our method would be grossly misleading with respect to dose.

RESULTS

For all 16 sampled dust collectors, our analysis with the cascade impactor simulation indicates distortions of negligible magnitude for purposes of dosimetry. In every case, the simulated data points closely approximate the distribution curve from which they were derived. This result reassures us that accepting at face value the sample points from the 1985 NKES study is a reasonable procedure for drawing conclusions about the form of the sampled distribution. It says nothing, of course, about the relationship of the distribution at the time of sampling with comparable distributions over time. And it does not assess possible effects of particle bounce. But it does strongly suggest, for example, that a curvilinear trend in a set of sample points is not the cascade impactor's distortion of an essentially lognormal distribution.

We show the results of the simulation for three of the sampled inlet ducts in Figures H-7, H-8, and H-9. In each figure, the curve is the constrained polynomial fit to the sampler data, which are shown as white-filled points. The black-filled points are the simulated cascade impactor data for the curve. The slight discrepancies between the cutpoint diameters for the sampling data and simulated points are apparent in the figures. These discrepancies were noted in the previous section and are possibly the result of the use of some alternative calculation or nomogram, instead of the table in the instrument manufacturer's literature. The unknown sampled distribution may have been less smooth than the fitted curve and may have differed from it to some degree in the upper tail, but it is unlikely to have deviated substantially from the fitted curve in the range of the data (barring unexpected influence of particle bounce), and the difference would have little effect on dose estimates. The three plotted examples represent a range of distribution types, from nearly lognormal to bimodal. One example is strongly weighted to smaller particle sizes. In each of these cases, these essential characteristics are very likely to have been present in the respective sampled distributions. Behavior of the distribution beyond the range of the data, of course, cannot be accounted for except by extrapolation, but the upper tail represents particles that approach and exceed non-respirable sizes and is of relatively little consequence for dosimetry.

CONCLUSIONS

The 16 measured inlet ducts of FMPC dust collectors have been used for calculations of deposition and dose. This appendix reviews questions of the sensitivity of the dose calculations to median particle aerodynamic diameter and the form of particle size distributions. It also examines possible distortions of the form of a particle size distribution measured by a cascade impactor of the type used in the 1985 NKES study at the FMPC. We draw the following conclusions:

(1) The median aerodynamic diameter is of much greater importance for estimating dose than details about the form of the particle size distribution.

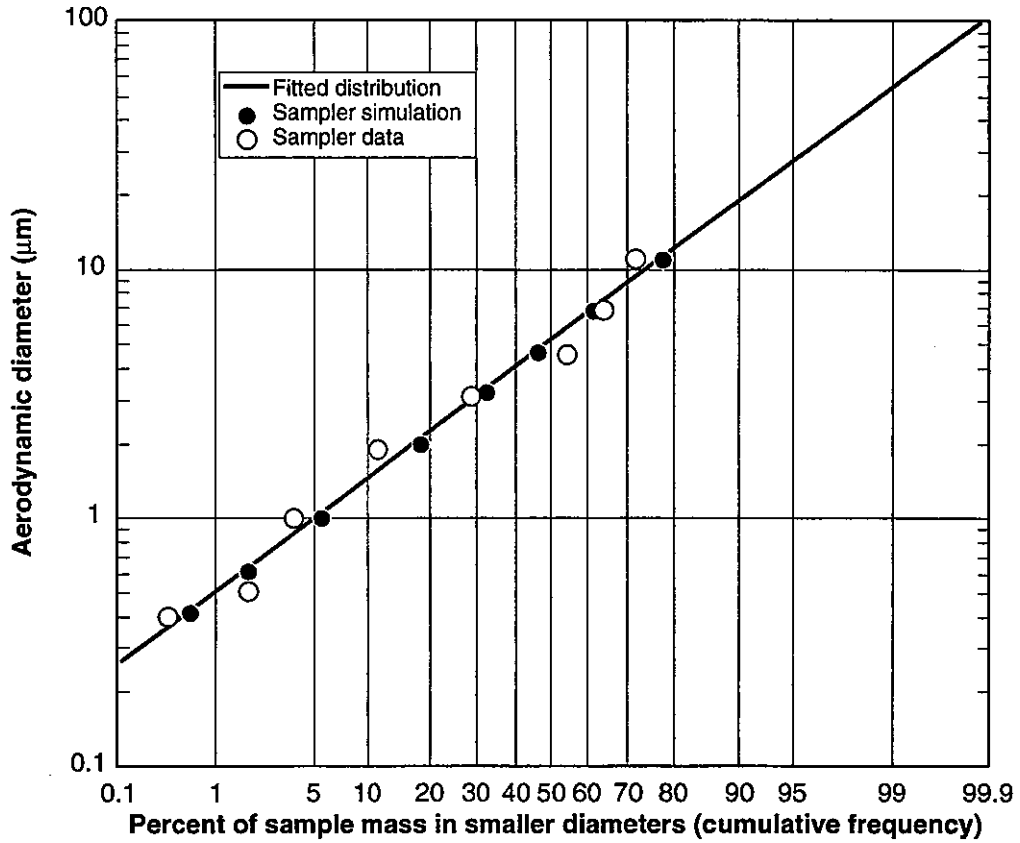

Figure H-7. Dust collector G4-5 inlet duct cascade impactor data, fitted distribution, and simulated cascade impactor response. This fitted distribution (curve) is essentially lognormal, reflecting the trend of the sampler data (white-filled points). The close proximity of the simulated response data (black-filled points) to the fitted curve indicates little instrument distortion of the sampled distribution's gross characteristics within and near the data range.

(2) For purposes of dosimetry, it is unlikely that the estimates of particle size distribution from the 1985 NKES study significantly distorted the input distributions to the sampler. Fluctuations in the distributions during the period of sampling (20–30 minutes for inlet ducts) would, of course, not have been detected by the measurements. But with the number of independently sampled stacks, it seems unlikely that such fluctuations could introduce a systematic bias that would seriously affect doses based on the releases from all stacks. There also exists a chance that particle bounce, which is not accounted for by cascade impactor theory, could have made median particle aerodynamic diameters seem smaller than they were, thus promoting an overestimation of dose to the lungs.

(3) Except for two stacks with smaller particles, the median aerodynamic diameters occurred in a cluster ranging from about 5 to about 15 μm. If this range were too high by a factor of two (which is unlikely), Figure H-3 indicates that the corrected dose to the lung from dust collector emissions would be about 50–70% higher. The stacks with smaller particles were Plant 4 G4-7 (2.0 μm) and Plant 5 G5-251 (0.54 μm).

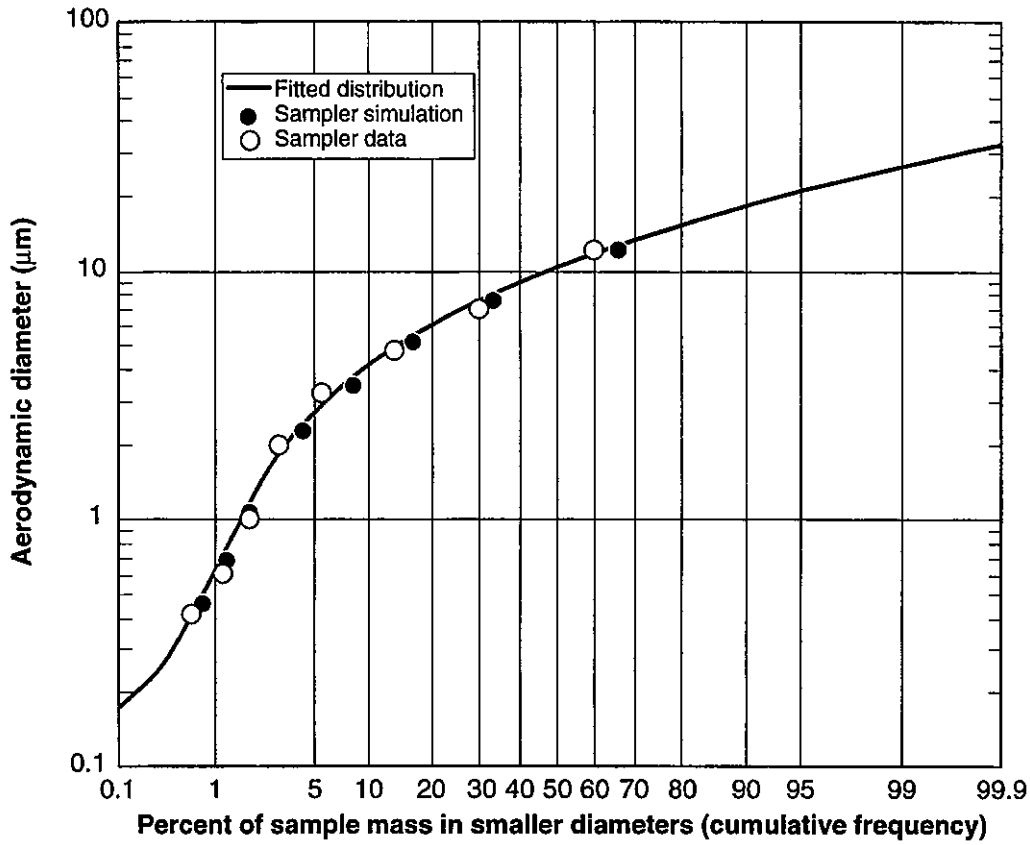

Figure H-8. Dust collector G5-249 inlet duct cascade impactor data, fitted distribution, and simulated cascade impactor response. This fitted distribution (curve) is bimodal (i.e., a plot of the relative frequency curve would show two maximum points). The fitted curve reflects the strong curvilinear trend and placement of the sampler data (white-filled points). The close proximity of the simulated response data (black-filled points) to the fitted curve indicates little instrument distortion of the sampled distribution's gross characteristics within and near the data range.

(4) The question of whether lognormal distributions should be substituted for the constrained cubic distributions is of something of a distraction. Figure H-2 should be a strong caution against uncritical use of the handbook technique.

REFERENCES

Boback M.W., T.A. Dugan, D.A. Fleming, R.B. Grant, and R.W. Keys. 1987. *History of FMPC Radionuclide Discharges.* Report FMPC-2082, Westinghouse Materials Company of Ohio, Cincinnati, Ohio.

Cheremisinoff P.N. and A.C. Morresi. 1978. *Air Pollution Sampling and Analysis Deskbook.* Ann Arbor Science Publishers, Inc., Ann Arbor, Michigan.

Crump J.G. and J.H. Seinfeld. 1982. "Further Results on Inversion of Aerosol Size Distribution Data: Higher-Order Sobolev Spaces and Constraints." *Aerosol Science and Technology* 1:363–369.

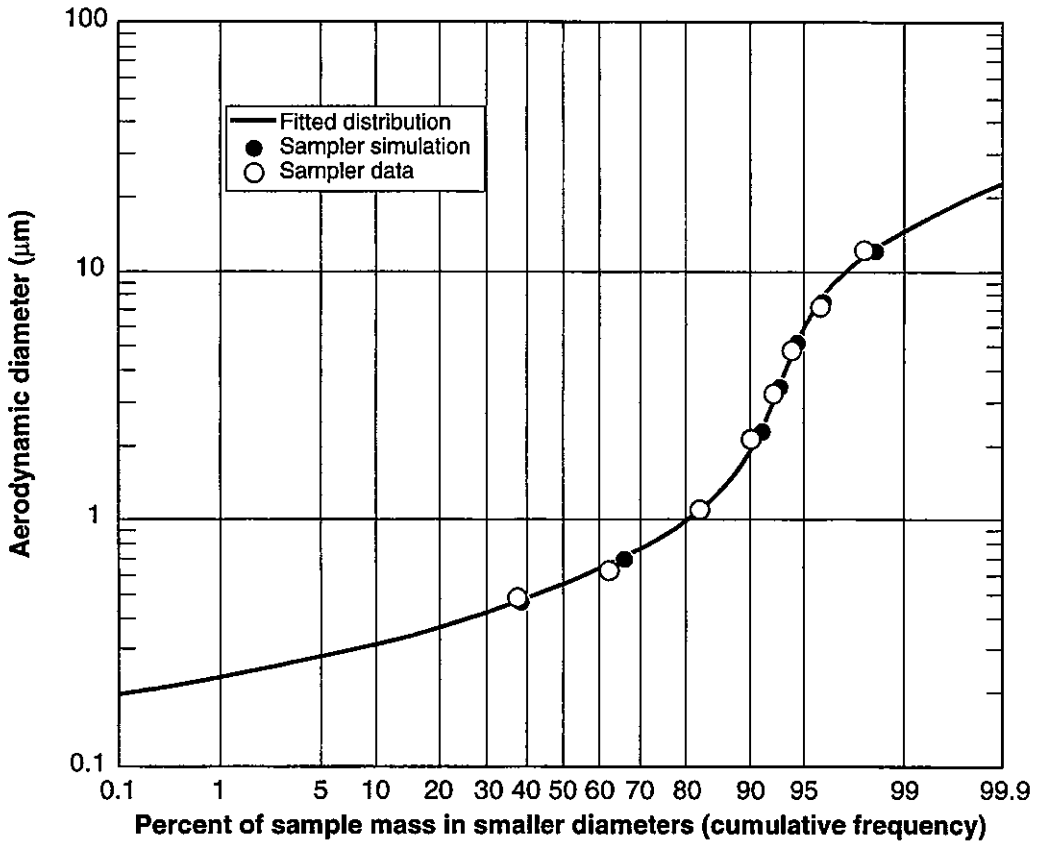

Figure H-9. Dust collector G5-251 inlet duct cascade impactor data, fitted distribution, and simulated cascade impactor response. This fitted distribution (curve) is weighted toward smaller particle sizes, with about 80% of the mass in submicron diameters. The trend is clearly indicated by the sampler data (white-filled points). The close proximity of the simulated response data (black-filled points) to the fitted curve indicates little instrument distortion of the sampled distribution's gross characteristics within and near the data range.

DallaValle J.M., C. Orr, Jr., and H.G. Blocker. 1951. "Fitting Bimodal Particle Size Distribution Curves — Comparison of Methods." *Industrial and Engineering Chemistry* **43**(6):1377–1380.

Hering S.V. 1989. "Inertial and Gravitational Collectors." In *Air Sampling Instruments for Evaluation of Atmospheric Contaminants,* 7th edition (S.V. Hering, Technical Editor), 337–364. American Conference of Government Industrial Hygienists, Cincinnati, Ohio.

International Commission on Radiological Protection. 1979. *Limits for Intakes of Radionuclides by Workers.* ICRP Publication 30 Part 1. *Ann. ICRP* **2**(3/4). Pergamon Press, Oxford.

Killough G.G., M.J. Case, K.R. Meyer, R.E. Moore, J.F. Rogers, S.K. Rope, D.W. Schmidt, B. Shleien, J.E. Till, and P.G. Voillequé. 1993. *The Fernald Dosimetry Reconstruction Project, Task 4: Environmental Pathways Analysis — Models and Validation.* Draft interim report for comment. Report CDC-3, Radiological Assessments Corporation, Neeses, South Carolina.

Knutson E.O. and P.J. Lioy. 1989. "Measurement and Presentation of Aerosol Size Distributions." In *Air Sampling Instruments for Evaluation of Atmospheric Contaminants,* 7th edition (S.V. Hering, Technical Editor), 59–72. American Conference of Government Industrial Hygienists, Cincinnati, Ohio.

Markowski G.R. 1987. "Improving Twomey's Algorithm for Inversion of Aerosol Measurement Data." *Aerosol Science and Technology* **7**:127–141.

Marple V.A. and Y.H. Liu. 1974. "Characteristics of Laminar Jet Impactors." *Environmental Science and Technology* **8**(7):648–654.

Reed, K.P. A study of the emissions of the process stacks at NLO: Plant #9, Plant #5-260, Plant #5-261. Unpublished report from Northern Kentucky Environmental Services (NKES) of a study commisioned by NLO; 1985.

Twomey S.J. 1975. "Comparison of Constrained Linear Inversion and Iterative Nonlinear Algorithm Applied to Indirect Estimation of Particle-Size Distributions." *Journal of Computational Physics* **18**:188–200.

Voillequé P.G., K.R. Meyer, D.W. Schmidt, S.K. Rope, G.G. Killough, M. Case, R.E. Moore, B. Shleien, and J.E. Till. 1995. *The Fernald Dosimetry Reconstruction Project, Tasks 2 and 3: Radionuclide Source Terms and Uncertainties.* Report CDC-5, Radiological Assessments Corporation, Neeses, South Carolina.

Winklmayr W., H.-C. Wang, and W. John. 1990. "Adaptation of the Twomey Algorithm to the Inversion of Cascade Impactor Data." *Aerosol Science and Technology* **13**:322–331.

APPENDIX I

DOSIMETRIC METHODS

INTRODUCTION

This appendix is intended as a reference for the dosimetric factors and related information that we have used to calculate radiation doses to the subjects of scenarios 1 through 9. For internal dose, we use the terms dose conversion factor and dose coefficient interchangeably, typically with units mrem pCi^{-1} or Sv Bq^{-1}. For direct external dose, we use the term dose-rate factor, and the units are dose rate per unit concentration of radioactivity in an exposure medium (e.g., mrem $year^{-1}$ per pCi m^{-3} for immersion in air, Sv $year^{-1}$ per Bq L^{-1} for submersion in water, Sv $year^{-1}$ per Bq m^{-2} for exposure to contaminated soil). It would have been impractical to convert all units in this appendix to a single system; rather, we present the reference tabulations in their original forms. We include Table I-1 to assist the reader in making conversions.

Dose coefficients depend on numerous factors, which include the radionuclide and its physical and chemical form, exposure mode, target organ, and the age (and possibly sex) of the exposed individual. Exposure modes vary according to whether the source of the radiation is internal or external to the body. Examples of exposure modes for internal dose are ingestion of contaminated food or water and inhalation of contaminated air. For external dose resulting from proximity to sources of penetrating radiations, examples of exposure modes are immersion in contaminated air or water and direct exposure to radionuclides in the soil. In the case of internal exposure by inhalation of particulate matter, the dose conversion factor also depends on the distribution of particle aerodynamic diameters. Figure I-1 summarizes properties of dosimetric factors used in this study.

Historically, the dosimetry of the decay products of radon (^{222}Rn) has been separated from that of other internal emitters. We maintain that separation in this report. Matters regarding the internal and environmental dosimetry of radon are discussed in the last section of this appendix.

Internal dose conversion factors summarize extensive dynamic calculations with physicochemical, anatomical, and metabolic models. For isotopes of uranium, thorium, radium, protactinium, actinium, and plutonium, the fundamental methodology is described in Publication 30 of the International Commission on Radiological Protection (ICRP) (ICRP 1979). We have extended this basic methodology in three ways. (1) Age-dependence has been taken into account to the extent possible at the time the database was compiled (1993), using data from ICRP Publication 56 Part 1 (ICRP 1990) for plutonium and tables from Cristy et al. (1986) for the isotopes of uranium, thorium, and radium. (2) Calculated internal doses have been tabulated according to linear energy transfer (LET), as low-LET absorbed dose and high-LET absorbed dose components for purposes of risk analysis. (3) In order to accommodate the needs of risk and power analysis for epidemiology, we have approximated annual fractional increments of 50-year dose commitments.

Table I-1. Useful Multipliers for Converting Radiation Dose and Radioactivity Units

From	To									
	Sv	mSv	rem	mrem	Ci	μCi	pCi	Bq	Sv Bq^{-1}	mrem pCi^{-1}
Sv	1	10^3	10^2	10^5						
mSv	10^{-3}	1	10^{-1}	10^2						
rem	10^{-2}	10	1	10^3						
mrem	10^{-5}	10^{-2}	10^{-3}	1						
Ci					1	10^6	10^{12}	3.7×10^{10}		
μCi					10^{-6}	1	10^6	3.7×10^4		
pCi					10^{-12}	10^{-6}	1	3.7×10^{-2}		
Bq					2.7×10^{-11}	2.7×10^{-5}	27	1		
Sv Bq^{-1}									1	3.7×10^3
mrem pCi^{-1}									2.7×10^{-4}	1

For radon decay products, we have restricted consideration of dose to the tracheobronchial epithelium (TBE). The dosimetric model for radon decay products is described in Publication No. 78 of the National Council on Radiation Protection and Measurements (NCRP) (NCRP 1984). The radon methodology takes into account the dependence of the dose on age and sex.

External dose rate factors apply to immersion in contaminated air, submersion in contaminated water, and exposure to contaminated ground surfaces. External irradiation involves only radiations of low linear energy transfer (LET), i.e., beta and photon radiations. Dose rate factors for these exposure modes were adopted from USDOE (1988). A more recent compilation of external dose rate factors is Eckerman and Ryman (1993), which was not yet available to us as we assembled the final database.

Refinements in internal dose estimation have also appeared since the database for this study was compiled. Most prominent, perhaps, is the newest respiratory tract model of the ICRP, described in Publication 66 (ICRP 1994). The change of a single component in a comprehensive model of radioactivity in the body, however, entails changes in the entire database of dosimetric factors calculated from the model. The calculations are extensive, and a tabulation that would meet the needs of this study could not be produced within its scope. These considerations help to explain our reluctance to commit the study to newer models and dosimetric factors only beginning to emerge from ICRP at the time our database had to be established. Although some preliminary calculations with the latest ICRP respiratory model might have been made at that time, extending such calculations to all radionuclides of interest and all organs with age dependence and annual increments of accrued dose was well beyond the reach of the study.

DECAY CHAINS

Environmental dose calculations involving the radionuclides released from the Feed Materials Production Center (FMPC) require that the dynamics of decay and formation of radioactive decay products of these radionuclides be considered. The calculations of decay chains are handled differently for different aspects of release, environmental transport, and dose.

Decay products formed while the radioactive precursors are resident in the production facility are included in the source term. The kinetics of decay products that form during

INTERNAL DOSE

Uranium and Related Radionuclides

Exposure parameters
Inhalation —
- Ambient air concentrations (pCi m^{-3}).
- Level of subject's physical activity (resting, light activity, vigorous activity).
- Distribution of particle aerodynamic diameters.
- Solubility (class D, W, Y for lung model; f_1 for GI tract model).

Ingestion —
- Concentrations in food and ingested soil (pCi kg^{-1}).
- Concentrations in drinking water (pCi L^{-1}).

Target tissues
Lungs (averaged dose), bone surfaces, kidneys, liver, red marrow, testes, ovaries. Dose to embryo/fetus: see Remark 2.

Sex dependence
None is taken into account by database.

Age dependence
Based on adjustment factors that multiply the tabulated adult organ dose to give the dose for the desired age group. The factors are specific to radionuclide and target organ and are tabulated for newborn; 3 months; and 1, 5, 10, and 15 years. Other ages are interpolated.

Resulting dose conversion factors
For specified set of parameter values, the result is presented as 50 annual increments of dose to the target tissue (mrem) corresponding to a unit intake of the specified radionuclide in the first year. Each year's increment is presented as a low-LET and a high-LET component.

Remarks
1. The dose to an organ from an internally distributed radionuclide is accrued over a period that depends on the half-life of the radionuclide, its properties affecting translocation, and its metabolic properties in systemic organs. If the half-life is short, the dose is delivered quickly (e.g., within a year for a half-life of a few weeks). If the half-life is very long, metabolism is dominant.
2. Dose to the embryo/fetus is estimated as the dose to the uterus of the mother during pregnancy.

EXTERNAL DOSE

Uranium and Related Radionuclides

Exposure parameters
Concentrations in air (pCi m^{-3}), surface soil (pCi g^{-1}), and water for swimming (pCi L^{-1}); distance from K-65 silos (m).

Target tissues
Lungs (averaged dose), bone surfaces, kidneys, liver, red marrow, testes, ovaries. Dose to embryo/fetus: see Remark.

Sex and age dependence
None is supported by the database.

Resulting dose conversion factors
For air, soil, and water: annual dose equivalent (mrem $year^{-1}$) for 1 year's exposure to contaminated medium. For K-65 silos: annual dose equivalent (mrem $year^{-1}$) for 1 year's residence at the specified location.

Remark
Dose to the embryo/fetus is estimated as the dose to the uterus of the mother during pregnancy.

Radon Decay Products

Target tissue: Tracheobronchial epithelium (TBE).

Exposure parameters
- Ambient air concentrations of RaA (attached), RaA* (unattached), RaB, and RaC.
- Level of subject's physical activity (resting, light activity).

Age and sex dependence
The NCRP model considers adult male, adult female, 10-year-old child (either sex), and infant (either sex).

Resulting dose conversion factors
For specified set of parameter values, the result is annual absorbed dose (mrad $year^{-1}$) to the TBE. This dose is dominated by the high-LET alpha component.

Remark
Radon decay products are short-lived. Dose is considered to be delivered within the year of exposure.

Figure I-1. Summary of properties of dosimetric factors. The heading "Uranium and Related Radionuclides" refers to isotopes of uranium, thorium, radium, protactinium, actinium, and plutonium, some of which appear as short-lived decay products.

the transport of progenitors through the enviornment are calculated by the environmental transport models, which keep track of the amount of each radionuclide in each environmental medium over time.

In the case of internal dose, the dose conversion factor implicitly accounts for the formation and decay of radioactive decay products after a radionuclide has entered the body. Internal dose is calculated separately for the intake of each decay product formed during transport and accounted for by the transport models (some decay products are known to form in negligible amounts during the environmental residence time and are not considered).

External dose rate factors are specific to single radionuclides (e.g., a dose rate factor for ^{238}U does not implicitly account for the formation of ^{234}Th). Formation of decay products in

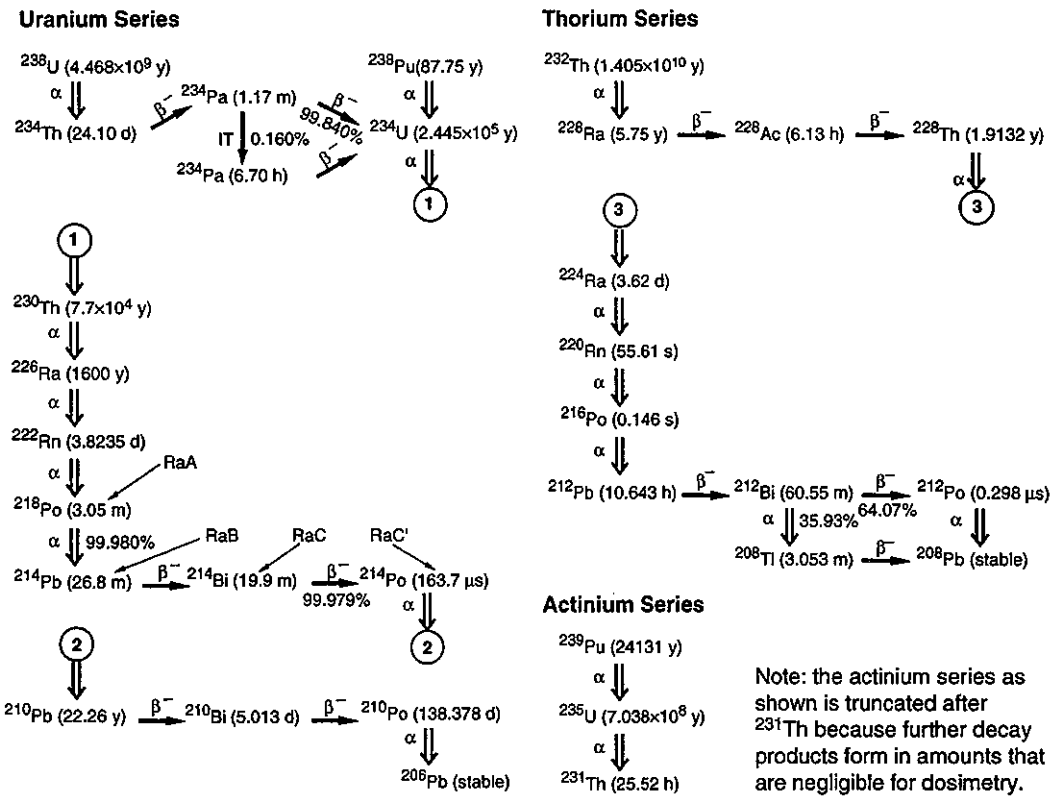

Figure I-2. Decay chains for radionuclides in the study. The chains shown are subchains of the uranium, thorium, and actinium series. In calculations involving these chains, further truncations are made at points below which negligible amounts of decay products would form. Note that for ^{222}Rn decay products in the uranium series, ^{214}Po (RaC') may always be assumed to be in secular equilibrium with ^{214}Bi (RaC). Decay products beyond ^{214}Po contribute negligibly to dose (source: Kocher 1981).

the relevant environmental media is calculated separately by the appropriate environmental model, each decay product is multiplied by its own dose rate factor, and the products are added to give the total dose rate.

The decay chains that are relevant to this study are shown in Figure I-2. The subchains actually used in the calculations are the result of truncating the complete chains at a point beyond which the inclusion of further decay products would not affect the dose estimates.

URANIUM, THORIUM, AND THEIR DECAY PRODUCTS

Internal Dose

For uranium and associated radionuclides, the internal dosimetry for this study is based principally on the methodology of ICRP Publication 30 (ICRP 1979), with some anatomical and physiological data based on data from ICRP Publication 23 (the Reference Man document, ICRP 1975). This methodology specifies models for estimating 50-year committed dose equivalent to each of a list of organs and tissues of the body. ICRP Publication 30 refers to ICRP Publication 26 (ICRP 1977) for the definition of a risk-weighted average of these organ com-

mitted dose equivalents, called the effective dose equivalent. Subsequent recommendations of the ICRP have replaced the effective dose equivalent with a modified set of organs and weights that are specified in ICRP Publication 60 (ICRP 1991), and the new quantity is called effective dose. In this study, we have used effective dose only as an average of dose equivalent over body tissues for making broad comparisons of dose to the subjects of scenarios 1 through 9 (the scenarios are described in Appendix J, and doses are tabulated in Appendix K). We have not used effective dose in the estimation of risk to the subjects of these scenarios.

The units of the dose conversion factors representing dose equivalent to specific organs and tissues and effective dose are Sv Bq^{-1} or the equivalent in conventional units (Table I-1). The interpretation is the dose equivalent to the target tissue per unit intake of the specified radionuclide into the body. The factors were calculated on the basis of a model for an individual who is a young adult at the time of an acute (instantaneous) intake, and the dose to the target organ accumulates for a period of 50 years after the intake. The dose conversion factors in the database do not furnish annual increments of the 50-year accumulation of dose, but annual increments are needed for the analysis of risk and epidemiological power. We calculated fractional annual increments separately with models similar to those underlying the calculation of the dose conversion factors in the database, with some necessary simplifications. Multiplying the fractional annual increments by the 50-year dose conversion factors provides the desired distribution of the dose over time. This calculation is discussed further at the end of this section.

The fundamental 50-year internal dose conversion factors for inhalation and ingestion that have been used in this study are listed in supplementary Tables I-1S through I-14S at the end of this appendix. These factors apply to adults and require modification for younger age groups, as we explain below. The tables were assembled from a database that is an extension of the one used for calculating tabulations in Federal Guidance Report No. 11 (Eckerman et al. 1988). The database was made available for this study by Dr. Keith F. Eckerman. The doses labeled "Effective (ICRP 60)" are the sum of the products of the ICRP Publication 30 organ dose equivalents and the weighting factors from ICRP Publication 60 (ICRP 1979, ICRP 1991).

High and low linear energy transfer. In computation of dose equivalent, different radiation types (e.g., alpha, beta and positron, photon) are weighted in accordance with a scheme that takes into account the linear energy transfer (LET) from the emitted particle into tissue (ICRP 1977, ICRP 1991). Absorbed dose does not take such weighting into account, but dose equivalent, by definition, weights the absorbed dose component for each radiation type with a quality factor Q. Recommendations of the ICRP have associated the quality factor for each radiation type with the linear energy transfer for that radiation type (ICRP 1977, ICRP 1991). For the radiation types of interest in this appendix, $Q = 1$ for beta, positron, and photon radiations (low LET), and $Q = 20$ for alpha radiations (high LET).

The quality factor has a broad correlation with radiation health effects but is inadequate for the risk analysis of this study. We required a breakdown of dose as absorbed dose for low-LET radiations and absorbed dose for high-LET radiations. However, the dosimetric database for the methodology of ICRP Publication 30 (ICRP 1979) had been tabulated as dose equivalent per unit intake, which means that the dose conversion factors were of the form $H = D_{low}Q_{low} + D_{high}Q_{high}$, where H is the dose equivalent factor (Sv Bq^{-1}), D_{low} and D_{high} are the absorbed dose components (Gy Bq^{-1}) for low- and high-LET radiations, respectively, and Q_{low} (= 1) and

Q_{high} (= 20) are the respective quality factors. Having only the number H available to us from the ICRP Publication 30 tabulation, we required additional information to infer the absorbed dose values D_{low} and D_{high} for our risk analysis.

The RADRISK program of the Environmental Protection Agency (EPA) provided tabulations of internal absorbed dose per unit intake for low- and high-LET radiations as required for a life-table analysis of risk from radiation exposure (Dunning et al. 1980). These numbers had not been selected initially for this study because their methodological basis was not completely consistent with that of the better known and internationally utilized ICRP Publication 30. But we were able to use the RADRISK tabulations to estimate the low- and high-LET breakdown of the ICRP Publication 30 database. We first calculated the fractions $f_{low} = D_{low}^{EPA}/(D_{low}^{EPA} + D_{high}^{EPA})$ and $f_{high} = 1 - f_{low}$; the superscript EPA refers to the RADRISK database. Then we estimated a total absorbed dose per unit intake $G = H/(f_{low} + Q_{high} f_{high})$ (Gy Bq^{-1}) where H (Sv Bq^{-1}) is the dose equivalent factor from the ICRP Publication 30 database and $Q_{high} = 20$. Finally, we calculated the estimates of the low- and high-LET components as $D_{low} = f_{low}G$ and $D_{high} = f_{high}G$. The implicit assumption is that although the dose equivalent values for the RADRISK and ICRP Publication 30 methodologies may differ, the fractional breakdown of absorbed dose into low- and high-LET components would be approximately the same. This assumption is a reasonable one, because of the similarity of the two methodologies with respect to the way the energy types enter the calculations.

Age and sex dependence. The dosimetric methodology of ICRP Publication 30 (ICRP 1979) is based on models for a hypothetical young male adult, although gonadal doses to males and females are separated as dose to testes and dose to ovaries. Breast and uterus are also included as target organs. With ICRP Publication 56 Part 1 (ICRP 1990) the Commission began the publication of dose conversion factors with age dependence for six age groups: 3 months; 1, 5, 10, and 15 years; and adult (≥20 years). The factors distinguish sexes only for gonadal tissues and breast, as noted above. At the time our database was compiled, the available ICRP documents listing age-dependent dose coefficients treated only a limited set of radionuclides that did not include uranium or thorium isotopes. For these isotopes, we have applied a tabulation of age conversion factors developed at the Oak Ridge National Laboratory (Cristy et al. 1986). This tabulation includes age conversion factors for ^{234}U, ^{235}U, ^{238}U, ^{228}Th, and ^{232}Th, but not ^{234}Th. The age conversion factors are presented as ratios for conversion of the adult dose to that of the desired group. The relevant age conversion factors for internal dose are shown in supplementary Tables I-15S through I-28S at the end of this appendix. In the case of ^{239}Pu, we adopted age-specific information from ICRP Publication 56 Par 1 (ICRP 1990). For the other radioisotopes considered (^{234}Th, ^{224}Ra, ^{226}Ra, ^{224}Ra, ^{234}Pa, ^{228}Ac), no comparable age-specific information was available, and the adult dose conversion factors are used in those cases. This is a relatively minor distortion, because most of the affected radionuclides are short-lived (the exceptions are ^{226}Ra and ^{224}Ra), and for short-lived radionuclides metabolic transfers are obscured by radioactive decay. In addition, crossfire gamma irradiation, which depends on anatomical dimensions, is usually not a dominant component of the dose. Finally, physiological parameters, such as breathing rates, consumption of drinking water, and dietary habits have been treated as age-specific for calculating intakes of all radionuclides. These parameters are discussed in the next section of this appendix (see page I-19). Thus, age-dependent factors have been considered to the extent permitted by the database.

Inhalation. Radiation dose from a radionuclide taken into the body by inhalation is calculated from assumptions about concentration of the radionuclide in the air that the subject breathes, the breathing rate, time spent breathing the contaminated air, other modifying factors, and a dose coefficient that expresses committed dose equivalent per unit intake of the radionuclide. The relationship can be indicated by the equation

$$D_H = \chi \cdot BR \cdot \Delta T \cdot U \cdot DC_H \quad \text{(I-1)}$$

where

D_H = 50-year committed dose (Sv) from breathing the radionuclide

χ = concentration of the radionuclide in air (Bq m^{-3})

BR = subject's breathing rate (m^3 day^{-1})

ΔT = time the subject spends breathing the contaminated air (days)

U = product of modifying factors, discussed below (dimensionless)

DC_H = dose coefficient expressing 50-year committed dose equivalent to a specific organ per unit intake by inhalation of the radionuclide (Sv Bq^{-1}).

In calculations for this study, the value of ΔT is typically 365 days to consider annual increments of exposure, which vary with the source term and other factors. The 50-year committed dose equivalent resulting from each year's exposure will also be broken into one-year increments; this procedure and the need for it are discussed later in the section. The air concentration χ is calculated by the air dispersion model and varies from year to year as the source term varies. The subject's breathing rate (BR) depends on physical activity (e.g., resting, light activity, vigorous exercise); an appropriate annual average is calculated according to each scenario's assumptions.

The product U of modifying factors generally adjusts the dose according to the exposure situation. Dose by inhalation is affected by times spent indoors and outdoors. Thus if f_{in} and f_{out} are fractions that partition the time into these two components, and if R is a ratio of indoor over outdoor air concentration of the airborne radionuclide, the appropriate modifying factor would be

$$U = f_{out} + f_{in}R. \quad \text{(I-2)}$$

when the factor χ in Equation I-1 refers to the outdoor air concentration. For all indoor exposures of all nine scenario subjects, the parameter R has been assigned the value $R = 0.7$ as a reasonable generic estimate. This value closely approximates the mean value 0.69 obtained for particulates in a seven-month study of a schoolroom in Denmark (Andersen 1972). A survey published by the Environmental Protection Agency (EPA) (Benson et al. 1972) indicates widely scattered results; $R = 0.7$ is above the median (between 0.5 and 0.6) for ratios based on mass concentrations (as opposed to particle count per unit volume). In the EPA review, nearly all of the data for concentrations by weight came from one study conducted in Hartford, Connecticut. The apparent trend for the Hartford study is not validated by the limited amount of data of the same kind from other cited studies (six plotted points with a median ratio of about 0.9). There are no clear patterns. (1) Our chosen factor 0.7 is halfway between 0.5 and 0.9, and (2) we assumed that in the 1950s and early 1960s, houses and schools in the rural community near

the FMPC had no less indoor-outdoor air exchange than the school in Denmark that was used for the study reported by Andersen (1972).

The inhalation dose coefficient DC_H of Equation I-1 comes from a database of previously calculated dosimetric information. This factor was calculated from radionuclide-specific physical and chemical data and dynamic models of the lungs and other organs. The lung model is of particular importance for inhalation dose, not only because the lungs are first and most directly exposed to the inhaled radioactivity, but also because the dynamic assumptions incorporated in the lung model determine the uptake over time of the radionuclide by other organs. We briefly review the ICRP lung model that is the basis for the inhalation dose coefficients used in this study.

The ICRP lung model of ICRP Publication 30 (ICRP 1979) is defined schematically by the table and diagram in Figure I-3. The model separates the respiratory tract into four major regions:

NP (nasal pharynx)

TB (tracheobronchial tree)

P (pulmonary region)

L (respiratory lymph nodes).

Each of the major regions is subdivided into two or more dynamic compartments, labeled by the letters a–j. Deposition is allocated first to the three major regions, which present surface area to the inspired air; the allocation fractions are denoted by D_{NP}, D_{TB}, and D_P. These deposition fractions are dependent on particle aerodynamic diameter (AD) for monodisperse aerosols and on the activity median aerodynamic diameter (AMAD) for aerosols with lognormal distributions of aerodynamic diameters. The values shown in Figure I-3 correspond to AMAD = 1 μm. For example, if 1 Bq of a radioactive aerosol with AMAD = 1 μm is inhaled, 0.3 Bq deposits in the nasal pharynx, 0.08 Bq deposits on the tracheobronchial tree, and 0.25 Bq deposits in the pulmonary region; the remainder is exhaled. For other values of AMAD, Figure I-4 shows curves constructed by the ICRP to represent the partitioned deposition of inhaled radioactivity for AMAD range 0.1 to 20 μm.

Within each of the three threshold regions, allocation to the compartments (a–b, c–d, e–h) is specified by the fractions F indicated in the table in Figure I-3. For example, compartments a and b would receive fractions $D_{NP}F_a$ and $D_{NP}F_b$, respectively, of the inhaled radioactivity. The clearance half-times for each compartment are listed in the columns labeled T in the table in Figure I-3. Quantities of radioactivity remaining in these two compartments over time (without radioactive decay) are given by the exponential functions $D_{NP}F_a \exp(-(\ln 2/T_a)t)$ and $D_{NP}F_b \exp(-(\ln 2/T_b)t)$, where t is the time since deposition. Analogous formulas for deposition and removal would apply to the tracheobronchial tree (c and d), except that there are two feedback paths from the pulmonary region (compartments f and g), which represent the mucociliary removal of radioactivity. This pulmonary material is subsequently brought up from the tracheobronchial passages, swallowed, and enters the gastrointestinal tract, where it is treated like ingested radioactivity. Direct calculation of the movement of radioactivity as it is represented by the ICRP lung model requires the formulation and solution of a coupled system of simultaneous ordinary differential equations. Radioactive decay chains further elaborate the calculation. The equations are given in ICRP Publication 30 Part 1 (ICRP 1979).

Region	Compartment	Clearance Class D T (day)	D F	W T (day)	W F	Y T (day)	Y F
NP	a	0.01	0.5	0.01	0.1	0.01	0.01
(D_{NP} = 0.30) [a]	b	0.01	0.5	0.40	0.9	0.40	0.99
TB	c	0.01	0.95	0.01	0.5	0.01	0.01
(D_{TB} = 0.08) [a]	d	0.2	0.05	0.2	0.5	0.2	0.99
	e	0.5	0.8	50	0.15	500	0.05
P	f	n.a.	n.a.	1.0	0.4	1.0	0.4
(D_P = 0.25) [a]	g	n.a.	n.a.	50	0.4	500	0.4
	h	0.5	0.2	50	0.05	500	0.15
L	i	0.5	1.0	50	1.0	1000	0.9
	j	n.a. [b]	n.a	n.a.	n.a.	infinite	0.1

[a] Deposition fractions for AMAD = 1 μm. [b] n.a. = not applicable.

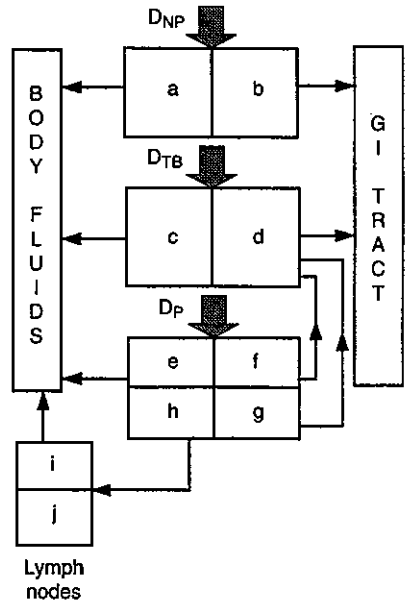

Figure I-3. The lung model of ICRP Publication 30. The columns D, W, and Y correspond, respectively, to rapid (days), intermediate (weeks), and slow (years) clearance of inspired material. The symbols T and F denote the biological half-time (days) and the fractional coefficient, respectively, corresponding to the compartment indicated by the subscript. The regional deposition fractions D_{NP}, D_{TB}, and D_P correspond to the nasal pharynx, tracheobronchial tree, and pulmonary regions, respectively, of the respiratory tract, and the values shown in the table are for particulate activity median aerodynamic diameter (AMAD) of 1 μm. Corresponding fractions for other values of the AMAD may be read from the graphs in Figure I–4.

It is important to keep in mind that the lung model determines not only the amounts of radioactivity in the various compartments of the respiratory tract over time, but that it also determines the rates of translocation of radioactivity from the lung into body fluids (principally blood), from which the radioactivity is taken up by systemic organs of the body. The transfer takes place primarily through direct absorption (from compartments a, c, e, and i shown in Figure I-3), but some material passes up the mucociliary ladder from the pulmonary region, through the tracheobronchial tree, and into the GI tract (f, g → d → GI in Figure I-3), where some of it is absorbed directly from the small intestine. Fractional uptake of inhaled radioactivity to other organs depends on how these processes are quantified. If an alternative model of the respiratory tract is introduced, doses to other organs also change.

The curves in Figure I-4 are intended to cover a range of lognormal distributions, presumably from geometric standard deviation (GSD) 1 (monodisperse) to 4.5. The ICRP Task Group on Lung Dynamics (Morrow et al. 1966) based its calculations for lognormal distributions on a tabulation of theoretical calculations for monodisperse aerosols over a range of tidal volumes (i.e., the volume of air inspired with each breath). The monodisperse results were then used in integrations over a variety of lognormal distributions. From these calculations, the Task Group concluded that when the mass median aerodynamic diameter (MMAD) of a distribution is spec-

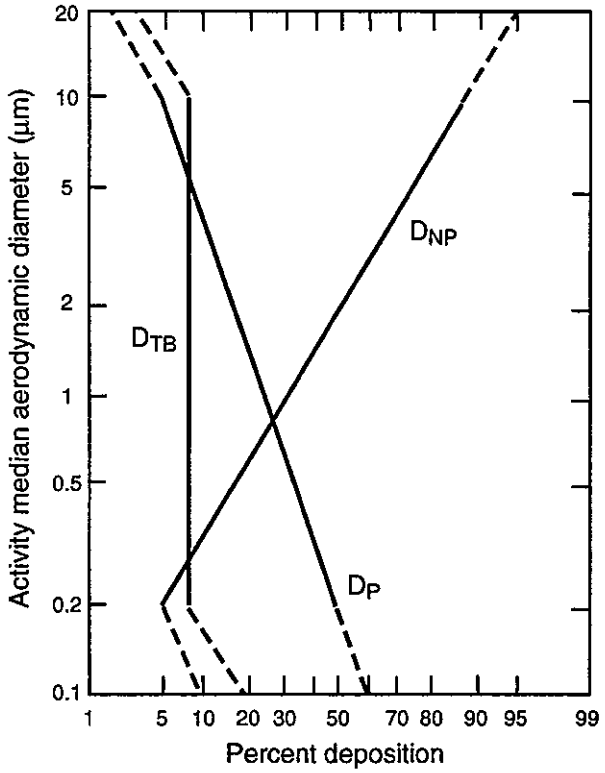

Figure I-4. Particulate deposition in the respiratory tract for the lung model of ICRP Publication 30 (ICRP 1979). The three curves are labeled to correspond to the three regional deposition fractions, for nasal pharynx (NP), tracheobronchial tree (TB), and pulmonary region (P). The model is defined for activity median aerodynamic diameters (AMAD) in the range from 0.2 to 10 μm, but the dashed segments of the curves indicate "provisional" extensions. The model is not recommended for use for distributions with AMAD less than 0.1 μm. The model assumes that each distribution is lognormal with geometric standard deviation less than 4.5.

ified, the deposition fraction is relatively insensitive to the GSD of the distribution, within the range 1.2–4.5. Figure I-5 is a redrawing of Figure 11 from Morrow et al. (1966), in which the three shaded regions bound the curves representing deposition fraction vs. MMAD when the GSD of the distribution varies between 1.2 and 4.5. For example, when MMAD = 2 μm, the vertical extent of the region labeled P in Figure I-5 indicates that the deposition fraction for the pulmonary region lies between 0.2 and 0.3 for GSD in the indicated range. At the expense of accepting this range of variability, it is possible to eliminate the GSD of the distribution as a parameter. Hence, curves such as those shown in Figure I-4, which were abstracted from calculations similar to those of the Task Group on Lung Dynamics, can be used to establish a generic functional relationship between the MMAD of the distribution particle diameters and fractional deposition in the three resipratory regions.

Within the uncertainties of the respiratory deposition models, the curves of Figure I-4 may reasonably be applied to a monodisperse aerosol for which every particle has aerodynamic diameter 1 μm or to a lognormal distribution with AMAD equal to 1 μm. The same deposition

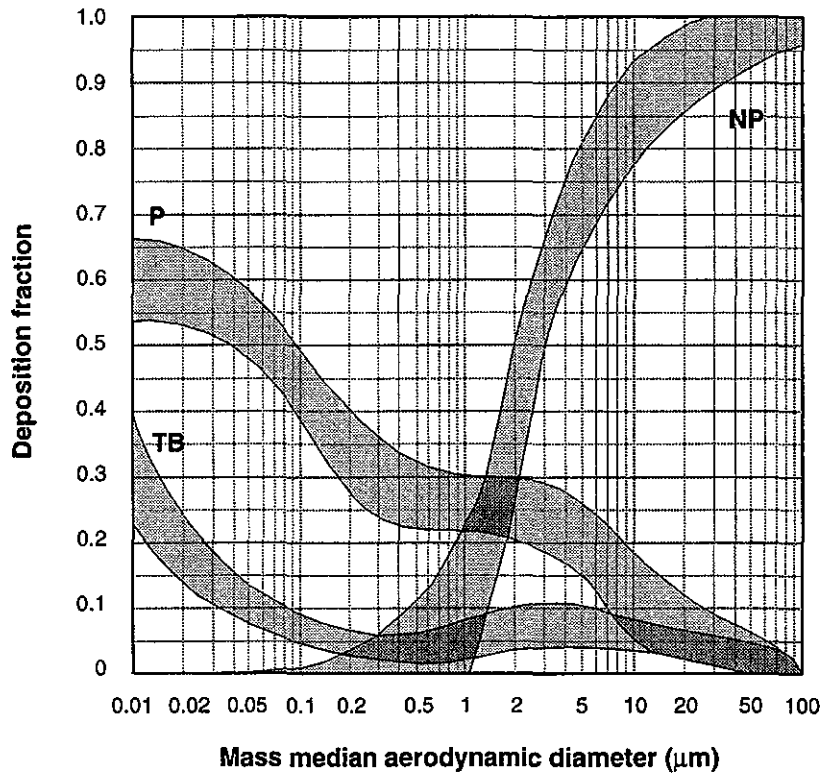

Figure I-5. Shaded regions that contain the curves of deposition vs. mass median aerodynamic diameter (MMAD) (μm) for lognormally distributed aerosols with geometric standard deviation ranging from 1.2 to 4.5. The curves correspond to the respiratory regions nasal pharynx (NP), tracheobronchial tree (TB), and pulmonary region (P). The figure is redrawn from Morrow et al. (1966). In the original calculations, the tidal volume was 1450 mL. The relatively small variability illustrated by these shaded regions for a specified MMAD makes possible the use of generic deposition curves such as those in Figure I-4 for any lognormally distribution of aerodynamic diameters with geometric standard deviations less than 4.5.

pattern would be predicted by the curves for the two cases. Anticipating that some particle size distributions in the study might not be lognormal, we devised a method of decomposing the distribution into a range of monodisperse components and applying the curves of Figure I-4 to each component to calculate a dose coefficient corresponding to the predicted deposition. The dose coefficients for all of the components are then averaged. Figure I-6 illustrates the process. In the figure, the mass has been divided into nine equal fractions, and the table beneath the figure associates an AD with each fraction. The distribution is thus approximated with nine monodisperse aerosols, with the AD of each component aerosol being determined by the distribution curve. Particle size–dependent dose conversion factors are calculated for each of the ADs according to deposition fractions from Figure I-4 by a method explained below, and the weighted average of the dose conversion factors is used in the computation of the inhalation dose.

The dependence of inhalation dose to systemic organs on the lung model implies a dependence on the deposition model and thus on particle AD. To avoid huge tabulations, organ-specific

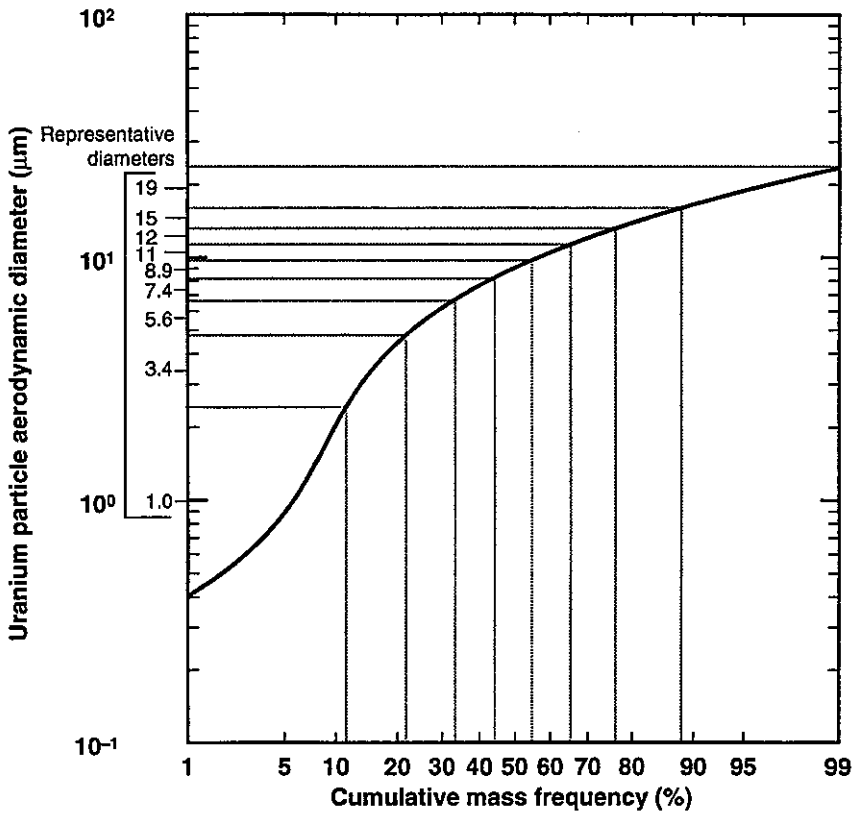

In this example, airborne uranium is divided into nine parts of equal mass. Each part is represented by the aerodynamic diameter that is the geometric mean of its range. Thus, the distribution is approximated by nine monodisperse aerosols. Corresponding dose coefficients are tabulated, and the average is used to estimate the dose.

Aerodynamic diameter (μm)	Lung dose coefficient (Sv Bq^{-1})	
19	2.25×10^{-5}	Dose to the lung per becquerel inhaled of class Y ^{238}U
15	3.29×10^{-5}	
12	4.38×10^{-5}	
11	4.82×10^{-5}	
8.9	5.86×10^{-5}	
7.4	6.85×10^{-5}	
5.6	8.57×10^{-5}	
3.4	1.24×10^{-4}	
1.0	2.66×10^{-4}	
Average	8.34×10^{-5}	

Figure I-6. Example of the dependence of inhalation dose on particle aerodynamic diameter (AD). The distribution of uranium is divided into nine equal parts, and each part is represented with the AD that is the median of its range. This amounts to an approximation of the continuous distribution by nine monodisperse aerosols. A dose coefficient is calculated for each AD, and the average of the dose coefficients is used to estimate the dose from inhalation. In general, the parts need not be of equal mass, but if not, a weighted average is used.

inhalation dose conversion factors have been computed for AMAD = 1 μm, together with organ-specific fractional weights d_{NP}, d_{TB}, and d_P ($d_{NP} + d_{TB} + d_P = 1$). These dose conversion factors and weights are shown in Tables I-1S through I-14S at the end of this appendix. To calculate the organ dose conversion factor for a particular AMAD value, use Figure I-4 (or an equivalent algorithm) to estimate the deposition fractions D_{NP}, D_{TB}, and D_P corresponding to that value.

The product of the correction factor CF, given by

$$\mathrm{CF} = \frac{D_{\mathrm{NP}}}{0.30} d_{\mathrm{NP}} + \frac{D_{\mathrm{TB}}}{0.08} d_{\mathrm{TB}} + \frac{D_{\mathrm{P}}}{0.25} d_{\mathrm{P}}, \tag{I-3}$$

and the tabulated 1-μm dose conversion factor gives the desired dose coefficient. For example, in Table I-1S, the entries for bone surface under Class Y are shown as 1.01×10^{-6} (7 2 91). (The parenthesized numbers are the fractions d_{NP}, d_{TB}, and d_{P}, expressed as percentages.) Suppose we wish to estimate the dose equivalent to bone surfaces following the intake by inhalation of 1 Bq of ^{238}U as a Class-Y aerosol with AMAD = 5 μm. From Figure I-4 we estimate $D_{\mathrm{NP}} = 0.74$, $D_{\mathrm{TB}} = 0.08$, and $D_{\mathrm{P}} = 0.088$. Substitution in Equation I-3 gives

$$\mathrm{CF} = \frac{0.74}{0.30} \times 0.07 + \frac{0.08}{0.08} \times 0.02 + \frac{0.088}{0.25} \times 0.91 = 0.513$$

so that the adjusted dose conversion factor for bone surface is

$$0.513 \times 1.01 \times 10^{-6} = 5.18 \times 10^{-7}.$$

Ingestion. Subjects of the nine scenarios (Appendix J) eat contaminated produce and animal products, and the subject of scenario 3 drinks contaminated well water. Children are also assumed to eat small amounts of radioactively contaminated dirt. Dose to an organ from ingesting a radionuclide can be written as follows:

$$D_{\mathrm{G}} = C \cdot Q \cdot U \cdot \mathrm{DC}_{\mathrm{G}} \tag{I-4}$$

where

D_{G} = 50-year committed dose equivalent to the organ (Sv)

C = concentration of the radionuclide in the ingested food, water, or soil (Bq kg^{-1} for food and soil, Bq L^{-1} for water and milk)

Q = total quantity of ingested food, water, or soil (kg for food and soil, L for water and milk)

U = product of modifying factors

DC_{G} = 50-year dose coefficient for ingestion of the radionuclide (Sv Bq^{-1}).

The concentration C of radioactivity in locally produced foods is calculated by the GARDEN model (Appendix A), coupled with the dynamic soil model (Appendix B), which in turn is coupled to atmospheric concentration and deposition, as well as to irrigation and watering of animals with water from contaminated sources. Levels of radioactivity in dirt ingested by children are given directly by the soil model. The only sources of contaminated drinking water were private wells south of the FMPC site, and assumed levels of contamination in drinking water for scenario 3 were based on a reconstruction of concentrations of radioactivity in Well 15. The total quantity Q of a foodstuff, drinking water, or soil is estimated as one year's intake, in order to give the committed dose equivalent resulting from annual exposures. The modifying factors U adjust the dose according to fractional amounts of diet or water consumption that are assumed to be from contaminated sources. It is easiest to think of applying Equation I-4 separately to each kind of food, to drinking water, and to ingestion of soil, with the appropriate modifying factor used in each version of the equation; the results are then summed to give the

total. The fraction of each dietary component that is assumed to come from contminated local food production varies among the nine scenarios, and the related modifying factor controls the variation.

The dose coefficient DC_G for ingestion of the radionuclide comes from a precalculated database of dosimetric information. The dose coefficient depends on dynamic models of the gastrointestinal (GI) tract and systemic organs. The dose coefficient for ingestion involves the ICRP model of the GI tract in two ways: (1) estimation of dose to the segments of the GI tract (stomach, small intestine, upper large intestine, and lower large intestine, abbreviated S, SI, ULI, and LLI, respectively), and (2) determination of the fraction of each unit amount of ingested radioactivity that is absorbed into body fluids and is thereby made available to systemic organs. The organ doses presented in this report do not include the segments of the GI tract as target organs, although our database and methodology do include them. The matter of uptake of radioactivity from the GI tract (specifically, from the SI) to the blood affects all doses (other than those from radon decay products), primarily from ingestion, but to a lesser extent, from inhalation.

The ICRP model of the GI tract is quantified in ICRP Publication 30 Part 1 (ICRP 1979). The model is of catenary structure, with the four segments represented by serially connected compartments. Radioactivity leaving one segment by first-order kinetics moves into the next. Absorption of radioactivity from the GI tract into the blood is assumed to occur exclusively in the SI, and this absorption is determined by a fraction f_1. The rate coefficient λ_B for absorption from the SI is given by the formula

$$\lambda_B = \frac{f_1 \lambda_{SI}}{1 - f_1} \tag{I-5}$$

where λ_{SI} is the rate coefficient governing the transfer of radioactivity from the SI to the ULI. When $f_1 = 1$, all radioactivity is assumed to move from the SI into body fluids, with none passing directly into the ULI. Figure I-7 shows the model schematically.

The ICRP GI tract model applies not only to radioactivity that enters the body by ingestion, but also to inhaled radioactivity that is brought up from the lungs by mucociliary action (arrows f and g in Figure I-3) and swallowed. Such radioactivity is subsequently passed directly to the GI tract model and treated the same as ingested material. Thus, the GI tract model plays a role in the calculation of dose from inhalation as well as from ingestion.

The GI tract absorption fraction f_1 depends on the chemical form of the radionuclide to which it applies, and values of this parameter are shown in Tables I-1S through I-14S, together with corresponding dose conversion factors.

Annual increments of committed dose. We have been required to calculate dose to each scenario subject in one-year increments over the period of FMPC operation (1951 through 1988). For external dose, this is a simple requirement, because each year's average concentration of a radionuclide in an exposure medium (e.g., air, water, or ground surface) need only be multiplied by the appropriate dose rate factor and a one-year time factor to give the annual dose from that exposure. For radon decay products (discussed in the last section of this appendix), the annual dose similarly depends directly on the air concentration of radon and each decay product averaged for the particular year, because of the short radiological half-lives of the decay products.

For uranium and thorium, however, it is somewhat more complicated to develop annual

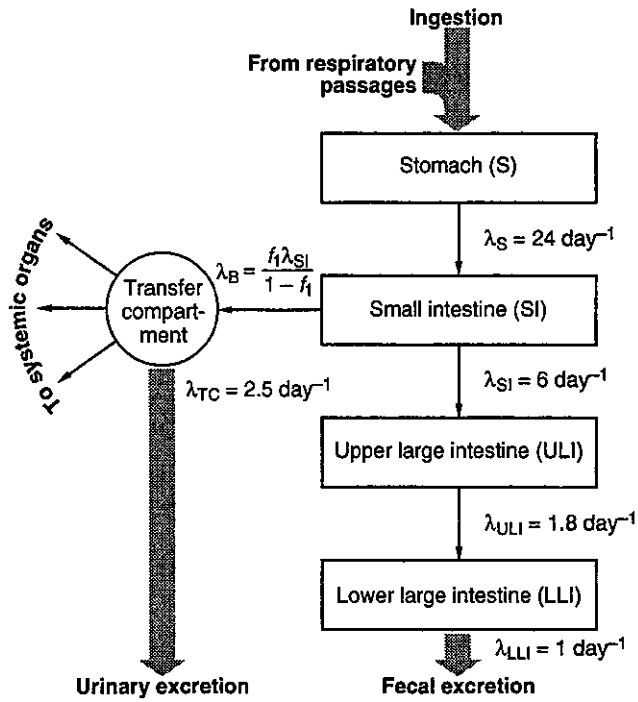

Figure I-7. The ICRP model of the gastrointestinal (GI) tract. Radioactivity may enter the GI tract by ingestion or from mucociliary clearance of inhaled material from the tracheobronchial and pulmonary regions of the respiratory passages. Radioactivity moves from each segment of the GI tract to the next by first-order kinetic processes. Absorption from the GI tract to the transfer compartment (essentially body fluids) is assumed to occur in the small intestine and is determined by a fraction f_1 that depends on the solubility of the radioactive material. This process determines the fractional uptake to systemic organs and thus influences their dose.

dose increments. As we have explained, internal dose coefficients are based on a model of acute intake and accumulation of dose to the organ or tissue of interest for a subsequent period of 50 years. Because the tabulated information does not provide annual increments of dose, we calculated fractional annual increments using models of intake, translocation, and metabolism similar to those on which the 50-year dose coefficients are based. Our simplifying assumption was that time-integrated radioactivity of the parent radionuclide in the organ of interest can be used for allocation of the dose to annual increments, with no consideration of decay products or crossfire irradiation among organs by gamma-emitting radionuclides. Thus, each dose coefficient may be regarded as the sum of 50 terms, where each term represents one year's increment of dose from the initial acute intake.

Instead of tabulating these annual fractional dose increments for the full variety of radionuclides, solubilities, and exposure modes, we illustrate them for inhalation dose coefficients for uranium (Table I-2). We compare the fractions for clearance classes W and Y and for each of the organs lung, GI tract, bone, and kidney. Class-W uranium clears rapidly (within weeks) from the lungs, and thus nearly all of the dose (99.3%) accrues to the lungs in the first year. The same is true of the GI tract, which is irradiated by radioactivity brought up from the lungs and swallowed. Bone has a long retention time, and consequently its dose accumulates slowly,

Table I-2. Annual Fractional Increments of 50-year Committed Dose Equivalent for Class-W and Class-Y Inhaled Uranium

	Annual fractional increment (%)							
	Class W				Class Y			
Year	Lung	GI tract	Bone	Kidney	Lung	GI tract	Bone	Kidney
1	99.30	100.00	8.23	52.55	32.93	96.53	1.61	11.33
2	0.69	0.00	4.96	7.57	18.37	2.20	1.97	8.15
3	0.01	0.00	4.70	6.20	11.85	0.81	2.52	8.32
4	0.00	0.00	4.47	5.23	8.43	0.29	2.94	8.08
5	0.00	0.00	4.25	4.42	6.33	0.11	3.25	7.59
6	0.00	0.00	4.04	3.73	4.87	0.04	3.46	6.98
7	0.00	0.00	3.84	3.15	3.79	0.01	3.59	6.33
8	0.00	0.00	3.65	2.66	2.96	0.01	3.65	5.67
9	0.00	0.00	3.47	2.25	2.31	0.00	3.66	5.03
10	0.00	0.00	3.30	1.90	1.81	0.00	3.63	4.43
11	0.00	0.00	3.13	1.61	1.41	0.00	3.57	3.89
12	0.00	0.00	2.98	1.36	1.10	0.00	3.48	3.39
13	0.00	0.00	2.83	1.15	0.86	0.00	3.38	2.95
14	0.00	0.00	2.69	0.97	0.67	0.00	3.27	2.56
15	0.00	0.00	2.56	0.82	0.52	0.00	3.15	2.21
16	0.00	0.00	2.43	0.69	0.40	0.00	3.03	1.91
17	0.00	0.00	2.31	0.58	0.31	0.00	2.91	1.64
18	0.00	0.00	2.20	0.49	0.24	0.00	2.79	1.41
19	0.00	0.00	2.09	0.42	0.19	0.00	2.66	1.21
20	0.00	0.00	1.99	0.35	0.15	0.00	2.55	1.03
21	0.00	0.00	1.89	0.30	0.11	0.00	2.43	0.88
22	0.00	0.00	1.80	0.25	0.09	0.00	2.32	0.76
23	0.00	0.00	1.71	0.21	0.07	0.00	2.21	0.64
24	0.00	0.00	1.62	0.18	0.05	0.00	2.10	0.55
25	0.00	0.00	1.54	0.15	0.04	0.00	2.00	0.47
26	0.00	0.00	1.47	0.13	0.03	0.00	1.91	0.40
27	0.00	0.00	1.39	0.11	0.03	0.00	1.82	0.34
28	0.00	0.00	1.33	0.09	0.02	0.00	1.73	0.29
29	0.00	0.00	1.26	0.08	0.02	0.00	1.64	0.24
30	0.00	0.00	1.20	0.07	0.01	0.00	1.56	0.21
31	0.00	0.00	1.14	0.06	0.01	0.00	1.49	0.18
32	0.00	0.00	1.08	0.05	0.01	0.00	1.41	0.15
33	0.00	0.00	1.03	0.04	0.01	0.00	1.35	0.13
34	0.00	0.00	0.98	0.03	0.00	0.00	1.28	0.11
35	0.00	0.00	0.93	0.03	0.00	0.00	1.22	0.09
36	0.00	0.00	0.88	0.02	0.00	0.00	1.16	0.08
37	0.00	0.00	0.84	0.02	0.00	0.00	1.10	0.07
38	0.00	0.00	0.80	0.02	0.00	0.00	1.05	0.06
39	0.00	0.00	0.76	0.01	0.00	0.00	0.99	0.05
40	0.00	0.00	0.72	0.01	0.00	0.00	0.95	0.04
41	0.00	0.00	0.69	0.01	0.00	0.00	0.90	0.03
42	0.00	0.00	0.65	0.01	0.00	0.00	0.85	0.03
43	0.00	0.00	0.62	0.01	0.00	0.00	0.81	0.02
44	0.00	0.00	0.59	0.01	0.00	0.00	0.77	0.02
45	0.00	0.00	0.56	0.01	0.00	0.00	0.73	0.02
46	0.00	0.00	0.53	0.00	0.00	0.00	0.70	0.01
47	0.00	0.00	0.51	0.00	0.00	0.00	0.66	0.01
48	0.00	0.00	0.48	0.00	0.00	0.00	0.63	0.01
49	0.00	0.00	0.46	0.00	0.00	0.00	0.60	0.01
50	0.00	0.00	0.44	0.00	0.00	0.00	0.57	0.01

which implies small annual increments (8.23% the first year). The removal of uranium from the kidney is faster than for bone, giving 52.55% of the dose in the first year, but some activity persists for years.

Class-Y uranium is released slowly from the lungs, and accordingly, Table I-2 shows annual

Table I-3. Sample Calculation of Dose with Annual Breakdown

	Annual dose (Sv) from exposure in year				
Year	1981	1982	1983	1984	Subtotal
1981	4.38×10^{-9}				4.38×10^{-9}
1982	3.09×10^{-9}	5.53×10^{-9}			8.62×10^{-9}
1983	1.33×10^{-9}	2.06×10^{-9}	3.69×10^{-9}		7.07×10^{-9}
1984	4.72×10^{-10}	6.64×10^{-10}	1.03×10^{-9}	1.84×10^{-9}	4.01×10^{-9}

lung increments of 1% and greater for 12 years. This slow clearance also distributes the dose to other organs over longer periods. The effect is least pronounced for inhaled material that moves from the lungs into the GI tract, because clearance of insoluble material from the upper respiratory passages is more rapid by mucociliary action than by absorption into body fluids (Figure I-3).

There are some shortcomings in using time-integrated radioactivity to estimate the annual fractional dose increments. Neglecting the buildup of radioactive decay products, which deliver dose at different rates, introduces a distortion, as does discounting crossfire radiations among organs by gamma emitting radionuclides. But the trends are correct, and we have no reason to believe that the distortions are large. An exact calculation would not have been feasible.

Decomposition of internal dose coefficients into sums of annual increments permits us to calculate and combine dose estimates in a pattern that is illustrated by Table I-3. This example considers an exposure that began in 1981 and lasted four years. The columns of the table represent hypothetical annual dose increments from exposure that occurred in the year that labels the column. For example, 3.69×10^{-9} Sv is the dose in 1983 from exposure in 1983, and 1.03×10^{-9} Sv is the dose in 1984 from exposure in 1983. When each row is added, the row sums represent the dose received in the corresponding year from exposures that occurred not only in that year, but also in previous years. For example, the sum of the entries in row 4 (4.01×10^{-9}) is the dose received in 1984 from exposures in 1981, 1982, 1983, and 1984. In effect, such a table is constructed to account for the years 1951 through 1988, and each entry represents a total dose to the organ of interest from all exposure modes, internal and external.

External Dose

Direct exposure to the radiation fields produced by concentrations of radioactivity outside of the body results in organ doses that we term external. External dose rates depend not only on the quantity of radioactivity in an environmental medium, but they also depend in a complicated way on the geometry, i.e., the spatial distribution of the radioactivity within the medium. Calculations based on standard geometries and on the photon energies and intensities of the radionuclides have been summarized in tables of dose rate factors corresponding to unit concentrations of radionuclides in the medium. Only radionuclides emitting gamma rays are likely to have significance as external sources of radiation in the circumstances envisioned by this study. The largest component of external dose comes from ^{214}Pb and ^{214}Bi, which are decay products of ^{222}Rn released from the K-65 silos. The external dose rate factors were taken from USDOE (1988) and are displayed in supplementary Tables I-29S through I-42S at the end of

this appendix.

We consider concentrations of radioactivity in air during transport of airborne releases. The geometry is defined by an infinite half-space extending upward from ground level, with a uniform distribution of radioactivity. The concentration of each radionuclide in the air is determined by the model calculation of dynamically varying air concentration at ground level. We did not calculate finite-plume adjustments, because of the relatively small magnitude of this dose component in comparison with total dose. We did consider shielding for the fraction of time the scenario subjects spent indoors, using the shielding factor 0.5 (USDOE 1988).

Swimming in contaminated water is an activity that could lead to external doses to scenario subjects. The geometry for this exposure is an infinite half-space with its upper boundary at the water surface, with a uniform distribution of radioactivity. Annual dose rates consider the fraction of time the subject spent swimming. The small magnitudes of doses from exposure to this medium made further adjustments unnecessary.

Contaminated ground surfaces are accounted for by dose rate factors that consider an infinite ground plane with uniformly distributed radioactivity on the surface. In our calculations, the area concentration of radioactivity is determined by the dynamically varying amount of each radionuclide in the 0.5-cm soil layer (Appendix B). We have made adjustments for shielding of subjects during time spent indoors, using the shielding factor 0.5 (USDOE 1988).

Direct external radiation doses from gamma-emitting radionuclides in the K-65 silos have been estimated and tabulated along with other external doses. In only one case (scenario 2) did the dose from this exposure exceed the external doses from exposure to the contaminated ground plain, and both are dominated by exposure to contaminated air. Even so, the estimated doses are of small magnitude relative to corresponding total doses. We made adjustments to account for shielding of the subject during time spent indoors, using the shielding factor 0.5, by analogy with exposure to air and ground surface. The methods for calculating dose from this external source are described in Appendix G.

Dose to the Embryo/Fetus

Dose to the embryo/fetus from radionuclides taken into the body of a pregnant woman is estimated as the dose to the uterus of the woman received during the nine-month gestation period. This is not a committed dose, accounting as it does only for dose received in-utero. After birth, the individual would continue to accrue dose from radioactivity incorporated in tissues from placental transfer during gestation, but there are no scenarios for these individuals to account for post-natal accrual (in any case, this gestational component of dose would likely be quickly dwarfed by dose from direct inhalation and ingestion of contaminated material if the individual's exposure environment remains similar to that of the mother during her pregnancy). The purpose of estimating the in-utero dose is to provide a basis for approximating risk to the embryo/fetus. Except for the specific time limitation to nine months, the calculation of this dose (i.e., dose to the uterus of the mother, as surrogate for the embryo/fetus) does not differ from that for other systemic organs. Dose components from both internal and external radioactivity are considered in the calculation. Results for the two scenario subjects (scenarios 1 and 6) who were pregnant during their exposure to radioactivity released from the FMPC are given in Appendix K.

PHYSIOLOGICAL PARAMETERS RELATED TO DOSE ESTIMATION

Intake rates of radionuclides in an environmental exposure medium (air, drinking water, food) depend on (1) the concentration of radioactivity in the medium and (2) the rate at which material is taken into the body. The second factor depends on assumptions about the physiology of the exposed individual. This information is often age- and sex-specific. In this appendix we give tabulated information for breathing rates (Table I-4), consumption rates of drinking water (Table I-5), and intake rates for basic dietary constituents (Table I-6).

This information has been used to estimate intakes of radioactivity for the nine exposure scenarios:

$$I = CQ \tag{I-6}$$

where

I = intake rate (Bq day^{-1})

C = concentration of radioactivity in the medium (Bq m^{-3} for air, Bq L^{-1} for drinking water or milk, and Bq kg^{-1} for foods)

Q = physiological consumption rate parameter (m^3 day^{-1} for air, L day^{-1} for drinking water or milk, and kg day^{-1} for foods).

Table I-4. Rates of Breathing (m^3 day^{-1}) by Age, Sex, and Exercise Level[a]

Age (years)	Male			Female		
	Resting	Light	Vigorous	Resting	Light	Vigorous
0	1.4	2.2	3.6	1.4	2.2	3.6
1	3.7	8.3	13.9	3.7	8.3	13.9
2–3	4.8	9.1	15.3	4.8	9.1	15.3
4	5.2	11.5	19.4	5.2	11.5	19.4
5	5.8	13.7	23.0	5.8	13.7	23.0
6–7	6.3	15.8	26.6	6.3	15.8	26.6
8–9	7.0	24.5	40.3	7.0	24.5	40.3
10–11	7.5	26.8	53.3	7.5	26.8	43.7
12–13	9.2	29.5	58.0	7.8	27.2	52.0
14	9.7	33.5	64.9	8.0	28.8	60.5
15	10.1	33.1	70.0	8.3	31.1	61.8
16–17	10.4	36.4	72.6	8.3	31.1	64.8
18–29	12.0	37.8	73.4	8.4	31.7	64.8
≥30	10.8	36.0	72.0	7.8	30.2	64.8

[a] Data are based Roy and Courtay (1991). Data for the vigorous exercise category were not given for ages newborn through five years. Extrapolations based on children aged 6–8 years were substituted for the missing data. The duration of activities at these levels is stated in each exposure scenario definition (Appendix J).

Table I-5. Drinking Water Consumption Rates by Age[a]

Age (years)	0	1–10	11–19	20–64	≥ 65
L day^{-1}	.323	.701	.907	1.27	1.34

[a] Note that these estimates are confined to tap water, presumably the contaminated source. The remaining fluid intake is from sources that are assumed to be uncontaminated (such as canned or bottled drinks) or is accounted for separately (e.g., milk from local production). The data are based on Roseberry and Burmaster (1992). No breakdown by sex was given.

The physiological data in Tables I-4 through I-6 are treated as reference information in the context of the nine exposure scenarios and related discussions. Although the data in these tables are based on statistical information about real populations, we do not treat these physiological data as sources of uncertainty in the calculations. They are, rather, static parameters in the definitions of the hypothetical subjects of the nine scenarios. Uncertainty analysis will accompany the application of this methodology to real populations.

Breathing rates, in m^3 day^{-1}, are listed by age, sex, and activity level in Table I-4. These numbers are used to calculate rates of intake by inhalation. Breathing rates vary with the level of activity, and average levels of indoor and outdoor activity are specified for each period and location in each of the scenarios.

Rates for consumption of drinking water are given as a function of age in Table I-5. These rates are taken as a generic representation of tap water consumption by each subject and thus do not represent total fluid intake.

In Table I-6, we have broken dietary information down into the following food types: vegetables, milk, beef, fish, poultry, and eggs. Beef is generic for beef, pork, and lamb, and the term fish is restricted to freshwater types. These categories correspond to the ones used with the nine scenarios.

Each consumption quantity shown in this appendix represents a total rate for the specified age, sex, and possibly other category. The scenarios define percentages of these total rates in order to account for the portions that are assumed to be contaminated with radioactivity from the FMPC or to ensure other compatibility with exposure assumptions. For garden produce and local animal products, these percentages are specified for each period and location. Inhalation intakes are affected by differences in indoor and outdoor levels of contamination and by the subject's assumed activity. Drinking water is an exception: if the source of drinking water for a given period and location is assumed to be contaminated, then all tap water that the subject drinks during that period and at that location is assumed to be contaminated at the level defined in a data file for that source. Contamination levels for water sources are specified as a function of time. The only contaminated drinking water source considered for the scenarios is a well affected by a groundwater plume that moved offsite south of the FMPC in the 1960s

Table I-6. Dietary Information by Sex and Age[a]

	Male						Female					
Age	Veg.	Milk	Beef	Fish	Poul.	Eggs	Veg.	Milk	Beef	Fish	Poul.	Eggs
0	.155	.273	.047	.001	.019	.006	.155	.271	.044	.001	.017	.004
1–4	.198	.375	.094	.007	.022	.020	.198	.378	.091	.006	.022	.019
5–9	.198	.453	.132	.011	.023	.018	.198	.435	.125	.010	.021	.016
10–14	.289	.503	.174	.013	.034	.021	.241	.403	.145	.013	.028	.017
15–19	.318	.500	.228	.016	.037	.031	.212	.311	.150	.017	.025	.018
20–24	.364	.291	.237	.020	.040	.032	.242	.191	.152	.017	.026	.024
25–29	.364	.239	.243	.024	.041	.033	.242	.182	.152	.018	.025	.023
30–39	.364	.278	.247	.020	.041	.038	.242	.153	.154	.019	.025	.023
40–59	.345	.197	.234	.023	.040	.038	.261	.150	.155	.021	.026	.024
≥60	.344	.214	.186	.020	.039	.037	.262	.181	.132	.016	.027	.023

[a] Dietary constituents and units of intake:

Vegetables (all types)	kg day^{-1}
Milk	L day^{-1}
Beef (generic for beef, pork, or lamb)	kg day^{-1}
Fish (freshwater)	kg day^{-1}
Poultry	kg day^{-1}
Eggs	kg day^{-1}.

The estimates are based on the study of Yang and Nelson (1986). For vegetables, the fractional breakdown by sex was estimated from Rupp (1980). We assume that half of the vegetables are root crops and half are leafy. Sex ratios for poultry were assumed to be the same as for meat; intakes are based on Tables 7 and 8 of Yang and Nelson (1986).

(Appendix F); this well involved only scenario 3.

RADON-222 AND ITS DECAY PRODUCTS

Because calculations for ^{222}Rn and its decay products are handled differently from those for airborne uranium, this section presents the methods associated with the kinetics of the ^{222}Rn decay chain and the estimation of dose to the tracheobronchial epithelium from the decay products. Most of the methodology is based on NCRP Publication No. 78 (NCRP 1984), and the reader may find additional detail for some of these topics in that reference. In this section, we refer to the dosimetric model from NCRP Publication No. 78 as "the NCRP dose model" or "the NCRP model." Methods for the kinetic decay chain calculations are not given in NCRP Publication No. 78. The equations for the decay chain have been formulated and solved by many researchers under various assumptions. For example, Raabe (1969) gives the explicit formulas for amounts of ^{218}Po, ^{214}Pb, ^{214}Bi, and the unattached amount of ^{218}Po, each normalized to the amount of ^{222}Rn, on the assumption that the amount of ^{222}Rn gas does not change during the time interval of interest. Thus, his equations may be interpreted as showing the ingrowth of the decay products, as well as the evolution of the attachment process for RaA,

in an environment in which the ^{222}Rn level is maintained at steady state and from which decay products are initially absent. We have formulated the equations to include the decay of the ^{222}Rn gas from an initial amount at the release point, and we present this formulation as we have derived and used it in the calculations.

The Radon-222 Decay Chain

The NCRP dose model considers dose from the radon decay products ^{218}Po (radium A or RaA), ^{214}Pb (radium B or RaB), and ^{214}Bi (radium C or RaC), and accordingly we restrict our calculations to ^{222}Rn and these decay products. The model implicitly accounts for ^{214}Po (radium C′ or RaC′, half-life 163.7 μs), which is always in secular equilibrium with ^{214}Bi; accordingly, we do not mention this decay product in calculations and formulas. In the time scales considered in this study, subsequent decay products (^{210}Pb, ^{210}Bi, and ^{210}Bi) form in negligible amounts.

The NCRP model assigns different weight to dose from transformations of RaA according to whether the nuclide is in a free ion state (unattached) or associated with an airborne dust particle or other condensation nucleus (attached). Radium A is considered to be formed initially as a free ion from the decay of ^{222}Rn. Free ions attach readily to available condensation nuclei, and the unattached RaA decreases at a rate that depends on mean particle diameter, particle count, and mean velocity of unattached RaA particles. Figure I-8 illustrates the process. Movement of RaA from the unattached to the attached state is governed by the attachment rate coefficient λ_S, given by

$$\lambda_S = \frac{S\bar{v}}{4} \quad s^{-1} \tag{I-7}$$

(NCRP 1984) where

$S = n\pi\bar{D}^2$ = surface area per unit volume ($cm^2\ cm^{-3}$) of condensation nuclei

$\bar{D}$ = diameter corresponding to the mean surface area of condensation nuclei (cm); the value $\bar{D}$ = 0.125 μm has been considered a typical average value for environmental atmospheres (NCRP 1984)

n = number concentration of condensation nuclei (cm^{-3}); indoor counts typically range from 15,000 to 120,000 condensation nuclei per cm^3 (NCRP 1984)

4 = ratio of spherical surface area to area of plane circular projection,

$\bar{v}$ = average velocity of unattached RaA ions = 1.38×10^4 cm s^{-1}.

Other decay products of ^{222}Rn exist in unattached and attached states, and the potential dosimetric significance of each state is discussed in NCRP Report No. 78 (NCRP 1984), but the NCRP dose model restricts consideration of the two states to RaA. When unattached RaB is considered, its compartment receives all unattached RaA and that fraction of attached RaA for which the recoil of the transformation breaks the bond with the condensation nucleus. The parameter indicating the probability of this dissociation is denoted by α_a and has been estimated as $\alpha_a = 0.81 \pm 0.07$ (NRCP 1984). Similar recoil fractions, β_b and β_c, can be postulated for the beta decay of RaB and RaC, but they would be small in comparison with α_a, which is associated with a higher-energy alpha particle that also has a much greater mass.

We note here for later reference that for a fixed airborne concentration of RaA, the NCRP dose model predicts dose to the tracheobronchial epithelium that increases with the fraction of

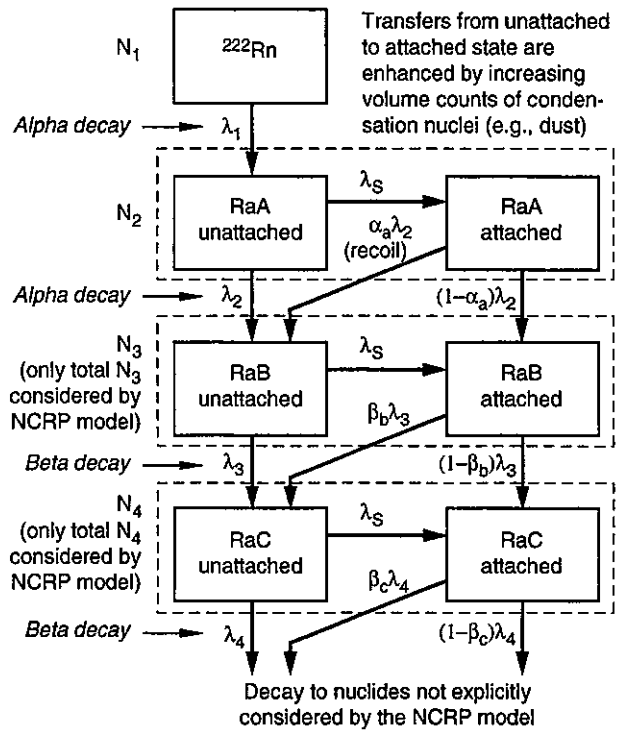

Figure I-8. Kinetics of the ^{222}Rn decay chain for the dosimetric model of NCRP Report No. 78. The decay of ^{222}Rn produces free ions of (unattached) RaA, which migrate to a state of attachment to condensation nuclei at a rate λ_S governed by the ambient count of available condensation nuclei. Both unattached and attached RaA contribute to unattached RaB; a fraction α_a of attached RaA is detached from the condensation nuclei by alpha recoil at the time of decay and become unattached RaB. The NCRP dose model, however, consolidates the two forms of RaB. Similar separations are indicated for subsequent decay products, but the NCRP model does not consider them.

the activity that is unattached (free ions are more efficient in delivering energy to the target tissue). Thus, higher particulate counts correspond, up to a point, to lower dose if the total RaA activity is held constant (the attachment coefficient λ_S increases with the particulate count n). We say up to a point, because with very high particulate counts, essentially all RaA would be associated with condensation nuclei, and further increases in the count would have negligible effect.

We now take up the ^{222}Rn decay chain kinetics. Because of the importance of the subject in the dose reconstruction, we present a scheme for making the calculations that is well suited to use with a spreadsheet, and we provide sample calculations to assist the reader in understanding the calculation procedure.

Decay chains are frequently characterized by systems of ordinary differential equations, one equation for each nuclide, with each dynamic variable representing the number of atoms of the respective nuclide. For ^{222}Rn and the decay products with which we are concerned, the equations take the form

$$\frac{dN_1}{dt} = -\lambda_1 N_1 \qquad \text{(I-8)}$$

$$\frac{dN_i}{dt} = -\lambda_i N_i + \lambda_{i-1} N_{i-1} \qquad i = 2, \ldots, 4 \tag{I-9}$$

where $N_1, \ldots, N_4$ denote the number of atoms of ^{222}Rn, RaA, RaB, and RaC, respectively, at time t. We prefer to deal with quantities of radioactivity, $A_i = \lambda_i N_i$ Bq (provided the rate coefficients λ_i have the units s^{-1}). Using this substitution, Equations I-8 and I-9 take the form

$$\frac{dA_1}{dt} = -\lambda_1 A_1 \tag{I-10}$$

$$\frac{dA_i}{dt} = -\lambda_i A_i + \lambda_i A_{i-1} \qquad i = 2, \ldots, 4 \tag{I-11}$$

(note the difference in form between the two systems) and for the initial activities we use the notation $A_1^0, \ldots, A_4^0$.

The simple structure of the system given by Equations I-10 and I-11 permits a recursive calculation for the solutions. The solution has the following form:

$$A_i = \sum_{k=1}^{i} c_{ik} \exp(-\lambda_k t) \tag{I-12}$$

where the array of coefficients c_{ik} may be calculated from the recursion

$$\begin{aligned} c_{ik} &= \frac{\lambda_i c_{i-1,k}}{\lambda_i - \lambda_k}, \qquad k < i \\ c_{ii} &= A_i^0 - \sum_{k=1}^{i-1} c_{ik}\,. \end{aligned} \tag{I-13}$$

To begin the recursion, set $c_{11} = A_1^0$. It is convenient to arrange the coefficients c_{ik} in a lower-triangular configuration, with rows indexed by values of i and columns by values of k. Such an arrangement (in a spreadsheet, for example) facilitates the calculation. Table I-7 shows the layout with the recursive formulas. To build the table, work by columns ($k = 1, \ldots, 4$), starting with the diagonal entry. In column 1, this is the initial quantity of ^{222}Rn, A_1^0. Proceeding down the column from the diagonal position to row 2, form the product of $\lambda_2/(\lambda_2 - \lambda_1)$ with the entry just above in row 1. Then move to row 3 and compute $\lambda_3/(\lambda_3 - \lambda_1)$ times the entry just above in row 2. When the first column has been filled, proceed to the second row of column 2 and compute the difference of A_2^0 (the initial activity of RaA) and the sum of all entries in the same row to the left of the diagonal (for column 2, there is only one entry to the left of the diagonal entry). Then proceed down the column as before, but using for row i the product of $\lambda_i/(\lambda_i - \lambda_2)$ and the entry immediately above. Complete the remaining columns similarly.

The middle panel of Table I-7 contains the values of the decay rate coefficients of ^{222}Rn, RaA, RaB, and RaC, expressed in reciprocal seconds. Once the coefficients c_{ik} in the main portion of the table have been computed, the amount of each species present at time t (expressed in seconds) is calculated by working across the row of species i and multiplying the coefficient in column k by $\exp(-\lambda_k t)$. For ^{222}Rn, there is a single term; for RaA, there are two terms; and so on. The sum of the products $c_{ik} \exp(-\lambda_k t)$ across row i gives the amount of nuclide i at time t (Equation I-12). This is shown in the bottom panel of Table I-7.

Table I-7. Tabular Calculation of the Decay Chain for ^{222}Rn, RaA, RaB, and RaC

	$k = 1$ (Rn)	$k = 2$ (RaA)	$k = 3$ (RaB)	$k = 4$ (RaC)
$i = 1$ (Rn)	$c_{11} = A_1^0$			
$i = 2$ (RaA)	$c_{21} = \frac{\lambda_2 c_{11}}{\lambda_2 - \lambda_1}$	$c_{22} = A_2^0 - c_{21}$		
$i = 3$ (RaB)	$c_{31} = \frac{\lambda_3 c_{21}}{\lambda_3 - \lambda_1}$	$c_{32} = \frac{\lambda_3 c_{22}}{\lambda_3 - \lambda_2}$	$c_{33} = A_3^0 - c_{31} - c_{32}$	
$i = 4$ (RaC)	$c_{41} = \frac{\lambda_4 c_{31}}{\lambda_4 - \lambda_1}$	$c_{42} = \frac{\lambda_4 c_{32}}{\lambda_4 - \lambda_2}$	$c_{43} = \frac{\lambda_4 c_{33}}{\lambda_4 - \lambda_3}$	$c_{44} = A_4^0 - c_{41} - c_{42} - c_{43}$
Terms (i = row)	$c_{i1} e^{-\lambda_1 t}$	$c_{i2} e^{-\lambda_2 t}$	$c_{i3} e^{-\lambda_3 t}$	$c_{i4} e^{-\lambda_4 t}$
λ (s^{-1})	2.10×10^{-6}	3.79×10^{-3}	4.31×10^{-4}	5.86×10^{-4}

Summation for each radionuclide (Equation I-12):

Rn	$A_1 = c_{11} e^{-\lambda_1 t}$
RaA	$A_2 = c_{21} e^{-\lambda_1 t} + c_{22} e^{-\lambda_2 t}$
RaB	$A_3 = c_{31} e^{-\lambda_1 t} + c_{32} e^{-\lambda_2 t} + c_{33} e^{-\lambda_3 t}$
RaC	$A_4 = c_{41} e^{-\lambda_1 t} + c_{42} e^{-\lambda_2 t} + c_{43} e^{-\lambda_3 t} + c_{44} e^{-\lambda_4 t}$

The coefficients c_{ik} are independent of the time t at which the evaluation is desired and consequently may be used to calculate the state of the decay chain for any value of t. But the c_{ik} do depend on the initial conditions A_i^0; therefore Table I-7 would have to be recomputed for each change in the initial equilibrium state. By preparing a table for each radionuclide in the chain, however, with a special set of initial values, it is possible to give data that are applicable to any set of initial conditions. Table I-8 contains an array for each of the four species. Each triangular subarray is computed by the rules given above, but the dimension of the subarray decreases by one with each step down the chain (RaA is 3 × 3, RaB is 2 × 2, and RaC has a single coefficient). Each subarray i is calculated with the initial conditions of $A_i^0 = 1$ and zero for the initial amount of each subsequent decay product. Thus, we are treating the initial amount of each species as a separate decay chain coming from an initial unit amount of its progenitor, and the coefficients in Table I-8 are independent of specific initial conditions. When the special separate decay chains are evaluated, their amounts are multiplied by the desired initial values for the full chain and corresponding nuclides in each subchain are added. For the reader's convenience, we show the decay rate coefficients λ_i (s^{-1}) in their appropriate columns in the bottom row of Table I-8. To illustrate the use of Table I-8 for a calculation, we turn to an example.

Table I-8. Coefficients for Calculating the ^{222}Rn Decay Chain

	Rn-222	RaA	RaB	RaC
Rn chain				
Rn-222	1			
RaA	1.0005544	−1.0005544		
RaB	1.00545336	0.12838313	−1.1338365	
RaC	1.00906948	−0.0234808	−4.2866334	3.30104478
RaA chain				
RaA		1		
RaB		−0.128312	0.128312	
RaC		0.0234678	0.48510213	−0.5085699
RaB chain				
RaB			1	
RaC			3.78064516	−3.7806452
RaC				1
λ (s^{-1})	2.10×10^{-6}	3.79×10^{-3}	4.31×10^{-4}	5.86×10^{-4}

Example I-1. We consider an initial ($t = 0$) activity ratio of ^{222}Rn : RaA : RaB : RaC = 1 : 0.6 : 0.3 : 0.2. We use Table I-8 to estimate the amount of each nuclide in the chain after one hour ($t = 3600$ s).

First, we calculate the quantities $\exp(-\lambda_i t)$ for the decay rate coefficients λ_i in the last row of Table I-8. Then in each row of the first subarray of Table I-8, we compute the sum of the products of the tabulated coefficients and the corresponding exponentials. These sums of products are given in the Rn-222 column of Table I-9, beginning at the ^{222}Rn row. For example, in the RaA row of Table I-9, the first-column entry is

$$0.99301754 = 1.0005544\exp(-\lambda_1 t) - 1.0005544\exp(-\lambda_2 t),$$

where the coefficients are from the RaA row of the first subarray in Table I-8, and the numeric values of the exponentials are given in Table I-9. We follow the same procedure in the second subarray of Table I-8. The results are tabulated in the RaA column of Table I-9, beginning in the RaA row. We repeat the procedure for the third and fourth subarrays of Table I-8. These results are in the RaB and RaC columns, respectively, of Table I-9.

The amount of each species after 3600 s is calculated from the entries in the columns labeled Rn-222, RaA, RaB, and RaC of Table I-9. In each row corresponding to a nuclide, sum the products of each row entry and the corresponding initial condition in the first row of the table. For example, the RaA activity in the last column of Table I-9

Table I-9. Radon Decay Chain One Hour (3600 s) after Initial State

	Rn-222	RaA	RaB	RaC	Activity at 3600 s
Initial conditions	1	0.6	0.3	0.2	
$\exp(-\lambda_i t)$	0.9924685	1.1871×10^{-6}	0.21190865	0.12128647	
Rn-222	0.9924685				0.9924685
RaA	0.99301754	1.1871×10^{-6}			0.99301825
RaB	0.75761118	0.02719027	0.21190865		0.83749794
RaC	0.49346702	0.041114713	0.3426103	0.12128647	0.64517623

is computed as

$$0.99301825 = 1 \times 0.99301754 + 0.6 \times 1.1871 \times 10^{-6}.$$

The final results are shown in the last column of Table I-9.

Unattached RaA

Example I-1 deals only with the total amount of RaA and does not consider disaggregation into the unattached and attached compartments that are indicated in Figure I-8. We denote the unattached radioactivity of RaA by the symbol A_2^*. The differential equation describing the kinetics shown in Figure I-8 (converted to activity units) is

$$\frac{dA_2^*}{dt} = \lambda_2 A_1 - (\lambda_2 + \lambda_S) A_2^* \tag{I-14}$$

and we use the symbol $(A_2^*)^0$ for the initial unattached activity. The symbol λ_S is the attachment rate coefficient of Equation I-7. By substituting $A_1 = A_1^0 \exp(-\lambda_1 t)$ (for ^{222}Rn) and solving Equation I-14, we obtain

$$A_2^* = (A_2^*)^0 \exp\big(-(\lambda_2 + \lambda_S)t\big) + \frac{A_1^0 \lambda_2}{\lambda_2 + \lambda_S - \lambda_1}\Big[\exp(-\lambda_1 t) - \exp\big(-(\lambda_2 + \lambda_S)t\big)\Big] \tag{I-15}$$

as the explicit equation for the unattached activity of RaA at time t. As before, quantities with the subscript 1 refer to ^{222}Rn.

Example I-2. We assume that ^{222}Rn and RaA are initially 1 and 0 Bq, respectively, and that the ambient count of condensation nuclei is 3×10^{10} m^{-3}. Using parameter values of $\bar{D}$ μm (mean aerosol diameter) and $\bar{v}$ cm s^{-1} (average speed of unattached decay products) cited after Equation I-7, we use Equation I-15 to calculate the amount of unattached RaA after 3600 s.

First it is necessary to calculate the attachment rate coefficient λ_S. From Equation I-7 (with appropriate conversions of units) the value is $\lambda_S = 0.0508\ s^{-1}$. Substituting this value, the initial values, and the decay rate coefficients λ_1 and λ_2 from Table I-8 into Equation I-15, we calculate the value $A_2^* = 0.0689$ Bq. Using the method of Example I-1, we also calculate the total amount of RaA after 3600 s as $A_2 = 0.9930$ Bq (Table I-9). Thus the amount attached to condensation nuclei is $A_2 - A_2^* = 0.9241$ Bq. The fraction $f_a = A_2^*/A_1 = 0.0694$ is essentially at equilibrium in atmospheres older than about two minutes for the parameters of this example. Equilibrium for f_a is given by the expression $\lambda_2/(\lambda_2 + \lambda_S - \lambda_1)$, which can be derived from Equation I-15 divided by the ^{222}Rn quantity, $A_1 = A_1^0 \exp(-\lambda_1 t)$ and by taking the limit as $t \to \infty$. We emphasize this point because the fraction of RaA that is unattached at the K-65 silos is unknown, but equilibration of f_a is rapid, and at moderate distances from the source a precise knowledge of the initial value is not necessary.

Indoor and Outdoor Concentrations of Radon-222 and Decay Products

A mass-balance model of air exchange is applied to distinguish between concentrations in air of ^{222}Rn and its decay products indoors and outdoors. We assume that the outdoor concentrations at a particular location have already been calculated from the air dispersion model and the decay chain equations discussed previously, in which the time variable corresponds to the mean time the released radioactivity requires to move from the source to the receptor location. Thus the outdoor proportions of radon and its decay products have evolved to an appropriate fraction of equilibrium as the radioactivity in the plume has moved downwind. For the calculations, the outdoor concentrations of ^{222}Rn and each decay product are assumed constant at the receptor location (they are interpreted as time averages for specific meteorological conditions). The model for indoor concentrations is given by the following steady-state expressions, which were derived from differential equations that quantify radioactive decay, attachment of ions to condensation nuclei, and indoor-outdoor air exchange:

Radon-222:
$$[A_1]_{in} = \lambda_e [A_1]_{out} (\lambda_1 + \lambda_e)^{-1} \quad \text{(I-16)}$$

RaA unattached:
$$[A_2^*]_{in} = \left(\lambda_2 [A_1]_{in} + \lambda_e [A_2^*]_{out}\right) (\lambda_2 + \lambda_S + \lambda_e + v_{unatt} A_S/V)^{-1} \quad \text{(I-17)}$$

RaA attached:
$$[A_2^-]_{in} = \left(\lambda_S [A_2^*]_{in} + \lambda_e [A_2^-]_{out}\right) (\lambda_2 + \lambda_e + v_{att} A_S/V)^{-1} \quad \text{(I-18)}$$

RaB:
$$[A_3]_{in} = \left(\lambda_3 ([A_2^*]_{in} + [A_2^-]_{in}) + \lambda_e [A_3]_{out}\right) (\lambda_3 + \lambda_e + v_{att} A_S/V)^{-1} \quad \text{(I-19)}$$

RaC:
$$[A_4]_{in} = \left(\lambda_4 [A_3]_{in} + \lambda_e [A_4]_{out}\right) (\lambda_4 + \lambda_e + v_{att} A_S/V)^{-1} \quad \text{(I-20)}$$

where

$[A_i]_{in}$ = indoor activity concentration (pCi m^{-3}) of nuclide i of the radon decay chain (index i has the values 1, 2, 3, and 4 corresponding to ^{222}Rn, RaA, RaB, and RaC, respectively)

$[A_i]_{out}$ = outdoor activity concentration (pCi m^{-3}) of nuclide i of the radon decay chain

$[A_2^*]$ = concentration of unattached RaA, and $[A_2^-]$ = attached activity of RaA ($[A_2] = [A_2^*] + [A_2^-]$)

λ_i = decay rate coefficient for nuclide i (s^{-1})

λ_e = fractional air exchange rate of the building with the outdoors (s^{-1}) (except for units, this parameter is the same as the quantity "air changes per hour," or ACH)

λ_S = fractional attachment rate (s^{-1}) for unattached RaA particles (Equation I-7)

v_{unatt} = deposition velocity ($m\ s^{-1}$) for plateout of unattached (free-ion) RaA on interior surfaces

v_{att} = deposition velocity ($m\ s^{-1}$) for plateout of attached radon decay products; this parameter depends on the size distribution of the condensation nuclei

A_S/V = indoor surface-to-volume ratio (m^{-1}).

Unattached fractions of RaB and RaC are not estimated, because the NCRP model does not use the partitioning for these species. As Equations I-19 and I-20 indicate, RaB and RaC are treated as if their unattached fractions were zero, and their deposition on indoor surfaces is governed by the parameter v_{att}.

Our estimate of the parameter λ_e in Equations I-16 through I-20 is based on a compilation of surveys of residences in the United States by climatic region reported by Murray and Burmaster (1995). For the region that includes Ohio, an empirical distribution of air changes per hour for all seasons has 50th percentile 0.40 h^{-1}, with 5th and 95th percentiles being given as 0.14 h^{-1} and 1.38 h^{-1}, respectively. These authors caution that how well the given distributions represent all dwellings in a region is not known. We also point out that the data are not strictly applicable to nonresidential buildings, but we have applied the median of this distribution to schools and workplaces, as well as to dwellings, in the nine scenarios of this task (Appendix J), i.e., for all buildings we assume $\lambda_e = 0.40/3600\ s^{-1}$. The sensitivity of dose estimates to this parameter is discussed in a subsequent subsection.

Simple calculations based on dimensions of rooms, ranging from 6 ft × 9 ft × 7 ft to 24 ft × 40 ft × 8 ft, give surface-to-volume ratios A_S/V ranging from about 1 m^{-1} to about 3 m^{-1}. This range includes both empty rooms and rooms with horizontal furniture surface area of one-third that of the floor (we included deposition on the floor under the furniture surfaces). We have chosen a nominal value of 2 m^{-1}, which is treated as a fixed reference value in all calculations. In a later subsection, we show the sensitivity of indoor dose estimates to variation of this parameter.

The deposition velocities v_{att} and v_{unatt} for indoor plateout depend on the state of attachment of the nuclide species. For attached species, the nominal value chosen for the condensation nuclei is 0.2 m h^{-1} (Knutson 1988). For unattached RaA, several experimental ranges have been cited; the range 5–10 m h^{-1}, with nominal value 8 m h^{-1}, has been suggested for exploratory calculations (Knutson 1988), and we have adopted this value for the dose calculations. Sensitivity analyses discussed in a subsequent subsection indicate little sensitivity of indoor/outdoor dose ratios to changes in v_{unatt} and moderate sensitivity to changes in v_{att}.

The NCRP Radon Dose Model

The NCRP dose model (NCRP 1984) estimates annual absorbed dose (mrad $year^{-1}$) to the tracheobronchial epithelium as a function of ambient air concentrations of $[A_2^*]$ (unattached RaA), $[A_2^-] = [A_2] - [A_2^*]$ (attached RaA), $[A_3]$ (RaB), and $[A_4]$ (RaC). (These notations were introduced in connection with Equations I-16 through I-20.) The dosimetry has been worked out for tissue at a depth of 22 μm below the surface of the bronchial epithelium, which is believed to be the shallowest locus of bronchial cell nuclei associated with bronchiogenic cancer (NCRP 1984). The NCRP dose conversion factors are given for the adult male and female and the 10-year-old child. Other ages are not given explicit treatment, but a calculation is

described that supports using the absorbed dose for the adult female as a surrogate for that of the one-year-old child (NCRP 1984). The absorbed dose-rate factors (DRFs) are expressed as follows in the notations of this appendix:

Male Adult:

Light activity: $$DRF = 0.98[A_2^*] + 0.029([A_2] - [A_2^*]) + 0.16[A_3] + 0.14[A_4] \quad \text{(I-21)}$$

Resting: $$DRF = 0.32[A_2^*] + 0.022([A_2] - [A_2^*]) + 0.12[A_3] + 0.10[A_4] \quad \text{(I-22)}$$

Female Adult:

Light activity: $$DRF = 0.82[A_2^*] + 0.029([A_2] - [A_2^*]) + 0.16[A_3] + 0.14[A_4] \quad \text{(I-23)}$$

Resting: $$DRF = 0.29[A_2^*] + 0.019([A_2] - [A_2^*]) + 0.10[A_3] + 0.09[A_4] \quad \text{(I-24)}$$

Child (10-year-old):

Light activity: $$DRF = 2.36[A_2^*] + 0.06([A_2] - [A_2^*]) + 0.26[A_3] + 0.28[A_4] \quad \text{(I-25)}$$

Resting: $$DRF = 0.54[A_2^*] + 0.04([A_2] - [A_2^*]) + 0.17[A_3] + 0.18[A_4]. \quad \text{(I-26)}$$

In Equations I-21 through I-26, the DRFs are in mrad year^{-1}, and $[A_2]$, $[A_3]$, and $[A_4]$ denote concentrations in air of radium A, radium B, and radium C, respectively, in pCi m^{-3}. The same units apply to $[A_2^*]$, the activity concentration of unattached RaA. To convert these absorbed doses to mrem, it is necessary to multiply by the quality factor 20 that is specified for alpha decay (ICRP 1991). Dose-rate factors for intermediate ages are estimated from Equations I-21 through I-26 by linear interpolation.

Sensitivity of Estimates of Dose to Parameter Values and Initial State

In order to apply the foregoing theory to calculations of dose from radon decay products, it is necessary to specify the equilibrium state of the radon decay chain at the point of release and the fraction of RaA that remains unattached. The subsequent equilibrium value of the unattached proportion of RaA depends on the count n of condensation nuclei per unit volume of air near the receptor. It is also necessary to consider the difference in dose rate between indoor and outdoor atmospheres. This difference is regulated by the parameter λ_e, which characterizes the air changes per hour inside a building, and by deposition velocities and other parameters that govern plateout of radon decay products on indoor surfaces (Equations I-16 through I-20). The following discussion explores the sensitivity of the dose calculation to each of these parameters.

The stage of equilibrium of the radon decay chain at the K-65 silos is unmeasured. The hypothetical extremes of pure radon gas, on the one hand, and complete equilibrium of radon and decay products, on the other hand, are highly improbable, although for the years before the K-65 silos were sealed, the latter hypothesis is likely to be nearer reality than the former. NCRP Report No. 78 (NCRP 1984) examines this question for environmental radon in the context of an activity ratio 1 : 0.9 : 0.7 : 0.7, which is considered environmentally typical, and a second

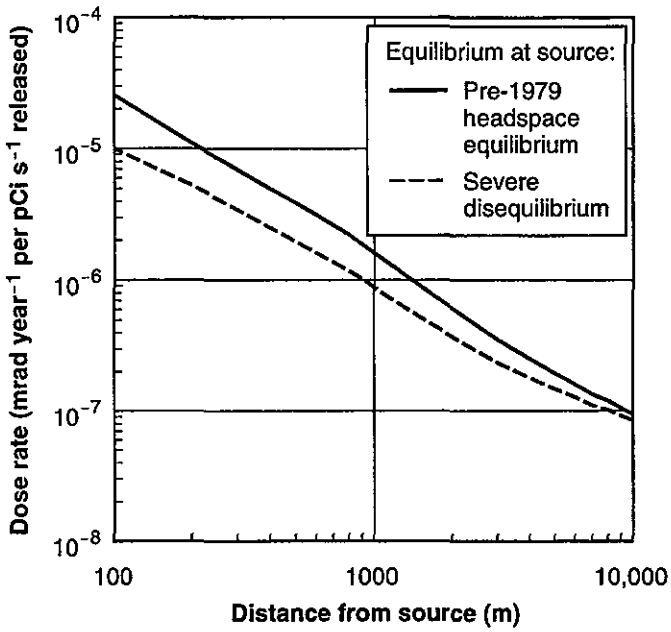

Figure I-9. Normalized annual radon dose for different assumed degrees of disequilibrium at the release point (K-65 silos). The dose corresponds to a normalized release rate of 1 pCi s^{-1} of radon gas. Release rates of the decay products are determined by the initial equilibrium that is assumed. The computed pre-1979 headspace equilibrium is 1 : 0.97 : 0.86 : 0.78, and severe disequilibrium is 1 : 0.6 : 0.3 : 0.2. The receptor is assumed to be an adult male engaged in light activity outdoors and located northeast of the source. At 1000 m from the source, the larger dose rate exceeds the smaller by a factor of about 2.8. Please note that this figure illustrates a dependence of radon dose on only two variables: distance from the source and initial equilibrium ratio. It does not represent the full range of possible dose rates from exposure to radon and its decay products. The radon dose calculations reported in this volume and in Appendix K take full account of age, sex, and fractions of time spent indoors and outdoors.

ratio 1 : 0.6 : 0.3 : 0.2, which is considered to constitute severe disequilibrium. The latter ratio corresponds to a dose rate that is about 50% of that produced by the former. Calculated concentrations of radon and decay products in the silo headspaces before sealing indicate a ratio of about 1 : 0.97 : 0.86 : 0.78, which somewhat exceeds the NCRP's environmentally typical level. We use this ratio at the point of release for pre-1979 dose estimates and the NCRP's environmentally typical ratio (1 : 0.9 : 0.7 : 0.7) at the point of release for estimates of radon dose after the silos were sealed (it is assumed that most of the decay products formed inside the sealed silos would plate out as the headspace gas diffuses through the concrete domes and walls). Please note that each of these ratios only provides an initial value as the radionuclides leave the silos; the subsequent evolution of the ratio is calculated as the plume moves downwind, and the evolved value is applied to the dose calculation at the receptor point. As the plume moves away from the source, the ratio asymptotically approaches full equilibrium. This convergence is illustrated by Figure I-9, which plots normalized dose rate as a function of distance for two initial ratios: the calculated pre-1979 headspace value and the NCRP's severe disequilibrium ratio.

The calculated pre-1979 headspace equilibrium is consistent with the environmental measurements that were available to us, and calculations based on it accurately reproduce gamma exposure rates that were measured on the silo domes before sealing took place. We know of no reason to assume that the level of equilibrium of the radon gas and decay products leaving the silos during this period was significantly inferior to this calculated value. (We are discussing a deterministic value of the ratio, but in the course of uncertainty calculations, the ratio varies from one Monte Carlo iteration to the next.)

Other mechanisms for altering the proportions of radon and its decay products in the airborne plume have been proposed. In its review of the draft of this task 6 report, the National Research Council (NRC) Committee on an Assessment of CDC Radiation studies suggested that the unattached RaA would be removed from the plume by attachment to dust particles, which the committee believed would have been abundantly suspended near the site by plant operations and construction. In fact, an analysis of measured particulates from 1971 through 1991 and particle size distributions typical of suspended soil particles indicated that the maximum likely effect on radon dose would be a reduction of perhaps 2% for an individual residing near the facility (the relatively large soil particles are not sufficiently numerous, in comparison with much smaller environmentally prevalent condensation nuclei, to produce the effect intuited by the committee). The analysis was reported by Killough et al. (1997, Attachment A).

In Example I-2, we referred to the rapid equilibration of the proportion of unattached RaA, i.e., the fraction A_2^*/A_1 as the plume moves downwind. As a practical matter, for offsite locations, the initial value of this quantity, f_a, has little effect on estimates of dose. We use a nominal value $f_a = 0.069$ for all calculations.

We approach the sensitivity of dose estimates to indoor plateout of radon decay products by considering ratios of annual indoor dose to annual outdoor dose (indoor/outdoor dose ratios) and the variation of these ratios with location, initial equilibrium state, and other parameter values. Table I-10 shows sensitivity comparisons of the indoor/outdoor dose ratios for joint variations in three pairs of parameters.

The first comparison shows that the indoor/outdoor dose ratio is relatively insensitive to distance. For the case of severe disequilibrium at the release source, only at distances from the source of about 5000 m is the equilibrium state sufficiently mature for plateout to reduce the ratio below 1.0; but in the case of the headspace equilibrium at the source, the ratio is less than unity at all distances shown in the table. The first comparison also indicates that the ratio is relatively insensitive to plateout of unattached decay products (maximum variation of 1.41/1.29 → 9%), at least for the nominal values of other parameters indicated for the comparison, and for both initial equilibrium states.

The second and third comparisons in Table I-10 indicate moderate sensitivity of the indoor/outdoor dose ratio to the air changes per hour (λ_e) when this parameter is varied between its 5th and 95th percentile values from the study of Murray and Burmaster (1995) that was discussed previously; the maximum variation is 0.77/0.61 → 26%. The greatest sensitivity is observed in varying the deposition velocity for the condensation nuclei (v_{att}); the largest variation is 0.97/0.61 → 59%. The maximum variation for the deposition velocity v_{unatt} is 0.88/0.70 → 26%. This contrast for the two deposition velocities is seen to be plausible when one considers that the greater effectiveness of unattached RaA in delivering dose to the tra-

Table I-10. Indoor/Outdoor Radon Dose Ratios: Sensitivity to Various Parameters[a]

	Severe disequilibrium at the source Rn : RaA : RaB : RaC = 1 : 0.6 : 0.3 : 0.2			Pre-1979 headspace equilibrium in the K-65 silos Rn : RaA : RaB : RaC = 1 : 0.97 : 0.86 : 0.78		
First comparison: $A_S/V = 2\ m^{-1}$, $\lambda_e = 0.4\ h^{-1}$, $v_{att} = 0.2\ m\ h^{-1}$						
	v_{unatt} (m h^{-1})			v_{unatt} (m h^{-1})		
Distance (m)	0	5	10	0	5	10
1000	1.41	1.35	1.29	0.86	0.83	0.80
5000	1.02	0.98	0.95	0.82	0.79	0.76
10,000	0.87	0.83	0.80	0.80	0.77	0.74
Second comparison: distance = 1000 m, $v_{unatt} = 5\ m\ h^{-1}$						
	λ_e (h^{-1})			λ_e (h^{-1})		
v_{att} (m h^{-1})	0.14	0.40	1.38	0.14	0.40	1.38
0.0	1.70	1.63	1.38	0.97	1.00	1.01
0.2	1.36	1.35	1.23	0.78	0.83	0.89
0.5	1.08	1.10	1.07	0.61	0.67	0.77
Third comparison: distance = 1000 m, $v_{unatt} = 5\ m\ h^{-1}$						
	λ_e (h^{-1})			λ_e (h^{-1})		
A_S/V m^{-1}	0.14	0.40	1.38	0.14	0.40	1.38
1	1.54	1.51	1.33	0.88	0.92	0.96
2	1.36	1.35	1.23	0.78	0.83	0.89
3	1.22	1.22	1.15	0.70	0.75	0.83

[a] All comparisons in this table are based on condensation nuclei count $n = 3 \times 10^{10}\ m^{-3}$. The subject is a male adult, and the dose estimate is based on "light activity" for both outdoors and indoors, to avoid confounding this variable with parameters affecting plateout. Table I-12 contrasts indoor and outdoor dose with different exercise states.

cheobronchial epithelium is offset by the relatively small fraction of activity that is typically in this state (about 7% for the dust counts that we take as nominal). Moreover, the term containing v_{unatt} in the denominator of Equation I-17 is dominated by the attachment rate coefficient ($\lambda_S \approx 0.05\ s^{-1}$, whereas $v_{unatt} \cdot A_S/V = 8 \times 2/3600\ s^{-1} \approx 0.004\ s^{-1}$). This diminishes sensitivity to v_{unatt}. On the other hand, the term with v_{att} in the denominators of Equations I-19 and I-20 is of comparable magnitude with the terms λ_i and λ_e, and this favors sensitivity to v_{att}, as Table I-10 indicates.

A final aspect of sensitivity of radon dose that affects both indoor and outdoor air is the count of condensation nuclei per unit air volume. Table I-10 was computed for a nominal count value of $3 \times 10^{10}\ m^{-3}$, which NCRP Publication No. 78 appears to consider environmentally typical. We have chosen this value as nominal for both indoor and outdoor calculations (an

Table I-11. Sensitivity of Cumulative Radon Dose (Sv) to Condensation Nuclei Count per Unit Volume

Other parameter values:		
	v_{att}	0.2 m h^{-1}
	v_{unatt}	8 m h^{-1}
	A_S/V	2 m^{-1}
	λ_e	0.4 h^{-1} (air changes per hour)

Count (m^{-3})	Dose (Sv)	Comment
1×10^9	6.1	Minimum for human activity
1×10^{10}	3.6	
1.5×10^{10}	3.4	Minimum for Figures 6.2 and 6.3 in NCRP (1984)
2×10^{10}	3.2	Taken to be a reasonable minimum value in NCRP (1984)
2.2×10^{10}	3.2	Estimate based on Fernald area particulate data for the period 1989–1991
3×10^{10}	3.0	Considered environmentally typical by NCRP (1984); adopted as nominal for this study
5×10^{10}	2.9	
1.2×10^{11}	2.8	Maximum for Figures 6.2 and 6.3 in NCRP (1984)
1×10^{12}	2.7	Maximum value considered in tables in NCRP (1984)

indoor value of 5×10^{10} might have been more representative of the few indoor measurements, but Table I-11 shows that the corresponding difference in dose is minor). Indoor ranges of this parameter span three orders of magnitude at the extreme and about one order of magnitude in indoor situations ranging from quiescence to routine human activity (NCRP 1984). Table I-11 shows cumulative radon dose estimates for exposure scenario 1 (Appendix J) corresponding to a range of values of the condensation nuclei count. As a practical matter, the sensitivity with respect to the nominal value of 3×10^{10} m^{-3} is about 21% (= $(3.4 - 2.8)/2.8 \times 100$), and most of this range is variability within the diurnal cycle of human activity rather than uncertainty with regard to long-term averages (see NCRP 1984, Figures 6.2 and 6.3).

Final Example of Dose Calculation for Radon Decay Products

We close the discussion of calculating dose from decay products of ^{222}Rn with an example that combines both environmental and dosimetric aspects of the problem. We return to the initial conditions of Example I-1 and estimate dose to a receptor 1 hour (3600 s) downwind.

Example I-3. Suppose the equilibrium state of radon and its decay products at the K-65 silos is Rn : RaA : RaB : RaC = 1 : 0.6 : 0.3 : 0.2 (the severe disequilibrium of NCRP Publication No. 78). We consider an average wind speed $\bar{u}$ = 2 m s^{-1} into a directional

sector with frequency $f = 0.12$ and a receptor at distance 7200 m in this direction. We assume that the diffusion factor for this distance is $\chi u/(Qf) = 3.2 \times 10^{-5}$ m^{-2} (Appendix M). We wish to estimate the annual dose (mrad year^{-1}) to a female adult who spends all of her time at this location, 90% indoors (for simplicity, we assume that time spent indoors is resting, and that time outdoors is spent in light activity). We assume a release rate of $Q = 1$ pCi s^{-1}.

First, we estimate the outdoor air concentration as

$$\chi = \frac{3.2 \times 10^{-5}\ \text{m}^{-2}}{2\ \text{m s}^{-1}} \times 0.12 \times 1\ \text{pCi s}^{-1} = 1.9 \times 10^{-6}\ \text{pCi m}^{-3}.$$

Table I-12 gives amounts of radon and each decay product at the receptor distance per pCi of radon released from the silos. Multiplying these entries by the concentration 1.9×10^{-6} pCi m^{-3} gives the respective concentrations in air of ^{222}Rn, RaA, RaB, and RaC, which are also shown in Table I-12. To convert these values to their indoor counterparts, we use Equations I-16 through I-20, with $\lambda_S = 0.0508$ s^{-1} (as computed in Example I-2), $v_{att} = 0.2$ m h^{-1}, $v_{unatt} = 8$ m h^{-1}, $\lambda_e = 0.4$ h^{-1}, and $A_S/V = 2$ m^{-1} (as shown in Table I-11). The indoor concentrations of radon and the decay products are shown in Table I-12. Note that at a distance 7200 m from the source, the indoor equilibrium appears less mature than the outdoor equilibrium. This effect is partly the result of the plateout of decay products indoors.

The final step is to use the outdoor and indoor air concentrations in Table I-12 with the NCRP radon dose model (Equations I-23 and I-24), together with the appropriate fractions that partition the time spent in each activity state (conveniently coinciding with indoors and outdoors for this example). The lower part of Table I-12 shows the results of these operations and the estimate of total annual dose per unit release rate.

Table I-12. Sample Calculation of Dose from Radon Decay Products[a]

	Radon chain at 7200 m relative to release of 1 pCi Rn-222	Concentrations (pCi m^{-3}) of Rn-222 and decay products at 7200 m	
	Outdoor	Outdoor	Indoor
Rn-222	0.9925	1.89×10^{-6}	1.85×10^{-6}
RaA (attached)	0.9241	1.76×10^{-6}	1.55×10^{-6}
RaA* (unattached)	0.0689	1.31×10^{-7}	1.19×10^{-7}
RaB	0.8375	1.59×10^{-6}	1.37×10^{-6}
RaC	0.6452	1.23×10^{-6}	1.16×10^{-6}
	Time fraction	Dose (mrad $year^{-1}$ per pCi s^{-1})	
Light activity (outdoor)	0.1	5.84×10^{-7}	
Resting (indoor)	0.9		3.06×10^{-7}
Total		3.34×10^{-7}	

[a] The data for the calculations in this table are given in Table I-3. The subject for whom the dose is estimated is a female adult. The basis for the dose estimates shown is an initial equilibrium ratio at the source of 1 : 0.6 : 0.3 : 0.2, which corresponds to "severe disequilibrium." If the calculations are repeated with the estimated headspace equilibrium ratio, 1 : 0.97 : 0.86 : 0.78, the total dose is 3.57×10^{-7} mrad $year^{-1}$ per pCi s^{-1} released, an increase of about 7%. The outdoor dose component increases by about 19% at the given distance from the source (Figure I-9).

REFERENCES

Andersen I. 1972. "Relationships between Outdoor and Indoor Air Pollution." Technical Note. *Atmospheric Environment* **6**: 275–278.

Benson F.B., J.J. Henderson, and D.E. Caldwell. 1972. *Indoor-Outdoor Air Pollution Relationships: A Literature Review.* Unnumbered report. U.S. Environmental Protection Agency, National Environmental Research Center, Research Triangle Park, North Carolina.

Cristy M.W., R.W. Leggett, D.E. Dunning, Jr., and K.F. Eckerman. 1986. *Relative Age-Specific Radiation Dose Commitment Factors for Major Radionuclides Released from Nuclear Fuel Facilities.* Report NUREG/CR-4628, ORNL/TM-9890, Oak Ridge National Laboratory, Oak Ridge, Tennessee.

Dunning D.E., Jr., R.W. Leggett, and M.G. Yalcintas. 1980. *A Combined Methodology for Estimating Dose Rates and Health Effects from Exposure to Radioactive Pollutants.* Report ORNL/TM-7105, Oak Ridge National Laboratory, Oak Ridge, Tennessee.

Eckerman K.F. and J.C. Ryman. 1993. *External Exposure to Radionuclides in Air, Water, and Soil.* Report EPA 402-R-93-081. Office of Radiation and Indoor Air, U.S. Environmental Protection Agency, Washington, D.C.

Eckerman K.F., A.B. Wolbarst, and A.C.B. Richardson. 1988. *Limiting Values of Radionuclide Intake and Air Concentration and Dose Conversion Factors for Inhalation, Submersion, and Ingestion.* Federal Guidance Report No. 11. U.S. Environmental Protection Agency, Office of Radiation Programs, Washington, D.C.

International Commission on Radiological Protection (ICRP). 1994. *Human Respiratory Tract Model for Radiological Protection.* ICRP Publication 66. Elsevier Science Limited, Oxford.

International Commission on Radiological Protection (ICRP). 1991. *1990 Recommendations of the International Commission on Radiological Protection.* ICRP Publication 60. *Ann. ICRP* **21**(1–3). Pergamon Press, Oxford.

International Commission on Radiological Protection (ICRP). 1990. *Age-Dependent Doses to Members of the Public from Intake of Radionuclides: Part 1.* ICRP Publication 56. *Ann. ICRP* **20**(2). Pergamon Press, Oxford.

International Commission on Radiological Protection (ICRP). 1979. *Limits for Intakes of Radionuclides by Workers.* ICRP Publication 30 Part 1. *Ann. ICRP* **2**(3/4). Pergamon Press, Oxford.

International Commission on Radiological Protection (ICRP). 1977. *Recommendations of the International Commission on Radiological Protection.* ICRP Publication 26. Pergamon Press, Oxford.

International Commission on Radiological Protection (ICRP). 1975. *Report of the Task Group on Reference Man.* ICRP Publication 23. Pergamon Press, Oxford.

Killough G.G., M.J. Case, K.R. Meyer, S.K. Rope, D.W. Schmidt, B. Shleien, W.K. Sinclair, P.G. Voillequé, and J.E. Till. 1997. *Responses to Comments from the National Academy of Sciences Related to Task 6 of the Fernald Dosimetry Reconstruction Project.* Report No. 4-CDC-Fernald-1997-FINAL, Radiological Assessments Corporation, Neeses, South Carolina.

Knutson E.O. 1988. "Modeling Indoor Concentrations of Radon's Decay Products." Chapter 5 in: Nazaroff W.W. and A.V. Nero, Jr., eds. *Radon and Its Decay Products in Indoor Air.* John Wiley and Sons, New York.

Kocher D.C. 1981. *Radioactive Decay Tables — A Handbook of Decay Data for Application to Radiation Dosimetry and Radiological Assessments.* Report DOE/TIC-11026, Technical Information Center, U.S. Department of Energy, Oak Ridge, Tennessee.

Morrow P.E., D.V. Bates, B.R. Fish, T.F. Hatch, and T.T. Mercer. 1966. "Deposition and Retention Models for Internal Dosimetry of the Human Respiratory Tract." *Health Physics* **12**: 173–207.

Murray D.M. and D.E. Burmaster. 1995. "Residential Air Exchange Rates in the United States: Empirical and Estimated Parametric Distributions by Season and Climatic Region." *Risk Analysis* **15**(4): 459–465.

National Council on Radiation Protection and Measurements (NCRP). 1984. *Evaluation of Occupational and Environmental Exposures to Radon and Radon Daughters in the United States.* NCRP Report No. 78, NCRP, Bethesda, Maryland.

Raabe O.G. 1969. "Concerning the Interactions that Occur between Radon Decay Products and Aerosols." *Health Physics* **17**: 177–185.

Roseberry A.M. and D.E. Burmaster. 1992. "Lognormal Distributions for Water Intake by Children." *Risk Analysis* **12**(1): 99–104.

Roy M. and C. Courtay. 1991. "Daily Activities and Breathing Parameters for Use in Respiratory Tract Dosimetry." *Radiation Protection Dosimetry* **3**: 179–186.

Rupp E.M. 1980. "Age Dependent Values of Dietary Intake for Assessing Human Exposures to Environmental Pollutants." *Health Physics* **39**: 151–163.

U.S. Department of Energy (USDOE). 1988. *External Dose-Rate Conversion Factors for Calculation of Dose to the Public.* Report DOE/EH-0070. Assistant Secretary for Environment, Safety, and Health, Office of Environmental Guidance and Compliance, Washington, D.C.

Yang Y.-Y. and C.B. Nelson. 1986. "An Estimation of Daily Food Usage Factors for Assessing Radionuclide Intakes in the U.S. Population." *Health Physics* **50**(2): 245–257.

Table I-1S. Internal Dose Conversion Factors for ^{238}U (Sv Bq^{-1})

U-238 T1/2 = 4.468E9y

	Inhalation			Oral	
	Class D f1 = 5.0E-02	Class W f1 = 5.0E-02	Class Y f1 = 2.0E-03	f1 = 5.0E-02	f1 = 2.0E-03
Adrenals	2.24E-08 (33 16 51)	6.77E-09 (30 29 41)	3.22E-09 (5 1 94)	2.31E-09	9.28E-11
Bld wall	2.22E-08 (33 16 51)	6.70E-09 (30 29 41)	2.38E-09 (7 2 91)	2.30E-09	9.46E-11
BSurface	9.78E-06 (33 16 51)	2.94E-06 (30 29 41)	1.01E-06 (7 2 91)	1.01E-06	4.04E-08
Breast	2.23E-08 (33 16 51)	6.74E-09 (30 29 41)	2.91E-09 (6 2 92)	2.31E-09	9.33E-11
ST wall	2.24E-08 (33 16 51)	7.30E-09 (31 27 42)	3.74E-09 (12 3 85)	3.28E-09	1.07E-09
SI wall	2.26E-08 (34 16 50)	8.09E-09 (33 25 42)	4.14E-09 (22 6 72)	4.65E-09	2.56E-09
ULI wall	2.44E-08 (38 15 47)	1.48E-08 (39 17 44)	1.24E-08 (37 10 53)	1.61E-08	1.46E-08
LLI wall	2.90E-08 (47 13 40)	3.20E-08 (43 12 45)	3.32E-08 (42 11 47)	4.57E-08	4.57E-08
Kidneys	4.01E-06 (33 16 51)	1.21E-06 (30 29 41)	4.27E-07 (7 2 91)	4.15E-07	1.66E-08
Liver	2.22E-08 (33 16 51)	6.73E-09 (30 29 41)	3.13E-09 (5 1 94)	2.30E-09	9.26E-11
Lungs	2.80E-07 (3 2 95)	1.42E-05 (0 0 100)	2.66E-04 (0 0 100)	2.30E-09	9.22E-11
Ovaries	2.23E-08 (33 16 51)	6.71E-09 (30 29 41)	2.42E-09 (7 2 91)	2.31E-09	1.02E-10
Pancreas	2.23E-08 (33 16 51)	6.74E-09 (30 29 41)	3.18E-09 (5 1 94)	2.30E-09	9.30E-11
R Marrow	6.58E-07 (33 16 51)	1.98E-07 (30 29 41)	6.88E-08 (7 2 91)	6.80E-08	2.72E-09
Skin	2.23E-08 (33 16 51)	6.71E-09 (30 29 41)	2.58E-09 (6 2 92)	2.30E-09	9.24E-11
Spleen	2.23E-08 (33 16 51)	6.74E-09 (30 29 41)	3.12E-09 (5 1 94)	2.30E-09	9.27E-11
Testes	2.22E-08 (33 16 51)	6.70E-09 (30 29 41)	2.37E-09 (7 2 91)	2.30E-09	9.39E-11
Thymus	2.22E-08 (33 16 51)	6.76E-09 (30 29 41)	3.78E-09 (4 1 95)	2.30E-09	9.20E-11
Thyroid	2.22E-08 (33 16 51)	6.71E-09 (30 29 41)	2.73E-09 (6 2 92)	2.30E-09	9.20E-11
Uterus	2.22E-08 (33 16 51)	6.70E-09 (30 29 41)	2.40E-09 (7 2 91)	2.30E-09	9.51E-11
Effective (ICRP60)	2.30E-07 (29 14 57)	1.77E-06 (1 1 98)	3.19E-05 (0 0 100)	2.58E-08	6.42E-09

Table I-2S. Internal Dose Conversion Factors for ^{235}U (Sv Bq^{-1})

U-235 T1/2 = 703.8E6y

	Inhalation			Oral	
	Class D f1 = 5.0E-02	Class W f1 = 5.0E-02	Class Y f1 = 2.0E-03	f1 = 5.0E-02	f1 = 2.0E-03
Adrenals	2.41E-08 (33 16 51)	7.50E-09 (29 28 43)	7.42E-09 (2 1 97)	2.50E-09	1.09E-10
Bld wall	2.35E-08 (33 16 51)	7.10E-09 (30 29 41)	2.60E-09 (7 2 91)	2.49E-09	1.65E-10
BSurface	1.01E-05 (33 16 51)	3.05E-06 (30 29 41)	1.05E-06 (7 2 91)	1.05E-06	4.20E-08
Breast	2.38E-08 (33 16 51)	7.33E-09 (29 28 43)	5.37E-09 (3 1 96)	2.49E-09	1.21E-10
ST wall	2.37E-08 (33 16 51)	7.90E-09 (31 26 43)	6.76E-09 (8 2 90)	3.56E-09	1.23E-09
SI wall	2.41E-08 (34 16 50)	8.67E-09 (34 25 41)	4.66E-09 (23 6 71)	5.24E-09	3.03E-09
ULI wall	2.61E-08 (39 15 46)	1.57E-08 (42 17 41)	1.31E-08 (41 11 48)	1.84E-08	1.69E-08
LLI wall	3.17E-08 (48 13 39)	3.38E-08 (48 12 40)	3.42E-08 (47 13 40)	5.31E-08	5.33E-08
Kidneys	4.19E-06 (33 16 51)	1.26E-06 (30 29 41)	4.45E-07 (7 2 91)	4.33E-07	1.73E-08
Liver	2.36E-08 (33 16 51)	7.37E-09 (29 28 43)	7.36E-09 (2 1 97)	2.46E-09	1.14E-10
Lungs	2.95E-07 (3 2 95)	1.48E-05 (0 0 100)	2.76E-04 (0 0 100)	2.46E-09	1.01E-10
Ovaries	2.37E-08 (33 16 51)	7.24E-09 (30 28 42)	2.84E-09 (9 2 89)	2.67E-09	3.34E-10
Pancreas	2.39E-08 (33 16 51)	7.44E-09 (29 28 43)	7.34E-09 (3 1 96)	2.49E-09	1.23E-10
R Marrow	6.58E-07 (33 16 51)	1.98E-07 (30 29 41)	7.15E-08 (7 2 91)	6.81E-08	2.78E-09
Skin	2.36E-08 (33 16 51)	7.17E-09 (30 29 41)	3.56E-09 (5 1 94)	2.45E-09	1.04E-10
Spleen	2.37E-08 (33 16 51)	7.36E-09 (29 28 43)	6.97E-09 (3 1 96)	2.46E-09	1.15E-10
Testes	2.36E-08 (33 16 51)	7.10E-09 (30 29 41)	2.52E-09 (7 2 91)	2.45E-09	1.15E-10
Thymus	2.35E-08 (33 16 51)	7.49E-09 (28 27 45)	1.04E-08 (2 0 98)	2.43E-09	9.81E-11
Thyroid	2.37E-08 (33 16 51)	7.22E-09 (30 29 41)	4.11E-09 (4 1 95)	2.45E-09	9.82E-11
Uterus	2.36E-08 (33 16 51)	7.14E-09 (30 29 41)	2.71E-09 (7 2 91)	2.52E-09	1.89E-10
Effective (ICRP60)	2.36E-07 (29 14 57)	1.84E-06 (1 1 98)	3.31E-05 (0 0 100)	2.73E-08	7.43E-09

Table I-3S. Internal Dose Conversion Factors for ^{234}U (Sv Bq^{-1})

U-234 T1/2 = 2.445E5y

	Inhalation			Oral	
	Class D f1 = 5.0E-02	Class W f1 = 5.0E-02	Class Y f1 = 2.0E-03	f1 = 5.0E-02	f1 = 2.0E-03
Adrenals	2.50E-08 (33 16 51)	7.52E-09 (30 29 41)	2.66E-09 (7 2 91)	2.58E-09	1.03E-10
Bld wall	2.50E-08 (33 16 51)	7.52E-09 (30 29 41)	2.65E-09 (7 2 91)	2.58E-09	1.03E-10
BSurface	1.09E-05 (33 16 51)	3.29E-06 (30 29 41)	1.13E-06 (7 2 91)	1.13E-06	4.52E-08
Breast	2.50E-08 (33 16 51)	7.52E-09 (30 29 41)	2.68E-09 (7 2 91)	2.58E-09	1.03E-10
ST wall	2.52E-08 (33 16 51)	8.09E-09 (32 27 41)	3.30E-09 (16 4 80)	3.70E-09	1.22E-09
SI wall	2.54E-08 (34 16 50)	8.87E-09 (33 26 41)	4.25E-09 (24 6 70)	5.23E-09	2.88E-09
ULI wall	2.74E-08 (38 15 47)	1.53E-08 (42 18 40)	1.19E-08 (42 11 47)	1.79E-08	1.62E-08
LLI wall	3.22E-08 (47 13 40)	3.15E-08 (47 13 40)	3.11E-08 (47 13 40)	4.95E-08	4.94E-08
Kidneys	4.52E-06 (33 16 51)	1.36E-06 (30 29 41)	4.79E-07 (7 2 91)	4.68E-07	1.87E-08
Liver	2.50E-08 (33 16 51)	7.52E-09 (30 29 41)	2.67E-09 (7 2 91)	2.58E-09	1.03E-10
Lungs	3.18E-07 (3 2 95)	1.60E-05 (0 0 100)	2.98E-04 (0 0 100)	2.58E-09	1.03E-10
Ovaries	2.50E-08 (33 16 51)	7.52E-09 (30 29 41)	2.65E-09 (7 2 91)	2.59E-09	1.06E-10
Pancreas	2.50E-08 (33 16 51)	7.52E-09 (30 29 41)	2.65E-09 (7 2 91)	2.58E-09	1.03E-10
R Marrow	6.98E-07 (33 16 51)	2.10E-07 (30 29 41)	7.22E-08 (7 2 91)	7.21E-08	2.88E-09
Skin	2.50E-08 (33 16 51)	7.52E-09 (30 29 41)	2.65E-09 (7 2 91)	2.58E-09	1.03E-10
Spleen	2.50E-08 (33 16 51)	7.52E-09 (30 29 41)	2.66E-09 (7 2 91)	2.58E-09	1.03E-10
Testes	2.50E-08 (33 16 51)	7.52E-09 (30 29 41)	2.65E-09 (7 2 91)	2.58E-09	1.03E-10
Thymus	2.50E-08 (33 16 51)	7.52E-09 (30 29 41)	2.66E-09 (7 2 91)	2.58E-09	1.03E-10
Thyroid	2.50E-08 (33 16 51)	7.52E-09 (30 29 41)	2.65E-09 (7 2 91)	2.58E-09	1.03E-10
Uterus	2.50E-08 (33 16 51)	7.52E-09 (30 29 41)	2.65E-09 (7 2 91)	2.58E-09	1.04E-10
Effective (ICRP60)	2.53E-07 (29 14 57)	1.99E-06 (1 1 98)	3.58E-05 (0 0 100)	2.82E-08	6.96E-09

Table I-4S. Internal Dose Conversion Factors for ^{234}Th (Sv Bq^{-1})

Th-234 T1/2 = 24.10d

	Inhalation		Oral
	Class W f1 = 2.0E-04	Class Y f1 = 2.0E-04	f1 = 2.0E-04
Adrenals	1.14E-10 (32 43 25)	2.24E-11 (18 5 77)	1.64E-12
Bld wall	1.02E-10 (37 46 17)	1.00E-11 (62 17 21)	9.15E-12
BSurface	7.83E-09 (35 47 18)	6.29E-10 (44 12 44)	2.08E-11
Breast	1.08E-10 (34 44 22)	1.66E-11 (28 8 64)	3.57E-12
ST wall	5.50E-10 (56 16 28)	4.99E-10 (61 16 23)	9.95E-10
SI wall	1.21E-09 (60 12 28)	1.21E-09 (62 17 21)	2.55E-09
ULI wall	6.48E-09 (61 10 29)	6.94E-09 (62 17 21)	1.47E-08
LLI wall	1.87E-08 (62 9 29)	2.03E-08 (62 17 21)	4.30E-08
Kidneys	1.06E-10 (35 45 20)	1.31E-11 (36 10 54)	3.71E-12
Liver	7.77E-10 (35 47 18)	5.91E-11 (48 13 39)	4.17E-12
Lungs	4.66E-08 (0 0 100)	6.39E-08 (0 0 100)	7.05E-13
Ovaries	1.13E-10 (39 43 18)	2.11E-11 (61 16 23)	3.12E-11
Pancreas	1.13E-10 (33 42 25)	2.33E-11 (20 6 74)	3.49E-12
R Marrow	4.18E-09 (36 47 17)	2.56E-10 (60 16 24)	1.84E-11
Skin	1.01E-10 (35 46 19)	9.93E-12 (39 11 50)	1.31E-12
Spleen	1.11E-10 (33 42 25)	2.15E-11 (21 6 73)	2.90E-12
Testes	9.93E-11 (36 48 16)	6.58E-12 (65 17 18)	2.53E-12
Thymus	1.19E-10 (30 39 31)	3.36E-11 (11 3 86)	4.15E-13
Thyroid	1.03E-10 (34 45 21)	1.27E-11 (28 8 64)	2.88E-13
Uterus	1.05E-10 (37 46 17)	1.21E-11 (61 16 23)	1.26E-11
Effective (ICRP60)	8.57E-09 (19 7 74)	1.02E-08 (15 5 80)	5.30E-09

Table I-5S. Internal Dose Conversion Factors for ^{232}Th (Sv Bq^{-1})

Th-232 T1/2 = 1.405E10y

	Inhalation			Oral
	Class W f1 = 2.0E-04	Class Y f1 = 2.0E-04		f1 = 2.0E-04
Adrenals	8.02E-07 (25 33 42)	6.34E-07 (3 1 96)		1.31E-09
Bld wall	7.41E-07 (25 33 42)	5.88E-07 (3 1 96)		1.21E-09
BSurface	1.11E-02 (25 33 42)	4.99E-03 (6 2 92)		1.85E-05
Breast	7.72E-07 (25 33 42)	6.14E-07 (3 1 96)		1.26E-09
ST wall	7.41E-07 (25 33 42)	6.06E-07 (3 1 96)		2.14E-09
SI wall	7.55E-07 (25 33 42)	5.98E-07 (3 1 96)		3.56E-09
ULI wall	7.58E-07 (25 32 43)	6.05E-07 (4 1 95)		1.47E-08
LLI wall	7.87E-07 (25 32 43)	6.27E-07 (5 1 94)		4.27E-08
Kidneys	7.65E-07 (25 33 42)	6.07E-07 (3 1 96)		1.25E-09
Liver	6.23E-06 (25 33 42)	5.04E-06 (3 1 96)		1.02E-08
Lungs	1.44E-05 (1 2 97)	9.40E-04 (0 0 100)		1.25E-09
Ovaries	7.62E-07 (25 33 42)	5.98E-07 (3 1 96)		1.25E-09
Pancreas	7.66E-07 (25 33 42)	6.21E-07 (3 1 96)		1.25E-09
R Marrow	8.93E-04 (25 33 42)	4.01E-04 (6 2 92)		1.48E-06
Skin	7.57E-07 (25 33 42)	6.01E-07 (3 1 96)		1.24E-09
Spleen	7.52E-07 (25 33 42)	6.12E-07 (3 1 96)		1.23E-09
Testes	7.55E-07 (25 33 42)	5.94E-07 (3 1 96)		1.23E-09
Thymus	7.51E-07 (25 33 42)	6.29E-07 (3 1 96)		1.23E-09
Thyroid	7.44E-07 (25 33 42)	5.99E-07 (3 1 96)		1.21E-09
Uterus	7.47E-07 (25 33 42)	5.92E-07 (3 1 96)		1.22E-09
Effective (ICRP60)	2.21E-04 (25 33 42)	2.11E-04 (3 1 96)		3.69E-07

Table I-6S. Internal Dose Conversion Factors for ^{231}Th (Sv Bq^{-1})

Th-231 T1/2 = 25.52h

	Inhalation			Oral
	Class W f1 = 2.0E-04	Class Y f1 = 2.0E-04		f1 = 2.0E-04
Adrenals	2.65E-12 (32 40 28)	9.91E-13 (16 9 75)		3.93E-13
Bld wall	2.62E-12 (51 42 7)	1.08E-12 (65 20 15)		2.89E-12
BSurface	9.22E-10 (29 40 31)	3.15E-10 (9 2 89)		3.17E-12
Breast	3.00E-12 (35 36 29)	1.42E-12 (27 12 61)		1.44E-12
ST wall	5.61E-11 (69 14 17)	6.44E-11 (66 20 14)		1.95E-10
SI wall	1.27E-10 (71 13 16)	1.48E-10 (67 20 13)		4.54E-10
ULI wall	5.26E-10 (72 12 16)	6.21E-10 (67 20 13)		1.90E-09
LLI wall	9.42E-10 (72 12 16)	1.12E-09 (67 20 13)		3.42E-09
Kidneys	2.33E-12 (43 46 11)	7.13E-13 (49 16 35)		1.26E-12
Liver	6.95E-12 (37 47 16)	1.81E-12 (25 10 65)		9.78E-13
Lungs	7.81E-10 (0 3 97)	8.75E-10 (0 5 95)		1.43E-13
Ovaries	7.62E-12 (64 23 13)	6.95E-12 (66 20 14)		2.08E-11
Pancreas	2.93E-12 (37 37 25)	1.34E-12 (34 13 53)		1.72E-12
R Marrow	7.88E-11 (30 39 31)	2.78E-11 (12 4 84)		5.30E-12
Skin	1.95E-12 (40 51 9)	3.56E-13 (38 13 49)		2.88E-13
Spleen	2.79E-12 (34 38 28)	1.19E-12 (24 11 65)		1.00E-12
Testes	1.91E-12 (44 52 4)	3.00E-13 (62 18 20)		5.24E-13
Thymus	2.99E-12 (26 36 38)	1.32E-12 (6 7 87)		3.39E-14
Thyroid	1.97E-12 (38 51 11)	3.09E-13 (25 10 65)		8.80E-15
Uterus	3.16E-12 (54 37 9)	1.73E-12 (65 20 15)		4.85E-12
Effective (ICRP60)	2.35E-10 (40 10 50)	2.56E-10 (38 13 49)		4.40E-10

Table I-7S. Internal Dose Conversion Factors for ^{230}Th (Sv Bq^{-1})

Th-230 T1/2 = 7.7E4y

	Inhalation		Oral
	Class W f1 = 2.0E-04	Class Y f1 = 2.0E-04	f1 = 2.0E-04
Adrenals	4.09E-07 (25 33 42)	1.73E-07 (6 2 92)	6.80E-10
Bld wall	4.08E-07 (25 33 42)	1.72E-07 (6 2 92)	6.80E-10
BSurface	2.16E-03 (25 33 42)	8.71E-04 (6 2 92)	3.60E-06
Breast	4.08E-07 (25 33 42)	1.72E-07 (6 2 92)	6.80E-10
ST wall	4.09E-07 (25 33 42)	1.73E-07 (6 2 92)	1.77E-09
SI wall	4.10E-07 (25 33 42)	1.74E-07 (6 2 92)	3.41E-09
ULI wall	4.16E-07 (26 33 41)	1.81E-07 (8 2 90)	1.65E-08
LLI wall	4.33E-07 (27 32 41)	2.00E-07 (12 3 85)	4.93E-08
Kidneys	4.08E-07 (25 33 42)	1.72E-07 (6 2 92)	6.80E-10
Liver	3.57E-06 (25 33 42)	1.51E-06 (6 2 92)	5.94E-09
Lungs	1.61E-05 (1 1 98)	3.00E-04 (0 0 100)	6.80E-10
Ovaries	4.08E-07 (25 33 42)	1.72E-07 (6 2 92)	6.82E-10
Pancreas	4.08E-07 (25 33 42)	1.73E-07 (6 2 92)	6.80E-10
R Marrow	1.73E-04 (25 33 42)	6.99E-05 (6 2 92)	2.89E-07
Skin	4.08E-07 (25 33 42)	1.72E-07 (6 2 92)	6.80E-10
Spleen	4.08E-07 (25 33 42)	1.72E-07 (6 2 92)	6.80E-10
Testes	4.08E-07 (25 33 42)	1.72E-07 (6 2 92)	6.80E-10
Thymus	4.08E-07 (25 33 42)	1.73E-07 (6 2 92)	6.80E-10
Thyroid	4.08E-07 (25 33 42)	1.72E-07 (6 2 92)	6.80E-10
Uterus	4.08E-07 (25 33 42)	1.72E-07 (6 2 92)	6.80E-10
Effective (ICRP60)	4.48E-05 (24 32 44)	5.33E-05 (2 1 97)	7.75E-08

Table I-8S. Internal Dose Conversion Factors for ^{228}Th (Sv Bq^{-1})

Th-228 T1/2 = 1.9131y

	Inhalation		Oral
	Class W f1 = 2.0E-04	Class Y f1 = 2.0E-04	f1 = 2.0E-04
Adrenals	1.35E-06 (26 34 40)	2.35E-07 (15 4 81)	2.32E-09
Bld wall	1.34E-06 (26 34 40)	2.25E-07 (16 4 80)	2.38E-09
BSurface	1.37E-03 (26 34 40)	2.29E-04 (16 4 80)	2.37E-06
Breast	1.35E-06 (26 34 40)	2.32E-07 (15 4 81)	2.33E-09
ST wall	1.35E-06 (26 34 40)	2.36E-07 (15 4 81)	3.64E-09
SI wall	1.35E-06 (26 34 40)	2.31E-07 (16 4 80)	6.07E-09
ULI wall	1.37E-06 (26 34 40)	2.53E-07 (18 5 77)	3.11E-08
LLI wall	1.44E-06 (27 32 41)	3.23E-07 (25 6 69)	1.32E-07
Kidneys	1.35E-06 (26 34 40)	2.30E-07 (15 4 81)	2.33E-09
Liver	1.17E-05 (26 34 40)	1.97E-06 (16 4 80)	2.01E-08
Lungs	9.48E-05 (0 1 99)	6.91E-04 (0 0 100)	2.31E-09
Ovaries	1.35E-06 (26 34 40)	2.26E-07 (16 4 80)	2.53E-09
Pancreas	1.35E-06 (26 34 40)	2.37E-07 (15 4 81)	2.32E-09
R Marrow	1.12E-04 (26 34 40)	1.87E-05 (16 4 80)	1.93E-07
Skin	1.34E-06 (26 34 40)	2.28E-07 (15 4 81)	2.31E-09
Spleen	1.34E-06 (26 34 40)	2.36E-07 (15 4 81)	2.32E-09
Testes	1.34E-06 (26 34 40)	2.25E-07 (16 4 80)	2.33E-09
Thymus	1.35E-06 (26 34 40)	2.44E-07 (14 4 82)	2.31E-09
Thyroid	1.34E-06 (26 34 40)	2.30E-07 (15 4 81)	2.30E-09
Uterus	1.34E-06 (26 34 40)	2.26E-07 (16 4 80)	2.38E-09
Effective (ICRP60)	4.01E-05 (19 24 57)	8.77E-05 (1 0 99)	6.55E-08

Table I-9S. Internal Dose Conversion Factors for ^{228}Ra (Sv Bq^{-1})

Ra-228 T1/2 = 5.75y	Inhalation				Oral
	Class W f1 = 2.0E-01				f1 = 2.0E-01
Adrenals	1.85E-07	(36	21	43)	1.58E-07
Bld wall	1.83E-07	(36	21	43)	1.57E-07
BSurface	6.51E-06	(38	21	41)	5.82E-06
Breast	1.84E-07	(36	21	43)	1.57E-07
ST wall	1.84E-07	(36	20	44)	1.57E-07
SI wall	1.84E-07	(36	21	43)	1.58E-07
ULI wall	1.87E-07	(36	20	44)	1.63E-07
LLI wall	1.96E-07	(37	20	43)	1.78E-07
Kidneys	1.83E-07	(36	21	43)	1.57E-07
Liver	1.84E-07	(36	20	44)	1.57E-07
Lungs	7.22E-06	(1	1	98)	1.57E-07
Ovaries	1.83E-07	(36	21	43)	1.58E-07
Pancreas	1.84E-07	(36	20	44)	1.57E-07
R Marrow	7.38E-07	(37	21	42)	6.53E-07
Skin	1.83E-07	(36	21	43)	1.57E-07
Spleen	1.84E-07	(36	21	43)	1.57E-07
Testes	1.83E-07	(36	21	43)	1.57E-07
Thymus	1.85E-07	(36	20	44)	1.57E-07
Thyroid	1.83E-07	(36	21	43)	1.57E-07
Uterus	1.83E-07	(36	21	43)	1.57E-07
Effective (IRP60)	1.16E-06	(10	6	84)	2.76E-07

Table I-10S. Internal Dose Conversion Factors for ^{226}Ra (Sv Bq^{-1})

Ra-226 T1/2 = 1600y	Ingestion				Oral
	Class W f1 = 2.0E-01				f1 = 2.0E-01
Adrenals	1.02E-07	(38	22	40)	9.19E-08
Bld wall	1.02E-07	(38	22	40)	9.15E-08
BSurface	7.59E-06	(38	22	40)	6.83E-06
Breast	1.02E-07	(38	22	40)	9.17E-08
ST wall	1.02E-07	(38	22	40)	9.25E-08
SI wall	1.03E-07	(38	21	41)	9.37E-08
ULI wall	1.08E-07	(39	21	40)	1.05E-07
LLI wall	1.22E-07	(41	19	41)	1.31E-07
Kidneys	1.02E-07	(38	22	40)	9.16E-08
Liver	1.02E-07	(38	22	40)	9.15E-08
Lungs	1.61E-05	(0	0	100)	9.16E-08
Ovaries	1.02E-07	(38	22	40)	9.16E-08
Pancreas	1.02E-07	(38	22	40)	9.17E-08
R Marrow	6.64E-07	(38	22	40)	5.98E-07
Skin	1.02E-07	(38	22	40)	9.16E-08
Spleen	1.02E-07	(38	22	40)	9.15E-08
Testes	1.02E-07	(38	22	40)	9.15E-08
Thymus	1.02E-07	(38	22	40)	9.15E-08
Thyroid	1.02E-07	(38	22	40)	9.15E-08
Uterus	1.02E-07	(38	22	40)	9.15E-08
Effective (ICRP60)	2.17E-06	(4	2	94)	2.25E-07

Table I-11S. Internal Dose Conversion Factors for ^{224}Ra (Sv Bq^{-1})

Ra-224 T1/2 = 3.66d	Inhalation	Oral
	Class W f1 = 2.0E-01	f1 = 2.0E-01
Adrenals	1.54E-08 (54 32 14)	2.06E-08
Bld wall	1.54E-08 (54 32 14)	2.08E-08
BSurface	1.17E-06 (54 33 13)	1.59E-06
Breast	1.54E-08 (54 32 14)	2.06E-08
ST wall	1.75E-08 (55 29 16)	2.49E-08
SI wall	1.98E-08 (57 27 16)	3.03E-08
ULI wall	4.09E-08 (62 18 20)	8.25E-08
LLI wall	8.36E-08 (65 14 21)	1.99E-07
Kidneys	1.54E-08 (54 32 14)	2.06E-08
Liver	1.54E-08 (54 32 14)	2.06E-08
Lungs	6.56E-06 (0 1 99)	2.05E-08
Ovaries	1.56E-08 (54 32 14)	2.12E-08
Pancreas	1.54E-08 (54 32 14)	2.06E-08
R Marrow	1.13E-07 (54 33 13)	1.52E-07
Skin	1.53E-08 (54 32 14)	2.06E-08
Spleen	1.54E-08 (54 32 14)	2.06E-08
Testes	1.53E-08 (54 32 14)	2.06E-08
Thymus	1.55E-08 (53 32 15)	2.05E-08
Thyroid	1.53E-08 (54 32 14)	2.05E-08
Uterus	1.54E-08 (54 32 14)	2.08E-08
Effective (ICRP60)	8.32E-07 (3 3 94)	7.41E-08

Table I-12S. Internal Dose Conversion Factors for ^{234}Pa (Sv Bq^{-1})

Pa-234 T1/2 = 6.70h	Inhalation		Oral
	Class W f1 = 1.0E-03	Class Y f1 = 1.0E-03	f1 = 1.0E-03
Adrenals	2.90E-11 (18 13 69)	2.93E-11 (16 15 69)	3.72E-11
Bld wall	1.45E-11 (71 16 13)	1.72E-11 (64 25 11)	9.06E-11
BSurface	8.24E-11 (38 48 14)	2.06E-11 (30 16 54)	2.74E-11
Brain	3.19E-12 (16 25 59)	2.28E-12 (4 13 83)	4.48E-13
Breast	2.03E-11 (29 13 58)	2.19E-11 (28 18 54)	4.99E-11
ST wall	1.33E-10 (65 15 20)	1.60E-10 (60 24 16)	7.80E-10
SI wall	2.22E-10 (74 16 10)	2.71E-10 (67 25 8)	1.48E-09
ULI wall	4.66E-10 (75 16 9)	5.70E-10 (67 25 8)	3.13E-09
LLI wall	3.63E-10 (75 16 9)	4.46E-10 (68 25 7)	2.46E-09
Kidneys	3.25E-11 (43 28 29)	2.51E-11 (43 20 37)	8.29E-11
Liver	4.55E-11 (29 26 45)	3.42E-11 (23 17 60)	5.88E-11
Lungs	8.46E-10 (0 7 93)	8.97E-10 (0 12 88)	1.51E-11
Ovaries	5.08E-11 (73 16 11)	6.13E-11 (66 25 9)	3.30E-10
Pancreas	3.89E-11 (32 13 55)	4.22E-11 (31 18 51)	1.06E-10
R Marrow	3.31E-11 (38 25 37)	2.74E-11 (37 19 44)	7.86E-11
Skin	9.56E-12 (25 13 62)	9.95E-12 (23 17 60)	1.87E-11
Spleen	3.07E-11 (27 12 61)	3.33E-11 (26 17 57)	7.04E-11
Testes	4.18E-12 (66 20 14)	4.56E-12 (63 25 12)	2.34E-11
Thymus	3.81E-11 (2 8 90)	4.00E-11 (2 13 85)	6.06E-12
Thyroid	1.20E-11 (3 9 88)	1.23E-11 (2 13 85)	1.86E-12
Uterus	2.87E-11 (72 16 12)	3.44E-11 (65 25 10)	1.83E-10
Effective (ICRP60)	1.84E-10 (30 11 59)	2.04E-10 (29 18 53)	5.57E-10

Table I-13S. Internal Dose Conversion Factors for ^{228}Ac (Sv Bq^{-1})

Ac-228 T1/2 = 6.13h

	Inhalation			Oral
	Class D f1 = 1.0E-03	Class W f1 = 1.0E-03	Class Y f1 = 1.0E-03	f1 = 1.0E-03
Adrenals	5.10E-11 (34 15 51)	2.26E-11 (21 22 57)	1.81E-11 (13 12 75)	1.80E-11
Bld wall	1.19E-11 (66 9 25)	7.49E-12 (62 20 18)	7.83E-12 (61 24 15)	4.09E-11
BSurface	1.43E-06 (32 16 52)	3.49E-07 (26 34 40)	5.93E-08 (17 4 79)	3.01E-09
Brain	1.27E-11 (33 17 50)	3.97E-12 (22 30 48)	1.96E-12 (6 8 86)	2.54E-13
Breast	2.11E-11 (39 12 49)	1.24E-11 (27 18 55)	1.28E-11 (22 14 64)	2.31E-11
ST wall	1.13E-10 (84 4 12)	9.94E-11 (67 16 17)	1.20E-10 (60 24 16)	6.21E-10
SI wall	1.79E-10 (93 3 4)	1.62E-10 (74 16 10)	1.95E-10 (66 26 8)	1.12E-09
ULI wall	3.76E-10 (95 2 3)	3.52E-10 (73 16 11)	4.27E-10 (67 25 8)	2.42E-09
LLI wall	2.87E-10 (97 2 1)	2.95E-10 (71 15 14)	3.52E-10 (66 24 10)	1.90E-09
Kidneys	3.70E-11 (42 14 44)	1.67E-11 (36 23 41)	1.38E-11 (34 17 49)	3.88E-11
Liver	3.77E-07 (32 16 52)	9.24E-08 (26 34 40)	1.57E-08 (17 4 79)	8.20E-10
Lungs	6.41E-10 (1 3 96)	3.47E-08 (0 0 100)	2.53E-07 (0 0 100)	7.34E-12
Ovaries	1.58E-08 (32 16 52)	3.90E-09 (26 34 40)	6.84E-10 (19 5 76)	1.79E-10
Pancreas	4.45E-11 (40 13 47)	2.48E-11 (30 19 51)	2.44E-11 (25 15 60)	5.05E-11
R Marrow	1.14E-07 (32 16 52)	2.80E-08 (26 34 40)	4.76E-09 (17 4 79)	2.75E-10
Skin	1.28E-11 (36 14 50)	6.59E-12 (24 20 56)	6.20E-12 (18 13 69)	8.84E-12
Spleen	2.21E-11 (39 10 51)	1.67E-11 (26 15 59)	1.95E-11 (20 14 66)	3.37E-11
Testes	1.58E-08 (32 16 52)	3.88E-09 (26 34 40)	6.59E-10 (17 5 78)	4.38E-11
Thymus	2.35E-11 (18 10 72)	2.11E-11 (5 11 84)	2.62E-11 (2 9 89)	3.06E-12
Thyroid	8.81E-12 (22 11 67)	6.77E-12 (7 13 80)	7.79E-12 (2 10 88)	9.39E-13
Uterus	2.00E-11 (74 7 19)	1.42E-11 (67 18 15)	1.57E-11 (63 24 13)	8.43E-11
Effective (ICRP60)	5.01E-08 (32 16 52)	1.65E-08 (20 25 55)	3.25E-08 (1 1 98)	4.50E-10

Table I-14S. Internal Dose Conversion Factors for ^{239}Pu (Sv Bq^{-1})

Pu-239 T1/2 = 24065y

	Inhalation		Oral		
	Class W f1 = 1.0E-03	Class Y f1 = 1.0E-05	f1 = 1.0E-03	f1 = 1.0E-04	f1 = 1.0E-05
Adrenals	9.54E-10 (25 33 42)	4.01E-10 (6 2 92)	7.92E-12	7.95E-13	8.28E-14
Bld wall	9.01E-10 (25 33 42)	3.74E-10 (6 2 92)	7.52E-12	7.98E-13	1.25E-13
BSurface	2.11E-03 (25 33 42)	8.21E-04 (6 2 92)	1.76E-05	1.76E-06	1.76E-07
Brain	9.23E-10 (25 33 42)	3.83E-10 (6 2 92)	7.66E-12	7.66E-13	7.66E-14
Breast	9.22E-10 (25 33 42)	3.99E-10 (6 2 92)	7.69E-12	8.09E-13	1.21E-13
ST wall	1.52E-09 (36 23 41)	1.07E-09 (35 9 56)	1.20E-09	1.19E-09	1.19E-09
SI wall	2.43E-09 (43 17 40)	2.10E-09 (43 12 45)	2.99E-09	2.99E-09	2.99E-09
ULI wall	9.72E-09 (51 10 39)	1.03E-08 (50 13 37)	1.73E-08	1.73E-08	1.73E-08
LLI wall	2.79E-08 (52 9 39)	3.10E-08 (51 14 35)	5.30E-08	5.31E-08	5.31E-08
Kidneys	9.21E-10 (25 33 42)	3.83E-10 (6 2 92)	7.66E-12	7.76E-13	8.78E-14
Liver	3.78E-04 (25 33 42)	1.51E-04 (6 2 92)	3.14E-06	3.14E-07	3.14E-08
Lungs	1.73E-05 (0 0 100)	3.23E-04 (0 0 100)	7.74E-12	7.75E-13	7.89E-14
Ovaries	3.18E-05 (25 33 42)	1.20E-05 (7 2 91)	2.64E-07	2.64E-08	2.64E-09
Pancreas	9.23E-10 (25 33 42)	3.86E-10 (6 2 92)	7.68E-12	7.89E-13	9.95E-14
R Marrow	1.69E-04 (25 33 42)	6.57E-05 (6 2 92)	1.41E-06	1.41E-07	1.41E-08
Skin	9.12E-10 (25 33 42)	3.79E-10 (6 2 92)	7.57E-12	7.63E-13	8.17E-14
Spleen	9.09E-10 (25 33 42)	3.84E-10 (6 2 92)	7.55E-12	7.64E-13	8.47E-14
Testes	3.18E-05 (25 33 42)	1.20E-05 (7 2 91)	2.64E-07	2.64E-08	2.64E-09
Thymus	9.05E-10 (25 33 42)	3.82E-10 (6 2 92)	7.51E-12	7.51E-13	7.54E-14
Thyroid	9.03E-10 (25 33 42)	3.75E-10 (6 2 92)	7.49E-12	7.49E-13	7.50E-14
Uterus	9.01E-10 (25 33 42)	3.74E-10 (6 2 92)	7.54E-12	8.11E-13	1.38E-13
Effective (ICRP60)	6.87E-05 (24 32 44)	6.48E-05 (2 1 97)	5.62E-07	6.20E-08	1.21E-08

Table I-15S. Age-Specific Ingestion DCFs for ^{238}U, Normalized to the Adult[a]

MODE	AGE	F1	EFF	ADREN	BL WALL	BRAIN	B SURF	BREAST	ST W	SI W	ULI W	LLI W	KIDNEY
S	NB	1.6E-1	110.	54.	54.	54.	180.	54.	51.	48.	35.	25.	53.
	3M	1.5E-1	74.	40.	40.	40.	120.	40.	38.	36.	27.	20.	39.
	1Y	1.0E-1	16.	15.	15.	15.	23.	15.	14.	13.	11.	8.6	11.
	5Y	7.0E-2	3.9	4.8	4.8	4.8	4.3	4.8	4.7	4.6	4.3	3.9	3.9
	10Y	8.0E-2	3.2	3.3	3.3	3.3	3.8	3.3	3.2	3.1	2.7	2.4	3.0
	15Y	9.0E-2	3.1	2.3	2.3	2.3	4.3	2.3	2.3	2.2	1.7	1.4	2.5
	20Y	5.0E-2	1.0	1.0	1.0	1.0	1.0	1.0	1.0	1.0	1.0	1.0	1.0
I	NB	6.4E-3	56.	54.	53.	54.	180.	53.	33.	25.	21.	20.	53.
	3M	6.0E-3	40.	40.	40.	40.	120.	40.	26.	20.	17.	16.	39.
	1Y	4.0E-3	11.	15.	14.	15.	23.	15.	9.4	8.6	8.0	7.4	11.
	5Y	2.8E-3	3.8	4.8	4.7	4.8	4.3	4.8	3.8	3.9	3.9	3.7	3.9
	10Y	3.2E-3	2.6	3.3	3.3	3.3	3.8	3.3	2.4	2.4	2.3	3.2	3.0
	15Y	3.6E-3	2.0	2.3	2.3	2.4	4.3	2.3	1.6	1.4	1.3	1.2	2.5
	20Y	2.0E-3	1.0	1.0	1.0	1.0	1.0	1.0	1.0	1.0	1.0	1.0	1.0

MODE	AGE	F1	LIVER	LUNGS	OVARIES	PANCR	ACT MAR	SKIN	SPLEEN	TESTES	THYMUS	THYROID	UTERUS
S	NB	1.6E-1	51.	54.	54.	54.	71.	54.	71.	54.	54.	54.	54.
	3M	1.5E-1	38.	40.	40.	40.	51.	40.	46.	40.	40.	40.	40.
	1Y	1.0E-1	13.	15.	15.	15.	9.8	15.	15.	15.	15.	15.	15.
	5Y	7.0E-2	4.4	4.8	4.8	4.8	2.4	4.8	5.0	4.8	4.8	4.8	4.8
	10Y	8.0E-2	3.3	3.3	3.3	3.3	2.1	3.3	3.8	3.3	3.3	3.3	3.3
	15Y	9.0E-2	2.5	2.4	2.3	2.3	2.0	2.3	3.1	2.3	2.3	2.3	2.3
	20Y	5.0E-2	1.0	1.0	1.0	1.0	1.0	1.0	1.0	1.0	1.0	1.0	1.0
I	NB	6.4E-3	51.	54.	52.	53.	71.	54.	71.	53.	54.	54.	53.
	3M	6.0E-3	38.	40.	39.	40.	51.	40.	46.	40.	40.	40.	40.
	1Y	4.0E-3	13.	15.	14.	15.	9.8	15.	15.	14.	15.	15.	14.
	5Y	2.8E-3	4.3	4.8	4.7	4.8	2.4	4.8	5.0	4.8	4.8	4.8	4.7
	10Y	3.2E-3	3.3	3.3	3.2	3.3	2.1	3.3	3.8	3.3	3.3	3.3	3.3
	15Y	3.6E-3	2.5	2.3	2.3	2.3	2.0	2.3	3.1	2.3	2.3	2.3	2.3
	20Y	2.0E-3	1.0	1.0	1.0	1.0	1.0	1.0	1.0	1.0	1.0	1.0	1.0

[a] Cristy et al. (1986).

Table I-16S. Age-Specific Ingestion DCFs for ^{235}U, Normalized to the Adult[a]

MODE	AGE	F1	EFF	ADREN	BL WALL	BRAIN	B SURF	BREAST	ST W	SI W	ULI W	LLI W	KIDNEY
S	NB	1.6E-1	110.	55.	55.	55.	190.	55.	53.	48.	34.	25.	55.
	3M	1.5E-1	77.	41.	41.	41.	130.	41.	39.	36.	26.	20.	41.
	1Y	1.0E-1	16.	15.	15.	15.	23.	15.	14.	13.	11.	8.5	11.
	5Y	7.0E-2	4.0	4.8	4.8	4.8	4.3	4.8	4.7	4.6	4.2	3.8	3.9
	10Y	8.0E-2	3.2	3.3	3.3	3.3	3.8	3.3	3.2	3.1	2.7	2.4	3.0
	15Y	9.0E-2	3.1	2.4	2.3	2.4	4.3	2.4	2.3	2.1	1.7	1.4	2.5
	20Y	5.0E-2	1.0	1.0	1.0	1.0	1.0	1.0	1.0	1.0	1.0	1.0	1.0
I	NB	6.4E-3	55.	55.	50.	55.	190.	53.	33.	24.	21.	19.	55.
	3M	6.0E-3	40.	41.	37.	41.	130.	39.	26.	19.	17.	16.	41.
	1Y	4.0E-3	11.	14.	13.	15.	23.	14.	9.2	8.4	7.9	7.4	11.
	5Y	2.8E-3	3.8	4.8	4.5	4.8	4.3	4.6	3.8	3.9	3.9	3.7	3.9
	10Y	3.2E-3	2.6	3.3	3.2	3.3	3.8	3.2	2.3	2.4	2.3	2.2	3.0
	15Y	3.6E-3	1.9	2.3	2.2	2.4	4.3	2.3	1.6	1.4	1.3	1.2	2.5
	20Y	2.0E-3	1.0	1.0	1.0	1.0	1.0	1.0	1.0	1.0	1.0	1.0	1.0

MODE	AGE	F1	LIVER	LUNGS	OVARIES	PANCR	ACT MAR	SKIN	SPLEEN	TESTES	THYMUS	THYROID	UTERUS
S	NB	1.6E-1	53.	55.	55.	55.	76.	55.	74.	55.	55.	55.	55.
	3M	1.5E-1	39.	41.	41.	41.	54.	41.	48.	41.	41.	41.	41.
	1Y	1.0E-1	13.	15.	14.	15.	10.	15.	15.	15.	15.	15.	15.
	5Y	7.0E-2	4.4	4.8	4.8	4.8	2.4	4.8	5.0	4.8	4.8	4.8	4.8
	10Y	8.0E-2	3.4	3.3	3.3	3.3	2.1	3.3	3.9	3.3	3.3	3.3	3.3
	15Y	9.0E-2	2.5	2.4	2.3	2.4	2.1	2.4	3.1	2.4	2.4	2.4	2.3
	20Y	5.0E-2	1.0	1.0	1.0	1.0	1.0	1.0	1.0	1.0	1.0	1.0	1.0
I	NB	6.4E-3	51.	55.	41.	53.	75.	55.	73.	54.	55.	55.	49.
	3M	6.0E-3	38.	41.	31.	40.	53.	41.	47.	40.	41.	41.	36.
	1Y	4.0E-3	13.	15.	11.	14.	9.9	15.	15.	14.	15.	15.	13.
	5Y	2.8E-3	4.4	4.8	4.1	4.7	2.4	4.8	5.0	4.8	4.8	4.8	4.5
	10Y	3.2E-3	3.3	3.3	2.8	3.3	2.1	3.3	3.8	3.3	3.3	3.3	3.1
	15Y	3.6E-3	2.4	2.4	2.0	2.3	2.0	2.3	3.1	2.3	2.4	2.4	2.2
	20Y	2.0E-3	1.0	1.0	1.0	1.0	1.0	1.0	1.0	1.0	1.0	1.0	1.0

[a] Cristy et al. (1986).

Table I-17S. Age-Specific Ingestion DCFs for ^{234}U, Normalized to the Adult[a]

MODE	AGE	F1	EFF	ADREN	BL WALL	BRAIN	B SURF	BREAST	ST W	SI W	ULI W	LLI W	KIDNEY
S	NB	1.6E-1	110.	56.	56.	56.	190.	56.	53.	49.	36.	26.	55.
	3M	1.5E-1	78.	41.	41.	41.	130.	41.	40.	37.	27.	20.	41.
	1Y	1.0E-1	16.	15.	15.	15.	23.	15.	14.	13.	11.	8.7	11.
	5Y	7.0E-2	4.0	4.8	4.8	4.8	4.3	4.8	4.7	4.6	4.3	3.9	3.9
	10Y	8.0E-2	3.2	3.4	3.4	3.4	3.8	3.4	3.2	3.2	2.8	2.4	3.0
	15Y	9.0E-2	3.1	2.4	2.4	2.4	4.3	2.4	2.3	2.2	1.8	1.5	2.5
	20Y	5.0E-2	1.0	1.0	1.0	1.0	1.0	1.0	1.0	1.0	1.0	1.0	1.0
I	NB	6.4E-3	59.	56.	56.	56.	190.	56.	34.	25.	21.	20.	55.
	3M	6.0E-3	42.	41.	41.	41.	130.	41.	26.	20.	17.	16.	41.
	1Y	4.0E-3	11.	15.	15.	15.	23.	15.	9.5	8.7	8.0	7.4	11.
	5Y	2.8E-3	3.8	4.8	4.8	4.8	4.3	4.8	3.8	3.9	3.9	3.7	3.9
	10Y	3.2E-3	2.6	3.4	3.4	3.4	3.8	3.4	2.4	2.4	2.3	2.2	3.0
	15Y	3.6E-3	2.0	2.4	2.4	2.4	4.3	2.4	1.6	1.4	1.3	1.2	2.5
	20Y	2.0E-3	1.0	1.0	1.0	1.0	1.0	1.0	1.0	1.0	1.0	1.0	1.0

MODE	AGE	F1	LIVER	LUNGS	OVARIES	PANCR	ACT MAR	SKIN	SPLEEN	TESTES	THYMUS	THYROID	UTERUS
S	NB	1.6E-1	53.	56.	56.	56.	76.	56.	74.	56.	56.	56.	56.
	3M	1.5E-1	39.	41.	41.	41.	54.	41.	48.	41.	41.	41.	41.
	1Y	1.0E-1	14.	15.	15.	15.	10.	15.	15.	15.	15.	15.	15.
	5Y	7.0E-2	4.4	4.4	4.8	4.8	2.4	4.8	5.0	4.8	4.4	4.8	4.4
	10Y	8.0E-2	3.4	3.4	3.4	3.4	2.1	3.4	3.9	3.4	3.4	3.4	3.4
	15Y	9.0E-2	2.5	2.4	2.4	2.4	2.1	2.4	3.1	2.4	2.4	2.4	2.4
	20Y	5.0E-2	1.0	1.0	1.0	1.0	1.0	1.0	1.0	1.0	1.0	1.0	1.0
I	NB	6.4E-3	53.	56.	56.	56.	76.	56.	74.	56.	56.	56.	56.
	3M	6.0E-3	39.	41.	41.	41.	54.	4.1	48.	41.	41.	41.	41.
	1Y	4.0E-3	14.	15.	15.	15.	10.	15.	15.	15.	15.	15.	15.
	5Y	2.8E-3	4.4	4.8	4.8	4.8	2.4	4.8	5.0	4.4	4.8	4.8	4.8
	10Y	3.2E-3	3.4	3.4	3.3	3.4	2.1	3.4	3.9	3.4	3.4	3.4	3.4
	15Y	3.6E-3	2.5	2.4	2.4	2.4	2.1	2.4	3.1	2.4	2.4	2.4	2.4
	20Y	2.0E-3	1.0	1.0	1.0	1.0	1.0	1.0	1.0	1.0	1.0	1.0	1.0

[a] Cristy et al. (1986).

Table I-18S. Age-Specific Ingestion DCFs for ^{232}Th, Normalized to the Adult[a]

MODE	AGE	F1	EFF	ADREN	BL WALL	BRAIN	B SURF	BREAST	ST W	SI W	ULI W	LLI W	KIDNEY
G	NB	1.0E-2	95.	160.	160.	160.	77.	160.	140.	120.	58.	34.	210.
	3M	5.0E-3	44.	73.	74.	73.	36.	73.	65.	56.	32.	22.	95.
	1Y	5.0E-4	4.0	6.4	6.4	6.3	3.3	6.4	6.5	6.8	7.4	7.3	8.1
	5Y	5.0E-4	3.1	4.5	4.5	4.5	2.7	4.5	4.4	4.3	4.1	3.8	5.5
	10Y	5.0E-4	2.6	3.6	3.6	3.6	2.5	3.6	3.3	3.2	2.7	2.3	4.0
	15Y	5.0E-4	2.4	2.6	2.6	2.6	2.3	2.6	2.4	2.2	1.6	1.4	2.8
	20Y	2.0E-4	1.0	1.0	1.0	1.0	1.0	1.0	1.0	1.0	1.0	1.0	1.0

MODE	AGE	F1	LIVER	LUNGS	OVARIES	PANCR	ACT MAR	SKIN	SPLEEN	TESTES	THYMUS	THYROID	UTERUS
G	NB	1.0E-2	240.	160.	160.	160.	170.	160.	300.	160.	160.	160.	160.
	3M	5.0E-3	110.	74.	74.	74.	76.	74.	140.	74.	74.	74.	74.
	1Y	5.0E-4	9.3	6.4	6.4	6.4	6.5	6.4	11.	6.4	6.4	6.4	6.4
	5Y	5.0E-4	5.9	4.5	4.5	4.5	4.3	4.5	6.7	4.5	4.5	4.5	4.5
	10Y	5.0E-4	4.1	3.6	3.6	3.6	3.1	3.6	4.3	3.6	3.6	3.6	3.6
	15Y	5.0E-4	2.8	2.6	2.6	2.6	2.4	2.6	2.9	2.6	2.6	2.6	2.6
	20Y	2.0E-4	1.0	1.0	1.0	1.0	1.0	1.0	1.0	1.0	1.0	1.0	1.0

[a] Cristy et al. (1986).

Table I-19S. Age-Specific Ingestion DCFs for ^{230}Th, Normalized to the Adult[a]

MODE	AGE	F1	EFF	ADREN	BL WALL	BRAIN	B SURF	BREAST	ST W	SI W	ULI W	LLI W	KIDNEY
G	NB	1.0E-2	88.	230.	230.	230.	69.	230.	170.	120.	51.	31.	280.
	3M	5.0E-3	40.	100.	100.	100.	32.	100.	78.	59.	29.	21.	120.
	1Y	5.0E-4	3.7	8.0	8.0	8.0	2.9	8.0	7.7	7.8	7.8	7.4	10.
	5Y	5.0E-4	2.8	4.7	4.7	4.7	2.4	4.7	4.3	4.2	4.0	3.7	6.1
	10Y	5.0E-4	2.4	3.1	3.1	3.1	2.3	3.1	2.8	2.7	2.4	2.2	3.9
	15Y	5.0E-4	2.2	2.3	2.3	2.3	2.2	2.3	2.0	1.8	1.4	1.3	2.7
	20Y	2.0E-4	1.0	1.0	1.0	1.0	1.0	1.0	1.0	1.0	1.0	1.0	1.0

MODE	AGE	F1	LIVER	LUNGS	OVARIES	PANCR	ACT MAR	SKIN	SPLEEN	TESTES	THYMUS	THYROID	UTERUS
G	NB	1.0E-2	320.	230.	230.	230.	200.	230.	380.	230.	230.	230.	230.
	3M	5.0E-3	140.	100.	100.	100.	87.	100.	170.	100.	100.	100.	100.
	1Y	5.0E-4	12.	8.1	8.1	8.0	7.2	8.1	13.	8.1	8.1	8.1	8.0
	5Y	5.0E-4	6.6	4.7	4.7	4.7	4.5	4.7	7.5	4.7	4.7	4.7	4.7
	10Y	5.0E-4	4.1	3.1	3.1	3.1	3.1	3.1	4.4	3.1	3.1	3.1	3.1
	15Y	5.0E-4	2.7	2.3	2.3	2.3	2.4	2.3	2.8	2.3	2.3	2.3	2.3
	20Y	2.0E-4	1.0	1.0	1.0	1.0	1.0	1.0	1.0	1.0	1.0	1.0	1.0

[a] Cristy et al. (1986).

Table I-20S. Age-Specific Ingestion DCFs for ^{228}Th, Normalized to the Adult[a]

MODE	AGE	F1	EFF	ADREN	BL WALL	BRAIN	B SURF	BREAST	ST W	SI W	ULI W	LLI W	KIDNEY
G	NB	1.0E-2	450.	150.	150.	150.	510.	150.	140.	110.	51.	27.	190.
	3M	5.0E-3	180.	71.	70.	71.	200.	70.	64.	55.	29.	19.	85.
	1Y	5.0E-4	14.	7.9	7.9	7.9	15.	7.9	7.8	7.7	7.7	7.3	8.0
	5Y	5.0E-4	6.4	4.3	4.3	4.3	6.5	4.3	4.2	4.1	4.0	3.7	4.4
	10Y	5.0E-4	3.8	2.7	2.7	2.7	4.1	2.7	2.6	2.5	2.4	2.2	3.1
	15Y	5.0E-4	2.6	1.9	1.9	1.9	2.9	1.9	1.9	1.7	1.4	1.3	2.4
	20Y	2.0E-4	1.0	1.0	1.0	1.0	1.0	1.0	1.0	1.0	1.0	1.0	1.0

MODE	AGE	F1	LIVER	LUNGS	OVARIES	PANCR	ACT MAR	SKIN	SPLEEN	TESTES	THYMUS	THYROID	UTERUS
G	NB	1.0E-2	250.	150.	150.	150.	800.	150.	390.	150.	150.	150.	150.
	3M	5.0E-3	110.	71.	69.	71.	300.	71.	160.	71.	71.	71.	70.
	1Y	5.0E-4	10.	7.9	7.9	7.9	20.	7.9	14.	7.9	7.9	7.9	7.9
	5Y	5.0E-4	5.3	4.3	4.3	4.3	9.1	4.3	7.1	4.3	4.3	4.3	4.3
	10Y	5.0E-4	3.5	2.7	2.7	2.7	4.7	2.7	4.3	2.7	2.7	2.7	2.7
	15Y	5.0E-4	2.5	1.9	1.9	1.9	2.9	1.9	2.8	1.9	1.9	1.9	1.9
	20Y	2.0E-4	1.0	1.0	1.0	1.0	1.0	1.0	1.0	1.0	1.0	1.0	1.0

[a] Cristy et al. (1986).

Table I-21S. Age-Specific Ingestion DCFs for ^{239}Pu, Normalized to the Adult[a,b]

Pu-239 Ingestion

	3 months	1 year	5 years	10 years	15 years	Adult
f1	1E-2	1E-3	1E-3	1E-3	1E-3	1E-3
Effective	14.43	1.44	1.13	1.03	1.01	1.00
Adrenals	46.15	3.77	2.31	1.46	1.08	1.00
Bl. Wall	46.15	3.77	2.31	1.46	1.08	1.00
Bone Surf.	10.00	1.00	1.00	0.94	1.06	1.00
Brain	46.15	3.77	2.31	1.46	1.08	1.00
Breast	46.15	3.77	2.31	1.46	1.08	1.00
S Wall	43.57	4.07	2.43	1.57	1.14	1.00
SI Wall	39.38	4.44	2.63	1.63	1.13	1.00
ULI Wall	26.67	6.00	3.23	1.97	1.20	1.00
LLI Wall	18.18	6.67	3.48	2.12	1.21	1.00
Kidneys	36.51	3.02	2.06	1.48	1.13	1.00
Liver	17.75	1.85	1.43	1.13	0.98	1.00
Lungs	46.15	3.77	2.38	1.54	1.08	1.00
Ovaries	9.58	1.00	1.04	1.04	1.13	1.00
Pancreas	46.15	3.77	2.31	1.46	1.08	1.00
R. Marrow	24.72	2.02	1.46	1.12	0.99	1.00
Skin	46.15	3.77	2.31	1.46	1.08	1.00
Spleen	46.15	3.77	2.31	1.46	1.08	1.00
Testes	15.00	1.46	1.29	1.13	1.13	1.00
Thymus	46.15	3.77	2.31	1.46	1.08	1.00
Thyroid	46.15	3.77	2.31	1.46	1.08	1.00
Uterus	46.15	3.77	2.31	1.46	1.08	1.00

[a] Cristy et al. (1986).

[b] Entries correspond to AMAD = 1 μm.

Table I-22S(a). Age-Specific Inhalation DCFs for ^{238}U, Normalized to the Adult[a]

MODE	AGE	AMAD	F1	EFF	ADREN	BL WALL	BRAIN	B SURF	BREAST	ST W	SI W	ULI W	LLI W	KIDNEY
D	NB	0.3	1.6E-1	34.	17.	17.	17.	58.	17.	17.	17.	17.	17.	17.
	3M	0.3	1.5E-1	25.	13.	13.	13.	42.	13.	13.	13.	13.	13.	13.
	1Y	0.3	1.0E-1	8.1	7.3	7.3	7.3	11.	7.3	7.3	7.3	7.3	7.3	5.5
	5Y	0.3	7.0E-2	2.9	3.4	3.4	3.4	3.1	3.4	3.4	3.4	3.4	3.4	2.8
	10Y	0.3	8.0E-2	2.1	2.1	2.1	2.1	2.4	2.1	2.1	2.1	2.1	2.1	1.9
	15Y	0.3	9.0E-2	1.8	1.3	1.3	1.3	2.4	1.3	1.3	1.3	1.3	1.3	1.4
	20Y	0.3	5.0E-2	1.0	1.0	1.0	1.0	1.0	1.0	1.0	1.0	1.0	1.0	1.0
D	NB	1.0	1.6E-1	35.	17.	17.	17.	59.	17.	17.	17.	17.	17.	17.
	3M	1.0	1.5E-1	26.	14.	14.	14.	43.	14.	14.	14.	14.	14.	14.
	1Y	1.0	1.0E-1	8.3	7.4	7.4	7.3	12.	7.4	7.4	7.4	7.4	7.4	5.6
	5Y	1.0	7.0E-2	2.9	3.4	3.4	3.4	3.1	3.4	3.4	3.4	3.4	3.4	2.8
	10Y	1.0	8.0E-2	2.1	2.1	2.1	2.1	2.4	2.1	2.1	2.1	2.1	2.1	1.9
	15Y	1.0	9.0E-2	1.8	1.3	1.3	1.3	2.4	1.3	1.3	1.3	1.3	1.3	1.4
	20Y	1.0	5.0E-2	1.0	1.0	1.0	1.0	1.0	1.0	1.0	1.0	1.0	1.0	1.0
D	NB	5.0	1.6E-1	37.	18.	18.	18.	62.	18.	18.	18.	18.	18.	18.
	3M	5.0	1.5E-1	27.	14.	14.	14.	44.	14.	14.	14.	14.	14.	14.
	1Y	5.0	1.0E-1	8.4	7.5	7.5	7.5	12.	7.5	7.5	7.5	7.5	7.5	5.7
	5Y	5.0	7.0E-2	2.9	3.5	3.5	3.5	3.1	3.5	3.5	3.5	3.5	3.5	2.8
	10Y	5.0	8.0E-2	2.1	2.1	2.1	2.1	2.4	2.1	2.1	2.1	2.1	2.1	1.9
	15Y	5.0	9.0E-2	1.8	1.3	1.3	1.3	2.4	1.3	1.3	1.3	1.3	1.3	1.4
	20Y	5.0	5.0E-2	1.0	1.0	1.0	1.0	1.0	1.0	1.0	1.0	1.0	1.0	1.0
W	NB	0.3	1.6E-1	18.	20.	20.	20.	64.	20.	20.	20.	19.	19.	19.
	3M	0.3	1.5E-1	14.	15.	15.	15.	43.	15.	15.	15.	15.	15.	15.
	1Y	0.3	1.0E-1	6.9	8.1	8.1	8.1	12.	8.1	8.1	8.1	8.0	8.0	6.2
	5Y	0.3	7.0E-2	3.3	3.6	3.6	3.6	3.2	3.6	3.6	3.6	3.6	3.6	2.9
	10Y	0.3	8.0E-2	2.2	2.2	2.2	2.2	2.6	2.2	2.2	2.2	2.2	2.2	2.0
	15Y	0.3	9.0E-2	1.5	1.4	1.4	1.4	2.6	1.4	1.4	1.4	1.4	1.4	1.5
	20Y	0.3	5.0E-2	1.0	1.0	1.0	1.0	1.0	1.0	1.0	1.0	1.0	1.0	1.0
W	NB	1.0	1.6E-1	20.	22.	22.	22.	72.	22.	22.	21.	21.	21.	21.
	3M	1.0	1.5E-1	15.	17.	17.	17.	49.	17.	17.	17.	16.	16.	16.
	1Y	1.0	1.0E-1	7.0	8.4	8.4	8.4	13.	8.4	8.4	8.4	8.2	8.2	6.4
	5Y	1.0	7.0E-2	3.3	3.6	3.6	3.6	3.2	3.6	3.6	3.6	3.7	3.7	2.9
	10Y	1.0	8.0E-2	2.2	2.3	2.3	2.3	2.6	2.3	2.3	2.3	2.3	2.3	2.1
	15Y	1.0	9.0E-2	1.6	1.5	1.5	1.5	2.7	1.5	1.5	1.5	1.4	1.4	1.5
	20Y	1.0	5.0E-2	1.0	1.0	1.0	1.0	1.0	1.0	1.0	1.0	1.0	1.0	1.0
W	NB	5.0	1.6E-1	26.	25.	25.	25.	84.	25.	25.	24.	23.	23.	24.
	3M	5.0	1.5E-1	20.	19.	19.	19.	58.	19.	19.	19.	18.	18.	19.
	1Y	5.0	1.0E-1	7.6	8.9	8.9	8.9	14.	8.9	8.9	8.8	8.6	8.6	6.7
	5Y	5.0	7.0E-2	3.3	3.7	3.7	3.7	3.3	3.7	3.7	3.7	3.7	3.7	3.0
	10Y	5.0	8.0E-2	2.2	2.4	2.4	2.4	2.7	2.4	2.4	2.3	2.3	2.3	2.1
	15Y	5.0	9.0E-2	1.7	1.5	1.5	1.5	2.8	1.5	1.5	1.5	1.5	1.5	1.6
	20Y	5.0	5.0E-2	1.0	1.0	1.0	1.0	1.0	1.0	1.0	1.0	1.0	1.0	1.0
Y	NB	0.3	6.4E-3	5.7	5.5	5.7	5.7	11.	5.6	5.8	6.3	8.6	8.6	4.9
	3M	0.3	6.0E-3	4.9	4.9	5.1	5.0	8.5	5.0	5.1	5.6	7.4	7.4	4.3
	1Y	0.3	4.0E-3	3.8	4.0	4.1	4.1	5.1	4.0	4.0	4.3	5.0	5.0	3.3
	5Y	0.3	2.8E-3	2.3	2.3	2.3	2.3	2.5	2.4	2.3	2.4	2.7	2.7	2.1
	10Y	0.3	3.2E-3	1.6	1.5	1.5	1.5	2.1	1.5	1.5	1.5	1.7	1.7	1.5
	15Y	0.3	3.6E-3	1.2	1.1	1.1	1.1	1.5	1.1	1.1	1.1	1.1	1.1	1.1
	20Y	0.3	2.0E-3	1.0	1.0	1.0	1.0	1.0	1.0	1.0	1.0	1.0	1.0	1.0
Y	NB	1.0	6.4E-3	5.7	6.6	6.8	6.8	15.	6.7	7.2	7.9	11.	11.	6.1
	3M	1.0	6.0E-3	4.9	5.7	5.9	5.9	12.	5.8	6.2	6.8	9.4	9.4	5.2
	1Y	1.0	4.0E-3	3.8	4.3	4.4	4.3	5.6	4.3	4.3	4.7	5.6	5.6	3.5
	5Y	1.0	2.8E-3	2.3	2.4	2.4	2.4	2.6	2.4	2.4	2.6	3.0	3.0	2.1
	10Y	1.0	3.2E-3	1.6	1.5	1.6	1.6	2.1	1.6	1.5	1.6	1.8	1.8	1.5
	15Y	1.0	3.6E-3	1.2	1.1	1.1	1.1	1.6	1.1	1.1	1.1	1.2	1.2	1.2
	20Y	1.0	2.0E-3	1.0	1.0	1.0	1.0	1.0	1.0	1.0	1.0	1.0	1.0	1.0
Y	NB	5.0	6.4E-3	5.7	11.	12.	12.	35.	12.	13.	14.	17.	17.	11.
	3M	5.0	6.0E-3	5.0	9.3	9.6	9.6	25.	9.4	10.	11.	14.	14.	9.0
	1Y	5.0	4.0E-3	3.8	5.5	5.6	5.6	8.0	5.6	5.6	6.1	7.0	7.0	4.4
	5Y	5.0	2.8E-3	2.3	2.8	2.8	2.8	2.8	2.8	2.8	3.0	3.5	3.5	2.4
	10Y	5.0	3.2E-3	1.6	1.8	1.8	1.8	2.3	1.8	1.8	1.9	2.1	2.1	1.7
	15Y	5.0	3.6E-3	1.2	1.2	1.2	1.2	1.9	1.2	1.2	1.2	1.3	1.3	1.3
	20Y	5.0	2.0E-3	1.0	1.0	1.0	1.0	1.0	1.0	1.0	1.0	1.0	1.0	1.0

[a] Cristy et al. (1986).

Table I-22S(b). Age-Specific Inhalation DCFs for ^{238}U, Normalized to the Adult[a]

MODE	AGE	AMAD	F1	LIVER	LUNGS	OVARIES	PANCR	ACT MAR	SKIN	SPLEEN	TESTES	THYMUS	THYROID	UTERUS
D	NB	0.3	1.6E-1	16.	19.	17.	17.	22.	17.	22.	17.	17.	17.	17.
	3M	0.3	1.5E-1	13.	16.	13.	13.	17.	13.	16.	13.	13.	13.	13.
	1Y	0.3	1.0E-1	6.7	7.0	7.3	7.3	4.9	7.3	7.4	7.3	7.3	7.3	7.3
	5Y	0.3	7.0E-2	3.1	3.4	3.4	3.4	1.7	3.4	3.6	3.4	3.4	3.4	3.4
	10Y	0.3	8.0E-2	2.1	2.2	2.1	2.1	1.3	2.1	2.4	2.1	2.1	2.1	2.1
	15Y	0.3	9.0E-2	1.4	1.5	1.3	1.3	1.1	1.3	1.7	1.3	1.3	1.3	1.3
	20Y	0.3	5.0E-2	1.0	1.0	1.0	1.0	1.0	1.0	1.0	1.0	1.0	1.0	1.0
D	NB	1.0	1.6E-1	16.	19.	17.	17.	23.	17.	23.	17.	17.	17.	17.
	3M	1.0	1.5E-1	13.	15.	14.	14.	17.	14.	16.	14.	14.	14.	14.
	1Y	1.0	1.0E-1	6.8	7.1	7.4	7.4	5.0	7.4	7.4	7.4	7.4	7.4	7.4
	5Y	1.0	7.0E-2	3.1	3.4	3.4	3.4	1.7	3.4	3.6	3.4	3.4	3.4	3.4
	10Y	1.0	8.0E-2	2.1	2.2	2.1	2.1	1.3	2.1	2.4	2.1	2.1	2.1	2.1
	15Y	1.0	9.0E-2	1.4	1.5	1.3	1.3	1.1	1.3	1.8	1.3	1.3	1.3	1.3
	20Y	1.0	5.0E-2	1.0	1.0	1.0	1.0	1.0	1.0	1.0	1.0	1.0	1.0	1.0
D	NB	5.0	1.6E-1	17.	19.	18.	18.	24.	18.	24.	18.	18.	18.	18.
	3M	5.0	1.5E-1	14.	15.	14.	14.	18.	14.	16.	14.	14.	14.	14.
	1Y	5.0	1.0E-1	6.9	7.3	7.5	7.5	5.1	7.5	7.6	7.5	7.5	7.5	7.5
	5Y	5.0	7.0E-2	3.2	3.4	3.5	3.5	1.7	3.5	3.6	3.5	3.5	3.5	3.5
	10Y	5.0	8.0E-2	2.1	2.2	2.1	2.1	1.3	2.1	2.4	2.1	2.1	2.1	2.1
	15Y	5.0	9.0E-2	1.4	1.4	1.3	1.3	1.2	1.3	1.8	1.3	1.3	1.3	1.3
	20Y	5.0	5.0E-2	1.0	1.0	1.0	1.0	1.0	1.0	1.0	1.0	1.0	1.0	1.0
W	NB	0.3	1.6E-1	18.	17.	20.	20.	25.	20.	25.	20.	20.	20.	20.
	3M	0.3	1.5E-1	14.	14.	15.	15.	18.	15.	17.	15.	15.	15.	15.
	1Y	0.3	1.0E-1	7.4	6.8	8.1	8.1	5.5	8.1	8.2	8.1	8.1	8.1	8.1
	5Y	0.3	7.0E-2	3.2	3.4	3.6	3.6	1.8	3.6	3.8	3.6	3.6	3.6	3.6
	10Y	0.3	8.0E-2	2.2	2.2	2.2	2.2	1.4	2.2	2.6	2.2	2.2	2.2	2.2
	15Y	0.3	9.0E-2	1.5	1.5	1.4	1.4	1.3	1.4	1.9	1.4	1.4	1.4	1.4
	20Y	0.3	5.0E-2	1.0	1.0	1.0	1.0	1.0	1.0	1.0	1.0	1.0	1.0	1.0
W	NB	1.0	1.6E-1	20.	17.	22.	22.	28.	22.	28.	22.	22.	22.	22.
	3M	1.0	1.5E-1	16.	14.	17.	17.	20.	17.	19.	17.	17.	17.	17.
	1Y	1.0	1.0E-1	7.7	6.8	8.4	8.4	5.7	8.4	8.5	8.4	8.4	8.4	8.4
	5Y	1.0	7.0E-2	3.3	3.4	3.6	3.6	1.9	3.6	3.8	3.6	3.6	3.6	3.6
	10Y	1.0	8.0E-2	2.3	2.2	2.3	2.3	1.4	2.3	2.6	2.3	2.3	2.3	2.3
	15Y	1.0	9.0E-2	1.6	1.5	1.5	1.5	1.3	1.5	1.9	1.5	1.5	1.5	1.5
	20Y	1.0	5.0E-2	1.0	1.0	1.0	1.0	1.0	1.0	1.0	1.0	1.0	1.0	1.0
W	NB	5.0	1.6E-1	23.	17.	25.	25.	32.	25.	33.	25.	25.	25.	25.
	3M	5.0	1.5E-1	18.	14.	19.	19.	24.	19.	22.	19.	19.	19.	19.
	1Y	5.0	1.0E-1	8.1	6.8	8.9	8.9	6.0	8.9	9.0	8.9	8.9	8.9	8.9
	5Y	5.0	7.0E-2	3.4	3.4	3.7	3.7	1.9	3.7	3.9	3.7	3.7	3.7	3.7
	10Y	5.0	8.0E-2	2.4	2.2	2.4	2.4	1.5	2.4	2.7	2.4	2.4	2.4	2.4
	15Y	5.0	9.0E-2	1.6	1.5	1.5	1.5	1.3	1.5	2.0	1.5	1.5	1.5	1.5
	20Y	5.0	5.0E-2	1.0	1.0	1.0	1.0	1.0	1.0	1.0	1.0	1.0	1.0	1.0
Y	NB	0.3	6.4E-3	5.1	5.7	5.7	5.5	4.8	5.6	6.2	5.7	5.3	5.6	5.7
	3M	0.3	6.0E-3	4.6	4.9	5.1	4.9	3.9	5.0	5.3	5.1	4.7	5.0	5.1
	1Y	0.3	4.0E-3	3.7	3.8	4.1	3.9	2.6	4.0	4.2	4.1	3.8	4.0	4.1
	5Y	0.3	2.8E-3	2.2	2.3	2.3	2.3	1.5	2.3	2.6	2.3	2.2	2.3	2.3
	10Y	0.3	3.2E-3	1.5	1.6	1.5	1.5	1.2	1.5	1.8	1.5	1.4	1.5	1.5
	15Y	0.3	3.6E-3	1.1	1.2	1.1	1.1	1.1	1.1	1.2	1.1	1.1	1.1	1.1
	20Y	0.3	2.0E-3	1.0	1.0	1.0	1.0	1.0	1.0	1.0	1.0	1.0	1.0	1.0
Y	NB	1.0	6.4E-3	6.1	5.7	6.8	6.6	6.4	6.7	7.7	6.8	6.3	6.7	6.8
	3M	1.0	6.0E-3	5.3	4.9	5.9	5.7	5.1	5.8	6.3	5.9	5.5	5.8	5.9
	1Y	1.0	4.0E-3	3.9	3.8	4.3	4.2	2.8	4.3	4.5	4.4	4.1	4.3	4.4
	5Y	1.0	2.8E-3	2.3	2.3	2.4	2.4	1.5	2.4	2.7	2.4	2.3	2.4	2.4
	10Y	1.0	3.2E-3	1.6	1.6	1.6	1.5	1.2	1.5	1.8	1.6	1.5	1.5	1.6
	15Y	1.0	3.6E-3	1.2	1.2	1.1	1.1	1.1	1.1	1.3	1.1	1.1	1.1	1.1
	20Y	1.0	2.0E-3	1.0	1.0	1.0	1.0	1.0	1.0	1.0	1.0	1.0	1.0	1.0
Y	NB	5.0	6.4E-3	10.	5.7	12.	11.	14.	12.	15.	12.	11.	12.	12.
	3M	5.0	6.0E-3	8.5	4.9	9.6	9.3	10.	9.5	11.	9.6	9.0	9.5	9.6
	1Y	5.0	4.0E-3	5.0	3.8	5.6	5.5	3.7	5.6	5.7	5.6	5.4	5.6	5.6
	5Y	5.0	2.8E-3	2.6	2.3	2.8	2.8	1.6	2.8	3.0	2.8	2.7	2.8	2.8
	10Y	5.0	3.2E-3	1.8	1.6	1.8	1.8	1.3	1.8	2.1	1.8	1.7	1.8	1.8
	15Y	5.0	3.6E-3	1.3	1.2	1.2	1.2	1.1	1.2	1.5	1.2	1.2	1.2	1.2
	20Y	5.0	2.0E-3	1.0	1.0	1.0	1.0	1.0	1.0	1.0	1.0	1.0	1.0	1.0

[a] Cristy et al. (1986).

Table I-23S(a). Age-Specific Inhalation DCFs for ^{235}U, Normalized to the Adult[a]

MODE	AGE	AMAD	F1	EFF	ADREN	BL WALL	BRAIN	B SURF	BREAST	ST W	SI W	ULI W	LLI W	KIDNEY
D	NB	0.3	1.6E-1	35.	17.	17.	17.	58.	17.	17.	17.	17.	17.	17.
	3M	0.3	1.5E-1	26.	13.	13.	13.	42.	13.	13.	13.	13.	13.	13.
	1Y	0.3	1.0E-1	8.2	7.3	7.3	7.3	11.	7.3	7.3	7.3	7.3	7.3	5.6
	5Y	0.3	7.0E-2	2.9	3.4	3.4	3.4	3.1	3.4	3.4	3.4	3.4	3.4	2.8
	10Y	0.3	8.0E-2	2.1	2.1	2.1	2.1	2.4	2.1	2.1	2.1	2.1	2.1	1.9
	15Y	0.3	9.0E-2	1.8	1.3	1.3	1.3	2.4	1.3	1.3	1.3	1.3	1.3	1.4
	20Y	0.3	5.0E-2	1.0	1.0	1.0	1.0	1.0	1.0	1.0	1.0	1.0	1.0	1.0
D	NB	1.0	1.6E-1	36.	17.	17.	17.	60.	17.	17.	17.	17.	17.	17.
	3M	1.0	1.5E-1	26.	14.	14.	14.	43.	14.	14.	14.	14.	14.	14.
	1Y	1.0	1.0E-1	8.3	7.4	7.4	7.4	12.	7.4	7.4	7.4	7.4	7.4	5.6
	5Y	1.0	7.0E-2	2.9	3.4	3.4	3.4	3.1	3.4	3.4	3.4	3.4	3.4	2.8
	10Y	1.0	8.0E-2	2.1	2.1	2.1	2.1	2.4	2.1	2.1	2.1	2.1	2.1	1.9
	15Y	1.0	9.0E-2	1.8	1.3	1.3	1.3	2.4	1.3	1.3	1.3	1.3	1.3	1.4
	20Y	1.0	5.0E-2	1.0	1.0	1.0	1.0	1.0	1.0	1.0	1.0	1.0	1.0	1.0
D	NB	5.0	1.6E-1	38.	18.	18.	18.	62.	18.	18.	18.	18.	18.	18.
	3M	5.0	1.5E-1	28.	14.	14.	14.	45.	14.	14.	14.	14.	14.	14.
	1Y	5.0	1.0E-1	8.5	7.5	7.5	7.5	12.	7.5	7.5	7.5	7.5	7.5	5.7
	5Y	5.0	7.0E-2	2.9	3.5	3.5	3.5	3.1	3.5	3.5	3.5	3.5	3.5	2.8
	10Y	5.0	8.0E-2	2.1	2.1	2.1	2.1	2.4	2.1	2.1	2.1	2.1	2.1	1.9
	15Y	5.0	9.0E-2	1.8	1.3	1.3	1.3	2.4	1.3	1.3	1.3	1.3	1.3	1.4
	20Y	5.0	5.0E-2	1.0	1.0	1.0	1.0	1.0	1.0	1.0	1.0	1.0	1.0	1.0
W	NB	0.3	1.6E-1	18.	20.	20.	20.	65.	20.	20.	20.	19.	18.	19.
	3M	0.3	1.5E-1	14.	15.	15.	15.	44.	15.	15.	15.	15.	15.	15.
	1Y	0.3	1.0E-1	6.9	8.1	8.1	8.1	13.	8.1	8.1	8.1	8.0	7.7	6.2
	5Y	0.3	7.0E-2	3.4	3.6	3.6	3.6	3.2	3.6	3.6	3.6	3.6	3.6	2.9
	10Y	0.3	8.0E-2	2.2	2.2	2.2	2.2	2.6	2.2	2.2	2.2	2.2	2.2	2.0
	15Y	0.3	9.0E-2	1.5	1.4	1.4	1.5	2.6	1.5	1.4	1.4	1.4	1.3	1.5
	20Y	0.3	5.0E-2	1.0	1.0	1.0	1.0	1.0	1.0	1.0	1.0	1.0	1.0	1.0
W	NB	1.0	1.6E-1	20.	22.	22.	22.	73.	22.	22.	21.	21.	20.	21.
	3M	1.0	1.5E-1	15.	17.	17.	17.	50.	17.	17.	17.	16.	16.	16.
	1Y	1.0	1.0E-1	7.1	8.4	8.4	8.4	13.	8.4	8.4	8.4	8.2	7.8	6.4
	5Y	1.0	7.0E-2	3.4	3.6	3.6	3.6	3.3	3.6	3.6	3.6	3.7	3.6	2.9
	10Y	1.0	8.0E-2	2.2	2.3	2.3	2.3	2.6	2.3	2.3	2.3	2.3	2.2	2.1
	15Y	1.0	9.0E-2	1.6	1.5	1.5	1.5	2.7	1.5	1.5	1.5	1.4	1.4	1.6
	20Y	1.0	5.0E-2	1.0	1.0	1.0	1.0	1.0	1.0	1.0	1.0	1.0	1.0	1.0
W	NB	5.0	1.6E-1	26.	25.	25.	25.	85.	25.	25.	24.	23.	21.	24.
	3M	5.0	1.5E-1	20.	19.	19.	19.	59.	19.	19.	19.	18.	17.	19.
	1Y	5.0	1.0E-1	7.6	8.9	8.9	8.9	14.	8.9	8.8	8.8	8.5	8.0	6.8
	5Y	5.0	7.0E-2	3.3	3.7	3.7	3.7	3.3	3.7	3.7	3.7	3.7	3.7	3.0
	10Y	5.0	8.0E-2	2.2	2.4	2.4	2.4	2.7	2.4	2.3	2.3	2.3	2.2	2.2
	15Y	5.0	9.0E-2	1.7	1.5	1.5	1.5	2.8	1.5	1.5	1.5	1.5	1.4	1.6
	20Y	5.0	5.0E-2	1.0	1.0	1.0	1.0	1.0	1.0	1.0	1.0	1.0	1.0	1.0
Y	NB	0.3	6.4E-3	5.7	5.6	5.7	5.7	11.	6.0	5.5	6.5	8.8	11.	5.0
	3M	0.3	6.0E-3	4.9	5.0	5.1	5.1	8.5	5.4	4.9	5.7	7.6	9.6	4.3
	1Y	0.3	4.0E-3	3.9	4.0	4.1	4.1	5.1	4.4	3.8	4.3	5.0	5.6	3.3
	5Y	0.3	2.8E-3	2.3	2.4	2.4	2.3	2.5	2.7	2.3	2.5	2.8	3.0	2.1
	10Y	0.3	3.2E-3	1.6	1.6	1.5	1.5	2.1	1.7	1.5	1.6	1.7	1.8	1.5
	15Y	0.3	3.6E-3	1.2	1.1	1.1	1.1	1.5	1.2	1.1	1.1	1.2	1.2	1.1
	20Y	0.3	2.0E-3	1.0	1.0	1.0	1.0	1.0	1.0	1.0	1.0	1.0	1.0	1.0
Y	NB	1.0	6.4E-3	5.7	6.4	6.9	6.8	16.	6.9	6.7	8.1	12.	14.	6.1
	3M	1.0	6.0E-3	5.0	5.6	6.0	5.9	12.	6.0	5.8	6.9	9.8	12.	5.2
	1Y	1.0	4.0E-3	3.9	4.2	4.4	4.4	5.7	4.6	4.1	4.7	5.7	6.2	3.5
	5Y	1.0	2.8E-3	2.3	2.5	2.4	2.4	2.6	2.7	2.3	2.6	3.0	3.2	2.1
	10Y	1.0	3.2E-3	1.6	1.6	1.6	1.6	2.1	1.7	1.5	1.6	1.8	2.0	1.5
	15Y	1.0	3.6E-3	1.2	1.2	1.1	1.1	1.6	1.2	1.1	1.2	1.2	1.2	1.2
	20Y	1.0	2.0E-3	1.0	1.0	1.0	1.0	1.0	1.0	1.0	1.0	1.0	1.0	1.0
Y	NB	5.0	6.4E-3	5.8	11.	12.	12.	36.	11.	12.	14.	17.	18.	11.
	3M	5.0	6.0E-3	5.0	8.6	9.6	9.6	25.	9.2	9.7	11.	14.	15.	9.0
	1Y	5.0	4.0E-3	3.9	5.3	5.7	5.6	8.1	5.7	5.4	6.1	7.0	7.1	4.4
	5Y	5.0	2.8E-3	2.3	2.8	2.8	2.8	2.8	3.0	2.7	3.1	3.5	3.5	2.4
	10Y	5.0	3.2E-3	1.6	1.8	1.8	1.8	2.3	1.9	1.7	1.9	2.1	2.1	1.7
	15Y	5.0	3.6E-3	1.2	1.2	1.2	1.2	1.9	1.3	1.2	1.2	1.3	1.2	1.3
	20Y	5.0	2.0E-3	1.0	1.0	1.0	1.0	1.0	1.0	1.0	1.0	1.0	1.0	1.0

[a] Cristy et al. (1986).

Table I-23S(b). Age-Specific Inhalation DCFs for ^{235}U, Normalized to the Adult[a]

MODE	AGE	AMAD	F1	LIVER	LUNGS	OVARIES	PANCR	ACT MAR	SKIN	SPLEEN	TESTES	THYMUS	THYROID	UTERUS
D	NB	0.3	1.6E-1	16.	19.	17.	17.	23.	17.	22.	17.	17.	17.	17.
	3M	0.3	1.5E-1	13.	16.	13.	13.	17.	13.	16.	13.	13.	13.	13.
	1Y	0.3	1.0E-1	6.7	7.1	7.3	7.3	5.0	7.3	7.4	7.3	7.3	7.3	7.3
	5Y	0.3	7.0E-2	3.1	3.5	3.4	3.4	1.7	3.4	3.6	3.4	3.4	3.4	3.4
	10Y	0.3	8.0E-2	2.1	2.2	2.1	2.1	1.3	2.1	2.4	2.1	2.1	2.1	2.1
	15Y	0.3	9.0E-2	1.4	1.5	1.3	1.3	1.1	1.3	1.7	1.3	1.3	1.3	1.3
	20Y	0.3	5.0E-2	1.0	1.0	1.0	1.0	1.0	1.0	1.0	1.0	1.0	1.0	1.0
D	NB	1.0	1.6E-1	16.	19.	17.	17.	23.	17.	23.	17.	17.	17.	17.
	3M	1.0	1.5E-1	13.	15.	14.	14.	18.	14.	16.	14.	14.	14.	14.
	1Y	1.0	1.0E-1	6.8	7.1	7.4	7.4	5.1	7.4	7.5	7.4	7.4	7.4	7.4
	5Y	1.0	7.0E-2	3.1	3.5	3.4	3.4	1.8	3.4	3.6	3.4	3.4	3.4	3.4
	10Y	1.0	8.0E-2	2.1	2.2	2.1	2.1	1.3	2.1	2.4	2.1	2.1	2.1	2.1
	15Y	1.0	9.0E-2	1.4	1.5	1.3	1.3	1.2	1.3	1.8	1.3	1.3	1.3	1.3
	20Y	1.0	5.0E-2	1.0	1.0	1.0	1.0	1.0	1.0	1.0	1.0	1.0	1.0	1.0
D	NB	5.0	1.6E-1	17.	19.	18.	18.	24.	18.	24.	18.	18.	18.	18.
	3M	5.0	1.5E-1	14.	15.	14.	14.	18.	14.	16.	14.	14.	14.	14.
	1Y	5.0	1.0E-1	6.9	7.3	7.5	7.5	5.2	7.5	7.6	7.5	7.5	7.5	7.5
	5Y	5.0	7.0E-2	3.2	3.5	3.5	3.5	1.8	3.5	3.6	3.5	3.5	3.5	3.5
	10Y	5.0	8.0E-2	2.1	2.2	2.1	2.1	1.4	2.1	2.5	2.1	2.1	2.1	2.1
	15Y	5.0	9.0E-2	1.4	1.4	1.3	1.3	1.2	1.3	1.8	1.3	1.3	1.3	1.3
	20Y	5.0	5.0E-2	1.0	1.0	1.0	1.0	1.0	1.0	1.0	1.0	1.0	1.0	1.0
W	NB	0.3	1.6E-1	18.	17.	20.	20.	26.	20.	25.	20.	19.	20.	20.
	3M	0.3	1.5E-1	14.	14.	15.	15.	18.	15.	17.	15.	15.	15.	15.
	1Y	0.3	1.0E-1	7.4	6.8	8.1	8.1	5.5	8.1	8.2	8.1	8.0	8.1	8.1
	5Y	0.3	7.0E-2	3.3	3.4	3.6	3.6	1.8	3.6	3.8	3.6	3.5	3.6	3.6
	10Y	0.3	8.0E-2	2.2	2.2	2.2	2.2	1.4	2.2	2.6	2.2	2.2	2.2	2.2
	15Y	0.3	9.0E-2	1.5	1.5	1.4	1.4	1.3	1.4	1.9	1.4	1.4	1.4	1.4
	20Y	0.3	5.0E-2	1.0	1.0	1.0	1.0	1.0	1.0	1.0	1.0	1.0	1.0	1.0
W	NB	1.0	1.6E-1	20.	17.	22.	22.	29.	22.	28.	22.	21.	22.	22.
	3M	1.0	1.5E-1	16.	14.	17.	17.	21.	17.	19.	17.	17.	17.	17.
	1Y	1.0	1.0E-1	7.7	6.8	8.4	8.4	5.7	8.4	8.5	8.4	8.4	8.4	8.4
	5Y	1.0	7.0E-2	3.3	3.4	3.6	3.6	1.9	3.6	3.8	3.6	3.6	3.6	3.6
	10Y	1.0	8.0E-2	2.3	2.2	2.3	2.3	1.5	2.3	2.6	2.3	2.3	2.3	2.3
	15Y	1.0	9.0E-2	1.6	1.5	1.5	1.5	1.3	1.5	2.0	1.5	1.5	1.5	1.5
	20Y	1.0	5.0E-2	1.0	1.0	1.0	1.0	1.0	1.0	1.0	1.0	1.0	1.0	1.0
W	NB	5.0	1.6E-1	23.	17.	25.	25.	33.	25.	33.	25.	25.	25.	25.
	3M	5.0	1.5E-1	18.	14.	19.	19.	24.	19.	22.	19.	19.	19.	19.
	1Y	5.0	1.0E-1	8.2	6.8	8.9	8.9	6.1	8.9	9.0	8.9	8.9	8.9	8.9
	5Y	5.0	7.0E-2	3.4	3.4	3.7	3.7	1.9	3.7	3.9	3.7	3.7	3.7	3.7
	10Y	5.0	8.0E-2	2.4	2.2	2.4	2.4	1.5	2.4	2.7	2.4	2.4	2.4	2.4
	15Y	5.0	9.0E-2	1.6	1.5	1.5	1.5	1.3	1.5	2.0	1.5	1.5	1.5	1.5
	20Y	5.0	5.0E-2	1.0	1.0	1.0	1.0	1.0	1.0	1.0	1.0	1.0	1.0	1.0
Y	NB	0.3	6.4E-3	4.8	5.6	5.8	5.2	4.8	5.4	6.0	5.7	4.5	5.8	5.8
	3M	0.3	6.0E-3	4.3	5.0	5.1	4.7	3.9	4.8	5.1	5.1	4.0	5.2	5.1
	1Y	0.3	4.0E-3	3.5	4.0	4.1	3.8	2.5	4.0	4.1	4.1	3.3	4.2	4.1
	5Y	0.3	2.8E-3	2.2	2.4	2.4	2.2	1.5	2.3	2.5	2.4	2.1	2.4	2.4
	10Y	0.3	3.2E-3	1.5	1.6	1.5	1.5	1.2	1.5	1.7	1.5	1.4	1.6	1.5
	15Y	0.3	3.6E-3	1.2	1.1	1.1	1.1	1.1	1.1	1.2	1.1	1.1	1.1	1.1
	20Y	0.3	2.0E-3	1.0	1.0	1.0	1.0	1.0	1.0	1.0	1.0	1.0	1.0	1.0
Y	NB	1.0	6.4E-3	5.4	6.4	6.9	6.1	6.4	6.3	7.3	6.9	5.2	6.8	6.9
	3M	1.0	6.0E-3	4.8	5.6	6.0	5.3	5.1	5.5	6.0	5.9	4.6	5.9	6.0
	1Y	1.0	4.0E-3	3.7	4.2	4.4	4.0	2.7	4.3	4.3	4.4	3.5	4.5	4.4
	5Y	1.0	2.8E-3	2.2	2.5	2.4	2.3	1.5	2.4	2.6	2.4	2.1	2.5	2.4
	10Y	1.0	3.2E-3	1.6	1.6	1.6	1.5	1.2	1.5	1.8	1.6	1.4	1.6	1.6
	15Y	1.0	3.6E-3	1.2	1.2	1.1	1.1	1.1	1.1	1.3	1.1	1.1	1.2	1.1
	20Y	1.0	2.0E-3	1.0	1.0	1.0	1.0	1.0	1.0	1.0	1.0	1.0	1.0	1.0
Y	NB	5.0	6.4E-3	8.8	11.	12.	10.	14.	11.	14.	12.	9.1	11.	12.
	3M	5.0	6.0E-3	7.3	8.6	9.6	8.4	11.	8.9	10.	9.7	7.5	9.4	9.6
	1Y	5.0	4.0E-3	4.5	5.3	5.6	5.1	3.7	5.5	5.5	5.7	4.6	5.6	5.7
	5Y	5.0	2.8E-3	2.5	2.8	2.8	2.6	1.6	2.8	2.9	2.8	2.5	2.8	2.8
	10Y	5.0	3.2E-3	1.7	1.8	1.8	1.7	1.3	1.8	2.0	1.8	1.6	1.8	1.8
	15Y	5.0	3.6E-3	1.3	1.2	1.2	1.2	1.2	1.2	1.5	1.2	1.2	1.2	1.2
	20Y	5.0	2.0E-3	1.0	1.0	1.0	1.0	1.0	1.0	1.0	1.0	1.0	1.0	1.0

[a] Cristy et al. (1986).

Table I-24S(a). Age-Specific Inhalation DCFs for ^{234}U, Normalized to the Adult[a]

MODE	AGE	AMAD	F1	EFF	ADREN	BL WALL	BRAIN	B SURF	BREAST	ST W	SI W	ULI W	LLI W	KIDNEY
D	NB	0.3	1.6E-1	35.	17.	17.	17.	58.	17.	17.	17.	17.	17.	17.
	3M	0.3	1.5E-1	26.	14.	14.	14.	42.	14.	14.	14.	14.	14.	13.
	1Y	0.3	1.0E-1	8.2	7.4	7.4	7.4	11.	7.4	7.4	7.4	7.4	7.4	5.6
	5Y	0.3	7.0E-2	2.9	3.4	3.4	3.4	3.1	3.4	3.4	3.4	3.4	3.4	2.8
	10Y	0.3	8.0E-2	2.1	2.1	2.1	2.1	2.4	2.1	2.1	2.1	2.1	2.1	1.9
	15Y	0.3	9.0E-2	1.8	1.3	1.3	1.3	2.4	1.3	1.3	1.3	1.3	1.3	1.4
	20Y	0.3	5.0E-2	1.0	1.0	1.0	1.0	1.0	1.0	1.0	1.0	1.0	1.0	1.0
D	NB	1.0	1.6E-1	36.	17.	17.	17.	60.	17.	17.	17.	17.	17.	17.
	3M	1.0	1.5E-1	26.	14.	14.	14.	43.	14.	14.	14.	14.	14.	14.
	1Y	1.0	1.0E-1	8.3	7.4	7.4	7.4	12.	7.4	7.4	7.4	7.4	7.4	5.6
	5Y	1.0	7.0E-2	2.9	3.5	3.5	3.5	3.1	3.5	3.5	3.5	3.5	3.5	2.8
	10Y	1.0	8.0E-2	2.1	2.1	2.1	2.1	2.4	2.1	2.1	2.1	2.1	2.1	1.9
	15Y	1.0	9.0E-2	1.8	1.3	1.3	1.3	2.4	1.3	1.3	1.3	1.3	1.3	1.4
	20Y	1.0	5.0E-2	1.0	1.0	1.0	1.0	1.0	1.0	1.0	1.0	1.0	1.0	1.0
D	NB	5.0	1.6E-1	38.	18.	18.	18.	62.	18.	18.	18.	18.	18.	18.
	3M	5.0	1.5E-1	28.	14.	14.	14.	44.	14.	14.	14.	14.	14.	14.
	1Y	5.0	1.0E-1	8.5	7.6	7.6	7.6	12.	7.6	7.6	7.6	7.6	7.5	5.7
	5Y	5.0	7.0E-2	2.9	3.5	3.5	3.5	3.1	3.5	3.5	3.5	3.5	3.5	2.8
	10Y	5.0	8.0E-2	2.1	2.1	2.1	2.1	2.4	2.1	2.1	2.1	2.1	2.1	1.9
	15Y	5.0	9.0E-2	1.8	1.3	1.3	1.3	2.4	1.3	1.3	1.3	1.3	1.3	1.4
	20Y	5.0	5.0E-2	1.0	1.0	1.0	1.0	1.0	1.0	1.0	1.0	1.0	1.0	1.0
W	NB	0.3	1.6E-1	18.	20.	20.	20.	65.	20.	20.	20.	19.	19.	19.
	3M	0.3	1.5E-1	14.	15.	15.	15.	44.	15.	15.	15.	15.	15.	15.
	1Y	0.3	1.0E-1	6.9	8.2	8.2	8.2	13.	8.2	8.2	8.1	8.1	7.8	6.2
	5Y	0.3	7.0E-2	3.4	3.6	3.6	3.6	3.2	3.6	3.6	3.6	3.6	3.6	2.9
	10Y	0.3	8.0E-2	2.2	2.2	2.2	2.2	2.6	2.2	2.2	2.2	2.2	2.2	2.0
	15Y	0.3	9.0E-2	1.5	1.4	1.4	1.4	2.6	1.4	1.4	1.4	1.4	1.4	1.5
	20Y	0.3	5.0E-2	1.0	1.0	1.0	1.0	1.0	1.0	1.0	1.0	1.0	1.0	1.0
W	NB	1.0	1.6E-1	20.	22.	22.	22.	73.	22.	22.	22.	21.	20.	21.
	3M	1.0	1.5E-1	15.	17.	17.	17.	50.	17.	17.	17.	16.	16.	16.
	1Y	1.0	1.0E-1	7.1	8.5	8.5	8.5	13.	8.5	8.4	8.4	8.3	7.9	6.4
	5Y	1.0	7.0E-2	3.4	3.6	3.6	3.6	3.3	3.6	3.6	3.6	3.7	3.6	2.9
	10Y	1.0	8.0E-2	2.2	2.3	2.3	2.3	2.6	2.3	2.3	2.3	2.3	2.2	2.1
	15Y	1.0	9.0E-2	1.6	1.5	1.5	1.5	2.7	1.5	1.5	1.5	1.4	1.4	1.6
	20Y	1.0	5.0E-2	1.0	1.0	1.0	1.0	1.0	1.0	1.0	1.0	1.0	1.0	1.0
W	NB	5.0	1.6E-1	26.	25.	25.	25.	85.	25.	25.	24.	23.	21.	24.
	3M	5.0	1.5E-1	20.	19.	19.	19.	59.	19.	19.	19.	18.	17.	19.
	1Y	5.0	1.0E-1	7.7	9.0	9.0	9.0	14.	9.0	8.9	8.9	8.6	8.4	6.8
	5Y	5.0	7.0E-2	3.3	3.7	3.7	3.7	3.3	3.7	3.7	3.7	3.7	3.7	3.0
	10Y	5.0	8.0E-2	2.2	2.4	2.4	2.4	2.7	2.4	2.4	2.4	2.3	2.3	2.2
	15Y	5.0	9.0E-2	1.7	1.5	1.5	1.5	2.8	1.5	1.5	1.5	1.5	1.4	1.6
	20Y	5.0	5.0E-2	1.0	1.0	1.0	1.0	1.0	1.0	1.0	1.0	1.0	1.0	1.0
Y	NB	0.3	6.4E-3	5.7	5.7	5.7	5.7	11.	5.7	6.0	6.3	8.6	11.	5.0
	3M	0.3	6.0E-3	4.9	5.1	5.1	5.1	8.6	5.1	5.3	5.6	7.4	9.3	4.3
	1Y	0.3	4.0E-3	3.8	4.1	4.1	4.1	5.1	4.1	4.1	4.3	4.9	5.5	3.3
	5Y	0.3	2.8E-3	2.3	2.4	2.4	2.4	2.6	2.4	2.4	2.4	2.7	3.0	2.1
	10Y	0.3	3.2E-3	1.6	1.5	1.5	1.5	2.1	1.5	1.5	1.5	1.7	1.8	1.5
	15Y	0.3	3.6E-3	1.2	1.1	1.1	1.1	1.5	1.1	1.1	1.1	1.1	1.2	1.1
	20Y	0.3	2.0E-3	1.0	1.0	1.0	1.0	1.0	1.0	1.0	1.0	1.0	1.0	1.0
Y	NB	1.0	6.4E-3	5.7	6.9	6.9	6.9	16.	6.8	7.5	8.0	11.	14.	6.1
	3M	1.0	6.0E-3	5.0	5.9	5.9	5.9	12.	5.9	6.4	6.8	9.6	12.	5.2
	1Y	1.0	4.0E-3	3.8	4.4	4.4	4.4	5.7	4.4	4.5	4.7	5.6	6.2	3.5
	5Y	1.0	2.8E-3	2.3	2.4	2.4	2.4	2.6	2.4	2.5	2.6	3.0	3.2	2.1
	10Y	1.0	3.2E-3	1.6	1.6	1.6	1.6	2.1	1.6	1.6	1.6	1.8	1.9	1.5
	15Y	1.0	3.6E-3	1.2	1.1	1.1	1.1	1.6	1.1	1.1	1.1	1.2	1.2	1.2
	20Y	1.0	2.0E-3	1.0	1.0	1.0	1.0	1.0	1.0	1.0	1.0	1.0	1.0	1.0
Y	NB	5.0	6.4E-3	5.8	12.	12.	12.	36.	12.	13.	17.	17.	18.	11.
	3M	5.0	6.0E-3	5.0	9.7	9.7	9.7	25.	9.7	11.	11.	14.	15.	9.1
	1Y	5.0	4.0E-3	3.9	5.7	5.7	5.7	8.1	5.7	5.8	6.1	7.0	7.1	4.4
	5Y	5.0	2.8E-3	2.3	2.8	2.8	2.8	2.8	2.8	2.9	3.1	3.5	3.5	2.4
	10Y	5.0	3.2E-3	1.6	1.8	1.8	1.8	2.3	1.8	1.8	1.9	2.1	2.1	1.7
	15Y	5.0	3.6E-3	1.2	1.2	1.2	1.2	1.9	1.2	1.3	1.2	1.3	1.2	1.3
	20Y	5.0	2.0E-3	1.0	1.0	1.0	1.0	1.0	1.0	1.0	1.0	1.0	1.0	1.0

[a] Cristy et al. (1986).

Table I-24S(b). Age-Specific Inhalation DCFs for ^{234}U, Normalized to the Adult[a]

MODE	AGE	AMAD	F1	LIVER	LUNGS	OVARIES	PANCR	ACT MAR	SKIN	SPLEEN	TESTES	THYMUS	THYROID	UTERUS
D	NB	0.3	1.6E-1	16.	19.	17.	17.	23.	17.	23.	17.	17.	17.	17.
	3M	0.3	1.5E-1	13.	16.	14.	14.	18.	14.	16.	14.	14.	14.	14.
	1Y	0.3	1.0E-1	6.8	7.1	7.4	7.4	5.0	7.4	7.4	7.4	7.4	7.4	7.4
	5Y	0.3	7.0E-2	3.1	3.4	3.4	3.4	1.8	3.4	3.6	3.4	3.4	3.4	3.4
	10Y	0.3	8.0E-2	2.1	2.2	2.1	2.1	1.3	2.1	2.4	2.1	2.1	2.1	2.1
	15Y	0.3	9.0E-2	1.4	1.5	1.3	1.3	1.1	1.3	1.7	1.3	1.3	1.3	1.3
	20Y	0.3	5.0E-2	1.0	1.0	1.0	1.0	1.0	1.0	1.0	1.0	1.0	1.0	1.0
D	NB	1.0	1.6E-1	17.	19.	17.	17.	24.	17.	23.	17.	17.	17.	17.
	3M	1.0	1.5E-1	13.	15.	14.	14.	18.	14.	16.	14.	14.	14.	14.
	1Y	1.0	1.0E-1	6.9	7.1	7.4	7.4	5.1	7.4	7.5	7.4	7.4	7.4	7.4
	5Y	1.0	7.0E-2	3.2	3.5	3.5	3.5	1.8	3.5	3.6	3.5	3.5	3.5	3.5
	10Y	1.0	8.0E-2	2.1	2.2	2.1	2.1	1.3	2.1	2.4	2.1	2.1	2.1	2.1
	15Y	1.0	9.0E-2	1.4	1.5	1.3	1.3	1.2	1.3	1.8	1.3	1.3	1.3	1.3
	20Y	1.0	5.0E-2	1.0	1.0	1.0	1.0	1.0	1.0	1.0	1.0	1.0	1.0	1.0
D	NB	5.0	1.6E-1	17.	19.	18.	18.	24.	18.	24.	18.	18.	18.	18.
	3M	5.0	1.5E-1	14.	15.	14.	14.	19.	14.	17.	14.	14.	14.	14.
	1Y	5.0	1.0E-1	7.0	7.3	7.6	7.6	5.2	7.6	7.6	7.6	7.6	7.6	7.6
	5Y	5.0	7.0E-2	3.2	3.5	3.5	3.5	1.8	3.5	3.6	3.5	3.5	3.5	3.5
	10Y	5.0	8.0E-2	2.1	2.2	2.1	2.1	1.4	2.1	2.5	2.1	2.1	2.1	2.1
	15Y	5.0	9.0E-2	1.4	1.4	1.3	1.3	1.2	1.3	1.8	1.3	1.3	1.3	1.3
	20Y	5.0	5.0E-2	1.0	1.0	1.0	1.0	1.0	1.0	1.0	1.0	1.0	1.0	1.0
W	NB	0.3	1.6E-1	19.	17.	20.	20.	26.	20.	25.	20.	20.	20.	20.
	3M	0.3	1.5E-1	15.	14.	15.	15.	18.	15.	17.	15.	15.	15.	15.
	1Y	0.3	1.0E-1	7.5	6.8	8.2	8.2	5.6	8.2	8.2	8.2	8.2	8.2	8.2
	5Y	0.3	7.0E-2	3.3	3.4	3.6	3.6	1.8	3.6	3.8	3.6	3.6	3.6	3.6
	10Y	0.3	8.0E-2	2.3	2.2	2.2	2.2	1.4	2.2	2.6	2.2	2.2	2.2	2.2
	15Y	0.3	9.0E-2	1.5	1.5	1.4	1.4	1.3	1.4	1.9	1.4	1.4	1.4	1.4
	20Y	0.3	5.0E-2	1.0	1.0	1.0	1.0	1.0	1.0	1.0	1.0	1.0	1.0	1.0
W	NB	1.0	1.6E-1	21.	17.	22.	22.	29.	22.	28.	22.	22.	22.	22.
	3M	1.0	1.5E-1	16.	14.	17.	17.	21.	17.	19.	17.	17.	17.	17.
	1Y	1.0	1.0E-1	7.8	6.8	8.5	8.5	5.8	8.5	8.5	8.5	8.5	8.5	8.5
	5Y	1.0	7.0E-2	3.3	3.4	3.6	3.6	1.9	3.6	3.8	3.6	3.6	3.6	3.6
	10Y	1.0	8.0E-2	2.3	2.2	2.3	2.3	1.5	2.3	2.7	2.3	2.3	2.3	2.3
	15Y	1.0	9.0E-2	1.6	1.5	1.5	1.5	1.3	1.5	2.0	1.5	1.5	1.5	1.5
	20Y	1.0	5.0E-2	1.0	1.0	1.0	1.0	1.0	1.0	1.0	1.0	1.0	1.0	1.0
W	NB	5.0	1.6E-1	24.	17.	25.	25.	33.	25.	33.	25.	25.	25.	25.
	3M	5.0	1.5E-1	18.	14.	19.	19.	25.	19.	22.	19.	19.	19.	19.
	1Y	5.0	1.0E-1	8.2	6.8	9.0	9.0	6.1	9.0	9.0	9.0	9.0	9.0	9.0
	5Y	5.0	7.0E-2	3.4	3.4	3.7	3.7	1.9	3.7	3.9	3.7	3.7	3.7	3.7
	10Y	5.0	8.0E-2	2.4	2.2	2.4	2.4	1.5	2.4	2.7	2.4	2.4	2.4	2.4
	15Y	5.0	9.0E-2	1.6	1.5	1.5	1.5	1.4	1.5	2.0	1.5	1.5	1.5	1.5
	20Y	5.0	5.0E-2	1.0	1.0	1.0	1.0	1.0	1.0	1.0	1.0	1.0	1.0	1.0
Y	NB	0.3	6.4E-3	5.4	5.7	5.7	5.7	4.8	5.7	6.3	5.7	5.7	5.7	5.7
	3M	0.3	6.0E-3	4.8	4.9	5.1	5.1	3.9	5.1	5.4	5.1	5.1	5.1	5.1
	1Y	0.3	4.0E-3	3.9	3.8	4.1	4.1	2.5	4.1	4.3	4.1	4.1	4.1	4.1
	5Y	0.3	2.8E-3	2.3	2.3	2.4	2.4	1.5	2.4	2.6	2.4	2.4	2.4	2.4
	10Y	0.3	3.2E-3	1.6	1.6	1.5	1.5	1.2	1.5	1.8	1.5	1.5	1.5	1.5
	15Y	0.3	3.6E-3	1.1	1.2	1.1	1.1	1.1	1.1	1.3	1.1	1.1	1.1	1.1
	20Y	0.3	2.0E-3	1.0	1.0	1.0	1.0	1.0	1.0	1.0	1.0	1.0	1.0	1.0
Y	NB	1.0	6.4E-3	6.5	5.7	6.9	6.9	6.6	6.9	7.9	6.9	6.9	6.9	6.9
	3M	1.0	6.0E-3	5.6	4.9	5.9	5.9	5.2	5.9	6.4	5.9	5.9	5.9	5.9
	1Y	1.0	4.0E-3	4.1	3.8	4.4	4.4	2.8	4.4	4.6	4.4	4.4	4.4	4.4
	5Y	1.0	2.8E-3	2.4	2.3	2.4	2.4	1.5	2.4	2.7	2.4	2.4	2.4	2.4
	10Y	1.0	3.2E-3	1.6	1.6	1.6	1.6	1.2	1.6	1.9	1.6	1.6	1.6	1.6
	15Y	1.0	3.6E-3	1.2	1.2	1.1	1.1	1.1	1.1	1.3	1.1	1.1	1.1	1.1
	20Y	1.0	2.0E-3	1.0	1.0	1.0	1.0	1.0	1.0	1.0	1.0	1.0	1.0	1.0
Y	NB	5.0	6.4E-3	11.	5.7	12.	12.	14.	12.	15.	12.	12.	12.	12.
	3M	5.0	6.0E-3	9.2	4.9	9.7	9.7	11.	9.7	11.	9.7	9.7	9.7	9.7
	1Y	5.0	4.0E-3	5.3	3.8	5.7	5.7	3.7	5.7	5.8	5.7	5.7	5.7	5.7
	5Y	5.0	2.8E-3	2.7	2.3	2.8	2.8	1.6	2.8	3.1	2.8	2.8	2.8	2.8
	10Y	5.0	3.2E-3	1.8	1.6	1.8	1.8	1.3	1.8	2.1	1.8	1.8	1.8	1.8
	15Y	5.0	3.6E-3	1.3	1.2	1.2	1.2	1.2	1.2	1.5	1.2	1.2	1.2	1.2
	20Y	5.0	2.0E-3	1.0	1.0	1.0	1.0	1.0	1.0	1.0	1.0	1.0	1.0	1.0

[a] Cristy et al. (1986).

Table I-25S(a). Age-Specific Inhalation DCFs for ^{232}Th, Normalized to the Adult[a]

MODE	AGE	AMAD	F1	EFF	ADREN	BL WALL	BRAIN	B SURF	BREAST	ST W	SI W	ULI W	LLI W	KIDNEY
W	NB	0.3	1.0E-2	2.2	3.2	3.2	3.2	1.6	3.2	3.2	3.2	3.2	3.3	4.1
	3M	0.3	5.0E-3	2.0	2.9	2.9	2.9	1.4	2.9	2.9	2.9	2.9	3.0	3.7
	1Y	0.3	5.0E-4	1.7	2.5	2.5	2.5	1.3	2.5	2.5	2.5	2.5	2.5	3.2
	5Y	0.3	5.0E-4	1.3	1.8	1.8	1.8	1.1	1.8	1.8	1.8	1.8	1.8	2.2
	10Y	0.3	5.0E-4	1.1	1.4	1.4	1.4	0.98	1.4	1.4	1.4	1.4	1.4	1.6
	15Y	0.3	5.0E-4	0.96	1.0	1.0	1.0	0.94	1.0	1.0	1.0	1.0	1.0	1.1
	20Y	0.3	2.0E-4	1.0	1.0	1.0	1.0	1.0	1.0	1.0	1.0	1.0	1.0	1.0
W	NB	1.0	1.0E-2	2.2	3.2	3.3	3.2	1.6	3.2	3.3	3.3	3.3	3.4	4.2
	3M	1.0	5.0E-3	2.0	2.9	3.0	2.9	1.5	2.9	3.0	3.0	0.00	3.0	3.8
	1Y	1.0	5.0E-4	1.7	2.5	2.5	2.5	1.3	2.5	2.5	2.5	2.5	2.6	3.2
	5Y	1.0	5.0E-4	1.2	1.8	1.8	1.8	1.1	1.8	1.8	1.8	1.8	1.8	2.2
	10Y	1.0	5.0E-4	1.1	1.4	1.4	1.4	0.98	1.4	1.4	1.4	1.4	1.4	1.6
	15Y	1.0	5.0E-4	0.96	1.0	1.0	1.0	0.94	1.0	1.0	1.0	1.0	1.0	1.1
	20Y	1.0	2.0E-4	1.0	1.0	1.0	1.0	1.0	1.0	1.0	1.0	1.0	1.0	1.0
W	NB	5.0	1.0E-2	2.1	3.3	3.4	3.3	1.6	3.4	3.4	3.4	3.4	3.5	4.4
	3M	5.0	5.0E-3	1.9	3.0	3.0	3.0	1.5	3.0	3.0	3.0	3.1	3.1	3.9
	1Y	5.0	5.0E-4	1.6	2.5	2.6	2.5	1.3	2.5	2.6	2.6	2.6	2.6	3.2
	5Y	5.0	5.0E-4	1.2	1.8	1.8	1.8	1.1	1.8	1.8	1.8	1.8	1.8	2.2
	10Y	5.0	5.0E-4	1.1	1.4	1.4	1.4	0.99	1.4	1.4	1.4	1.4	1.4	1.6
	15Y	5.0	5.0E-4	0.95	1.0	1.0	1.0	0.94	1.0	1.0	1.0	1.0	1.0	1.1
	20Y	5.0	2.0E-4	1.0	1.0	1.0	1.0	1.0	1.0	1.0	1.0	1.0	1.0	1.0
Y	NB	0.3	1.0E-2	2.5	2.0	2.0	2.0	1.3	2.0	2.0	2.0	2.0	2.1	2.5
	3M	0.3	5.0E-3	2.3	1.9	1.9	1.9	1.2	1.9	1.9	1.9	1.9	2.0	2.3
	1Y	0.3	5.0E-4	2.0	1.7	1.7	1.7	1.2	1.7	1.7	1.7	1.7	1.8	2.1
	5Y	0.3	5.0E-4	1.5	1.4	1.4	1.4	1.0	1.4	1.4	1.4	1.4	1.4	1.6
	10Y	0.3	5.0E-4	1.2	1.2	1.2	1.2	1.0	1.2	1.2	1.2	1.2	1.2	1.3
	15Y	0.3	5.0E-4	1.0	1.0	1.0	1.0	1.0	1.0	1.0	1.0	1.0	1.0	1.1
	20Y	0.3	2.0E-4	1.0	1.0	1.0	1.0	1.0	1.0	1.0	1.0	1.0	1.0	1.0
Y	NB	1.0	1.0E-2	2.5	2.2	2.2	2.2	1.4	2.2	2.2	2.2	2.3	2.4	2.8
	3M	1.0	5.0E-3	2.3	2.0	2.2	2.0	1.3	2.0	2.0	2.0	2.1	2.2	2.5
	1Y	1.0	5.0E-4	2.0	1.8	1.8	1.8	1.2	1.8	1.8	1.8	1.8	1.8	2.2
	5Y	1.0	5.0E-4	1.5	1.4	1.4	1.4	1.0	1.4	1.4	1.4	1.4	1.4	1.6
	10Y	1.0	5.0E-4	1.2	1.2	1.2	1.2	1.0	1.2	1.2	1.2	1.2	1.2	1.3
	15Y	1.0	5.0E-4	1.0	1.0	1.0	1.0	0.99	1.0	1.0	1.0	1.0	1.0	1.1
	20Y	1.0	2.0E-4	1.0	1.0	1.0	1.0	1.0	1.0	1.0	1.0	1.0	1.0	1.0
Y	NB	5.0	1.0E-2	2.7	3.2	3.2	3.2	1.9	3.2	3.2	3.2	3.4	3.9	4.1
	3M	5.0	5.0E-3	2.4	2.6	2.6	2.5	1.5	2.6	2.6	2.6	2.8	3.2	3.3
	1Y	5.0	5.0E-4	2.0	2.0	2.0	2.0	1.2	2.0	2.0	2.0	2.1	2.2	2.5
	5Y	5.0	5.0E-4	1.4	1.5	1.5	1.5	1.1	1.5	1.5	1.5	1.5	1.6	1.8
	10Y	5.0	5.0E-4	1.2	1.3	1.3	1.3	1.0	1.3	1.3	1.3	1.3	1.3	1.4
	15Y	5.0	5.0E-4	1.0	1.0	1.0	1.0	0.99	1.0	1.0	1.0	1.1	1.1	1.1
	20Y	5.0	2.0E-4	1.0	1.0	1.0	1.0	1.0	1.0	1.0	1.0	1.0	1.0	1.0

[a] Cristy et al. (1986).

Table I-25S(b). Age-Specific Inhalation DCFs for ^{232}Th, Normalized to the Adult[a]

MODE	AGE	AMAD	F1	LIVER	LUNGS	OVARIES	PANCR	ACT MAR	SKIN	SPLEEN	TESTES	THYMUS	THYROID	UTERUS
W	NB	0.3	1.0E-2	4.8	15.	3.2	3.2	3.3	3.2	5.9	3.2	3.2	3.2	3.2
	3M	0.3	5.0E-3	4.3	12.	2.9	2.9	3.0	2.9	5.3	2.9	2.9	2.9	2.9
	1Y	0.3	5.0E-4	3.7	6.3	2.5	2.5	2.6	2.5	4.4	2.5	2.5	2.5	2.5
	5Y	0.3	5.0E-4	2.3	3.2	1.8	1.8	1.7	1.8	2.7	1.8	1.8	1.8	1.8
	10Y	0.3	5.0E-4	1.6	2.1	1.4	1.4	1.2	1.4	1.7	1.4	1.4	1.4	1.4
	15Y	0.3	5.0E-4	1.1	1.5	1.0	1.0	0.97	1.0	1.1	1.0	1.0	1.0	1.0
	20Y	0.3	2.0E-4	1.0	1.0	1.0	1.0	1.0	1.0	1.0	1.0	1.0	1.0	1.0
W	NB	1.0	1.0E-2	4.9	14.	3.3	3.2	3.4	3.3	6.1	3.3	3.3	3.3	3.3
	3M	1.0	5.0E-3	4.4	12.	3.0	2.9	3.0	3.0	5.4	0.00	3.0	3.0	3.0
	1Y	1.0	5.0E-4	3.7	6.0	2.5	2.5	2.6	2.5	4.4	2.5	2.5	2.5	2.5
	5Y	1.0	5.0E-4	2.4	3.1	1.8	1.8	1.7	1.8	2.7	1.8	1.8	1.8	1.8
	10Y	1.0	5.0E-4	1.6	2.0	1.4	1.4	1.2	1.4	1.7	1.4	1.4	1.4	1.4
	15Y	1.0	5.0E-4	1.1	1.4	1.0	1.0	0.97	1.0	1.1	1.0	1.0	1.0	1.0
	20Y	1.0	2.0E-4	1.0	1.0	1.0	1.0	1.0	1.0	1.0	1.0	1.0	1.0	1.0
W	NB	5.0	1.0E-2	5.1	11.	3.4	3.4	3.5	3.4	6.3	3.4	3.4	3.4	3.4
	3M	5.0	5.0E-3	4.5	9.2	3.0	3.0	3.1	0.00	5.5	3.0	3.0	3.0	3.0
	1Y	5.0	5.0E-4	3.7	5.1	2.5	2.5	2.6	2.6	4.4	2.6	2.6	2.6	2.6
	5Y	5.0	5.0E-4	2.4	2.7	1.8	1.8	1.7	1.8	2.7	1.8	1.8	1.8	1.8
	10Y	5.0	5.0E-4	1.6	1.9	1.4	1.4	1.3	1.4	1.7	1.4	1.4	1.4	1.4
	15Y	5.0	5.0E-4	1.1	1.3	1.0	1.0	0.98	1.0	1.1	1.0	1.0	1.0	1.0
	20Y	5.0	2.0E-4	1.0	1.0	1.0	1.0	1.0	1.0	1.0	1.0	1.0	1.0	1.0
Y	NB	0.3	1.0E-2	2.8	2.9	2.0	2.0	2.3	2.0	3.4	2.0	2.0	2.0	2.0
	3M	0.3	5.0E-3	2.6	2.7	1.9	1.9	2.2	1.9	3.1	1.9	1.9	1.9	1.9
	1Y	0.3	5.0E-4	2.3	2.3	1.7	1.7	2.0	1.7	2.8	1.7	1.7	1.7	1.7
	5Y	0.3	5.0E-4	1.7	1.6	1.4	1.4	1.4	1.4	1.9	1.4	1.4	1.4	1.4
	10Y	0.3	5.0E-4	1.3	1.3	1.2	1.2	1.2	1.2	1.4	1.2	1.2	1.2	1.2
	15Y	0.3	5.0E-4	1.1	1.1	1.0	1.0	1.0	1.0	1.1	1.0	1.0	1.0	1.0
	20Y	0.3	2.0E-4	1.0	1.0	1.0	1.0	1.0	1.0	1.0	1.0	1.0	1.0	1.0
Y	NB	1.0	1.0E-2	3.1	2.9	2.2	2.2	2.6	2.2	3.8	2.2	2.2	2.2	2.2
	3M	1.0	5.0E-3	2.8	2.7	2.0	2.0	2.3	2.0	3.4	2.0	2.0	2.0	2.0
	1Y	1.0	5.0E-4	2.4	2.3	1.8	1.8	2.0	1.8	2.8	1.8	1.8	1.8	1.8
	5Y	1.0	5.0E-4	1.7	1.6	1.4	1.4	1.5	1.4	1.9	1.4	1.4	1.4	1.4
	10Y	1.0	5.0E-4	1.3	1.3	1.2	1.2	1.2	1.2	1.4	1.2	1.2	1.2	1.2
	15Y	1.0	5.0E-4	1.1	1.1	1.0	1.0	1.0	1.0	1.1	1.0	1.0	1.0	1.0
	20Y	1.0	2.0E-4	1.0	1.0	1.0	1.0	1.0	1.0	1.0	1.0	1.0	1.0	1.0
Y	NB	5.0	1.0E-2	4.7	2.9	3.2	3.2	3.7	3.2	5.9	3.2	3.2	3.2	3.2
	3M	5.0	5.0E-3	3.7	2.7	2.6	2.6	2.9	2.6	4.6	2.9	2.5	2.6	2.6
	1Y	5.0	5.0E-4	2.8	2.3	2.0	2.0	2.2	2.0	3.3	2.0	2.0	2.0	2.0
	5Y	5.0	5.0E-4	1.9	1.6	1.5	1.5	1.5	1.5	2.1	1.5	1.5	1.5	1.5
	10Y	5.0	5.0E-4	1.4	1.3	1.3	1.3	1.2	1.3	1.5	1.3	1.3	1.3	1.3
	15Y	5.0	5.0E-4	1.1	1.1	1.0	1.0	1.0	1.0	1.1	1.0	1.0	1.0	1.0
	20Y	5.0	2.0E-4	1.0	1.0	1.0	1.0	1.0	1.0	1.0	1.0	1.0	1.0	1.0

[a] Cristy et al. (1986).

Table I-26S(a). Age-Specific Inhalation DCFs for ^{230}Th, Normalized to the Adult[a]

MODE	AGE	AMAD	F1	EFF	ADREN	BL WALL	BRAIN	B SURF	BREAST	ST W	SI W	ULI W	LLI W	KIDNEY
W	NB	0.3	1.0E-2	2.1	4.3	4.3	4.3	1.4	4.3	4.3	4.3	4.3	4.4	5.2
	3M	0.3	5.0E-3	1.9	3.8	3.8	3.8	1.2	3.8	3.8	3.8	3.8	3.9	4.6
	1Y	0.3	5.0E-4	1.5	3.1	3.1	3.1	1.1	3.1	3.1	3.1	3.1	3.1	3.8
	5Y	0.3	5.0E-4	1.1	1.8	1.8	1.8	0.95	1.8	1.8	1.8	1.8	1.9	2.4
	10Y	0.3	5.0E-4	0.99	1.2	1.2	1.2	0.90	1.2	1.2	1.2	1.2	1.2	1.5
	15Y	0.3	5.0E-4	0.91	0.92	0.92	0.92	0.88	0.92	0.92	0.92	0.92	0.92	1.1
	20Y	0.3	2.0E-4	1.0	1.0	1.0	1.0	1.0	1.0	1.0	1.0	1.0	1.0	1.0
W	NB	1.0	1.0E-2	2.0	4.4	4.4	4.4	1.4	4.4	4.4	4.4	4.5	4.6	5.4
	3M	1.0	5.0E-3	1.8	3.9	3.9	3.9	1.3	3.9	3.9	3.9	3.9	4.0	4.7
	1Y	1.0	5.0E-4	1.5	3.1	3.1	3.1	1.1	3.1	3.1	3.1	3.1	3.2	3.9
	5Y	1.0	5.0E-4	1.1	1.8	1.8	1.8	0.95	1.8	1.8	1.8	1.9	1.9	2.4
	10Y	1.0	5.0E-4	0.98	1.2	1.2	1.2	0.90	1.2	1.2	1.2	1.2	1.3	1.6
	15Y	1.0	5.0E-4	0.91	0.91	0.91	0.91	0.88	0.91	0.91	0.91	0.92	0.92	1.1
	20Y	1.0	2.0E-4	1.0	1.0	1.0	1.0	1.0	1.0	1.0	1.0	1.0	1.0	1.0
W	NB	5.0	1.0E-2	1.9	4.6	4.6	4.6	1.4	4.6	4.6	4.6	4.7	4.9	5.6
	3M	5.0	5.0E-3	1.7	4.0	4.0	4.0	1.3	4.0	4.0	4.0	4.0	4.2	4.9
	1Y	5.0	5.0E-4	1.4	3.1	3.1	3.1	1.1	3.1	3.1	3.1	3.2	3.2	3.9
	5Y	5.0	5.0E-4	1.1	1.9	1.9	1.9	0.95	1.9	1.9	1.9	1.9	1.9	2.4
	10Y	5.0	5.0E-4	0.96	1.2	1.2	1.2	0.90	1.2	1.2	1.2	1.2	1.3	1.6
	15Y	5.0	5.0E-4	0.89	0.91	0.91	0.91	0.88	0.91	0.91	0.91	0.91	0.92	1.1
	20Y	5.0	2.0E-4	1.0	1.0	1.0	1.0	1.0	1.0	1.0	1.0	1.0	1.0	1.0
Y	NB	0.3	1.0E-2	3.4	2.5	2.5	2.5	1.1	2.5	2.5	2.5	2.6	2.8	3.1
	3M	0.3	5.0E-3	3.0	2.3	2.3	2.3	1.0	2.3	2.3	2.3	2.4	2.5	2.9
	1Y	0.3	5.0E-4	2.4	2.0	2.0	2.0	0.98	2.0	2.0	2.0	2.0	2.1	2.5
	5Y	0.3	5.0E-4	1.6	1.4	1.4	1.4	0.93	1.4	1.4	1.4	1.4	1.4	1.8
	10Y	0.3	5.0E-4	1.3	1.1	1.1	1.1	0.95	1.1	1.1	1.1	1.1	1.1	1.3
	15Y	0.3	5.0E-4	1.1	0.99	0.99	0.99	0.98	0.99	0.99	0.99	0.99	1.0	1.0
	20Y	0.3	2.0E-4	1.0	1.0	1.0	1.0	1.0	1.0	1.0	1.0	1.0	1.0	1.0
Y	NB	1.0	1.0E-2	3.4	2.9	2.9	2.9	1.2	2.9	2.9	2.9	3.1	3.4	3.6
	3M	1.0	5.0E-3	3.0	2.5	2.5	2.5	1.1	2.5	2.5	2.5	2.7	3.0	3.1
	1Y	1.0	5.0E-4	2.4	2.1	2.1	2.1	1.0	2.1	2.1	2.1	2.1	2.3	2.6
	5Y	1.0	5.0E-4	1.6	1.4	1.4	1.4	0.93	1.4	1.4	1.4	1.5	1.5	1.8
	10Y	1.0	5.0E-4	1.3	1.1	1.1	1.1	0.95	1.1	1.1	1.1	1.1	1.1	1.3
	15Y	1.0	5.0E-4	1.1	0.99	0.99	0.99	0.98	0.99	0.99	0.99	0.99	1.0	1.1
	20Y	1.0	2.0E-4	1.0	1.0	1.0	1.0	1.0	1.0	1.0	1.0	1.0	1.0	1.0
Y	NB	5.0	1.0E-2	3.4	4.5	4.5	4.5	1.6	4.5	4.6	4.6	5.1	6.2	5.6
	3M	5.0	5.0E-3	2.8	3.4	3.4	3.4	1.3	3.4	3.5	3.5	3.9	4.8	4.2
	1Y	5.0	5.0E-4	2.2	2.4	2.4	2.4	1.1	2.4	2.4	2.4	2.6	3.0	3.0
	5Y	5.0	5.0E-4	1.5	1.6	1.6	1.6	0.95	1.6	1.6	1.6	1.7	1.8	2.0
	10Y	5.0	5.0E-4	1.2	1.2	1.2	1.2	0.94	1.2	1.2	1.2	1.2	1.3	1.4
	15Y	5.0	5.0E-4	1.0	0.97	0.97	0.97	0.95	0.97	0.97	0.98	0.99	1.0	1.1
	20Y	5.0	2.0E-4	1.0	1.0	1.0	1.0	1.0	1.0	1.0	1.0	1.0	1.0	1.0

[a] Cristy et al. (1986).

Table I-26S(b). Age-Specific Inhalation DCFs for ^{230}Th, Normalized to the Adult[a]

MODE	AGE	AMAD	F1	LIVER	LUNGS	OVARIES	PANCR	ACT MAR	SKIN	SPLEEN	TESTES	THYMUS	THYROID	UTERUS
W	NB	0.3	1.0E-2	6.0	16.	4.3	4.3	3.7	4.3	7.0	4.3	4.3	4.3	4.3
	3M	0.3	5.0E-3	5.3	13.	3.8	3.8	3.3	3.8	6.2	3.8	3.8	3.8	3.8
	1Y	0.3	5.0E-4	4.4	6.6	3.1	3.1	2.8	3.1	5.0	3.1	3.1	3.1	3.1
	5Y	0.3	5.0E-4	2.6	3.3	1.8	1.8	1.8	1.8	2.9	1.8	1.8	1.8	1.8
	10Y	0.3	5.0E-4	1.6	2.1	1.2	1.2	1.2	1.2	1.7	1.2	1.2	1.2	1.2
	15Y	0.3	5.0E-4	1.1	1.5	0.92	0.92	0.97	0.92	1.1	0.92	0.92	0.92	0.92
	20Y	0.3	2.0E-4	1.0	1.0	1.0	1.0	1.0	1.0	1.0	1.0	1.0	1.0	1.0
W	NB	1.0	1.0E-2	6.2	16.	4.4	4.4	3.8	4.4	7.3	4.4	4.4	4.4	4.4
	3M	1.0	5.0E-3	5.4	13.	3.9	3.9	3.3	3.9	6.3	3.9	3.9	3.9	3.9
	1Y	1.0	5.0E-4	4.4	6.4	3.1	3.1	2.8	3.1	5.1	3.1	3.1	3.1	3.1
	5Y	1.0	5.0E-4	2.6	3.3	1.8	1.8	1.8	1.8	2.9	1.8	1.8	1.8	1.8
	10Y	1.0	5.0E-4	1.6	2.1	1.2	1.2	1.2	1.2	1.7	1.2	1.2	1.2	1.2
	15Y	1.0	5.0E-4	1.1	1.5	0.91	0.91	0.96	0.91	1.1	0.91	0.91	0.91	0.91
	20Y	1.0	2.0E-4	1.0	1.0	1.0	1.0	1.0	1.0	1.0	1.0	1.0	1.0	1.0
W	NB	5.0	1.0E-2	6.4	14.	4.6	4.6	4.0	4.6	7.6	4.6	4.6	4.6	4.6
	3M	5.0	5.0E-3	5.6	11.	4.0	4.0	3.4	4.0	6.5	4.0	4.0	4.0	4.0
	1Y	5.0	5.0E-4	4.5	5.9	3.1	3.1	2.8	3.1	5.1	3.1	3.1	3.1	3.1
	5Y	5.0	5.0E-4	2.6	3.0	1.9	1.9	1.8	1.9	2.9	1.9	1.9	1.9	1.9
	10Y	5.0	5.0E-4	1.6	2.0	1.2	1.2	1.2	1.2	1.8	1.2	1.2	1.2	1.2
	15Y	5.0	5.0E-4	1.1	1.4	0.91	0.91	0.96	0.91	1.1	0.91	0.91	0.91	0.91
	20Y	5.0	2.0E-4	1.0	1.0	1.0	1.0	1.0	1.0	1.0	1.0	1.0	1.0	1.0
Y	NB	0.3	1.0E-2	3.5	5.7	2.5	2.5	2.3	2.5	4.0	2.5	2.5	2.5	2.5
	3M	0.3	5.0E-3	3.2	4.9	2.3	2.3	2.1	2.3	3.6	2.3	2.3	2.3	2.3
	1Y	0.3	5.0E-4	2.8	3.8	2.0	2.0	1.9	2.0	3.1	2.0	2.0	2.0	2.0
	5Y	0.3	5.0E-4	1.9	2.3	1.4	1.4	1.4	1.4	2.0	1.4	1.4	1.4	1.4
	10Y	0.3	5.0E-4	1.3	1.6	1.1	1.1	1.1	1.1	1.4	1.1	1.1	1.1	1.1
	15Y	0.3	5.0E-4	1.0	1.2	0.99	0.99	1.0	0.99	1.1	0.99	0.99	0.99	0.99
	20Y	0.3	2.0E-4	1.0	1.0	1.0	1.0	1.0	1.0	1.0	1.0	1.0	1.0	1.0
Y	NB	1.0	1.0E-2	4.0	5.7	2.9	2.9	2.6	2.9	4.6	2.9	2.9	2.9	2.9
	3M	1.0	5.0E-3	3.5	4.9	2.5	2.5	2.3	2.5	4.0	2.5	2.5	2.5	2.5
	1Y	1.0	5.0E-4	2.9	3.8	2.1	2.1	2.0	2.1	3.3	2.1	2.1	2.1	2.1
	5Y	1.0	5.0E-4	1.9	2.3	1.4	1.4	1.4	1.4	2.1	1.4	1.4	1.4	1.4
	10Y	1.0	5.0E-4	1.3	1.6	1.1	1.1	1.1	1.1	1.4	1.1	1.1	1.1	1.1
	15Y	1.0	5.0E-4	1.1	1.2	0.99	0.99	1.0	0.99	1.1	0.99	0.99	0.99	0.99
	20Y	1.0	2.0E-4	1.0	1.0	1.0	1.0	1.0	1.0	1.0	1.0	1.0	1.0	1.0
Y	NB	5.0	1.0E-2	6.3	5.7	4.5	4.5	4.1	4.5	7.4	4.5	4.5	4.5	4.5
	3M	5.0	5.0E-3	4.8	4.9	3.4	3.4	3.1	3.4	5.5	3.4	3.4	3.4	3.4
	1Y	5.0	5.0E-4	3.4	3.8	2.4	2.4	2.2	2.4	3.8	2.4	2.4	2.4	2.4
	5Y	5.0	5.0E-4	2.1	2.3	1.6	1.6	1.5	1.6	2.4	1.6	1.6	1.6	1.6
	10Y	5.0	5.0E-4	1.4	1.6	1.2	1.2	1.2	1.2	1.5	1.2	1.2	1.2	1.2
	15Y	5.0	5.0E-4	1.1	1.2	0.97	0.97	1.0	0.97	1.1	0.97	0.97	0.97	0.97
	20Y	5.0	2.0E-4	1.0	1.0	1.0	1.0	1.0	1.0	1.0	1.0	1.0	1.0	1.0

[a] Cristy et al. (1986).

Table I-27S(a). Age-Specific Inhalation DCFs for ^{228}Th, Normalized to the Adult[a]

MODE	AGE	AMAD	F1	EFF	ADREN	BL WALL	BRAIN	B SURF	BREAST	ST W	SI W	ULI W	LLI W	KIDNEY
W	NB	0.3	1.0E-2	13.	3.8	3.8	3.8	9.9	3.8	3.8	3.8	3.9	4.0	4.6
	3M	0.3	5.0E-3	10.	3.4	3.4	3.4	7.7	3.4	3.4	3.4	3.4	3.5	3.9
	1Y	0.3	5.0E-4	6.1	2.8	2.8	2.8	5.5	2.8	2.8	2.8	2.8	2.9	3.1
	5Y	0.3	5.0E-4	3.0	1.7	1.7	1.7	2.6	1.7	1.7	1.7	1.7	1.7	1.9
	10Y	0.3	5.0E-4	1.8	1.0	1.0	1.0	1.6	1.0	1.0	1.0	1.0	1.1	1.3
	15Y	0.3	5.0E-4	1.2	0.81	0.81	0.81	1.1	0.81	0.81	0.81	0.81	0.81	0.99
	20Y	0.3	2.0E-4	1.0	1.0	1.0	1.0	1.0	1.0	1.0	1.0	1.0	1.0	1.0
W	NB	1.0	1.0E-2	12.	3.9	3.9	3.9	10.	3.9	3.9	3.9	4.0	4.1	4.7
	3M	1.0	5.0E-3	9.7	3.4	3.4	3.4	8.0	3.4	3.4	3.4	3.5	3.6	4.0
	1Y	1.0	5.0E-4	6.0	2.8	2.8	2.8	5.5	2.8	2.8	2.8	2.8	2.9	3.1
	5Y	1.0	5.0E-4	2.9	1.7	1.7	1.7	2.6	1.7	1.7	1.7	1.7	1.7	1.9
	10Y	1.0	5.0E-4	1.8	1.0	1.0	1.0	1.6	1.0	1.0	1.0	1.0	1.1	1.3
	15Y	1.0	5.0E-4	1.2	0.80	0.80	0.80	1.1	0.80	0.80	0.80	0.81	0.81	0.99
	20Y	1.0	2.0E-4	1.0	1.0	1.0	1.0	1.0	1.0	1.0	1.0	1.0	1.0	1.0
W	NB	5.0	1.0E-2	12.	4.0	4.0	4.0	11.	4.0	4.0	4.0	4.1	4.3	4.9
	3M	5.0	5.0E-3	9.1	3.5	3.5	3.5	8.3	3.5	3.5	3.5	3.5	3.7	4.1
	1Y	5.0	5.0E-4	5.9	2.8	2.8	2.8	5.5	2.8	2.8	2.8	2.8	2.9	3.1
	5Y	5.0	5.0E-4	2.8	1.7	1.7	1.7	2.6	1.7	1.7	1.7	1.7	1.8	1.9
	10Y	5.0	5.0E-4	1.7	1.0	1.0	1.0	1.6	1.0	1.0	1.0	1.1	1.1	1.3
	15Y	5.0	5.0E-4	1.2	0.80	0.80	0.80	1.1	0.80	0.80	0.80	0.80	0.81	0.99
	20Y	5.0	2.0E-4	1.0	1.0	1.0	1.0	1.0	1.0	1.0	1.0	1.0	1.0	1.0
Y	NB	0.3	1.0E-2	9.7	3.5	3.4	3.4	7.3	3.5	3.4	3.4	3.6	4.2	3.9
	3M	0.3	5.0E-3	8.0	3.0	2.9	2.9	5.8	3.0	3.0	3.0	3.1	3.6	3.3
	1Y	0.3	5.0E-4	5.7	2.5	2.4	2.4	4.3	2.5	2.4	2.4	2.5	2.7	2.6
	5Y	0.3	5.0E-4	3.0	1.5	1.5	1.5	2.3	1.6	1.5	1.5	1.6	1.7	1.7
	10Y	0.3	5.0E-4	2.0	1.0	0.98	0.98	1.5	1.0	0.98	0.98	1.0	1.1	1.2
	15Y	0.3	5.0E-4	1.4	0.91	0.90	0.90	1.1	0.91	0.90	0.90	0.91	0.92	1.0
	20Y	0.3	2.0E-4	1.0	1.0	1.0	1.0	1.0	1.0	1.0	1.0	1.0	1.0	1.0
Y	NB	1.0	1.0E-2	9.9	4.1	4.0	4.0	9.4	4.1	4.1	4.1	4.4	5.4	4.7
	3M	1.0	5.0E-3	8.1	3.4	3.3	3.3	6.8	3.3	3.3	3.3	3.6	4.4	3.7
	1Y	1.0	5.0E-4	5.7	2.5	2.5	2.5	4.5	2.5	2.5	2.5	2.6	3.0	2.7
	5Y	1.0	5.0E-4	3.0	1.6	1.5	1.5	2.4	1.6	1.6	1.6	1.6	1.8	1.7
	10Y	1.0	5.0E-4	2.0	1.0	1.0	1.0	1.5	1.0	1.0	1.0	1.0	1.1	1.2
	15Y	1.0	5.0E-4	1.4	0.90	0.89	0.89	1.1	0.90	0.89	0.89	0.90	0.92	1.0
	20Y	1.0	2.0E-4	1.0	1.0	1.0	1.0	1.0	1.0	1.0	1.0	1.0	1.0	1.0
Y	NB	5.0	1.0E-2	11.	6.0	6.0	6.0	15.	6.0	6.0	6.1	6.6	8.3	7.2
	3M	5.0	5.0E-3	8.4	4.4	4.3	4.3	9.7	4.4	4.4	4.4	4.9	6.4	5.0
	1Y	5.0	5.0E-4	5.7	2.8	2.8	2.8	5.2	2.8	2.8	2.8	3.0	3.7	3.0
	5Y	5.0	5.0E-4	3.0	1.7	1.7	1.7	2.6	1.7	1.7	1.7	1.8	2.1	1.8
	10Y	5.0	5.0E-4	2.0	1.1	1.1	1.1	1.6	1.1	1.1	1.1	1.1	1.3	1.3
	15Y	5.0	5.0E-4	1.4	0.87	0.86	0.86	1.1	0.87	0.87	0.87	0.88	0.93	1.0
	20Y	5.0	2.0E-4	1.0	1.0	1.0	1.0	1.0	1.0	1.0	1.0	1.0	1.0	1.0

[a] Cristy et al. (1986).

Table I-27S(b). Age-Specific Inhalation DCFs for ^{228}Th, Normalized to the Adult[a]

MODE	AGE	AMAD	F1	LIVER	LUNGS	OVARIES	PANCR	ACT MAR	SKIN	SPLEEN	TESTES	THYMUS	THYROID	UTERUS
W	NB	0.3	1.0E-2	5.9	17.	3.8	3.8	16.	3.8	8.6	3.8	3.8	3.8	3.8
	3M	0.3	5.0E-3	5.0	13.	3.4	3.4	12.	3.4	7.2	3.4	3.4	3.4	3.4
	1Y	0.3	5.0E-4	4.0	6.7	2.8	2.8	8.2	2.8	5.4	2.8	2.8	2.8	2.8
	5Y	0.3	5.0E-4	2.2	3.3	1.7	1.7	3.8	1.7	3.0	1.7	1.7	1.7	1.7
	10Y	0.3	5.0E-4	1.4	2.1	1.0	1.0	1.9	1.0	1.8	1.0	1.0	1.0	1.0
	15Y	0.3	5.0E-4	1.0	1.5	0.81	0.81	1.2	0.81	1.2	0.81	0.81	0.81	0.81
	20Y	0.3	2.0E-4	1.0	1.0	1.0	1.0	1.0	1.0	1.0	1.0	1.0	1.0	1.0
W	NB	1.0	1.0E-2	6.1	16.	3.9	3.9	17.	3.9	9.0	3.9	3.9	3.9	3.9
	3M	1.0	5.0E-3	5.1	13.	3.4	3.4	12.	3.4	7.4	3.4	3.4	3.4	3.4
	1Y	1.0	5.0E-4	4.0	6.6	2.8	2.8	8.3	2.8	5.4	2.8	2.8	2.8	2.8
	5Y	1.0	5.0E-4	2.2	3.3	1.7	1.7	3.8	1.7	3.0	1.7	1.7	1.7	1.7
	10Y	1.0	5.0E-4	1.4	2.1	1.0	1.0	1.9	1.0	1.8	1.0	1.0	1.0	1.0
	15Y	1.0	5.0E-4	1.0	1.5	0.80	0.80	1.2	0.80	1.2	0.80	0.80	0.80	0.80
	20Y	1.0	2.0E-4	1.0	1.0	1.0	1.0	1.0	1.0	1.0	1.0	1.0	1.0	1.0
W	NB	5.0	1.0E-2	6.3	15.	4.0	4.0	18.	4.0	9.4	4.0	4.0	4.0	4.0
	3M	5.0	5.0E-3	5.3	12.	3.5	3.5	13.	3.5	7.6	3.5	3.5	3.5	3.5
	1Y	5.0	5.0E-4	4.0	6.3	2.8	2.8	8.3	2.8	5.5	2.8	2.8	2.8	2.8
	5Y	5.0	5.0E-4	2.2	3.2	1.7	1.7	3.8	1.7	3.0	1.7	1.7	1.7	1.7
	10Y	5.0	5.0E-4	1.4	2.0	1.0	1.0	1.9	1.0	1.8	1.0	1.0	1.0	1.0
	15Y	5.0	5.0E-4	1.0	1.4	0.80	0.80	1.2	0.80	1.2	0.80	0.80	0.80	0.80
	20Y	5.0	2.0E-4	1.0	1.0	1.0	1.0	1.0	1.0	1.0	1.0	1.0	1.0	1.0
Y	NB	0.3	1.0E-2	4.9	9.9	3.4	3.4	11.	3.4	6.8	3.4	3.4	3.4	3.4
	3M	0.3	5.0E-3	4.1	8.2	2.9	3.0	8.6	2.9	5.6	2.9	2.9	3.0	2.9
	1Y	0.3	5.0E-4	3.2	5.7	2.4	2.4	6.3	2.4	4.4	2.4	2.4	2.4	2.4
	5Y	0.3	5.0E-4	2.0	3.1	1.5	1.5	3.2	1.5	2.6	1.5	1.5	1.5	1.5
	10Y	0.3	5.0E-4	1.3	2.0	0.98	0.99	1.7	0.98	1.6	0.98	0.99	0.99	0.98
	15Y	0.3	5.0E-4	1.0	1.4	0.90	0.91	1.1	0.90	1.1	0.90	0.91	0.90	0.90
	20Y	0.3	2.0E-4	1.0	1.0	1.0	1.0	1.0	1.0	1.0	1.0	1.0	1.0	1.0
Y	NB	1.0	1.0E-2	6.0	9.9	4.0	4.1	14.	4.0	8.4	4.0	4.0	4.1	4.0
	3M	1.0	5.0E-3	4.7	8.2	3.3	3.3	10.	3.3	6.5	3.3	3.3	3.3	3.3
	1Y	1.0	5.0E-4	3.4	5.7	2.5	2.5	6.7	2.5	4.6	2.5	2.5	2.5	2.5
	5Y	1.0	5.0E-4	2.0	3.1	1.5	1.6	3.3	1.5	2.7	1.5	1.6	1.6	1.5
	10Y	1.0	5.0E-4	1.3	2.0	1.0	1.0	1.7	1.0	1.6	1.0	1.0	1.0	1.0
	15Y	1.0	5.0E-4	1.0	1.4	0.89	0.90	1.1	0.89	1.1	0.89	0.90	0.89	0.89
	20Y	1.0	2.0E-4	1.0	1.0	1.0	1.0	1.0	1.0	1.0	1.0	1.0	1.0	1.0
Y	NB	5.0	1.0E-2	9.1	9.9	6.0	6.0	24.	6.0	13.	6.0	5.9	6.0	6.0
	3M	5.0	5.0E-3	6.3	8.2	4.3	4.3	14.	4.3	8.9	4.3	4.3	4.3	4.3
	1Y	5.0	5.0E-4	3.8	5.7	2.8	2.8	7.6	2.8	5.2	2.8	2.8	2.8	2.8
	5Y	5.0	5.0E-4	2.2	3.1	1.7	1.7	3.6	1.7	2.9	1.7	1.7	1.7	1.7
	10Y	5.0	5.0E-4	1.4	2.0	1.1	1.1	1.9	1.1	1.7	1.1	1.1	1.1	1.1
	15Y	5.0	5.0E-4	1.0	1.4	0.86	0.86	1.2	0.86	1.2	0.86	0.87	0.86	0.86
	20Y	5.0	2.0E-4	1.0	1.0	1.0	1.0	1.0	1.0	1.0	1.0	1.0	1.0	1.0

[a] Cristy et al. (1986).

Table I-28S. Age-Specific Inhalation DCFs for ^{239}Pu, Normalized to the Adult[a]

Pu-239 Class W AMAD=1 micron

	3 months	1 year	5 years	10 years	15 years	Adult
Effective	1.58	1.42	1.17	1.00	1.00	1.00
Adrenals	4.80	3.87	2.40	1.53	1.13	1.00
Bl. Wall	4.80	3.87	2.40	1.53	1.13	1.00
Bone Surf.	1.00	1.00	0.95	0.95	1.00	1.00
Brain	4.80	3.87	2.40	1.53	1.13	1.00
Breast	4.80	3.87	2.40	1.53	1.13	1.00
S Wall	4.80	3.87	2.40	1.53	1.13	1.00
SI Wall	4.80	3.87	2.40	1.53	1.13	1.00
ULI Wall	4.87	3.87	2.40	1.60	1.13	1.00
LLI Wall	4.69	3.75	2.31	1.50	1.06	1.00
Kidneys	3.68	3.03	2.11	1.45	1.12	1.00
Liver	1.88	1.83	1.42	1.15	0.98	1.00
Lungs	9.47	6.32	3.26	2.11	1.47	1.00
Ovaries	1.00	1.00	1.03	1.03	1.10	1.00
Pancreas	4.80	3.87	2.40	1.53	1.13	1.00
R. Marrow	2.45	2.00	1.45	1.09	1.00	1.00
Skin	4.80	3.87	2.40	1.53	1.13	1.00
Spleen	4.80	3.87	2.40	1.53	1.13	1.00
Testes	1.55	1.45	1.31	1.10	1.10	1.00
Thymus	4.80	3.87	2.40	1.53	1.13	1.00
Thyroid	4.80	3.87	2.40	1.53	1.13	1.00
Uterus	4.80	3.87	2.40	1.53	1.13	1.00

[a] ICRP (1990).

Table I-29S. External Dose-Rate Conversion Factors for $^{238}U^{a}$

U-238 4.468E9 y

	Submersion (Gy-m3/Bq-y)	Immersion (Gy-m3/Bq-y)	Ground Plane (Gy-m2/Bq-y)
Effective	1.39E-10	3.46E-13	1.75E-11
Adrenals	5.78E-11	1.41E-13	3.14E-12
Bl Wall	5.62E-11	1.36E-13	1.47E-12
Brain	5.51E-11	1.33E-13	1.63E-12
Breast	4.19E-10	1.06E-12	8.03E-11
Heart	4.95E-11	1.20E-13	1.57E-12
S Wall	5.38E-11	1.30E-13	1.95E-12
SI Wall	4.38E-11	1.06E-13	1.16E-12
ULI Wall	5.19E-11	1.25E-13	1.36E-12
LLI Wall	4.79E-11	1.21E-13	2.14E-12
Kidneys	5.92E-11	1.43E-13	1.58E-12
Liver	5.59E-11	1.35E-13	1.53E-12
Lungs	6.78E-11	1.65E-13	3.27E-12
Marrow	1.15E-10	2.78E-13	4.14E-12
R Marrow	3.81E-11	9.27E-14	1.50E-12
Ovaries	4.86E-11	1.18E-13	2.06E-12
Pancreas	4.03E-11	9.78E-14	2.04E-12
B Surf	1.22E-10	2.97E-13	5.65E-12
Spleen	5.22E-11	1.26E-13	1.91E-12
Testes	1.45E-10	3.57E-13	1.50E-11
Thymus	7.43E-11	1.80E-13	1.95E-12
Thyroid	1.02E-10	2.46E-13	4.24E-12
Uterus	4.32E-11	1.05E-13	1.14E-12
Skin	6.78E-10	1.69E-12	1.43E-10

[a] USDOE (1988).

Table I-30S. External Dose-Rate Conversion Factors for $^{235}U^{a}$

U-235 7.038E8 y

	Submersion (Gy-m3/Bq-y)	Immersion (Gy-m3/Bq-y)	Ground Plane (Gy-m2/Bq-y)
Effective	2.07E-07	4.62E-10	4.59E-09
Adrenals	1.71E-07	3.81E-10	3.76E-09
Bl Wall	1.56E-07	3.49E-10	3.46E-09
Brain	1.67E-07	3.73E-10	3.68E-09
Breast	2.58E-07	5.76E-10	5.95E-09
Heart	1.53E-07	3.41E-10	3.38E-09
S Wall	1.54E-07	3.43E-10	3.41E-09
SI Wall	1.35E-07	3.00E-10	2.97E-09
ULI Wall	1.62E-07	3.62E-10	3.59E-09
LLI Wall	1.51E-07	3.38E-10	3.32E-09
Kidneys	1.60E-07	3.57E-10	3.51E-09
Liver	1.56E-07	3.49E-10	3.43E-09
Lungs	1.71E-07	3.81E-10	3.76E-09
Marrow	2.47E-07	5.51E-10	5.46E-09
R Marrow	1.64E-07	3.65E-10	3.59E-09
Ovaries	1.35E-07	3.03E-10	3.00E-09
Pancreas	1.31E-07	2.92E-10	2.89E-09
B Surf	2.53E-07	5.65E-10	5.59E-09
Spleen	1.55E-07	3.46E-10	3.43E-09
Testes	2.36E-07	5.27E-10	5.24E-09
Thymus	1.81E-07	4.03E-10	4.00E-09
Thyroid	2.30E-07	5.14E-10	5.08E-09
Uterus	1.38E-07	3.05E-10	3.03E-09
Skin	2.64E-07	5.81E-10	6.14E-09

[a] USDOE (1988).

Table I-31S. External Dose-Rate Conversion Factors for ^{234}U[a]

U-234 2.445E5 y

	Submersion (Gy-m3/Bq-y)	Immersion (Gy-m3/Bq-y)	Ground Plane (Gy-m2/Bq-y)
Effective	2.05E-10	5.00E-13	2.18E-11
Adrenals	9.97E-11	2.37E-13	4.49E-12
Bl Wall	9.51E-11	2.25E-13	2.49E-12
Brain	9.30E-11	2.19E-13	2.62E-12
Breast	5.54E-10	1.38E-12	9.70E-11
Heart	8.49E-11	2.00E-13	2.51E-12
S Wall	9.11E-11	2.16E-13	3.00E-12
SI Wall	7.51E-11	1.77E-13	1.96E-12
ULI Wall	9.16E-11	2.16E-13	2.37E-12
LLI Wall	8.62E-11	2.04E-13	3.22E-12
Kidneys	1.01E-10	2.40E-13	2.70E-12
Liver	9.35E-11	2.21E-13	2.52E-12
Lungs	1.11E-10	2.65E-13	4.70E-12
Marrow	1.81E-10	4.32E-13	6.43E-12
R Marrow	7.46E-11	1.75E-13	2.47E-12
Ovaries	8.19E-11	1.95E-13	3.08E-12
Pancreas	7.14E-11	1.69E-13	3.00E-12
B Surf	1.92E-10	4.57E-13	7.97E-12
Spleen	8.95E-11	2.12E-13	2.95E-12
Testes	2.19E-10	5.32E-13	1.91E-11
Thymus	1.21E-10	2.86E-13	3.19E-12
Thyroid	1.64E-10	3.92E-13	6.24E-12
Uterus	7.41E-11	1.75E-13	1.90E-12
Skin	8.84E-10	2.16E-12	1.72E-10

[a] USDOE (1988).

Table I-32S. External Dose-Rate Conversion Factors for ^{234}Th[a]

Th-234 24.10 d

	Submersion (Gy-m3/Bq-y)	Immersion (Gy-m3/Bq-y)	Ground Plane (Gy-m2/Bq-y)
Effective	1.04E-08	2.44E-11	2.69E-10
Adrenals	7.27E-09	1.71E-11	1.79E-10
Bl Wall	7.41E-09	1.74E-11	1.81E-10
Brain	7.49E-09	1.76E-11	1.83E-10
Breast	1.48E-08	3.49E-11	4.41E-10
Heart	6.78E-09	1.60E-11	1.66E-10
S Wall	7.03E-09	1.65E-11	1.72E-10
SI Wall	5.97E-09	1.41E-11	1.46E-10
ULI Wall	7.32E-09	1.72E-11	1.79E-10
LLI Wall	6.54E-09	1.53E-11	1.60E-10
Kidneys	7.62E-09	1.79E-11	1.86E-10
Liver	7.32E-09	1.72E-11	1.79E-10
Lungs	8.14E-09	1.91E-11	2.00E-10
Marrow	1.39E-08	3.27E-11	3.41E-10
R Marrow	5.70E-09	1.34E-11	1.39E-10
Ovaries	6.14E-09	1.44E-11	1.51E-10
Pancreas	5.30E-09	1.24E-11	1.30E-10
B Surf	1.43E-08	3.35E-11	3.54E-10
Spleen	6.92E-09	1.63E-11	1.70E-10
Testes	1.22E-08	2.89E-11	3.14E-10
Thymus	9.41E-09	2.21E-11	2.30E-10
Thyroid	1.21E-08	2.84E-11	2.97E-10
Uterus	6.03E-09	1.42E-11	1.47E-10
Skin	2.38E-08	4.30E-11	4.78E-10

[a] USDOE (1988).

Table I-33S. External Dose-Rate Conversion Factors for ^{232}Th[a]

Th-232	1.4405E10 y		
	Submersion (Gy-m3/Bq-y)	Immersion (Gy-m3/Bq-y)	Ground Plane (Gy-m2/Bq-y)
Effective	2.50E-10	6.03E-13	1.79E-11
Adrenals	1.41E-10	3.53E-13	4.86E-12
Bl Wall	1.44E-10	3.43E-13	3.76E-12
Brain	1.40E-10	3.32E-13	3.76E-12
Breast	5.41E-10	1.34E-12	7.35E-11
Heart	1.27E-10	3.00E-13	3.46E-12
S Wall	1.35E-10	3.19E-13	3.86E-12
SI Wall	1.14E-10	2.69E-13	2.95E-12
ULI Wall	1.37E-10	3.24E-13	3.54E-12
LLI Wall	1.25E-10	2.97E-13	3.81E-12
Kidneys	1.52E-10	3.62E-13	4.00E-12
Liver	1.42E-10	3.38E-13	3.73E-12
Lungs	1.61E-10	3.84E-13	5.30E-12
Marrow	2.70E-10	6.49E-13	8.08E-12
R Marrow	1.06E-10	2.50E-13	3.05E-12
Ovaries	1.20E-10	2.84E-13	3.68E-12
Pancreas	1.01E-10	2.40E-13	3.32E-12
B Surf	2.81E-10	6.76E-13	9.19E-12
Spleen	1.32E-10	3.14E-13	3.78E-12
Testes	2.78E-10	6.73E-13	1.58E-11
Thymus	1.85E-10	4.41E-13	4.86E-12
Thyroid	2.41E-10	5.76E-13	7.38E-12
Uterus	1.12E-10	2.66E-13	2.92E-12
Skin	7.89E-10	1.90E-12	1.31E-10

[a] USDOE (1988).

Table I-34S. External Dose-Rate Conversion Factors for ^{231}Th[a]

Th-231	25.52 h		
	Submersion (Gy-m3/Bq-y)	Immersion (Gy-m3/Bq-y)	Ground Plane (Gy-m2/Bq-y)
Effective	1.56E-08	3.68E-11	5.14E-10
Adrenals	1.05E-08	2.46E-11	2.73E-10
Bl Wall	1.05E-08	2.46E-11	2.59E-10
Brain	1.06E-08	2.47E-11	2.58E-10
Breast	2.48E-08	5.92E-11	1.24E-09
Heart	9.65E-09	2.25E-11	2.36E-10
S Wall	1.00E-08	2.34E-11	2.50E-10
SI Wall	8.46E-09	1.98E-11	2.05E-10
ULI Wall	1.06E-08	2.49E-11	2.63E-10
LLI Wall	9.38E-09	2.19E-11	2.37E-10
Kidneys	1.10E-08	2.59E-11	2.78E-10
Liver	1.03E-08	2.42E-11	2.53E-10
Lungs	1.16E-08	2.73E-11	3.00E-10
Marrow	1.96E-08	4.59E-11	4.97E-10
R Marrow	8.30E-09	1.94E-11	2.05E-10
Ovaries	8.78E-09	2.06E-11	2.23E-10
Pancreas	7.65E-09	1.79E-11	1.96E-10
B Surf	2.02E-08	4.73E-11	5.22E-10
Spleen	9.89E-09	2.31E-11	2.46E-10
Testes	1.84E-08	4.35E-11	5.73E-10
Thymus	1.31E-08	3.08E-11	3.22E-10
Thyroid	1.73E-08	4.05E-11	4.49E-10
Uterus	8.49E-09	1.98E-11	2.04E-10
Skin	7.78E-08	1.16E-10	1.74E-09

[a] USDOE (1988).

Table I-35S. External Dose-Rate Conversion Factors for ^{230}Th[a]

Th-230 7.7E4 y

	Submersion (Gy-m3/Bq-y)	Immersion (Gy-m3/Bq-y)	Ground Plane (Gy-m2/Bq-y)
Effective	5.24E-10	1.24E-12	2.44E-11
Adrenals	3.43E-10	8.03E-13	9.54E-12
Bl Wall	3.46E-10	8.14E-13	8.46E-12
Brain	3.49E-10	8.16E-13	8.62E-12
Breast	9.14E-10	2.20E-12	8.24E-11
Heart	3.14E-10	7.35E-13	7.84E-12
S Wall	3.27E-10	7.68E-13	8.35E-12
SI Wall	2.81E-10	6.57E-13	6.84E-12
ULI Wall	3.35E-10	7.86E-13	8.16E-12
LLI Wall	3.05E-10	7.16E-13	8.03E-12
Kidneys	3.59E-10	8.43E-13	8.78E-12
Liver	3.43E-10	8.05E-13	8.43E-12
Lungs	3.81E-10	8.97E-13	1.04E-11
Marrow	6.32E-10	1.49E-12	1.65E-11
R Marrow	2.76E-10	6.41E-13	6.97E-12
Ovaries	2.89E-10	6.78E-13	7.62E-12
Pancreas	2.51E-10	5.86E-13	6.81E-12
B Surf	6.51E-10	1.54E-12	1.78E-11
Spleen	3.22E-10	7.57E-13	8.24E-12
Testes	6.00E-10	1.42E-12	2.34E-11
Thymus	4.38E-10	1.03E-12	1.07E-11
Thyroid	5.59E-10	1.32E-12	1.48E-11
Uterus	2.81E-10	6.59E-13	6.86E-12
Skin	1.09E-09	2.66E-12	1.39E-10

[a] USDOE (1988).

Table I-36S. External Dose-Rate Conversion Factors for ^{228}Th[a]

Th-228 1.9132 y

	Submersion (Gy-m3/Bq-y)	Immersion (Gy-m3/Bq-y)	Ground Plane (Gy-m2/Bq-y)
Effective	2.65E-09	6.08E-12	7.43E-11
Adrenals	2.00E-09	4.57E-12	4.73E-11
Bl Wall	1.92E-09	4.41E-12	4.43E-11
Brain	2.01E-09	4.59E-12	4.65E-11
Breast	3.70E-09	8.57E-12	1.54E-10
Heart	1.83E-09	4.19E-12	4.21E-11
S Wall	1.86E-09	4.27E-12	4.32E-11
SI Wall	1.62E-09	3.68E-12	3.73E-11
ULI Wall	1.95E-09	4.46E-12	4.51E-11
LLI Wall	1.78E-09	4.08E-12	4.16E-11
Kidneys	1.97E-09	4.49E-12	4.54E-11
Liver	1.92E-09	4.38E-12	4.43E-11
Lungs	2.11E-09	4.81E-12	5.00E-11
Marrow	3.32E-09	7.59E-12	7.78E-11
R Marrow	1.76E-09	4.00E-12	4.05E-11
Ovaries	1.64E-09	3.76E-12	3.84E-11
Pancreas	1.50E-09	3.43E-12	3.54E-11
B Surf	3.41E-09	7.81E-12	8.11E-11
Spleen	1.86E-09	4.24E-12	4.32E-11
Testes	3.05E-09	7.00E-12	8.03E-11
Thymus	2.33E-09	5.32E-12	5.38E-11
Thyroid	2.97E-09	6.81E-12	7.00E-11
Uterus	1.64E-09	3.73E-12	3.78E-11
Skin	4.14E-09	9.16E-12	2.16E-10

[a] USDOE (1988).

Table I-37S. External Dose-Rate Conversion Factors for $^{228}Ra^{a}$

Ra-228 5.75 y

	Submersion (Gy-m3/Bq-y)	Immersion (Gy-m3/Bq-y)	Ground Plane (Gy-m2/Bq-y)
Effective	8.65E-17	2.17E-19	1.80E-17
Adrenals	6.22E-18	1.56E-20	1.30E-18
Bl Wall	1.12E-24	2.81E-27	2.34E-25
Brain	4.97E-19	1.24E-21	1.04E-19
Breast	4.86E-16	1.22E-18	1.02E-16
Heart	8.11E-19	2.03E-21	1.69E-19
S Wall	1.27E-18	3.19E-21	2.64E-19
SI Wall	1.05E-20	2.62E-23	2.18E-21
ULI Wall	1.54E-20	3.86E-23	3.22E-21
LLI Wall	2.55E-18	6.41E-21	5.32E-19
Kidneys	7.46E-21	1.87E-23	1.55E-21
Liver	6.05E-20	1.51E-22	1.26E-20
Lungs	4.92E-18	1.23E-20	1.02E-18
Marrow	2.95E-18	7.41E-21	6.16E-19
R Marrow	1.61E-18	4.05E-21	3.38E-19
Ovaries	2.44E-18	6.11E-21	5.08E-19
Pancreas	3.62E-18	9.11E-21	7.57E-19
B Surf	7.97E-18	2.00E-20	1.66E-18
Spleen	1.40E-18	3.51E-21	2.92E-19
Testes	4.51E-17	1.13E-19	9.41E-18
Thymus	1.04E-21	2.60E-24	2.17E-22
Thyroid	3.11E-18	7.78E-21	6.49E-19
Uterus	4.54E-22	1.14E-24	9.46E-23
Skin	1.04E-15	2.60E-18	2.17E-16

[a] USDOE (1988).

Table I-38S. External Dose-Rate Conversion Factors for $^{226}Ra^{a}$

Ra-226 1600 y

	Submersion (Gy-m3/Bq-y)	Immersion (Gy-m3/Bq-y)	Ground Plane (Gy-m2/Bq-y)
Effective	9.22E-09	2.05E-11	2.04E-10
Adrenals	7.62E-09	1.69E-11	1.68E-10
Bl Wall	7.00E-09	1.56E-11	1.54E-10
Brain	7.46E-09	1.66E-11	1.64E-10
Breast	1.15E-08	2.55E-11	2.58E-10
Heart	6.81E-09	1.52E-11	1.50E-10
S Wall	6.86E-09	1.53E-11	1.52E-10
SI Wall	6.03E-09	1.34E-11	1.33E-10
ULI Wall	7.24E-09	1.61E-11	1.59E-10
LLI Wall	6.73E-09	1.50E-11	1.49E-10
Kidneys	7.16E-09	1.59E-11	1.58E-10
Liver	6.97E-09	1.55E-11	1.54E-10
Lungs	7.62E-09	1.69E-11	1.68E-10
Marrow	1.09E-08	2.44E-11	2.42E-10
R Marrow	7.32E-09	1.63E-11	1.61E-10
Ovaries	6.08E-09	1.35E-11	1.34E-10
Pancreas	5.86E-09	1.31E-11	1.29E-10
B Surf	1.12E-08	2.50E-11	2.48E-10
Spleen	6.92E-09	1.54E-11	1.53E-10
Testes	1.05E-08	2.35E-11	2.33E-10
Thymus	8.08E-09	1.80E-11	1.78E-10
Thyroid	1.02E-08	2.28E-11	2.26E-10
Uterus	6.14E-09	1.37E-11	1.35E-10
Skin	1.50E-08	2.92E-11	2.64E-10

[a] USDOE (1988).

Table I-39S. External Dose-Rate Conversion Factors for ^{224}Ra[a]

Ra-224 3.62 d

	Submersion (Gy-m3/Bq-y)	Immersion (Gy-m3/Bq-y)	Ground Plane (Gy-m2/Bq-y)
Effective	1.36E-08	3.00E-11	2.97E-10
Adrenals	1.15E-08	2.54E-11	2.51E-10
Bl Wall	1.06E-08	2.33E-11	2.30E-10
Brain	1.14E-08	2.50E-11	2.47E-10
Breast	1.62E-08	3.59E-11	3.57E-10
Heart	1.03E-08	2.26E-11	2.24E-10
S Wall	1.04E-08	2.29E-11	2.26E-10
SI Wall	9.19E-09	2.03E-11	2.01E-10
ULI Wall	1.09E-08	2.40E-11	2.37E-10
LLI Wall	1.02E-08	2.25E-11	2.23E-10
Kidneys	1.09E-08	2.40E-11	2.37E-10
Liver	1.05E-08	2.32E-11	2.29E-10
Lungs	1.14E-08	2.52E-11	2.49E-10
Marrow	1.54E-08	3.38E-11	3.35E-10
R Marrow	1.15E-08	2.54E-11	2.51E-10
Ovaries	9.38E-09	2.06E-11	2.04E-10
Pancreas	9.00E-09	1.98E-11	1.96E-10
B Surf	1.57E-08	2.46E-11	3.41E-10
Spleen	1.04E-08	2.30E-11	2.28E-10
Testes	1.56E-08	3.43E-11	3.41E-10
Thymus	1.19E-08	2.61E-11	2.59E-10
Thyroid	1.49E-08	3.30E-11	3.24E-10
Uterus	9.30E-09	2.05E-11	2.02E-10
Skin	2.02E-08	4.11E-11	3.81E-10

[a] USDOE (1988).

Table I-40S. External Dose-Rate Conversion Factors for ^{234}Pa[a]

Pa-234 6.7 h

	Submersion (Gy-m3/Bq-y)	Immersion (Gy-m3/Bq-y)	Ground Plane (Gy-m2/Bq-y)
Effective	2.73E-06	5.95E-09	5.27E-08
Adrenals	2.34E-06	5.08E-09	4.49E-08
Bl Wall	2.27E-06	4.92E-09	4.35E-08
Brain	2.54E-06	5.15E-09	4.86E-08
Breast	2.95E-06	6.43E-09	5.78E-08
Heart	2.24E-06	4.86E-09	4.27E-08
S Wall	2.23E-06	4.84E-09	4.27E-08
SI Wall	2.03E-06	4.41E-09	3.89E-08
ULI Wall	2.38E-06	5.16E-09	4.57E-08
LLI Wall	2.19E-06	4.76E-09	4.19E-08
Kidneys	2.38E-06	5.16E-09	4.54E-08
Liver	2.26E-06	4.89E-09	4.32E-08
Lungs	2.42E-06	5.24E-09	4.62E-08
Marrow	2.69E-06	5.84E-09	5.19E-08
R Marrow	2.43E-06	5.27E-09	4.65E-08
Ovaries	2.16E-06	4.70E-09	4.14E-08
Pancreas	1.95E-06	4.22E-09	3.73E-08
B Surf	2.73E-06	5.95E-09	5.30E-08
Spleen	2.19E-06	4.76E-09	4.19E-08
Testes	3.22E-06	6.97E-09	6.16E-08
Thymus	2.54E-06	5.49E-09	4.86E-08
Thyroid	3.05E-06	6.62E-09	5.86E-08
Uterus	1.98E-06	4.30E-09	3.78E-08
Skin	4.27E-06	8.59E-09	1.09E-07

[a] USDOE (1988).

Table I-41S. External Dose-Rate Conversion Factors for $^{228}Ac^{a}$

Ac-228	6.13 h		
	Submersion (Gy-m3/Bq-y)	Immersion (Gy-m3/Bq-y)	Ground Plane (Gy-m2/Bq-y)
Effective	1.30E-06	2.81E-09	2.45E-08
Adrenals	1.11E-06	2.41E-09	2.09E-08
Bl Wall	1.08E-06	3.35E-09	2.04E-08
Brain	1.21E-06	2.63E-09	2.28E-08
Breast	1.39E-06	3.00E-09	2.65E-08
Heart	1.07E-06	2.32E-09	2.01E-08
S Wall	1.06E-06	2.30E-09	1.99E-08
SI Wall	9.73E-07	2.11E-09	1.82E-08
ULI Wall	1.14E-06	2.46E-09	2.14E-08
LLI Wall	1.05E-06	2.27E-09	1.97E-08
Kidneys	1.14E-06	2.46E-09	2.13E-08
Liver	1.08E-06	2.34E-09	2.02E-08
Lungs	1.15E-06	2.49E-09	2.16E-08
Marrow	1.26E-06	2.73E-09	2.38E-08
R Marrow	1.16E-06	2.52E-09	2.18E-08
Ovaries	1.03E-06	2.24E-09	1.94E-08
Pancreas	9.30E-07	2.02E-09	1.75E-08
B Surf	1.28E-06	2.78E-09	2.42E-08
Spleen	1.05E-06	2.27E-09	1.96E-08
Testes	1.52E-06	3.30E-09	2.86E-08
Thymus	1.21E-06	2.61E-09	2.26E-08
Thyroid	1.45E-06	3.14E-09	2.73E-08
Uterus	9.46E-07	2.05E-09	1.77E-08
Skin	2.45E-06	4.54E-09	1.36E-07

[a] USDOE (1988).

Table I-42S. External Dose-Rate Conversion Factors for $^{239}Pu^{a}$

Pu-239	23,131 y		
	Submersion (Gy-m3/Bq-y)	Immersion (Gy-m3/Bq-y)	Ground Plane (Gy-m2/Bq-y)
Effective	1.10E-10	2.62E-13	1.02E-11
Adrenals	6.30E-11	1.45E-13	2.41E-12
Bl Wall	5.54E-11	1.26E-13	1.25E-12
Brain	5.92E-11	1.35E-13	1.46E-12
Breast	2.70E-11	6.65E-13	4.38E-11
Heart	5.49E-11	1.25E-13	1.42E-12
S Wall	5.59E-11	1.28E-13	1.63E-12
SI Wall	4.68E-11	1.07E-13	1.08E-12
ULI Wall	5.84E-11	1.33E-13	1.32E-12
LLI Wall	5.49E-11	1.26E-13	1.76E-12
Kidneys	5.62E-11	1.29E-13	1.31E-12
Liver	5.54E-11	1.26E-13	1.31E-12
Lungs	6.54E-11	1.51E-13	2.42E-12
Marrow	1.03E-10	2.36E-13	3.24E-12
R Marrow	5.27E-11	1.21E-13	1.51E-12
Ovaries	4.97E-11	1.14E-13	1.62E-12
Pancreas	4.68E-11	1.08E-13	1.66E-12
B Surf	1.08E-11	2.49E-13	3.97E-12
Spleen	5.62E-11	1.29E-13	1.63E-12
Testes	1.17E-10	2.76E-13	9.35E-12
Thymus	6.73E-11	1.54E-13	1.53E-12
Thyroid	9.16E-11	2.11E-13	3.14E-12
Uterus	4.76E-11	1.09E-13	1.08E-12
Skin	3.92E-10	9.18E-13	7.57E-11

[a] USDOE (1988).

Table I-43S. External Dose-Rate Conversion Factors for ^{214}Pb, ^{214}Bi, and ^{214}Po for Submersion in Air (Gy year^{-1} (Bq m^{-3})$^{-1}$)[a,b]

Organ	^{214}Pb	^{214}Bi	^{214}Po
Effective	3.35×10^{-7}	2.18×10^{-6}	1.17×10^{-10}
Adrenals	2.84×10^{-7}	1.85×10^{-6}	1.01×10^{-10}
Bladder Wall	2.66×10^{-7}	1.84×10^{-6}	9.76×10^{-11}
Brain	2.89×10^{-7}	2.07×10^{-6}	1.10×10^{-10}
Breast	3.86×10^{-7}	2.32×10^{-6}	1.24×10^{-10}
S Wall	2.61×10^{-7}	1.80×10^{-6}	9.59×10^{-11}
SI Wall	2.32×10^{-7}	1.68×10^{-6}	8.70×10^{-11}
ULI Wall	2.73×10^{-7}	1.94×10^{-6}	1.02×10^{-10}
LLI Wall	2.55×10^{-7}	1.79×10^{-6}	9.41×10^{-11}
Kidneys	2.76×10^{-7}	1.94×10^{-6}	1.02×10^{-10}
Liver	2.65×10^{-7}	1.84×10^{-6}	9.70×10^{-11}
Lungs	2.86×10^{-7}	1.95×10^{-6}	1.04×10^{-10}
R. Marrow	2.89×10^{-7}	1.97×10^{-6}	1.05×10^{-10}
Ovaries	2.43×10^{-7}	1.73×10^{-6}	9.43×10^{-11}
Pancreas	2.26×10^{-7}	1.59×10^{-6}	8.35×10^{-11}
Bone Surfaces	3.70×10^{-7}	2.09×10^{-6}	1.15×10^{-10}
Spleen	2.60×10^{-7}	1.78×10^{-6}	9.41×10^{-11}
Testes	3.89×10^{-7}	2.55×10^{-6}	1.37×10^{-10}
Thymus	2.95×10^{-7}	2.02×10^{-6}	1.09×10^{-10}
Thyroid	3.68×10^{-7}	2.39×10^{-6}	1.31×10^{-10}
Uterus	2.32×10^{-7}	1.64×10^{-6}	8.43×10^{-11}
Skin	8.78×10^{-7}	4.24×10^{-6}	1.59×10^{-10}

[a] USDOE (1988).
[b] Half lives: ^{214}Pb 26.8 m
^{214}Bi 19.9 m
^{214}Po 0.000164 s.

APPENDIX J

SPECIFICATIONS OF THE NINE EXPOSURE SCENARIOS

The radiation dose that a person living near the Feed Materials Production Center (FMPC) might have received depends on a number of factors, such as residence and work locations, length of time in the area, lifestyle, diet, and the source of some foods (for example, local gardens or uncontaminated food from distant locations). To consider these features of a person's life, we developed exposure scenarios for nine representative residents of the FMPC area, for which representative dose estimates could be made. These scenarios incorporate some typical lifestyles and food habits of residents in the area and specify the applicable home, school, and work locations. These scenarios can help some individuals estimate dose ranges for themselves by finding lifestyle profiles that most closely match their backgrounds. The scenarios are not designed to include all conceivable lifestyles of residents who lived in this region during the time of the FMPC operations. Rather, they serve as guides to a range of potential profiles of people in the area.

Tables J-1 through J-9 summarize the nine exposure scenarios quantitatively in terms of the model parameters that specify them. Each scenario is divided into several periods of time, and each parameter can change from one period to the next.

Within each period, there is at least one primary location where most of the individual's time was spent; in most periods, there are two locations, such as home and school. The proportions of time spent in the locations are specified as parameters and are further broken down into time spent indoors and outdoors, because concentrations of airborne radioactivity in releases from the Feed Materials Production Center (FMPC) usually would have been higher outdoors.

The indices of activity for indoors and outdoors refer to parameters for indicating breathing rates in response to the subject's vigor of exercise during each period and at each location. The scale, ranging on a continuum from 0 for resting (slow breathing), to 1 for light activity (moderate breathing), and to 2 for heavy activity (rapid breathing), is calibrated to age- and sex-specific physiological models of respiration (Appendix I).

For airborne particulates, the parameter labeled indoor particulate factor is a fraction that is multiplied by the outdoor concentration of radioactivity to estimate the corresponding indoor concentration. By contrast, the parameter called air turnover is a fractional hourly replacement of the air in a building and is applied only to the incursion and removal of radon and its decay products indoors. Both parameters compensate for the effect of the enclosure in reducing indoor air concentration of radioactivity below outdoor levels. This reduction is taken into account in estimating the component of dose for times the subjects are assumed to have spent indoors. The generic values of these parameters that are shown in Tables J-1 through J-9 are discussed in Appendix I.

Each of Tables J-1 through J-9 is divided into two parts. The first part, which begins with a simple description of the scenario, gives summary information about the individual: sex, date of birth, location of the home, schools attended and their locations, location of the place of employment, and identification of any assumed sources of contaminated water that affect the

scenario. The second part of each table lists the parameters that define the scenario and shows each parameter value for each period and location.

The primary location of the subject is a variable of particular interest in all scenarios. In general, the dose decreases with increasing distance from the point of release of radioactive materials, but direction is also important because of the predominantly southwesterly wind direction (which blows toward the northeast). The points of release on the FMPC site are numerous, and for purposes of indicating distances of receptor points from the site, we use the distance of the receptor point from the center of the FMPC production area. Thus, scenarios 1, 2, and 3 feature primary locations within about 2 km from the site; scenarios 5, 7, and 9 are based on primary locations that are 8–10 km from the site; and scenarios 4, 6 and 8 are intermediate with respect to primary location (3–4 km from the site).

Spatial factors other than distance from the site are also potentially important in estimating the dose. Nearness to the K-65 silos, which are located toward the western site boundary, was also considered (scenario 2) because of the possibility of enhanced dose from ^{222}Rn (radon) decay products. As the calculations turned out, the subjects of scenarios 1 and 2 received about the same cumulative dose from radon decay products (Appendix K); the prevalence of the southwesterly winds compensated for the greater distance of the residence of scenario 1 from the K-65 silos.

In scenario 3, the subject is assumed to have drunk water from a well contaminated by the groundwater plume that migrated off the site in the mid 1960s (the well is assumed to be Well 15; see Appendix F). Consumption of local garden produce and animal products is considered in scenarios 1–4 and 6–8, and the irrigation of the vegetable garden with water from the Great Miami River is assumed in scenarios 6 and 7. As an extreme case, irrigation of home-grown produce with water from Paddy's Run Creek is assumed in scenario 2 (any irrigation from this creek is highly unlikely; it is dry much of the year, but the assumption provides a level of contamination from irrigation that is unlikely to be exceeded). External exposure from swimming in contaminated water is taken into account in scenarios 1–4 and 6–8. In general, the assumed levels of radioactivity are based on those observed in the Great Miami River, but in scenarios 2 and 3 we have considered the possibility that the subject as a preschool child (Period 1) might have played in the water or mud of Paddy's Run south of the site.

Ingestion of contaminated soil particles is considered in all scenarios. This exposure pathway includes the eating of dirt by small children and for all age groups ingesting particles of soil that adhere to incompletely washed produce and from other accidental sources. Table J-10 shows the age-specific relationship, based on data of Kimbrough et al. (1983).

Scenarios 1 and 6 hypothesize a pregnancy when the subjects were 18 years of age. A period of nine months is specified for each pregnancy, and the dose to the embryo/fetus is estimated on the basis of each subject's exposure during this period.

The scenarios consider people who were infants or children at the time the exposure began in order to allow for the effects of age-dependence in the dosimetry and to permit as long a period as possible for the accrual of cumulative dose. Older persons, whose dose and risk would generally be smaller, were not included in these scenarios.

REFERENCES

Kimbrough R.D., H. Falk, P. Steher, and G. Fries. 1983. "Health Implications of 2,3,7,8-Tetrachlorodibenzodioxin (TDCC) Contamination of Residential Soil." In *Proceedings of Public Health Risks of the Dioxins,* October 19–20, 1983. William Kaufman, Los Angeles, California.

Table J-1. Scenario 1

Location and habits tend to maximize exposure to airborne uranium and to radon.

Sex	F
Born	1946
Home	1.7 km NE
Schools	Elda Elementary (EE) 4.7 km ENE Hamilton-Cleaves Middle School, Ross High School (HCR) 6 km NE
Work	In the home
Contaminated water sources	Great Miami River (GMR)

	Period 1 1946–1951	Period 2 1951–1957		Period 3 1957–1964		Period 4[a] 1964–1965	Period 5 1965–1989
Location	Home	Home	EE	Home	HCR	Home	Home
Time indoors (%)	80	67	14	67	14	83	83
Indoor activity index[b]	0.5	1	1	1	1	1	1
Time outdoors (%)	20	15	4	15	4	17	17
Outdoor activity index[b]	1.5	1.5	1.5	1.5	1.5	1.5	1.5
Indoor particulate factor	0.7	0.7	0.7	0.7	0.7	0.7	0.7
Air turnover ($hour^{-1}$)	0.4	0.4	0.4	0.4	0.4	0.4	0.4
Contaminated drinking water source	none	none	none	none	none	none	none
Contaminated irrigation water source	none	none	none	none	none	none	none
Irrigation volume ($L\ m^{-2}\ day^{-1}$)	0.5	0.5	0	0.5	0	0.5	0.5
Contaminated vegetables (% of intake)	50	50	0	50	0	50	50
Contaminated milk (% of intake)	100	100	0	100	0	100	100
Contaminated beef (% of intake)	50	50	0	50	0	50	50
Contaminated poultry (% of intake)	50	50	0	50	0	50	50
Contaminated eggs (% of intake)	100	100	0	100	0	100	100
Contaminated fish (% of intake)	50	50	0	50	0	50	50
Contaminated water source for fish	GMR	GMR	none	GMR	none	GMR	GMR
Swimming (% of time)	2	2	0	2	0	0	0
Contaminated water source for swimming	GMR	GMR	none	GMR	none	GMR	GMR
Ingested soil ($g\ day^{-1}$)	5	0.1	0.1	0.1	0.1	0.05	0.05

[a] Pregnancy.
[b] Varies continuously from 0 (resting) to 1 (light activity) to 2 (vigorous activity).

Table J-2. Scenario 2

Location near FMPC radon source (K-65 silos). Subject lived west of FMPC site across Paddy's Run Road.

Sex	M
Born	1/1/1951
Home	2 km W
Schools	Elda Elementary (EE) 4.7 km ENE Hamilton-Cleaves Middle School, Ross High School (HCR) 6 km NE
Work	In Hamilton, 12 km N (outside of assessment domain)
Contaminated water sources	Paddy's Run (PADRUN), Great Miami River (GMR)

	Period 1 1951–1956	Period 2 1956–1962		Period 3 1962–1969		Period 4 1969–1989	
Location	Home	Home	EE	Home	HCR	Home	Work[a]
Time indoors (%)	83	67	14	67	14	60	24
Indoor activity index[b]	0.5	1	1	1	1	1	0.5
Time outdoors (%)	17	15	4	15	4	15	1
Outdoor activity index[b]	1.5	1.5	1.5	1.5	1.5	1.5	1
Indoor particulate factor	0.7	0.7	0.7	0.7	0.7	0.7	0.7
Air turnover ($hour^{-1}$)	0.4	0.4	0.4	0.4	0.4	0.4	0.4
Contaminated drinking water source	none	none	none	none	none	none	none
Contaminated irrigation water source	PADRUN	PADRUN	none	PADRUN	none	PADRUN	none
Irrigation volume ($L\ m^{-2}\ day^{-1}$)	0.25	0.25	0	0.25	0	0.25	0
Contaminated vegetables (% of intake)	50	50	0	50	0	50	0
Contaminated milk (% of intake)	50	50	0	50	0	50	0
Contaminated beef (% of intake)	0	0	0	0	0	0	0
Contaminated poultry (% of intake)	50	50	0	50	0	50	0
Contaminated eggs (% of intake)	100	100	0	100	0	100	0
Contaminated fish (% of intake)	0	0	0	0	0	0	0
Contaminated water source for fish	none	none	none	none	none	none	none
Swimming (% of time)	1	2	0	2	0	0	0
Contaminated water source for swimming	PADRUN	GMR	none	GMR	none	GMR	none
Ingested soil ($g\ day^{-1}$)	5	0.1	0.1	0.1	0.1	0.05	0.05

[a] Work location is outside the assessment domain; thus no dose is calculated for this location.
[b] Varies continuously from 0 (resting) to 1 (light activity) to 2 (vigorous activity).

Table J-3. Scenario 3

In addition to airborne uranium and radon exposure, subject drank water from contaminated well water south of the FMPC site across Willey Road.

Sex	M
Born	1/1/1951
Home	2 km S
Schools	Elda Elementary (EE) 4.7 km ENE Hamilton-Cleaves Middle School, Ross High School (HCR) 6 km NE
Work	1.5 km SE (WORK3)
Contaminated water sources	Paddy's Run (PADRUN), Great Miami River (GMR), and Well 15 (WELL)

	Period 1 1951–1956	Period 2 1956–1962		Period 3 1962–1969		Period 4 1969–1989	
Location	Home	Home	EE	Home	HCR	Home	WORK3
Time indoors (%)	83	67	14	67	14	60	15
Indoor activity index[a]	0.5	1	1	1	1	1	1
Time outdoors (%)	17	15	4	15	4	15	10
Outdoor activity index[a]	1.5	1.5	1.5	1.5	1.5	1.5	1.5
Indoor particulate factor	0.7	0.7	0.7	0.7	0.7	0.7	0.7
Air turnover ($hour^{-1}$)	0.4	0.4	0.4	0.4	0.4	0.4	0.4
Contaminated drinking water source	none[b]	none[b]	none	WELL	none	WELL	WELL
Contaminated irrigation water source	none	none	none	none	none	none	none
Irrigation volume ($L\ m^{-2}\ day^{-1}$)	0.5	0.5	0	0.5	0	0.5	0
Contaminated vegetables (% of intake)	50	50	0	50	0	50	0
Contaminated milk (% of intake)	100	100	0	100	0	100	0
Contaminated beef (% of intake)	0	0	0	0	0	0	0
Contaminated poultry (% of intake)	50	50	0	50	0	50	0
Contaminated eggs (% of intake)	100	100	0	100	0	100	0
Contaminated fish (% of intake)	0	0	0	0	0	0	0
Contaminated water source for fish	none	none	none	none	none	none	none
Swimming (% of time)	1	2	0	2	0	0	0
Contaminated water source for swimming	PADRUN	GMR	none	GMR	none	GMR	none
Ingested soil ($g\ day^{-1}$)	5	0.1	0.1	0.1	0.1	0.05	0.1

[a] Varies continuously from 0 (resting) to 1 (light activity) to 2 (vigorous activity).
[b] Groundwater plume did not leave the FMPC site during this period.

Table J-4. Scenario 4

Exposure to airborne uranium from 1960–1978. The subject was raised in Ross and left the area after high school.

Sex	F
Born	7/15/1960
Home	4 km ENE
Schools	Elda Elementary (EE) 4.7 km ENE Hamilton-Cleaves Middle School, Ross High School (HCR) 6 km NE
Work	N/A — left the assessment domain in 1978
Contaminated water sources	Great Miami River (GMR)

	Period 1 1960–1965	Period 2 1965–1971		Period 3 1971–1978	
Location	Home	Home	EE	Home	HCR
Time indoors (%)	83	67	14	67	14
Indoor activity index[a]	0.5	1	1	1	1
Time outdoors (%)	17	15	4	15	4
Outdoor activity index[a]	1.5	1.5	1.5	1.5	1.5
Indoor particulate factor	0.7	0.7	0.7	0.7	0.7
Air turnover ($hour^{-1}$)	0.4	0.4	0.4	0.4	0.4
Contaminated drinking water source	none	none	none	none	none
Contaminated irrigation water source	none	none	none	none	none
Irrigation volume ($L\ m^{-2}\ day^{-1}$)	0.5	0.5	0	0.5	0
Contaminated vegetables (% of intake)	10	10	0	10	0
Contaminated milk (% of intake)	10	10	0	10	0
Contaminated beef (% of intake)	0	0	0	0	0
Contaminated poultry (% of intake)	0	0	0	0	0
Contaminated eggs (% of intake)	10	10	0	10	0
Contaminated fish (% of intake)	0	0	0	0	0
Contaminated water source for fish	none	none	none	none	none
Swimming (% of time)	0	2	0	2	0
Contaminated water source for swimming	none	GMR	none	GMR	none
Ingested soil ($g\ day^{-1}$)	5	0.1	0.1	0.1	0.1

[a] Varies continuously from 0 (resting) to 1 (light activity) to 2 (vigorous activity).

Table J-5. Scenario 5

Low exposure. The subject resided near the boundary of the assessment domain to the north.

Sex	M
Born	1/1/1951
Home	8 km N
Schools	Morgan Elementary (ME) 6.2 km NW Hamilton-Cleaves Middle School, Ross High School (HCR) 6 km NE
Work	In Hamilton, 12 km N (outside assessment domain)
Contaminated water sources	None

	Period 1 1951–1956	Period 2 1956–1962		Period 3 1962–1969		Period 4 1969–1989	
Location	Home	Home	ME	Home	HCR	Home	Work[a]
Time indoors (%)	83	67	14	67	14	60	24
Indoor activity index[b]	0.5	1	1	1	1	1	0.5
Time outdoors (%)	17	15	4	15	4	15	1
Outdoor activity index[b]	1.5	1.5	1.5	1.5	1.5	1.5	1
Indoor particulate factor	0.7	0.7	0.7	0.7	0.7	0.7	0.7
Air turnover ($hour^{-1}$)	0.4	0.4	0.4	0.4	0.4	0.4	0.4
Contaminated drinking water source	none	none	none	none	none	none	none
Contaminated irrigation water source	none	none	none	none	none	none	none
Irrigation volume ($L\ m^{-2}\ day^{-1}$)	0.5	0.5	0	0.5	0	0.5	0
Contaminated vegetables (% of intake)	0	0	0	0	0	0	0
Contaminated milk (% of intake)	0	0	0	0	0	0	0
Contaminated beef (% of intake)	0	0	0	0	0	0	0
Contaminated poultry (% of intake)	0	0	0	0	0	0	0
Contaminated eggs (% of intake)	0	0	0	0	0	0	0
Contaminated fish (% of intake)	0	0	0	0	0	0	0
Contaminated water sourcce for fish	none	none	none	none	none	none	none
Swimming (% of time)	0	0	0	0	0	0	0
Contaminated water source for swimming	none	none	none	none	none	none	none
Ingested soil ($g\ day^{-1}$)	5	0.1	0.1	0.1	0.1	0.05	0.05

[a] Work location is outside the assessment domain; no dose has been estimated for exposure incurred there.
[b] Varies continuously from 0 (resting) to 1 (light activity) to 2 (vigorous activity).

Table J-6. Scenario 6

Consumption of vegetables from a garden irrigated with river water. The subject's residence and garden were located 3 km ESE from FMPC site.

Sex	F
Born	1/1/1946
Home	3 km ESE
Schools	Elda Elementary (EE) 4.7 km ENE Hamilton-Cleaves Middle School, Ross High School (HCR) 6 km NE
Work	Family farm
Contaminated water sources	Great Miami River (GMR)

	Period 1 1946–1951	Period 2 1951–1957		Period 3 1957–1964		Period 4[a] 1964–1965	Period 5 1965–1989
Location	Home	Home	EE	Home	HCR	Home	Home
Time indoors (%)	80	67	14	67	14	83	83
Indoor activity index[b]	0.5	1	1	1	1	1	1
Time outdoors (%)	20	15	4	15	4	17	17
Outdoor activity index[b]	1.5	1.5	1.5	1.5	1.5	1.5	1.5
Indoor particulate factor	0.7	0.7	0.7	0.7	0.7	0.7	0.7
Air turnover ($hour^{-1}$)	0.4	0.4	0.4	0.4	0.4	0.4	0.4
Contaminated drinking water source	none	none	none	none	none	none	none
Contaminated irrigation water source	GMR	GMR	none	GMR	none	GMR	GMR
Irrigation volume ($L\ m^{-2}\ day^{-1}$)	0.5	0.5	0	0.5	0	0.5	0.5
Contaminated vegetables (% of intake)	50	50	0	50	0	50	50
Contaminated milk (% of intake)	100	100	0	100	0	100	100
Contaminated beef (% of intake)	50	50	0	50	0	50	50
Contaminated poultry (% of intake)	50	50	0	50	0	50	50
Contaminated eggs (% of intake)	100	100	0	100	0	100	100
Contaminated fish (% of intake)	50	50	0	50	0	50	50
Contaminated water source for fish	GMR	GMR	none	GMR	none	GMR	GMR
Swimming (% of time)	2	2	0	2	0	0	0
Contaminated water source for swimming	GMR	GMR	none	GMR	none	GMR	GMR
Ingested soil ($g\ day^{-1}$)	5	0.1	0.1	0.1	0.1	0.05	0.05

[a] Pregnancy.
[b] Varies continuously from 0 (resting) to 1 (light activity) to 2 (vigorous activity).

Table J-7. Scenario 7

Subject lived 10 km S of FMPC site and consumed vegetables from a garden irrigated with river water.

Sex	M
Born	1/1/1951
Home	10 km S (near boundary of assessment domain)
Schools	Elda Elementary (EE) 4.7 km ENE Hamilton-Cleaves Middle School, Ross High School (HCR) 6 km NE
Work	In Miamitown near home (WORK7)
Contaminated water source	Paddy's Run (PADRUN), Great Miami River (GMR)

	Period 1 1951–1956	Period 2 1956–1962		Period 3 1962–1969		Period 4 1969–1989	
Location	Home	Home	EE	Home	HCR	Home	WORK7
Time indoors (%)	83	67	14	67	14	60	24
Indoor activity index[a]	0.5	1	1	1	1	1	0.5
Time outdoors (%)	17	15	4	15	4	15	1
Outdoor activity index[a]	1.5	1.5	1.5	1.5	1.5	1.5	1
Indoor particulate factor	0.7	0.7	0.7	0.7	0.7	0.7	0.7
Air turnover ($hour^{-1}$)	0.4	0.4	0.4	0.4	0.4	0.4	0.4
Contaminated drinking water source	none	none	none	none	none	none	none
Contaminated irrigation water source	GMR	GMR	none	GMR	none	PADRUN	none
Irrigation volume ($L\ m^{-2}\ day^{-1}$)	0.5	0.5	0	0.5	0	0.5	0
Contaminated vegetables (% of intake	50	50	0	50	0	50	0
Contaminated milk (% of intake)	10	50	0	50	0	50	0
Contaminated beef (% of intake)	0	0	0	0	0	0	0
Contaminated poultry (% of intake)	50	50	0	50	0	50	0
Contaminated eggs (% of intake)	10	100	0	100	0	100	0
Contaminated fish (% of intake)	50	50	0	50	0	50	0
Contaminated water source for fish	GMR	GMR	none	GMR	none	GMR	none
Swimming (% of time)	2	2	0	2	0	0	0
Contaminated water source for swimming	GMR	GMR	none	GMR	none	GMR	none
Ingested soil ($g\ day^{-1}$)	5	0.1	0	0.1	0	0.05	0

[a] Varies continuously from 0 (resting) to 1 (light activity) to 2 (vigorous activity).

Table J-8. Scenario 8

As a 5–year old in 1975, the subject moved with his family to Ross (4 km ENE from FMPC site) and attended Ross schools.

Sex	M
Born	1/1/1970
Home	4 km ENE
Schools	Elda Elementary (EE) 4.7 km ENE Hamilton-Cleaves Middle School, Ross High School (HCR) 6 km NE
Work	None before end of exposure period (high school graduation in 1988)
Contaminated water sources	Great Miami River (GMR)

	Period 1 1975–1981		Period 2 1981–1989	
Location	Home	EE	Home	HCR
Time indoors (%)	67	14	67	14
Indoor activity index[a]	1	1	1	1
Time outdoors (%)	15	4	15	4
Outdoor activity index[a]	1.5	1.5	1.5	1.5
Indoor particulate factor	0.7	0.7	0.7	0.7
Air turnover ($hour^{-1}$)	0.4	0.4	0.4	0.4
Contaminated drinking water source	none	none	none	none
Contaminated irrigation water source	none	none	none	none
Irrigation volume ($L\ m^{-2}\ day^{-1}$)	0.5	0	0.5	0
Contaminated vegetables (% of intake)	10	0	10	0
Contaminated milk (% of intake)	10	0	10	0
Contaminated beef (% of intake)	0	0	0	0
Contaminated poultry (% of intake)	0	0	0	0
Contaminated eggs (% of intake)	10	0	10	0
Contaminated fish (% of intake)	0	0	0	0
Contaminated water source for fish	none	none	none	none
Swimming (% of time)	0	0	0	0
Contaminated water source for swimming	GMR	none	GMR	none
Ingested soil ($g\ day^{-1}$)	0.1	0	0.1	0

[a] Varies continuously from 0 (resting) to 1 (light activity) to 2 (vigorous activity).

Table J-9. Scenario 9

Exposure to airborne uranium while attending Ross schools. Subject's family lived near the assessment domain boundary NE of the FMPC.

Sex	M
Born	1/1/1951
Home	10 km NE (near boundary of the assessment domain)
Schools	Elda Elementary (EE) 4.7 km ENE Hamilton-Cleaves Middle School, Ross High School (HCR) 6 km NE
Work	None; left the area after high school graduation in 1969
Contaminated water sources	None

	Period 1 1951–1956	Period 2 1956–1962		Period 3 1962–1969	
Location	Home	Home	EE	Home	HCR
Time indoors (%)	83	67	14	67	14
Indoor activity index[a]	0.5	1	1	1	1
Time outdoors (%)	17	15	4	15	4
Outdoor activity index[a]	1.5	1.5	1.5	1.5	1.5
Indoor particulate factor	0.7	0.7	0.7	0.7	0.7
Air turnover ($hour^{-1}$)	0.4	0.4	0.4	0.4	0.4
Contaminated drinking water source	none	none	none	none	none
Contaminated irrigation water source	none	none	none	none	none
Irrigation volume ($L\ m^{-2}\ day^{-1}$)	0.5	0.5	0	0.5	0
Contaminated vegetables (% of intake)	0	0	0	0	0
Contaminated milk (% of intake)	0	0	0	0	0
Contaminated beef (% of intake)	0	0	0	0	0
Contaminated poultry (% of intake)	0	0	0	0	0
Contaminated eggs (% of intake)	0	0	0	0	0
Contaminated fish (% of intake)	0	0	0	0	0
Contaminated water source for fish	none	none	none	none	none
Swimming (% of time)	0	0	0	0	0
Contaminated water source for swimming	none	none	none	none	none
Ingested soil ($g\ day^{-1}$)	5	0.1	0	0.1	0

[a] Varies continuously from 0 (resting) to 1 (light activity) to 2 (vigorous activity).

Table J-10. Soil Ingestion by Age[a]

Age group	Soil ingested ($mg\ day^{-1}$)
newborn	0
9–18 mo.	1,000
1.5–3.5 yr.	10,000
3.5–5 yr.	1,000
≥5 yr.	100

[a] From Kimbrough et al. (1983).

APPENDIX K

DOSE ESTIMATES FOR MEMBERS OF THE PUBLIC RESIDING NEAR THE FEED MATERIALS PRODUCTION CENTER

INTRODUCTION

Dose estimates vary considerably according to the exposure history of individuals. In general, dose to an individual might be expected to decrease with increasing distance of the individual's place of residence from the source of airborne releases of radioactivity. Various factors, however, can interfere with this simple dependence of dose on distance. For example, time spent at school may alter the estimate of dose from inhalation; similarly, consumption of local produce raised at a location other than one's residence would give different dose estimates from those based on produce raised in the home garden.

In order to present a sense of the variation of dose estimates with different assumptions about an individual's history of exposure to radioactivity released from the Feed Materials Production Center (FMPC), we have defined nine sets of assumptions, called *exposure scenarios* (or simply *scenarios*). Details of the scenarios are given in Appendix J. These scenarios portray a range of possible activities of people residing in the assessment domain. Each scenario corresponds to one individual. The exposure levels associated with the scenarios range from typical to uncommon combinations of exposure factors. The scenarios are based on hypothetical rather than real individuals, but they contain elements to which many people who have lived near the FMPC may be able to relate their own experiences.

> NOTE. We emphasize that terms such as person, individual and subject used in discussing the nine scenarios refer only to fictitious characters whose activities illustrate exposure and dose; these terms do **not** refer to real people.

We begin by outlining the principal types of exposure of members of the public to FMPC radioactivity. We separate the exposures into two groups, according to the radionuclides involved. Exposures in the first group of come from the uranium isotopes (^{234}U, ^{235}U, and ^{238}U), thorium isotopes from thorium production (treated generically as ^{232}Th), and decay products of these radionuclides (Figure 1); we ordinarily refer to this group as simply "uranium." The second group of exposures is associated with ^{222}Rn and its decay products; ^{222}Rn is produced by the decay of ^{226}Ra contained primarily in the K-65 silos west of the FMPC production area. We note that relatively small quantities of ^{222}Rn and its decay products were emitted from drums stored on a pad in the production area for about two years in the early 1950s. These emissions have been considered in dose estimates, but they are negligible relative to subsequent emissions from the K-65 silos, and in discussions of radon emissions, we usually omit mention of them. The following outline gives the main exposure pathways associated with these two groups of radionuclides:

1. Uranium, thorium, and their decay products released to the air as particulates, released to surface waters, or forming as decay products in the soil, surface water, or ground water
   - Primary inhalation of airborne material that has not yet deposited on the ground

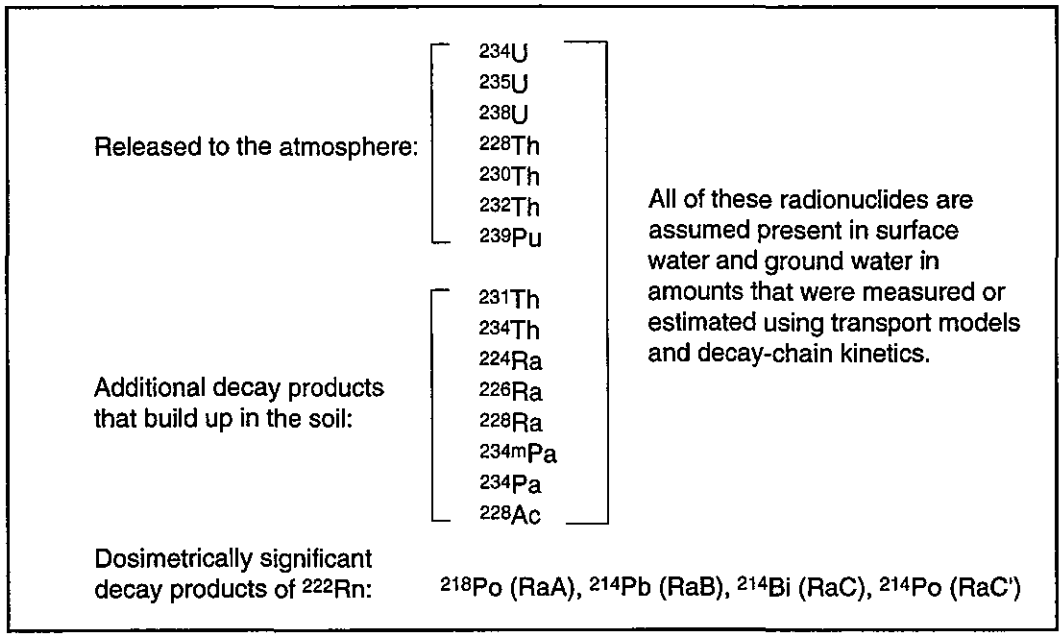

Figure K-1. List of radionuclides affecting the exposures in scenarios 1–9.

- Secondary inhalation of resuspended material
- Consumption of contaminated drinking water and contaminated food from garden or locally produced animal products
- External exposure to gamma-emitting radionuclides
  - — Immersion in contaminated air
  - — Standing on contaminated ground
  - — Swimming in contaminated water

2. Radon from the K-65 silos
   - Inhalation of radon decay products
   - External exposure to gamma rays from K-65 silos
   - External exposure to gamma rays from airborne radon decay products ^{214}Pb and ^{214}Bi.

Doses for each scenario will be broken down into some of the components indicated by this outline.

EXPOSURE SCENARIOS

The nine exposure scenarios were developed in order to indicate the effects of different combinations of magnitudes of the exposure factors outlined above. In each case, we tried to choose plausible magnitudes of exposure, even for scenarios that exhibit an extreme feature (such as nearness to the release source or the use of a contaminated well). Scenarios that feature low exposures complement those with high extremes to indicate a range. All scenarios consider only exposure to FMPC releases, and the exposure must have occurred within the assessment domain during the years 1951–1988. Note that the nine scenarios consider young

people, who were infants or children at the time the exposure began and whose collective risk situation would tend to be maximum (they would have more years of potential exposure and more years for health effects to express themselves). Older persons, whose risk would likely be less, were not included in these scenarios.

Table K-1 summarizes the scenarios in terms of some of their distinguishing characteristics. These characteristics are related to the exposure pathways outlined above, and they influence the estimates of dose in various degrees. The distance and direction of the subject's principal location from the center of the FMPC site have an important correlation with exposure to primary pathways, such as inhalation of airborne radioactivity. Age, and to a lesser extent, sex influence the dose, and both are considered in the methodology to the extent that the dosimetric database supports the distinction (Appendix I). The number of years the subject resided in the assessment domain during the period of plant operation is obviously related to the total dose. Local garden produce and animal products constitute an exposure pathway for dose by ingestion. These pathways are quantified in terms of percentages of a subject's total intakes of various food types that are assumed to be contaminated by the following processes:

- Deposition of airborne radionuclides on plant surfaces
- Irrigation of plants with contaminated water
- Uptake of radioactivity from the soil through the roots of plants
- Incorporation of radionuclides into animal products by the animal's consumption of contaminated forage, drinking water, and (in the case of poultry) contaminated soil
- Incorporation of radionuclides into the flesh of fish caught from contaminated streams.

Contaminated drinking water is a possible exposure pathway, although the only mechanism considered is the use of water from wells that were contaminated by the groundwater plume that migrated offsite to the south in the mid-1960s. Table K-1 quantifies the scenarios in terms of most of these exposure pathways so that different scenarios may be compared at a glance. Note that scenario 3 is the one that includes exposure to uranium-contaminated well water. Additional information is given in Tables J-1 through J-9 in Appendix J. Scenario 3 is discussed in Appendix R with regard to the chemical toxicity of uranium in the kidneys.

Primary location of the subject relative to the point of release is a variable of particular interest in all scenarios. Not only the distance, but also the direction of the subject's location from the center of the FMPC production area, is important in estimating exposure and dose. In general, the dose decreases with increasing distance from the point of release of radioactive materials. In addition, predominantly southwesterly winds (i.e., blowing from the southwesterly directions) enhance airborne transport of radionuclides into northeastern sectors. Hence, a subject located at a given distance northeast of the FMPC may have received a higher dose from airborne radioactivity than one at the same distance but in another direction. Table K-1 shows that the scenarios consider locations at different distances and directions from the FMPC. Nearness to the K-65 silos, which are located toward the western site boundary, was also considered (scenario 2) because of the possibility of enhanced dose from decay products of ^{222}Rn.

External exposure from swimming in contaminated water is taken into account in scenarios 1–4, 6, and 7, and ingestion of contaminated soil particles is considered in all scenarios.

Table K-1. Summary of the Nine Scenarios for FMPC Dose Calculations

Scenario (description)	Distance from FMPC (km)	Direction	Date of birth	Sex	Years at location	Intake from local source (%)[a]						Contaminated water[b]	
						Veg.	Milk	Meat	Poultry	Eggs	Fish[c]	Drink	Irrigate
1 (maximum)	1.7	NE	1-1-46	F	42	50	100	50	50	100	50	no	no
2 (radon)	2	W	1-1-51	M	38	50	50	0	50	100	0	no	PADRUN
3 (well water)	2	S	1-1-51	M	38	50	100	0	50	100	0	WELL	WELL
4 (average)	4[d]	ENE	7-15-60	F	18[e]	10	10	0	0	10	0	no	no
5 (worked outside domain)	8	N	1-1-51	M	38	0	0	0	0	0	0	no	no
6 (irrigated with river water)	3	ESE	1-1-46	F	42	50	100	50	50	100	50	no	GMR
7 (irrigated with river water)	10	S	1-1-51	M	38	50	10	0	0	10	50	no	GMR
8 (lived in Ross 1970s and 1980s)	4	ENE	1-1-70	M	13[f]	10	10	0	0	10	0	no	no
9 (lived 10 km; school in Ross)	10	NE	1-1-51	M	18[g]	0	0	0	0	0	0	no	no

[a] These values are rough estimates based on conversations with local residents. Six vegetables grown in this area that contribute the bulk of garden consumption by hypothetical individuals are lettuce, onions, potatoes, sweet corn, beans, and tomatoes.

[b] GMR = Great Miami River; PADRUN = Paddy's Run; WELL = contaminated well water from the mid 1960s to 1988. An irrigation rate of 0.5 L m^{-2} day^{-1} is assumed for river water and 0.25 L m^{-2} day^{-1} for irrigation with water from Paddy's Run.

[c] Contaminated fish for scenarios 1, 6, and 7 are assumed to have been caught from the Great Miami River.

[d] In Ross.

[e] Left the area after high school graduation in 1978.

[f] Came to Ross in September 1975.

[g] Left the area after high school graduation in 1968.

These pathways are not shown in Table K-1, but details are given in Appendix J. Other external pathways (i.e., gamma exposure from airborne radioactivity and standing on contaminated ground) are considered in all scenarios. The extent of exposure to these pathways is controlled by the subject's division of time between indoors and outdoors. Parameters related to the subject's habits are shown in Appendix J.

The results of dose calculations based on the nine scenarios depend implicitly on other quantitative information, which is outlined as follows:

1. Source terms
   - — Airborne release of particulates. Detailed information is given in the Task 2/3 report (Voillequé et al. 1995).
   - — Airborne release of radon and its decay products. Detailed information is given in the Task 2/3 report.
   - — Levels of radionuclides in the Great Miami River. Appendix E, Table E-1
   - — Levels of radionuclides in Paddy's Run. Appendix E, Table E-2
   - — Levels of radionuclides in Well 15. Appendix F, Table F-1
   - — External dose rate from gamma radiation from the K-65 silos as a function of distance from the source. Appendix G, Table G-1
2. Age-dependent physiological data
   - — Breathing rates. Appendix I, Table I-4
   - — Consumption of drinking water Appendix I, Table I-5

— Consumption of basic food types. Appendix I, Table I-6

3. Ambient atmospheric dust loadings. Used, together with model-predicted concentrations of radionuclides in soil, to estimate concentrations of resuspended radionuclides in ambient air. Appendix D, Table D-2

DOSE ESTIMATES FOR THE NINE SCENARIOS

The nominal estimates of dose for the nine scenarios are tabulated in considerable breakdown detail in Table K-2. By nominal, we mean that the estimate is based on a deterministic calculation and does not represent the mean, 50th percentile, or other central measure of an uncertainty distribution. Each entry in Table K-2 is a cumulative value for all years of exposure experienced by the subject of a scenario. The table is a reproduction of a computer spreadsheet that contains the several components of dose to a list of target organs for each scenario. The columns of Table K-2 are arranged according to the outline given in the introductory discussion of this appendix.

Note that for each organ listed in Table K-2, except for the effective dose (ICRP 1991), there are two lines in the table. The first of the two lines contains estimates of absorbed dose (marked with the abbreviation "Ab" and given in units of gray or Gy) and (where it is applicable) gives the low-LET and high-LET components (LET means linear energy transfer; see Appendix I). External doses consisting of gamma and x-rays are exclusively low-LET, whereas internal dose from alpha emitting radionuclides generally contains a component of low-LET in addition to a component of high-LET radiation. The breakdown into these two components is important in analyzing risk.

The second of the two lines associated with an organ in Table K-2 (marked DE and given in units of sievert or Sv) expresses dose to the organ in terms of dose equivalent, which is a weighted sum of the low-LET and high-LET components, where the weights are quality factors corresponding to the respective radiation types. In accordance with the recommendation of ICRP Publication 26 (ICRP 1977) and ICRP Publication 60 (ICRP 1991), the quality factor for photon emissions (gamma rays and x-rays) and electrons (beta rays and positrons) is 1, and the quality factor for alpha emissions is 20. Thus, for the emissions represented in Table K-2, low-LET emissions are weighted 1 and high-LET emissions are weighted 20 (dose equivalent = 1×low-LET absorbed dose + 20×high-LET absorbed dose). For radon decay products, the preponderant component of dose is high-LET, and consequently the two lines in the radon column differ by a factor of 20. The quality factor scheme just described for dose equivalent is broadly correlated with the risk of fatal cancer associated with each type of radiation, but the risk analysis for this study proceeds directly from an analysis of low- and high-LET components of absorbed dose to different organs and tissues. The dose equivalent values are presented here because of their prevalence in environmental dosimetry and their familiarity to many readers.

Table K-3 illustrates the annual accumulation of the components of the dose to the subject of scenario 1. The table shows a breakdown of dose to the lungs by years of plant operation (1951–1988, column 1). The breakdown by columns is the same for Tables K-2 and K-3. This annual resolution of the calculation is required for epidemiological power and risk analysis. A table similar to Table K-3 could be produced for each scenario and each target organ, but much of the time-trend information is shown more clearly in Figures K-2 through K-4.

Table K-2. Cumulative Radiation Dose Estimates for the Nine Scenarios

		Airborne particulates				Ingestion		External (low LET)				Uranium	Radon
	Dose											total DE	progeny
Target	type	Primary		Resuspended						Ground	K-65	(Sv)	(high LET)
organ	and units	Low LET	High LET	Low LET	High LET	Low LET	High LET	Air	Water	Surface	Silos		
Scenario 1													
Lung	Ab (Gy)	1.3E-3	1.8E-2	1.8E-5	2.4E-4	4.4E-7	3.2E-6	1.8E-3	5.2E-13	4.8E-6	1.0E-9		1.5E-1
	DE (Sv)	3.5E-1		4.9E-3		6.5E-5		1.8E-3	5.2E-13	4.8E-6	1.0E-9	3.6E-1	3.0
Bone	Ab (Gy)	1.0E-4	3.4E-3	4.7E-7	3.6E-5	4.0E-4	2.1E-3	2.0E-3	7.8E-13	7.2E-6	1.4E-9		
	DE (Sv)	6.8E-2		7.1E-4		4.3E-2		2.0E-3	7.8E-13	7.2E-6	1.4E-9	1.1E-1	
Kidney	Ab (Gy)	9.6E-6	9.8E-5	3.8E-8	3.5E-7	3.9E-5	4.2E-4	1.8E-3	4.9E-13	4.3E-6	1.0E-9		
	DE (Sv)	2.0E-3		7.1E-6		8.4E-3		1.8E-3	4.9E-13	4.3E-6	1.0E-9	1.2E-2	
Liver	Ab (Gy)	1.7E-6	7.6E-6	1.8E-8	8.2E-8	5.9E-7	5.3E-6	1.7E-3	4.8E-13	4.2E-6	1.0E-9		
	DE (Sv)	1.5E-4		1.7E-6		1.1E-4		1.7E-3	4.8E-13	4.2E-6	1.0E-9	2.0E-3	
Ovaries	Ab (Gy)	3.6E-7	1.3E-6	3.1E-9	1.1E-8	9.8E-7	3.3E-6	1.6E-3	4.2E-13	3.8E-6	9.6E-10		
	DE (Sv)	2.7E-5		2.2E-7		6.6E-5		1.6E-3	4.2E-13	3.8E-6	9.6E-10	1.7E-3	
Rmarrow	Ab (Gy)	2.9E-5	4.0E-4	1.6E-7	4.3E-6	1.0E-4	1.6E-4	1.8E-3	5.0E-13	4.4E-6	1.1E-9		
	DE (Sv)	8.0E-3		8.5E-5		3.2E-3		1.8E-3	5.0E-13	4.4E-6	1.1E-9	1.3E-2	
Testes	Ab (Gy)	2.3E-7	1.3E-6	1.8E-9	1.1E-8	4.4E-7	3.2E-6	2.3E-3	7.3E-13	7.7E-6	1.1E-9		
	DE (Sv)	2.7E-5		2.2E-7		6.5E-5		2.3E-3	7.3E-13	7.7E-6	1.1E-9	2.4E-3	
Effective	DE (Sv)	4.3E-2		5.9E-4		1.2E-3		2.0E-3	6.4E-13	7.2E-6	1.1E-9	4.7E-2	
Scenario 2													
Lung	Ab (Gy)	3.7E-4	5.0E-3	5.3E-6	7.1E-5	1.3E-7	1.1E-6	1.6E-3	2.2E-12	1.7E-6	2.1E-6		1.5E-1
	DE (Sv)	1.0E-1		1.4E-3		2.2E-5		1.6E-3	2.2E-12	1.7E-6	2.1E-6	1.0E-1	3.0
Bone	Ab (Gy)	2.2E-5	9.1E-4	1.3E-7	9.6E-6	1.5E-4	7.4E-4	1.8E-3	3.3E-12	2.5E-6	2.9E-6		
	DE (Sv)	1.8E-2		1.9E-4		1.5E-2		1.8E-3	3.3E-12	2.5E-6	2.9E-6	3.5E-2	
Kidney	Ab (Gy)	2.0E-6	2.0E-5	1.1E-8	1.0E-7	1.4E-5	1.5E-4	1.6E-3	2.1E-12	1.5E-6	2.1E-6		
	DE (Sv)	4.1E-4		2.0E-6		3.1E-3		1.6E-3	2.1E-12	1.5E-6	2.1E-6	5.1E-3	
Liver	Ab (Gy)	4.9E-7	2.3E-6	5.2E-9	2.5E-8	1.8E-7	2.0E-6	1.5E-3	2.0E-12	1.5E-6	2.1E-6		
	DE (Sv)	4.7E-5		5.0E-7		4.0E-5		1.5E-3	2.0E-12	1.5E-6	2.1E-6	1.6E-3	
Ovaries	Ab (Gy)	9.9E-8	3.6E-7	9.2E-10	3.2E-9	3.4E-7	1.1E-6	1.4E-3	1.7E-12	1.3E-6	2.0E-6		
	DE (Sv)	7.2E-6		6.4E-8		2.3E-5		1.4E-3	1.7E-12	1.3E-6	2.0E-6	1.4E-3	
Rmarrow	Ab (Gy)	6.3E-6	1.2E-4	4.2E-8	1.2E-6	3.7E-5	5.9E-5	1.7E-3	2.1E-12	1.5E-6	2.2E-6		
	DE (Sv)	2.3E-3		2.4E-5		1.2E-3		1.7E-3	2.1E-12	1.5E-6	2.2E-6	5.2E-3	
Testes	Ab (Gy)	6.1E-8	3.6E-7	5.3E-10	3.2E-9	1.3E-7	1.1E-6	2.1E-3	3.1E-12	2.7E-6	2.3E-6		
	DE (Sv)	7.3E-6		6.5E-8		2.2E-5		2.1E-3	3.1E-12	2.7E-6	2.3E-6	2.1E-3	
Effective	DE (Sv)	1.2E-2		1.7E-4		4.7E-4		1.8E-3	2.7E-12	2.5E-6	2.2E-6	1.4E-2	
Scenario 3													
Lung	Ab (Gy)	3.3E-4	4.4E-3	5.2E-6	7.0E-5	2.9E-6	2.1E-5	1.2E-3	2.2E-12	1.6E-6	1.4E-8		1.1E-1
	DE (Sv)	8.9E-2		1.4E-3		4.3E-4		1.2E-3	2.2E-12	1.6E-6	1.4E-8	9.2E-2	2.1
Bone	Ab (Gy)	1.9E-5	8.8E-4	1.3E-7	9.6E-6	1.0E-3	1.1E-2	1.4E-3	3.3E-12	2.4E-6	1.9E-8		
	DE (Sv)	1.8E-2		1.9E-4		2.1E-1		1.4E-3	3.3E-12	2.4E-6	1.9E-8	2.3E-1	
Kidney	Ab (Gy)	1.8E-6	1.7E-5	1.1E-8	9.9E-8	2.0E-4	2.0E-3	1.2E-3	2.1E-12	1.5E-6	1.4E-8		
	DE (Sv)	3.5E-4		2.0E-6		4.1E-2		1.2E-3	2.1E-12	1.5E-6	1.4E-8	4.3E-2	
Liver	Ab (Gy)	4.4E-7	2.2E-6	5.2E-9	2.5E-8	3.7E-6	5.1E-5	1.2E-3	2.0E-12	1.4E-6	1.4E-8		
	DE (Sv)	4.5E-5		5.0E-7		1.0E-3		1.2E-3	2.0E-12	1.4E-6	1.4E-8	2.2E-3	
Ovaries	Ab (Gy)	8.9E-8	3.3E-7	9.1E-10	3.2E-9	6.7E-6	2.2E-5	1.1E-3	1.7E-12	1.3E-6	1.3E-8		
	DE (Sv)	6.7E-6		6.4E-8		4.5E-4		1.1E-3	1.7E-12	1.3E-6	1.3E-8	1.6E-3	
Rmarrow	Ab (Gy)	5.6E-6	1.2E-4	4.2E-8	1.3E-6	6.6E-4	1.8E-3	1.3E-3	2.1E-12	1.5E-6	1.5E-8		
	DE (Sv)	2.4E-3		2.5E-5		3.7E-2		1.3E-3	2.1E-12	1.5E-6	1.5E-8	4.1E-2	
Testes	Ab (Gy)	5.4E-8	3.3E-7	5.2E-10	3.2E-9	2.9E-6	2.2E-5	1.6E-3	3.1E-12	2.6E-6	1.5E-8		
	DE (Sv)	6.7E-6		6.5E-8		4.3E-4		1.6E-3	3.1E-12	2.6E-6	1.5E-8	2.0E-3	
Effective	DE (Sv)	1.1E-2		1.7E-4		1.3E-2		1.4E-3	2.7E-12	2.4E-6	1.4E-8	2.6E-2	

Figure K-2 shows annual releases of uranium (Voillequé et al. 1995) and scenario 1 dose response curves for the lungs, bone surfaces, and kidneys. The subject of scenario 1 lived at the same location in the assessment domain (about 1.7 km NE of the center of the production area) throughout the entire period of plant operation, although her school environment (about 4 km NE of the center of the production area; see Appendix J) exposed her to different dose rates from those she would have experienced at home. Her exposure to uranium was greatest during the 1950s and early 1960s when releases peaked, but the dose from each increment of intake (e.g., intake from one day's exposure) is accrued over a longer period because of the retention of some radionuclides in the body. The result is a smoothing of the annual dose curves relative to the uranium release curve. Some long-lived radionuclides, such as uranium, are removed more slowly from bone than from soft tissues, and the effect shown by Figure K-2 is a longer buildup and much more gradual decrease of annual dose, even after the uranium release has

Table K-2. Cumulative Radiation Dose Estimates for the Nine Scenarios (continued)

		Airborne particulates				Ingestion		External (low LET)				Uranium	Radon
	Dose											total DE	progeny
Target	type	Primary		Resuspended						Ground	K-65	(Sv)	(high LET)
organ	and units	Low LET	High LET	Low LET	High LET	Low LET	High LET	Air	Water	Surface	Silos		
Scenario 4													
Lung	Ab (Gy)	1.3E-4	1.7E-3	1.8E-6	2.4E-5	2.9E-7	1.9E-6	6.7E-4	1.8E-13	1.1E-6	5.4E-17		6.2E-2
	DE (Sv)	3.5E-2		4.9E-4		3.8E-5		6.7E-4	1.8E-13	1.1E-6	5.4E-17	3.6E-2	1.2
Bone	Ab (Gy)	6.4E-6	3.4E-4	4.1E-8	2.5E-6	1.7E-4	2.0E-3	7.4E-4	2.6E-13	1.6E-6	7.3E-17		
	DE (Sv)	6.8E-3		5.1E-5		4.0E-2		7.4E-4	2.6E-13	1.6E-6	7.3E-17	4.8E-2	
Kidney	Ab (Gy)	4.8E-7	4.6E-6	3.5E-9	3.3E-8	8.5E-6	8.9E-5	6.6E-4	1.6E-13	9.5E-7	5.3E-17		
	DE (Sv)	9.3E-5		6.6E-7		1.8E-3		6.6E-4	1.6E-13	9.5E-7	5.3E-17	2.6E-3	
Liver	Ab (Gy)	1.8E-7	9.5E-7	1.8E-9	8.3E-9	5.0E-7	8.8E-6	6.3E-4	1.6E-13	9.3E-7	5.2E-17		
	DE (Sv)	1.9E-5		1.7E-7		1.8E-4		6.3E-4	1.6E-13	9.3E-7	5.2E-17	8.3E-4	
Ovaries	Ab (Gy)	3.4E-8	1.2E-7	3.1E-10	1.0E-9	1.2E-6	1.9E-6	5.9E-4	1.4E-13	8.3E-7	4.9E-17		
	DE (Sv)	2.5E-6		2.1E-8		3.9E-5		5.9E-4	1.4E-13	8.3E-7	4.9E-17	6.3E-4	
Rmarrow	Ab (Gy)	1.9E-6	5.3E-5	1.4E-8	4.0E-7	3.9E-5	3.3E-4	6.8E-4	1.7E-13	9.7E-7	5.5E-17		
	DE (Sv)	1.1E-3		8.0E-6		6.7E-3		6.8E-4	1.7E-13	9.7E-7	5.5E-17	8.5E-3	
Testes	Ab (Gy)	2.0E-8	1.3E-7	1.9E-10	1.1E-9	3.3E-7	1.9E-6	8.8E-4	2.5E-13	1.7E-6	5.8E-17		
	DE (Sv)	2.6E-6		2.2E-8		3.8E-5		8.8E-4	2.5E-13	1.7E-6	5.8E-17	9.2E-4	
Effective	DE (Sv)	4.1E-3		5.6E-5		1.5E-3		7.5E-4	2.2E-13	1.6E-6	5.4E-17	6.4E-3	
Scenario 5													
Lung	Ab (Gy)	1.1E-4	1.4E-3	1.5E-6	2.0E-5	3.0E-9	1.7E-8	1.9E-4	0	4.6E-7	1.1E-20		1.6E-2
	DE (Sv)	2.9E-2		4.1E-4		3.4E-7		1.9E-4	0	4.6E-7	1.1E-20	3.0E-2	3.2E-1
Bone	Ab (Gy)	6.0E-6	2.6E-4	3.7E-8	2.8E-6	8.4E-7	1.3E-5	2.0E-4	0	7.0E-7	1.5E-20		
	DE (Sv)	5.3E-3		5.7E-5		2.6E-4		2.0E-4	0	7.0E-7	1.5E-20	5.8E-3	
Kidney	Ab (Gy)	5.7E-7	5.7E-6	3.0E-9	2.9E-8	7.3E-8	7.4E-7	1.8E-4	0	4.2E-7	1.1E-20		
	DE (Sv)	1.1E-4		5.7E-7		1.5E-5		1.8E-4	0	4.2E-7	1.1E-20	3.1E-4	
Liver	Ab (Gy)	1.4E-7	7.0E-7	1.5E-9	7.4E-9	4.2E-9	4.5E-8	1.7E-4	0	4.1E-7	1.0E-20		
	DE (Sv)	1.4E-5		1.5E-7		9.0E-7		1.7E-4	0	4.1E-7	1.0E-20	1.9E-4	
Ovaries	Ab (Gy)	2.8E-8	1.0E-7	2.6E-10	9.3E-10	1.2E-8	1.7E-8	1.6E-4	0	3.7E-7	9.9E-21		
	DE (Sv)	2.1E-6		1.9E-8		3.6E-7		1.6E-4	0	3.7E-7	9.9E-21	1.6E-4	
Rmarrow	Ab (Gy)	1.8E-6	3.4E-5	1.2E-8	3.6E-7	2.1E-7	1.6E-6	1.9E-4	0	4.3E-7	1.1E-20		
	DE (Sv)	6.8E-4		7.2E-6		3.3E-5		1.9E-4	0	4.3E-7	1.1E-20	9.1E-4	
Testes	Ab (Gy)	1.7E-8	1.0E-7	1.5E-10	9.4E-10	3.4E-9	1.7E-8	2.4E-4	0	7.5E-7	1.2E-20		
	DE (Sv)	2.1E-6		1.9E-8		3.4E-7		2.4E-4	0	7.5E-7	1.2E-20	2.4E-4	
Effective	DE (Sv)	3.5E-3		4.9E-5		1.3E-5		2.1E-4	0	7.0E-7	1.1E-20	3.8E-3	
Scenario 6													
Lung	Ab (Gy)	6.7E-4	9.0E-3	8.9E-6	1.2E-4	2.7E-7	1.8E-6	1.2E-3	5.2E-13	2.4E-6	1.5E-13		9.8E-2
	DE (Sv)	1.8E-1		2.4E-3		3.6E-5		1.2E-3	5.2E-13	2.4E-6	1.5E-13	1.8E-1	2.0
Bone	Ab (Gy)	5.4E-5	1.7E-3	2.3E-7	1.8E-5	2.0E-4	1.1E-3	1.3E-3	7.7E-13	3.6E-6	2.0E-13		
	DE (Sv)	3.5E-2		3.5E-4		2.2E-2		1.3E-3	7.7E-13	3.6E-6	2.0E-13	5.9E-2	
Kidney	Ab (Gy)	5.0E-6	5.1E-5	1.9E-8	1.8E-7	1.9E-5	2.0E-4	1.2E-3	4.8E-13	2.1E-6	1.5E-13		
	DE (Sv)	1.0E-3		3.5E-6		4.1E-3		1.2E-3	4.8E-13	2.1E-6	1.5E-13	6.3E-3	
Liver	Ab (Gy)	8.9E-7	3.9E-6	8.8E-9	4.1E-8	3.4E-7	3.0E-6	1.1E-3	4.7E-13	2.1E-6	1.4E-13		
	DE (Sv)	7.9E-5		8.2E-7		6.0E-5		1.1E-3	4.7E-13	2.1E-6	1.4E-13	1.2E-3	
Ovaries	Ab (Gy)	1.9E-7	6.9E-7	1.6E-9	5.4E-9	5.6E-7	1.8E-6	1.1E-3	4.1E-13	1.9E-6	1.4E-13		
	DE (Sv)	1.4E-5		1.1E-7		3.7E-5		1.1E-3	4.1E-13	1.9E-6	1.4E-13	1.2E-3	
Rmarrow	Ab (Gy)	1.5E-5	2.1E-4	7.7E-8	2.1E-6	5.1E-5	8.5E-5	1.2E-3	4.9E-13	2.2E-6	1.5E-13		
	DE (Sv)	4.1E-3		4.2E-5		1.8E-3		1.2E-3	4.9E-13	2.2E-6	1.5E-13	7.1E-3	
Testes	Ab (Gy)	1.2E-7	6.9E-7	8.8E-10	5.4E-9	2.6E-7	1.8E-6	1.6E-3	7.2E-13	3.8E-6	1.6E-13		
	DE (Sv)	1.4E-5		1.1E-7		3.6E-5		1.6E-3	7.2E-13	3.8E-6	1.6E-13	1.7E-3	
Effective	DE (Sv)	2.2E-2		2.9E-4		6.5E-4		1.3E-3	6.4E-13	3.6E-6	1.5E-13	2.4E-2	

declined drastically. The dosimetric data for each year take account of the subject's age during that year, but this effect is not obvious in Figure K-2.

Figure K-3 compares radon release from the K-65 silos over time with the dose from radon decay products to the tracheobronchial epithelium (TBE) for the subject of scenario 1. This figure shows a much clearer correlation of annual radon dose with annual radon release because of the short half-lives of the radon decay products. The annual dose curve shows some effect of age dependence in the years before 1966 (the year when the subject was 20 years of age), with annual doses that are higher relative to emissions than for subsequent years. In 1979, the

Table K-2. Cumulative Radiation Dose Estimates for the Nine Scenarios (continued)

		Airborne particulates				Ingestion		External (low LET)				Uranium	Radon
	Dose											total DE	progeny
Target	type	Primary		Resuspended						Ground	K-65	(Sv)	(high LET)
organ	and units	Low LET	High LET	Low LET	High LET	Low LET	High LET	Air	Water	Surface	Silos		
Scenario 7													
Lung	Ab (Gy)	9.8E-5	1.3E-3	1.5E-6	2.0E-5	1.8E-7	8.8E-7	1.5E-4	6.8E-13	4.4E-7	1.3E-19		1.4E-2
	DE (Sv)	2.7E-2		4.1E-4		1.8E-5		1.5E-4	6.8E-13	4.4E-7	1.3E-19	2.8E-2	2.7E-1
Bone	Ab (Gy)	5.3E-6	2.5E-4	3.8E-8	2.8E-6	3.6E-5	3.2E-4	1.7E-4	1.0E-12	6.7E-7	1.7E-19		
	DE (Sv)	4.9E-3		5.6E-5		6.4E-3		1.7E-4	1.0E-12	6.7E-7	1.7E-19	1.2E-2	
Kidney	Ab (Gy)	4.8E-7	4.8E-6	3.0E-9	2.9E-8	3.2E-6	3.3E-5	1.5E-4	6.4E-13	4.0E-7	1.3E-19		
	DE (Sv)	9.7E-5		5.7E-7		6.5E-4		1.5E-4	6.4E-13	4.0E-7	1.3E-19	9.0E-4	
Liver	Ab (Gy)	1.3E-7	6.4E-7	1.5E-9	7.3E-9	2.0E-7	1.6E-6	1.4E-4	6.2E-13	3.9E-7	1.2E-19		
	DE (Sv)	1.3E-5		1.5E-7		3.3E-5		1.4E-4	6.2E-13	3.9E-7	1.2E-19	1.9E-4	
Ovaries	Ab (Gy)	2.6E-8	9.3E-8	2.6E-10	9.1E-10	3.2E-7	8.9E-7	1.3E-4	5.4E-13	3.5E-7	1.2E-19		
	DE (Sv)	1.9E-6		1.9E-8		1.8E-5		1.3E-4	5.4E-13	3.5E-7	1.2E-19	1.5E-4	
Rmarrow	Ab (Gy)	1.5E-6	3.1E-5	1.2E-8	3.5E-7	1.1E-5	3.9E-5	1.5E-4	6.4E-13	4.1E-7	1.3E-19		
	DE (Sv)	6.2E-4		7.0E-6		7.8E-4		1.5E-4	6.4E-13	4.1E-7	1.3E-19	1.6E-3	
Testes	Ab (Gy)	1.5E-8	9.3E-8	1.5E-10	9.3E-10	1.8E-7	8.9E-7	2.0E-4	9.5E-13	7.1E-7	1.4E-19		
	DE (Sv)	1.9E-6		1.9E-8		1.8E-5		2.0E-4	9.5E-13	7.1E-7	1.4E-19	2.2E-4	
Effective	DE (Sv)	3.3E-3		4.9E-5		2.3E-4		1.7E-4	8.4E-13	6.6E-7	1.3E-19	3.7E-3	
Scenario 8													
Lung	Ab (Gy)	1.9E-5	2.5E-4	2.4E-7	3.2E-6	4.4E-9	2.3E-8	1.8E-4	0	1.1E-7	2.0E-18		1.9E-2
	DE (Sv)	5.1E-3		6.4E-5		4.7E-7		1.8E-4	0	1.1E-7	2.0E-18	5.3E-3	3.8E-1
Bone	Ab (Gy)	4.3E-7	2.0E-5	2.4E-9	1.2E-7	8.4E-7	6.0E-6	1.9E-4	0	1.7E-7	2.7E-18		
	DE (Sv)	3.9E-4		2.3E-6		1.2E-4		1.9E-4	0	1.7E-7	2.7E-18	7.0E-4	
Kidney	Ab (Gy)	7.0E-8	7.0E-7	3.8E-10	3.6E-9	1.3E-7	1.3E-6	1.7E-4	0	1.0E-7	2.0E-18		
	DE (Sv)	1.4E-5		7.2E-8		2.7E-5		1.7E-4	0	1.0E-7	2.0E-18	2.1E-4	
Liver	Ab (Gy)	1.7E-8	9.7E-8	1.7E-10	7.1E-10	5.6E-9	4.3E-8	1.7E-4	0	1.0E-7	1.9E-18		
	DE (Sv)	2.0E-6		1.4E-8		8.7E-7		1.7E-4	0	1.0E-7	1.9E-18	1.7E-4	
Ovaries	Ab (Gy)	3.6E-9	1.4E-8	3.0E-11	9.2E-11	1.1E-8	2.4E-8	1.6E-4	0	8.9E-8	1.9E-18		
	DE (Sv)	2.8E-7		1.9E-9		4.8E-7		1.6E-4	0	8.9E-8	1.9E-18	1.6E-4	
Rmarrow	Ab (Gy)	2.2E-7	4.5E-6	1.3E-9	3.0E-8	3.5E-7	1.1E-6	1.8E-4	0	1.0E-7	2.1E-18		
	DE (Sv)	9.0E-5		6.0E-7		2.2E-5		1.8E-4	0	1.0E-7	2.1E-18	2.9E-4	
Testes	Ab (Gy)	2.2E-9	1.4E-8	1.8E-11	9.2E-11	4.4E-9	2.3E-8	2.3E-4	0	1.8E-7	2.2E-18		
	DE (Sv)	2.7E-7		1.9E-9		4.7E-7		2.3E-4	0	1.8E-7	2.2E-18	2.3E-4	
Effective	DE (Sv)	4.7E-4		6.1E-6		8.2E-6		2.0E-4	0	1.7E-7	2.0E-18	6.8E-4	
Scenario 9													
Lung	Ab (Gy)	2.1E-4	2.9E-3	3.0E-6	4.1E-5	3.5E-9	2.1E-8	3.0E-4	0	9.5E-7	1.3E-19		2.9E-2
	DE (Sv)	5.8E-2		8.3E-4		4.3E-7		3.0E-4	0	9.5E-7	1.3E-19	5.9E-2	5.7E-1
Bone	Ab (Gy)	1.3E-5	4.8E-4	7.9E-8	5.6E-6	1.3E-6	1.9E-5	3.3E-4	0	1.4E-6	1.7E-19		
	DE (Sv)	9.7E-3		1.1E-4		3.7E-4		3.3E-4	0	1.4E-6	1.7E-19	1.1E-2	
Kidney	Ab (Gy)	1.2E-6	1.2E-5	6.2E-9	5.9E-8	1.3E-7	1.3E-6	3.0E-4	0	8.6E-7	1.3E-19		
	DE (Sv)	2.4E-4		1.2E-6		2.6E-5		3.0E-4	0	8.6E-7	1.3E-19	5.7E-4	
Liver	Ab (Gy)	2.8E-7	1.3E-6	3.0E-9	1.4E-8	5.2E-9	6.2E-8	2.8E-4	0	8.4E-7	1.2E-19		
	DE (Sv)	2.6E-5		2.9E-7		1.2E-6		2.8E-4	0	8.4E-7	1.2E-19	3.1E-4	
Ovaries	Ab (Gy)	5.7E-8	2.0E-7	5.3E-10	1.8E-9	1.8E-8	2.2E-8	2.6E-4	0	7.5E-7	1.2E-19		
	DE (Sv)	4.0E-6		3.7E-8		4.6E-7		2.6E-4	0	7.5E-7	1.2E-19	2.7E-4	
Rmarrow	Ab (Gy)	3.6E-6	5.7E-5	2.4E-8	6.8E-7	3.3E-7	2.4E-6	3.0E-4	0	8.7E-7	1.3E-19		
	DE (Sv)	1.1E-3		1.4E-5		4.8E-5		3.0E-4	0	8.7E-7	1.3E-19	1.5E-3	
Testes	Ab (Gy)	3.5E-8	2.0E-7	3.1E-10	1.8E-9	4.1E-9	2.1E-8	3.9E-4	0	1.5E-6	1.4E-19		
	DE (Sv)	4.0E-6		3.7E-8		4.3E-7		3.9E-4	0	1.5E-6	1.4E-19	4.0E-4	
Effective	DE (Sv)	7.1E-3		1.0E-4		1.9E-5		3.4E-4	0	1.4E-6	1.3E-19	7.6E-3	

K-65 silos were sealed, reducing the rates of emission and consequent dose by more than an order of magnitude.

Table K-4 is the principal summary of dose from uranium and associated radionuclides to the subjects of scenarios 1–9 with propagated uncertainties. Each dose estimate represents the median (50th percentile) of the total and cumulative dose to the individual, i.e., total of all components (such as inhalation, ingestion, and direct external dose) and cumulative over all years of plant operation (1951–1988). The propagated uncertainty from all applicable sources (e.g., release, atmospheric dispersion, and GARDEN model parameters) is indicated by the 5th and 95th percentiles of the distribution, which are included in Table K-4. The dose is shown for the lungs, bone surfaces, kidneys, liver, red marrow, testes, and ovaries, and the effective dose to the whole body is also recorded, although (as we have mentioned previously)

Table K-3. Absorbed Dose (Gy) by Year to the Subject of Scenario 1

Year	Airborne particulates				Ingestion		External				Radon
	Primary		Resuspended						Ground		
	Low LET	High LET	Low LET	High LET	Low LET	High LET	Air	Water	surface	K-65 silos	
1951	2.6E-8	3.3E-7	1.1E-10	1.4E-9	2.7E-11	2.0E-10	8.8E-7	0	1.4E-10	0	7.9E-5
1952	2.1E-7	3.0E-6	2.2E-9	2.8E-8	5.8E-10	4.8E-9	2.3E-5	2.0E-14	1.9E-9	7.5E-13	2.3E-3
1953	9.1E-6	1.2E-4	7.1E-8	9.1E-7	4.8E-9	3.9E-8	4.0E-5	3.4E-14	7.8E-8	5.0E-11	4.5E-3
1954	5.3E-5	7.0E-4	4.6E-7	6.1E-6	3.1E-8	2.1E-7	5.2E-5	3.2E-14	3.1E-7	5.3E-11	6.2E-3
1955	1.1E-4	1.5E-3	1.0E-6	1.4E-5	6.3E-8	4.8E-7	5.2E-5	2.3E-14	5.6E-7	5.3E-11	6.6E-3
1956	1.1E-4	1.4E-3	1.2E-6	1.6E-5	4.3E-8	3.1E-7	5.2E-5	2.9E-14	4.3E-7	5.3E-11	6.6E-3
1957	9.3E-5	1.2E-3	1.3E-6	1.7E-5	3.8E-8	2.6E-7	5.1E-5	2.9E-14	3.4E-7	8.3E-11	6.5E-3
1958	8.2E-5	1.1E-3	1.2E-6	1.6E-5	2.5E-8	2.0E-7	5.4E-5	1.6E-14	3.1E-7	8.4E-11	6.5E-3
1959	8.0E-5	1.1E-3	1.3E-6	1.7E-5	2.5E-8	2.0E-7	6.3E-5	2.3E-14	3.3E-7	8.4E-11	7.1E-3
1960	7.5E-5	1.0E-3	1.2E-6	1.6E-5	2.5E-8	2.0E-7	6.3E-5	8.1E-14	3.4E-7	8.4E-11	7.1E-3
1961	7.9E-5	1.1E-3	1.3E-6	1.7E-5	2.3E-8	1.9E-7	6.3E-5	6.8E-14	3.8E-7	8.4E-11	6.2E-3
1962	7.4E-5	1.0E-3	1.2E-6	1.6E-5	1.9E-8	1.6E-7	6.3E-5	5.7E-14	2.6E-7	8.4E-11	5.8E-3
1963	7.1E-5	9.7E-4	1.1E-6	1.5E-5	1.5E-8	1.2E-7	6.3E-5	7.7E-14	2.5E-7	8.4E-11	5.4E-3
1964	6.3E-5	8.6E-4	9.6E-7	1.3E-5	2.0E-8	1.4E-7	6.6E-5	3.4E-14	2.0E-7	2.4E-11	5.8E-3
1965	5.1E-5	6.9E-4	7.7E-7	1.1E-5	1.6E-8	1.0E-7	6.9E-5	0	9.5E-8	7.3E-13	5.2E-3
1966	4.1E-5	5.5E-4	6.2E-7	8.4E-6	1.2E-8	8.1E-8	7.0E-5	0	5.8E-8	7.4E-13	4.8E-3
1967	3.6E-5	4.9E-4	5.3E-7	7.2E-6	1.0E-8	6.8E-8	7.0E-5	0	7.5E-8	7.4E-13	4.8E-3
1968	3.5E-5	4.7E-4	5.1E-7	6.8E-6	9.3E-9	6.3E-8	7.0E-5	0	1.0E-7	7.4E-13	4.8E-3
1969	2.8E-5	3.9E-4	4.2E-7	5.8E-6	7.7E-9	5.1E-8	7.0E-5	0	5.4E-8	7.4E-13	4.8E-3
1970	2.4E-5	3.3E-4	3.5E-7	4.8E-6	6.6E-9	4.4E-8	7.0E-5	0	3.7E-8	7.4E-13	4.8E-3
1971	2.0E-5	2.8E-4	2.9E-7	4.0E-6	6.4E-9	4.0E-8	7.0E-5	0	3.2E-8	7.4E-13	4.8E-3
1972	1.9E-5	2.6E-4	2.7E-7	3.7E-6	5.0E-9	3.3E-8	7.0E-5	0	5.5E-8	7.4E-13	4.8E-3
1973	1.9E-5	2.5E-4	2.7E-7	3.6E-6	4.5E-9	2.9E-8	7.0E-5	0	7.8E-8	7.4E-13	4.8E-3
1974	1.8E-5	2.5E-4	2.8E-7	3.6E-6	3.9E-9	2.6E-8	7.0E-5	0	8.8E-8	7.4E-13	4.8E-3
1975	1.9E-5	2.5E-4	2.9E-7	3.8E-6	3.6E-9	2.4E-8	7.0E-5	0	1.0E-7	7.4E-13	4.8E-3
1976	1.8E-5	2.4E-4	2.8E-7	3.7E-6	3.4E-9	2.2E-8	7.0E-5	0	8.9E-8	7.4E-13	4.8E-3
1977	1.5E-5	1.9E-4	2.3E-7	3.0E-6	3.5E-9	2.2E-8	7.0E-5	0	4.5E-8	7.4E-13	4.8E-3
1978	1.1E-5	1.4E-4	1.7E-7	2.3E-6	2.5E-9	1.6E-8	7.0E-5	0	1.1E-8	7.4E-13	4.8E-3
1979	8.5E-6	1.1E-4	1.3E-7	1.8E-6	2.2E-9	1.4E-8	4.0E-5	0	9.2E-9	1.2E-11	2.7E-3
1980	6.9E-6	9.3E-5	1.0E-7	1.4E-6	1.9E-9	1.2E-8	8.7E-6	0	6.9E-9	2.3E-11	6.5E-4
1981	5.8E-6	7.9E-5	8.5E-8	1.1E-6	1.8E-9	1.1E-8	8.7E-6	0	8.2E-9	2.3E-11	6.5E-4
1982	5.2E-6	6.9E-5	7.3E-8	9.7E-7	1.8E-9	1.1E-8	8.7E-6	0	1.0E-8	2.3E-11	6.5E-4
1983	4.6E-6	6.2E-5	6.2E-8	8.3E-7	1.9E-9	1.1E-8	8.7E-6	0	1.1E-8	2.3E-11	6.5E-4
1984	5.0E-6	6.7E-5	6.2E-8	8.2E-7	1.8E-9	1.0E-8	8.7E-6	0	2.1E-8	2.3E-11	6.5E-4
1985	4.1E-6	5.5E-5	5.0E-8	6.6E-7	1.7E-9	9.5E-9	8.7E-6	0	9.2E-9	2.3E-11	6.5E-4
1986	3.6E-6	4.8E-5	4.2E-8	5.6E-7	1.3E-9	7.8E-9	8.7E-6	0	8.4E-9	2.3E-11	6.5E-4
1987	3.0E-6	4.1E-5	3.5E-8	4.7E-7	1.8E-9	9.5E-9	3.6E-13	0	6.5E-9	2.3E-11	6.5E-4
1988	2.4E-6	3.3E-5	2.9E-8	3.9E-7	2.0E-9	1.0E-8	2.4E-6	0	4.5E-9	2.3E-11	1.8E-4
Totals:											
Ab (Gy)	1.3E-3	1.8E-2	1.8E-5	2.4E-4	4.4E-7	3.2E-6	1.8E-3	5.2E-13	4.8E-6	1.0E-9	1.5E-1
DE (Sv)	3.5E-1		4.9E-3		6.5E-5		1.8E-3	5.2E-13	4.8E-6	1.0E-9	3.0

no use of effective dose has been made for risk analysis. Table K-5 gives similar information for radon decay products, but the target tissue for the radon decay chain is restricted to the tracheobronchial epithelium.

Please note that the 50th percentiles in Tables K-4 and K-5 differ from the corresponding nominal values reported in previous tables. These percentiles are statistical estimates that depend in a nonlinear way on some of the uncertain model parameters. Also, arithmetic operations carried out on random variables in Monte Carlo modeling do not necessarily preserve distribution properties; for example, the 50th percentile of the sum of, say, 38 random variables with skewed distributions (representing dose in each year of FMPC operation), in general, is not the same as the sum of the 50th percentile of each of the random variables.

Even though we have not used the effective dose for risk analysis in this study, the effective

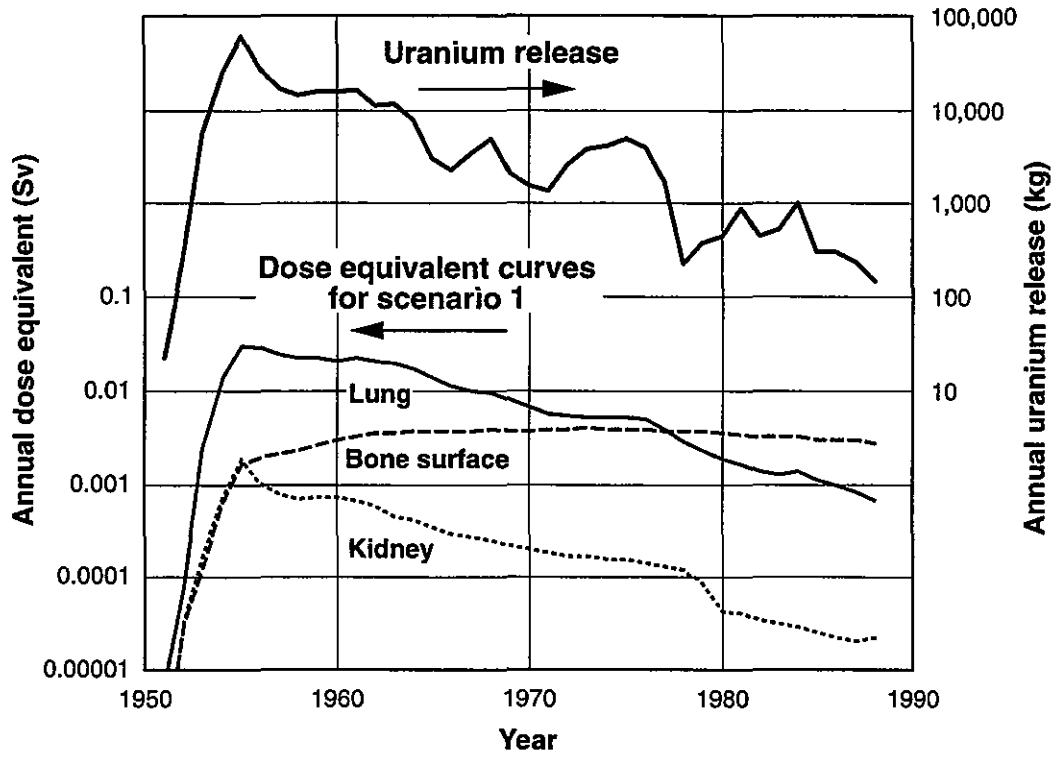

Figure K-2. Uranium organ doses for scenario 1, shown with uranium releases from the FMPC. The dose response curves correlate generally with the uranium releases over time but are smoothed by the accumulation of residual dose resulting from delayed removal of the radionuclides from the organs. Bone surfaces have a longer retention time for uranium than softer tissues and consequently show a response with a longer buildup and more gradual decrease.

dose is a useful measure for comparing combinations of exposures experienced by different individuals. Using this measure, we may easily compare exposures of subjects of the nine scenarios to sources of radiation originating at the FMPC. Figure K-4 shows the annual effective dose by year for each of the nine scenarios. The effective dose shown in the figure includes internal and external dose from uranium and associated radionuclides and the contribution of radon decay products to the dose to the tracheobronchial epithelium. The effective dose for inhaled radon decay products was calculated as the product of the dose equivalent to the tracheobronchial epithelium and the weighting factor $w_{TBE} = 0.08$ (ICRP 1981).

Figure K-4 provides some useful points of comparison. First, notice the general similarity of the trends expressed by the curves for all scenarios but 4, 8, and 9, except for the different vertical displacements of the curves. These vertical displacements are mainly the result of the distance of each subject's residence from the FMPC production area. The subjects of these six scenarios resided in the assessment domain throughout the years of plant operation (1951–1988), and their maximum age difference was five years (Table K-2). Except for scenario 5, all of these subjects had some consumption of locally contaminated food.

A comparison of Figures K-4 and K-3 shows the strong influence of the radon component on the effective dose. The abrupt decrease in annual dose between 1979 and 1980, when the

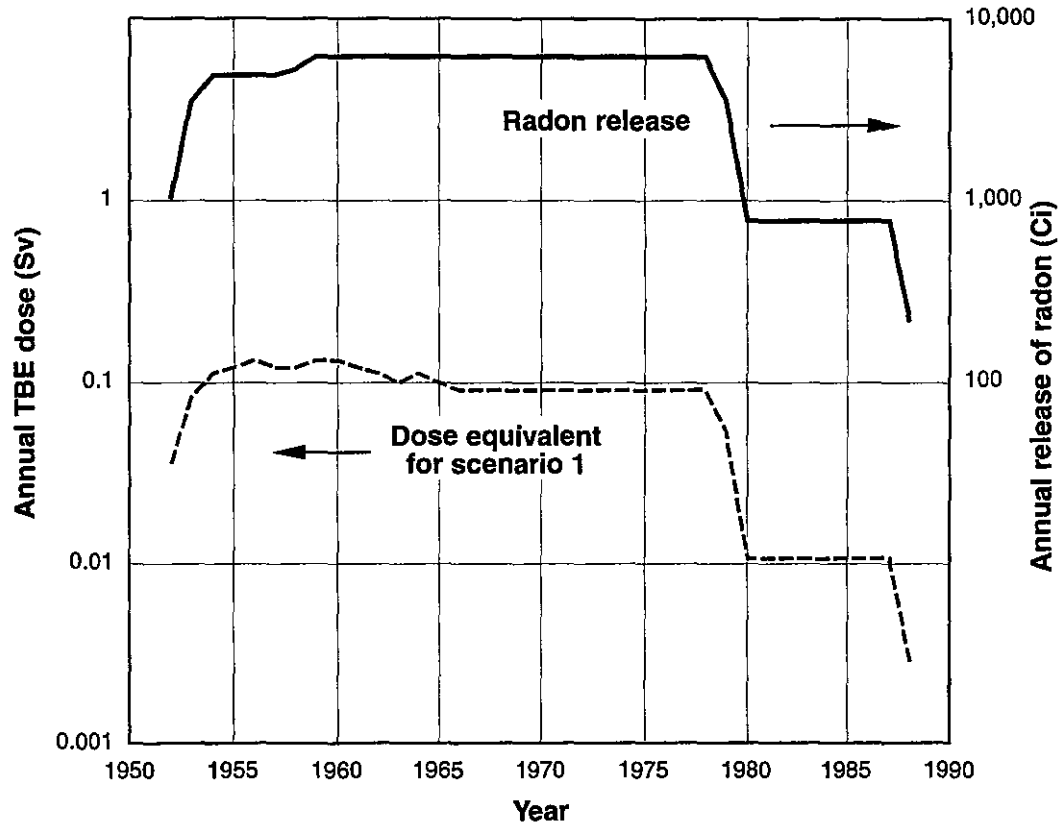

Figure K-3. Radon dose to the tracheobronchial epithelium for the subject of scenario 1, shown with radon release from the K-65 silos from 1952 through 1988. The period before 1966 shows the effect of age dependence of the dose.

K-65 silos were sealed, is visible in the curves for all scenarios except 9. This subject left the area in 1968.

Scenario 2 was originally intended to present the maximum radon exposure. The subject of scenario 1, however, turns out to have about the same cumulative dose from radon decay products because of the prevalence of the southwesterly winds that blew from the K-65 silos toward the home of this subject. Although subject 1 is five years older than subject 2, the two annual dose curves cross in the early 1960s. For most of the 1960s and 1970s, the annual dose for scenario 2 exceeds that for scenario 1; part of the explanation for this effect is the higher annual radon dose for the child-adolescent (scenario 2) during this period, who would have been 10 years old in 1961 (see Appendix I for a discussion of age dependence of radon dose).

The curve for scenario 9 in Figure K-4 shows a steep decline after 1968 because the subject finished high school in that year and left the assessment domain. After 1968, the curve shows only the annual increments of residual dose to which the subject was already committed by his exposure through 1968. This residual dose is principally from inhalation of uranium and other long-lived radionuclides. Radon decay products would show no residual dose because of their short half-lives.

The subject of scenario 3 regularly ingested water from a contaminated well during the South Plume migration, beginning in the middle 1960s. The passing of the uranium plume

Table K-4. Total and Cumulative Uranium[a] Dose (Sv) to Subjects of Scenarios 1–9 with Percentiles of Propagated Uncertainty Distribution

Scenario	Percentile	Target organ							
		Lung	Bone	Kidney	Liver	Red Marrow	Testes	Ovaries	Effective[b]
1	5	0.14	0.078	0.0064	0.00076	0.0094		0.00056	0.021
	50	0.46	0.17	0.016	0.0023	0.02		0.0019	0.061
	95	1.4	0.43	0.043	0.0085	0.051		0.0076	0.18
2	5	0.044	0.027	0.0033	0.00062	0.0036	0.00074		0.0074
	50	0.15	0.057	0.0071	0.0019	0.008	0.0024		0.021
	95	0.42	0.12	0.015	0.0071	0.021	0.0096		0.057
3	5	0.046	0.22	0.041	0.0016	0.04	0.0011		0.019
	50	0.13	0.26	0.045	0.0027	0.044	0.0027		0.031
	95	0.36	0.33	0.056	0.0066	0.054	0.0081		0.061
4	5	0.015	0.032	0.0016	0.00036	0.0057		0.00021	0.004
	50	0.048	0.075	0.0035	0.0011	0.013		0.00074	0.0093
	95	0.14	0.19	0.0087	0.0031	0.034		0.0025	0.022
5	5	0.012	0.0034	0.00017	0.00008	0.00056	0.00009		0.0017
	50	0.04	0.0095	0.00044	0.00024	0.0015	0.00029		0.0053
	95	0.11	0.025	0.0012	0.00084	0.0039	0.0012		0.014
6	5	0.078	0.043	0.0035	0.00047	0.005		0.00035	0.011
	50	0.24	0.091	0.0084	0.0015	0.011		0.0012	0.033
	95	0.67	0.22	0.021	0.0048	0.028		0.0044	0.088
7	5	0.013	0.0098	0.00069	0.00011	0.0013	0.0001		0.0021
	50	0.04	0.016	0.0012	0.00025	0.0022	0.00029		0.0055
	95	0.096	0.029	0.0022	0.00071	0.0041	0.00092		0.012
8	5	0.002	0.00044	0.0001	0.00005	0.00016	0.00007		0.0003
	50	0.007	0.0011	0.00027	0.00021	0.00043	0.00028		0.00096
	95	0.02	0.0033	0.001	0.00092	0.0014	0.0013		0.0025
9	5	0.025	0.0058	0.00032	0.00013	0.00094	0.00012		0.0035
	50	0.085	0.016	0.0008	0.0004	0.0023	0.00051		0.011
	95	0.24	0.044	0.0025	0.0017	0.0064	0.0023		0.03

[a] The doses include contributions from all radionuclides and decay products listed in Fig. K-1, except ^{222}Rn and its decay products.

[b] The effective doses in this table do not include radon decay products.

through the groundwater that supplied the subject's well is fairly obvious from the curve, although one has to look carefully at the figure to distinguish this curve from two others during this period. Scenario 3 is based on consumption of water from Well 15, which had the highest measured concentrations of the wells sampled. The part of scenario 3 that shows the peak and some of the decline is based on a conservative reconstruction of the earlier part of the period of plume migration, for which there were no data (see Appendix F and Appendix R; the latter appendix discusses the reconstruction of the concentration curve for the well and the chemical toxicity of uranium to the kidneys for scenario 3).

Scenarios 4 and 8 describe subjects who were born or came to live in the assessment domain after the peak releases of uranium in the middle 1950s. The subject of scenario 4 was born in 1960 and lived in Ross, about 4 km NE of the FMPC production area. She left the area after graduating from high school in 1978. The peculiar shape of the curve may show some dependence of the dose on age as the subject matured. Her breathing rate and respiratory tidal volume increased as she approached maturity, and these parameters increased her dose

Table K-5. Cumulative Dose (Sv) to Tracheobronchial Epithelium from Releases of Radon From the FMPC

		Percentiles of estimated dose		
Scenario	Nominal	5th	50th	95th
1	3.0	0.98	3.6	14
2	3.0	0.98	3.6	13
3	2.1	0.89	2.6	10
4	1.2	0.40	1.5	7.2
5	0.32	0.10	0.42	1.9
6	2.0	0.53	2.2	9.2
7	0.27	0.12	0.38	1.5
8	0.39	0.10	0.44	2.2
9	0.57	0.17	0.84	4.8

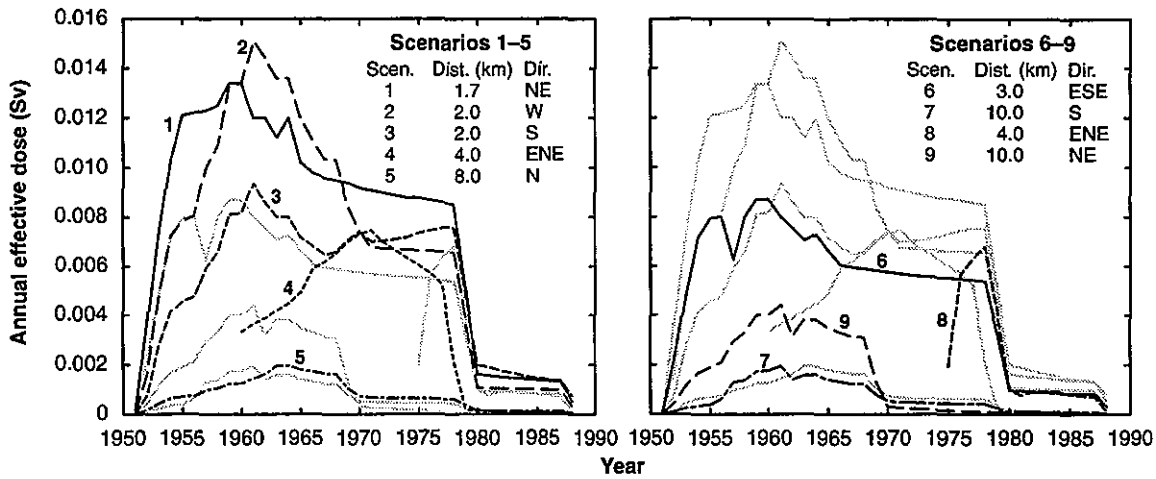

Figure K-4. Annual effective dose (Sv) for uranium and radon to the subjects of the nine scenarios. Distances and directions from the center of the FMPC production area are shown to illustrate the dependence of the dose on the subject's primary residence. Note that the subjects of scenarios 4 and 8 were born or moved to the assessment domain after the peak releases of the 1950s. The subject of scenario 9 left the area after high school graduation in 1968; residual dose from radon would have ceased promptly, but some dose from uranium retained in tissues would have continued to accrue.

from inhaled radioactivity. The radon component reaches a maximum at 10 years of age, in 1970, and declines gradually until maturity. After the subject's departure from the region in 1978, the annual dose decreases because it is sustained only by residual radioactivity from long-lived radionuclides in the body, with no new exposure. The subject of scenario 8 came, as a five-year-old child, to live in Ross in September 1975, when the dose curve begins (the low

dose for 1975 is due in part to the four-month exposure during that year). The annual dose increases by a combination of exposure to radioactivity from the FMPC and the age-specific respiratory factors, and it declines abruptly when the sealing of the K-65 silos reduces the radon component.

Another broad comparison of effective dose from uranium and radon is shown in Figure K-5. The stacked-bar chart in the figure indicates the amount of each scenario's cumulative effective dose (Sv) that came from each of four exposure modes:

- Ingestion of uranium with food and drinking water
- External dose from transported gamma-emitting radionuclides and the K-65 silos
- Direct inhalation of airborne uranium (excluding inhalation of resuspended uranium)
- Inhalation of radon decay products.

We remind the reader that the term uranium in the foregoing list is used generically for all of the radionuclides in Figure K-1 except radon decay products. It is obvious from Figure K-5 that radon decay products account for at least 85% of the effective dose in every scenario. The reader should bear in mind that there is substantial uncertainty in each component of this dose, as Tables K-4 and K-5 indicate, and this translates into some uncertainty for the proportions. In addition, we repeat the caution that effective dose is a broad measure that is not used for risk assessment in this study. Even so, we believe Figure K-5 provides a useful perspective for assessing the patterns of exposure and dose.

DOSE TO THE EMBRYO/FETUS

The subjects of two scenarios (1 and 6; see Appendix J) carried pregnancies to term during 1964–1965. The components of the estimated absorbed dose to the embryo/fetus for these two cases are shown in Table K-6. These dose estimates are based on the corresponding components of absorbed dose that accrued to the uterus of the mother during the nine months of gestation. They do not account for residual dose after birth from radionuclides retained in the tissues from uptake during gestation. Their purpose is to serve as a basis for estimating risk to the embryo/fetus that might result from the mother's exposure to radionuclides from the FMPC.

REFERENCES

International Commission on Radiological Protection (ICRP). 1991. *1990 Recommendations of the International Commission on Radiological Protection.* ICRP Publication 60. *Ann. ICRP* **21**(1–3). Pergamon Press, Oxford, UK.

International Commission on Radiological Protection (ICRP). 1981. *Limits for Inhalation of Radon Daughters by Workers.* ICRP Publication 32. Pergamon Press, Oxford, UK.

International Commission on Radiological Protection (ICRP). 1977. *Recommendations of the International Commission on Radiological Protection.* ICRP Publication 26. Pergamon Press, Oxford, UK.

Voillequé P.G., K.R. Meyer, D.W. Schmidt, S.K. Rope, G.G. Killough, M. Case, R.E. Moore, B. Shleien, and J.E. Till. 1995. *The Fernald Dosimetry Reconstruction Project Tasks 2 and 3 — Radionuclide Source Terms and Uncertainties. RAC* Report CDC-5. Radiological Assessments Corporation, Neeses, South Carolina.

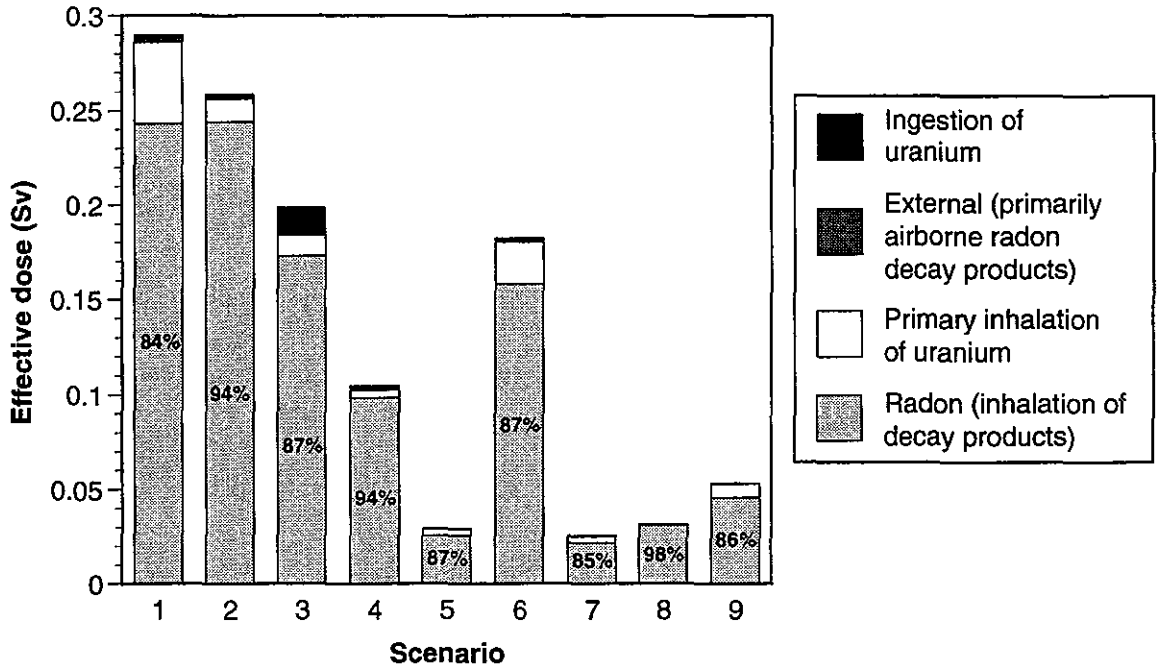

Figure K-5. Cumulative effective dose (Sv) broken down into four exposure modes for scenarios 1 through 9. The term "uranium" in the legend refers to all radionuclides in Figure K-1 except radon decay products. The percentages refer to radon dose components as fractions of the total effective doses for the respective scenarios.

Table K-6. Absorbed Dose to Embryo/Fetus (Gy) for Scenarios 1 and 6

		Internal dose		External dose
Scenario	Percentile	Low-LET[a]	High-LET	Low-LET
1	5	3.1×10^{-9}	1.4×10^{-8}	3.4×10^{-8}
	50	1.1×10^{-8}	4.8×10^{-8}	1.2×10^{-7}
	95	3.9×10^{-8}	1.7×10^{-7}	4.3×10^{-7}
6	5	3.6×10^{-9}	1.5×10^{-8}	2.1×10^{-8}
	50	9.4×10^{-9}	3.9×10^{-8}	5.5×10^{-8}
	95	2.5×10^{-8}	1.0×10^{-7}	1.4×10^{-7}

[a] LET = linear energy transfer.

APPENDIX L

DETERMINATION OF AIR SAMPLER COLLECTION EFFICIENCY

INTRODUCTION

This appendix estimates the efficiency of the ambient air samplers used around the Feed Materials Production Center (FMPC) in collecting particulates of uranium. One important use of the historic air monitoring data in the Fernald Dosimetry Reconstruction Project is to compare these measurements with model predictions, a process called "validation." Validation of model predictions with available measurements gives confidence in the model's ability to predict concentrations of Fernald-released materials at locations and times when no measurements were available. The concepts and results of the validation exercises in this study are discussed in the main text and in Appendix N.

Before using the measurements from the monitoring program, sources of uncertainty and bias had to be examined. These topics were addressed in Appendix L of our Task 4 report (Killough et al. 1993). The collection efficiency of the ambient samplers was determined to be the most significant source of bias. The focus of the Task 4 report was the 3-year period 1960–1962. Measurements were compared with predictions on a monthly time scale during that 3-year period. Since that time, the decision was made to develop source terms on an annual basis because of limitations in the data needed to reconstruct releases through plant scrubbers (Voillequé et al. 1995). Therefore, this appendix presents the collection efficiency of the ambient air samplers on an *annual* time scale for the entire 30-year period of routine air monitoring (1958–1988). The reader is referred to our Task 5 report (Shleien et al. 1995), Appendix B, Part 2, for detailed tables of concentrations of uranium in air and for a description of the air sampling methods. Detailed tables of validation results are presented in Appendix N of this report. A map of the air sampling locations is included in the validation section of Volume I.

METHOD FOR QUANTITATIVE ASSESSMENT OF COLLECTION EFFICIENCY

The uranium emitted from FMPC facilities was associated with a wide range of particle sizes. These particle-size distributions were estimated as part of the reconstruction of source terms (Voillequé et al. 1995). In our Task 4 methodology report, we focused our assessment of the bias of the perimeter air samplers on the collection efficiency of high-volume air samplers as a function of particle size. Because there were no site-specific studies, we turned to the scientific literature for information. A number of literature sources on aerosol sampling of ambient air were reviewed (May et al. 1976, Pattenden and Wiffen 1977, Wedding et al. 1977, Agarwal and Liu 1980, Liu and Pui 1981, Vrins and Hofschreuder 1983, Vincent 1989, Garland and Nicholson 1991). The work of Wedding et al. proved most applicable to our situation, providing quantitative measurements of collection efficiency for the standard American high-volume air sampler for particle sizes up to 50 μm aerodynamic diameter (Table L-1). (The aerodynamic diameter is the diameter of a sphere of unit density that has the same gravitational settling velocity as the particle. The physical diameter of a particle is its aerodynamic diameter divided by the square root of the particle density.)

Table L-1. Sampling Effectiveness (% of Total Aerosol Collected) of High-Volume Air Sampler at 4.6 m s^{-1} (Wedding et al. 1977)

Particle aerodynamic diameter (μm) and sampler orientation[a]							
5		15		30		50	
0°	45°	0°	45°	0°	45°	0°	45°
97%	100%	35%	55%	18%	41%	7%	34%

[a] Sampler orientation of 0° is defined as the situation with the high-volume roof ridge parallel to the air flow. The high-volume sampler is extremely sensitive to the angle of approaching wind and is more efficient at 45° than at 0°.

To evaluate the Fernald sampler collection efficiency, we first estimated the uranium particle-size distributions at the locations of each air sampler. This calculation took into account the source term particle-size characteristics, as well as the differential deposition of particles between the release points and the samplers according to particle diameters and densities. The particle-size distributions at the location of the samplers were output from the environmental transport and dosimetry model. This model takes into account the evolution of particle-size distributions resulting from deposition during travel of the released material away from the sources.

Crystal Ball® software (Decisioneering 1993) was used to perform an uncertainty analysis of the collection efficiency of the perimeter air samplers based on our estimates of the particle-size distributions and the collection efficiencies published by Wedding et al. (Table L-1). The efficiency distribution shape was assumed to be triangular with the minimum, maximum, and most likely values shown in Table L-2. Minimum and maximum values for each interval were taken directly from Wedding et al. (1977); the most likely value was obtained by averaging their sampler efficiencies bracketing that size range. For example, the most likely efficiency value for the 15–30 μm range was the average of 35, 55, 18, and 41% (Table L-1), which is 37% (Table L-2). Monte Carlo sampling of the distributions was performed for 1000 trials.

Table L-2. Distributions of Collection Efficiency Used in Uncertainty Analysis

Aerodynamic diameter (μm)	Collection efficiency (%)		
	Minimum	Most likely	Maximum
<5	97	98	100
5–15	35	72	100
15–30	18	37	55
30–50	7	25	41
>50	0	10	34

RESULTS OF ASSESSMENT OF COLLECTION EFFICIENCY

The uranium particle-size distribution was estimated annually for each of the four perimeter sampler locations between 1958–1971 and for the boundary stations after 1971. Table L-3 presents the long-term average particle-size distributions at the locations of the air samplers. The estimated distribution was somewhat different for each year depending on the source term mixture for that year. The standard deviations in Table L-3 reflect this year-to-year variation.

Compared with our initial assessment in the Task 4 report (Killough et al. 1993), these final particle-size distributions at the point of the samplers do not have a large percentage of uranium in the larger size fractions. Previously, the predicted particle-size distribution at the site perimeter included over 30% of the uranium mass in the >50 μm fraction; whereas, now that fraction is less than 10% of the total mass (Table L-3). This difference probably resulted from the reduction in the overall estimates of releases from the scrubbers, the source of the largest particles, compared to the draft interim source-term estimates for 1960–1962 (Voillequé et al. 1991). In addition, we are now using a surface depletion model for deposition of uranium particulates, as opposed to the source depletion model that was used earlier in the project.

Table L-3. Predicted Long-term Average Particle-Size Distributions at the Perimeter and Boundary Air Sampler Locations[a]

	Percentage of uranium in aerodynamic particle size interval[b]				
Location	0–5 μm	5–15 μm	15–30 μm	30–50 μm	>50 μm
NE	52 ± 3	28 ± 6	7 ± 1	5 ± 2	8 ± 3
SE	52 ± 3	27 ± 6	8 ± 2	5 ± 2	8 ± 3
SW	50 ± 3	27 ± 6	9 ± 2	5 ± 2	9 ± 3
NW	48 ± 3	26 ± 6	14 ± 4	4 ± 2	7 ± 3
BS–1	47 ± 7	25 ± 10	13 ± 8	5 ± 4	9 ± 4
BS–2	50 ± 6	26 ± 10	9 ± 5	6 ± 4	9 ± 5
BS–3	50 ± 6	26 ± 11	9 ± 4	6 ± 4	9 ± 5
BS–4	49 ± 6	26 ± 10	10 ± 5	6 ± 4	9 ± 4
BS–5	49 ± 6	26 ± 10	10 ± 5	6 ± 4	9 ± 5
BS–6	45 ± 7	25 ± 9	16 ± 10	5 ± 4	8 ± 4
BS–7	49 ± 6	26 ± 10	11 ± 6	6 ± 4	9 ± 4

[a] Operating time interval for the four perimeter stations (listed first) was 1958–1971, and was 1972–1988 for the boundary stations (BS–#). The uncertainty shown is the standard deviation of the values for those years.

[b] Totals do not always equal 100% because the percentages shown are the averages for any given particle-size category over the period of years that the station operated. The totals for any given location and year always equal 100%.

The results of the uncertainty analysis of sampler collection efficiency are presented in Table L-4 for the perimeter stations and Table L-5 for the boundary stations. The changes in particle-size distributions discussed above have resulted in overall higher collection efficiencies and fewer differences in efficiencies among years and among different sampler locations than was previously expected based on the methods development in Killough et al. (1993). On average, the collection efficiency of the high-volume air samplers for uranium particulates from the FMPC is estimated to be between 70 and 75% (Tables L-4 and L-5).

Table L-4. Collection Efficiencies[a] (%) for Monitoring of Uranium in Air at the FMPC Perimeter

Year	NE		SE		SW		NW	
1958	75	± 4	75	± 4	74	± 4	73	± 4
1959	75	± 3	76	± 3	75	± 3	74	± 3
1960	72	± 3	72	± 3	71	± 3	70	± 3
1961	73	± 3	73	± 3	71	± 3	70	± 2
1962	74	± 4	74	± 3	73	± 3	71	± 3
1963	76	± 4	76	± 4	75	± 4	73	± 4
1964	76	± 4	76	± 4	75	± 4	72	± 4
1965	78	± 4	78	± 4	76	± 4	73	± 4
1966	77	± 4	77	± 4	75	± 4	72	± 4
1967	77	± 4	77	± 4	76	± 4	76	± 4
1968	76	± 5	76	± 4	75	± 4	76	± 4
1969	75	± 5	75	± 5	74	± 5	74	± 4
1970	75	± 3	76	± 5	75	± 5	75	± 5
1971	73	± 3	73	± 3	72	± 3	72	± 3
All	75	± 2	75	± 2	74	± 2	73	± 2

[a] Mean and standard deviation.

Table L-5. Collection Efficiencies[a] (%) for Monitoring of Uranium in Air at the FMPC Boundary

Year	BS-1		BS-2		BS-3		BS-4		BS-5		BS-6		BS-7	
1972	75	± 3	75	± 3	75	± 3	75	± 3	74	± 3	74	± 3	75	± 3
1973	72	± 3	72	± 3	72	± 3	72	± 3	72	± 3	72	± 3	72	± 3
1974	71	± 2	71	± 3	72	± 3	71	± 3	71	± 3	71	± 3	72	± 3
1975	72	± 3	72	± 3	72	± 3	71	± 3	71	± 3	71	± 3	72	± 3
1976	71	± 2	71	± 2	71	± 2	71	± 2	71	± 2	71	± 2	72	± 2
1977	71	± 3	71	± 3	72	± 3	71	± 3	71	± 3	70	± 3	71	± 3
1978	74	± 5	76	± 5	76	± 5	75	± 5	75	± 5	71	± 5	75	± 5
1979	70	± 4	71	± 4	72	± 4	71	± 4	70	± 4	68	± 4	71	± 4
1980	73	± 5	75	± 6	75	± 6	74	± 6	74	± 6	71	± 5	74	± 5
1981	71	± 6	71	± 6	72	± 6	71	± 6	71	± 6	69	± 6	71	± 6
1982	73	± 6	74	± 6	74	± 6	74	± 6	74	± 6	71	± 5	74	± 6
1983	72	± 4	73	± 4	74	± 4	73	± 4	73	± 4	70	± 4	73	± 4
1984	74	± 4	74	± 4	75	± 4	74	± 4	74	± 4	72	± 4	74	± 4
1985	74	± 4	77	± 4	77	± 4	76	± 4	76	± 4	72	± 4	76	± 4
1986	72	± 3	75	± 3	75	± 3	74	± 3	74	± 3	70	± 3	74	± 3
1987	71	± 3	74	± 3	74	± 3	73	± 3	73	± 3	68	± 3	73	± 3
1988	64	± 3	69	± 2	70	± 2	67	± 2	67	± 3	61	± 3	67	± 3
All	72	± 2	73	± 2	73	± 2	72	± 2	72	± 2	70	± 3	73	± 3

[a] Mean and standard deviation.

APPLICATION OF COLLECTION EFFICIENCY ESTIMATES

Our model predictions for the uranium concentrations in air at receptor locations around the FMPC are annual estimates. Therefore, we needed to produce annual average measured concentrations for comparison with the predictions. Beginning with the original analytical data sheets containing the monitoring data for each week and location (Shleien et al. 1993), we computed annual average concentrations of uranium in air for each sampler location and year. The annual average concentrations are tabulated in Appendix N, and details are presented there. These measured concentrations were divided by the fractional sampler collection efficiency for that location and year to obtain a "corrected" air concentration. To illustrate, the annual average measured concentration of uranium at the NE sampler location in 1964 was 211 femtocuries uranium per cubic meter air (fCi m^{-3}). The corrected annual average air concentration is 211 ÷ 0.76 (from Table L-4), or 278 fCi m^{-3}. These corrected annual average air concentrations were used in the validation exercises described in Appendix N and Volume I. The uncertainty in determining the collection efficiency is included in the overall measurement uncertainty in the model calibration and uncertainty assessment (Appendix M).

This analysis of bias in historic air sampling data has been particularly important for the validation work of this study. However, it should be emphasized that the negative bias (roughly 25%, because of collection efficiency of the air samplers) is not important from a radiation protection standpoint. The particle-size range that is most important for internal dose assessment should have been efficiently collected by the samplers.

REFERENCES

Agarwal J.K. and B.Y.H. Liu. 1980. "A Criterion for Accurate Aerosol Sampling in Calm Air." *Am. Ind. Hyg. Assoc. J.* **41**:191–197.

Decisioneering. 1993. *Crystal Ball® Version 3.0 for Windows. User's Manual.* Decisioneering, Inc., Boulder, Colorado.

Garland J.A. and K.W. Nicholson. 1991. "A Review of Methods for Sampling Large Airborne Particles and Associated Radioactivity." *J. Aerosol Sci.* **22**:479–499.

Killough G.G., M.J. Case, K.R. Meyer, R.E. Moore, J.F. Rogers, S.K. Rope, D.W. Schmidt, B. Shleien, J.E. Till, and P.G. Voillequé. 1993. *The Fernald Dosimetry Reconstruction Project. Task 4. Environmental Pathways — Models and Validation.* RAC Report CDC-3. Radiological Assessments Corporation, Neeses, South Carolina.

Liu B.Y.H. and D.Y.H. Pui. 1981. "Aerosol Sampling Inlets and Inhalable Particles." *Atmos. Environ.* **15**:589–600.

May K.R., M.P. Pomeroy and S. Hibbs. 1976. "Sampling Techniques for Large Windborne Particles." *J. Aerosol. Sci.* **7**:53–62.

Pattenden N.J. and R.D. Wiffen. 1977. "The Particle Size Dependence of the Collection Efficiency of an Environmental Aerosol Sampler." *Atmos. Environ.* **11**:677-81.

Shleien B., S.K. Rope, M.J. Case, G.G. Killough, K.R. Meyer, R.E. Moore, D.W. Schmidt, J.E. Till, and P.G. Voillequé. 1995. *The Fernald Dosimetry Reconstruction Project. Task 5. Review of Historic Data and Assessments for the FMPC.* RAC Report CDC-4. Radiological Assessments Corporation, Neeses, South Carolina.

Vincent J.H. 1989. "Sampling for Aerosols in the Ambient Atmosphere," Chapter 15 in *Aerosol Sampling: Science and Practice.* John Wiley, Chichester.

Voillequé P.G., K.R. Meyer, D.W. Schmidt, G.G. Killough, R.E. Moore, V.I. Ichimura, S.K. Rope, B. Shleien, and J.E. Till. 1991. *The Fernald Dosimetry Reconstruction Project. Tasks 2 and 3. Radionuclide Source Terms and Uncertainties — 1960–1962.* RAC Report CDC-2. Radiological Assessments Corporation, Neeses, South Carolina.

Voillequé P.G., K.R. Meyer, D.W. Schmidt, S.K. Rope, G.G. Killough, M. Case, R.E. Moore, B. Shleien, and J.E. Till. 1995. *The Fernald Dosimetry Reconstruction Project. Tasks 2 and 3. Radionuclide Source Terms and Uncertainties.* RAC Report CDC-5. Radiological Assessments Corporation, Neeses, South Carolina.

Vrins E. and P. Hofschreuder. 1983. "Sampling Total Suspended Particulate Matter." *J. Aerosol Sci.* **14**:318–322.

Wedding J.B., A.R. McFarland, and J.E. Cermak. 1977. "Large Particle Collection Characteristics of Ambient Aerosol Samplers." *Envir. Sci. Technol.* **11**:387–390.

APPENDIX M

AIR DISPERSION MODELS FOR THE PRODUCTION AREA AND THE K-65 SILOS

INTRODUCTION

Uranium isotopes and other radionuclides were released to the air from the production area of the Feed Materials Production Center (FMPC) during its years of operation (1951 through 1988). Radon-222 (radon) and its decay products were vented to the atmosphere from the K-65 silos west of the production area in the years before the silos were sealed in 1979; in subsequent years these radionuclides continued to escape through cracks in the containment, but at lower rates. These releases of radioactivity to the atmosphere from the production area and the K-65 silos account directly for most of the offsite dose estimated in this study, i.e., dose by inhalation of airborne radioactivity. The airborne releases of uranium and other radionuclides from the production area are also coupled to ingestion dose from consumption of garden crops contaminated by deposition of radioactive particulates and consumption of animal products contaminated by the animal's grazing where deposition has occurred.

The purposes of this appendix are to explain our approach to estimating atmospheric dispersion of radioactivity released from the FMPC, to assess parametric uncertainties in the estimates, and to describe the supporting models and data. We have calibrated atmospheric diffusion models by parameter estimation and regression techniques, using air monitoring data for uranium and radon measured in the environment around the FMPC. This empirical approach differs somewhat from typical atmospheric dispersion calculations supporting prospective assessments that are intended to demonstrate compliance with environmental health protection standards or other criteria. The nature and requirements of dose reconstruction are quite different from studies of that kind and impose different demands on air dispersion modeling. We go into these questions in a discussion section at the end of this appendix (page M-69).

In 1986 and 1987, the network of uranium air monitoring stations on the FMPC site was extended by the addition of six stations, giving coverage at distances of more than 6 km from the center of the production area. A seventh new station was put into service in 1988. We considered data from these stations for the years 1986–1988. When these data are adjusted for the magnitude of the release, wind speed, and wind-direction frequency, they provide a coherent picture of atmospheric dispersion of uranium released from the production area. The data include the effects of plume depletion resulting from wet and dry deposition, and these processes were taken into account in calibrating the model. Once the basic atmospheric dispersion model had been calibrated, that model could be combined with the source term and meteorological data to estimate offsite concentrations for all years of plant operation. Uncertainties indicated by regression estimates of calibration parameters, residual uncertainties, and uncertainties in the source term and meteorological data have been estimated and propagated through the predictive calculations and ultimately show up as components of uncertainty in dose and risk.

Systematic air monitoring of radon near the FMPC was not undertaken until the 1980s after the K-65 silos were sealed. Nevertheless, two datasets from that period give us a sense of the air dispersion of radon released from the K-65 silos. One dataset is compiled from routine monitoring by FMPC personnel at the site boundary stations (BS-1 through BS-7, which on average are about 1 km from the center of the production area; see Figure N-9 in Appendix N). This monitoring began in July 1980. The second dataset is based on a nearly complete sequence of measurements covering a one-year period. These measurements were taken as part of a study by Mound Laboratory that spanned 1984–1986. Most of the stations in the Mound study were placed nearer to the K-65 silos than the boundary stations where the FMPC monitoring took place. The combined data from these two datasets, with background subtracted, and adjusted for rate of release, wind speed, and wind-direction frequency, show a clear trend out to about 2 km from the point of release. The radon data show greater uncertainty than the uranium data, the source-to-receptor distance they cover is not as great, and the calibration of the transport model using regression methods with the Mound and FMPC data is more complex. The uncertainty is propagated through the concentration predictions to dose and risk from radon decay products.

Thus there are distinct but similar empirical approaches to modeling the dispersion of airborne releases from two types of FMPC sources. The production area is about 1 km^2 with numerous building clusters that create complicated patterns of windflow and turbulence, whereas the K-65 silos are relatively isolated and present a simpler and more compact source. In this appendix, we first describe in some detail the methods used to derive the uranium dispersion model from the air monitoring data. Next we develop the radon air dispersion model from the Mound and the FMPC radon data. Because of the complexity of the radon data analysis, we discuss it in a separate section that begins on page M-37.

The meteorological data that enter into all air dispersion calculations are based on measurements taken from an instrumented tower operated on the FMPC site since mid-1986. The siting of the tower, the brevity of the data record, and other aspects of the meteorological dataset have given rise to questions concerning its validity. In Task 4 (Killough et al. 1993) we expended considerable effort examining this dataset and comparing it with possible surrogates. We have also developed a method for estimating the uncertainty that arises from using this five-year composite dataset to model air concentrations in earlier years. In a section of this appendix (beginning on page M-51), we review the Task 4 analysis of the dataset and present the uncertainty method. On the basis of this analysis, we concluded that its shortcomings notwithstanding, this dataset represents the most specific and authentic information applicable to airborne releases from the FMPC. Accordingly, we have used it in all calculations of airborne transport of historical releases.

We end the appendix with a discussion of uncertainties, including a recapitulation of the simulated sources of uncertainty that affect the prediction of air concentrations.

Readers of the Task 4 report will notice that our approach to atmospheric modeling has changed in the interim. In the case of transport of airborne uranium, the change was primarily motivated by the discovery that the air monitoring data for the years 1986 through 1988, when analyzed appropriately, gave a clear picture of the trend of air concentration with distance from the center of the site (at the time the Task 4 report was written, it was not

possible to analyze these data, because estimates of uranium releases during 1986–1988 were not yet available). When these data were adjusted for uranium released, wind speed, and wind directional frequency, their trend with distance from the production area was particularly well fitted by the "ski-jump" profile of a circular area source model, with plume depletion from deposition being accounted for by a surface depletion model. The model adopted is based on a Gaussian plume with a source radius of 450 m, which approximates the part of the production area where most releases originated. There are plausible physical reasons that this kind of model should give a good representation of releases from the FMPC production area. This fact and the need to incorporate objective site-specific estimates of uncertainty into the model predictions led us to combine the calibration of the model with statistical methods that provided the basis of such an uncertainty analysis for airborne uranium.

We extended the same general approach to modeling atmospheric dispersion of radon released from the K-65 silos, although the circular area source assumed for these releases is of much smaller radius (50 m) than that used for the production area. The radon data taken in the 1980s present greater scatter than do the uranium data, they are representative of smaller distances from the point of release, and they are affected by statistical difficulties of subtracting background estimates from measurements of small magnitude. Thus, there is greater uncertainty in air concentration predictions for radon than for uranium. There are other technical differences in the calibrations of the uranium and radon air dispersion models that are described in this appendix. Even so, the two approaches have in common the estimation of the uncertainty distribution of a model calibration factor. The basis for the estimation is regression, in combination with the analysis of exogenous uncertainties in the data.

SOME PRELIMINARY MATTERS

Estimation of past air concentrations of radioactivity at specified locations in the FMPC assessment domain is required for dose reconstruction. The air concentrations are directly applicable to dose by inhalation, and in the case of uranium, the air pathway is coupled by deposition of radioactivity from the airborne plume to contamination of crops and animal products. The amount of material that deposits on crops and pasture grass must be estimated for purposes of estimating intake by ingestion of contaminated food. But deposition also depletes the concentration in the plume, and the extent of the plume depletion must be estimated as part of the process of predicting air concentrations.

For both uranium and radon, there are air monitoring data to which each model's performance must be related, either by calibration (minimization of bias) in advance of the assessment or by validation (comparison of predictions with data) after assessment. We have considered data of both types for uranium and primarily calibration data for radon.

Model structures, parameters, and calibration procedures introduce uncertainties into the predictions. We are required to analyze uncertainties and estimate their propagation into the model predictions. Our fundamental rule is to seek to minimize bias in the predictions and to express conservatism by increasing the variances of uncertainty distributions.

Uncertainties are represented by model parameters that are treated as random variables. In our approach, these uncertainties are not retrofitted to a model, but rather the model is developed from a stochastic point of view, with both the mathematical forms and the distribution parameters receiving equal emphasis.

The first step is the selection of a generic transport and diffusion model that expresses the basic physical processes as we believe they apply to the assessment at hand. In the case of uranium, the model must include quantitative estimation of plume depletion, because the calibration data have been affected in a significant way by deposition. As we pointed out in the introduction, we have chosen Gaussian area source models for both uranium and radon.

The second step of the process is calibration, in which model bias with respect to a specified set of data is minimized, in the sense of least squares, by a regression procedure. This step introduces into the model a calibration factor, which is itself an uncertainty distribution. This distribution is estimated partly by the regression and partly by an auxiliary analysis that considers exogenous uncertainties that are introduced into the data by preliminary adjustments and transformations to a suitable form for the calibration.

In additional steps, we analyze uncertainties associated with using the calibrated model to predict air concentrations at specific locations in the assessment domain at specific times (our time resolution is one year, and consequently we are predicting annual averages of concentration). These uncertainties are related to the release, deposition parameters, the use of a temporally limited meteorological dataset to make predictions for years outside its scope, and the model's inability to transcend idealized limitations and represent irregularities that have not been quantified in detail, such as the real source geometry, the real terrain, and inhomogeneous transfer of heat between the air and the soil. When random variables that are broadly representative of these uncertainties are incorporated into the model, together with the factor determined by the calibration, the result can be viewed as a stochastic model whose value is an uncertainty distribution for the air concentration rather than a point estimate. Calculation of the output distribution requires Monte Carlo methods, which are based on sampling the component random variables that express the model uncertainties.

The Model Equations

We now write the equation that expresses the concentration of uranium at a specified location and in a particular year:

$$\chi_{d,m,t}(x) = \left(\sum_{r=1}^{R} Q_{r,m,t} \right) \cdot \mathrm{CF} \cdot \varphi_{\mathrm{met},t} \varphi_{\mathrm{resid}} \sum_{q=1}^{6} \sum_{s=\mathrm{A}}^{\mathrm{F}} \frac{f_{q,d,s}}{u_q} D_s(x) \theta_s \left(x, \frac{v_{q,s,m} \varphi_{\mathrm{dep}} + \bar{J} W_{\mathrm{r}}}{u_q} \right) . \quad \text{(M-1)}$$

We are not going to define every symbol in complete detail in this section. Rather, we want to give a general view of the model's structure, with its deterministic and stochastic parameters. The concentration at ground level is χ (pCi m^{-3}), and x (m) is the distance from the center of the circular source region to the receptor. We define the indices:

d one of 16 directional sectors, which are defined on page M-9. Knowing the distance x and the value of d determines the location of the receptor, to within the angular resolution of the model

m particle size class. For purposes of deposition and inhalation dose (Appendix I), particle aerodynamic diameters are handled in discrete classes or intervals, with a representative diameter for each interval

t year (1951, 1952,...,1958)

r release source for uranium (there are more than 30)

q wind speed class. There are six discrete classes, represented by wind speeds 1, 3, 5, 7, 9, and 11 m s^{-1}

s Pasquill-Gifford stability class. There are six, labeled A through F, with A being the most unstable (corresponding to rapid horizontal and vertical dispersion of the plume as it moves downwind and generally lower concentrations at a ground-lever receptor for a ground-level source) and F the most stable (slow horizontal and vertical dispersion with generally higher concentrations at the receptor).

Thus, we see that $\chi_{d,m,t}(x)$ specifies a direction and distance (d, x), a particle size class (m), and a year (t).

The source term is $Q_{r,m,t}$ (pCi s^{-1}), which is summed over the specific uranium sources ($r = 1,...,R$).

Let us skip to the double summation, which represents a weighted average of the product of the functions D_s and θ_s divided by wind speed u_q over the six wind speed classes and the six stability classes. The weight fraction, $f_{q,d,s}$, depends on wind speed class, direction (which is fixed), and stability class and comes from the meteorological database, which is discussed in a later section (page M-51). The quantity D_s is called a diffusion function, and its units are m^{-2}. We defer further discussion of it, except to say that the quotient D_s / u_q can be thought of as an air concentration, without the effects of deposition, from a source that emits 1 pCi s^{-1} during atmospheric conditions of stability class s while the wind blows from the source to the receptor with wind speed u_q. The fractional factor θ_s corrects the predicted concentration for the effects of plume depletion from deposition. This factor is based on a surface depletion model that is a function of the stability s, the distance x from the source, and the quotient of total deposition divided by the wind speed. The terms in the numerator of that quotient are the dry deposition velocity $v_{q,s,m}$ (m s^{-1}) and the wet deposition velocity, which is represented by the product of the average rainfall rate $\overline{J}$ and a washout ratio W_r (we leave φ_{dep} for later). We discuss wet and dry deposition in subsequent sections (page M-11).

The remaining quantities in Equation M-1 are random variables representing uncertainties that affect the calibration and predictions. The first, CF, is determined by the regression procedure that calibrates the model to the air monitoring data designated for that purpose. The distribution of CF turns out, as we shall see in a later section (page M-18), to be (approximately) lognormal. The geometric mean of CF is the value that minimizes the bias of the model with respect to the calibration data (in the hope that the low bias extends to predictions in general, and validations tend to indicate this). The geometric standard deviation of CF quantifies uncertainty in the calibration process itself.

The random variable $\varphi_{met,t}$ accounts for uncertainty in the meteorological dataset, particularly uncertainty that is related to using a composite dataset for five recent years (1987–1991) to estimate concentrations for a much longer period (1951–1988). Its dependence on the year (t) indicates that it is sampled independently for successive years.

The random variable φ_{resid} is based on the distribution of residuals for the regression that calibrates the model. We interpret this uncertainty as being related to the model's inapplicability to such factors as irregularities in terrain and inhomogeneities in the heat exchange between the air and the ground; it could also account for a lack of detail in modeling the source region. The distribution of this factor, which is also determined from the regression procedure, is approximately lognormal. This distribution is sampled only once for each Monte Carlo cycle, by which we mean that the value remains the same for all 38 simulated years.

In the parentheses following the depletion fraction θ_s is the random variable φ_{dep}. This random variable provides an uncertainty distribution for the dry deposition velocity $v_{q,s,m}$. The washout ratio for wet deposition, W_r, is also a random variable. The random variables associated with deposition are sampled once at the beginning of each Monte Carlo cycle, because they are intended to simulate a lack of knowledge of the true time-averaged values rather than year-to-year variability.

The summation of the uranium release rates $Q_{r,m,t}$ (pCi s^{-1}) over all sources (r) also represents a random variable. For each year (t) and each release point (r), an uncertainty distribution for the release was estimated as part of Task 2/3 (Voillequé et al. 1995). These estimates are used for both calibration (1986–1988) and prediction of air concentrations (all years of operation).

The equation for the ground-level concentration of radon is of similar form and has many of the same quantities. It is simpler because we do not explicitly model deposition for radon and its decay products. This equation is

$$\chi_{d,t}(x) = Q_t \cdot \mathrm{CF}(x) \cdot \varphi_{met,t}\varphi_{resid} \sum_{q=1}^{6} \sum_{s=A}^{F} \frac{f_{q,d,s}}{u_q} D_s(x) \ , \qquad \text{(M-2)}$$

where the calibration factor CF now depends on the distance x from the source, there is no particle size index (m) as there was for uranium, and there is not an explicit plume depletion factor (θ_s in Equation M-1 for uranium). The release term Q_t is for a single source and release rate (this is a slight oversimplification; the full details will be given in a later section on page M-30 and following). And finally, the diffusion function $D_s(x)$ is also based on a Gaussian plume model for a circular area source, but the radius (50 m) is much smaller than the one for the uranium dispersion model (450 m). In other respects, the symbols shown are analogous to their counterparts in Equation M-1. The methods for calibrating the model represented by Equation M-2 to the radon air monitoring data have some features in common with those used for uranium, but there are also important differences. We discuss each procedure in some detail in a later section (page M-13 and following for uranium; page M-30 and following for radon).

Remarks about Uncertainty Distributions

We have tried to derive uncertainty distributions for the models in accordance with principles that provide a rationale for each choice. This is not to say that the process is free of judgments; it is not. Because we seek to minimize bias in the predictions of air concentrations (and thus in the dose estimates that are based on the air concentrations), we express conservatism by increasing variances in uncertainty distributions. This statement is an indication of procedure rather than a formal definition of the relationship of results to the models and their uncertain parameters. In deriving an uncertainty distribution, it is better to arrive at one with a variance that is too large than one with a variance that we are not sure is large enough. On the other hand, we do not resolve indecision in the modeling process by deliberately overpredicting the central estimate of an outcome (e.g., dose). Such upward biasing of predictions is justified in some types of assessment analysis, but in deference to the epidemiological power analysis to which this methodology is to be applied, we must avoid the practice in this assessment.

We often favor the use of lognormal distributions because of the simplicity of calculating their composites when independent random variables are multiplied or divided. This preference is not based on a technical limitation — we can and do use Monte Carlo methods to estimate composites of arbitrary distributions — but rather to provide the reader with familiar distributions characterized by two easily interpreted parameters instead of distributions requiring a set of percentiles or a frequency plot or cumulative curve for presentation. Exercising this preference is appropriate when the composite random variable is not biased by it and has a variance at least as large as the more authentic composite. Some useful properties of lognormal distributions are given here to assist readers in following the presentations. The following rules have been derived from theory presented by Aitchison and Brown (1969).

(1) The product of a constant c (nonstochastic quantity) and a lognormally-distributed random variable with geometric mean GM = 1 and geometric standard deviation GSD is lognormally distributed with geometric mean = c and geometric standard deviation GSD. This rule makes it convenient to transform a nonstochastic parameter in a model to a lognormal random variable by multiplying it by a lognormal random variable with geometric mean 1 (this is the effect of the random variables denoted by φ in Equations M-1 and M-2).

(2) The product of N independently distributed lognormal random variables is lognormal. The geometric mean of the product is the product of the geometric means, and the geometric standard deviation of the product is

$$\mathrm{GSD} = \exp\left(\sqrt{(\ln \mathrm{GSD}_1)^2 + \cdots + (\ln \mathrm{GSD}_N)^2}\right). \qquad \text{(M-3)}$$

If, instead of a product, we have a combination of products and quotients of the N independently distributed lognormal random variables, the geometric mean is the same combination of the geometric means of the factors, and the geometric standard deviation of the combination is given by Equation M-3.

(3) The (arithmetic) mean α and standard deviation β of a lognormal distribution are related to the geometric mean GM and geometric standard deviation GSD by the equations

$$\alpha = GM \cdot \exp\left(\frac{1}{2}(\ln GSD)^2\right), \quad \beta = \alpha\sqrt{\exp\left((\ln GSD)^2\right) - 1}\ . \tag{M-4}$$

From the second of these two equations, we see that the coefficient of variation ($CV = \beta / \alpha$) depends only on GSD and is given by the radical quantity. [Note that α and β do not refer to the underlying normal distribution; the parameters of that distribution are mean $\mu = \ln(GM)$ and $\sigma = \ln(GSD)$].

(4) If the 50th and 95th percentiles (v_{50} and v_{95}, respectively) of a distribution are given, the lognormal distribution with the same corresponding percentiles has geometric mean GM = v_{50} and $GSD = (v_{95} / v_{50})^{1/1.65}$ (1.65 is the 95th percentile of the standard normal distribution). This rule is useful for approximating skewed distributions with known 50th and 95th percentiles by lognormal distributions with the same corresponding percentiles.

The sum of lognormally distributed random variables is, regrettably, not lognormally distributed, whether the terms are independent or not. The central limit theorem tells us that under fairly general conditions, the distribution function of the Z-transformed arithmetic average of independently distributed random variables (not necessarily of the same distribution type) converges to the standard normal distribution as the number of terms in the average tends to infinity (Kendall and Stuart 1969). This result is often interpreted to mean that the sum of a moderately large number of random variables is approximately normally distributed, irrespective of the distribution types of the individual terms. (It is also invoked to claim that a product of not necessarily lognormal factors is approximately lognormal.) As a practical matter, such an assumption may turn out to be wrong; the sum may require far more terms than the investigator has available for the normal approximation to be valid. Our experience with sums of (not necessarily independent) lognormally distributed random variables has been that the distribution of the sum, even though not analytically lognormal, is sometimes very well fitted by a lognormal distribution, with the criterion being a succession of tests of fit. This point is illustrated in Example M-1, beginning on page M-65. For some purposes, even a fit that is marginal by analytic standards may be adequate.

THE GAUSSIAN MODEL FOR A CIRCULAR AREA SOURCE REGION

The FMPC production area and the K-65 silos are both treated as ground-level circular area release sources, but the two circles have different radii. We apply the Gaussian plume model for a ground-level point source and integrate over the circular region. The well-known point source model is

$$C_{PS}(x,y,\xi,\eta) = \frac{Qf}{\pi\sigma_y(x-\xi)\sigma_z(x-\xi)u}\exp\left(-\frac{(y-\eta)^2}{2\sigma_y^2(x-\xi)}\right), \tag{M-5}$$

where the point (ξ,η) is the source and (x,y) is the ground-level receptor. The value of C_{PS} is the air concentration at ground level (pCi m^{-3}). A reference for this model is Hanna et al. (1982); our formula is obtained from theirs by putting $h = z = 0$ (both source and receptor are

at ground level) and replacing x and y by the distances $x-\xi$ and $y-\eta$, respectively. The symbol Q denotes a unit release rate (1 pCi s^{-1}), f is a fractional wind-direction frequency, u is wind speed from source to receptor (m s^{-1}), and the functions σ_y and σ_z are horizontal and vertical dispersion coefficients, respectively (m), expressed as functions of the source-to-receptor distance $x-\xi$. Integrating $C_{PS}(x,y,\xi,\eta)$ over the circular source region and dividing by the area gives

$$C_A(x,y,\rho)=\frac{1}{\pi\rho^2}\int_{-\rho}^{\rho}\int_{-\sqrt{\rho^2-\xi^2}}^{\sqrt{\rho^2-\xi^2}} C_{PS}(x,y,\xi,\eta)\,d\eta\,d\xi \qquad \text{(M-6)}$$

where ρ (m) is the radius of the circular region with its center at the origin of the coordinate system. The quantity $C_A(x,y,\rho)$ is the ground-level air concentration at the point (x,y) resulting from the release of 1 pCi s^{-1} from the circular area, with the magnitude of the release being distributed uniformly over the circlar region. After substitution of Equation M-5, the double integral on the right of Equation M-6 can be put in terms of the cumulative standard normal probability distribution function $P(X)$ as follows:

$$C_A(x,y,\rho)=\frac{\sqrt{2}Qf}{\pi^{3/2}\rho^2 u}\int_{-\rho}^{\min(\rho,x)}\frac{1}{\sigma_z(x-\xi)}\left[P\left(\frac{y+\sqrt{\rho^2-\xi^2}}{\sigma_y(x-\xi)}\right)-P\left(\frac{y-\sqrt{\rho^2-\xi^2}}{\sigma_y(x-\xi)}\right)\right]d\xi \qquad \text{(M-7)}$$

where the upper limit of the integral allows for receptor points within the source region. The function $P(X)$ is defined by the equation

$$P(X)=\frac{1}{\sqrt{2\pi}}\int_{-\infty}^{X} e^{-x^2/2}\,dx. \qquad \text{(M-8)}$$

An analytic approximation of $P(X)$ (e.g., Abramowitz and Stegun 1968, Equation 26.2.19) reduces computing the integral of Equation M-7 to a one-dimensional numerical integration.

Equation M-7 presupposes a fixed wind direction for the fraction f of the period to which the formula is applied. Wind directions are defined in terms of 16 discrete wind sectors with the release source at the center (Figure M-1). When the receptor point is in a given sector (for example, NE), the wind direction is associated with the reciprocal sector (in the example, SW). We implement the model so that when the wind blows into the receptor sector, the concentration is uniform across the sector (in the direction perpendicular to the radial centerline) and zero outside the sector. Within the sector, as a function of distance from the center of the area source, we use Equation M-7 with $y=0$ as a profile of concentration. The plume emanating from a circular source of radius 450 m is, of course, wider than the sector for some distance outward, and there is consequently a greater overlapping when the wind blows into adjacent sectors than is the case for point source models. The calibration that we will describe subsequently (page 13) accounts implicitly for this overlapping.

With point source models, sector averaging is commonly used for long-term (annual) averages of air concentrations, such as we will be estimating. The purpose is to account for the variations of plume direction within the receptor sector and thus the corresponding variations in predicted concentration at the receptor point. The usual procedure is to

integrate the plume formula crosswind (i.e., from $y = -\infty$ to $+\infty$) and to divide by the sector width as a function of the distance x (e.g., Hanna et al. 1982). This approach works well with point source models, because the plume width is comparable to the sector width at most distances. In the case of a large circular area source, however, this procedure is inappropriate. Sector averaging of the circular area source model produces a steep profile that is similar to that of a point source model. It appears unlikely that such a procedure would lead to a concentration profile that would be physically representative of long-term average concentrations consistent with the circular area source model. A more realistic (and elaborate) averaging scheme would have to be worked out to account not only for plume oscillations within the receptor sector but also for the effects of overlap as the plume oscillates in neighboring sectors. Because of our calibration procedure, we have chosen instead to assume that the profile shape (but not the absolute magnitude) is similar to the centerline shape of the circular area source model (Equation M-7) and to allow the calibration to fix the magnitude. When deposition is accounted for, this method gives very good agreement with the trend of the data.

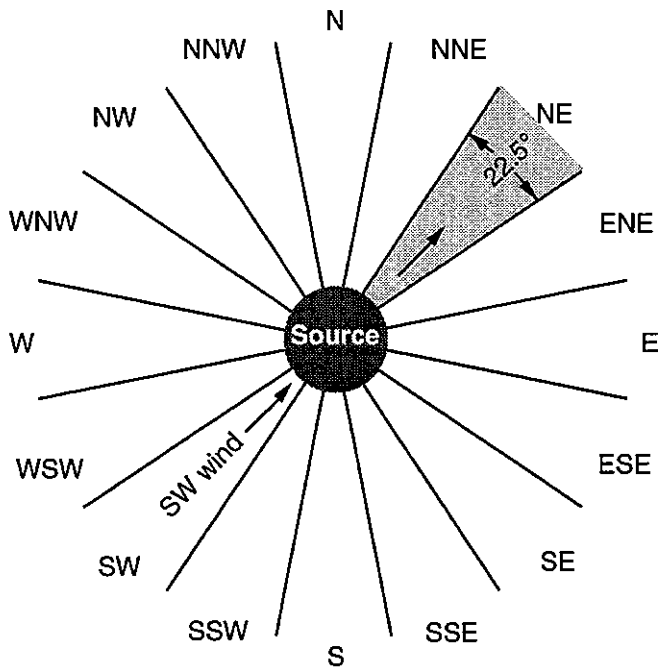

Figure M-1. Layout of 16 wind sectors for atmospheric dispersion calculations. The wind direction is associated with the sector from which the wind blows across the source. Thus the sector in which a receptor is located and the sector representing the wind direction are reciprocal (differ by 180°).

We used numerical integration to tabulate the integral as a function of x for each of the Pasquill-Gifford atmospheric stability classes A–F. Separate tabulations were prepared for the values of the radius ρ corresponding to each source region (i.e., the production area and the K-65 silos). The computer performs logarithmic interpolation to obtain values

corresponding to nontabular distances. We used Briggs's formulas (rural version) for the dispersion coefficients σ_y and σ_z (Hanna et al. 1982).

AIRBORNE RELEASES FROM THE PRODUCTION AREA

Deposition

Parameters for wet and dry deposition were discussed in considerable detail in the Task 4 report (Killough et al. 1993) and will be summarized here. Since the Task 4 report appeared, we have changed our approach to plume depletion from a source depletion model to a surface depletion model, which we describe in this section.

Dry deposition. Dry deposition of airborne particles occurs when some of the particles make contact with a stationary surface and adhere (at least temporarily; the return of some of the deposited particles to the airflow is resuspension). Dry deposition is modeled by means of a (dry) deposition velocity v_d (m s^{-1}), and the deposition rate is assumed to be the product of v_d and the air concentration near the ground (typical units of deposition rate are pCi m^{-2} s^{-1}). The deposition velocity of a particle depends on (a) the aerodynamic diameter of the particle, (b) the wind speed near the ground, (c) the atmospheric stability class (A–F), and (d) a parameter related to the roughness attributes of the terrain (e.g., ground cover). The deposition velocity includes gravitational settling, which dominates other physical processes for particles of aerodynamic diameter 10 μm and larger.

In deriving the dry deposition velocity v_d, we employed the model of Sehmel and Hodgson (1980) for surface transfer, which is derived from regressions on wind-tunnel data. Other components of the deposition velocity are combined with the surface transfer by an electrical resistance analogy. Values of v_d for particles of density 7 g cm^{-3} are given for various physical diameters, wind speeds, and atmospheric stability classes A–F in Table G-3 of the Task 4 report. In general, the deposition velocity increases with particle diameter and with wind speed; there is a slight decrease in deposition velocity with increasing atmospheric stability (i.e., moving from A to F). The deposition model incorporated in our dispersion models takes these dependencies fully into account, through the algorithms given in Appendix G of the Task 4 report. Appendix G of the Task 4 report also describes a check of the theoretical deposition velocities against empirical deposition velocities estimated from measurements of uranium on gummed film and air concentrations measured by high-volume samplers located near the gummed-film sampling locations. These results showed a very satisfactory correspondence with theoretical values.

Wet deposition. Wet deposition can be modeled by an experimentally determined washout ratio

$$W_r = C_r / C_a \tag{M-9}$$

where C_r is the concentration of a tracer in precipitation (mg cm^{-3}) and C_a is the concentration of the tracer in air (mg cm^{-3}) at a reference height, taken as 1 m. A wet deposition velocity can then be defined as

$$v_w = W_r J \tag{M-10}$$

where J is precipitation rate, say in m s^{-1}, so that v_w has the same units as the dry deposition v_d defined above.

Estimates of washout ratios are available from numerous studies. Hanna et al. (1982) note that about half of the values of the washout ratios in the extensive survey of McMahon and Denison (1979) lie in the range 3×10^5 to 1×10^6, with median about 6×10^5. To test the appropriateness of these values for modeling wet deposition near the FMPC, we derived a site-specific washout ratio for uranium in air near the FMPC from measurements of uranium in air and uranium in rain. The measurements were taken during the period 1961–1967. The middle half of these observations lie between 3.1×10^5 and 1.1×10^6, with median 5.6×10^5. Thus, there is excellent agreement between the local measurements and those reported in the literature. Further details are given in Appendix H of the Task 4 report.

Plume depletion. As particles are removed from the airborne plume by wet and dry deposition processes, the air concentration diminishes. Accounting for deposition and plume depletion is particularly important for uranium and other particulates released from the production area. For radon and decay products released from the K-65 silos, the radon data used in the calibration implicitly account for deposition of radon from the plume, and we have made no attempt to remove this influence from the radon air dispersion model. For uranium, however, it is necessary to derive a pre-deposition model in order to take into account different combinations of particle sizes that require different deposition velocities.

To adjust the uranium air concentrations, we use a surface depletion model adapted from a formulation by Horst (1977). The model is described by an integral equation

$$\overline{\chi}(x)=\frac{Qf}{u}\overline{D}_A(x)-\frac{v}{u}\int_0^x\overline{\chi}(\xi)\overline{D}_{PS}(x-\xi)\,d\xi \qquad \text{(M-11)}$$

where v is the sum of the wet and dry deposition velocities (m s^{-1}), and the bars indicate crosswind integration. This model depletes the plume by integration of a negative source at ground level from 0 to distance x; the effect is to diffuse a material deficit into the plume. The crosswind-integrated solution $\overline{\chi}(x)$ has units pCi m^{-2}. The function $\overline{D}_A(x)$ (m^{-1}) is a crosswind-integrated diffusion function based on the area source model of Equation M-7, where we assume the plume has a rectangular cross section. The first term is just the crosswind integral of the undepleted concentration, which we represent as

$$\frac{Qf}{u}\overline{D}_A(x)=C_A(x,0,\rho)\times \text{ sector width at } x, \qquad \text{(M-12)}$$

where $C_A(x,0,\rho)$ is from Equation M-7 (since the concentration is constant across the sector and zero outside, the crosswind integral is the constant value multiplied by the sector width). The crosswind-integrated diffusion function $\overline{D}_{PS}$ is derived from the point-source Gaussian plume at ground level (Equation M-5); its form is

$$\overline{D}_{PS}(x)=\sqrt{\frac{2}{\pi}}\frac{1}{\sigma_z(x)}. \qquad \text{(M-13)}$$

We solved a discrete version of the integral equation (M-11) by recursion, using a small spatial step (5 m). Finally, for each x we divided the solution by the crosswind-integrated concentration without depletion (Equation M-12) to obtain a suspension ratio (SR):

$$\mathrm{SR}(x) = \frac{\overline{\chi}(x)}{(Qf/u)\overline{D}_{\mathrm{A}}(x)}. \qquad \text{(M-14)}$$

It can be shown that the suspension ratio depends on the ratio v/u rather than on each of v and u independently (Horst 1977). Hence, we are able to tabulate SR by atmospheric stability (A–F), v/u, and distance x. In the calculations, the computer interpolates in these tables of SR to adjust the predicted downwind concentrations for plume depletion.

Our application of the surface depletion model differs from the approach of Horst (1977) in the following respects: (1) In his presentation, both diffusion functions in his counterpart of our Equation M-11 correspond to the point-source Gaussian plume. (2) His formulation is more general in order to permit an arbitrary release height and receptor height; we take both heights to be ground level.

Calibration of the Air Dispersion Model to Uranium Data

Figure N-9 (Appendix N) shows the locations of high-volume air samplers that were used for uranium measurements near the FMPC. Boundary stations BS1–BS7 were established in 1972. In 1986, two stations (AMS8 and AMS9) were added to the boundary stations (BS1–BS7), in 1987 four more stations (AMS10–AMS13) were brought on line, and AMS14 was put in service into 1988. After the expansion of the air monitoring program, all location numbers were preceded by "AMS" rather than "BS," which was previously used for the boundary stations. The data from these stations, which range in location from about 500 m to more than 6 km from the center of the production area, offer a much better opportunity for calibrating the air dispersion model than was available with earlier data. We have based our calibration on the data taken during the years 1986 through 1988. The year 1986 provides two new stations in the NE quadrant (AMS8 and AMS9) that are nearer the production area than the boundary stations. In 1987 and 1988, the added stations AMS10–AMS14 gave the first systematic sampling at distances beyond the boundary stations. After 1988, the data would not have beenuseful, because FMPC operations had been discontinued, and the measured air concentrations would have resulted primarily from resuspended uranium and unquantified trace amounts of uranium in air filters or other laboratory equipment.

Functional form of the air dispersion model for uranium. The air dispersion model to be fitted to the uranium air monitoring data is the diffusion function based on the circular area source model of Equation M-7 with $y = 0$,

$$D_{\mathrm{A}}(x,\rho) = \frac{K \cdot C_{\mathrm{A}}(x,0,\rho)\cdot u}{Qf} = \frac{K\sqrt{2}}{\pi^{3/2}\rho^2} \int_{-\rho}^{\min(\rho,x)} \frac{1}{\sigma_z(x-\xi)} \left[2P\left(\frac{\sqrt{\rho^2-\xi^2}}{\sigma_y(x-\xi)} \right) - 1 \right] d\xi , \qquad \text{(M-15)}$$

where $D_{\mathrm{A}}(x,\rho)$ has units m^{-2}. The calibration factor K is to be determined from the data, which are transformed from concentration to diffusion by the factor $u/(Qf)$. This

transformation removes dependence on wind speed, wind directional frequency, and release rate and lets us view the data as a function of distance from the source and atmospheric stability. Hilsmeier and Gifford (1962) plotted point source dispersion models as diffusion functions. The value of the source radius ρ is taken as 450 m, giving an area of 0.64 km^2, which corresponds approximately to the part of the production area where the emission sources are concentrated. The uranium release rate Q for each year of sampling is based on the source term reconstruction of Task 2/3 (Voillequé et al. 1995). The fractional wind direction frequency f is from the five-year composite FMPC meteorological dataset, which is discussed in another section of this appendix (page M-51); the value of f is specific to the sampling location and corresponds to the direction of wind blowing from the center of the production area to the sampler location. The wind speed u is also based on the five-year composite FMPC meteorological dataset and is the average wind speed for the direction of the wind blowing from the center of the production area toward the sampler location.

The estimate of the parameter K takes plume depletion from deposition into account, using the suspension ratio SR(x) defined previously (Equation M-14). The suspension ratio depends on the deposition velocity of the uranium particles, which is based on the distribution of particle aerodynamic diameters in the plume. In the full calculation, there are 20 particle size distributions, but it was impractical to carry out the estimation of K in this level of detail. We reduced uranium particles in the source term to three broad categories and estimated an average deposition velocity for each category. The three categories correspond to releases from (1) air ducts fitted with dust collectors (DC), (2) large particles reentrained from the scrubbers (Plant 2/3 and Plant 8), and (3) small particles that penetrated the scrubbers (Plant 2/3 and Plant 8). We refer to the two categories of scrubber particles as (2) reentrained and (3) penetrating. Table M-1 shows the estimated dry deposition velocities for the three categories and the percentage of the uranium released during 1986–1988 belonging to each category. A footnote of Table M-1 shows the average wet deposition velocity for 1986–1988.

Fitting the diffusion model to the air monitoring data. The estimation problem consists of finding the distribution of the parameter K that gives the best fit of the diffusion function of Equation M-15 (averaged over stability classes A through F) to the data. This can be expressed as a least-squares problem

$$\sum_{i=1}^{N}\left[\ln(\chi_i u_i / (Qf_i)) - \ln KD_i\right]^2 = \text{minimum}\ , \qquad \text{(M-16)}$$

where χ_i is the measured concentration of uranium in the air at sampling station i, N is the number of sampling stations, and the stability-averaged diffusion function with plume depletion is

$$D_i = \sum_{k=\mathrm{A}}^{\mathrm{F}} \alpha_k D_{\mathrm{A}k}(x_i,\rho) \sum_{j=1}^{3} p_j \mathrm{SR}(x_i, v_j / u_i). \qquad \text{(M-17)}$$

Table M-1. Partitioning of Uranium Releases 1986–1988 for Calibration of the Uranium Air Dispersion Model

Component of release	Percent	Total deposition velocity v [a] (m s^{-1})
Dust collectors	23	0.0235
Scrubbers		
Reentrained	57	0.28
Penetrating	20	0.021

[a] Total deposition velocity $v = v_d + v_w$. Wet deposition v_w varied with rainfall. For 1986–1988, we estimated an average value of $v_w = 0.017$ m s^{-1}.

As noted, the index i corresponds to the sampling location; x_i is the distance from the center of the production area to sampling station i. The α_k are normalized frequencies of the stability classes A–F. The quantity $D_{Ak}(x_i,\rho)$ is the circular area source diffusion function (Equation M-15, except for the factor K) at distance x_i for stability k. The three broad categories of particle sizes are indexed by j, and p_j is the fraction of the release during 1986–1988 that was in category j. The suspension ratio $SR(x_i, v_j / u_i)$, which adjusts for plume depletion, depends on the distance x_i and the ratio of deposition velocity and wind speed, as noted previously; v_j denotes the total (dry plus wet) deposition velocity from Table M-1. Table M-2 shows the concentrations χ_i and other quantities that appear in Equations M-16 and M-17. The concentrations shown in Table M-2 have been adjusted for resuspended uranium, sampler efficiency, and analytic error. We discuss the adjustments below (page M-18).

For a single-parameter estimation of the form defined by Equations M-16 and M-17, it is possible to show that

$$K = \exp\left(\frac{1}{N}\sum_{i=1}^{N} \ln\frac{\chi_i u_i / (Qf_i)}{D_i}\right). \qquad \text{(M-18)}$$

minimizes the sum of the squares in Equation M-16.

Parametric uncertainty in the fitted model. Figure M-2 shows the plotted diffusion data from Table M-2 and the fitted diffusion function. The gray band around the curve (5th and 95th percentiles) shown in the figure corresponds to parametric estimation of diffusion as a function of the distance x from the source center (i.e., calibration of the model). This band represents the distribution of the calibration factor K. The bounds reflect a broader uncertainty distribution than what would be predicted by the residuals alone. The enlarged distribution considers (1) uncertainties introduced in the process of adjusting the gross concentrations, (2) uncertainties in the wind speed and wind-direction frequencies used in transforming the data to diffusion, (3) uncertainties in the release estimates (Q) for 1986–1988, and (4) uncertainty in estimated plume depletion due to deposition.

Table M-2. Conversion of Measured Air Concentrations of Uranium to Diffusion Units[a]

Station	Distance (km)	Wind direction	Wind directional frequency	Wind speed ($m\ s^{-1}$)	Year	Adjusted concentration ($fCi\ m^{-3}$)	Diffusion (m^{-2})
AMS1	0.9	S	0.043	2.24	1986	4.01	2.9×10^{-5}
					1987	4.39	4.1×10^{-5}
					1988	3.82	6.3×10^{-5}
AMS2	1.3	SW	0.127	2.20	1986	3.56	8.6×10^{-6}
					1987	3.61	1.1×10^{-5}
					1988	3.13	1.7×10^{-5}
AMS3	0.7	W	0.105	2.16	1986	6.49	1.9×10^{-5}
					1987	6.91	2.6×10^{-5}
					1988	2.92	1.9×10^{-5}
AMS4	1.4	NNW	0.054	2.19	1986	2.17	1.2×10^{-5}
					1987	2.03	1.5×10^{-5}
					1988	0.81	1.1×10^{-5}
AMS5	1.3	NE	0.044	2.43	1986	2.00	1.6×10^{-5}
					1987	2.07	2.1×10^{-5}
					1988	0.90	1.6×10^{-5}
AMS6	1.1	ENE	0.072	2.23	1986	2.12	9.1×10^{-6}
					1987	2.92	1.6×10^{-5}
					1988	0.96	9.5×10^{-6}
AMS7	1.6	ESE	0.022	1.29	1986	1.14	9.5×10^{-6}
					1987	1.64	1.8×10^{-5}
					1988	0.53	1.0×10^{-5}
AMS8	0.8	SW	0.127	2.20	1986	9.82	2.4×10^{-5}
					1987	9.01	2.8×10^{-5}
					1988	5.45	3.0×10^{-5}
AMS9	0.5	SW	0.127	2.20	1986	16.80	4.1×10^{-5}
					1987	15.40	4.8×10^{-5}
					1988	7.26	4.0×10^{-5}
AMS10	2.4	N	0.041	2.64	1987	0.91	1.1×10^{-5}
					1988	0.26	5.3×10^{-6}
AMS11	4.1	NE	0.044	2.43	1987	0.93	9.3×10^{-6}
					1988	0.35	6.2×10^{-6}

[a] Footnote is on the next page.

Table M-2. Conversion of Measured Air Concentrations of Uranium to Diffusion Units (continued)[a]

Station	Distance (km)	Wind direction	Wind directional frequency	Wind speed (m s^{-1})	Year	Adjusted concentration (fCi m^{-3})	Diffusion (m^{-2})
AMS12	6.2	SE	0.017	1.44	1987	0.26	3.9×10^{-6}
					1988	0.16	4.2×10^{-6}
AMS13	4.6	WSW	0.111	1.95	1987	1.70	5.4×10^{-6}
					1988	0.89	5.0×10^{-6}
AMS14	4.8	WSW	0.111	1.95	1988	0.78	4.4×10^{-6}

[a] The conversion is given by $D = \chi u / (Qf)$, where D is diffusion (m^{-2}), χ is adjusted concentration (fCi m^{-3}), u is wind speed (m s^{-1}), f is the frequency of the wind direction from the source to the receptor (dimensionless), and Q (fCi s^{-1}) is the annual average release rate that produced the measured concentration. Adjustment of the air concentrations is explained in the next section. Lognormally approximated distributions of Q (total uranium) are

Year		1986	1987	1988
Q (fCi s^{-1})	GM	7.15×10^{6}	5.55×10^{6}	3.12×10^{6}
	GSD	1.35	1.29	1.46

We treat the distributions of these uncertainties as being independent of each other and independent of the distribution of the residuals. We formulate this model as follows: K is a random variable such that

$$\ln\left(\frac{\chi_i u_i / (Qf_i)}{D(x_i)}\right) = \ln K + \ln\varepsilon + \ln\eta \qquad \text{(M-19)}$$

where the uncertainties ε and η are independently distributed, and where the expected values of $\ln\varepsilon$ and $\ln\eta$ are zero. The distribution of η is a composite of items (1)–(4) on page 15. The distributions of the individual components are discussed below (page M-23). The composite distribution is lognormal with GSD = 2. It accounts for exogenous uncertainties that were introduced into the data points by adjusting the measured air concentrations and transforming them to diffusion. It also accounts for uncertain deposition parameters in the model that are not estimated by the regression.

The distribution of ε is not assumed a priori but is estimated by bootstrap sampling of the residuals (Efron 1982). A composite sampling operation, based on the model of Equation M-19, is carried out by Monte Carlo methods. We summarize the steps as follows:

(1) Compute the sample mean

$$\overline{\ln K} = \frac{1}{N}\sum_{i=1}^{N}\ln\left(\frac{\chi_i u_i / (Qf_i)}{D_i}\right).$$

(2) Compute the residuals

$$\ln \varepsilon_i = \ln\left(\frac{\chi_i u_i / (Qf_i)}{D_i}\right) - \overline{\ln K}, \quad i = 1,\cdots,N.$$

(3) Perform Monte Carlo trials for $b = 1,2,\cdots,B$. At each trial draw two independent samples:

A. Draw a sample of size N from the distribution of the residuals (i.e., $\ln\varepsilon$) by the bootstrap method: assign equal probabilities to all residuals of step (2) and at each iteration, choose N of the residuals at random with replacement. Denote this sample by $(\ln\varepsilon_{b1}, \ln\varepsilon_{b2}, \cdots, \ln\varepsilon_{bN})$.

B. Draw a corresponding sample of size N from the known distribution of $\ln\eta$ (normal, since η is lognormal). Denote this sample by $(\ln\eta_{b1}, \ln\eta_{b2}, \cdots, \ln\eta_{bN})$.

The estimate of K for iteration b is

$$K_b = \exp\left(\frac{1}{N}\sum_{i=1}^{N}\left[\ln\left(\frac{\chi_i u_i / (Qf_i)}{D_i}\right) - \ln\varepsilon_{bi} - \ln\eta_{bi}\right]\right).$$

This process estimates the distribution of the geometric mean (GM) of K as estimated by the data. Using 1000 iterations ($B = 1000$), we found that the aggregate of iterates was well fitted by the lognormal distribution with geometric mean (GM) = 3.47 and geometric standard deviation (GSD) = 1.15. The nominal estimate from the data (i.e., the value obtained from the initial regression) is K = 3.48 (Equation M-18). The shaded area of Figure M-2 corresponds to the uncertainty band defined by the 5th and 95th percentiles of this lognormal distribution. This uncertainty in the diffusion function is propagated through all air dispersion calculations of uranium that use this dispersion model. The residual distribution (dashed lines) is also propagated as a component of uncertainty. Interpretation of this component is discussed in a later section (page M-57).

If we made the prior assumption that the residuals are a sample from a normal distribution, the need for Monte Carlo calculations in the foregoing procedure would be eliminated. Our primary reason for describing and carrying out the process in the manner presented is to emphasize the residuals and to show the parallel with a similar process for estimating two regression parameters when we fit a model to the radon data (page M-30). In each case, the bootstrap method frees us of the necessity to make any prior assumption about the form of the distribution of the residuals.

It is very important to realize that the gray uncertainty band in Figure M-2 represents only uncertainty related to parameterizing the theoretical diffusion curve (calibration). This 90% band excludes about half of the observations. Additional components of uncertainty, including one based on the residuals, are introduced when the curve is used to predict specific air concentrations. These uncertainties are discussed in a later section (page M-57).

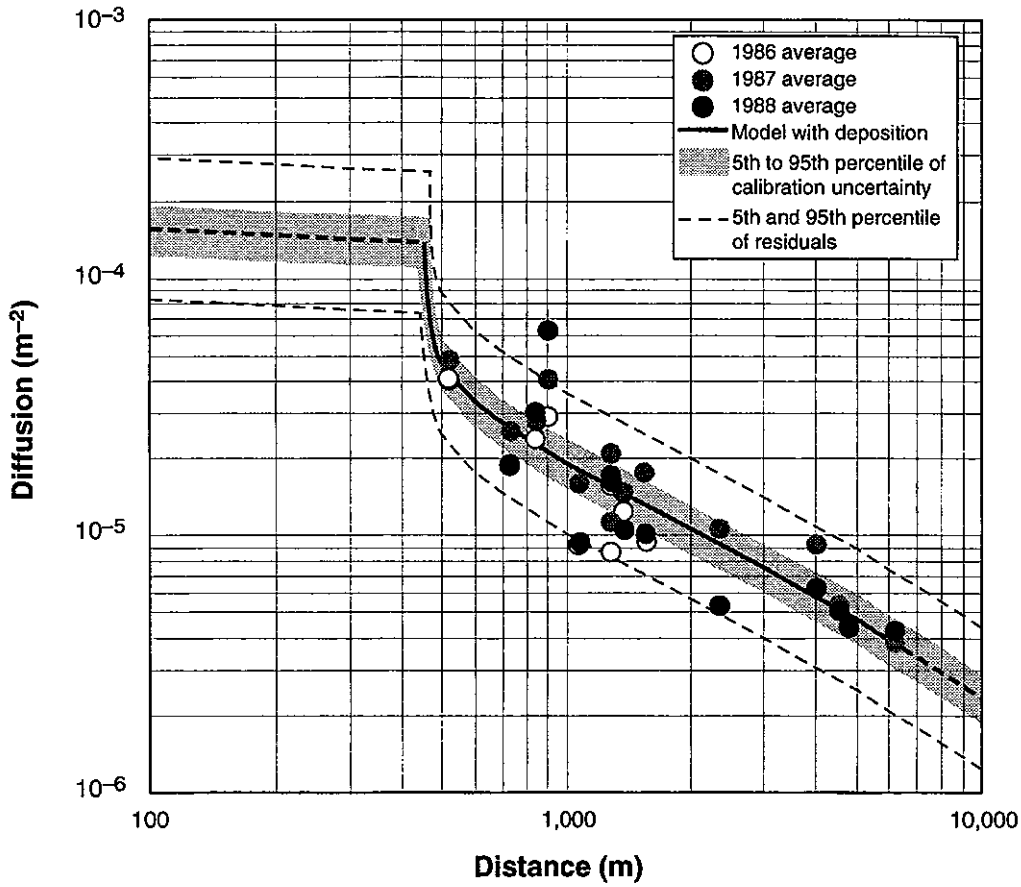

Figure M-2. Diffusion function for uranium fitted to air monitoring data taken during 1986–1988. Distance is measured from the center of the FMPC production area. The model is based on a Gaussian area source model for a circular region of radius 450 m, corresponding approximately to the part of the FMPC production area where the release sources are located. The data reflect the reduction of air concentrations by deposition of uranium from the plume; the model uses surface depletion to simulate the reduced concentrations. The gray band indicates a 90% confidence interval for the calibration (i.e., determining the diffusion curve), and the dashed lines show the 5th and 95th percentiles of the distribution of the residuals.

Adjusting measured air concentrations for resuspension, analytical error, and sampler inefficiency. Figure M-3 illustrates the corrections and adjustments that were made to the uranium air monitoring data before use in the model calibration. The first set of corrections illustrated in this schematic are discussed in Appendix N. The second set of adjustments are addressed in this appendix.

The equation describing the adjustment of the gross annual average concentrations is:

$$\chi'_{i,t} = (\chi_{i,t} / \Psi_t - d_{i,t} S_i \Phi / 1000) / E_{i,t} \qquad \text{(M-20)}$$

where

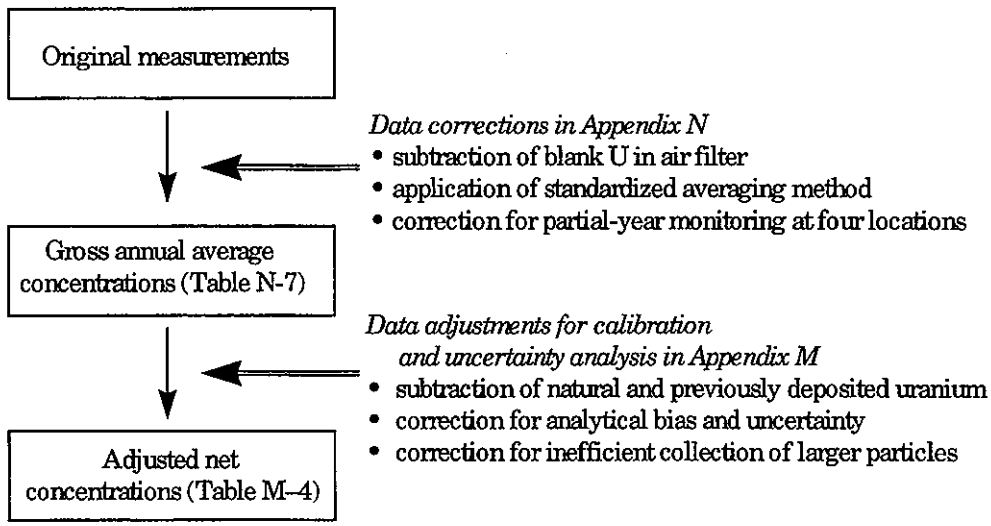

Figure M-3. Monitoring data from the three-year period, 1986–1988, were used for calibration of the model for uranium dispersion from the FMPC. The schematic illustrates the corrections and adjustments made to the original measurements of uranium in air before use in atmospheric dispersion model calibration and uncertainty analysis.

$\chi'_{i,t}$ = adjusted net concentration at sampler location i due to direct releases during year t (fCi U m^{-3} air)

$\chi_{i,t}$ = gross annual average concentration at location i for year t (fCi U m^{-3} air)

Ψ_t = analytical bias and uncertainty factor for year t (unitless)

$d_{i,t}$ = dust loading at location i for year t (µg soil m^{-3} air)

S_i = concentration of U in soil at sampler location i in 1986–1988 (pCi U g^{-1} soil)

Φ = soil uncertainty factor (unitless)

1000 = unit conversion factor = pCi $(fCi)^{-1} \times \mu g\ g^{-1} = 10^{-3} \times 10^{6}$

$E_{i,t}$ = fractional air sampler collection efficiency at location i in year t (unitless).

The amount of uranium in air from natural background uranium in soil, as well as uranium previously deposited on soil from FMPC releases, can be viewed as the "non-direct" component to the gross concentration measured in air. For calibration, we needed an estimate of the net concentration in air at a sampling station from the *current* year's releases of uranium. Although relatively unimportant historically, non-direct contributions to uranium in air were expected to be more important in these last three years of our study, when the releases of uranium were small. To estimate the non-direct contribution to uranium in air, we used site-specific measurements of uranium in soil at each sampler location and measurements of dust loading in air during the three years. Because the non-direct component of uranium in air was due to suspension of uranium-bearing soil particles, it was assumed that the dust in air at a given sampling location had an equal uranium concentra-

tion (per gram) as the surface soil at that location. Thus, in equation M-20, the non-direct component is represented by the product $d_{i,t}S_i$.

The concentrations of uranium in soil at the boundary stations, S_i, are given in Appendix C; the average of the measurements made in 1986–1988 was used in this analysis. For two stations, AMS8 and AMS9, we had no measurements of uranium in soil for 1986–1988. The soil concentrations at those two locations were estimated using the relative dispersion factor at those locations compared to location AMS2 (Table M-3). The concentrations of uranium in soil at the relatively distant locations AMS10–AMS14 were represented by a background average of 2.2 pCi U g^{-1}. Because the uranium in soil is not known with certainty, we included a soil uncertainty factor, Φ, which has a geometric mean of 1.0 and a geometric standard deviation (GSD) of 1.4. This GSD was observed by Myrick et al. (1983) in a background survey of uranium in soils from Ohio.

Table M-3. Relative Dispersion Parameters (χ/Q) for Locations AMS8 and AMS9, Used to Estimate Concentrations of Uranium in Soil, for Resuspension Contribution to Uranium in Air

Location	χ/Q Relative to Location AMS2
AMS8	1.4
AMS9	5.0

In addition to subtracting the non-direct component of the gross uranium concentration, a correction was made for measurement bias due to inefficient collection of larger particles. This issue is discussed in more detail in Appendix L, in the context of validation of results with earlier monitoring data. An analytical bias and uncertainty factor (Ψ_t) was included, based on quality assurance results from the two laboratories used during those three years (Table N-10). Uncertainties in both the collection efficiency and the analytical factor were propagated through the computation of adjusted net concentrations of uranium in air.

Table M-4 presents the numerical values of the parameters used for each location and year, as well as the adjusted net concentrations of uranium in air. The Crystal Ball uncertainty analysis software (Decisioneering 1993) was used to propagate uncertainties in Equation M-20, where the uncertain input parameters were $d_{i,t}$, Φ, Ψ_t, and $E_{i,t}$. The last three columns in Table M-4 present percentile values of the output uncertainty distribution for net adjusted uranium concentrations. These distributions of values were used in the model calibration. Table M-5 summarizes the sources of uncertainty and the measures of dispersion of the corresponding distributions that were propagated through each line of Table M-4. To obtain a single distribution for conservative representation of uncertainty in the data adjustments of Table M-4, we used the largest ratio of the 95th divided by the 50th percentile (1.42) and assumed a lognormal distribution, for which the GSD would be 1.24 ($= 1.42^{1/1.65}$). In the calibration of the air dispersion model, this distribution is one of the four components of the exogenous term $\ln \eta$ (Equation M-19). The remaining components and the composite uncertainty distribution are discussed in the next subsection.

Table M–4. Computation of Adjusted Net Uranium Concentrations in Air Used in Model Calibration[a]

Location	Year	S_i pCi g^{-1}	$d_{i,t}$ µg m^{-3}	$d_{i,t}S_i$ fCi m^{-3}	$\chi_{i,t}$ fCi m^{-3}	Ψ_t	$E_{i,t}$	$\chi'_{i,t}$ (fCi m^{-3})[b]	$\chi'_{i,t}$ (fCi m^{-3}) Percentiles of Distribution		
									5%	50%	95%
BS1	1986	4.0	33.3	0.13	2.84	1.04	0.65	4.00	3.40	4.01	4.80
BS2	1986	8.93	33.6	0.30	2.87	1.04	0.69	3.56	2.95	3.56	4.33
BS3	1986	44.6	37.1	1.65	6.15	1.04	0.67	6.36	4.63	6.49	8.31
BS4	1986	5.2	38.6	0.20	1.74	1.04	0.68	2.17	1.80	2.17	2.64
BS5	1986	5.7	32.4	0.18	1.58	1.04	0.67	1.99	1.65	2.00	2.42
BS6	1986	7.07	36.2	0.26	1.71	1.04	0.66	2.10	1.71	2.12	2.57
BS7	1986	3.63	31.9	0.12	0.92	1.04	0.68	1.13	0.94	1.14	1.38
AMS8	1986	12.5	33.5	0.42	7.33	1.04	0.68	9.75	8.38	9.82	11.6
AMS9	1986	44.6	36.5	1.63	13.21	1.04	0.66	16.8	13.8	16.8	20.5
BS1	1987	4.0	29	0.12	3.31	1.13	0.64	4.40	3.71	4.39	5.32
BS2	1987	8.93	31.9	0.28	3.08	1.13	0.68	3.59	2.98	3.61	4.33
BS3	1987	44.6	31.9	1.42	6.76	1.13	0.67	6.81	5.15	6.91	8.75
BS4	1987	5.2	34.7	0.18	1.75	1.13	0.68	2.01	1.66	2.03	2.49
BS5	1987	5.7	30.7	0.17	1.77	1.13	0.67	2.08	1.72	2.07	2.55
BS6	1987	7.07	33.5	0.24	2.39	1.13	0.65	2.89	2.40	2.92	3.55
BS7	1987	3.63	34.8	0.13	1.4	1.13	0.68	1.64	1.36	1.64	2.00
AMS8	1987	12.5	34.5	0.43	7.37	1.13	0.67	9.09	7.68	9.01	10.8
AMS9	1987	44.6	37.8	1.68	13.32	1.13	0.66	15.3	12.2	15.4	18.9
AMS10	1987	2.2	47.2	0.10	0.67	0.91	0.7	0.90	0.75	0.91	1.08
AMS11	1987	2.2	42.3	0.09	0.7	0.91	0.73	0.93	0.78	0.93	1.10
AMS12	1987	2.2	35.2	0.08	0.25	0.91	0.79	0.25	0.18	0.26	0.32
AMS13	1987	2.2	44.5	0.10	1.26	0.91	0.76	1.69	1.46	1.70	1.98
BS1	1988	4.0	31.6	0.13	2.6	1.06	0.61	3.81	3.29	3.82	4.56
BS2	1988	8.93	38.2	0.34	2.57	1.06	0.67	3.11	2.59	3.13	3.73
BS3	1988	44.6	35.7	1.59	3.59	1.06	0.65	2.76	1.20	2.92	4.15
BS4	1988	5.2	39.4	0.20	0.77	1.06	0.66	0.79	0.58	0.81	1.03
BS5	1988	5.7	36.6	0.21	0.83	1.06	0.65	0.88	0.65	0.90	1.13
BS6	1988	7.07	36.6	0.26	0.9	1.06	0.63	0.94	0.66	0.96	1.22
BS7	1988	3.63	37.3	0.14	0.5	1.06	0.65	0.52	0.37	0.53	0.67
AMS8	1988	12.5	39.8	0.50	4.32	1.06	0.66	5.42	4.58	5.45	6.37
AMS9	1988	44.6	40.8	1.82	6.78	1.06	0.64	7.15	4.92	7.26	9.36
AMS10	1988	2.2	51	0.11	0.25	0.89	0.68	0.25	0.15	0.26	0.35
AMS11	1988	2.2	40.9	0.09	0.3	0.89	0.72	0.34	0.25	0.35	0.44
AMS12	1988	2.2	37.8	0.08	0.18	0.89	0.78	0.15	0.09	0.16	0.22
AMS13	1988	2.2	48.7	0.11	0.69	0.89	0.76	0.88	0.73	0.89	1.05
AMS14	1988	2.2	37.1	0.08	0.6	0.89	0.76	0.78	0.66	0.78	0.93

[a] See text for explanation of parameter symbols.

[b] Nominal values. Percentile values from uncertainty analysis were used in calibration.

Table M-5. Sources of Uncertainty in Adjusting Uranium Air Monitoring Data

Quantity	Distribution type	Measure of dispersion	Value or range
Air sampler efficiencies	Normal	CV[a]	2.8 – 8.6%[b]
Resuspension			
Soil uncertainty factor	Lognormal	GSD[c]	1.4[d]
Dust loading	Normal	CV[a]	2%[e]
Analytical uncertainty factor	Normal	CV[a]	7%[f]
Meteorological data (1987–1991)			
Wind speed	Lognormal	GSD[c]	1.07 – 1.16
Wind directional frequency	Lognormal	GSD[c]	1.03 – 1.25
FMPC airborne releases (1986–1988)	Lognormal	GSD[c]	1.29 – 1.46
Composite	—	95th/50th percentile	1.16 – 1.42
	Lognormal	Maximum GSD[c, g]	1.24

[a] Coefficient of variation = standard deviation / mean.

[b] The calibration efficiency was determined separately for each sampler and year (see Appendix L). The range of the CV for all combinations for 1986–1988 is shown.

[c] Geometric standard deviation.

[d] This GSD was observed by Myrick et al. (1983) in a background survey of uranium in soils from Ohio.

[e] Killough et al. (1993) Appendix O. Data are from boundary air monitoring stations for 1986–1988.

[f] Based on a review of the fluorimetric analytical method [see Killough et al. (1993) Appendix L].

[g] The maximum is for all years (1986–1988) and sampler locations.

Combining exogenous uncertainties for the air dispersion model calibration. Equation M-19 presented two uncertainty terms for the model calibration. The first ($\ln \varepsilon$) corresponded to regression residuals, i.e., intrinsic factors related to sampling. The second ($\ln \eta$) was characterized as a combination of exogenous or external factors introduced by data adjustments, transformation to diffusion, and uncertain parameters in the diffusion model. We described the data adjustment uncertainties and their composite in the previous subsection. We now combine all of the uncertainties represented by the term $\ln \eta$ in Equation M-19. As noted in the discussion of that equation, these uncertainties are

(1) uncertainties introduced in the process of adjusting the gross concentrations (discussed in the previous subsection)
(2) uncertainties in the ratio f / u of wind-direction frequencies divided by wind speed, used in transforming the data to diffusion
(3) uncertainties in the uranium release estimates Q for 1986–1988
(4) uncertainty in the estimated plume depletion due to deposition.

Table M-6 relates the exogenous uncertainty random variable η to these factors and summarizes the properties of the distributions of the factors. We have assumed lognormality for each distribution, which implies (because only products and quotients are involved) that the composite distribution is lognormal.

Table M-6. Exogenous Uncertainties in Calibrating the Air Dispersion Model for Uranium

Exogenous uncertainty $\eta = \frac{\chi}{Q \cdot (f/u) \cdot KD^* \varphi_{dep}}$,

where D^* = diffusion adjusted for deposition
K = calibration factor to be determined by regression

Symbol	Quantity	GSD
χ	Adjusted air concentration (pCi m^{-3})	1.24[a]
Q	Release rate during calibration period (pCi s^{-1})	1.46[b]
f/u	Ratio of wind directional frequency over wind speed (s m^{-1})	1.27[c]
φ_{dep}	Plume depletion uncertainty (dimensionless)	1.74[d]
η	Composite (Equation M-3)	2.1

[a] Table M-5.

[b] Footnote to Table M-2. The maximum GSD for the three years is used.

[c] Based on an estimate of year-to-year variability of f/u for each wind direction during 1987–1991, using the FMPC meteorological dataset. The GSD shown is the maximum for all wind directions.

[d] Derived from the assumption that deposition velocities are known to within a factor of 3 (i.e., 95th/50th percentile = 3). With the surface depletion model we used, a factor of 3 in the deposition velocity corresponds to a factor between 2 and 3 in fractional depletion over most of the range of v/u, where v is total deposition velocity. We assume an uncertainty factor of 2.5 in fractional depletion (i.e., 95th/50th percentile = 2.5). If the distribution is lognormal, this assumption gives GSD = $2.5^{1/1.65}$ = 1.74.

DISPERSION OF RADON FROM THE K-65 SILOS

Using air monitoring data for radon to model air dispersion of radon and its decay products released from the K-65 silos west of the production area is similar in some respects to the corresponding problem for uranium released from the production area, but quite different in others. The general form of the postulated diffusion model is the same, and there are radon monitoring data from stations located at various distances from the point of release. But the radon data differ from the uranium data in quality, relationship to release rates, difficulty of separating releases from background at some stations, and spatial and temporal coverage. Nevertheless, these data indicate a coherent trend in diffusion vs. distance from the source and must be carefully integrated into the reconstruction of radon air concentrations and dose.

Overview

The details of the derivations associated with calibrating the radon dispersion model tend to be confusing. It is helpful to have a sense of where the discussion is going before plunging into it. This overview is intended to convey such a sense while postponing the intricacies of the reasoning.

We need to make a preliminary point. The fundamental form of the diffusion function is the circular area-source Gaussian model previously applied to uranium (Equation M-15). There are two differences: (1) the circular area is much smaller, $\rho = 50$ m, corresponding approximately to the areas of the domes and some of the surrounding berms; and (2) the calibration factor K in Equation M-15 is replaced by a function of two parameters that are determined by regression. When we speak of diffusion functions below, they are like $D_A(x,\rho)$ in Equation M-15 with exceptions (1) and (2) as noted. Remember that $D_A(x,\rho)$ depends on stability class through the diffusion coefficients σ_y and σ_z (Equation M-15).

We begin this overview by observing that three models are needed to simulate air dispersion of radon released from the K-65 silos. The models are based on the same Gaussian area-source prototype, but they differ in calibration. These calibrations must account for

1. Releases that occur at a constant rate 24 hours per day, corresponding to the years before 1980 when radon was vented to the atmosphere through penetrations in the K-65 silo domes
2. Release rates that differ between day and night, with one model calibrated for each. These models would apply to the 1980s, when different release mechanisms dominated according to the time of day.

After the penetrations in the silo domes were sealed in June 25, 1979, releases were substantially reduced. But daytime and nighttime release rates were no longer equal, because heating of the gas in the head space increased the pressure and enhanced rates of leakage of radon through cracks in the containment (for convenience, we refer to this mechanism as thermal pumping). The other component of release during this period was diffusion through these cracks, and this diffusion is assumed to occur at a constant rate 24 hours per day. Thus, during the day, the release is thermal pumping + diffusion; during the night, the release is diffusion only. Table M-7 shows the estimated release rate for each mechanism. The mechanisms and the methods of estimation are described in Appendix J of Voillequé et al. (1995).

Table M-7. Estimated Annual Releases of Radon from the K-65 Silos (Ci year^{-1})

Release type	5th percentile	Median	95th percentile
Unconstrained (before July 1979)	4200	6200	8700
Constrained (after July 1979)			
Thermal pumping (daytime)	230	810	1600
Diffusion (24 hours)	72	130	240

The following equations, which are based on median values from Table M-7, give nominal release rates for the unconstrained period (before July 1979) and the daytime and nighttime components for the constrained period:

$$Q_{24\text{-h}} = \frac{6200 \text{ Ci year}^{-1} \times 10^{12} \text{ pCi Ci}^{-1}}{3.154 \times 10^{7} \text{ s year}^{-1}} = 1.97 \times 10^{8} \text{ pCi s}^{-1} \qquad \text{(M-21)}$$

$$Q_{\text{day}} = \frac{(810 \times 2 + 130) \text{ Ci year}^{-1} \times 10^{12} \text{ pCi Ci}^{-1}}{3.154 \times 10^{7} \text{ s year}^{-1}} = 5.55 \times 10^{7} \text{ pCi s}^{-1} \qquad \text{(M-22)}$$

$$Q_{\text{night}} = \frac{130 \text{ Ci year}^{-1} \times 10^{12} \text{ pCi Ci}^{-1}}{3.154 \times 10^{7} \text{ s year}^{-1}} = 4.12 \times 10^{6} \text{ pCi s}^{-1} \qquad \text{(M-23)}$$

In Equation M-22, the value 810 Ci year^{-1} is multiplied by 2 because the annual average includes nighttime, when the thermal pumping is assumed to be zero.

Now suppose we have diffusion models, $D_{24\text{-h}}$, D_{day}, and D_{night}, that are calibrated to correspond to the respective release periods of Equations M-21 through M-23. Then average concentrations at a given location for the periods of unconstrained and constrained releases could be predicted as follows:

Pre 1980: $$\chi_{24\text{-h}} = (Qf / u)_{24\text{-h}} D_{24\text{-h}} \qquad \text{(M-24)}$$

and

1980s: $$\chi_{24\text{-h}} = \frac{1}{2}(\chi_{\text{day}} + \chi_{\text{night}}) = \frac{1}{2}\left[\left(\frac{Qf}{u}\right)_{\text{day}} D_{\text{day}} + \left(\frac{Qf}{u}\right)_{\text{night}} D_{\text{night}}\right]. \qquad \text{(M-25)}$$

The radon data from systematic observations at a variety of locations belong to the period of constrained releases (Equation M-25); observations in the pre-1980 period of unconstrained releases are fragmentary. Because of (1) the differences in the daytime and nighttime release rates and (2) the different meteorological frequencies for night and day, Equation M-25 expresses the relationships that must be considered in the calibration. It is not possible to calibrate a daytime and a nighttime component separately, because the data represent averages over longer periods that include both day and night. Thus, the data cannot be directly resolved into these components. Another complication is the necessity to subtract estimates of background radon from the measured concentrations, so that the quantities $\chi_{24\text{-h}}$ of Equations M-24 and M-25 may be interpreted as net concentrations (i.e., representing radon attributable to K-65 releases only). The next section of this appendix (beginning on page M-37) gives details about the analysis of the radon data, and in particular, estimation of net concentrations from gross measurements.

Let us assume for the moment that a calibration can be carried out with Equation M-25 to estimate the component diffusion functions D_{day} and D_{night}. Then it is reasonable to combine these components to estimate dispersion for the pre-1980 period as follows:

$$D_{24\text{-h}} = \left(\frac{\chi u}{Qf}\right)_{24\text{-h}} = \frac{1}{2}\left[\left(\frac{f}{u}\right)_{\text{day}} D_{\text{day}} + \left(\frac{f}{u}\right)_{\text{night}} D_{\text{night}}\right] \cdot \left(\frac{f}{u}\right)_{24\text{-h}}^{-1} \qquad \text{(M-26)}$$

This equation follows from the assumption that $Q_{\text{day}} = Q_{\text{night}} = Q_{24\text{-h}}$ during the pre-1980 period of unconstrained releases. Details of this calibration follow, and Equation M-25 is fundamental to the derivation.

Daytime vs. Nighttime Releases

There are two major datasets based on radon air monitoring near the FMPC during the 1980s. The first consists of measurements taken by Mound Laboratory during 1984–1986 at 17 stations located, for the most part, within the site boundary. The second dataset is based on FMPC environmental monitoring of radon, which consists of measurements taken at the site boundary stations (BS1–BS7, about 1 km from the center of the production area, on average) during the years 1981 through 1987.

These two datasets present important contrasts. The Mound data, because of the proximity of the sampling stations to the K-65 silos, generally show higher radon concentrations than do the FMPC data, which are closer to background levels. When the FMPC data are averaged over the seven years of observation, the average for each station exceeds the background average. At all boundary stations except two, however, Fisher's least significant difference test (Snedecor and Cochran 1967) cannot distinguish the average net value (station minus background) from zero at the 5% level. The two exceptions are BS6 (marginal; the probability of a larger difference is actually 5.3%) and BS7 (decisive; the probability of a larger difference is 1.3%). Also, four of the 14 Mound Laboratory sampling stations gave results that the least significant difference test failed to distinguish from background: stations 9, 10, 13, and 15. But it is important to remember that the seven-year-average net concentrations for the FMPC boundary station data and the one-year average net concentrations for the Mound stations are statistically unbiased estimates of net air concentrations for the respective stations and sampling periods. Moreover, these data are not interpreted in isolation, but as part of a spatial trend that is supported by the aggregate of both the Mound and the FMPC datasets. And the visual trend (Figure M-4) shows none of the locally erratic signs that usually are seen when some of the measurements lose all significance. Accordingly, we submit that in this larger context, the data that are statistically indistinguishable from background should not be discarded as if they were invalid.

We see that the gray uncertainty band in Figure M-4 excludes about one-third of the observations, just as the corresponding band for the uranium curve excluded about half of the uranium data points. It must be borne in mind that the shaded region in Figure M-4 represents only uncertainty in parameterizing the theoretical curve (calibration); it does not represent all of the uncertainty associated with using the curve to predict air concentrations at various locations over time. Additional components of uncertainty are discussed in a later section of this appendix (page M-57).

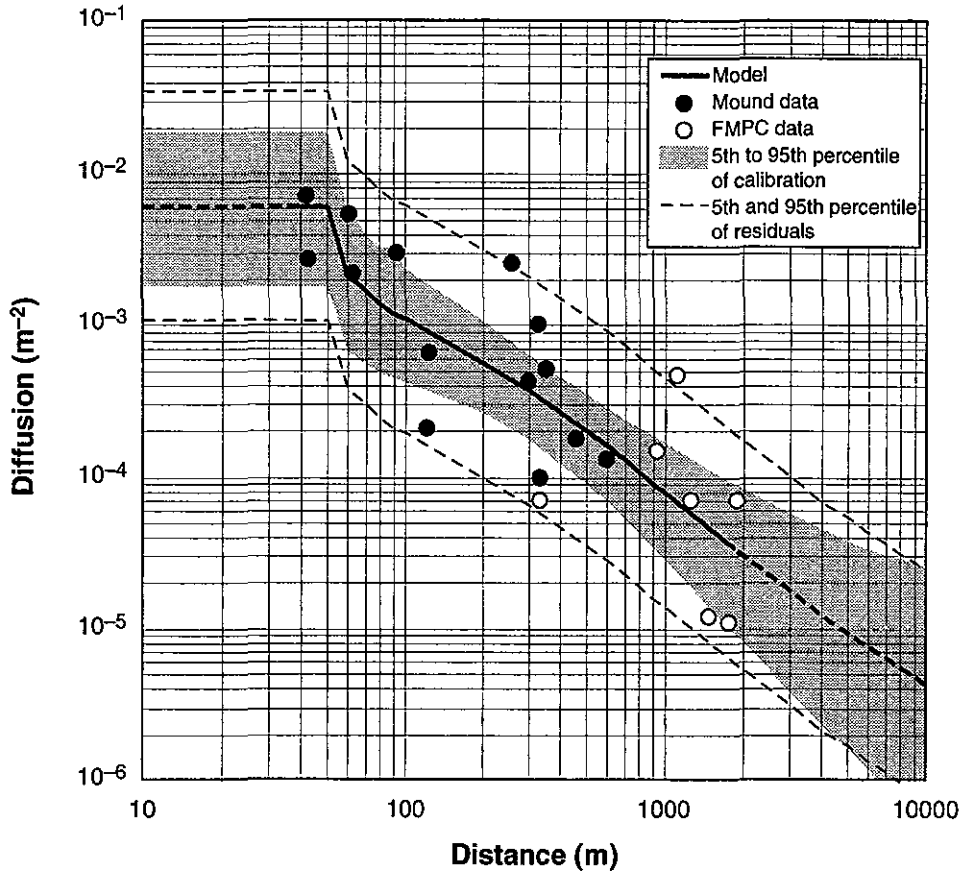

Figure M-4. Daytime diffusion data and circular area-source model for radon released from the K-65 silos. The Mound Laboratory data (black points) represent the period July 2, 1985 through July 2, 1986. The FMPC boundary station data (white points) represent quarterly cumulative samples at BS1–BS7 from 1981 through 1987, averaged over the seven-year period. The vertical dimension of the shaded area is a 90% confidence interval based on uncertainties in quantities used to convert concentrations to diffusion units (including release rates during the 1980s), on estimates of uncertainty in the data, and on residual uncertainty in a two-parameter regression of the area-source model on the data. This band represents uncertainty in the calibration (determination of the curve). The dashed lines show the 5th and 95th percentiles of the distribution of residuals.

Table M-8 shows fractional frequencies of the atmospheric stability classes based on the five-year annual-average FMPC meteorological dataset in the column labeled 24-hour. The least-stable categories belong to daytime and the most-stable to nighttime. If we begin at class A and add frequencies, we see that classes A–D account for 47% of the time. Thus, we make the break between day and night between classes D and E (technically, we should associate a small fraction of class E with daytime and the complementary fraction with nighttime, but the distortion from not doing so is minor). For daytime, then, we renormalize the frequencies of classes A–D so that they sum to 1; for nighttime, we do the same for classes E and F. The normalized frequencies are shown in Table M-8.

Table M-8. Frequencies of the Pasquill-Gifford Stability Classes in the FMPC Five-Year Meteorological Dataset

Class	24-hour	Daytime	Nighttime
A	0.0637	0.1347	
B	0.0310	0.0656	
C	0.0446	0.0942	
D	0.3340	0.7056	
E	0.2881		0.5470
F	0.2385		0.4530
Total	0.9999	1.0001	1.0000

We now express the diffusion functions for day and night at downwind distance x as

$$D_{\text{day}}(x) = K\left(\frac{x}{\rho}\right)^c \sum_{k=\text{A}}^{\text{D}} \alpha_k^{\text{day}} D_{\text{A}k}(x,\rho), \quad D_{\text{night}}(x) = K\left(\frac{x}{\rho}\right)^c \sum_{k=\text{E}}^{\text{F}} \alpha_k^{\text{night}} D_{\text{A}k}(x,\rho) \qquad \text{(M-27)}$$

where α^{day} and α^{night} are the stability frequencies for daytime and nighttime, respectively, from Table M-8, and the function $D_{\text{A}k}(x,\rho)$ is based on Equation M-15 with σ_y and σ_z corresponding to stability Class k. The calibration factor K that appears in Equation M-15 is replaced by the expression $K(x/\rho)^c$, which is to be applied jointly to the two functions in Equation M-27; the joint distribution of the parameters K and c is to be estimated from the data by regression. We will return to the interpretation of this factor in a subsequent section, beginning on page M-34.

We have said that Equation M-25 is fundamental to the transformation of the data to diffusion. Let us consider the sampling station i at distance $x = x_i$ from the source and rewrite Equation M-25 as follows:

$$\chi(x_i) = \frac{1}{2}\left[\left(\frac{Qf}{u}\right)_{\text{day}} D_{\text{day}}(x_i) + \left(\frac{Qf}{u}\right)_{\text{night}} D_{\text{night}}(x_i)\right] = \frac{D_{\text{day}}(x_i)}{2}\left[\left(\frac{Qf}{u}\right)_{\text{day}} + r(x_i)\cdot\left(\frac{Qf}{u}\right)_{\text{night}}\right]. \qquad \text{(M-28)}$$

The function $r(x)$ is the ratio of the functions D_{night} and D_{day}:

$$r(x) = \frac{\sum_{k=\text{E}}^{\text{F}} \alpha_k^{\text{night}} D_{\text{A}k}(x,\rho)}{\sum_{k=\text{A}}^{\text{D}} \alpha_k^{\text{day}} D_{\text{A}k}(x,\rho)}. \qquad \text{(M-29)}$$

The adjustment factor $K(x/\rho)^c$ cancels from the ratio, and hence $r(x)$ is independent of the (as yet) unknown parameters K and c. Solving Equation M-29 for D_{day}, and evaluating for $x = x_i$, we get

$$D_{\text{day},i} = \frac{\chi(x_i)}{\frac{1}{2}\left[\left(\frac{Qf}{u}\right)_{\text{day},i} + r(x_i)\cdot\left(\frac{Qf}{u}\right)_{\text{night},i}\right]} . \qquad \text{(M-30)}$$

The release rates Q_{day} and Q_{night} were calculated in Equations M-22 and M-23, respectively. For each monitoring station, Table M-9 gives the meteorological ratios f/u for day and night and the measured radon concentrations $\chi(x_i)$. With these data and the calculated values of $r(x_i)$, Equation M-30 transforms the measured air concentrations to daytime diffusion. These values are the ones plotted in Figure M-4. The next step is to fit the function $D_{\text{day}}(x)$, as shown in Equation M-27, to the plotted diffusion points. This is done by using regression to estimate the parameters K and c. Once these parameters are known, D_{night} is also known (Equation M-27).

Calibration of the Air Dispersion Model to the Mound and FMPC Radon Data

We now describe the regression procedure that fits the model $D_{\text{day}}(x;K,c)$ of Equation M-27 to the combined dataset. In fact, the regression is carried out a large number of times (1000) in Monte Carlo trials to simulate bootstrap sampling from the residuals and sampling from a lognormal distribution that represents uncertainties in the radon data and exogenous uncertainties in other data that were used to perform the transformation from concentration to diffusion. The result is an uncertainty distribution for the mean air concentration at each distance from the source, as well as a joint uncertainty distribution for K and c. The process is analogous to the one that was performed for uranium, but now there are two parameters to be estimated rather than one, and consequently we must discuss the estimation in terms of regression. However, we formulated the uranium parameter estimation in terms of least-squares of residuals (Equation M-16), and the parallels should be apparent.

We formulate the basic problem as a residual least-squares optimization for $D_{\text{day}}(x;K,c)$ and the diffusion-converted radon data:

$$\sum_{i=1}^{N}\left[\ln D_{\text{day},i} - \ln D_{\text{day}}(x;K,c)\right]^2 = \text{minimum} , \qquad \text{(M-31)}$$

where the daytime diffusion value at station i, $D_{\text{day},i}$, is given by Equation M-30, and the function $D_{\text{day}}(x;K,c)$ is defined by Equation M-27. When the logarithm is applied to the factor $K(x/\rho)^c$, the expression in the brackets could be rearranged in the form of a linear regression for the parameters K and c, but rewriting the equation would serve no purpose in this discussion. The regression estimates an uncertainty distribution expressed by the residuals, but as with uranium, we consider additional uncertainty that has been introduced by conversions and by the data themselves. We rewrite the model as

Table M-9. Transformation of 1980s Radon Data to Diffusion

Station	Distance (m)	f/u (s m^{-1}) Day	f/u (s m^{-1}) Night	Concentration (pCi m^{-3})	Diffusion (m^{-2}) Day	Diffusion (m^{-2}) Night	Ratio
MLM3	42	0.025	0.046	7700	6.2×10^{-3}	3.5×10^{-2}	5.6
MLM1	43	0.046	0.097	5500	2.3×10^{-3}	1.3×10^{-2}	5.6
MLM4	61	0.020	0.036	4400	4.5×10^{-3}	2.5×10^{-2}	5.6
MLM2	63	0.024	0.021	1900	2.0×10^{-3}	1.1×10^{-2}	5.6
MLM5	93	0.044	0.068	5300	2.6×10^{-3}	1.5×10^{-2}	5.6
MLM13	121	0.027	0.016	180	2.0×10^{-4}	1.1×10^{-3}	5.6
MLM6	124	0.046	0.097	1400	5.7×10^{-4}	3.2×10^{-3}	5.6
MLM12	261	0.011	0.019	1200	2.2×10^{-3}	1.4×10^{-2}	6.1
MLM7	301	0.046	0.097	950	3.7×10^{-4}	2.4×10^{-3}	6.3
MLM11	325	0.020	0.036	910	8.8×10^{-4}	5.7×10^{-3}	6.4
BS6	332	0.048	0.045	130	6.6×10^{-5}	4.3×10^{-4}	6.5
MLM15	334	0.048	0.045	180	9.3×10^{-5}	6.0×10^{-4}	6.5
MLM8	351	0.033	0.094	920	4.2×10^{-4}	2.8×10^{-3}	6.6
MLM9	455	0.052	0.110	500	1.6×10^{-4}	1.2×10^{-3}	7.1
MLM10	599	0.058	0.108	400	1.2×10^{-4}	9.2×10^{-4}	7.8
BS5	924	0.024	0.021	140	1.4×10^{-4}	1.2×10^{-3}	8.6
BS7	1121	0.014	0.022	320	4.1×10^{-4}	3.6×10^{-3}	8.8
BS1	1262	0.044	0.068	160	6.3×10^{-5}	5.6×10^{-4}	8.9
BS3	1468	0.046	0.097	34	1.1×10^{-5}	9.9×10^{-5}	9.1
BS4	1762	0.029	0.081	21	9.0×10^{-6}	8.3×10^{-5}	9.3
BS2	1905	0.058	0.108	240	6.4×10^{-5}	6.0×10^{-4}	9.4

$$\ln D_{\text{day},i} = \ln D_{\text{day}}(x_i;K,c) + \ln\varepsilon + \ln\eta \ , \qquad \text{(M-32)}$$

where $\ln\varepsilon$ has expected value zero and is associated with the residuals; $\ln\eta$ is assumed to be normally distributed, independently of $\ln\varepsilon$, with expected value zero, and is estimated in advance from uncertainties related to the data and their transformation to diffusion. We will return to the details about the distribution of $\ln\eta$, but for the time being, let us assume that this distribution is known and is available for Monte Carlo sampling. As we did for uranium, we sample the residuals by a bootstrap method (Efron 1982). The method does not require us to make prior assumptions about the form of the distribution (except that it has mean zero, as noted above). The steps in the procedure are as follows:

(1) Perform the regression of Equation M-31 to obtain parameter estimates K_0 and c_0.

(2) Estimate the residuals

$$\ln\varepsilon_{0i} = \ln D_{\text{day},i} - \ln D_{\text{day}}(x_i;K_0,c_0) \ , \quad i = 1,\cdots,N.$$

(3) Perform Monte Carlo trials for $b = 1,2,\cdots,B$. At each trial draw two independent samples:

A. Draw a bootstrap sample of size N from the distribution of the residuals obtained in step (2). To do this, assign equal probabilities to all residuals and sample with replacement until N are obtained. Denote this sample by $(\ln \varepsilon_{b1}, \ln \varepsilon_{b2}, \cdots, \ln \varepsilon_{bN})$.
B. Draw a corresponding sample of size N from the known distribution of $\ln \eta$. Denote this sample by $(\ln \eta_{b1}, \ln \eta_{b2}, \cdots, \ln \eta_{bN})$.

Define D^*_{bi} by

$$\ln D^*_{bi} = \ln D_{\text{day},i} - \ln \varepsilon_{bi} - \ln \eta_{bi}\,, \quad i = 1, \cdots, N$$

and perform the regression

$$\sum_{i=1}^{N} \left[\ln D^*_{bi} - \ln D_{\text{day}}(x_i; K, c)\right]^2 = \text{minimum}$$

for the parameters K_b and c_b, which are stored for later analysis. Also save the predicted diffusion estimates at each of a specified set of distances, say $X_1, \cdots, X_M$ (we use capital letters to distinguish these locations from the sampling stations; $X_1, \cdots, X_M$ range from 10 m to 10,000 m in logarithmic intervals and are used for plotting). We store the predicted values

$$D_{\text{day}}(X_j; K_b, c_b), \quad j = 1, \cdots, M$$

for each Monte Carlo trial b. The distributions shown by these latter samples permit us to draw the uncertainty band (the gray area in Figure M-4) about the nominal model curve $Y = D_{\text{day}}(X; K_0, c_0)$, where $10 \text{ m} \le X \le 10{,}000 \text{ m}$.

The nominal curve drawn in Figure M-4 is the curve that results from the initial regression, before the Monte Carlo trials begin. The nominal parameter estimates are K_0 = 0.612 and c_0 = 0.213. The set of residuals based on this curve and the original data are used repeatedly for the bootstrap samples, which differ randomly from one Monte Carlo trial to the next. The second error term in Equation M-32, $\ln \eta$, is an exogenous uncertainty component that is included in the analysis. It is to this latter distribution that we turn next.

The two parts of the uncertainty expressed by η are (1) the radon air concentration measurements and (2) parameters used in transforming the net concentrations to diffusion (quantities that appear in the denominator in Equation M-30). We begin with (1).

As we have noted previously, the Mound data and the FMPC data are sets with distinct characteristics. The Mound data represent one year, and the FMPC data (as aggregated for this purpose) represent seven years. In each case, we assume that we are estimating the long-term behavior of a dynamic system. The relative error in the net concentrations is large at the boundary stations, because at those distances from the K-65 silos, the measured concentrations are not much above background. The coefficients of variation (CV = standard deviation divided by mean) of the net concentrations for the boundary stations average 2.5. For the Mound data, the CVs are much less, because the measurements are generally well above background. Details about the sampling and the data analysis are given in the next section (page M-37), but for now we wish to emphasize the strategy.

One approach to consolidating the two datasets for regression would be to use a weighting scheme to compensate for the greater uncertainty in the FMPC data. Such schemes, however, usually apply to situations where it is the residuals that appear to come from more than one distribution, rather than an exogenous uncertainty term such as we are introducing here. Instead, we have chosen to assume that the average CV for the FMPC data (2.5, noted in the previous paragraph) should apply to all of the net-concentration data, FMPC and Mound alike. This approach has the effect of increasing the overall estimate of the data uncertainty, in conformity with the principle of expressing conservatism in uncertainty estimates.

We assume, then, that the distribution for data uncertainty is lognormal with CV = 2.5. For any lognormal distribution,

$$\mathrm{CV} = \sqrt{\exp(\sigma^2) - 1} \tag{M-33}$$

(Equation M-4), where $\sigma = \ln(\mathrm{GSD})$ is the standard deviation of the underlying normal distribution. Solving for GSD, we have

$$\mathrm{GSD} = \exp\left(\sqrt{\ln\left(\mathrm{CV}^2 + 1\right)}\right). \tag{M-34}$$

For CV = 2.5, GSD = 4.1. This is the value we assign for uncertainty in the data (the numerator of Equation M-30).

Part (2) of the uncertainty is associated with transformation of net air concentrations to diffusion. This transformation is given by Equation M-30, and the denominator contains the quantities whose individual uncertainties are to be combined. These quantities are Q_{day}, Q_{night}, $(f/u)_{\mathrm{day}}$, $(f/u)_{\mathrm{night}}$ and the ratio $r(x)$. The distributions of Q_{day} and Q_{night} are based on Table M-7 and Equations M-22 and M-23; we approximated the distributions with lognormal distributions based on ratios of the tabulated 95th and 50th percentiles from Table M-19. Distributions of $(f/u)_{\mathrm{day}}$ and $(f/u)_{\mathrm{night}}$ were assumed to be normal, with parameters estimated from the five-year composite meteorological dataset for the FMPC. The diffusion ratio $r(x)$ was assumed to be lognormally distributed with GM = 6.5 and 95th percentile equal to 1.5 times the GM, corresponding to a GSD of 1.3; this is a somewhat arbitrary assumption suggested by the aggregate of values of the ratio at the sampling stations (Table M-9). Using these distributions with Monte Carlo simulations, we obtained an empirical distribution for the denominator of Equation M-30 that was approximated by a lognormal distribution with GSD = 1.4.

Thus, we have in Equation M-30 a quotient of independent lognormal distributions with numerator GSD = 4.1 and denominator GSD = 1.4. The quotient is also lognormally distributed, with GSD given by

$$\mathrm{GSD} = \exp\left(\sqrt{(\ln 4.1)^2 + (\ln 1.4)^2}\right) = 4.3\,. \tag{M-35}$$

This is the GSD we used to define the distribution of η in Equation M-32 and in the description of the Monte Carlo trials. Table M-10 summarizes the components of uncertainty in this calculation.

Another component of uncertainty not considered in Table M-10 is related to the use of a five-year composite meteorological dataset from recent years (1987–1991) to estimate frequencies for earlier years. As we mentioned in the introduction, such a component has been estimated. It is introduced into the dose calculation at the point where air dispersion is simulated, but it is not treated as a part of the basic diffusion function. This component of uncertainty is discussed in a later section of this appendix (page M-51).

Table M-10. Uncertainty Distributions of Quantities Related to the Air Transport Model for Radon Released from the K-65 Silos

Quantity	Distribution type	Mean or GM	SD or GSD
$r(x)$	lognormal	6.5	1.3
Q_{day} pCi s^{-1}	lognormal	5.6×10^{7}	1.4
Q_{night} pCi s^{-1}	lognormal	4.2×10^{6}	1.5
$(f/u)_{day}$ s m^{-1}	normal	3.8×10^{-2}	3.3×10^{-3}
$(f/u)_{night}$ s m^{-1}	normal	7.4×10^{-2}	1.2×10^{-2}
Data	lognormal	—	4.1
Conversion	lognormal	—	1.4
Residuals	lognormal	—	2.8

Interpretations of the Fitted Air Dispersion Models

Figures M-2 and M-4 show atmospheric diffusion curves fitted to data. The curves are derived from plume models that are based on rudimentary physics (mass conservation and gradient-driven diffusion) and empirical parameter estimation (Briggs's curves for σ_y and σ_z, from Hanna et al. 1982). As presented in the literature, these models generally have no disposable parameters for fitting. For our purposes, we added a calibration factor K, which can be interpreted as moving the logarithmically plotted model curve upward ($K > 1$) or downward ($K < 1$) without changing its shape. This multiplication is the only parametric adjustment that was made in order to fit the uranium model.

In the case of radon, a second degree of freedom was included in the regression in the form of a parameter c, which appeared in the factor $K(x/\rho)^c$. Varying c shears the logarithmically plotted curve vertically upward or downward about the point where $x = \rho$, the radius of the circular source region. We do not include the portion of the curve inside the source region in the shearing transformation. Figure M-5 illustrates these two movements. These transformations can be interpreted, in part, as local adjustments to the dispersion coefficients σ_y and σ_z.

The uranium regression was based on a single multiplicative parameter for two principal reasons. The first reason is practical: it would have been computationally difficult to

accommodate the surface-depletion deposition model into a regression that varied the slope of the curve, because although the suspension ratio SR does not depend on the multiplicative parameter K, SR would depend on the value of c. But the second and more important point is that the added degree of freedom is hardly necessary for the uranium data. Figure M-2 indicates that the direction of the fitted curve is about right with respect to the aggregate of the data, and the primary function of this shear parameter would be to increase the uncertainty bounds as the distance from the source increases. But the uranium data cover a large fraction of the assessment domain's radius, and it is only beyond 6 km that the uncertainty bounds would begin to diverge appreciably. At those distances, concentration estimates will be about an order of magnitude lower than at the site boundary, and conservatism in other uncertainty estimates will likely compensate.

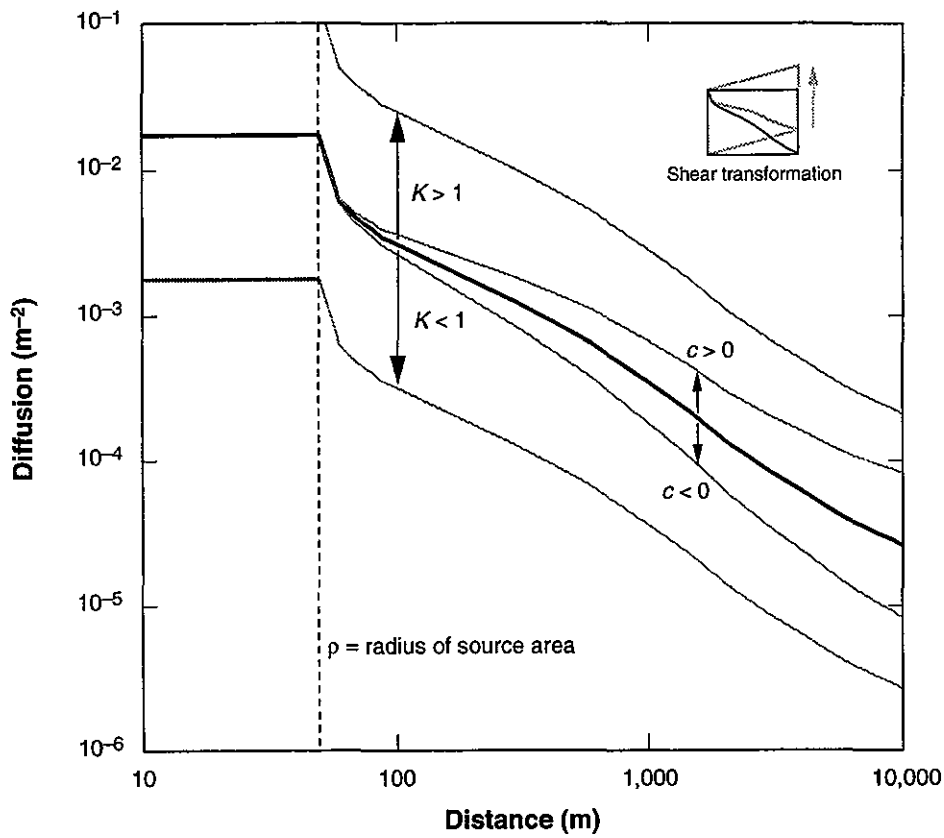

Figure M-5. Parameters used in fitting the circular area-source diffusion models to the uranium and radon data. The uranium model uses only the parameter K, which displaces the curve vertically. The radon model uses both K and a parameter c, which applies a shear transformation to the portion of the curve beyond the source region.

The radon regression is another matter entirely. The radon data cover distances less than 2 km from the K-65 silos, and the data are subject to greater exogenous and residual uncertainties than the uranium data. The complication from deposition is not present with

the radon calculation. Thus it is practical and important to carry out the two-parameter regressions in this case.

Some justification of the choice of a particular form of Gaussian plume–based model curve may be needed, apart from practical success. This is not a rigid prescription, and there may be other choices that would have reached a similar goal. We offer the following rationale.

For the uranium coming from the production area, the source complex is not well characterized for the kind of deterministic calculation that depends explicitly on the definition of each source (e.g., building or stack) by parameters such as building size, stack height (above ground and above roof), stack diameter, gas exit velocity and temperature, and ambient temperature. Apart from the physical dimensions, which are known, most of these data are fragmentary or nonexistent for most of the years of operation of the FMPC. Appendices I and J of the Task 4 report explain calculations that we performed to discriminate between plume rise and entrainment of the plume in building wake cavities. These calculations were based on prescriptions of Briggs (1969), Briggs (1974), and Hanna et al. (1982), with the fragmentary data just alluded to and the meteorological data of the FMPC. The results of the calculations almost invariably pointed to entrainment of the plumes in the building wakes (as opposed to plumes that would rise by momentum and thermal buoyancy), suggesting that the transport might well be simulated as if the releases came from ground level. The buildings are large and the stack exhausts generally are not high above the rooftops, conditions which favor the entrainment. In addition, many of the stacks were fitted with rain covers (although this aspect was not taken into account explicitly in the calculations). There are more than thirty release points distributed within a production area in which the proximity of many large buildings creates complex patterns of turbulence in the airflow. These factors pointed reasonably toward a diffusion curve based on a relatively large ground-level area source. A circle was chosen for directional symmetry. We also did exploratory calculations with cylindrical volume sources of various heights, but the shapes of the resulting diffusion curves (apart from scale factors) were very similar to those produced by circular areas, and we saw no advantage to pursuing the more complicated model. We took the size of the circular source region to be similar to that part of the production area where most of the emitting buildings were located, and although there is some latitude in this choice, we did not attempt to optimize it. We settled on a circle with radius 450 m.

In the case of the radon releases, judgment and exploratory calculations with point-source models suggested the use of a ground-level area-source model. Each silo has an interior radius of about 40 ft = 12 m (Task 4 report, Appendix P). The radius of a circle with twice the area (two silos) is $12 \times \sqrt{2} = 17$ m. We somewhat arbitrarily tripled this radius to 50 m in order to include the plane projection of the area of the berms, considering the possibility of appreciable diffusion of radon through cracks in the lateral containment walls and through the soil of the berms to the surface (this hypothesis, of course, applies to the 1980s, when the calibration measurements were made, but is less realistic before 1980). The shape of the berms would smooth the windflow over the silos, making the windfield more like one over a plane surface without obstructions than about an elevated locus of release. As

with uranium, the exact size of the source area is not critical to the estimates of concentration and dose.

MEASURED RADON CONCENTRATIONS AND UNCERTAINTIES

Overview

The available environmental monitoring data for radon in air around the FMPC have been described in the Task 4 report and final report of Task 5 (Shleien et al. 1995). The earliest environmental radon monitoring near the FMPC was conducted at a limited number of locations in 1978–1979. This monitoring and the other major monitoring programs are briefly summarized in Table M-11. Additional details about these monitoring programs were provided in the Task 4 and Task 5 reports.

Of these four major radon monitoring data sets, not all are equally useful for calibrations of the radon air dispersion model. For our calibrations, we would prefer environmental monitoring at many locations, particularly at different distances from the K-65 Silos, and over a long time period, so that multiple annual average concentrations could be evaluated. The preliminary monitoring of 1978–1979 does not meet either of these criteria. That monitoring was performed for a relatively short period, and primarily at a single location. In the Task 5 report (Shleien et al. 1995), results of monitoring by the Ohio Department of Health (ODH) were considered to be less useful than the FMPC routine monitoring, because of a number of unusable results and higher uncertainties in the ODH results. However, the Mound monitoring was performed at a large range of locations, from less than 100 m to about 2000 m from the Silos. The monitoring was performed long enough to calculate annual average concentrations. The FMPC monitoring was performed primarily along the boundary of the site, and thus the range of distances is not as extensive as for the Mound monitoring. But, the routine monitoring was performed from 1980 onward, providing many complete years of data. For our calibrations, we have used the Mound and FMPC routine monitoring data sets.

Table M-11. Brief Summary of Major Data Sets of Environmental Radon Monitoring Around the FMPC

Data set	Years	Locations	Instruments,[a] sampling periods
Preliminary FMPC	1978–1980	Primarily at boundary air monitoring station 6.	PERMs, 4–21 days, some gaps between. Some grab samples.
FMPC Routine	1980–present	Seven boundary air monitoring stations. Background. More stations added, especially in 1987	Alpha-track, quarterly.
Mound	1984–1986	Seventeen onsite locations, from less than 100 m to about 2000 m from Silos. Three nearby residences.	PERMs, one to two weeks.
Ohio Department of Health (ODH)	1985–1989	Twelve stations on the site boundary.	Alpha-track, 3–12 months.

[a] Passive environmental radon monitors (PERMs) and alpha-track detectors are both passive radon gas monitors. To record the radon concentration, PERMs use a negatively charged electrode and a thermoluminescent dosimeter (TLD), while alpha-track detectors use a plastic that is etched by alpha particles. Additional details are provided in the Task 4 and Task 5 reports (Killough et al. 1993 and Shleien et al. 1995).

The time period of monitoring results to be used for calibrations of the radon air dispersion model is dependent on the periods for which we have obtained useful monitoring data, and on the periods into which the source term has been separated. Essentially all of the monitoring data were taken in the period after the silo domes were sealed in 1979. From our source term report (Voillequé et al. 1995), a single radon release rate from the K-65 Silos was estimated to apply to the period July 1979 through December 1987. Radon releases are only estimated through 1988 (in accordance with the objectives of the project). Thus, the period July 1979–December 1987 includes most of the time period of concern for radon releases, for which we have environmental monitoring data. We thus perform calibrations of the radon air dispersion model using estimated source terms and monitoring data within this period, July 1979–December 1987.

FMPC Routine Monitoring

The FMPC established its routine radon monitoring program in July 1980 at the six boundary air monitoring stations, then called BS1 through BS6 (Boback and Ross 1981). Alpha-track detectors, configured as passive radon gas detectors, were typically exposed for about three months, although variations in exposure times occurred.

In 1981 the program was expanded to include sampling at the new seventh boundary station, BS-7, and two background stations (Fleming et al. 1982). In 1986, the seven boundary air monitoring stations were renamed AMS1 through AMS7, and further

expansion added monitoring at two onsite locations, AMS8 and AMS9, and three offsite locations, AMS10, AMS11, and AMS13 (WMCO 1987). In 1987 the program was expanded greatly to include sampling at 16 locations on the site boundary (called FMPC A through FMPC P), 16 locations on the fenceline around the K-65 Silos (called K65 A through K65 P), two other onsite locations on the west side of the production area, four background stations, and a few residences near the FMPC, in addition to the air monitoring stations AMS1–AMS13 (WMCO 1988). The program continued with only minor changes through at least 1990 (WMCO 1989, Dugan et al. 1990, and Byrne et al. 1991).

Data from the expanded boundary and offsite stations are only available for a single year (1987) in our period of interest. As we see later, the low radon concentrations at these distances creates large uncertainties in net concentrations for a single year of data, but the seven previous boundary stations (AMS1 through AMS7) provide a potentially useful data set, with seven years of data. The onsite stations added in 1986 and 1987 are generally similar to locations monitored by Mound, and data from these stations will not add significantly to our available data. For these reasons, the only data to be used further in the calibration work are from the boundary stations AMS1 through AMS7 (Figure M-6).

Measured Gross Concentrations. Much of the available data for the routine radon monitoring has been obtained from the annual environmental monitoring reports. However, more detailed results have been obtained for some periods of the FMPC radon monitoring. A handwritten spreadsheet (Anonymous circa 1984) provides a compilation of the individual detector results of the program for June 13, 1980, through December 27, 1983. These individual results were reported in Table ES-4, Appendix E, of the Task 5 report (Shleien et al. 1995). Computer file copies of the FMPC alpha track monitoring data for 1987–1992 (only part of 1992) have also been received, directly from the FMPC (Byrne 1992). These computer files include the individual measurements for locations reported in the environmental monitoring reports and also for some locations not reported in annual reports. We examined the FMPC routine radon monitoring program previously, in our report of Task 5 (Shleien et al. 1995), and some additional details can be found there.

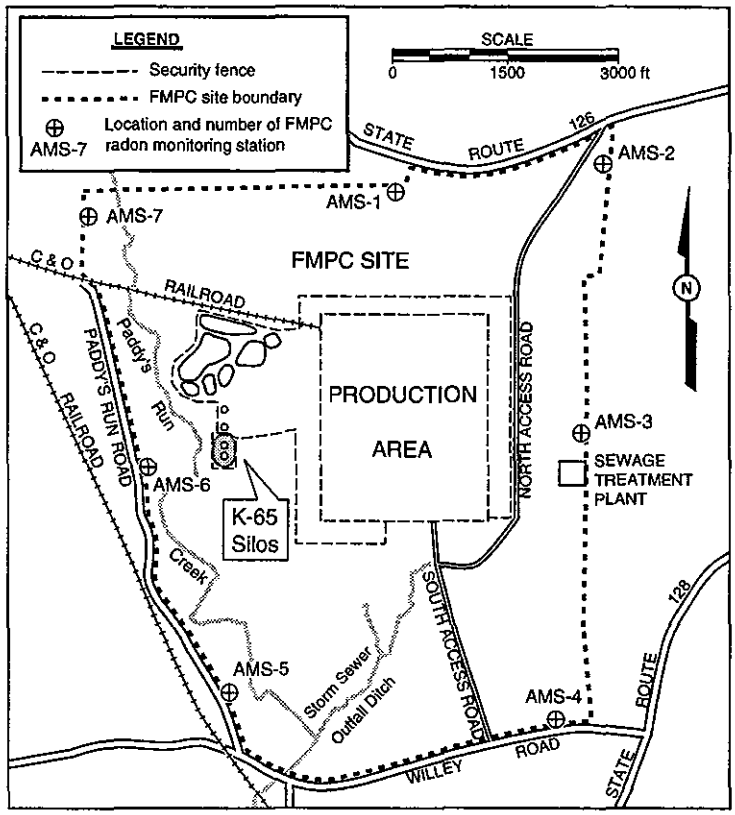

Figure M-6. Locations of the boundary air monitoring stations in relation to the K-65 silos. The boundary stations, AMS 1–7, were the primary radon monitoring locations for the FMPC routine monitoring program through 1986. These boundary stations are the same as those formerly called stations BS-1 through BS-7.

Because individual results are not available for all years of the monitoring, we use annual average concentrations, which are reported in the annual environmental monitoring reports. The annual average radon concentrations at boundary stations AMS1 through AMS7 for the period 1981–1987 are shown in Table M-12 (Fleming et al. 1982, Fleming and Ross 1983, Fleming and Ross 1984, Facemire et al. 1985, Aas et al. 1986, WMCO 1987, WMCO 1988). For 1981, background measurements were only made for the last three quarters of the year (see later discussion). Thus, for 1981 we recalculated average concentrations based on these three quarters only, from the individual results mentioned above. The values reported for 1984 were geometric means, but details of the individual results from 1984 were not available; we use the values as if they were arithmetic means.

Table M-12. Average Annual Measured Radon Concentrations (pCi L^{-1}) at FMPC Boundary Air Monitoring Stations [a]

Year	AMS1	AMS2	AMS3	AMS4	AMS5	AMS6	AMS7
1981[b]	0.78	0.80	0.47	0.48	0.23	0.65	0.76
1982	0.79	0.91	0.66	0.90	0.94	1.01	1.07
1983	0.65	0.77	0.76	0.65	1.05	0.82	0.91
1984[c]	0.917	0.801	0.843	0.591	0.970	0.584	0.717
1985	0.81	0.82	0.28	0.56	0.80	0.66[d]	1.01
1986	0.64	0.84	0.68	0.55	0.58	0.65	0.96
1987	0.54	0.46	1.12	1.02	0.60	1.26	0.66

[a] Results obtained from annual environmental monitoring reports, except as noted.
[b] Results for 1981 are based on the last three quarters of data, to be compatible with the background concentrations, which were only measured for these three quarters.
[c] The "average" values for 1984 were geometric means, but we treat them as arithmetic means.
[d] This is the average of values given for two stations, BS6A and BS6B.

Calculations of net concentrations and uncertainties. As we are interested in Rn concentrations due to releases from the K-65 Silos, we must determine net concentrations (above background) from the gross measurements. Calculating the "best estimate" values of the net, annual average radon concentrations for each monitoring station is straightforward. Annual average background concentrations are subtracted from the gross annual average concentrations at the location. Then net concentrations for the whole period 1981–1987 are just the means of the annual values.

Although estimating the uncertainties in the net concentrations is conceptually straightforward, the implementation is somewhat more complicated. Our general approach is first to estimate uncertainties in the gross and background annual average concentrations that we have obtained from the annual environmental monitoring reports. These uncertainties are then propagated through the calculations of net concentrations. We assume that the basic annual average concentrations (gross and background) follow normal distributions, and we use standard error propagation formulas. In most cases, the values calculated are means, and the uncertainties reported are uncertainties of the mean, and are given as estimates of one standard deviation of the associated mean value.

The two types of uncertainty that can be quantified for the FMPC routine radon monitoring data are due to (1) random sampling errors and (2) instrument and analytical uncertainties. The two uncertainties are considered independent, and are combined as follows:

$$S_{\text{Total}} = \sqrt{(S_{\text{RSE}})^2 + (S_{\text{inst}})^2} \qquad \text{(M-36)}$$

where

S_{Total} = the total uncertainty, expressed as one standard deviation.

S_{RSE} = the uncertainty, expressed as one standard deviation, due to random sampling error.

S_{inst} = the uncertainty, expressed as one standard deviation, due to instrument and analytical uncertainties.

For calculating the uncertainty in a mean value from random sampling errors, we use the usual equation, taken from Gilbert (1987):

$$S_{RSE}(\bar{x}) = S\sqrt{\frac{1-f}{n}} \qquad \text{(M-37)}$$

where

$S_{RSE}(\bar{x})$ = the uncertainty, expressed as one standard deviation, of the mean value $\bar{x}$, due to random sampling errors.

$\bar{x}$ = $\frac{1}{n}\sum_i x_i$, the arithmetic mean of the values x_i.

S = the sample standard deviation of the measurements of x_i.

n = the number of sampling units in the population that were sampled.

N = the total number of sampling units in the population.

f = $\frac{n}{N}$, the fraction of the sampling units that were sampled.

For the gross measurements of radon concentration at the boundary stations, measurements were taken continuously, with each measurement taken over a three-month period. The alpha-track instruments are time integrating, and instruments were replaced by their successors with no significant time gap. Thus, for estimating the average annual gross concentration at a given boundary station, the sampling units are considered to be three month–long measurements at the station. In a given year, there are then four sampling units, and all four sampling units have been sampled. So, $n = N = 4$, and $f = 1$. Thus the uncertainty due to random sampling error is zero.

For gross concentrations at the boundary stations, then, the only uncertainties considered are instrument and analytical uncertainties. The detailed compilation of individual measurements of Byrne (1992) indicates that during 1987 and 1988, there was a single location at which five replicate instruments were used for each quarterly measurement period. The location was called FMPC K, and was on the western site boundary, roughly 200 m south of boundary station AMS6. The results of these replicates can be used to estimate the instrument and analytical uncertainties. For each quarterly period we calculated the coefficient of variation (CV) of the five replicate measurements. Table M-13 shows the replicate measurements, the mean, the standard deviation, and the CV.

Table M-13. FMPC Routine Monitoring: Replicate Measurements of Radon Concentration in Air (pCi L^{-1})

	1987				1988			
Replicate	1st qtr	2nd qtr	3rd qtr	4th qtr	1st qtr	2nd qtr	3rd qtr	4th qtr
1	0.2	5.2	13.0	6.5	0.3	1.3	1.8	0.9
2	3.2	1.3	1.1	1.1	0.3	1.8	1.1	0.9
3	0.8	4.1	0.7	1.2	0.3	1.1	1.3	1.0
4	5.7	6.3	0.0	11.5	0.6	1.8	1.2	1.0
5	3.8	0.3	2.3	4.8	0.3	3.4	0.8	1.3
mean	2.74	3.44	3.42	5.02	0.36	1.88	1.24	1.02
standard deviation	2.25	2.56	5.42	4.31	0.134	0.904	0.365	0.164
coefficient of variation (%)	82.2	74.3	158.5	85.8	37.3	48.1	29.4	16.1

From the calculations in Table M-13, the average CV for 1987 and 1988 is 66%, and the average CV for 1987 is 100%. The average CVs are assumed to represent the instrument uncertainties that would apply to any single quarterly measurement. Since we do not, in general, have individual quarterly results, we assume that each quarterly result is equal to the average value for that year. The instrument uncertainty in the average annual concentration is then calculated by standard error propagation techniques to be

$$S_{\text{inst}}\left(\bar{x}_{jk}\right) = \frac{\sqrt{\sum_{i=1}^{m_j}\left(S_{\text{inst}}\left(x_{ijk}\right)\right)^2}}{m_j} = \frac{\sqrt{m_j}}{m_j} CV_j \bar{x}_{jk} \qquad \text{(M-38)}$$

where

x_{ijk} = quarterly radon concentration measurement (unknown) for quarter i of year j, at location k.

$\bar{x}_{jk}$ = the average radon concentration for year j and location k (results from annual environmental monitoring reports, as shown in Table M-12.

CV_j = the coefficient of variation applicable to year j.

m_j = the number of quarterly measurements for year j.

The values of m and CVj require different values for different years. In 1981, we used only three quarters of monitoring data, to be comparable with the background measurements for this year, which were only performed for three quarters. In 1987, the FMPC started placing duplicate detectors at each location. Thus, for 1987, the number of measurements at each location for 1987 is eight. Based on data compiled in our Task 5 report (Shleien et al. 1995), during 1981–1983 only one detector was used per location. For 1984–1986 the number

of detectors per location has not been determined; for uncertainty calculation purposes, we assume one detector. The values of m_j and CV_j are shown in Table M-14.

Table M-14. Values to Be Used in Calculating Instrument Uncertainties for FMPC Monitoring

Years	Value of m_j	Value of CV_j
1981	3	66%
1982–1986	4	66%
1987	8	100%

For the background measurements, there are infinitely many possible locations that could be sampled to estimate the background concentration of radon around the FMPC. Thus, in Equation M-37, f would be zero, and so, unlike for the gross measurements at the boundary stations, the uncertainty due to random sampling errors is not zero. The FMPC measured radon concentrations at two or more locations that they deemed representative of background. For estimating the random sampling uncertainties in the background concentrations, we treat each average annual measurement as one sampling unit. The random sampling uncertainty is calculated using Equation M-37, with $n = 2$ for most years. The instrument uncertainties in the background measurements are estimated as described for the gross measurements at the boundary stations.

Table M-15 is a compilation of the average annual radon concentrations at the background locations for 1981–1987, taken from the annual environmental monitoring reports (Fleming et al. 1982, Fleming and Ross 1983, Fleming and Ross 1984, Facemire et al. 1985, Aas et al. 1986, WMCO 1987, WMCO 1988).

The instrument and random sampling uncertainties for the background concentration measurements are calculated as described above, using the measured average annual concentrations given in Table M-15. The total uncertainty in the background measurements is calculated by combining the random sampling and instrument uncertainties, as in Equation M-36. The calculated uncertainties are shown in Table M-16.

Table M-15. Average Background Concentrations of Radon in Air, from FMPC Annual Environmental Monitoring Reports

	Average measured background concentration (pCi L^{-1}) at location [a]:								
Year	8 mi ENE	5 mi WNW	OS1 5 km	OS2 3 km	AMSBK1 10.5 km[b]	AMSBK2 6.4 km[b]	BKGD1 34 km	BKGD2 25 km	Mean
1981	0.67 [c]	0.36 [d]							0.59 [e]
1982	0.56	0.66							0.61
1983	0.77	0.61							0.69
1984	0.836 [f]	0.357 [f]							0.596
1985			0.59	0.37					0.48
1986					0.60	0.57			0.58
1987					0.66	0.80	0.43	0.76	0.66

[a] Data from annual environmental monitoring reports. Distances are from the FMPC to the monitoring location.
[b] In 1986, these locations were called OS1 and OS2, but distances are the same as AMSBK1 and AMSBK2.
[c] This value was based on three quarterly measurements.
[d] This value was based on only a single quarterly measurement.
[e] Weighted to account for one average based on three quarters and one based on one quarter.
[f] Averages reported for 1984 were geometric means. We use them as if they were arithmetic means. The additional significant figures are as reported in the original source document.

Table M-16. Calculated Means and Uncertainties (pCi L^{-1}) of FMPC Background Radon Measurements

		Calculated uncertainties		
Year	mean	S_{inst}	S_{RSE}	S_{Total}
1981	0.59	0.174	0.155	0.233
1982	0.61	0.143	0.050	0.151
1983	0.69	0.161	0.085	0.182
1984	0.596	0.150	0.240	0.283
1985	0.48	0.115	0.110	0.159
1986	0.58	0.137	0.015	0.137
1987	0.66	0.120	0.083	0.146

The net annual average radon concentrations for the boundary station monitoring are calculated by subtracting the annual average background concentrations from the gross concentrations. The uncertainty in the net concentrations is calculated by usual error propagation methods from the uncertainties in the gross and background concentrations, which were described earlier. The calculated net concentrations and associated uncertainties are shown in Table M-17. Of the annual average concentrations, it is seen that in many cases the uncertainties (one standard deviation) are of the same magnitude as the values. A number of the estimates are less than zero. For use in the calibrations, we calculate the mean net concentrations for the seven-year period 1981–1987. Again, uncertainties for these values

are calculated with standard error propagation methods. These mean concentrations for the entire period are also given in Table M-17.

Table M-17. Calculated Net Radon Concentrations and Uncertainties (Uncert) (pCi L^{-1}) for the FMPC Routine Monitoring at Boundary Stations, 1981–1987 [a]

	AMS1		AMS2		AMS3		AMS4		AMS5		AMS6		AMS7	
Year	Value	Uncert	Value	Uncert	Value	Uncert	Value	Uncert	Value	Uncert	Value	Uncert	Value	Uncert
1981	0.187	0.377	0.212	0.385	-0.126	0.293	-0.112	0.296	-0.361	0.249	0.059	0.340	0.168	0.372
1982	0.18	0.301	0.30	0.336	0.05	0.265	0.29	0.333	0.33	0.345	0.40	0.366	0.46	0.384
1983	-0.035	0.281	0.085	0.313	0.075	0.310	-0.035	0.281	0.365	0.391	0.135	0.326	0.225	0.351
1984	0.320	0.414	0.204	0.387	0.246	0.397	-0.006	0.343	0.374	0.427	-0.012	0.342	0.120	0.369
1985	0.33	0.311	0.34	0.314	-0.20	0.184	0.08	0.244	0.32	0.308	0.185	0.271	0.53	0.369
1986	0.055	0.252	0.255	0.309	0.095	0.263	-0.035	0.228	-0.005	0.236	0.065	0.255	0.375	0.345
1987	-0.122	0.239	-0.202	0.217	0.458	0.418	0.358	0.386	-0.062	0.256	0.598	0.464	-0.0025	0.273
1981–1987	0.131	0.120	0.171	0.124	0.0854	0.118	0.0772	0.116	0.137	0.122	0.204	0.130	0.268	0.134

[a] Uncertainties are estimates of one standard deviation of the associated value.

Mound Monitoring

Personnel from the Mound facility, which is a DOE facility in Miamisburg, Ohio, established a radon monitoring network at the FMPC in September 1984 (Hagee et al. 1985). Mound used Passive Environmental Radon Monitors (PERMs), which measure time-integrated radon concentrations. Continual replacements of the PERMs after one- to two-week exposure periods resulted in essentially continuous monitoring at the locations. Mound initially monitored at six onsite locations, quickly expanded to 17 onsite locations at varying distances from the K-65 Silos, and later added three offsite locations. Preliminary monitoring was performed for September 20, 1984 through February 5, 1985, and was described in a Mound report (Hagee et al. 1985). Routine monitoring was then performed for July 2, 1985, through October 3, 1986. A letter with attached tables provides detailed results for this routine monitoring period (Jenkins 1986). An Oak Ridge National Laboratory report (Berven and Cottrell 1987) summarizes all results of the Mound monitoring. Some additional details are discussed in the draft report of Task 4 (Killough et al. 1993).

The source terms for ^{222}Rn releases from the K-65 Silos were developed for an annual time resolution (Voillequé et al. 1995). Therefore, we wish to use annual average concentrations for air dispersion model calibrations. From the Mound data, the longest uninterrupted set of data is from July 2, 1985, through October 3, 1986. Within this period, monitoring at one of the intermediate distance locations was terminated on June 4, 1986. Thus, in order to use all of the data from this location, we use the data from July 2, 1985, through July 2, 1986.

The results of the individual Mound measurements for July 2, 1985, through October 3, 1986, taken from Jenkins (1986), are presented in Table M-1S, at the end of this Appendix. The onsite monitoring locations are shown in Figure M-7 (from Hagee et al. 1985).

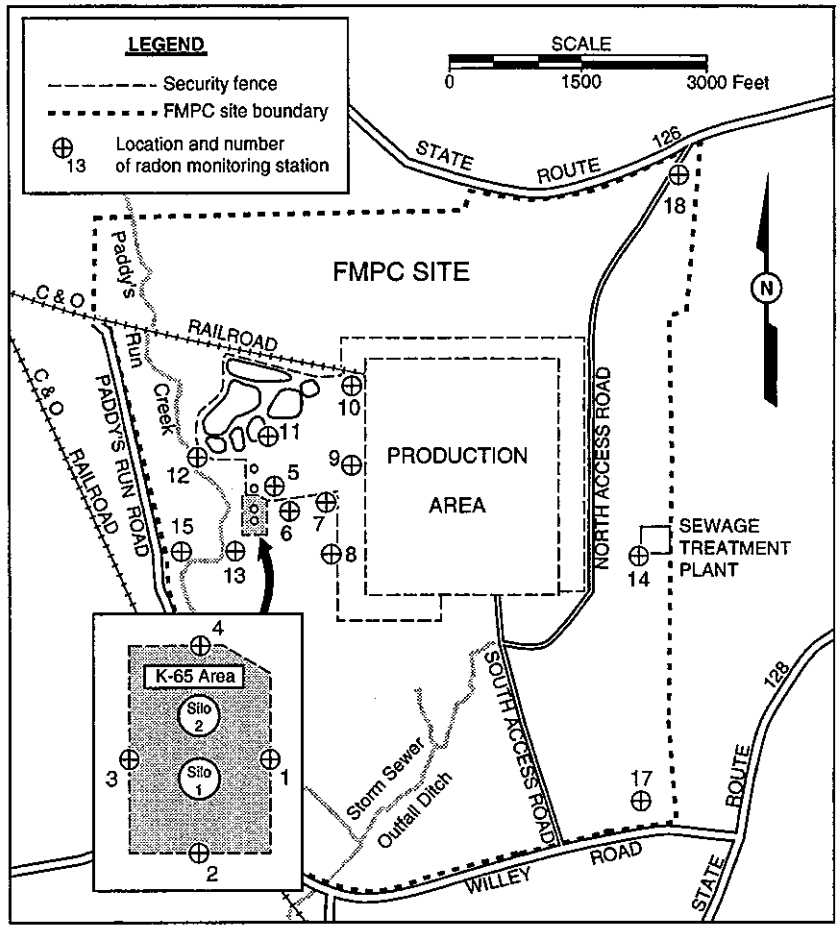

Figure M-7. Onsite monitoring locations of the Mound radon monitoring program on the FMPC site from September 1984 to October 1986 (from Hagee et al. 1985). Locations 19, 20, and 21 are offsite and not shown here.

To use the Mound monitoring data, annual average concentrations must first be calculated. In Table M-1S it can be seen that from July 2, 1985, through July 2, 1986, there were a few cases when no measurement is reported in the source document (Jenkins 1986). We assume that in these cases no valid measurement was obtained. We further assume that, since there are only a small number of such occurrences, the lack of these data points does not contribute to any significant bias in an annual average concentration. Because individual measurements represent different exposure times, the annual average concentrations are calculated as time-weighted averages of the individual measurements.

Background concentrations for the Mound data. As for the FMPC data, we must determine net concentrations for the Mound data by subtracting a background concentration from the gross measurements. In the Mound monitoring network, there were not any locations specifically chosen to represent background (Hagee et al. 1985). We identified three simple options that could reasonably be used to estimate a background concentration for the Mound monitoring: (1) use background concentrations measured for the same period by the

FMPC routine radon monitoring program, (2) use concentrations measured at the offsite locations monitored by Mound, or (3) use concentrations measured by Mound along the eastern boundary of the FMPC. The third option was used in the draft report of Task 4 (Killough et al. 1993).

The FMPC did perform background radon monitoring during this time, as part of their routine monitoring program. However, these measurements were made using alpha track detectors, while the Mound measurements used PERMs. We feel that it is inappropriate to make direct comparisons of radon concentrations measured with different instruments, without knowledge of a quantitative relationship between results from one type and results from the other. Our evaluations of the results of radon monitoring around the FMPC site and past experience performing environmental radon measurements lead us to judge that the results of measurements by one method may be biased relative to the results of another method. Thus the FMPC background measurements are rejected for use with the Mound monitoring data.

We could find very little information about the locations of the offsite monitoring performed by Mound. Results for these locations, 19, 20, and 21, are provided by Jenkins (1986), but the locations are not described. The Oak Ridge National Laboratory report (Berven and Cottrell 1987) indicates that location 21 was the nearest residence, and that locations 19 and 20 were other residences. No other information was found. If location 21 was the residence nearest to the K-65 Silos, then it is along Paddy's Run Road, in the general area of Mound location 15 (or FMPC routine monitoring boundary station 6) and within about 500 m of the silos. Thus, location 21 can not be considered representative of background radon concentrations. Locations 19 and 20 are unknown to us, and there is no indication that they were chosen to represent background. Based on measurements for the period October 1, 1985 (when measurements at the offsite locations started), through October 3, 1986, the average concentration at locations 19 and 20 was 0.58 pCi L^{-1} (the concentration at location 21 was even higher, 0.90 pCi L^{-1}) compared to the average of 0.47 pCi L^{-1} for locations 14, 17, and 18. The concentrations at the offsite locations thus appear slightly higher than at the eastern boundary locations. Because of these two factors, it appears that the offsite Mound monitoring locations are not representative of background.

The first Mound report (Hagee et al. 1985) indicated that the concentrations measured at locations 14, 17, and 18 were in the background range. These locations, all on the east boundary of the FMPC site (see Figure M-7), are the farthest from the K-65 Silos, at distances of 1400–2000 m, and in the draft report of Task 4 (Killough et al. 1993) we assumed these stations were representative of background. However, the FMPC monitored radon in air at its boundary stations AMS 2, AMS 3, and AMS 4, which are located similarly to Mound locations 18, 14, and 17, respectively. Results for these three boundary stations appear to be slightly elevated above background (see Table M-17). In addition, based on radon releases from the K-65 Silos, predicted radon concentrations at the three Mound stations on the eastern boundary are greater than zero. Thus, it does not seem reasonable to assume that stations 14, 17, and 18 are representative of background radon concentrations.

None of the three simple options for estimating background radon concentrations seems satisfactory. Therefore, we used a slightly more complicated method, that makes use of the

background concentrations measured in the FMPC monitoring and the fact that the three Mound monitoring stations on the eastern site boundary are relatively close to the FMPC boundary stations on the same boundary. We assume that the ratio of background concentration to concentrations at the boundary locations is the same for the two monitoring programs. Thus, for the FMPC monitoring, we calculate ratios of the background concentration to the concentration at each of locations AMS2, AMS3, and AMS4. These ratios are then multiplied by the concentrations measured by Mound at stations 18, 14, and 17, respectively, to estimate what the background concentration for the Mound monitoring was. This method allows us to use the background concentrations measured by the FMPC program, with a correction to account for the different instruments used in the two programs.

Uncertainties in concentrations. The Mound radon monitoring was only performed for a relatively short period, compared to the FMPC monitoring. As discussed earlier, we are only working with measurements from a one-year period. For our calibrations, the concentration we would like to estimate for each location is a mean, net concentration that would serve as a generic mean for any year in the period 1980–1987. Thus our uncertainty estimate must include a component for the random sampling error related to having samples from only a portion of the period of interest. For the Mound monitoring, which used PERMs for the measurements, instrument uncertainties are unknown, but are thought to be relatively small (unlike for the alpha-track detectors used in the FMPC monitoring). We thus assume that the instrument uncertainties are negligible.

Thus, for these Mound data, the only component of uncertainty to be calculated is that due to random sampling error. For the period of data we evaluate, July 2, 1985, through July 2, 1986, there were 43 one- to two-week sampling periods. For purposes of calculating the uncertainties, we assume that the 43 time periods are randomly distributed over the period of interest 1980–1987. Then the random sampling error is calculated using Equation M-36, given earlier. In this case, however, the number of potential sampling units, N, is essentially infinite, which gives f approaching zero. We assume that f equals zero, so the equation reduces to:

$$S_{RSE}(\bar{x}) = \frac{S}{\sqrt{n}} \qquad \text{(M-39)}$$

The uncertainties are calculated in this manner for all of the gross annual mean concentrations first. These uncertainties are propagated through the remainder of the calculations by assuming that the annual mean values follow normal distributions and by using standard error propagation formulas. In most cases, the values we calculate are mean values, so the uncertainties reported are uncertainties of the mean, and are given as estimates of one standard deviation of the associated mean value. One additional uncertainty calculation is performed for the determination of background concentrations, and this calculation is described below.

Results of net concentration calculations. To estimate the background radon concentration, we first calculate the adjustment factors, based on ratios of background to location concentrations from the FMPC monitoring data. These calculations are shown in Table M-18. The ratios of background concentration to location concentration are based on

the average annual gross concentrations (Table M-12) and average annual background concentrations (Table M-15) from the FMPC monitoring. The mean ratios are the adjustment factors by which the Mound eastern boundary station concentrations are multiplied to estimate the background concentration. The calculation of estimated background is shown in Table M-19.

Table M-18. Calculation of Adjustment Factors, from FMPC Monitoring Data

	Ratio background to location concentrations		
Year	AMS2	AMS3	AMS4
1981	0.736	1.270	1.232
1982	0.670	0.924	0.678
1983	0.890	0.901	1.054
1984	0.745	0.708	1.009
1985	0.585	1.714	0.857
1986	0.696	0.860	1.064
1987	1.440	0.592	0.650
mean	0.823	0.996	0.935
standard deviation	0.287	0.381	0.215

Table M-19. Calculations of Estimated Background Radon Concentration to Be Applied to Mound Monitoring Results [a]

		Mound measured concentration (pCi L^{-1})		Adjustment factor		Estimated background concentration (pCi L^{-1})	
Mound location	FMPC location	Value	Uncertainty	Value	Uncertainty	Value	Uncertainty
14	AMS-3	0.364	0.0361	0.996	0.381	0.362	0.143
17	AMS-4	0.471	0.0356	0.935	0.215	0.440	0.107
18	AMS-2	0.559	0.0621	0.823	0.287	0.460	0.168
mean						0.421	0.0818

[a] We provide extra significant figures here, as values will be used in further calculations.

The estimated mean background concentration given in Table M-19, 0.421 pCi L^{-1}, will be used in calculating net concentrations at the other Mound monitoring stations. The uncertainty given in Table M-19 is the estimated standard deviation of the mean value, calculated by propagating the uncertainties from the predecessor values. To ensure that the uncertainty in this value is not underestimated, we also perform an alternative calculation of the standard deviation of the mean background concentration. We assume that each of the three estimates of the background concentration from the three locations is an equally valid estimate of the true value. The sample standard deviation for the three values is calculated,

and then the standard deviation of the mean is calculated to be 0.0298 pCi L^{-1}. The standard deviation estimated through propagation of error, 0.0818 pCi L^{-1}, is higher, so it will be used for further calculations.

Once the annual average gross radon concentration for each station is calculated, calculating the net concentrations is straightforward. The results are shown in Table M-20. These net concentrations are used in the model calibration exercises.

Table M-20. Calculated Net Radon Concentrations and Uncertainties from the Mound Monitoring of July 2, 1985, through July 2, 1986 (pCi L^{-1}) [a]

Mound Location	Concentration	Uncertainty	Mound Location	Concentration	Uncertainty
1	5.52	0.427	10	0.396	0.101
2	1.87	0.251	11	0.906	0.145
3	7.69	0.842	12	1.19	0.152
4	4.36	0.422	13	0.184	0.100
5	5.26	0.462	14	[b]	
6	1.37	0.150	15	0.180	0.102
7	0.948	0.168	17	[b]	
8	0.922	0.147	18	[b]	
9	0.498	0.109			

[a] Uncertainties are estimates of one standard deviation of the associated value.
[b] Data from Stations 14, 17, and 18 were used to estimate the background concentration. Thus, no net concentrations are calculated for these stations.

METEOROLOGICAL DATA

The meteorological datasets considered for use in this study were originally records of hourly observations of twenty or more variables, measured and recorded by instrumentation installed on towers. For use in the calculations, the data are put into the form of joint frequency tables (JFTs) of wind speed (m s^{-1}), wind direction (one of 16 radial sectors), and Pasquill-Gifford atmospheric stability (A–F). We originally considered working with a monthly time resolution, but the cruder resolution of the uranium source term and the even coarser resolution of the source term of radon from the K-65 silos made any time step of less than one year excessive.

Concerns about the FMPC Dataset

Ideally, we would use a JFT specifically computed for each calendar year of the study's simulation of FMPC operations (1951–1988). Regional airport datasets go back to the 1940s. By contrast, the meteorological tower on the FMPC site was constructed in 1985 and began regular operation with full instrumentation at two heights (10 m and 60 m) in mid-1986. We examined the full dataset from the Cincinnati Airport (January 1948 through December

1991), data for January 1987 through December 1990 from the Dayton Airport (a longer record was available, but it was not acquired), data recorded at Oxford, Ohio (January 1981 through December 1990), and the FMPC tower data (August 1986 through December 1991). The Oxford dataset was useful for comparisons of regional wind speeds and wind directions, but it was never considered as a surrogate for the study because of the brevity of its record, the difficulty of estimating stability from the information that was recorded, and peculiarities of the terrain in the vicinity of the tower.

In Appendix E of the Task 4 report, we gave detailed information about comparisons among these datasets. The data from the two airports are similar, but it is fair to say that by almost any measure, the difference between the FMPC tower dataset and the data from either airport (Cincinnati in particular, since it has most often been used or advocated for FMPC assessments) is significant. The wind speeds at Cincinnati are higher than at the FMPC by about a factor of two on average. This is not altogether surprising, given the fact that major airports are located in open spaces, whereas the FMPC site is somewhat sheltered by nearby ridges with tops to about 70 m above the level of the production area, except for gaps to the southwest and northeast. The FMPC dataset also assigns higher weight to the stable E and F classes and lower weight to the neutral D class than the Cincinnati dataset. This comparison is complicated by the fact that the stabilities were computed differently in the two datasets: the FMPC stabilities are estimated from the temperature gradient between 10 m and 60 m of altitude, whereas the Cincinnati stabilities are based on a scheme that uses wind speed and an insolation index (negative for nighttime) based on solar angle, cloud cover, and ceiling (Turner 1964). Other investigators have noted important differences in the local meteorology that call into question substituting the Cincinnati dataset for the FMPC dataset (Pendergrass 1987).

Nevertheless, there are difficulties with using the FMPC dataset. Several criticisms have been raised against it:

(1) The brief duration of the record (5 years at the time the database for this project was compiled) gives concern about the adequacy of this dataset to estimate air concentrations in the years before 1987.

(2) There are numerous gaps in the 5-year record, which are the result of lightning, maintenance downtime, and other operational problems associated with the tower instrumentation and the computer system that recorded the data. It is reasonable to express concern about whether these gaps might distort the JFT.

(3) It has been alleged that the tower is poorly sited and may not be representative of local and regional wind patterns. In particular, it has been suggested that a pine tree plantation located on the FMPC property west of the tower would bias wind speed estimates. A report by a National Oceanic and Atmospheric Administration (NOAA) survey team (Pendergrass 1987) failed to mention the pine trees, but the report identified drainage flows through Paddy's Run and other complex wind patterns that indicated a need for additional towers on the site to support real-time plume travel projections in the event of an operational accident. However, plant operations ended in 1988, and presumably no action was taken on the recommendations of the NOAA team.

There is some validity in each of these criticisms of the FMPC dataset, and we have sought remedies to the extent we believe they are possible. We take the criticisms in order.

The brief duration of the record is a severe limitation. A typical approach in such cases is to establish a correlation between the FMPC dataset and the same 5 years of data from a suggested alternative, say Cincinnati, and to apply the correlation to earlier years of Cincinnati data to estimate corresponding values for the FMPC (the wind speed, wind direction, and stability at the FMPC site would be predicted for each hour by the joint values of the same three variables at Cincinnati). We chose to approach this problem in a simpler fashion, which also makes use of the Cincinnati data. In our approach, the five-year composite dataset for the FMPC is used to estimate meteorological frequencies for periods before 1987, but an uncertainty is applied to the estimates of air concentration. This uncertainty distribution is based on how well the Cincinnati composite data for 1987–1991 estimate earlier air concentrations as calculated by Cincinnati data specific to the earlier years. Details of the approach are given later in this section (page M-54).

The gaps in the FMPC record are, of course, worrisome. After examining lists of their occurrences, we concluded that their appearance was sufficiently random to justify ignoring them in the preparation of JFTs. The gaps would be of greater concern in calculations that proceed on an hourly basis. We are not persuaded that attempts to fill in the gaps by interpolation or similar devices would add credibility to the dataset, and we elected not to do so.

The siting of the meteorological tower is an appropriate concern, but one for which no clear remedy presents itself. The NOAA survey team took 21 days of observations in November 1987 using 14 portable towers (Pendergrass 1987). Their report stated that the data indicated possibly significant differences between the FMPC site and each of the two nearby airports (Cincinnati and Dayton, about 30 and 60 km distant, respectively). Doubts were raised about the suitability of the existing tower to support real-time forecasts of plume travel in emergency situations, but the very different question of suitability of the tower data for this dose reconstruction study was obviously not addressed. The NOAA survey identified drainage flows down Paddy's Run and episodes of diverging wind directions between the valley floor and nearby ridgetops, but it could not quantify frequencies of these phenomena and associate them with longer-term estimation of air concentrations over a wide area. The survey report did not mention the pine tree plantation west of the tower, but this issue was raised in a review by the Fernald Environmental Restoration Management Corporation (FERMCO) of the Task 4 report. There is, of course, the possibility that these trees affected the wind speed at the tower to some degree during the recording period (1987–1991). But in examining land-use maps, we found that about one-third of the area of the assessment domain was forested, and several bands of forest traverse the northeast quadrant. The effectiveness of the windbreaks afforded by these natural growths may have been comparable to the pine trees west of the tower. We are led to conclude that any attenuation of predicted wind speed caused by the pine tree plantation may not represent a distortion for the assessment domain as a whole. In any case, we judge that the FMPC dataset is likely a better representation of the assessment domain than data from the Cincinnati airport, which is situated in a flat open space on a bluff south of the Ohio river. The authenticity of the FMPC

tower dataset cannot be dismissed, despite its manifest shortcomings. Accepting its possible but unknown biases is preferable to making adjustments that are at best speculative or substituting a surrogate dataset from a distant sampling station (e.g., Cincinnati). And we remind the reader that our calibrations and comparisons of simulations of environmental concentrations with measurements (validations), although they provide no absolute guarantees, still furnish a level of insurance against gross errors in the meteorological database, as well as in the models and other data.

Monte Carlo Estimation of Uncertainty Using the Five-Year Composite Dataset

Early concern about the brevity of the FMPC meteorological record led us to examine the long-term Cincinnati record for measures of year-to-year variation. The question we are asking is, how well does a five-year composite JFT (1987–1991) represent the years 1951–1986. We have such a five-year composite JFT for the FMPC data, but there are no FMPC data for the earlier years. However, we can test the question for the Cincinnati data, provided we can formulate the comparison precisely. Specifically,

(1) We form a five-year composite JFT with the Cincinnati data for 1987–1991.
(2) For each of the years 1951–1991, we compare concentration estimates based on the JFT for that year with concentration estimates based on the five year composite JFT.

What requires further definition is how the comparisons in (2) are to be made. In order to make such comparisons, we needed a function of the dataset that was related in a reasonable way to what we are trying to predict. We chose to use the normalized ground-level concentration χ/Q predicted by a point-source centerline Gaussian plume model with release height 10 m (the height at which the wind measurements for each dataset were taken). Plume depletion due to deposition was not considered. The generic equation is

$$\chi/Q = \frac{1}{\pi u \sigma_y \sigma_z} \exp\left(-\frac{H^2}{2\sigma_z^2}\right) \qquad \text{(M-40)}$$

where u is the wind speed (m s^{-1}) and $H = 10$ m is the release height. The diffusion coefficients σ_y and σ_z depend on the distance from the source and on the stability class (A–F), but these dependencies are not shown explicitly. The interpretation of Equation M-40 is the steady-state concentration for a unit release rate for a wind that blows from source to receptor 100% of the time with wind speed and stability fixed. For our calculations, χ/Q is multiplied by frequencies from the JFT and averaged over wind speed and stability, taking into account the fraction of the time the wind blows from the source to the receptor.

For comparing the five-year composite dataset with a specific previous year (e.g., 1951), we proceeded as follows:

A. We defined a grid consisting of receptor points throughout the FMPC assessment domain. We used 10 radial distances from the center of the production area, ranging from 1000 to 10,000 m in 1000-m increments. We placed 10 such points in each of the 16 wind sectors, for a total of 160 points. The point source was located at the center of the circular domain.

B. We used the five-year composite Cincinnati dataset and the plume model to compute χ / Q for each of the 160 receptor grid points.
C. We used the Cincinnati JFT for the specific year (e.g., 1951) and the point-source Gaussian plume model to compute χ / Q for each of the 160 receptor grid points.
D. For each of the 160 grid points we computed R = result of B divided by result of C. The ratio R may be thought of as a predicted-to-observed (P/O) ratio, where predicted corresponds to the five-year composite dataset.
E. We formed an empirical distribution of the 160 P/O ratios from D and computed statistics. It is not unreasonable to assume that this distribution is lognormal, so we estimated and tabulated the GM and GSD.
F. We repeated the foregoing steps for each of the years 1951 through 1991.

Figure M-8 shows the 5th, 50th, and 95th percentiles of the P/O distribution plotted against the predicted year. The plot has the expected characteristics, with the extreme percentiles diverging as we go backward in time from the composite period. The GMs fluctuate around the line P/O = 1, although in the aggregate they indicate some under-prediction. Table M-21 shows the GM and GSD for each year.

If the five-year composite JFT for the FMPC data may be assumed to have the same stochastic relationship to the unknown FMPC JFTs for past years, the information in Figure M-8 and Table M-21 can be used to assign uncertainties to predictions of air concentrations based on the recent composite FMPC JFT. We consider this a reasonable assumption, and we have applied it to the calculations of air concentration. We define a multiplicative uncertainty factor for each receptor point and each year of the simulation period. The factors are identically and independently distributed for different locations and years. We generate their distribution with the following sampling scheme:

(1) Noting from Figure M-8 that the maximum range in the GMs is a factor of two, we sample a random GM from a log-uniform distribution with minimum $1/\sqrt{2}$ and maximum $\sqrt{2}$.
(2) Using the GM from step (1) and GSD = 1.61 (the maximum GSD from Table M-21), we sample from the lognormal distribution with these parameters.
(3) We store the value from step (2) and repeat the process.

This somewhat conservative procedure takes account of year-to-year variability in the GM of the P/O ratios, as well as uncertainty associated with location. To a sample of size 1,000, we fitted a lognormal distribution with GM = 1.0 and GSD = 1.7 (note, however, that the distribution defined by the sampling procedure is not analytically lognormal). This GSD has 95th/50th percentile ratio 2.4. Please note that this distribution applies to all receptor points and to all 38 years of plant operation. Sampling from this distribution amounts to sampling from a lognormal distribution whose geometric mean is itself an uncertain parameter [compare Hoffman and Hammonds (1994)].

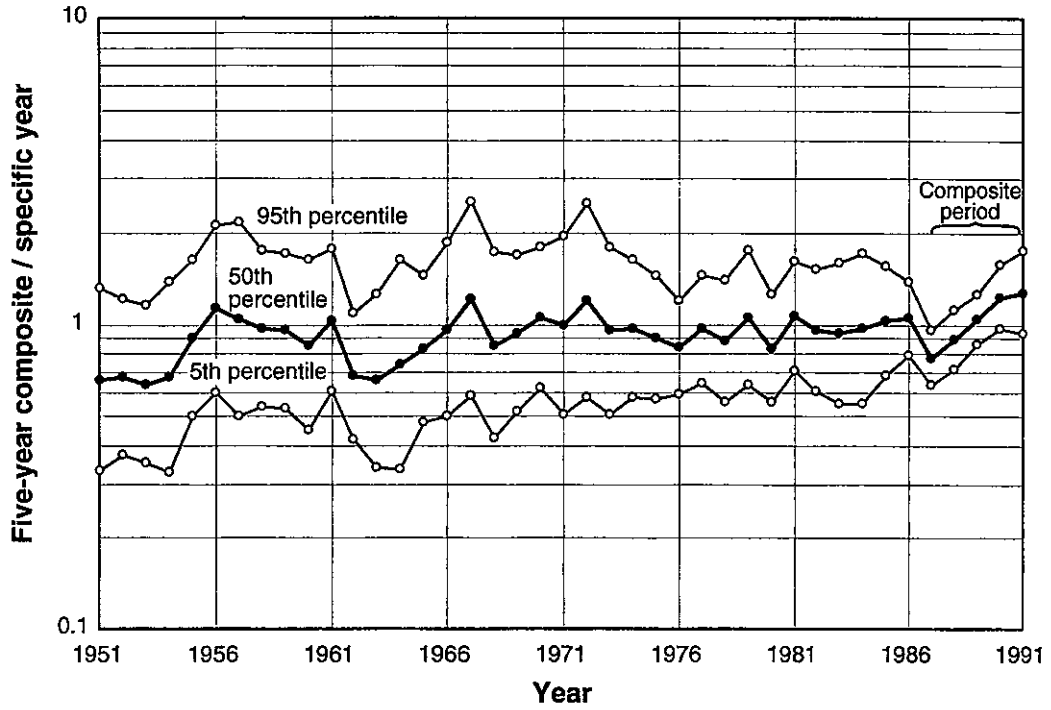

Figure M-8. Distributions of P/O ratios of χ / Q calculated with Cincinnati JFT data. Predicted (P) corresponds to the five-year composite JFT for 1987–1991; observed (O) corresponds to the JFT for a specific year. As one would expect, during the composite period, the 50th percentiles average about 1, and the extreme percentiles are closer together than for earlier years.

Table M-21. Distributions of Predicted/Observed Ratios for Prediction of Past Air Concentrations with 1987–1991 Composite Cincinnati Joint Frequency Meteorological Data

Year	GM	GSD	Year	GM	GSD	Year	GM	GSD
1951	0.66	1.52	1965	0.83	1.40	1979	1.05	1.36
1952	0.68	1.43	1966	0.96	1.49	1980	0.84	1.28
1953	0.64	1.44	1967	1.21	1.56	1981	1.07	1.29
1954	0.67	1.55	1968	0.85	1.53	1982	0.96	1.32
1955	0.90	1.43	1969	0.94	1.43	1983	0.94	1.38
1956	1.13	1.47	1970	1.05	1.38	1984	0.97	1.41
1957	1.04	1.56	1971	1.00	1.50	1985	1.03	1.28
1958	0.97	1.43	1972	1.20	1.56	1986	1.05	1.18
1959	0.95	1.43	1973	0.95	1.47	1987	0.78	1.13
1960	0.86	1.47	1974	0.97	1.37	1988	0.90	1.15
1961	1.04	1.38	1975	0.91	1.32	1989	1.05	1.12
1962	0.68	1.33	1976	0.84	1.24	1990	1.23	1.16
1963	0.66	1.49	1977	0.97	1.28	1991	1.28	1.21
1964	0.74	1.61	1978	0.88	1.32			

For each Monte Carlo iteration in the calculation, this uncertainty is applied year by year to the estimated air concentration at each receptor location. Receptor locations are assumed independent. This uncertainty is propagated through all calculations that depend on air concentrations and corresponds to a component of uncertainty in computed scenario doses.

The foregoing discussion summarizes our treatment of uncertainties related to the use of meteorological data collected at the FMPC tower. The procedure just described, of course, does not explicitly formulate a component of uncertainty that responds to some of the concerns raised about this dataset. We believe, however, that the procedure is sufficiently conservative to allow implicitly for these concerns. For reference, we provide a listing of the five-year (1987–1991) composite annual JFT for the FMPC data (Table M-22). Similar listings of composite JFTs for each month are shown in Appendix E of the Task 4 report.

OTHER UNCERTAINTIES

Two remaining sources of uncertainty associated with atmospheric dispersion have to do with (1) deposition and (2) local effects that lead to inaccurate predictions of air concentration by the diffusion curves of Figures M-2 and M-4.

Wet deposition is modeled with a wet deposition velocity based on a washout ratio. In the discussion of wet deposition beginning on page M-11, we reported FMPC measurements of uranium in precipitation with a range that spanned the second and third quartiles. For the simulations, we represent the washout ratio by the lognormal distribution with GM = 6×10^5 and GSD = 2.14, corresponding to 25th and 75th percentiles 3.6×10^5 and 1×10^6, respectively. These values agree approximately with the reported range and the literature.

Dry deposition is based on a theory of dry deposition velocities that depend on particle diameter, roughness height, stability class, and wind speed near the ground (this appendix, page M-11; Killough et al. 1993, Appendix G). Deposition is calculated for ranges of particle diameter, stability and wind speed, and the particle size distribution and the JFT are used to average the results. On each Monte Carlo iteration, we calculate a random multiplicative uncertainty factor for deposition velocity. This factor is lognormal with GM = 1 and GSD = 1.95, which gives a 95th/50th percentile ratio of 3. The choice of this distribution is partly subjective; it is not as large as the scatter shown in the review of Sehmel (1980), but it is reasonable to assume that the particulate matter dealt with in our study is somewhat less heterogeneous than in the review.

Item (2) of the introductory paragraph of this section is related to the diffusion curves of Figures M-2 and M-4. The gray uncertainty bands about those curves represent uncertainty in the measurement of diffusion as a function of distance using the data at hand. In Figure M-2, the vertical extent of the band is based on $\sigma / \sqrt{N}$, where σ is a composite standard deviation for the logarithms of the residuals and the exogenous uncertainties (1986–1988 uranium releases, resuspended uranium, sampler efficiency, plume depletion), and N is the number of observations (38). In ordinary sampling, $\sigma / \sqrt{N}$ is the standard deviation of the sample mean, sometimes called the standard error. In the present context, it is the standard error for calibrating the diffusion curve by the regression procedure.

Table M-22. Composite Meteorological Frequencies for FMPC, Annual 1987–1991

	Wind speed range (m s^{-1})								Wind speed range (m s^{-1})						
	0–2	2–4	4–6	6–8	8–10	>10	Total		0–2	2–4	4–6	6–8	8–10	>10	Total
Class A frequency 0.06374								**Class B** frequency 0.03104							
N	.00548	.01482	.01201	.00000	.00000	.00000	.03231	N	.00805	.03271	.00926	.00152	.00000	.00000	.05154
NNE	.01088	.01509	.01007	.00122	.00039	.00000	.03765	NNE	.00641	.01174	.01408	.00155	.00000	.00000	.03378
NE	.01762	.03981	.00770	.00040	.00000	.00000	.06553	NE	.01023	.03650	.01330	.00000	.00000	.00000	.06003
ENE	.03891	.05314	.00520	.00076	.00000	.00000	.09801	ENE	.01626	.03749	.00680	.00165	.00000	.00000	.06220
E	.02178	.01596	.00253	.00000	.00000	.00037	.04064	E	.02043	.01399	.00392	.00000	.00000	.00000	.03834
ESE	.01375	.00688	.00000	.00000	.00000	.00000	.02063	ESE	.01107	.00770	.00000	.00000	.00000	.00000	.01877
SE	.00655	.00266	.00000	.00000	.00000	.00037	.00958	SE	.00447	.00318	.00000	.00000	.00000	.00000	.00765
SSE	.00969	.00368	.00073	.00037	.00000	.00000	.01447	SSE	.01028	.00223	.00224	.00076	.00000	.00000	.01551
S	.01113	.01689	.00216	.00000	.00000	.00000	.03018	S	.01420	.01538	.00270	.00000	.00000	.00000	.03228
SSW	.01794	.07121	.02186	.00000	.00000	.00000	.11101	SSW	.02268	.06206	.02160	.00224	.00078	.00000	.10936
SW	.03382	.06934	.03479	.00144	.00000	.00000	.13939	SW	.02935	.08052	.03092	.00237	.00000	.00000	.14316
WSW	.03371	.07260	.01689	.00076	.00000	.00000	.12396	WSW	.02726	.06730	.02381	.00115	.00000	.00000	.11952
W	.01979	.07220	.03010	.00193	.00000	.00000	.12402	W	.02246	.05246	.02933	.00076	.00000	.00000	.10501
WNW	.01514	.03295	.01853	.00284	.00000	.00000	.06946	WNW	.01431	.02885	.02122	.00155	.00000	.00000	.06593
NW	.01352	.02184	.00831	.00000	.00000	.00000	.04367	NW	.01743	.03522	.02236	.00000	.00000	.00000	.07501
NNW	.00874	.01790	.01203	.00037	.00000	.00045	.03949	NNW	.01163	.03677	.01269	.00083	.00000	.00000	.06192
Total	.27846	.52697	.18289	.01010	.00039	.00119	1.0000	Total	.24650	.52410	.21422	.01440	.00078	.00000	1.0000
Class C frequency 0.04458								**Class D** frequency 0.33399							
N	.01227	.03159	.01054	.00218	.00000	.00000	.05658	N	.01134	.03947	.01233	.00078	.00000	.00000	.06392
NNE	.00980	.02674	.00873	.00054	.00000	.00000	.04581	NNE	.01592	.03649	.01141	.00159	.00000	.00000	.06541
NE	.01186	.03378	.01465	.00166	.00000	.00000	.06195	NE	.02317	.04119	.00989	.00049	.00000	.00000	.07474
ENE	.03285	.03767	.00390	.00384	.00000	.00000	.07826	ENE	.03055	.05437	.01459	.00175	.00000	.00000	.10126
E	.02593	.01519	.00164	.00052	.00000	.00000	.04328	E	.02105	.01234	.00098	.00000	.00007	.00000	.03444
ESE	.01684	.00817	.00000	.00000	.00000	.00000	.02501	ESE	.01403	.00364	.00007	.00000	.00000	.00000	.01774
SE	.01176	.00769	.00000	.00000	.00000	.00000	.01945	SE	.00989	.00574	.00021	.00000	.00000	.00000	.01584
SSE	.00631	.00918	.00158	.00000	.00000	.00000	.01707	SSE	.01216	.00912	.00224	.00014	.00000	.00000	.02366
S	.00808	.02267	.00335	.00000	.00000	.00000	.03410	S	.01447	.01962	.00607	.00065	.00000	.00000	.04081
SSW	.00801	.05529	.01609	.00111	.00054	.00000	.08104	SSW	.02734	.04451	.01655	.00255	.00000	.00000	.09095
SW	.03041	.08680	.02257	.00310	.00000	.00000	.14288	SW	.03739	.05062	.01209	.00162	.00028	.00014	.10214
WSW	.03214	.06748	.01674	.00186	.00000	.00000	.11822	WSW	.03529	.03460	.01015	.00272	.00051	.00007	.08334
W	.01979	.04125	.01882	.00279	.00000	.00000	.08265	W	.02737	.04350	.01889	.00201	.00000	.00000	.09177
WNW	.01738	.03271	.01579	.00275	.00000	.00000	.06863	WNW	.01829	.03857	.01588	.00181	.00000	.00000	.07455
NW	.01357	.03517	.02017	.00000	.00057	.00000	.06948	NW	.01753	.02915	.01249	.00037	.00022	.00000	.05976
NNW	.01429	.03023	.01053	.00058	.00000	.00000	.05563	NNW	.01588	.03314	.00946	.00108	.00015	.00000	.05971
Total	.27127	.54160	.16508	.02093	.00111	.00000	1.0000	Total	.33165	.49607	.15329	.01755	.00123	.00020	1.0000
Class E frequency 0.28810								**Class F** frequency 0.23854							
N	.02250	.01139	.00099	.00008	.00000	.00000	.03496	N	.01479	.00042	.00000	.00000	.00011	.00022	.01554
NNE	.01278	.00914	.00150	.00017	.00000	.00000	.02359	NNE	.01584	.00010	.00024	.00000	.00000	.00000	.01618
NE	.01626	.00819	.00061	.00000	.00000	.00000	.02506	NE	.01582	.00000	.00000	.00000	.00000	.00000	.01582
ENE	.04355	.02127	.00122	.00000	.00000	.00000	.06604	ENE	.03651	.00268	.00000	.00000	.00000	.00000	.03919
E	.03378	.00459	.00017	.00000	.00000	.00000	.03854	E	.05881	.00010	.00000	.00000	.00000	.00000	.05891
ESE	.01528	.00240	.00000	.00000	.00000	.00000	.01768	ESE	.03339	.00000	.00000	.00000	.00000	.00010	.03349
SE	.01811	.00320	.00032	.00000	.00000	.00000	.02163	SE	.01867	.00010	.00000	.00000	.00000	.00000	.01877
SSE	.02090	.01010	.00146	.00016	.00000	.00000	.03262	SSE	.02029	.00015	.00000	.00000	.00000	.00000	.02044
S	.03069	.02700	.00655	.00143	.00000	.00000	.06567	S	.02967	.00078	.00000	.00000	.00000	.00000	.03045
SSW	.05250	.05278	.01530	.00177	.00016	.00000	.12251	SSW	.06088	.00226	.00011	.00000	.00000	.00000	.06325
SW	.09163	.06151	.01053	.00067	.00008	.00000	.16442	SW	.09926	.00425	.00000	.00000	.00000	.00000	.10351
WSW	.08408	.02649	.00617	.00123	.00000	.00000	.11797	WSW	.12584	.00284	.00000	.00000	.00000	.00000	.12868
W	.05896	.03287	.00730	.00046	.00000	.00000	.09959	W	.12743	.00122	.00000	.00000	.00000	.00000	.12865
WNW	.04197	.02673	.00582	.00032	.00000	.00000	.07484	WNW	.14417	.00020	.00000	.00000	.00000	.00000	.14437
NW	.03663	.01442	.00222	.00016	.00000	.00000	.05343	NW	.12380	.00031	.00000	.00000	.00000	.00000	.12411
NNW	.02943	.01004	.00174	.00025	.00000	.00000	.04146	NNW	.05745	.00120	.00000	.00000	.00000	.00000	.05865
Total	.60905	.32212	.06189	.00670	.00024	.00000	1.0000	Total	.98262	.01660	.00035	.00000	.00011	.00032	1.0000

In Figure M-2, the gray uncertainty band excludes about half of the observations, and this fact may lead the reader to ask whether the band accounts adequately for uncertainty associated with the diffusion curve. The answer is that the process of determining the theoretical curve calibration must be distinguished from using the curve for estimating air

concentrations. In the latter connection, not only the band of calibration uncertainty, but other uncertain quantities—such as the source term, deposition, and meteorological parameters—must be considered. And there is yet another source of uncertainty that is related to the ability of the curve to predict air concentrations at specific locations within the assessment domain.

The diffusion curve represents a theoretical ideal of diffusion that would exist if the area distribution of the source were as postulated, if local atmospheric behavior remained typical of 1986–1988, and if the terrain were level and free of obstructions and did not exchange heat with the atmosphere at different rates in different locations. In the real assessment domain, all of these assumptions are violated in various ways which cannot be quantified in detail, but the residuals estimate the aggregated effects of these and other deviations from the ideal. We treat this component of uncertainty separately in estimating air concentrations, and to represent it we use a lognormal approximation of the distribution of the residuals for the uranium curve of Figure M-2 (GSD = 1.47). For want of a better name, we refer to this component as residual uncertainty.

We use the residual uncertainty determined from the uranium monitoring to estimate air concentrations of both uranium and radon. Radon residuals, of course, are also available and have a GSD that is nearly twice the one for uranium. The decision to apply the uranium residuals to both predictions was influenced by the following considerations:

(1) The uranium data cover a range of 500 m to 6000 m from their source center, whereas the radon data extend from 40 m to 2000 m from the K-65 silos. Thus, the uranium residuals may be more typical of locations throughout the assessment domain, where exposed individuals lived, attended school, and worked.
(2) The radon residuals show considerable scatter that results partly from uncertainty in measuring net concentrations at low levels. The uranium residuals are less affected by background adjustments. Some of the scatter in the Mound radon data (Figure M-4, black circles) may be attributable to proximity of the monitors to the source.
(3) The uncertainty band around the radon diffusion curve (Figure M-4) reflects more conservatism than the uncertainty band around the uranium curve (Figure M-2). The added conservatism came from extending the large coefficients of variation estimated for the boundary stations to the Mound data (see Equation M-34 and the numeric values following the equation). This extra conservatism compensates somewhat for our not applying larger residual uncertainty to estimates of radon concentrations.

The residual uncertainties for different receptor locations are assumed to be independent. A number is drawn for each receptor location at the beginning of each Monte Carlo cycle (a Monte Carlo cycle includes all 38 simulated years of plant operation). The sample is a multiplicative factor with the residual GSD (1.47) and is multiplied by the randomly predicted air concentration for the location for each year of plant operation.

RECAPITULATION OF UNCERTAINTIES

Figure M-9 presents the uncertainties described in this appendix in a schematic arrangement that indicates their origin and propagation. Figure M-10 (uranium) and M-11 (radon) relate the distributions to the equations associated with the estimation of air concentrations.

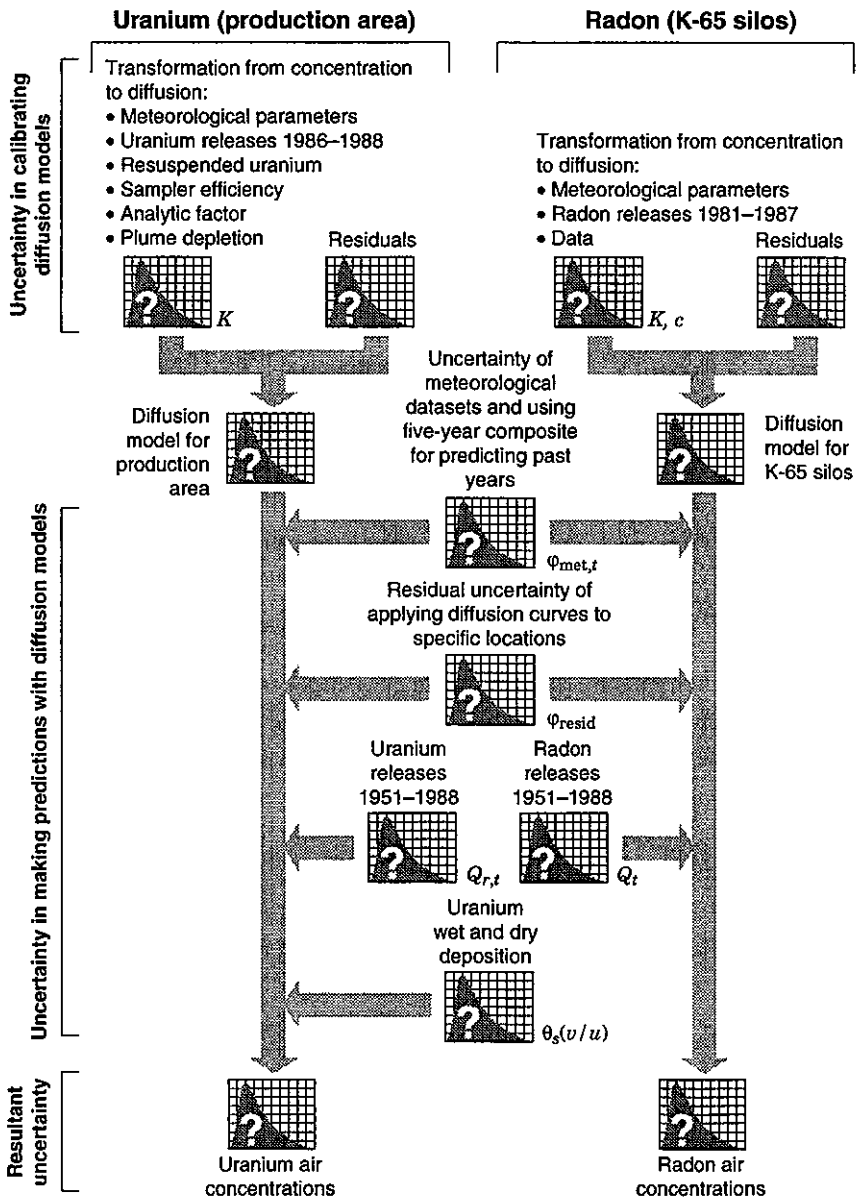

Figure M-9. Uncertainties associated with atmospheric dispersion from the FMPC production area and the K-65 silos. The symbols to the lower right of some icons are defined in Figures M-10 and M-11.

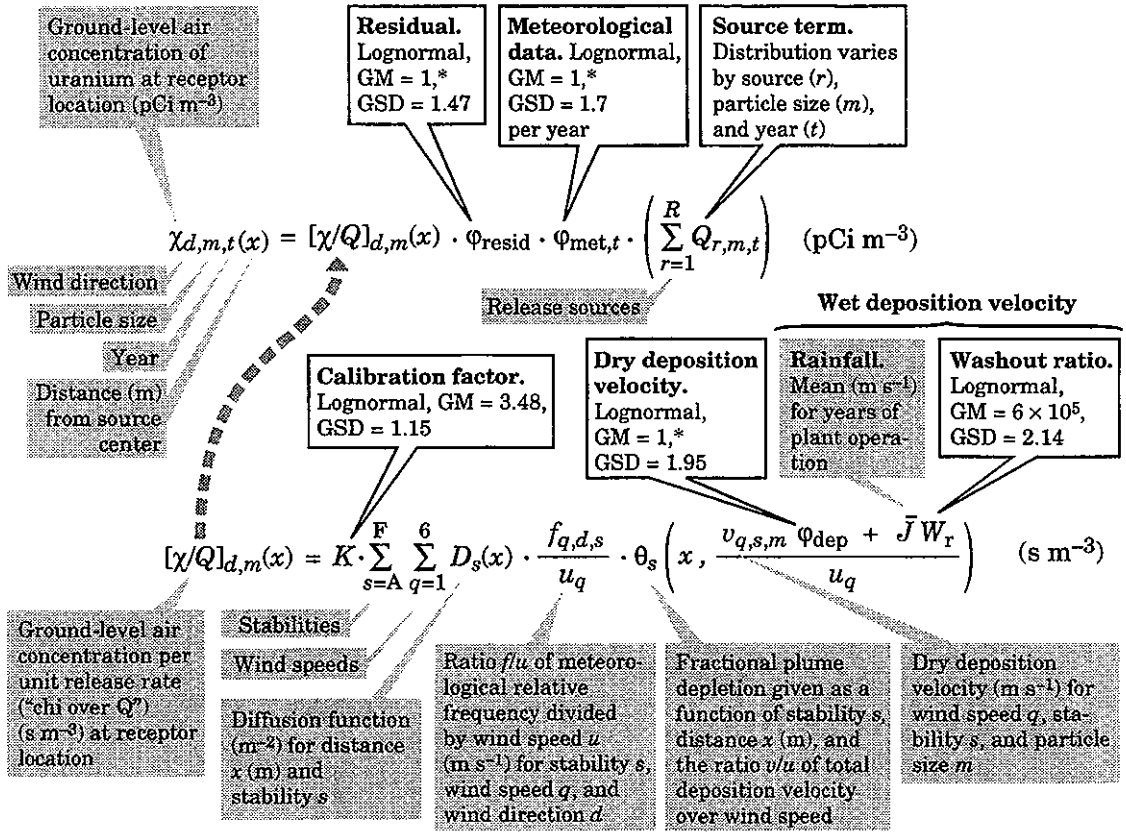

* The random variables denoted by φ (with subscripts) are lognormally distributed multiplicative uncertainty factors, with geometric mean 1. For any nonstochastic quantity C, the product $C\varphi$ is lognormally distributed with geometric mean C and geometric standard deviation (GSD) equal to the GSD of φ.

Legend

Random variables

Deterministic quantities

List of indices

q	Wind speed (6 categories: 1, 3, 5, 7, 9, 11 m s^{-1})
d	Wind direction (16 sectors of 22.5°)
s	Atmospheric stability (classes A, . . . , F)
m	Particle size category
t	Year (1951–1988)

Figure M-10. Uncertainties in uranium air concentrations. This figure expresses the calculation of the air concentration in terms of its equation, with random variables (uncertain quantities) and deterministic quantities.

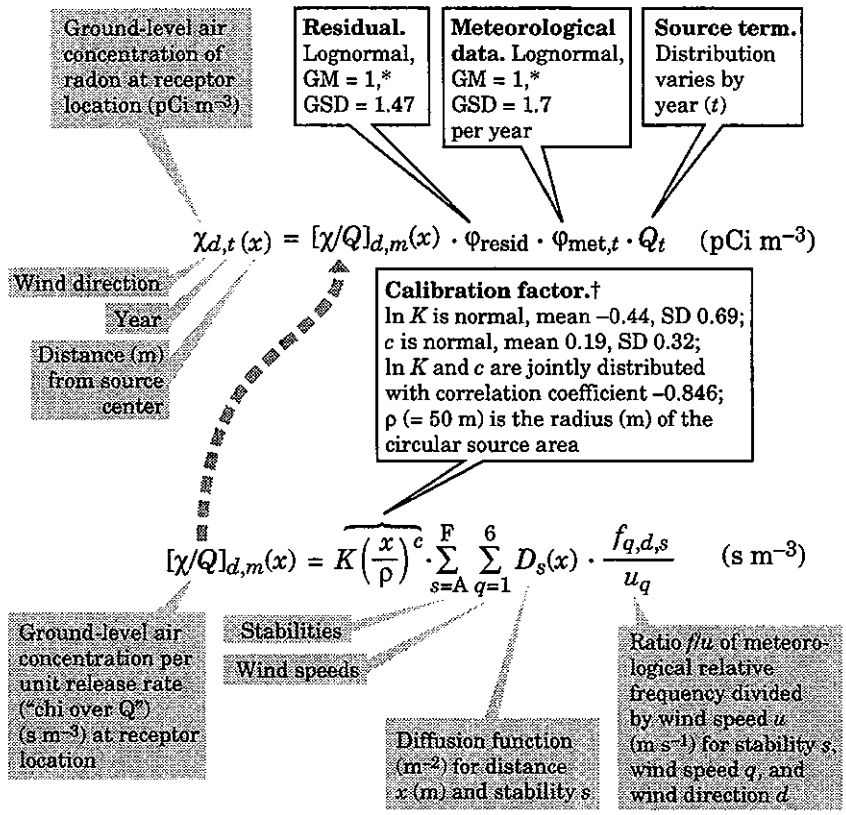

* The random variables denoted by φ (with subscripts) are lognormally distributed multiplicative uncertainty factors, with geometric mean 1. For any nonstochastic quantity C, the product $C\varphi$ is lognormally distributed with geometric mean C and geometric standard deviation (GSD) equal to the GSD of φ.

† The calibration factor may also be treated as a multiplicative lognormally distributed factor with GM and GSD given as a function of the distance x (m) by the following table:

Distance (m)	40	100	200	500	1,000	2,000	5,000	10,000
GM	0.62	0.74	0.84	1.0	1.1	1.3	1.6	1.8
GSD	2.1	1.7	1.5	1.5	1.7	2.0	2.6	3.2

Legend

Random variables

Deterministic quantities

List of indices

q	Wind speed (6 categories: 1, 3, 5, 7, 9, 11 m s^{-1})
d	Wind direction (16 sectors of 22.5°)
s	Atmospheric stability (classes A, . . . , F)
m	Particle size category
t	Year (1951–1988)

Figure M-11. Uncertainties in radon air concentrations. This figure expresses the calculation of the air concentration in terms of its equation, with random variables (uncertain quantities) and deterministic quantities.

Figure M-9 emphasizes the contrast in the two main aspects of uncertainty that have been treated in this appendix: (1) calibration and (2) making predictions with the calibrated diffusion function. Each aspect contributes a component to the total uncertainty in any

prediction. Within each aspect, there are similarities and differences between uranium and radon. We review these similarities and differences in the following subsections and close with an example.

Calibration

For both uranium and radon, transformations of the data to diffusion introduce an exogenous component of uncertainty, in addition to the intrinsic component expressed by the residuals. In both cases, meteorological parameters and release rates for the calibration period contribute to this component. Uranium is unique in requiring adjustments to the data to account for resuspension and sampler efficiency, each with its own uncertainty, and in addition there is an uncertainty factor for laboratory analysis of uranium samples. Also in the case of uranium, we give explicit treatment to deposition; for radon, the effects of deposition are left implicit. Some of the radon data have the unique problem of having magnitudes near background level during the calibration period. Inclusion of these data introduces, by way of the exogenous uncertainty term, a large calibration uncertainty component that is not present for uranium. We also estimate two calibration parameters for radon, in place of just one for uranium. The additional degree of freedom for radon permits the width of the calibration uncertainty band to increase as the distance from the source exceeds that of the farthest sampling locations (Figure M-4). Figure M-12 reviews the calibration process and the distributions involved in a generic way that applies to both uranium and radon.

Predictions

Figure M-9 indicates, in addition to the calibration uncertainties which are propagated through the calculations, three uncertainties that are introduced into the predictions for both uranium and radon:

1. Uncertainty in meteorological datasets ($\varphi_{met,t}$ in Figures M-10 and M-11), particularly the uncertainty arising from using the five-year composite meteorological dataset (based on 1987–1991) for predictions of specific years
2. The distribution of the residuals (φ_{resid} in Figures M-10 and M-11), derived from the uranium calibration. Applied to both uranium and radon, this distribution is interpreted to compensate for mispredictions from such local variations as terrain, obstructions, and nonuniform air-soil thermal interactions
3. Uncertainties in the release of uranium or radon, as the case may be, for each year of the simulation and, in the case of uranium, for each separate source ($Q_{r,m,t}$ for uranium source r in Figure M-10 and Q_t for radon released from the K-65 silos in Figure M-11).

A fourth uncertainty is applied only to uranium. This is the uncertainty in the amount of plume depletion that occurs as a result of wet and dry deposition. This effect also influenced the uranium calibration and was handled in a simple way. For predictions, the uncertainties are applied directly to the dry deposition velocities (uncertainty factor φ_{dep} that multiplies the dry deposition velocity in Figure M-10) and for wet deposition they are expressed in the lognormally distributed washout ratio (W_r in Figure M-10) and the rainfall rate $\overline{J}$, which is

the mean of random variables that simulate each year's rainfall (the product $\overline{J}W_r$ is the wet deposition velocity and is shown in Figure M-10). The total (random) deposition velocity determines the plume depletion through the surface depletion model (which also depends on the atmospheric stability, the distance from the source, and the wind speed; see Figure M-10).

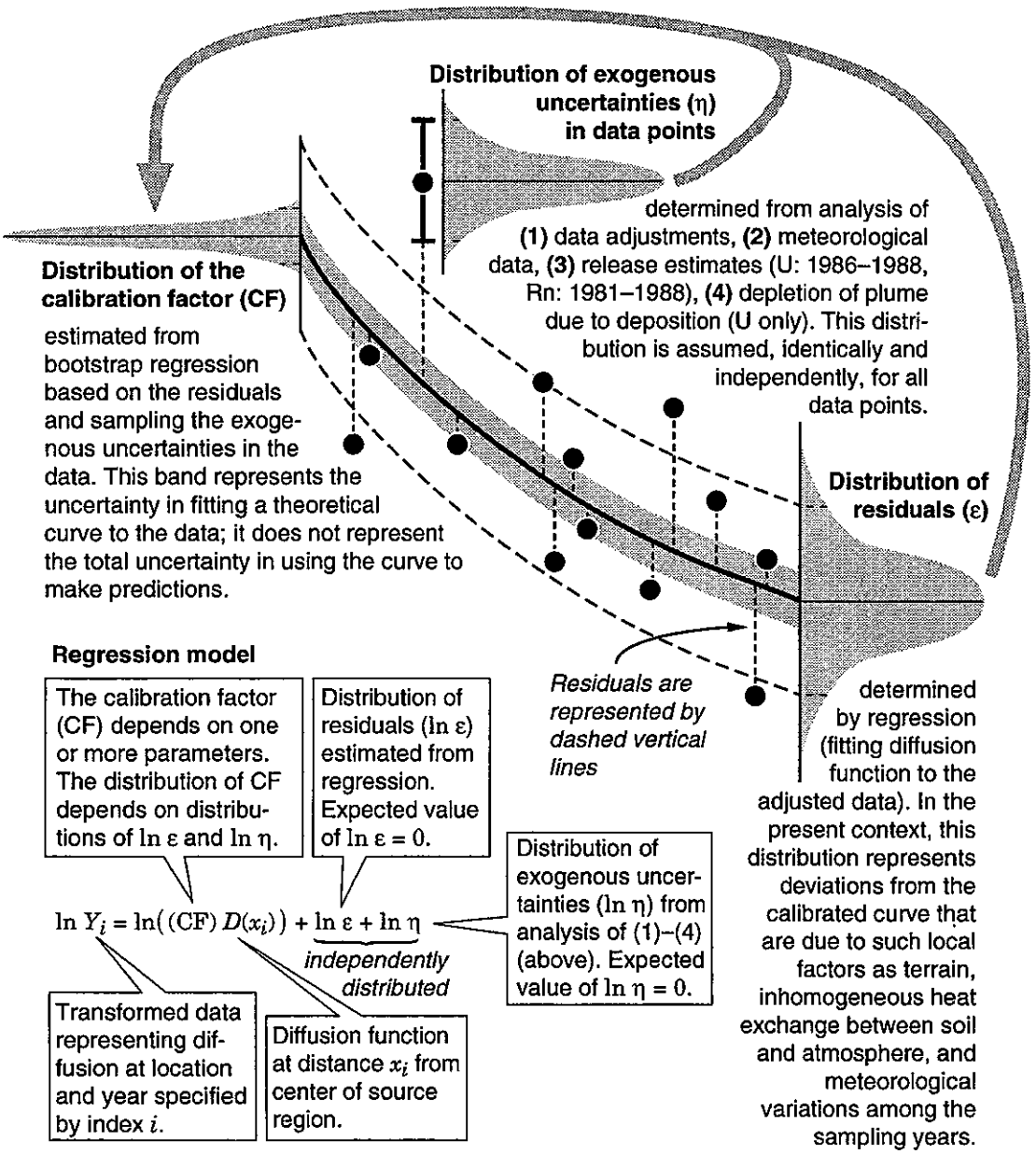

Figure M-12. Review of the uncertainty distributions and regression procedure used to calibrate the uranium and radon air dispersion models to site-specific data.

Some of the uncertainties show an explicit dependence on the year t of the prediction. This is an important point, because in the Monte Carlo simulations, such an uncertainty will be sampled independently once for each of the 38 simulated years. In some cases, the distribution is the same for all years (e.g., the meteorological uncertainty factor $\varphi_{met,t}$ in Figures M-10 and M-11), and in other cases the form of the distribution varies from year to year (e.g., the release term $Q_{r,m,t}$ for uranium in Figure M10 and Q_t for radon in Figure M-11). Thus we have two operational classes of uncertainties: those that are sampled once for each Monte Carlo cycle and those that are sampled once for each year within each Monte Carlo cycle. This structure complicates the analysis of the simulation and in most cases makes it impossible to determine the resultant distributions in explicit analytic form (e.g., the sum of 38 years of annual dose), even when the 38 component distributions are of tractable analytic form, such as lognormal. This point is illustrated in the following example.

Example M-1. We consider a simplified calculation of annual air concentration, annual dose, and cumulative dose for 38 years to an individual at a receptor point 1,000 m northeast of a source of airborne natural uranium, of inhalation class Y, and particle size specified by AMAD = 2 μm. Figure M-12 gives all data and results of the calculation. Unlike the real source term, the distribution of the release rate (item D in Figure M-12) is assumed to be the same for all years (this, of course, does not mean that the random releases will be the same from year to year).

The calculation follows a simplified form of the equation in Figure M-10. We take stability D as an average and do not sum over stabilities. Similarly, we use an average of the meteorological ratio f / u and do not sum over wind speed categories. The diffusion KD is estimated for x = 1,000 m from Figure M-2 and shown in the upper right hand corner of Figure M-13 (the GSD corresponds to the calibration uncertainty and is shown in Figure M-10). The distribution of φ_{resid} is shown in Figure M-10. The uncertainty of the plume depletion fraction θ is handled as in the uranium calibration (expressed in Table M-6 as φ_{dep}). The meteorological ratio f / u is treated as a deterministic quantity; its uncertainty is considered to be included in the factor $\varphi_{met,t}$ (item E in Figure M-13). The product (composite) of the factors KD, φ_{resid}, θ, and f / u is the normalized air concentration $[\chi / Q]\varphi_{resid}$ (item C in Figure M-13). This is the stochastic factor that will be used to calculate air concentration from each year's release rate. Note that the distribution of $[\chi / Q]\varphi_{resid}$ does not depend on the year; it is sampled only once during each Monte Carlo cycle.

Columns 1–4 in the lower left hand corner of Figure M-13 suggest the calculation, as it might be arranged in a spreadsheet. The reversed letters and numerals above the columns indicate the operations that are carried out to compute the entries in each column. The values shown in columns 1 and 2 are the geometric means of the distributions that the entries represent. The entries shown in columns 3 and 4 have been calculated deterministically from columns 1 and 2 and from other geometric means as indicated by the reversed letters and numerals. The point is that each

constant entry in each column is the stand-in for a distribution. In columns 1 and 2, the distributions are as specified in the headings. In columns 3 and 4, the distributions are composites of other distributions as indicated.

SAMPLE CALCULATION OF URANIUM AIR CONCENTRATION AND DOSE

Basic data

Receptor location	1,000 m NE
Material	Natural U, Class Y
Particle AMAD	2 μm
Annual release	6,750 kg
	1.67×10^{11} Bq
(A) Dose factor*	1.77×10^{-4} Sv Bq^{-1}
(B) Breathing	8,395 m^3 year^{-1}

* Committed dose equivalent to lungs for inhaled class Y with AMAD 2 μm; ^{238}U factor used as surrogate for natural U

Calculation layout (below)

Columns 1 and 2 are specified distributions. Distributions in columns 3 and 4 are calculated as indicated:

Lognormal stochastic factors for 38-year simulation

	GM	GSD
Diffusion KD (m^{-2})	1.92×10^{-5}	1.15
Residual factor φ_{resid}	1	1.47
Plume depletion θ	1	1.74
Met. ratio f / u (s m^{-3})	0.0846	—
(C) $[\chi / Q] \cdot \varphi_{resid}$ (s m^{-3})	1.62×10^{-6}	1.99

Stochastic factors with independent lognormal distributions for each year

	GM	GSD
(D) Release rate Q_t (Bq s^{-1})	5.28×10^3	1.73
(E) Met. uncertainty $\varphi_{met,t}$	1	1.7

Year	1 = (D) Q_t (Bq s^{-1})	2 = (E) $\varphi_{met,t}$	3 = 1 × 2 × (C) Concentration (Bq m^{-3})	4 = 3 × (A) × (B) Annual dose (Sv)
1951	5.28×10^3	1	8.55×10^{-3}	1.27×10^{-2}
1952	5.28×10^3	1	8.55×10^{-3}	1.27×10^{-2}
1953	5.28×10^3	1	8.55×10^{-3}	1.27×10^{-2}
⋮	⋮	⋮	⋮	⋮
1986	5.28×10^3	1	8.55×10^{-3}	1.27×10^{-2}
1987	5.28×10^3	1	8.55×10^{-3}	1.27×10^{-2}
1988	5.28×10^3	1	8.55×10^{-3}	1.27×10^{-2}
Cumulative dose (Sv)				4.83×10^{-1}

Distributions obtained by Monte Carlo calculations

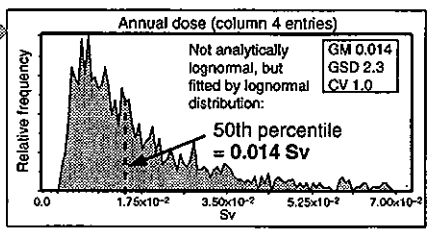

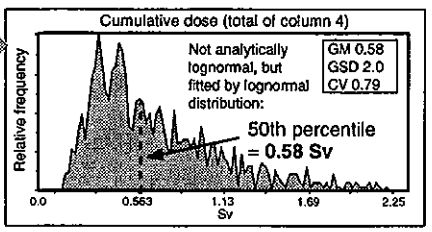

Factors for the 38 years are identically and independently distributed. The values shown are the geometric means.

Calculated deterministic values are not equal to the 50th percentiles of their respective distributions.

Figure M-13. Data and calculations for Example M-1. The text of the example relates distributions and other quantities to their sources in other parts of this appendix.

The distributions Q_t are the same for all years t, as are the distributions $\varphi_{met,t}$. But each of these distributions is sampled independently from year to year. For calculating the entries in column 3 (air concentrations), we begin a Monte Carlo cycle by (1) sampling $[\chi / Q]\varphi_{resid}$, then (2) independently for each t, sampling Q_t and

$\varphi_{met,t}$ and forming the product $Q_t \cdot \varphi_{met,t} \cdot [\chi / Q]\varphi_{resid}$, which is the entry in column 3. Thus $[\chi / Q]\varphi_{resid}$ is sampled only once in a Monte Carlo cycle, whereas 38 stochastic values of the air concentration (column 3) are realized. A result of this two-stage sampling is that the concentrations in column 3 are not independently distributed. We return to this point later.

Two additional factors are needed for dose: the dose conversion factor (in this case, committed dose equivalent to the lung per unit intake, item A in the upper left corner of Figure M-13) and the breathing rate (item B). These factors have appropriate units, so that their product, multiplied by column 3, gives the annual committed dose equivalent (column 4). The entries in column 4, however, are not independently distributed because of the factor $[\chi / Q]\varphi_{resid}$, as noted previously. The distribution of each year's column 4 entry, obtained by Monte Carlo sampling with Crystal Ball™, is shown in the first of the two insets in the lower right hand corner of Figure M-13. Although it is not analytically lognormal, this distribution is well fitted by a lognormal distribution with GM = 0.014 Sv, GSD = 2.3, and CV (coefficient of variation) 1.0.

The total of column 4 represents the cumulative committed dose equivalent, which is realized once for each Monte Carlo cycle. The distribution of cumulative dose is shown in the second of the two insets in the lower right hand corner of Figure M-13. This distribution, like the terms of which it is the composite, is not analytically lognormal, but it is well fitted by the lognormal distribution with GM = 0.58 Sv, GSD = 2.0, and CV = 0.79. Notice the decrease in the GSD and the CV from the component distributions. If the terms were independently distributed, the fractional reduction in the CV would be $1/\sqrt{38}$, but in this case the magnitude of the reduction is affected by the correlation of the terms. Even so, there is some reduction in relative variability. The standard deviation of the sum is larger than that of the terms, but it is smaller as a percentage of the mean. For this example, we can do the following analysis:

The variance σ_T^2 of the total can be expressed as

$$\sigma_T^2 = \sum_{i=1}^{N} \sigma_i^2 + 2\sum_{i<j} \rho_{i,j}\sigma_i\sigma_j = N\sigma^2[1+\rho(N-1)] \qquad \text{(M-41)}$$

where $\sigma = \sigma_i = \sigma_j$ for all $i, j = 1,2,\cdots,N$ (= 38, the number of years of operation) and $\rho = \rho_{i,j}$, the common pairwise correlation coefficient for the annual dose in different years [the decomposition represented by the first equation of M-41 is shown in virtually all texts on mathematical statistics; for example, Wilks (1962)]. Now, if we can estimate the variance of the annual and cumulative doses from the geometric means and geometric standard deviations shown in Figure M-13, we can use Equation M-41 to calculate the correlation coefficient ρ. Using the conversion given

by Equation M-4 with the values of GM and GSD from the two insets in Figure M-13, we find that $\sigma_T = 0.580$ and $\sigma = 0.0198$. Substituting these values into Equation M-41, we find that $\rho = 0.583$. If we denote the coefficients of variation for the annual doses and the cumulative dose by CV and CV_T, respectively, we may use Equation M-41 and the fact that the mean of the cumulative dose is N times the mean of each annual dose to show that

$$CV_T = \frac{CV}{\sqrt{N}}\sqrt{1+\rho(N-1)} \; . \qquad \text{(M-42)}$$

If the annual doses were uncorrelated ($\rho = 0$), the coefficient of variation of the cumulative dose would be about one-sixth that of the annual doses ($1/\sqrt{38}$) or about 16%. In fact, we see from Figure M-13 that CV_T is 79%, and the difference is brought about by the moderate correlations between annual doses ($\rho = 0.583$). If the correlation coefficient approaches 1, the coefficients of variation for annual doses and cumulative dose approach equality.

A final point is illustrated by this example. The sum of the deterministically calculated entries in column 4 of Figure M-13 is less than the 50th percentile of the distribution of the cumulative dose shown in the bottom inset. The results of deterministic calculations with complex models do not, in general, agree with the central measures (e.g., 50th percentiles) of the corresponding results in the calculations with uncertainties. The extent of the discrepancy depends on various factors, including the nonlinearity of the model with respect to important parameters that are treated as uncertain. In this example, summing 50th percentiles for the 38 years in a deterministic calculation gives a result less than the 50th percentile of the distribution of the sum. This is not an accident. It is the result of a general property of the geometric mean, which, loosely stated, is that the geometric mean of a sum exceeds (or, in exceptional cases, may be equal to) the sum of the geometric means. In mathematical language and notation, we may state a precise form of the result as follows: If $A_1 = (a_{12},\ldots,a_{1M}),\ldots,A_N = (a_{N1},\ldots,a_{NM})$ are N vectors of M positive numbers each, and $\Sigma A_i = (\Sigma a_{i1},\ldots,\Sigma a_{iM})$ is their vector sum, then if $\mathbf{G}$ denotes the geometric mean,

$$\mathbf{G}(A_1)+\cdots+\mathbf{G}(A_N) < \mathbf{G}(\Sigma A_i) \; . \qquad \text{(M-43)}$$

The exception is that equality holds if every vector A_i is proportional to all other vectors A_j ($j \neq i$). This result is Theorem 10 from Hardy et al. (1959). In our context, N is 38 years of plant operation, and M is the sample size for an uncertainty analysis. As stated, the result shows that for any sample drawn from each year and added to provide a corresponding sample for the total, the sum of the sample geometric means for all years is less than the geometric mean of the total. If the distributions for the individual years are approximately lognormal (or log-triangular or log-uniform, or any other log-symmetric distribution), the geometric mean of a sample estimates the 50th percentile, and for a large sample, we would expect the approximation to be

close. Similarly, if the sample distribution of the total (e.g., the cumulative dose) is well fitted by a lognormal (or other log-symmetric) distribution (as is the case in Figure M-13, bottom inset), the geometric mean of the sample estimates the 50th percentile of the total. The inequality of geometric means holds for every sample, large or small, but the relationship with 50th percentiles is dependent on the form of the distributions. This analysis provides insight into one important source of disparity between 50th percentiles of uncertain results based on totals and corresponding deterministic values computed from 50th percentiles of the terms. This kind of disparity frequently occurs in the results of this study because the results are summations over the 38 years of plant operation.

DISCUSSION

The methods described in this appendix for modeling atmospheric dispersion of uranium released from the FMPC production area and radon released from the K-65 silos is based on well-known statistical methods (some of relatively recent origin), Gaussian plume dispersion models, representation of uncertainties with probability distributions, and Monte Carlo sampling techniques. Reduced to their components, the methods are conventional. Some readers might find the calibration unexpected, particularly its use of regression methods to estimate uncertainty distributions. However, it is most likely the context that is unfamiliar rather than the methods of analysis. Many, if not most, past applications of atmospheric transport modeling in environmental assessments have been prospective. Often, they have been based on generic model calculations, in which the source term, a meteorological joint frequency table, and some source parameters having to do with effective release heights were used with one of the available computer programs.

The FMPC production area is ill-characterized with respect to some of the source parameters, such as stack gas velocities and temperatures. Calculations with such fragmentary data as were obtained suggested that rooftop releases within the production area would have been drawn down into building wake cavities and otherwise dispersed by turbulent airflow within the complex of structures. This result pointed to a ground-level area source air dispersion model as an appropriate candidate. The availability of the 1986–1988 uranium air monitoring data for source-to-receptor distances ranging from 500 m to more than 6,000 m provided an excellent opportunity for calibrating the model to annual average concentrations and directly estimating uncertainty distributions associated with the calibrated model. For most prospective studies, such an analysis would be impossible. There are important differences between prospective studies and reconstructive assessments (dose reconstruction, in particular) that should be noted here.

Prospective studies envision facilities that have yet to be built or remediations that have yet to be carried out. Accordingly, there tends to be an absence of measurements that relate air concentrations to releases from the unbuilt facility or the not-yet restored land. The methodology applied to such prospective calculations (1) anticipates the probable overestimation of concentrations, (2) incorporates assumptions about source terms, buildings, and activities that may not yet exist, and (3) expects ultimately to present predicted concen-

trations that are below thresholds with margins of safety built into them. In appropriate contexts (e.g., protection of the public health and safety), such methodologies have validity.

Dose reconstruction, on the other hand, is quite different: (a) because it is retrospective, it has no direct connection with environmental health protection (no one can be protected retroactively); (b) it frequently provides information that will be used in epidemiological analysis to test for a statistical relationship between exposure to environmental pollutants and incidence of disease in exposed populations; and (c) it usually has available some data that are contemporaneous with and directly related to some of the quantities being estimated. However, (d) there may not be prior information about levels of exposure; such information must come from extensive analysis of data, historical documents, and histories of exposed individuals and populations. Thus (because of a and b), dose reconstruction may seek to minimize bias in its estimates of exposure and dose, and it must accompany these estimates with expressions of uncertainty. Whereas prospective studies tend to deal with uncertainty by making pessimistic assumptions that will likely exaggerate exposure or dose, dose reconstruction generally may not deliberately bias its estimates of exposure or dose, but instead must express conservatism by broadening uncertainty bounds. In view of c, dose reconstruction is obligated to scrutinize the data available to it, and from the aggregate of such data, to draw the best conclusions that its tools and the quality of the data permit. And keeping d in mind, we should not embrace protocols designed for other purposes without assurance that their implicit assumptions and ranges of validity fit the project at hand. These principles are applicable to all aspects of this dose reconstruction, but they apply in particular to air dispersion modeling. We have kept them very much in mind as we have worked out the approach described in this appendix.

REFERENCES

Aas C.A., D.L. Jones, and R.W. Keys. 1986. *Feed Materials Production Center Environmental Monitoring Annual Report for 1985*. Rep. FMPC-2047, Special, UC-41, Westinghouse Materials Company of Ohio, Cincinnati, Ohio.

Abramowitz M. and I. Stegun. 1968. *Handbook of Mathematical Functions*. Dover Publications, Inc., New York, NY.

Aitchison J. and J.A.C. Brown. 1969. *The Lognormal Distribution*. The University Press, Cambridge.

Anonymous. Circa 1984. *FMPC Radon (Terradex) Results*. Handwritten spreadsheet of radon concentrations.

Berven B.A. and W.D. Cottrell. 1987. *Review of Radiological Data for the K-65 Storage Silos at the Feed Materials Production Center, Fernald, Ohio*. Rep. ORNL/M-2110, Oak Ridge National Laboratory, Oak Ridge, Tennessee.

Boback M.W. and K.N. Ross. 1981. *Feed Materials Production Center Environmental Monitoring Annual Report for 1980*. Rep. NLCO-1168, Special, NLO, Inc., Cincinnati, Ohio.

Briggs G.A. 1974. "Diffusion Estimation for Small Emissions." In *Atmospheric Turbulence and Diffusion Laboratory 1973 Annual Report*, ATDL-106.

Briggs G.A. 1969. *Plume Rise*. Report TID-25075, U.S. Atomic Energy Commission Office of Information Services. Available from National Technical Information Service.

Byrne J.M. 1992. Letter, with enclosed computer disks, to Duane W. Schmidt, dated August 31, 1992. Reference number WEMCO:EM:EMON:92-1274, Westinghouse Environmental Management Company of Ohio, Cincinnati, Ohio.

Byrne J.M., T.A. Dugan, and J.S. Oberjohn. 1991. *Feed Materials Production Center Annual Environmental Report for Calendar Year 1990*. Rep. FMPC-2245, Special, UC-707, Westinghouse Materials Company of Ohio, Cincinnati, Ohio.

Decisioneering Inc. 1993. *Crystal Ball Version 3.0*. 1380 Lawrence Street, Denver, Colorado.

Dugan T.A., G.L. Gels, J.S. Oberjohn, and L.K. Rogers. 1990. *Feed Materials Production Center Annual Environmental Report for Calendar Year 1989*. Rep. FMPC-2200, Special, UC-707, Westinghouse Materials Company of Ohio, Cincinnati, Ohio.

Efron B. 1982. *The Jackknife, the Bootstrap and Other Resampling Plans*. CBMS 38, Society for Industrial and Applied Mathematics, Philadelphia, Pennsylvania.

Facemire C.F., D.L. Jones, and R.W. Keys. 1985. *Feed Materials Production Center Environmental Monitoring Annual Report for 1984*. Rep. NLCO-2028, Special, UC-41, NLO, Inc., Cincinnati, Ohio.

Fleming D.A. and K.N. Ross. 1983. *Feed Materials Production Center Environmental Monitoring Annual Report for 1982*. Rep. NLCO-1187, Special, UC-41, NLO, Inc., Cincinnati, Ohio.

Fleming D.A. and K.N. Ross. 1984. *Feed Materials Production Center Environmental Monitoring Annual Report for 1983*. Rep. NLCO-2018, Special, UC-41, NLO, Inc., Cincinnati, Ohio.

Fleming D.A., M.W. Boback, and K.N. Ross. 1982. *Feed Materials Production Center Environmental Monitoring Annual Report for 1981*. Rep. NLCO-1180, Special, UC-41, NLO, Inc., Cincinnati, Ohio.

Gilbert R.O. 1987. *Statistical Methods for Environmental Pollution Monitoring*. Van Nostrand Reinhold, New York.

Hagee G.R., P.H. Jenkins, P.J. Gephart, and C.R. Rudy. 1985. *Radon and Radon Flux Measurements at the Feed Materials Production Center, Fernald, Ohio*. Rep. MLM-MU-85-68-0001, Mound, Monsanto Research Corporation, Miamisburg, Ohio.

Hanna S.R., G.A. Briggs, and R.P. Hosker, Jr. 1982. *Handbook on Atmospheric Diffusion*. Report DOE/TIC-11223 (DE82002045), U.S. Department of Energy (NTIS).

Hardy G.H., J.E. Littlewood, and G. Pólya. 1959. *Inequalities*. University Press, Cambridge, UK.

Hilsmeier W.F. and F.A. Gifford, Jr. 1962. *Graphs for Estimating Atmospheric Dispersion*. USAEC Report ORO-545, Weather Bureau, Oak Ridge, Tennessee. Curves reprinted in *Meteorology and Atomic Energy 1968* (D.H. Slade, Ed.), pp. 411–413 (1988).

Hoffman F.O. and J.S. Hammonds. 1994. "Propagation of Uncertainty in Risk Assessments: The Need to Distinguish Between Uncertainty Due to Lack of Knowledge and Uncertainty Due to Variability." *Risk Analysis* **14**(5): 707–712.

Horst T.W. 1977. "A Surface Depletion Model for Deposition from a Gaussian Plume." *Atmospheric Environment* **11**: 41–46.

Jenkins P.H. 1986. Letter to Woodrow D. Cottrell, Oak Ridge National Laboratory, dated November 21, 1986. Mound, Monsanto Research Corporation, Miamisburg, Ohio.

Kendall M.G. and A. Stuart. 1969. *The Advanced Theory of Statistics, Volume 1: Distribution Theory* (Third Edition). Hafner Publishing Company, New York.

Killough G.G., M.J. Case, K.R. Meyer, R.E. Moore, J.F. Rogers, S.K. Rope, D.W. Schmidt, B. Shleien, J.E. Till, and P.G. Voillequé. 1993. *The Fernald Dosimetry Reconstruction Project, Task 4, Environmental Pathways — Models and Validation.* Draft report for comment, dated March 1993. Rep. CDC-3, Radiological Assessments Corporation, Neeses, South Carolina.

McMahon T.A. and P.J. Denison. 1979. "Empirical Atmospheric Deposition Parameters — A Survey." *Atmospheric Environment* **13**: 571–585.

Myrick T.E., B.A. Berven, and F.F. Haywood. 1983. "Determination of Concentrations of Selected Radionuclides in Surface Soil in the U.S." *Health Physics* **45**(3): 631–642.

Pendergrass W.R. 1987. *Meteorological Site Survey — Feed Materials Production Center, Fernald, Ohio.* Unpublished report, Atmospheric Turbulence and Diffusion Division, Air Resources Laboratory, National Oceanic and Atmospheric Administration, Oak Ridge, Tennessee.

Sehmel G.A. 1980. "Particle and Gas Dry Deposition: A Review." *Atmospheric Environment* **14**:983–1011.

Sehmel G.A. and W.H. Hodgson. 1980. "A Model for predicting Dry Deposition of Particles and Gases to Environmental Surfaces," in *Implications of Clean Air Ammendments of 1977 and of Energy Considerations for Air Pollution Control.* Symposium Series #196, vol. 76, American Institute of Chemical Engineers Symposium Series.

Shleien B., S.K. Rope, M.J. Case, G.G. Killough, K.R. Meyer, R.E. Moore, D.W. Schmidt, J.E. Till, and P.G. Voillequé. 1995. *The Fernald Dosimetry Reconstruction Project, Task 5. Review of Historic Data and Assessments for the FMPC.* Rep. CDC-4, Radiological Assessments Corporation, Neeses, South Carolina.

Turner D.B. 1964. "A Diffusion Model for an Urban Area." *Journal of Applied Meteorology* **3**: 83–91.

Voillequé P.G., K.R. Meyer, D.W. Schmidt, S.K. Rope, G.G. Killough, M. Case, R.E. Moore, B. Shleien, and J.E. Till. 1995. *The Fernald Dosimetry Reconstruction Project, Tasks 2 and 3, Radionuclide Source Terms And Uncertainties.* Rep. CDC-5, Radiological Assessments Corporation, Neeses, South Carolina.

Wilks S.S. 1962. *Mathematical Statistics.* John Wiley and Sons, Inc., New York.

WMCO (Westinghouse Materials Company of Ohio). 1987. *Feed Materials Production Center Environmental Monitoring Annual Report for 1986.* Rep. FMPC-2076, Special, UC-41, WMCO, Cincinnati, Ohio.

WMCO (Westinghouse Materials Company of Ohio). 1988. *Feed Materials Production Center Environmental Monitoring Annual Report for 1987.* Rep. FMPC-2135, Special, UC-41, WMCO, Cincinnati, Ohio.

WMCO (Westinghouse Materials Company of Ohio). 1989. *Feed Materials Production Center Environmental Monitoring Annual Report for 1988.* Rep. FMPC-2173, Special, UC-707, WMCO, Cincinnati, Ohio.

Table M-1S. Concentrations of ^{222}Rn Measured by Mound Monitoring Program at the FMPC from July 2, 1985 through October 3, 1986 (pCi L^{-1}) [a]

Monitoring period		Monitoring location									
From:	To:	1	2	3	4	5	6	7	8	9	10
07/02/85	07/18/85	4.7	1.7	2.8	2.7	6.4	1.6	1.9	0.80	1.1	0.69
07/18/85	08/02/85	4.0	1.3	5.8	2.2	3.2	1.3	1.5	0.71	0.73	0.37
08/02/85	08/08/85	1.4	1.1	8.0	6.3	2.5	0.74	1.6	0.76	0.93	0.78
08/08/85	08/15/85	5.0	1.7	8.1	3.9	5.2	1.2	0.87	0.88	0.97	0.28
08/15/85	08/29/85	4.2	1.6	5.7	4.2	3.8	1.2	1.2	0.57	1.2	0.79
08/29/85	09/05/85	8.0	1.7	5.1	3.9	8.2	1.4	1.4	0.67	0.56	0.61
09/05/85	09/12/85	5.4	1.9	2.1	4.0	7.0	1.4	1.9	1.1	1.3	0.69
09/12/85	09/19/85	3.8	2.1	25	5.5	5.9	2.4	3.9	2.7	2.1	1.1
09/19/85	10/01/85	6.4	2.7	9.9	11	8.3	2.8	3.2	1.7	2.1	2.3
10/01/85	10/09/85	8.4	2.0	14	4.3	6.5	3.4	4.2	2.5	1.4	1.0
10/09/85	10/23/85	3.7	2.9	9.3	5.6	5.7	1.2	1.9	1.4	1.6	1.3
10/23/85	11/06/85	1.6	2.0	19	1.7	1.3	0.88	0.55	0.75	0.38	
11/06/85	11/13/85	2.9	2.0	7.1	6.1	5.5	1.3	0.85	0.69	0.57	1.2
11/13/85	11/27/85	4.1	1.8	14	4.5	5.2	1.3	0.80	0.94	0.44	0.38
11/27/85	12/04/85	1.5	2.1	9.5	3.1	0.99	0.53	0.19	0.28	0.12	0.32
12/04/85	12/11/85	7.3	8.9	14	14	11	3.5	1.8	2.8	1.1	0.69
12/11/85	12/19/85	3.3	2.1	3.6	3.8	3.3	0.94	0.56	0.64	0.69	0.85
12/19/85	01/02/86	7.3	1.4	2.8	3.1	8.5	2.5	0.88	1.2	0.63	0.70
01/02/86	01/08/86	3.1	1.7	6.1	6.0	2.9	0.86	0.74	0.96	0.61	0.96
01/08/86	01/15/86	7.9	2.5	3.6	2.0	5.8	2.9	1.5	1.8	0.48	0.77
01/15/86	01/22/86	4.1	1.5	5.2	11	5.2	0.95	1.1	1.4	0.68	1.0
01/22/86	01/29/86	4.8	1.1	7	3.2	1.6	1.2	0.85	0.99	0.15	0.31
01/29/86	02/05/86	2.5	1.6	12	4.3	3.4	1.3	0.76	0.98	0.51	1.1
02/05/86	02/12/86	4.8	1.6	2.1	0.99	1.1	1.2	0.43	0.62	0.45	0.25
02/12/86	02/19/86	8.4	6.9	22	12	6.2	1.1	1.8	4.2	0.72	0.72
02/19/86	02/27/86	8.8	3.0	7.1	4.9	4.0	1.7	0.48	0.96	0.51	0.30
02/27/86	03/05/86	7.0	2.3	1.2	4.0	2.7	2.9	1.0	1.1	0.43	0.32
03/05/86	03/12/86	4.6	1.7	4.7	6.7	5.3	0.94	0.24	0.40	0.49	0.67
03/12/86	03/19/86	5.1	3.3	10.	4.4	4.8	2.4	0.56	0.93	0.56	0.48
03/19/86	03/26/86	7.3	2.7	3.4	5.2	6.1	2.2	0.47	1.1	0.69	0.67
03/26/86	04/02/86	7.5	2.7	4.1	3.3	15	3.5	1.5	2.6	0.97	1.3
04/02/86	04/09/86	9.7	2.2	12	3.8	9.2	1.8		1.5	1.5	1.2
04/09/86	04/16/86	8.6	1.2	6.8	3.0	2.7	2.6	1.9	1.5	0.86	0.74
04/16/86	04/29/86	12	4.4	6.3	5.1	5.1	2.0	1.9	2.4	1.2	1.2
04/29/86	05/07/86	7.6	5.3	2.4	5.2	7.4	2.7	1.6	2.5	0.54	1.2
05/07/86	05/14/86	7.0	1.9	18	2.2	4.6	1.6	0.97	1.2	0.97	0.67
05/14/86	05/21/86	4.5	0.61	1.5	5.5	6.7	1.4	0.54	1.1	0.83	0.48
05/21/86	05/28/86	7.2	1.8	9.9	5.4	5.2	2.3	1.5	1.8	1.1	1.1
05/28/86	06/04/86	9.1		11		7.4	2.9	1.6	2.6	1.2	0.91
06/04/86	06/11/86	7.4	0.97	5.8	5.5	9.5	1.1		1.1	0.76	0.60
06/11/86	06/18/86		1.9	3.1	4.3	13	2.0		1.4	1.6	0.79
06/18/86	06/25/86	12	1.7	9.3	3.8	7.7	2.9		1.6	1.4	1.1
06/25/86	07/02/86	11	1.6	7.1	5.1	6.8	2.5		1.7	1.6	0.76
07/02/86	07/08/86	8.0	2.7	1.4	5.4	10.	2.0		1.6	1.1	1.1
07/08/86	07/16/86	7.5	1.1	3.4	2.3	7.4	1.3		0.96	0.91	0.55
07/16/86	07/23/86	15	1.1	3.3	2.9	6.2	3.1		1.4	1.3	0.88
07/23/86	07/30/86	8.2	2.0	7.8	2.9	5.1	2.2		2.1	1.2	1.3
07/30/86	08/06/86	10.	1.5	6.2	3.0	3.8	2.6		2.2	2.0	1.4
08/06/86	08/13/86	8.4	1.9	3.4	2.8	5.2	2.9		2.2	1.1	1.1
08/13/86	08/20/86	5.5	1.3	4.9	3.0	5.5	1.7		1.8	1.5	0.93
08/20/86	08/27/86	4.2	1.9	7.3	2.6	4.7	1.4		1.4	1.6	1.1
08/27/86	09/03/86	2.3	2.5	11	3.0	2.2	1.8		2.4	2.0	1.2
09/03/86	09/10/86	7.5	1.8	5.7	4.4	5.5	2.8		1.8	1.7	1.2
09/10/86	09/17/86	4.0	0.77	5.6	3.7	5.2	0.67		0.74	0.36	1.1
09/17/86	09/24/86	4.2		6.3	2.7	6.1	1.7		1.1	1.0	0.78
09/24/86	10/03/86	4.8	0.85	3.2	4.3	9.5	1.3		1.2	1.2	0.85

[a] Ref: Jenkins 1986. Single gaps in data indicate that no measurement was reported for the period.

Table M-1S. Concentrations of ^{222}Rn Measured by Mound Monitoring Program at the FMPC from July 2, 1985 through October 3, 1986 (pCi L^{-1}) [a] (continued)

Monitoring period		Monitoring location									
From:	To:	11	12	13	14	15	17	18	19	20	21
07/02/85	07/18/85	0.89	0.95	0.41	0.31	0.42	0.47	0.44			
07/18/85	08/02/85	0.72	0.95	0.45		0.65	0.51	0.68			
08/02/85	08/08/85	1.7	1.5	0.36	0.36	0.80	0.50	0.67			
08/08/85	08/15/85	0.59	0.73	0.58	0.35	0.67	0.58	0.47			
08/15/85	08/29/85	1.1	0.99	0.33	0.39	0.56	0.52	0.65			
08/29/85	09/05/85	0.93	1.5	0.39	0.56	0.73	0.59				
09/05/85	09/12/85	1.2	1.3	0.61	0.3	0.52	0.53	0.61			
09/12/85	09/19/85	2.1	2.5	1.1	1.1	2.1	1.0	2.2			
09/19/85	10/01/85	2.9	3.4	1.1	0.99	1.9	1.0	1.3			
10/01/85	10/09/85	2.6	2.7	1.2	1.1	1.5	1.1	1.4	1.1	1.1	2.1
10/09/85	10/23/85	2.2	2.1	0.84	0.43	0.82	0.58	0.83	0.96	0.86	1.6
10/23/85	11/06/85	0.86	1.1	0.40	0.28	0.82	0.35	0.37	0.50	0.30	0.56
11/06/85	11/13/85	0.94	1.7	0.47	0.2	0.43	0.19	0.30	0.32	0.19	0.41
11/13/85	11/27/85	0.49	0.81	0.57	0.27	0.58	0.24	0.33	0.54	0.32	0.55
11/27/85	12/04/85	0.31		0.30	0.17	0.25	0.57	0.16	0.18	0.19	0.14
12/04/85	12/11/85	1.3	2.2	2.4	0.69	0.67	0.98	0.59	0.85	0.63	1.2
12/11/85	12/19/85	0.84	0.87	0.51	0.18	0.21	0.22	0.23	0.35	0.15	0.29
12/19/85	01/02/86	0.73	0.70	0.48	0.29	0.34	0.34	0.29	0.42	0.24	0.29
01/02/86	01/08/86	0.85	1.6	0.66	0.23	0.28	0.25	0.39	0.44	0.34	0.25
01/08/86	01/15/86	0.70	1.4	0.69	0.42	0.39	0.44	0.39	0.63	0.32	0.60
01/15/86	01/22/86	1.2	2.2	0.38	0.38	0.44	0.36	0.27	0.72	0.44	0.40
01/22/86	01/29/86	0.44	1.1	0.27	0.26	0.43	0.25	0.32	0.41	0.25	0.41
01/29/86	02/05/86	0.74	1.2	0.51	0.34	0.65	0.30	0.31	0.41	0.38	0.26
02/05/86	02/12/86	0.24	0.36	0.26	0.11	0.15	0.15	0.18	0.26	0.17	0.17
02/12/86	02/19/86	2.6	4.7	0.83	0.29	0.54	0.38	0.37	0.67	0.43	0.88
02/19/86	02/27/86	0.89	1.2	0.38	0.18	0.22	0.21	0.24	0.35	0.23	0.32
02/27/86	03/05/86	0.66	1.0	0.27	0.30	0.20	0.27	0.15	0.27	0.29	
03/05/86	03/12/86	0.80	1.3	0.14	0.10	0.12	0.19	0.23	0.40	0.31	0.20
03/12/86	03/19/86	0.63	1.9	0.33	0.17	0.45	0.29	0.19	0.43	0.47	0.63
03/19/86	03/26/86	1.0	1.2	0.35	0.13	0.24	0.22	0.31	0.47	0.28	0.53
03/26/86	04/02/86	1.4	2.5	0.81	0.42	0.74	0.51	0.56	0.72	0.69	1.3
04/02/86	04/09/86	1.6	2.6	0.69	0.23	0.56	0.47	0.50	0.81	0.67	1.2
04/09/86	04/16/86	1.2	1.8	0.48	0.39	0.53	0.48	0.39	0.52	0.49	0.90
04/16/86	04/29/86	1.8	1.8	0.88	0.24	0.47	0.55	0.66	0.77	0.78	1.1
04/29/86	05/07/86	1.7	2.1	1.0	0.48	0.65	0.73		0.61	0.53	1.2
05/07/86	05/14/86	1.0	1.4	0.46	0.16	0.51	0.37	0.47	0.49	0.52	0.75
05/14/86	05/21/86	1.3	0.49	0.23	0.23	0.23	0.21	0.46	0.25	0.25	0.50
05/21/86	05/28/86	2.4	2.3	0.72	0.30	0.54	0.48	0.46	0.58	0.54	0.84
05/28/86	06/04/86	3.4	1.9	0.68	0.44	0.65	0.59	0.91	0.54	0.62	1.1
06/04/86	06/11/86	2.1	2.5	0.30	0.13	0.30	0.26	0.38	0.50	0.35	0.64
06/11/86	06/18/86	2.7	1.6	0.83	0.40	0.49	0.55	0.89	0.65	0.63	1.0
06/18/86	06/25/86	2.7	1.9	0.73	0.31	0.52	0.57	0.88	0.86	0.83	1.1
06/25/86	07/02/86	1.4	2.2	0.69	0.47	0.70	0.64	1.1	0.75	0.68	1.1
07/02/86	07/08/86	1.4	1.0	0.65	0.23	0.51	0.74	1.0	0.75	0.69	1.4
07/08/86	07/16/86	0.68	1.2	0.34	0.17	0.51	0.32	0.47	0.41	0.41	0.71
07/16/86	07/23/86	1.2	1.4	0.35		0.25	0.40	0.44	0.17	0.65	0.66
07/23/86	07/30/86	1.4	2.0	0.78	0.41	1.1	0.84	0.99	0.86	0.83	1.7
07/30/86	08/06/86	3.1	2.1	0.63	0.32	1.0	1.0	1.4	1.2	1.3	2.1
08/06/86	08/13/86	2.2	2.8	0.66	0.41	1.1	0.77	0.64	0.73	0.70	1.5
08/13/86	08/20/86	1.9	2.3	0.77	0.30	0.73	0.85	0.76	0.80	1.1	1.4
08/20/86	08/27/86	2.1	2.0	0.95	0.68	1.3	0.82	0.86	1.2	0.69	1.5
08/27/86	09/03/86	2.6	2.3	1.5	0.51	0.79	0.92	1.3	1.1	1.2	1.5
09/03/86	09/10/86	3.6	2.7	1.2	0.70	1.5	0.74	1.4	1.2	1.2	1.8
09/10/86	09/17/86	1.5	1.6	0.36	0.29	0.61	0.46	0.95	0.53	0.74	0.91
09/17/86	09/24/86	2.4	2.7	0.56	0.53	0.54	0.62	0.75	0.80	0.43	1.3
09/24/86	10/03/86	1.2	0.53	0.82	0.16	0.38	0.37	0.65	0.62	0.43	0.82

[a] Ref: Jenkins 1986. Single gaps in data indicate that no measurement was reported for the period.

APPENDIX N

DETAILED VALIDATION RESULTS

INTRODUCTION

Validation data refers to data that can be used to check predictions of the source term and environmental transport calculations. In Task 5 of the project, we compiled many environmental monitoring data sets that could potentially be used for validation exercises (Shleien et al. 1995). In this report we present and analyze the data sets that are most useful for validating or corroborating our predictions of the atmospheric release and transport of radon and uranium particulates from the Feed Materials Production Center (FMPC). Introductory material on validation concepts is presented in Volume I, as is a summary of results of the validation exercises. Details of the data and analyses are presented in this appendix. One important criterion for data to be used for validation purposes is that it should be independent of data used to develop source terms and environmental transport models. The data evaluated here meet this criterion. Relative to the importance of radon releases to doses to people around the site, validation data for radon releases appear lacking in quantity and quality. However, we have tried to evaluate all available radon monitoring; the sparse data reflect the limited radon monitoring at the FMPC in the earlier years of operation (through the 1970s).

RADON VALIDATION DATA

Much of the data on measured concentrations of radon in air around the FMPC has been used in Appendix M for the dispersion model calibration. There are some additional data which can be used to provide validation, or perhaps at least qualitative corroboration, of radon release and transport calculations. This section evaluates data of four types that we believe are useful in evaluating the radon predictions:

- Radon flux measured on the K-65 silo domes. These data are used to develop a lower bound estimate of the daytime radon release rate from the silos that is applicable to the 1980–1987 period. The lower bound can be compared with our current estimates of release rates.
- Hourly measurements of radon in air very close to the silos. These data show the diurnal patterns of radon concentrations and show a significant change from the pattern of 1986 and 1987 to the pattern of 1991. The pattern for 1986 and 1987 qualitatively corroborates our predicted higher releases during daylight hours for 1980–1987.
- Time-integrated measurements of radon in air before and after the silo dome penetrations were sealed (which occurred June 25, 1979). A limited number of measurements were made, essentially all at boundary station BS-6 in 1979–1980. These data show a large decrease in radon concentration after the silos were sealed.

This provides some corroboration of the large decrease in our estimated release rates between the periods 1959–June 1979 and July 1979–1987.

- Grab samples of radon daughters in air before the sealing of silo penetrations. These data provide qualitative corroboration for parameters used to estimate releases of radon daughters from the K-65 silos.

Measurements of Radon Flux on K-65 Silo Domes

In 1984, personnel from the Mound facility (a U.S. Department of Energy facility in Miamisburg, Ohio) made measurements of the radon flux density emitted from the domes of the K-65 silos. Because of limitations of the data set (mentioned later), we felt initially that the data could not be used directly to estimate the radon release rate from the silos. However, reevaluation of the data indicates that the results are useful for validation comparisons with our estimated radon release rates. The results can be used to estimate a lower bound on total radon emissions from the silo domes.

For emissions of radon from an area source (such as the domes of the silos), differences exist in terminology used to describe the release rates. Emission measurements are commonly reported in units of activity per unit area and per unit time (such as pCi m^{-2} s^{-1}). Such quantities are accurately referred to as "flux density" or "fluence rate," but they are also commonly referred to simply as "flux." As the Mound report of the measurements (Hagee et al. 1985) uses the common term "flux," we also use the common term in this discussion.

The radon flux measurements performed by Mound on the silo domes are described in Hagee et al. (1985). Mound used an accumulator method, which involves collecting radon in a closed container placed on a surface, followed by measuring the radon accumulated in the container. Charcoal canisters (using activated charcoal to adsorb the radon), approximately 4 in. diameter by 1½ in. tall, were used. A pliable caulking material was used between the silo dome surface and the charcoal canister to ensure a tight seal between the surfaces. The canister design also incorporated a feature to minimize transfer of contamination (radon daughters) from the dome surface to the charcoal unit of the canister.

The radon flux measurements were made on October 18 and 24, 1984. Because of the very high radon emission rate from the domes, Mound made preliminary radon flux measurements to investigate possible saturation of the charcoal. Based on these preliminary results, it was decided that appropriate exposure times for the canisters were about 2 hours for measurements on intact areas of the silo domes, and less than 1 hour for cracked areas of the domes, which had higher radon emission rates. The Mound report does not indicate the time of day of the flux measurements. It seems logical that since nothing was noted to the contrary, the measurements were probably made during normal working hours. We thus assume that the measurements were made during daylight hours.

Twenty-four locations were selected on each of the two K-65 silo domes. The approximate locations are shown in Figure N-1, based on figures in Hagee et al. (1985). On each silo, 12 locations were placed along north-south and east-west lines. The report states, "Essentially, all of these canisters were on intact concrete showing no serious cracks or fissures" (Hagee et al. 1985). The report further describes the other locations for each silo, "The remaining twelve locations were chosen in areas which had obvious cracks or fissures." From these

descriptions, we believe that all of the measurement locations are biased, half toward intact concrete, which presumably would exhibit lower radon emission rates (on the average), and half toward obvious cracks, which presumably would exhibit higher emission rates. There is no information about the fractions of the silo domes that are represented by "intact concrete" and by cracks and fissures. Because of this and because none of the sampling locations can be considered random or unbiased, we think it is not feasible to use the measurements to directly estimate total radon emissions from the silo domes. Also, because nothing is known about the area that might be represented by cracked concrete, we think it is not feasible to use the measurements on cracked concrete to estimate a *reasonable* upper bound on releases.

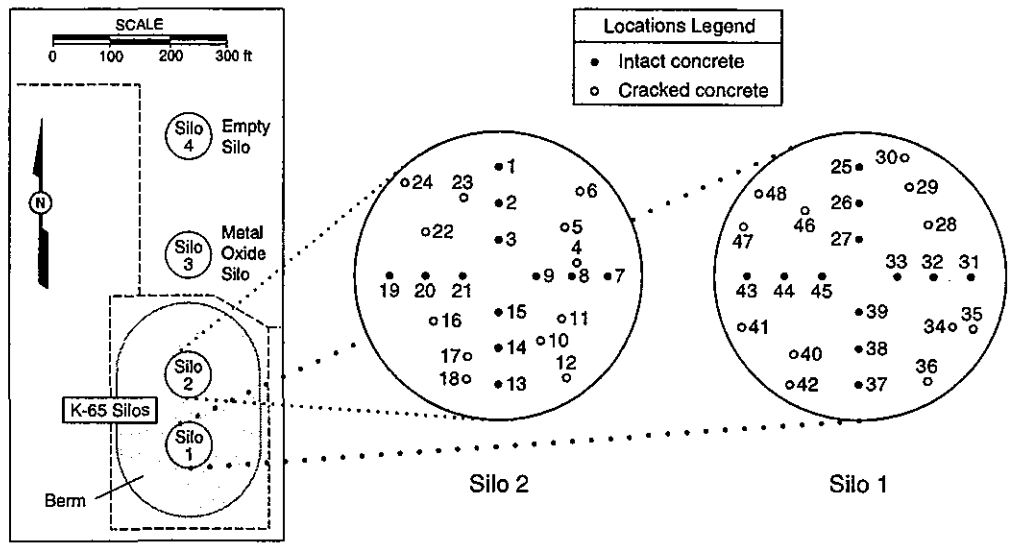

Figure N-1. Locations of the Mound radon flux measurements on the K-65 silo domes in October 1984 (Hagee et al. 1985). Cracked concrete contains obvious cracks, and intact concrete is without significant cracks.

Because of the air exchange mechanism for releases from the silos, based on thermal expansion of silo head space gases (Voillequé et al. 1995), the radon flux from the silo domes is expected to be much greater on areas of concrete having cracks. We thus consider the flux measurements on what was thought to be intact concrete to be biased toward lower emission rates than the average for the silo domes. So, we use the flux measurements made on intact concrete to calculate a lower bound on total radon releases through the silo domes. The Mound report (Hagee et al. 1985) also noted the "... existence of severe radon release around most of the metal protrusions on top of the tanks ..." This provides more evidence that using the flux measurements from only intact concrete areas will definitely result in a lower-bound estimate of radon releases from the silos.

Results of the Mound radon flux measurements on the K-65 silo domes are shown in Table N-1 (Hagee et al. 1985). For 25% of the measurements, a duplicate result was also given, and these results are also shown. The exact nature of the duplicates was not provided in Hagee et al. (1985).

Table N-1. Radon Flux Measurements (pCi m^{-2} s^{-1}) on the K-65 Silo Domes, Performed by Mound in October 1984

		Flux measurements					Flux measurements		
Location	Condition[a]	First	Duplicate	Mean	Location	Condition[a]	First	Duplicate	Mean
1	intact	2.2×10^3		2.2×10^3	25	intact	1.8×10^2	1.6×10^3	8.9×10^2
2	intact	1.3×10^2		1.3×10^2	26	intact	1.3×10^5		1.3×10^5
3	intact	5.8×10^1	1.3×10^1	3.6×10^1	27	intact	3.1×10^4		3.1×10^4
4	cracks	7.5×10^2		7.5×10^2	28	cracks	2.4×10^1	1.4×10^2	8.2×10^1
5	cracks	6.2×10^2		6.2×10^2	29	cracks	1.1×10^4		1.1×10^4
6	cracks	2.8×10^2		2.8×10^2	30	cracks	7.1×10^1		7.1×10^1
7	intact	1.1×10^2		1.1×10^2	31	intact	6.2×10^1	1.6×10^2	1.1×10^2
8	intact	9.8×10^1		9.8×10^1	32	intact	9.3×10^1		9.3×10^1
9	intact	6.4×10^1	3.4×10^2	2.0×10^2	33	intact	2.4×10^3		2.4×10^3
10	cracks	3.9×10^3		3.9×10^3	34	cracks	9.0×10^5		9.0×10^5
11	cracks	3.7×10^4		3.7×10^4	35	cracks	2.1×10^5		2.1×10^5
12	cracks	1.9×10^7		1.9×10^7	36	cracks	6.9×10^6	1.4×10^7	1.0×10^7
13	intact	4.3×10^3		4.3×10^3	37	intact	3.3×10^2		3.3×10^2
14	intact	8.4×10^2		8.4×10^2	38	intact	5.3×10^2		5.3×10^2
15	intact	6.3×10^1	1.7×10^3	8.8×10^2	39	intact	1.3×10^2		1.3×10^2
16	cracks	7.7×10^1	1.1×10^3	5.9×10^2	40	cracks	1.7×10^4	8.8×10^4	5.3×10^4
17	cracks	3.1×10^4		3.1×10^4	41	cracks	3.2×10^3		3.2×10^3
18	cracks	8.3×10^6	2.5×10^7	1.7×10^7	42	cracks	2.2×10^2		2.2×10^2
19	intact	2.1×10^2		2.1×10^2	43	intact	2.9×10^1		2.9×10^1
20	intact	7.7×10^1		7.7×10^1	44	intact	9.6×10^1		9.6×10^1
21	intact	8.2×10^1		8.2×10^1	45	intact	3.3×10^1	1.0×10^2	6.7×10^1
22	cracks	5.0×10^2		5.0×10^2	46	cracks	6.4×10^3		6.4×10^3
23	cracks	6.6×10^2		6.6×10^2	47	cracks	2.3×10^4		2.3×10^4
24	cracks	1.6×10^7	2.8×10^7	2.2×10^7	48	cracks	1.0×10^2		1.0×10^2

[a] "Intact" indicates concrete without serious cracks or fissures; "cracks" indicates concrete with obvious cracks or fissures.

To estimate a lower bound, we assume that the intact concrete is representative of the entire surfaces of the silo domes. The lower-bound estimate of radon releases through the silo domes is then calculated as the average radon flux measured for intact concrete, multiplied by the total surface area of the two silo domes. We first briefly consider the distribution of flux measurements. Figure N-2 shows a log-probability plot of the individual flux measurements on intact concrete. The distribution appears reasonably similar to a lognormal distribution, and we note in particular that the highest flux values appear consistent with the overall distribution. For the intact concrete areas, the mean measured radon flux (from Table N-1) is 7290 pCi m^{-2} s^{-1}, and the standard deviation is 26,900 pCi m^{-2} s^{-1}. With 24 measurement locations (n = 24), the standard error of the mean is thus 5490 pCi m^{-2} s^{-1}.

In our Task 2/3 report, the surface area of the silo domes was determined to be 5300 ft^2 per silo. For the two silos, this is equivalent to a total surface area of 985 m^2. Thus, the lower-bound estimate of total radon releases from the silo domes is (7290 pCi m^{-2} s^{-1}) × (985 m^2) = 7×10^6 pCi s^{-1}. From the standard error of the mean flux, the standard deviation of this release rate is 5.4×10^6 pCi s^{-1}.

This lower-bound estimate can be compared with our current estimates of radon releases from the silos, as calculated in the Task 2/3 report (Voillequé et al. 1995). For the period 1980–1987, our estimates are annual radon releases of 130 Ci through diffusion and 810 Ci through air exchange. (These are best estimate values; the uncertainties are discussed in the

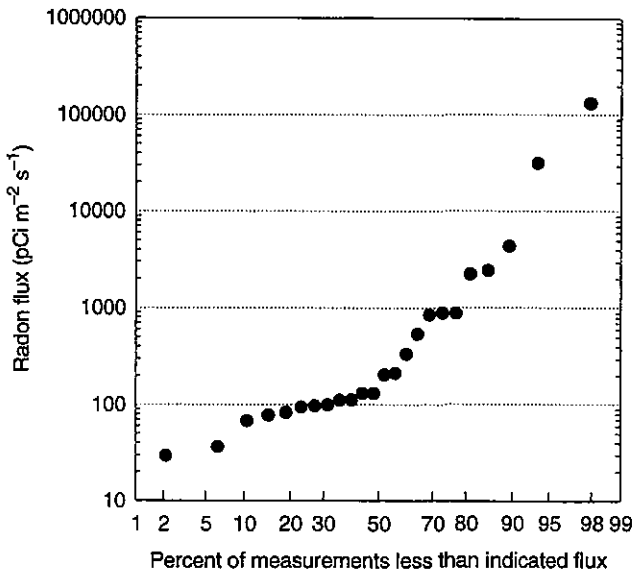

Figure N-2. Distribution of radon flux measured on intact concrete of the K-65 silo domes. Each point represents the average flux for a single location (Table N-1).

Task 2/3 report.) The air exchange releases are believed to occur during daylight hours only. To convert the annual release through air exchange to a *rate*, we multiply by two (assuming one-half of a day is daylight). With units conversions, our estimates are release rates of 4.12×10^6 pCi s^{-1} through diffusion and 5.13×10^7 pCi s^{-1} through air exchange for a total of 5.54×10^7 pCi s^{-1} during daylight hours. In Figure N-3, the 90% probability range of the lower-bound release estimate, based on the mean and standard error of the mean of the flux measurements, is compared to the ranges of predicted release rates from diffusion and air exchange release.

The lower-bound estimate of radon releases, based on the flux measurements, is less than our current estimate of total radon releases from the silos but ranges to greater than our current estimate of diffusion releases from the silos. Two conclusions can be made from this comparison. First, the general magnitude of the lower-bound estimate from the Mound flux monitoring in 1984 is consistent with our current estimate of total radon releases. Second, the magnitude of the lower-bound estimate is also consistent with the existence of air exchange releases (or some release in addition to diffusion releases). We acknowledge that the radon flux measurements represent a limited data set, but the general consistency in results is reassuring.

Hourly Measurements of Radon in Air Near K-65 Silos

Hourly measurements of radon in air can be useful in examining the diurnal variations in radon concentrations. Diurnal changes in meteorological conditions (generally winds are more calm at night) can produce diurnal patterns in radon concentrations. In the presence of a constant radon source term, these meteorological changes produce higher nighttime radon concentrations (less dispersion) and lower daytime concentrations (more dispersion).

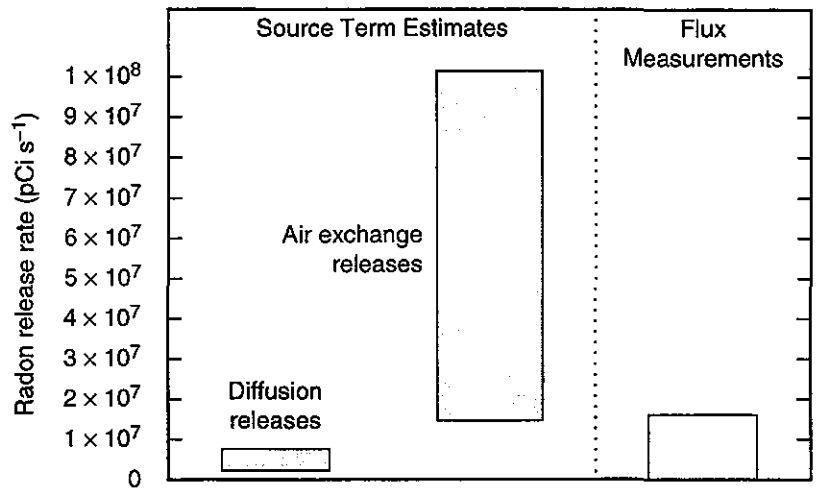

Figure N-3. Comparison of predicted radon release rates from the K-65 silos for daylight hours during 1980–1987 with a lower-bound estimate of release rate based on flux measurements made by Mound in 1984. Each box represents the 90% probability range (5th to 95th percentiles for predictions, and ± 1.645 standard errors of the mean for the flux measurements).

However, for our estimated radon releases from the K-65 silos for 1980–1987, we have predicted release rates that are significantly higher during daylight hours. Thus, for radon concentrations near the K-65 silos for this period, we would expect a nonstandard diurnal pattern of higher concentrations in daylight hours when the release rates are higher. The hourly concentration measurements should be useful to corroborate or refute such a pattern. Results of hourly radon measurements were discussed briefly in the Task 2/3 report (Voillequé et al. 1995); the information here is expanded from that discussion.

The hourly measurements we discuss here are often referred to in FMPC reports as continuous or "real-time" measurements. They are measurements of concentrations of radon in air that diffuses into the measuring instrument, with the results integrated over 1-hour periods. The instruments used have not been specified in all of the reports, but from conversations with staff at the FMPC it appears that Eberline RGMs (radon gas monitors) and Pylon radon gas monitoring instruments have been used.

Document searches, which included discussions with FMPC staff involved in the radon monitoring programs at the site, resulted in only a few sources that provide hourly radon measurement data for the 1980–1987 period. In April 1986, there was an incident that released radon from the K-65 silos at rates higher than the routine rate for the period. The Incident Investigation Report for this event compiled hourly radon measurements at one location near the silos for April 23–25, 1986 (DOE 1986). The exact location of the monitoring was not provided in the report, but it was described as being about 35 ft from the point of the radon discharge from the silos (during this event, the radon was vented through pipes that were connected to the silo domes and apparently extended down the sides of the berm around the silos). From photographs in the report, it appears that an air monitoring station was located to the east of the K-65 silos, somewhat outside of the fence surrounding the silos (see

Figure N-4). This may have been the location of the hourly radon monitoring. Results are shown in Table N-2. Most of the results of this monitoring were presented only as plots (DOE 1986), so the plots were digitized to obtain many of the values shown in the table.

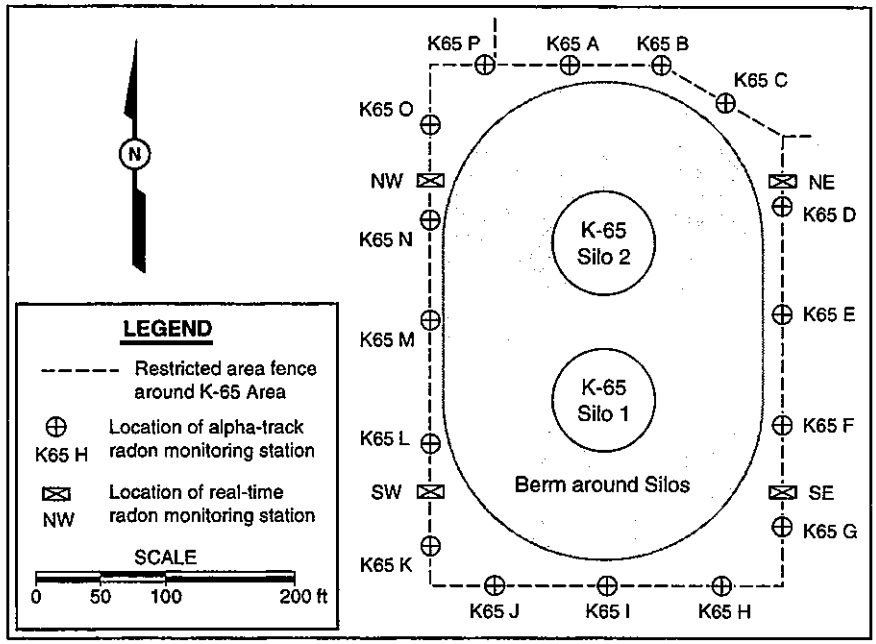

Figure N-4. Locations of FMPC hourly radon monitoring (real-time monitors) on the fenceline of the K-65 area. The locations of real-time monitors shown are for the 1987 and 1991 data, although the locations are approximate and may have changed (especially the northeast and southeast stations). For 1986, the precise location is not known, but probably was on the east side, outside the fenceline (see text).

In November 1987, a Radon Treatment System (RTS) was installed at the K-65 silos to remove radon daughters from air in the silo head spaces (Grumski and Shanks 1988). This system was installed in advance of the work in December 1987 to apply a layer of expanded foam to the domes of the silos. The initial work on the silo domes included the replacement of some of the flanges on the silo domes (to allow connection of pipes to carry air to the RTS). During the flange changeout operations and early operations of the RTS, hourly radon monitoring was performed. The flanges on Silo 1 were replaced on November 4, and radon monitoring results were reported for November 3–5 (Grumski 1987). Three locations were monitored: on the northeast, northwest, and southwest sides of the K-65 area fenceline (Figure N-4). Results are shown in Table N-3. The results of this monitoring were presented only as plots (Grumski 1987), so the plots were digitized to obtain the values shown in the table.

Table N-2. Hourly Radon Concentrations (pCi L^{-1}) Measured for Three Days at One Location [a]

Time	April 23, 1986	April 24, 1986	April 25, 1986
01:00		4.0 [b]	4.0 [b]
02:00		4.0 [b]	4.0 [b]
03:00		4.0 [b]	4.0 [b]
04:00		3.2	3.2
05:00		3.6	3.6
06:00		4.5	4.5
07:00		4	4.0
08:00		2.8	2.8
09:00		11.10 [c]	5.01 [c]
10:00	7.3	10.10 [c]	26.10 [c]
11:00	26	7.90 [c]	110.00 [c]
12:00	31	11.90 [c]	309.00 [c]
13:00	17	5.52 [c]	471.00 [c]
14:00	16	3.33 [c]	694.00 [c]
15:00	36	5.31 [c]	333.00 [c]
16:00	11	3.33 [c]	156.00 [c]
17:00	4.9	1.90 [c]	87.80 [c]
18:00	2.0	1.06 [c]	37.00 [c]
19:00	2.0	1.2	14
20:00	2.0	1.2	3.1
21:00	2.4	1.2	4.5
22:00	2.8	2.8	4.0
23:00	4.0 [b]	4.0 [b]	4.0 [b]
00:00	4.0 [b]	4.0 [b]	4.0 [b]

[a] Location was probably on the east side of the K-65 area (see text). Unless otherwise noted, data were digitized from figures in DOE (1986). Digitizing resolution was the equivalent of about 0.4 pCi L^{-1}. Blanks in table indicate that no data were available.

[b] In digitizing these data points, it was impossible to differentiate the symbols and lines representing different days. In these cases, all uncertain days were assigned the same value.

[c] Data obtained from table (not digitized) in DOE (1986).

The flanges on Silo 2 were replaced on November 12, 1987, and hourly radon monitoring results were reported for November 11–13 (Grumski and Shanks 1988). Four locations were monitored: on the northeast, northwest, southwest, and southeast sides of the K-65 area fenceline (Figure N-4). Results are shown in Table N-4. The results of this monitoring were presented only as plots (Grumski and Shanks 1988), so the plots were digitized to obtain the values shown in the table.

Additional hourly monitoring data are available for times later in November and in early December 1987 (Grumski and Shanks 1988). However, these later measurements were made while the RTS was operating, and thus may not be representative of the typical concentration patterns for the period 1980–1987, before installation of the foam layer. We believe that the 9 days of data compiled here provide a reasonable picture of the diurnal pattern in radon concentrations near the silos, so the later results are not examined here.

Table N-3. Hourly Radon Concentrations (pCi L^{-1}) Measured for Three Days at Three Locations [a]

Time	November 3, 1987			November 4, 1987			November 5, 1987		
	NE	NW	SW	NE	NW	SW	NE	NW	SW
01:00	2.7	2.7	3.6	8.2	3.2	2.3	5.0	3.2	0.9
02:00	4.1	2.7	4.1	11	3.6	3.2	5.4	1.4	0.9
03:00	4.6	2.7	4.6	9.1	5.0	3.6	4.5	3.6	0.9
04:00	5.0	2.7	5.0	7.3	5.0	3.6	7.3	3.2	0.9
05:00	7.7	2.7	4.6	8.2	4.1	3.6	7.3	3.2	0.4
06:00	7.3	3.2	4.6	12	4.1	3.6	5.9	3.2	0.9
07:00	7.3	3.6	4.6	9.1	4.5	4.1	5.5	3.2	0.9
08:00	5.5	3.6	5.5	7.7	5.5	4.5	5.0	3.6	1.8
09:00	3.6	3.6	3.6	4.5	4.5	2.7	3.6	2.7	
10:00	3.2	5.0	2.7	5.9	2.7	1.4	11	1.8	
11:00	1.4	9.1	1.4	17	1.4	0.9	14	0.9	
12:00	17	6.4	0.9	19	0.9	0.4	12	0.4	
13:00	17	2.7	0.5	47	0.4	0.4	33	0.4	
14:00	25	0.9	0.5	52	0.4	0.4	51	0.4	
15:00	18	0.9	0.9	58	0.4	0.4	54	0.4	
16:00	13	1.4	0.9	28	0.4	0.4	45	0.4	
17:00	113	223	0.5	17	0.9	0.9	34	0.4	
18:00	45	108	0.5	4.5	1.4	1.4	12	0.4	
19:00	20	36	0.9	3.2	0.9	1.8	5.0	0.9	
20:00	10	13	1.8	4.5	1.8	1.8	3.2	0.4	
21:00	7.7	5.5	2.3	5.0	2.3	2.3	3.2	1.4	
22:00	9.1	3.2	3.2	5.0	2.7	0.9	2.3	1.4	
23:00	9.1	3.2	3.2	5.0	3.2	0.9	0.9	0.9	
00:00	9.5	3.2	3.2	4.5	3.2	0.9	0.4	0.4	

[a] Locations are shown in Figure N-4. Data were digitized from figures in Grumski (1987). Digitizing resolution was the equivalent of about 0.45 pCi L^{-1}. Blanks in table indicate that no data were available.

Hourly radon monitoring near the K-65 silos apparently became routine in 1988 (Byrne 1992a), and we have obtained detailed, tabulated results for October 1991, in computer spreadsheet files (Byrne 1992b). Again, four locations were monitored: on the northeast, northwest, southwest, and southeast sides of the K-65 area fenceline (Figure N-4). Results are shown in Table N-5.

Figure N-5 plots the hourly measurements from 1986 and early November 1987. The measurements show prominent peak radon concentrations, generally from 15 to 225 pCi L^{-1}, that occurred during daylight and early evening hours, primarily from 10 am to 8 pm. We note that the extremely high concentration measured on April 25, 1986, was during the "incident" (unplanned release) in which radon releases were higher than the routine releases. At other times of the day, concentrations were less than 10 pCi L^{-1}. Monitoring stations to the east of the silos tended to exhibit the highest radon concentrations, as expected based on predominant wind directions at the FMPC (from the southwest). At the southwest location, concentrations were often low during the day, and there were no high peak concentrations. This could be due to the generally upwind location.

Figure N-6 plots the hourly measurements from the first 9 days of October 1991. The measurements again show prominent peak radon concentrations, from 13 to 99 pCi L^{-1} for these 9 days. However, these peak concentrations generally occurred during late night to

Table N-4. Hourly Radon Concentrations (pCi L^{-1}) Measured for Three Days at Four Locations [a,b]

	November 11, 1987				November 12, 1987				November 13, 1987			
Time	NE	NW	SW	SE	NE	NW	SW	SE	NE	NW	SW	SE
01:00					3.1	3.1	3.1	3.1	1.5	1.5	1.5	1.5
02:00					3.6	3.6	3.6	3.6	1.5	1.5	1.5	1.5
03:00					5.1	4.6	4.6	4.6	1.0	1.0	1.0	1.0
04:00					4.6	4.6	4.6	4.6	1.5	1.5	1.5	1.5
05:00					4.1	4.1	4.1	8.7	1.5	1.5	1.5	1.5
06:00					4.1	4.1	4.1	6.7	1.0	1.0	1.0	1.0
07:00					5.1	3.6	3.6	5.1	1.5	1.5	1.5	1.5
08:00					4.1	4.1	4.1	4.1	2.0	1.5	1.5	1.5
09:00					3.6	3.6	3.6	3.6	3.0	1.0	1.0	1.0
10:00					7.7	1.5	1.5	1.5	7.9	0.5	0.5	0.5
11:00					12	0.5	0.5	0.5	15	0.5	0.5	0.5
12:00	0.5	0.5	0.5		13	1.0	1.0	1.0	12	0.5	0.5	0.5
13:00	0.5	0.5	0.5	3.5	14	0.5	0.5	0.5	10	0.5	0.5	0.5
14:00	1.0	1.0	1.0	9.9	27	2.6	2.6	2.6	14	0.5	0.5	0.5
15:00	1.0	1.0	1.0	14	25	0.5	0.5	0.5	7.9	0.5	0.5	0.5
16:00	3.5	1.0	1.0	25	17	0.5	0.5	0.5	8.9	0.5	0.5	0.5
17:00	1.5	1.5	1.5	14	13	0.5	0.5	0.5	9.8	0.5	0.5	3.0
18:00	0.5	0.5	0.5	5.4	4.6	0.5	0.5	0.5	3.4	1.0	1.0	1.0
19:00	1.5	1.5	1.5	3.0	2.0	0.5	0.5	0.5	2.0	1.5	1.5	1.5
20:00	2.0	2.0	2.0	1.5	1.0	1.0	1.0	1.0	1.0	1.0	1.0	1.0
21:00	2.5	2.0	2.0	2.0	1.0	1.0	1.0	1.0	1.0	1.0	1.0	1.0
22:00	3.5	2.5	2.5	2.5	1.0	1.0	1.0	1.0	2.0	2.0	2.0	2.0
23:00	4.4	3.0	3.0	3.0	1.0	1.0	1.0	1.0	3.0	3.0	3.0	3.0
00:00	3.5	3.5	3.5	3.5	1.0	1.0	1.0	1.0	3.0	3.0	3.0	3.0

[a] Locations are shown in Figure N-4. Data were digitized from figures in Grumski and Shanks (1988). Digitizing resolution was the equivalent of about 0.5 pCi L^{-1}. Blanks in table indicate that no data were available.

[b] For many of the data points compiled here, it was extremely difficult, or impossible, to differentiate the symbols and lines representing different locations. In such cases, all uncertain locations were assigned the same value. This does not apply to results for locations that were clearly elevated relative to the other locations.

morning hours. At other times of the day, concentrations were again less than 10 pCi L^{-1}. During the 9 days shown, monitoring results were often only available from one or two of the four stations. However, the highest concentrations should be expected at the northeast station (which is shown) because it is in the predominant wind direction from the silos.

For 1980–1987, the period after penetrations in the K-65 silo domes were sealed and before the foam layer was applied to the domes, our radon release estimates include daylight releases resulting from thermal expansion of silo head space gases and subsequent air exchange release from the silos. The daylight-only air exchange release rate is predicted to be much higher than the rate of diffusion releases, which are thought to occur over the whole day. The result is predicted radon release rates that are much higher for daylight hours (5.55×10^7 pCi s^{-1}) than for nighttime (4.12×10^6 pCi s^{-1}) (see Appendix M). For 1988 (and through October 1991), our calculations indicate that the thermally induced air exchange releases during daylight hours had been reduced to very low levels because of the insulating ability of the foam layer applied to the silo domes in December 1987 (see Appendix J of the Task 2/3 report: Voillequé et al. 1995). Thus, for 1988 and later years, radon releases are thought to occur at a relatively constant rate during the day.

The diurnal pattern in radon concentrations measured in October 1991, with peak concentrations at night and in the morning (Figure N-6), is generally consistent with the

Table N-5. Hourly Radon Concentrations (pCi L^{-1}) after Addition of Foam Layer to K-65 Silos: Nine Days of October 1991 Data at Three Locations [a]

	October 1, 1991			October 2, 1991			October 3, 1991			October 4, 1991			October 5, 1991		
Time	NE	NW	SW	NE	NW	SW	NE	NW	SW	NE	NW	SW	NE	NW	SW
01:00	56.9	6.5		7.8	4.2	3.4	13.7			99.2			0.4		
02:00	69.1	8.5	3.3	5.6	3.6	3.6	58.3			77.9			0.4		
03:00	62.6	6.4	5.8	5.6	4.0	3.6	31.0			31.1			0.6		
04:00	65.1	7.0	5.8	13.2	4.4	3.1	43.3			14.0			0.7		
05:00	48.5	9.6	4.3	12.3	5.1	3.6	20.9			5.8			0.9		
06:00	34.7	6.1	4.7	7.8	4.6	3.6	11.4			2.6			2.8		
07:00	25.2	5.6	7.9	6.2	4.5	4.4	6.4			1.7			1.5		
08:00	22.4	5.0	6.0	8.5	4.8	3.8	3.5			1.6			1.0		
09:00	11.9	4.3	5.3	5.0		3.9	1.9			1.2			1.6		
10:00	5.8	2.6	4.3				1.1			1.1			0.9		
11:00	3.3	2.2	3.5	2.5			1.2			1.6			0.7		
12:00	2.4	1.6	1.7	1.8			1.6			1.5			0.7		
13:00	2.9	1.2	1.2	6.7			1.8			1.3			0.9		
14:00	4.4	1.1	0.8	8.4			3.2			1.2			1.0		
15:00	5.0	0.8	0.6	4.4			4.5			1.0			0.9		
16:00	4.3	1.0	0.5	3.4			3.5			0.8			0.9		
17:00	3.3	1.0	0.6	2.0			11.0			0.6			0.6		
18:00	2.2	1.1	0.4	1.0			6.1			0.4			1.1		
19:00	1.8	1.8	0.4	0.7			5.4			0.3			1.9		
20:00	5.2	2.8	1.0	5.2			22.6			0.3			5.6		
21:00	7.0	3.2	2.2	27.1			23.7			0.3			16.6		
22:00	9.4	3.3	6.4	34.9			11.8			0.3			18.7		
23:00	8.0	3.5	6.0	21.3			16.6			0.3			20.9		
00:00	7.5	3.5	5.0	12.4			15.2			0.3			27.2		

[a] Locations are shown in Figure N-4. Data were obtained (in electronic spreadsheet) from Byrne (1992a). The instrument at the SE location was out of service for the time period compiled here; this location is not shown in the table. Single blanks in table indicate that no data were available, with no reason given. Long gaps in data for NW and SW locations were noted as "tech error" in the source document (Byrne 1992a).

predicted relatively constant radon release rate, because the more stable conditions at night would tend to result in less dispersion and thus higher concentrations. However, the diurnal pattern in radon concentrations measured in 1986 and early November 1987 showed peak concentrations in daylight hours (Figure N-5). This pattern is consistent with higher radon release rates during daylight hours. We believe that patterns seen for the two different periods provides strong evidence that for 1980–1987 the radon release rate was much higher in daytime than at night. Though we make no quantitative comparisons, this provides qualitative corroboration of the predicted daylight release rates (from thermally induced air exchange) that are very large relative to nighttime release rates.

Early Time-Integrated Measurements of Radon in Air at Boundary Station BS-6

One of the most important structural changes to the K-65 silos that must be considered in estimating radon source terms is the sealing of penetrations of the silo domes, which occurred June 25, 1979 (details are provided in Appendix Q, Volume II, this report). Our predicted radon release rates decrease by a large factor (of about 6.5 for median estimated releases) after the silos were sealed. Radon measurements made both before and after the sealing would thus be quite useful for comparison with the predicted release rates.

Table N-5. Hourly Radon Concentrations (pCi L^{-1}) after Addition of Foam Layer to K-65 Silos: Nine Days of October 1991 Data at Three Locations (continued) [a]

	October 6, 1991			October 7, 1991			October 8, 1991			October 9, 1991		
Time	NE	NW	SW	NE	NW	SW	NE	NW	SW	NE	NW	SW
01:00	72.5			4.9		4.3	30.7		4.7	61.6		3.2
02:00	49.2			9.7		3.9	34.0		4.7	48.4		3.8
03:00	24.2			14.3		5.0	61.1		4.4	39.5		3.8
04:00	19.8		3.0	21.6		6.1	83.9		4.6	50.7		4.3
05:00	13.4		2.2	24.6		5.8				34.9		4.7
06:00	10.8			25.3		7.8			4.5	22.3		5.2
07:00	15.2		2.2	21.7		8.8			5.4	20.9		7.1
08:00	32.2		2.1	15.9		6.9			5.7	15.2		6.7
09:00	18.9		2.0	10.7		5.7			5.5	11.6		5.9
10:00	8.7		1.8	6.0		4.9			5.2	7.9		3.3
11:00	4.1		1.5	3.7		2.9			3.4	6.9		2.0
12:00	2.7		1.3	2.6		1.9			1.8	5.8		1.6
13:00	1.6		1.3	3.0		1.5			1.6	5.4		0.9
14:00	1.5		1.4	4.0		1.3			1.4	4.4	1.5	0.6
15:00	1.7		1.3	4.8		1.3	1.9		1.3	4.7	1.2	0.6
16:00	0.9		1.3	4.3		1.1	1.3		1.4	5.7	1.0	0.7
17:00	0.7		1.3	3.7		1.3	2.0		0.9	3.5	1.2	0.4
18:00	0.8		1.5	3.8		1.4	1.2		1.2	2.8	1.1	0.6
19:00	0.8		1.4	3.8		1.2	1.1		1.1	1.8	1.2	0.7
20:00	1.0		1.5	18.3		2.7	1.1		1.5	2.0	1.8	0.9
21:00	2.7		1.7	22.1		4.1	2.2		2.1	4.4	1.7	0.7
22:00	9.5		2.3	24.2		5.5	1.4		3.8	2.9	1.3	0.9
23:00	8.8		3.1	29.8		4.9	3.6		4.0	3.3	1.7	1.1
00:00	6.4		5.6	28.2		19.9	31.2		3.2	6.1	1.8	0.9

[a] Locations are shown in Figure N-4. Data were obtained (in electronic spreadsheet) from Byrne (1992a). The instrument at the SE location was out of service for the time period compiled here; this location is not shown in the table. Long gaps in data for NW and SW locations (not NE) were noted as "tech error" in the source document (Byrne 1992a). Other blanks in table here indicate that no data were available, with no reason given.

Most of the useful, available monitoring data for radon in air around the FMPC were described in the draft report of Task 4 (Killough et al. 1993) and the final report of Task 5 (Shleien et al. 1995). There is only a small amount of data for the period before the sealing of the silos. This early radon monitoring is discussed in detail in the Task 5 report (Shleien et al. 1995), and the following information is summarized from that report.

One of the types of early radon monitoring was time-integrated measurements of ^{222}Rn, made using passive radon monitors thought to be the same as those commonly called passive environmental radon monitors (PERMs). The measurements were made in 1978–1980, though most were in 1979. Individual measurements encompassed periods of 1 day to 3 weeks. Because all but two of the measurements were taken at boundary station BS-6, we only consider those measurements at BS-6. Figure N-7 shows the locations of the boundary air monitoring stations for 1978–1980. Results of the individual measurements at BS-6 are shown in Figure N-8, along with average concentrations calculated for the periods before and after sealing. We note that in the Task 5 report we did not know the exact date the silos were sealed. We now know that the sealing was completed June 25, 1979 (see Appendix Q). With this knowledge, the average radon concentration after sealing is updated (below) from the Task 5 value, to now include the correct individual values.

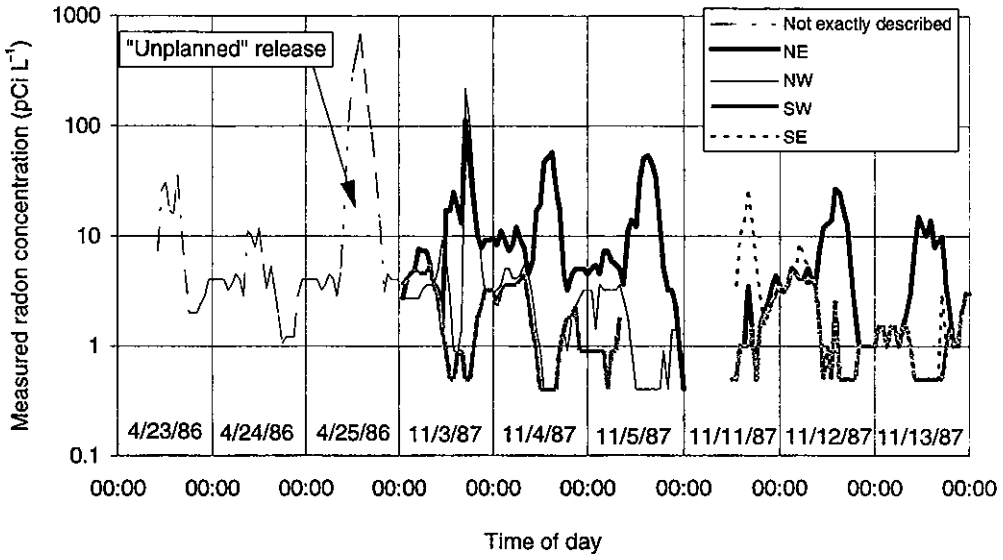

Figure N-5. Hourly measurements of radon concentration in air near the K-65 silos, made during 9 days in the period 1980–1987, before the foam layer was installed on the silo domes. The "unplanned" release on April 25, 1986 was a nonroutine occurrence and should not be considered typical. Vertical lines on the graph represent midnight. Note that all days shown are not contiguous in time; there are three groups of 3 consecutive days. See text for discussion about the "not exactly described" location for the 1986 measurements.

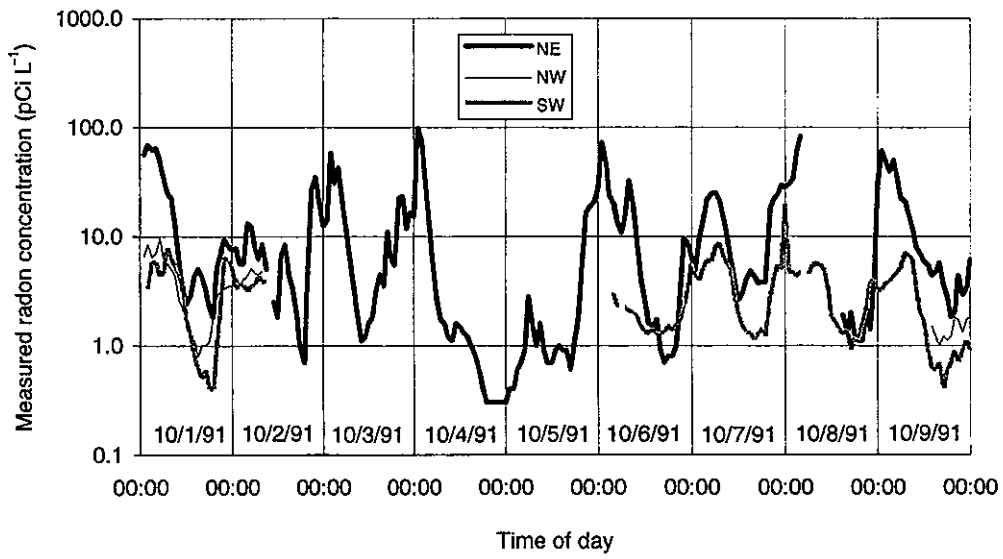

Figure N-6. Some hourly measurements of radon concentration in air near the K-65 silos, in the period after the foam layer was installed on the silo domes. Though data from all of October 1991 have been obtained, we only show the first 9 days, as a representative fraction. Vertical lines on the graph represent midnight.

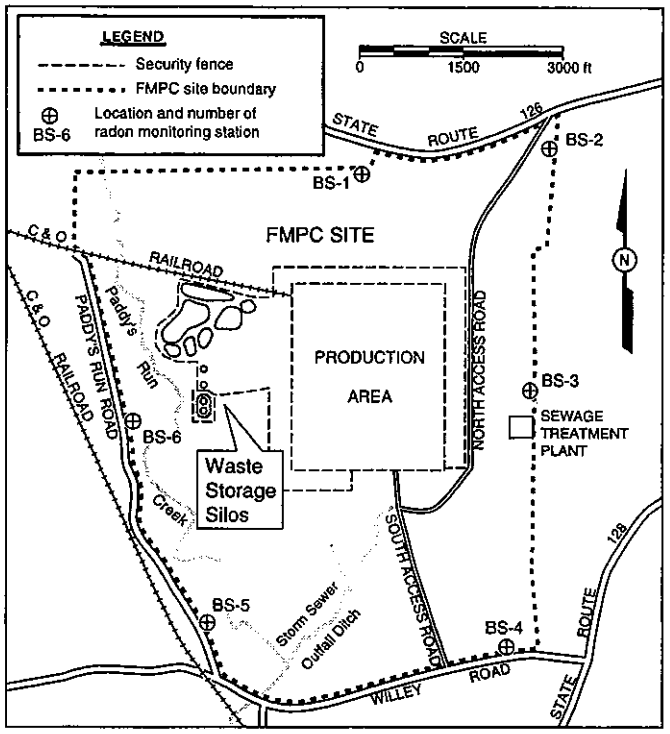

Figure N-7. Locations of the boundary air sampling stations of the FMPC site during 1978–1980. These were the primary monitoring locations used in the early radon monitoring at the FMPC, with particular emphasis on BS-6, the monitoring station closest to the K-65 silos.

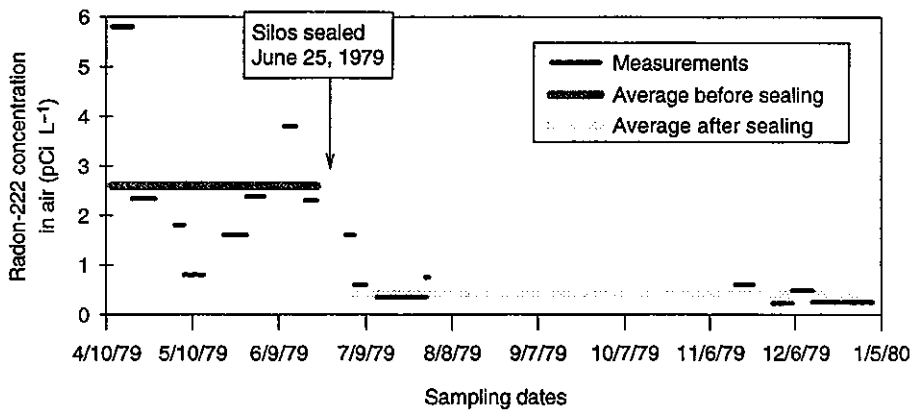

Figure N-8. Concentrations of ^{222}Rn in air at boundary air monitoring station BS-6 before and after the penetrations in the domes of the K-65 silos were sealed. Station BS-6 is about 300 m west of the K-65 silos. Averages shown are time-weighted gross concentrations. The before-sealing average (2.6 pCi L^{-1}) includes results through June 22, 1979, and the after-sealing average (0.42 pCi L^{-1}) includes results of July 2, 1979, and later.

From these individual measurements, the time-weighted average, gross concentrations (shown in Figure N-8) were 2.6 pCi L^{-1} for the period before sealing and 0.42 pCi L^{-1} for the period after sealing. There were no concurrent measurements of background radon concentrations, so we developed estimates for the background (see Shleien et al. 1995 for details). Net concentrations were then estimated to be 2.0 ± 0.9 pCi L^{-1} before sealing and -0.03 ± 0.34 pCi L^{-1} after sealing, where the "±" values define a 90% confidence interval (± 1.645 standard deviations). The magnitude of the decrease in concentration is difficult to ascertain from the data because of the large uncertainties. However, the results show a large decrease in measured radon concentration at BS-6 after the penetrations in the K-65 silo domes were sealed, which is strong evidence that radon release rates were significantly higher before the sealing than after the sealing. This provides qualitative corroboration of the *predicted* significantly increased radon releases for the period before the silo sealing.

Early Grab Measurements of Radon Daughters in Air at Boundary Station BS-6

The early radon monitoring also included some grab (short sampling period of 30 minutes) air filter samples analyzed for radon daughters. Details about these measurements can also be found in the report of Task 5 (Shleien et al. 1995). These radon daughter grab samples were taken during September and October 1978, primarily at boundary station BS-6 (see Figure N-7).

Of the 15 samples taken at BS-6, one result was about seven times higher than all other results, and thus seems suspect. If this extreme value is neglected, the average reported concentration is 1.9 pCi L^{-1}. If the extreme value is included, the mean concentration is 4.3 pCi L^{-1}. These results were originally reported as concentrations of ^{222}Rn, but because of the sampling technique (filters extracted radon daughters from air) they were really estimates of the average concentration of each of the short-lived daughters of ^{222}Rn. Since the measurements were only 30-minute grab samples, a *detailed* comparison with predicted values (which would be based on a longer time resolution) is not warranted.. However, a rough comparison to measured *radon* concentrations may be of some use.

If no short-lived daughters were released with the radon from the K-65 silos, based on travel time we would expect the net radon daughter concentrations at BS-6 to be only about one-tenth the net concentration of radon. This is because BS-6 is relatively close to the silos and the transport time is short, so the ingrowth of daughters during transport is very slight. Of course, if the daughters are released in equilibrium with radon, their concentrations at BS-6 would be essentially equal to that of radon. The average measured daughter concentration of 1.9 (or 4.3) pCi L^{-1} is significantly above the expected background and in the range of the average measured gross concentrations of ^{222}Rn for the period before the sealing of silo penetrations, 2.6 pCi L^{-1} (see previous section). This rough equivalence of radon and radon daughter concentrations indicates that radon daughters were probably released in appreciable fractions of equilibrium. It thus provides some corroboration of the estimation, in the final Task 2/3 report (Voillequé et al. 1995), that the radon daughters were released in quantities almost in equilibrium with ^{222}Rn for this period before the sealing of the silos (1959–1979).

URANIUM VALIDATION RESULTS

Data Completeness and Computation of Average Concentrations of Uranium in Air

Because our predicted air concentrations were developed based on an annual resolution, it was necessary to produce annual average concentrations for the historic measurements made by the FMPC monitoring program. This section presents detailed information relating to how those averages were produced.

Perimeter air monitoring stations (1958–1971). All averages were derived from the most original source available, the analytical data sheets, on which the amounts of uranium on each air filter were recorded. Air monitoring before 1958 was conducted for less than 1% of the year, so production of an annual average from that small coverage was not warranted. In 1958, monitoring data from the security guard posts were combined so that they could be included with the reduced monitoring program, which continued between 1959 and 1971 at the four corners of the FMPC perimeter security fence. [See Shleien et al. (1995) for the history of the air monitoring program.] Data from the southwest and west guard stations from 1958 were combined and reported as southwest; the northwest and north were reported as northwest; the northeast and east were reported as northeast; and the southeast and south were combined as southeast.

During this period, the minimum detectable concentration (MDC) for uranium in air was 10 femtocuries per cubic meter (fCi m^{-3}). The occasional values which were less than the MDC were assigned a value of 1/2 MDC (5 fCi m^{-3}) when computing averages. This procedure resulted in little or no difference in the annual averages because there were very few measurements less than the MDC. Table N-6 illustrates how many individual measurements were reported as <10 fCi m^{-3}, as well as other information about data completeness.

Especially for data collected during the early years, we sometimes invalidated individual sample results because of suspect sampling conditions such as the following, which were noted by the sampling or analytical technicians on the analytical data sheets:

- defective pump
- uncertain sample volume or time
- partial loss of sample
- filters came loose.

The number of invalid samples is indicated in Table N-6.

A weekly sample datum was included in the year in which the sample ending date fell, e.g. the samples ending 1/2/76 were included in the 1976 annual average. The December 1971 data were omitted from our computation of the annual average for that year because testing was being conducted to prepare for the change of monitoring locations from the perimeter to the boundary stations. Table N-7 presents the annual average concentrations of uranium in air at the perimeter stations, as reconstructed from the analytical data sheets.

Table N-6. Data Completeness and Detectability at Perimeter Monitoring Stations (Uranium in Air)

		Monitoring Stations											
		SW			NW			NE			SE		
Year	n[a]	# NA[b]	# IV[c]	# <[d]	# NA	# IV	# <	# NA	# IV	# <	# NA	# IV	# <
1958	26	5	1	0	3	2	0	5	0	0	5	0	0
1959	21	7	0	0	10	0	0	2	0	0	2	0	0
1960	28	15	0	0	1	1	0	1	1	0	12	0	0
1961	46	10	1	0	3	2	0	0	3	0	5	2	0
1962	53	0	0	0	0	5	0	2	3	0	2	4	0
1963	52	1	0	0	2	0	0	0	1	0	1	0	0
1964	51	0	1	0	1	2	1	0	2	0	1	3	0
1965	53	1	0	2	1	0	3	1	0	0	0	0	1
1966	55	1	0	0	3	0	1	1	1	0	1	0	1
1967	51	0	0	1	0	0	1	0	0	0	0	0	0
1968	52	21	0	0	0	0	0	0	0	0	0	0	0
1969	48	2	0	0	0	1	1	0	0	2	1	0	1
1970	52	0	0	1	0	0	0	0	0	0	0	0	0
1971	47	1	1	1	2	0	0	0	0	1	3	0	0

[a] n= Total number of sample collection periods during that year. During this time, each sample was a duration of 2.3 days with a weekly frequency. Special sampling sometimes increased the total number of collection periods above 52 or 53 per year. The total number of valid data points for a sampler is n – #NA – #IV.

[b] # NA = Number of missing samples, or "not available."

[c] # IV = Number of samples invalidated due to suspected sample problem (see Shleien et al. 1995).

[d] # < = Number of samples less than detection limit of 10 fCi m^{-3}.

Table N-7. Annual Average Concentrations of Uranium in Air (fCi m^{-3}) Measured at Perimeter Air Monitoring Stations[a]

	Monitoring Stations			
Year	SW	NW	NE	SE
1958	95	109	339	163
1959	131	94	109	65
1960	346	165	170	173
1961	154	115	182	140
1962	234	70	145	158
1963	260	113	293	209
1964	223	90	211	162
1965	89	39	123	68
1966	130	38	112	76
1967	130	43	120	96
1968	166	97	130	141
1969	166	49	88	90
1970	86	36	64	36
1971	48	38	39	32

[a] Uncorrected for sampler collection efficiency. Annual averages were determined from individual weekly measurements recorded on analytical data sheets. Before 1958, air monitoring was too infrequent to compute an annual average (Shleien et al. 1995). All concentrations are based on a constant activity-per-mass of 6.8×10^{-7} Ci U g^{-1} U.

These perimeter stations were dismantled and replaced with boundary monitoring stations in 1972.

Boundary air monitoring stations (1972–1985). The MDC improved when air monitoring was moved to the boundary stations, due mainly to the continuous sampling, which resulted in a larger volume of air being drawn per sample. The MDC values reported in the annual environmental monitoring reports were: 1971–1972, 10 fCi m^{-3}; 1973–1974, 0.6 fCi m^{-3}; 1975–1980, 0.4 fCi m^{-3}; and 1981–1983, 0.1 fCi m^{-3}. The FMPC was apparently not taking credit for the increased sample volume in the reported detection limits for 1971–1972, which should have been improved (lowered) relative to the perimeter sampling. At any rate, none of the sample results reported during the 1972–1984 period were less than the MDC. In contrast to the perimeter sampling interval, only one boundary sample at boundary station BS–4 in 1972 was invalidated. During this time, the site typically would not report a result if there was a problem with sampling or analysis, so we counted that sample as "not available" rather than "invalid." Table N-8 shows the number of missing data points during this period.

Table N-8. Data Completeness at Boundary Stations (Uranium in Air)[a]

		Monitoring Stations						
Year	n[b]	BS–1	BS–2	BS–3	BS–4	BS–5	BS–6	BS–7[c]
1972	47	6	3	7	2[d]	5	3	47
1973	52	0	0	4	1	5	2	38
1974	51	0	0	0	0	0	1	49
1975	52	1	0	0	0	1	0	52
1976	42	1	1	0	1	1	1	14
1977	52	0	0	0	0	0	1	52
1978	52	0	0	0	0	1	0	52
1979	51	2	1	1	1	1	3	51
1980	52	1	0	0	1	0	0	52
1981	51	0	0	0	0	0	0	2
1982	51	0	0	0	0	0	0	0
1983	52	0	0	0	0	0	0	0
1984	53	0	0	0	0	0	0	0

[a] Values in table are the number of samples not available. The total number of valid data points for any given year and location can be determined by subtracting the number of samples not available for that location from the total number of sample collection periods (n) in that year.

[b] n = Total number of sample collection periods during that year. During this time, air sampling was continuous with a weekly filter collection frequency.

[c] Monitoring did not begin at BS–7 until June 1973 and operated sporadically after that until 1981.

[d] Includes one invalid data point.

Table N-9 presents the annual average concentrations of uranium in air at the boundary stations, as reconstructed from the analytical data sheets.

Table N-9. Annual Average Concentrations of Uranium in Air (fCi m^{-3}) Measured at Boundary Air Monitoring Stations[a]

	Monitoring Stations						
Year	BS–1	BS–2	BS–3	BS–4	BS–5	BS–6	BS–7
1972	11.92	12.03	18.34	5.81	7.09	18.80	
1973	20.53	17.46	24.70	6.23	7.04	18.06	26.03
1974	22.08	17.19	17.25	4.84	7.21	12.16	12.59
1975	25.10	22.16	27.15	7.66	9.14	17.67	
1976	21.12	12.64	17.70	5.36	5.88	10.54	12.28
1977	11.65	8.26	12.94	4.11	5.24	5.07	
1978	8.19	8.63	16.74	5.19	10.37	7.01	
1979	13.28	7.72	19.30	8.12	10.77	9.16	
1980	4.17	3.53	4.62	3.48	3.01	4.05	
1981	7.96	8.75	10.93	3.61	5.28	5.01	2.69
1982	15.64	8.75	14.40	4.28	7.24	7.92	4.05
1983	21.45	14.51	24.75	8.61	9.94	11.35	4.85
1984	17.18	12.84	22.07	4.72	6.42	9.61	4.42
1985	2.96	3.11	5.57	2.13	2.21	2.47	1.11

[a] Uncorrected for sampler collection efficiency. Through 1984, annual averages were determined from individual weekly measurements recorded on analytical data sheets. All concentrations were corrected to a constant activity-per-mass of 6.8×10^{-7} Ci U per gram of U (the FMPC used two different reporting protocols during this time period). Annual averages for 1985 were obtained from the annual environmental report, because analytical data sheets were not located.

Expanded air monitoring program (1986–1988). This section explains how we determined the annual average concentrations of uranium in air for 1986–1988, when the air monitoring program expanded beyond the boundary stations to include stations closer and further from the FMPC (Figure N-9). Data from this expanded program were used to calibrate the air dispersion model (Appendix M). Before conducting that calibration exercise, we had obtained annual average concentrations of uranium in air at these air monitoring stations from the annual environmental reports for 1985 through 1988 (Aas et al. 1987, Gels and Lojek 1988, Gels et al. 1989), because weekly analytical data sheets had not been located.

Because of the importance of the model calibration exercise to this study, we undertook a more thorough investigation of the air monitoring data from 1986–1988. More original sources of information were examined to determine the appropriateness of published average concentrations for our purposes. Electronic spreadsheet files of the weekly measurements for all 3 years were obtained from the Fernald site (Byrne 1995). Analytical data sheets for weekly measurements of uranium in air at the boundary stations 1 through 7 were located for 1986, and the electronic spreadsheet values were checked against those paper records. During examination of these original sources of information, several important issues arose.

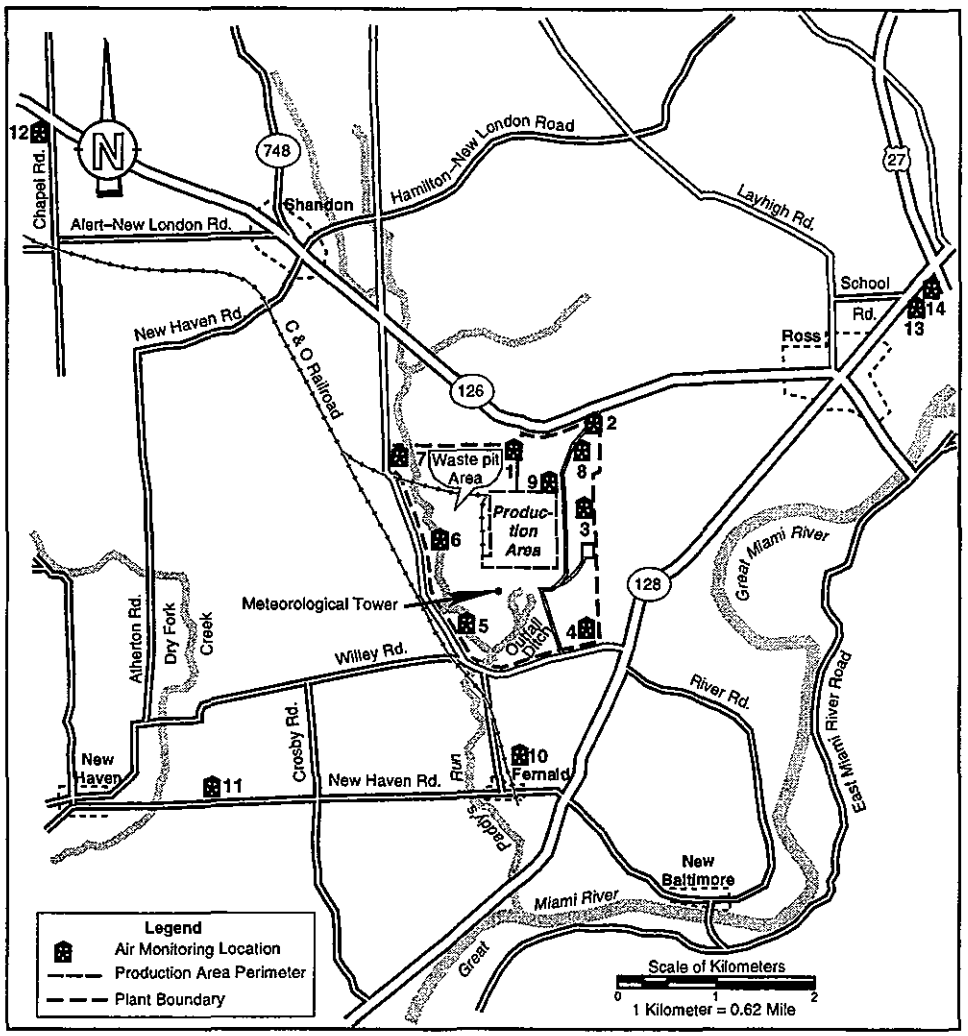

Figure N-9. Locations of high-volume air monitoring stations (AMS) in 1986–1988.

The first issue involved the reporting and use of blank values, which represented the micrograms of uranium measured in a blank filter. Offsite samples from 1987 and 1988 (AMS–10 through AMS–14) always had a blank filter value, which was determined each week, that was subtracted from the sample result before computing the airborne uranium concentrations. However, for the boundary and onsite stations (AMS–1 through AMS–9), the blank was not subtracted consistently by the FMPC before reporting the annual average concentrations.

The first recording of blank filter results from the FMPC lab that we located was the set of analytical data sheets for onsite air samples in 1986. For all analytical data sheets through 1984, which we had examined thoroughly and used to derive our annual averages of uranium in air, there had been no blank analysis results recorded. Although blanks were run, they were not subtracted from the gross measurements in 1986 or 1987, but they were subtracted in 1988. From examination of the electronic spreadsheets, it also appeared that an inconsistent method (geometric versus arithmetic average) was used to compute the annual average concentrations that had been reported by the site for these 3 years.

Because of the considerable reporting inconsistencies during these years, we recomputed all the average concentrations for 1986–1988 using a uniform method, correcting for filter blanks. In 1986, the blank value for each week's analyses was taken from the analytical data sheets. For 1987, we did not have the weekly blank values, so an average value of 3.6 micrograms (µg) uranium per filter (the 90% confidence interval was 0.5–7), from the 1986 set was subtracted from the 1987 measurements before computing the weekly concentrations. Out of 468 filters in 1987, the amounts of uranium per filter ranged from 2 to 1500 µg, with a median of 47 µg. Thus, the estimated blank value represented less than 10% of the total uranium for over half of the analyses of air filters in 1987.

Another potential problem with the air monitoring data was that the uranium analyses for offsite air monitoring stations (number AMS-10 and larger) were always analyzed by an outside contracted laboratory, not by the FMPC. Therefore, there was a concern that the results from stations AMS-1 through AMS-9 may not be comparable to the others. However, examination of summary quality assurance data did not indicate a major analytical bias, although there is considerable scatter in the data. Quality assurance programs were in place for both laboratories. For example, at least 10% of the samples analyzed by the FMPC in 1987 and 1988 were control samples, which included standards, spikes, and blanks. The control samples were analyzed along with the field samples (Gels et al. 1989). (The 1986 environmental report does not give a percentage of control samples.) Accuracy of uranium in air analysis was determined by spiked samples. The site also participated in intercomparison programs with other organizations. The intercomparison results for 1988 are presented in Table N-10.

In 1988, the FMPC submitted quality assurance samples to the commercial laboratory that conducted the offsite air filter analyses. Known amounts of uranium were added to the control samples in the range of amounts typically detected at those stations. Analytical results from the contract laboratory's quality assurance samples are shown in Table N-10. Their performance was considered satisfactory for analyses at environmental levels although results in 1987 were better (Gels et al. 1989).

Table N-10. Results of Data Quality Assessments for Analyses of Uranium in Air in 1986–1988 (reported in FMPC Annual Environmental Reports)

	Year		
Data quality test	1986	1987	1988
DOE Quality Assurance Program (FMPC result / EML[a] result)	Water, soil, and air; range not given; average 1.04	Water, soil, and air; range not given; average 1.13	Water and air; range 0.95–1.13; average 1.06
Blind spike of uranium in air filters (contract lab result / spike amount)	Samples from late 1986 were reported as combined with the 1987 samples	number 25; average 0.91; range 0.57 to 1.35	number 25; average 0.89; range 0.4 to 1.6

[a] EML is the Environmental Measurements Laboratory of the Department of Energy, in New York City.

During 1987, a series of four air filters from AMS–3 were split in thirds and analyzed by the FMPC, the contract laboratory, and a U.S. Environmental Protection Agency laboratory.

Gels and Lojek (1988) states that "although the analytical methods used by the three laboratories differed, the results of the analyses were generally within the measurement errors reported by the respective laboratories." In summary, we concluded that potential analytical bias resulting from the use of two laboratories was not an overriding concern in use of these data, and that the uncertainty and bias in the analytical determination would be included as part of the overall uncertainty analysis for the uranium dispersion model (Appendix M).

Another complication in the use of these data for the calibration exercise became apparent after examining the weekly monitoring results (Figure N-10). It was clear that the source term, as reflected by the monitoring data, was not uniform during this time, particularly in 1988. In fact, over half of the annual release was believed to have occurred over a 4-week period in June 1988, as a result of UO_3 gulping operations at the Plant 2/3 refinery (Gels et al. 1989). The emissions were identified from the high concentrations of uranium measured in ambient air beginning the first week in June. After discovering the source of the problem, the process was shut down on June 30 and remained out of service for the remainder of the year. Ross (AMS–13) was the offsite station that was most impacted; however, all stations except AMS–12, to the NW, showed the maximum weekly concentration during the middle two weeks in June 1988 (Figure N-11).

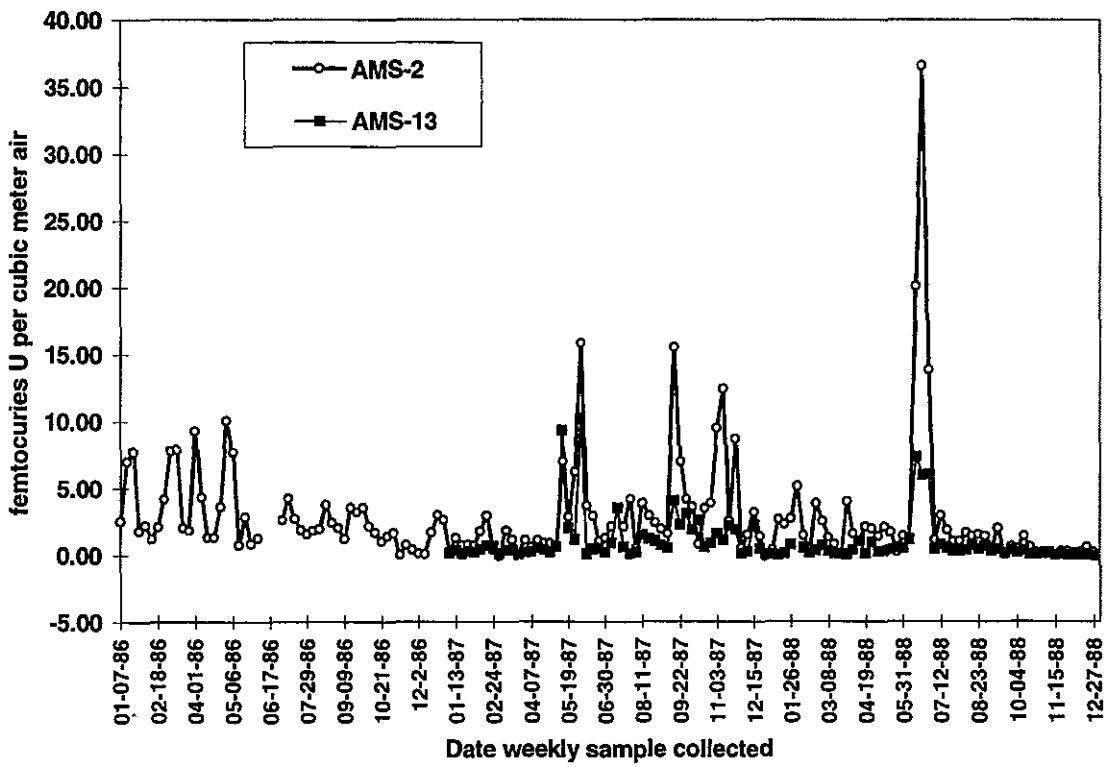

Figure N-10. Weekly measurements of uranium in air at the NE boundary (AMS–2) and at Elda School in Ross (AMS–13) during 1986–1988. Ross was the offsite station that was most affected by the June 1988 releases, although all of the offsite stations showed some elevated concentrations (Figure N-11).

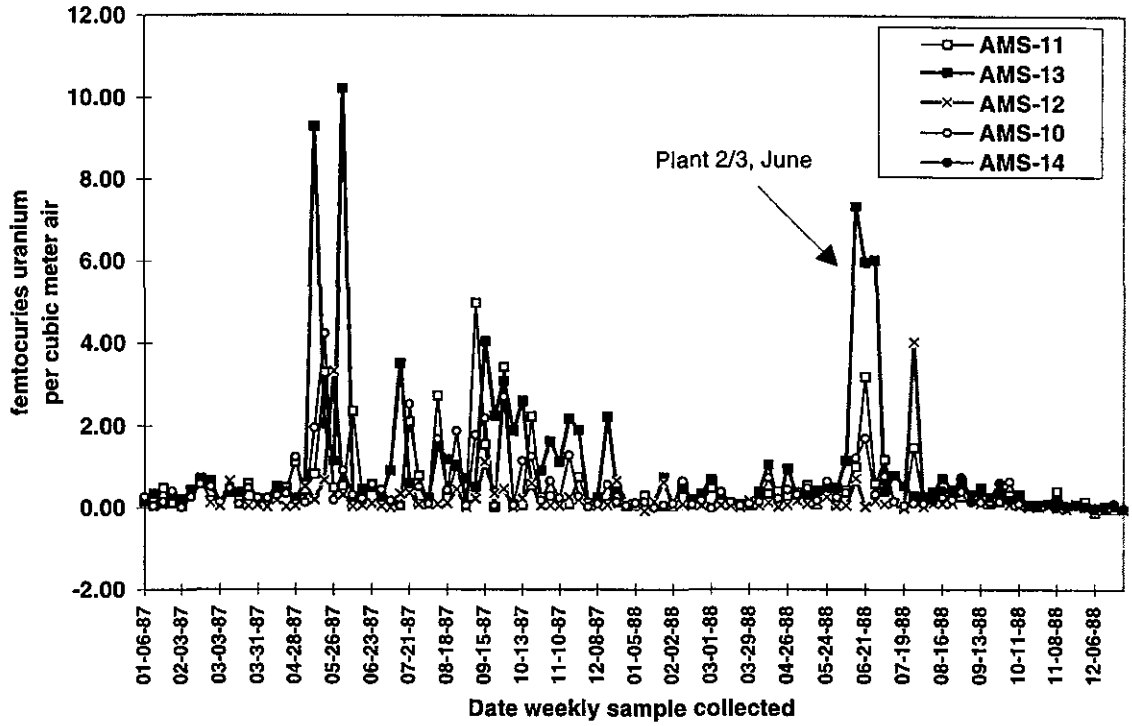

Figure N-11. Weekly measurements of uranium in air from offsite stations in 1987–1988. See Figure N-9 for locations. These offsite stations were not in service before 1987.

Because of the non-uniform source term, we made a correction to the annual averages for four locations to account for the fact that monitoring was only conducted there for part of the year (Table N-11). All other stations were operating continuously throughout the year. The partial-year average was multiplied by a correction factor obtained from stations that were operating the entire year. This correction cleared up the discrepancy between the 1988 averages from AMS–13 and AMS–14, which are physically very close to each other. The approximately three-fold difference between the annual average concentrations at AMS–13 and AMS–14 was not discussed in the annual environmental report. Now it is clear that the reason for the difference in those averages is that AMS–14 was not in place until the latter part of that year, after the majority of the releases had occurred.

Table N-12 summarizes the completeness, detectability, and average concentrations of uranium in air for 1986–1988. If the gross amount of uranium on the filter was less than the blank value, then a negative concentration would be obtained. Most concentrations were greater than zero. The largest percentage of non-positive concentrations was 10% at AMS–12 in 1988 (Table N-12). In computing average concentrations, all net concentrations, including negative values, were included.

These average concentrations for 1986–1988 were used in the calibration of the air dispersion model used for uranium releases from the FMPC (Appendix M). For the calibration exercise, the averages were adjusted to correct for air sampler collection efficiency, analytical bias, and resuspension of natural and previously-deposited uranium. These adjustments are discussed in Appendix M.

Table N-11. Correction for Partial-Year Monitoring at Four Air Monitoring Stations in 1986–1988

Sampler and year	Average before partial-year correction (fCi m^{-3})	Correction factor	Average after partial-year correction (fCi m^{-3})
AMS–8 in 1986	4.62	1.6, based on year-long record at BS–2	7.33
AMS–9 in 1986	8.32	1.6, based on year-long record at BS–2	13.21
AMS–12 in 1987	0.28	0.89, based on year-long record at other offsite stations	0.25
AMS–14 in 1988	0.20	3.0, based on year-long record at AMS–13	0.60

Table N-12. Completeness, Detectability, and Annual Average Concentrations (fCi m^{-3}) of Uranium at Air Montitoring Stations in 1986–1988[a]

	Year								
	1986			1987			1988		
Location	n	n ≤ 0	Average	n	n ≤ 0	Average	n	n ≤ 0	Average
Onsite [b]									
AMS-1	49	1	2.84	52	0	3.31	52	1	2.60
AMS-2	50	1	2.87	51	2	3.08	52	2	2.57
AMS-3	50	0	6.15	52	0	6.76	51	0	3.59
AMS-4	53	0	1.74	52	0	1.75	52	2	0.77
AMS-5	49	0	1.58	52	0	1.77	52	2	0.83
AMS-6	47	0	1.71	52	0	2.39	51	0	0.90
AMS-7	52	0	0.92	52	2	1.40	52	2	0.50
AMS-8	20	0	7.33[d]	52	1	7.37	52	1	4.32
AMS-9	18	0	13.21[d]	52	0	13.32	52	0	6.78
Offsite [c]									
AMS-10	0	0	NS	52	0	0.67	52	3	0.25
AMS-11	0	0	NS	52	0	0.7	52	4	0.3
AMS-12	0	0	NS	45	0	0.25[d]	51	5	0.18
AMS-13	0	0	NS	52	0	1.26	51	1	0.69
AMS-14	0	0	NS	0	0	NS	21	2	0.60[d]

[a]Arithmetic average, reconstructed from weekly measurements. Laboratory blank values subtracted. n=total number of samples; n ≤ 0 indicates the number of samples that were zero or less after blank was subtracted; NS= no sample.

[b]Onsite samples analyzed by FMPC laboratory.

[c]Offsite samples analyzed by outside contracted laboratory.

[d]Monitoring not conducted for entire year. Measured average was adjusted to produce an estimate of the true annual average as described in text and Table N-11.

Uranium in Air at Perimeter and Boundary Monitoring Stations

The concepts of the validation of predicted results by comparison with environmental measurements are discussed in the main text (Volume I) of this report. Tables N-13 through N-24 and Figures N-12 through N-20 present the detailed results of these comparisons for uranium in air at the perimeter and boundary locations between 1958 and 1988. The computation of the air sampler collection efficiency is presented in Appendix L. The "background" line shown on the validation plots is the uranium concentration measured in air at Columbus, Ohio, by the U.S. Environmental Protection Agency.

Table N-13. Computation of Correlation and Bias for Predicted and Observed Concentrations of Uranium in Air at Northeast Perimeter Station[a]

Year	Observed concen. (fCi m^{-3})	Collection efficiency	Corrected observed (fCi m^{-3})	Corrected observed (mg m^{-3})	Predicted (mg m^{-3})	ln (O)	ln (P)	P/O	ln P/O
1958	339	75	452	6.64E-04	1.20E-03	-7.32E+00	-6.73E+00	1.81	0.59
1959	109	75	145	2.14E-04	1.20E-03	-8.45E+00	-6.73E+00	5.62	1.73
1960	170	72	236	3.47E-04	1.10E-03	-7.97E+00	-6.81E+00	3.17	1.15
1961	182	73	249	3.66E-04	1.20E-03	-7.91E+00	-6.73E+00	3.27	1.19
1962	145	74	196	2.88E-04	8.70E-04	-8.15E+00	-7.05E+00	3.02	1.11
1963	293	76	386	5.67E-04	1.10E-03	-7.48E+00	-6.81E+00	1.94	0.66
1964	211	76	278	4.08E-04	7.10E-04	-7.80E+00	-7.25E+00	1.74	0.55
1965	123	78	158	2.32E-04	3.20E-04	-8.37E+00	-8.05E+00	1.38	0.32
1966	112	77	145	2.14E-04	2.20E-04	-8.45E+00	-8.42E+00	1.03	0.03
1967	120	77	156	2.29E-04	3.10E-04	-8.38E+00	-8.08E+00	1.35	0.30
1968	130	76	171	2.51E-04	4.10E-04	-8.29E+00	-7.80E+00	1.63	0.49
1969	88	75	117	1.72E-04	1.90E-04	-8.67E+00	-8.57E+00	1.10	0.10
1970	64	75	85	1.25E-04	1.60E-04	-8.98E+00	-8.74E+00	1.28	0.24
1971	39	73	53	7.85E-05	9.50E-05	-9.45E+00	-9.26E+00	1.21	0.19
							Average	2.11	0.62
							Standard deviation	1.27	0.50

[a]Geometric bias = exp(0.62) = 1.86; correlation between ln(O) and ln(P) = 0.85.

Table N-14. Computation of Correlation and Bias for Predicted and Observed Concentrations of Uranium in Air at Southeast Perimeter Station[a]

Year	Observed concen. (fCi m^{-3})	Collection efficiency	Corrected observed (fCi m^{-3})	Corrected observed (mg m^{-3})	Predicted (mg m^{-3})	ln (O)	ln (P)	P/O	ln P/O
1958	163	75	217	3.19E-04	6.80E-04	-8.05E+00	-7.29E+00	2.13	0.76
1959	65	76	86	1.26E-04	7.10E-04	-8.98E+00	-7.25E+00	5.65	1.73
1960	173	72	240	3.53E-04	6.60E-04	-7.95E+00	-7.32E+00	1.87	0.63
1961	140	73	192	2.82E-04	6.70E-04	-8.17E+00	-7.31E+00	2.38	0.87
1962	158	74	214	3.14E-04	5.10E-04	-8.07E+00	-7.58E+00	1.62	0.49
1963	209	76	275	4.04E-04	6.20E-04	-7.81E+00	-7.39E+00	1.53	0.43
1964	162	76	213	3.13E-04	4.10E-04	-8.07E+00	-7.80E+00	1.31	0.27
1965	68	78	87	1.28E-04	1.90E-04	-8.96E+00	-8.57E+00	1.48	0.39
1966	76	77	99	1.45E-04	1.30E-04	-8.84E+00	-8.95E+00	0.90	-0.11
1967	96	77	125	1.83E-04	1.80E-04	-8.60E+00	-8.62E+00	0.98	-0.02
1968	141	76	186	2.73E-04	2.40E-04	-8.21E+00	-8.33E+00	0.88	-0.13
1969	90	75	120	1.76E-04	1.10E-04	-8.64E+00	-9.12E+00	0.62	-0.47
1970	36	76	47	6.96E-05	9.00E-05	-9.57E+00	-9.32E+00	1.29	0.26
1971	32	73	44	6.44E-05	5.50E-05	-9.65E+00	-9.81E+00	0.85	-0.16
							Average	1.68	0.35
							Standard deviation	1.25	0.55

[a] Geometric bias = exp(0.35) = 1.42; correlation between ln(O) and ln(P) = 0.79.

Table N-15. Computation of Correlation and Bias for Predicted and Observed Concentrations of Uranium in Air at Southwest Perimeter Station[a]

Year	Observed concen. (fCi m^{-3})	Collection efficiency	Corrected observed (fCi m^{-3})	Corrected observed (mg m^{-3})	Predicted (mg m^{-3})	ln (O)	ln (P)	P/O	ln P/O
1958	74	128	130	1.89E-04	4.00E-04	-8.58E+00	-7.82E+00	2.12	0.75
1959	75	175	177	2.57E-04	4.20E-04	-8.27E+00	-7.78E+00	1.64	0.49
1960	71	487	474	7.16E-04	3.90E-04	-7.24E+00	-7.85E+00	0.54	-0.61
1961	71	217	211	3.19E-04	4.00E-04	-8.05E+00	-7.82E+00	1.25	0.23
1962	73	321	321	4.71E-04	3.00E-04	-7.66E+00	-8.11E+00	0.64	-0.45
1963	75	347	347	5.10E-04	3.70E-04	-7.58E+00	-7.90E+00	0.73	-0.32
1964	75	297	293	4.37E-04	2.50E-04	-7.74E+00	-8.29E+00	0.57	-0.56
1965	76	117	120	1.72E-04	1.10E-04	-8.67E+00	-9.12E+00	0.64	-0.45
1966	75	173	181	2.55E-04	7.90E-05	-8.28E+00	-9.45E+00	0.31	-1.17
1967	76	171	181	2.51E-04	1.00E-04	-8.29E+00	-9.21E+00	0.40	-0.92
1968	75	221	227	3.25E-04	1.40E-04	-8.03E+00	-8.87E+00	0.43	-0.84
1969	74	224	231	3.30E-04	6.30E-05	-8.02E+00	-9.67E+00	0.19	-1.66
1970	75	115	118	1.69E-04	5.30E-05	-8.69E+00	-9.85E+00	0.31	-1.16
1971	72	67	71	9.80E-05	3.20E-05	-9.23E+00	-1.03E+01	0.33	-1.12
							Average	0.72	-0.56
							Standard deviation	0.56	0.68

[a] Geometric bias = exp(-0.56) = 0.57; correlation between ln(O) and ln(P) = 0.65.

Table N-16. Computation of Correlation and Bias for Predicted and Observed Concentrations of Uranium in Air at Northwest Perimeter Station[a]

Year	Observed concen. (fCi m^{-3})	Collection efficiency	Corrected observed (fCi m^{-3})	Corrected observed (mg m^{-3})	Predicted (mg m^{-3})	ln (O)	ln (P)	P/O	ln P/O
1958	109	73	149	2.19E-04	2.20E-04	-8.42E+00	-8.42E+00	1.00	0.00
1959	94	74	127	1.87E-04	2.20E-04	-8.59E+00	-8.42E+00	1.18	0.16
1960	165	70	236	3.47E-04	2.10E-04	-7.97E+00	-8.47E+00	0.61	-0.50
1961	115	70	164	2.42E-04	2.20E-04	-8.33E+00	-8.42E+00	0.91	-0.09
1962	70	71	99	1.45E-04	1.70E-04	-8.84E+00	-8.68E+00	1.17	0.16
1963	113	73	155	2.28E-04	2.00E-04	-8.39E+00	-8.52E+00	0.88	-0.13
1964	90	72	125	1.84E-04	1.40E-04	-8.60E+00	-8.87E+00	0.76	-0.27
1965	39	73	53	7.85E-05	6.70E-05	-9.45E+00	-9.61E+00	0.85	-0.16
1966	38	72	53	7.76E-05	4.70E-05	-9.46E+00	-9.97E+00	0.61	-0.50
1967	43	76	57	8.32E-05	5.30E-05	-9.39E+00	-9.85E+00	0.64	-0.45
1968	97	76	128	1.88E-04	7.00E-05	-8.58E+00	-9.57E+00	0.37	-0.99
1969	49	74	66	9.73E-05	3.20E-05	-9.24E+00	-1.03E+01	0.33	-1.11
1970	36	75	48	7.06E-05	2.70E-05	-9.56E+00	-1.05E+01	0.38	-0.96
1971	38	72	53	7.76E-05	1.70E-05	-9.46E+00	-1.10E+01	0.22	-1.52
							Average	0.71	-0.45
							Standard deviation	0.31	0.51

[a] Geometric bias = exp(-0.45) = 0.64; correlation between ln(O) and ln(P) = 0.86.

Figure N-12 illustrates the temporal trend in P/O ratio for uranium in air at the four perimeter stations. This type of trend analysis can help separate model bias from source term bias. There appears to be a downward slope to the temporal trend, that is, the predictions decrease more rapidly than the observations. One explanation is that the source terms for the early part of this period, especially 1959–1962, are overestimated.

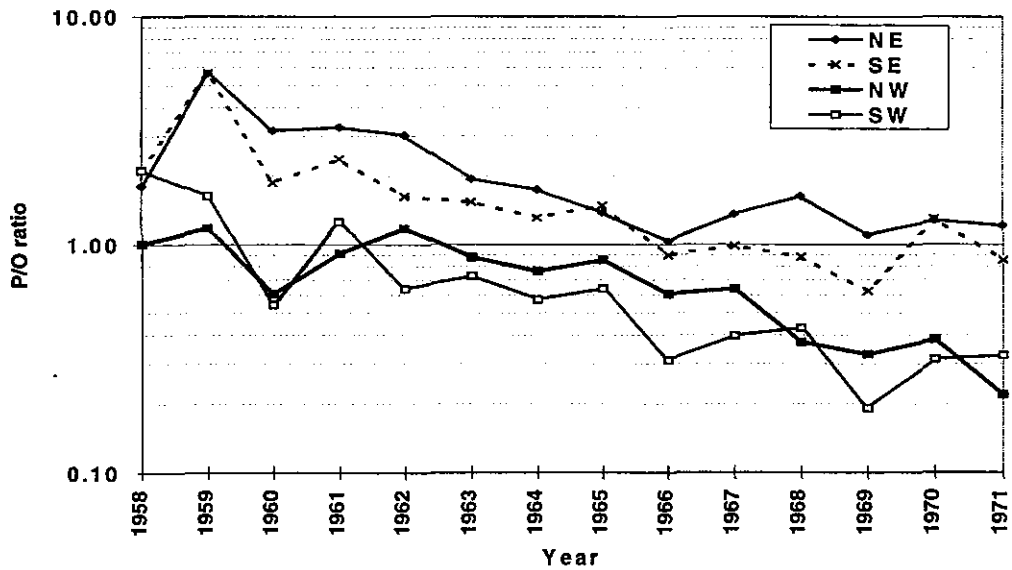

Figure N-12. Temporal trend in P/O ratio at four perimeter stations.

Table N-17. Computation of Correlation and Bias for Predicted and Observed Concentrations of Uranium in Air at Boundary Station BS–1[a]

Year	Observed concen. (fCi m^{-3})	Collection efficiency	Corrected observed (fCi m^{-3})	Corrected observed (mg m^{-3})	Predicted (mg m^{-3})	ln (O)	ln (P)	P/O	ln P/O
1972	11.92	75	15.90	2.34E-05	3.60E-05	-1.07E+01	-1.02E+01	1.54	0.43
1973	20.53	72	28.51	4.19E-05	4.50E-05	-1.01E+01	-1.00E+01	1.07	0.07
1974	22.08	71	31.10	4.57E-05	4.60E-05	-9.99E+00	-9.99E+00	1.01	0.01
1975	25.10	72	34.86	5.12E-05	5.50E-05	-9.88E+00	-9.81E+00	1.07	0.07
1976	21.12	71	29.75	4.37E-05	4.40E-05	-1.00E+01	-1.00E+01	1.01	0.01
1977	11.65	71	16.40	2.41E-05	1.90E-05	-1.06E+01	-1.09E+01	0.79	-0.24
1978	8.19	74	11.06	1.63E-05	5.30E-06	-1.10E+01	-1.21E+01	0.33	-1.12
1979	13.28	70	18.97	2.79E-05	5.80E-06	-1.05E+01	-1.21E+01	0.21	-1.57
1980	4.17	73	5.71	8.4E-06	7.90E-06	-1.17E+01	-1.17E+01	0.94	-0.06
1981	7.96	71	11.21	1.65E-05	1.20E-05	-1.10E+01	-1.13E+01	0.73	-0.32
1982	15.64	73	21.43	3.15E-05	9.60E-06	-1.04E+01	-1.16E+01	0.30	-1.19
1983	21.45	72	29.79	4.38E-05	8.10E-06	-1.00E+01	-1.17E+01	0.18	-1.69
1984	17.18	74	23.22	3.41E-05	1.60E-05	-1.03E+01	-1.10E+01	0.47	-0.76
1985	2.96	74	4.00	5.88E-06	6.50E-06	-1.20E+01	-1.19E+01	1.11	0.10
1986	2.84	72	3.94	5.8E-06	5.70E-06	-1.21E+01	-1.21E+01	0.98	-0.02
1987	3.31	71	4.66	6.85E-06	4.40E-06	-1.19E+01	-1.23E+01	0.64	-0.44
1988	2.60	64	4.06	5.97E-06	2.60E-06	-1.20E+01	-1.29E+01	0.44	-0.83
							Average	0.77	-0.44
							Standard deviation	0.41	0.64

[a] Geometric bias = exp(-0.44) = 0.64; correlation between ln(O) and ln(P) = 0.62.

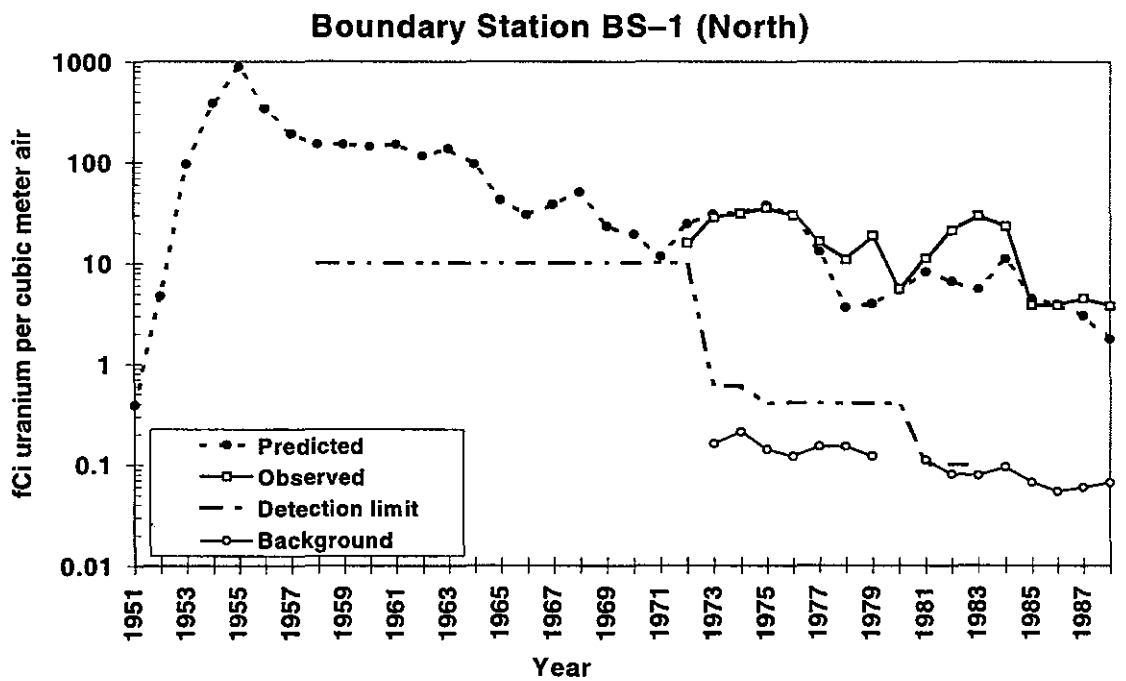

Figure N-13. Summary of observed and predicted concentrations of uranium in air at Boundary Station BS–1, north of the FMPC.

Table N-18. Computation of Correlation and Bias for Predicted and Observed Concentrations of Uranium in Air at Boundary Station BS–2[a]

Year	Observed concen. (fCi m^{-3})	Collection efficiency	Corrected observed (fCi m^{-3})	Corrected observed (mg m^{-3})	Predicted (mg m^{-3})	ln (O)	ln (P)	P/O	ln P/O
1972	12.03	75	16.04	2.36E-05	7.30E-05	-1.07E+01	-9.53E+00	3.10	1.13
1973	17.46	72	24.25	3.56E-05	9.20E-05	-1.02E+01	-9.29E+00	2.58	0.95
1974	17.19	71	24.21	3.56E-05	9.30E-05	-1.02E+01	-9.28E+00	2.61	0.96
1975	22.16	72	30.78	4.53E-05	1.10E-04	-1.00E+01	-9.12E+00	2.43	0.89
1976	12.64	71	17.81	2.62E-05	8.80E-05	-1.06E+01	-9.34E+00	3.36	1.21
1977	8.26	71	11.64	1.71E-05	3.90E-05	-1.10E+01	-1.02E+01	2.28	0.82
1978	8.63	76	11.36	1.67E-05	9.80E-06	-1.10E+01	-1.15E+01	0.59	-0.53
1979	7.72	71	10.87	1.6E-05	1.10E-05	-1.10E+01	-1.14E+01	0.69	-0.37
1980	3.53	75	4.71	6.93E-06	1.50E-05	-1.19E+01	-1.11E+01	2.17	0.77
1981	8.75	71	12.32	1.81E-05	2.20E-05	-1.09E+01	-1.07E+01	1.21	0.19
1982	8.75	74	11.83	1.74E-05	1.80E-05	-1.10E+01	-1.09E+01	1.04	0.03
1983	14.51	73	19.88	2.92E-05	1.50E-05	-1.04E+01	-1.11E+01	0.51	-0.67
1984	12.84	74	17.35	2.55E-05	3.10E-05	-1.06E+01	-1.04E+01	1.22	0.20
1985	3.11	77	4.04	5.94E-06	1.20E-05	-1.20E+01	-1.13E+01	2.02	0.70
1986	2.87	75	3.83	5.63E-06	1.00E-05	-1.21E+01	-1.15E+01	1.78	0.58
1987	3.08	74	4.16	6.12E-06	7.70E-06	-1.20E+01	-1.18E+01	1.26	0.23
1988	2.57	69	3.72	5.48E-06	3.90E-06	-1.21E+01	-1.25E+01	0.71	-0.34
							Average	1.84	0.45
							Standard deviation	0.95	0.64

[a]**Geometric bias = exp(0.45) = 1.57; correlation between ln(O) and ln(P) = 0.72.**

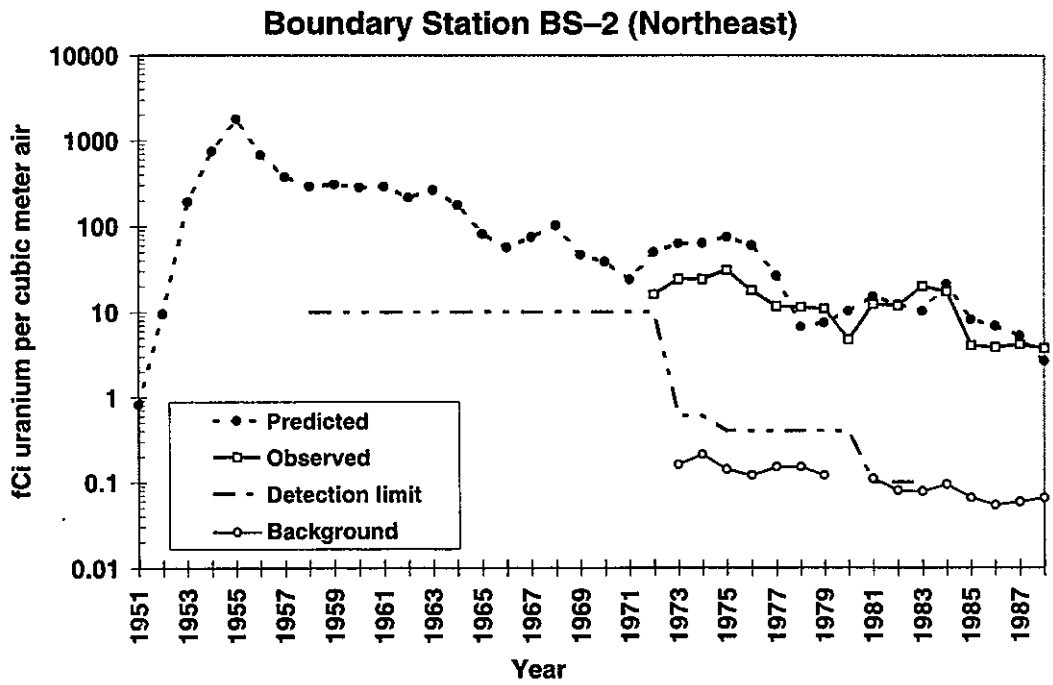

Figure N-14. Summary of observed and predicted concentrations of uranium in air at Boundary Station BS–2, northeast of the FMPC.

Table N-19. Computation of Correlation and Bias for Predicted and Observed Concentrations of Uranium in Air at Boundary Station BS–3[a]

Year	Observed concen. (fCi m^{-3})	Collection efficiency	Corrected observed (fCi m^{-3})	Corrected observed (mg m^{-3})	Predicted (mg m^{-3})	ln (O)	ln (P)	P/O	ln P/O
1972	18.34	75	24.45	3.59E-05	1.00E-04	-1.02E+01	-9.21E+00	2.78	1.02
1973	24.70	72	34.31	5.04E-05	1.30E-04	-9.89E+00	-8.95E+00	2.58	0.95
1974	17.25	72	23.96	3.52E-05	1.30E-04	-1.03E+01	-8.95E+00	3.69	1.31
1975	27.15	72	37.71	5.54E-05	1.60E-04	-9.80E+00	-8.74E+00	2.89	1.06
1976	17.70	71	24.93	3.66E-05	1.30E-04	-1.02E+01	-8.95E+00	3.55	1.27
1977	12.94	72	17.97	2.64E-05	5.60E-05	-1.05E+01	-9.79E+00	2.12	0.75
1978	16.74	76	22.02	3.24E-05	1.40E-05	-1.03E+01	-1.12E+01	0.43	-0.84
1979	19.30	72	26.81	3.94E-05	1.50E-05	-1.01E+01	-1.11E+01	0.38	-0.97
1980	4.62	75	6.16	9.06E-06	2.10E-05	-1.16E+01	-1.08E+01	2.32	0.84
1981	10.93	72	15.18	2.23E-05	3.20E-05	-1.07E+01	-1.03E+01	1.43	0.36
1982	14.40	74	19.46	2.86E-05	2.60E-05	-1.05E+01	-1.06E+01	0.91	-0.10
1983	24.75	74	33.44	4.92E-05	2.20E-05	-9.92E+00	-1.07E+01	0.45	-0.80
1984	22.07	75	29.43	4.33E-05	4.40E-05	-1.00E+01	-1.00E+01	1.02	0.02
1985	5.57	77	7.23	1.06E-05	1.70E-05	-1.15E+01	-1.10E+01	1.60	0.47
1986	6.15	75	8.20	1.21E-05	1.40E-05	-1.13E+01	-1.12E+01	1.16	0.15
1987	6.76	74	9.14	1.34E-05	1.10E-05	-1.12E+01	-1.14E+01	0.82	-0.20
1988	3.59	70	5.13	7.54E-06	5.40E-06	-1.18E+01	-1.21E+01	0.72	-0.33
							Average	1.87	0.38
							Standard deviation	1.14	0.80

[a]**Geometric bias = exp(0.38) = 1.46; correlation between ln(O) and ln(P) = 0.50.**

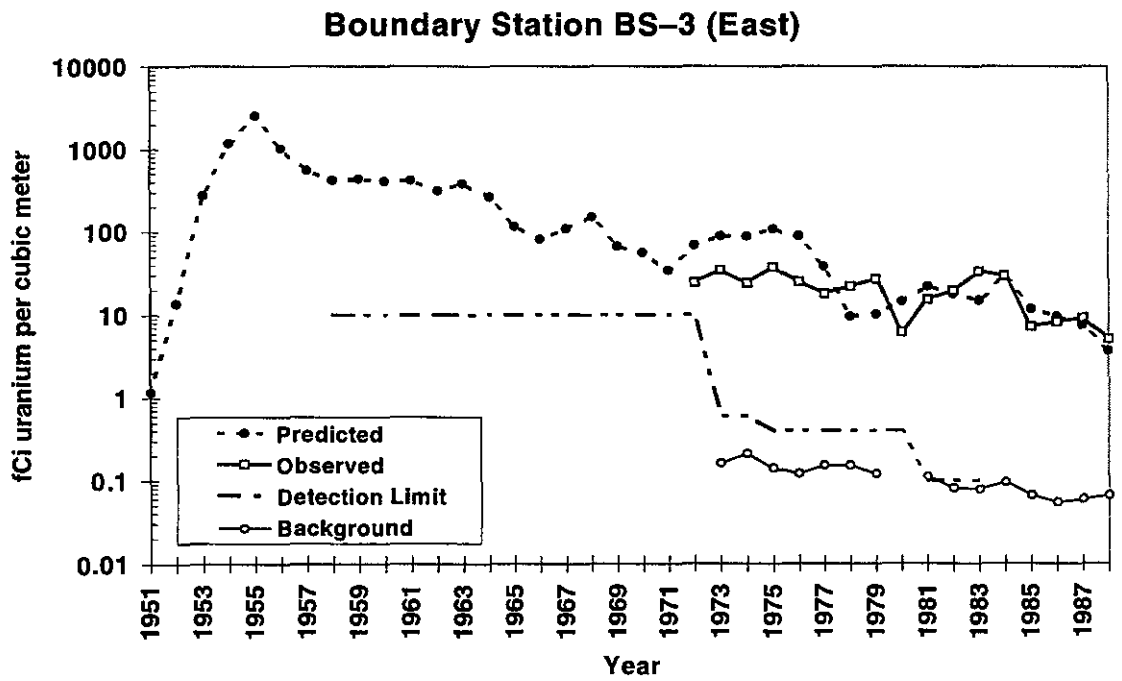

Figure N-15. Summary of observed and predicted concentrations of uranium in air at Boundary Station BS–3, east of the FMPC.

Table N-20. Computation of Correlation and Bias for Predicted and Observed Concentrations of Uranium in Air at Boundary Station BS–4[a]

Year	Observed concen. (fCi m^{-3})	Collection efficiency	Corrected observed (fCi m^{-3})	Corrected observed (mg m^{-3})	Predicted (mg m^{-3})	ln (O)	ln (P)	P/O	ln P/O
1972	5.81	75	7.74	1.14E-05	2.90E-05	-1.14E+01	-1.04E+01	2.55	0.94
1973	6.23	72	8.65	1.27E-05	3.70E-05	-1.13E+01	-1.02E+01	2.91	1.07
1974	4.84	71	6.82	1.00E-05	3.80E-05	-1.15E+01	-1.02E+01	3.79	1.33
1975	7.66	71	10.79	1.59E-05	4.50E-05	-1.11E+01	-1.00E+01	2.84	1.04
1976	5.36	71	7.56	1.11E-05	3.60E-05	-1.14E+01	-1.02E+01	3.24	1.18
1977	4.11	71	5.80	8.52E-06	1.60E-05	-1.17E+01	-1.10E+01	1.88	0.63
1978	5.19	75	6.92	1.02E-05	4.10E-06	-1.15E+01	-1.24E+01	0.40	-0.91
1979	8.12	71	11.44	1.68E-05	4.50E-06	-1.10E+01	-1.23E+01	0.27	-1.32
1980	3.48	74	4.70	6.91E-06	6.10E-06	-1.19E+01	-1.20E+01	0.88	-0.12
1981	3.61	71	5.08	7.47E-06	9.20E-06	-1.18E+01	-1.16E+01	1.23	0.21
1982	4.28	74	5.78	8.5E-06	7.50E-06	-1.17E+01	-1.18E+01	0.88	-0.13
1983	8.61	73	11.80	1.73E-05	6.30E-06	-1.10E+01	-1.20E+01	0.36	-1.01
1984	4.72	74	6.38	9.38E-06	1.30E-05	-1.16E+01	-1.13E+01	1.39	0.33
1985	2.13	76	2.80	4.12E-06	4.90E-06	-1.24E+01	-1.22E+01	1.19	0.17
1986	1.74	74	2.35	3.46E-06	4.30E-06	-1.26E+01	-1.24E+01	1.24	0.22
1987	1.75	73	2.40	3.52E-06	3.20E-06	-1.26E+01	-1.27E+01	0.91	-0.10
1988	0.77	67	1.15	1.69E-06	1.70E-06	-1.33E+01	-1.33E+01	1.01	0.01
							Average	1.70	0.24
							Standard deviation	1.17	0.86

[a]Geometric bias = exp(0.24) = 1.28; correlation between ln(O) and ln(P) = 0.30.

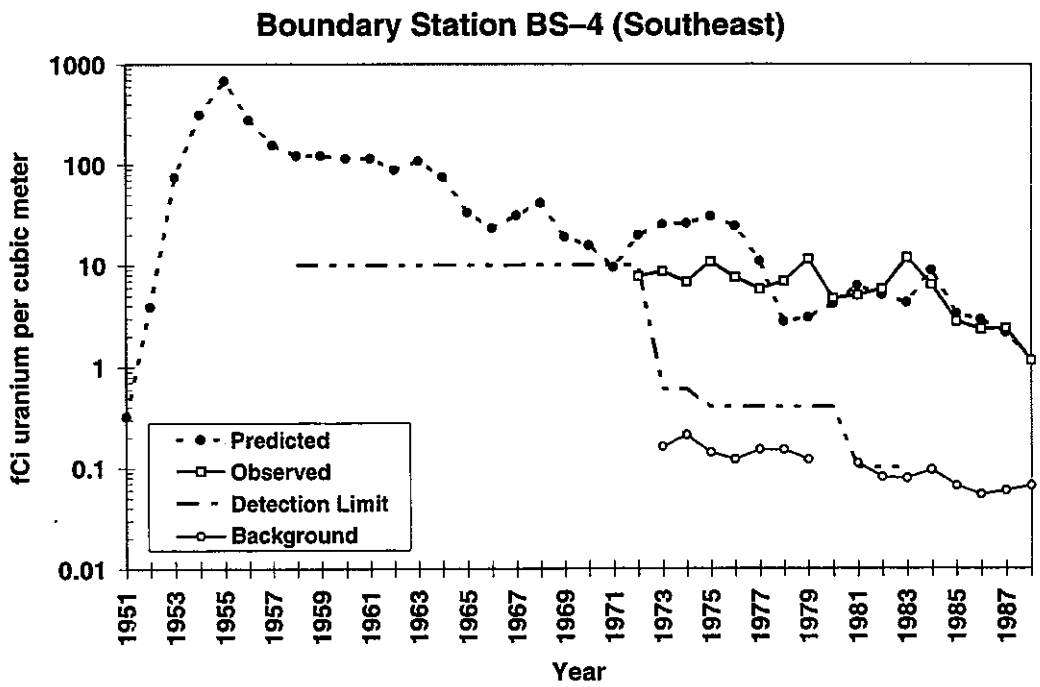

Figure N-16. Summary of observed and predicted concentrations of uranium in air at Boundary Station BS–4, southeast of the FMPC.

Table N-21. Computation of Correlation and Bias for Predicted and Observed Concentrations of Uranium in Air at Boundary Station BS–5[a]

Year	Observed concen. (fCi m^{-3})	Collection efficiency	Corrected observed (fCi m^{-3})	Corrected observed (mg m^{-3})	Predicted (mg m^{-3})	ln (O)	ln (P)	P/O	ln P/O
1972	7.09	74	9.58	1.41E-05	2.40E-05	-1.12E+01	-1.06E+01	1.71	0.53
1973	7.04	72	9.78	1.44E-05	3.00E-05	-1.12E+01	-1.04E+01	2.09	0.74
1974	7.21	71	10.15	1.49E-05	3.10E-05	-1.11E+01	-1.04E+01	2.08	0.73
1975	9.14	71	12.88	1.89E-05	3.70E-05	-1.09E+01	-1.02E+01	1.95	0.67
1976	5.88	71	8.28	1.22E-05	2.90E-05	-1.13E+01	-1.04E+01	2.38	0.87
1977	5.24	71	7.38	1.08E-05	1.30E-05	-1.14E+01	-1.13E+01	1.20	0.18
1978	10.37	75	13.82	2.03E-05	3.40E-06	-1.08E+01	-1.26E+01	0.17	-1.79
1979	10.77	70	15.38	2.26E-05	3.70E-06	-1.07E+01	-1.25E+01	0.16	-1.81
1980	3.01	74	4.07	5.99E-06	5.00E-06	-1.20E+01	-1.22E+01	0.84	-0.18
1981	5.28	71	7.43	1.09E-05	7.40E-06	-1.14E+01	-1.18E+01	0.68	-0.39
1982	7.24	74	9.78	1.44E-05	6.10E-06	-1.11E+01	-1.20E+01	0.42	-0.86
1983	9.94	73	13.61	2E-05	5.10E-06	-1.08E+01	-1.22E+01	0.25	-1.37
1984	6.42	74	8.68	1.28E-05	1.00E-05	-1.13E+01	-1.15E+01	0.78	-0.24
1985	2.21	76	2.91	4.27E-06	4.00E-06	-1.24E+01	-1.24E+01	0.94	-0.07
1986	1.58	74	2.14	3.14E-06	3.40E-06	-1.27E+01	-1.26E+01	1.08	0.08
1987	1.77	73	2.42	3.56E-06	2.60E-06	-1.25E+01	-1.29E+01	0.73	-0.32
1988	0.83	67	1.24	1.82E-06	1.40E-06	-1.32E+01	-1.35E+01	0.77	-0.26
							Average	1.12	-0.21
							Standard deviation	0.78	0.93

[a]**Geometric bias = exp(-0.21) = 0.81; correlation between ln(O) and ln(P) = 0.18.**

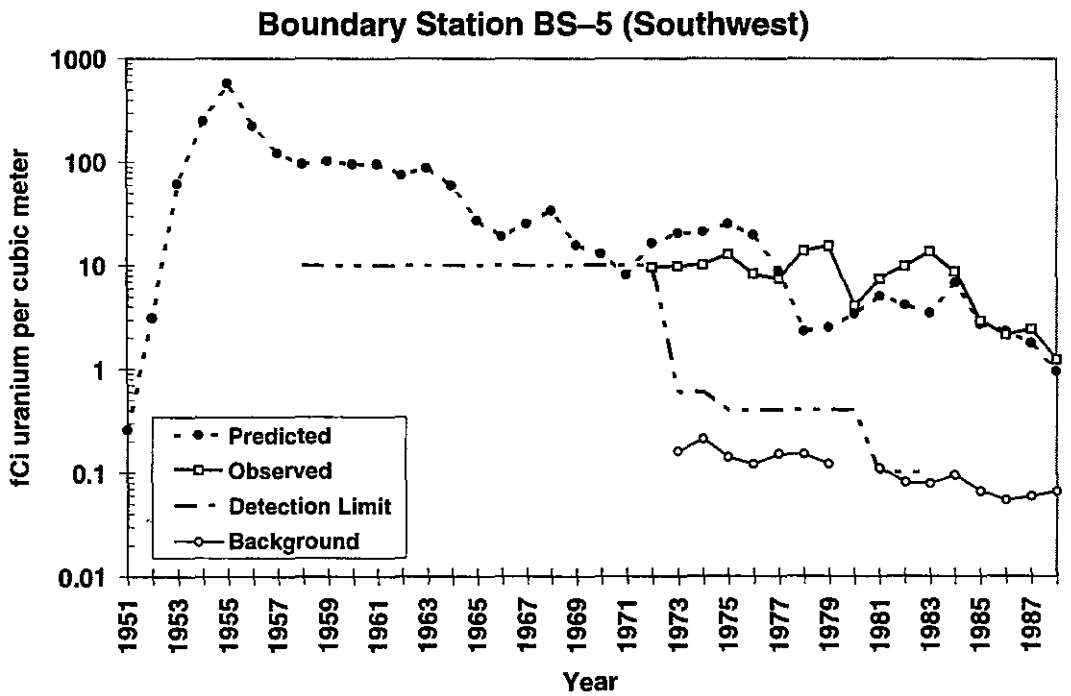

Figure N-17. Summary of observed and predicted concentrations of uranium in air at Boundary Station BS–5, southwest of the FMPC.

Table N-22. Computation of Correlation and Bias for Predicted and Observed Concentrations of Uranium in Air at Boundary Station BS–6[a]

Year	Observed concen. (fCi m^{-3})	Collection efficiency	Corrected observed (fCi m^{-3})	Corrected observed (mg m^{-3})	Predicted (mg m^{-3})	ln (O)	ln (P)	P/O	ln P/O
1972	18.80	74	25.40	3.73E-05	5.00E-05	-1.02E+01	-9.90E+00	1.34	0.29
1973	18.06	72	25.08	3.69E-05	6.20E-05	-1.02E+01	-9.69E+00	1.68	0.52
1974	12.16	71	17.13	2.52E-05	6.30E-05	-1.06E+01	-9.67E+00	2.50	0.92
1975	17.67	71	24.89	3.66E-05	7.50E-05	-1.02E+01	-9.50E+00	2.05	0.72
1976	10.54	71	14.85	2.18E-05	6.00E-05	-1.07E+01	-9.72E+00	2.75	1.01
1977	5.07	70	7.24	1.06E-05	2.70E-05	-1.15E+01	-1.05E+01	2.54	0.93
1978	7.01	71	9.88	1.45E-05	7.80E-06	-1.11E+01	-1.18E+01	0.54	-0.62
1979	9.16	68	13.48	1.98E-05	8.60E-06	-1.08E+01	-1.17E+01	0.43	-0.83
1980	4.05	71	5.71	8.4E-06	1.20E-05	-1.17E+01	-1.13E+01	1.43	0.36
1981	5.01	69	7.27	1.07E-05	1.70E-05	-1.14E+01	-1.10E+01	1.59	0.46
1982	7.92	71	11.16	1.64E-05	1.40E-05	-1.10E+01	-1.12E+01	0.85	-0.16
1983	11.35	70	16.21	2.38E-05	1.20E-05	-1.06E+01	-1.13E+01	0.50	-0.69
1984	9.61	72	13.35	1.96E-05	2.20E-05	-1.08E+01	-1.07E+01	1.12	0.11
1985	2.47	72	3.43	5.04E-06	9.60E-06	-1.22E+01	-1.16E+01	1.90	0.64
1986	1.71	70	2.44	3.59E-06	8.50E-06	-1.25E+01	-1.17E+01	2.37	0.86
1987	2.39	68	3.51	5.17E-06	6.80E-06	-1.22E+01	-1.19E+01	1.32	0.27
1988	0.90	61	1.48	2.17E-06	4.30E-06	-1.30E+01	-1.24E+01	1.98	0.68
							Average	1.52	0.26
							Standard deviation	0.77	0.62

[a]**Geometric bias = exp(0.26) = 1.30; correlation between ln(O) and ln(P) = 0.67.**

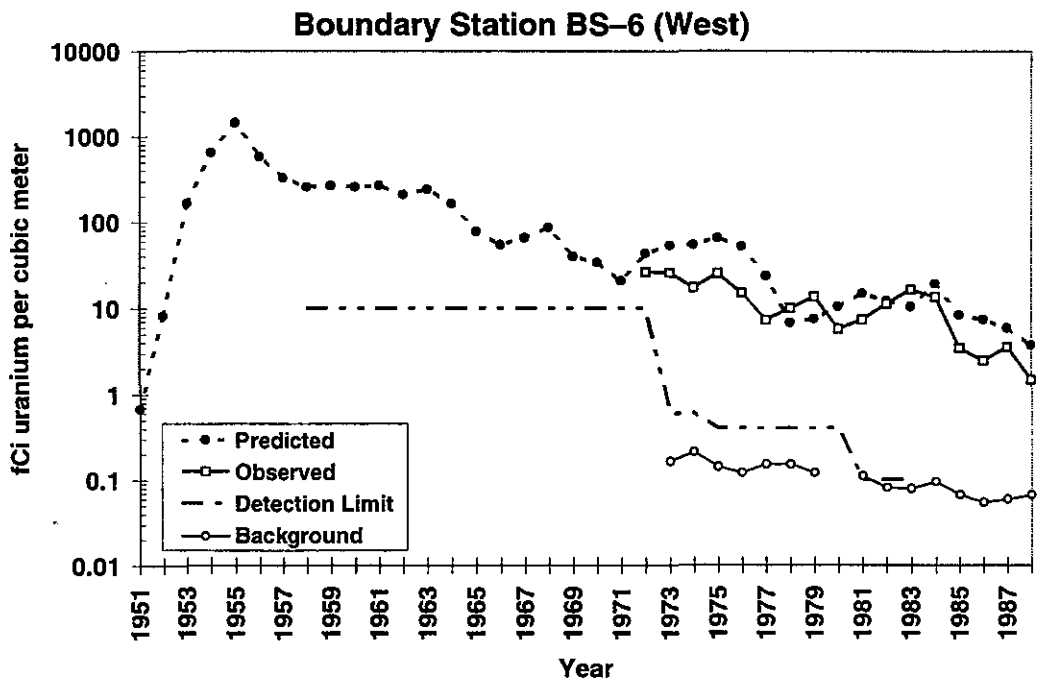

Figure N-18. Summary of observed and predicted concentrations of uranium in air at Boundary Station BS–6, west of the FMPC.

Table N-23. Computation of Correlation and Bias for Predicted and Observed Concentrations of Uranium in Air at Boundary Station BS–7[a]

Year	Observed concen. (fCi m^{-3})	Collection efficiency	Corrected observed (fCi m^{-3})	Corrected observed (mg m^{-3})	Predicted (mg m^{-3})	ln (O)	ln (P)	P/O	ln P/O
1972		75			1.20E-05		-1.13E+01		
1973	26.03	72	36.15	5.31E-05	1.60E-05	-9.84E+00	-1.10E+01	0.30	-1.20
1974	12.59	72	17.48	2.57E-05	1.60E-05	-1.06E+01	-1.10E+01	0.62	-0.47
1975		72			1.90E-05		-1.09E+01		
1976	12.28	72	17.06	2.51E-05	1.50E-05	-1.06E+01	-1.11E+01	0.60	-0.51
1977		71			6.60E-06		-1.19E+01		
1978		75			1.70E-06		-1.33E+01		
1979		71			1.90E-06		-1.32E+01		
1980		74			2.60E-06		-1.29E+01		
1981	2.69	71	3.78	5.56E-06	3.90E-06	-1.21E+01	-1.25E+01	0.70	-0.36
1982	4.05	74	5.47	8.05E-06	3.20E-06	-1.17E+01	-1.27E+01	0.40	-0.92
1983	4.85	73	6.65	9.78E-06	2.70E-06	-1.15E+01	-1.28E+01	0.28	-1.29
1984	4.42	74	5.98	8.79E-06	5.30E-06	-1.16E+01	-1.21E+01	0.60	-0.51
1985	1.11	76	1.46	2.15E-06	2.10E-06	-1.31E+01	-1.31E+01	0.98	-0.02
1986	0.92	74	1.24	1.83E-06	1.80E-06	-1.32E+01	-1.32E+01	0.98	-0.02
1987	1.40	73	1.92	2.82E-06	1.40E-06	-1.28E+01	-1.35E+01	0.50	-0.70
1988	0.50	67	0.75	1.1E-06	7.30E-07	-1.37E+01	-1.41E+01	0.67	-0.41
							Average	0.56	-0.66
							Standard deviation	0.23	0.44

[a]Geometric bias = exp(-0.66) = 0.52; correlation between ln(O) and ln(P) = 0.90.

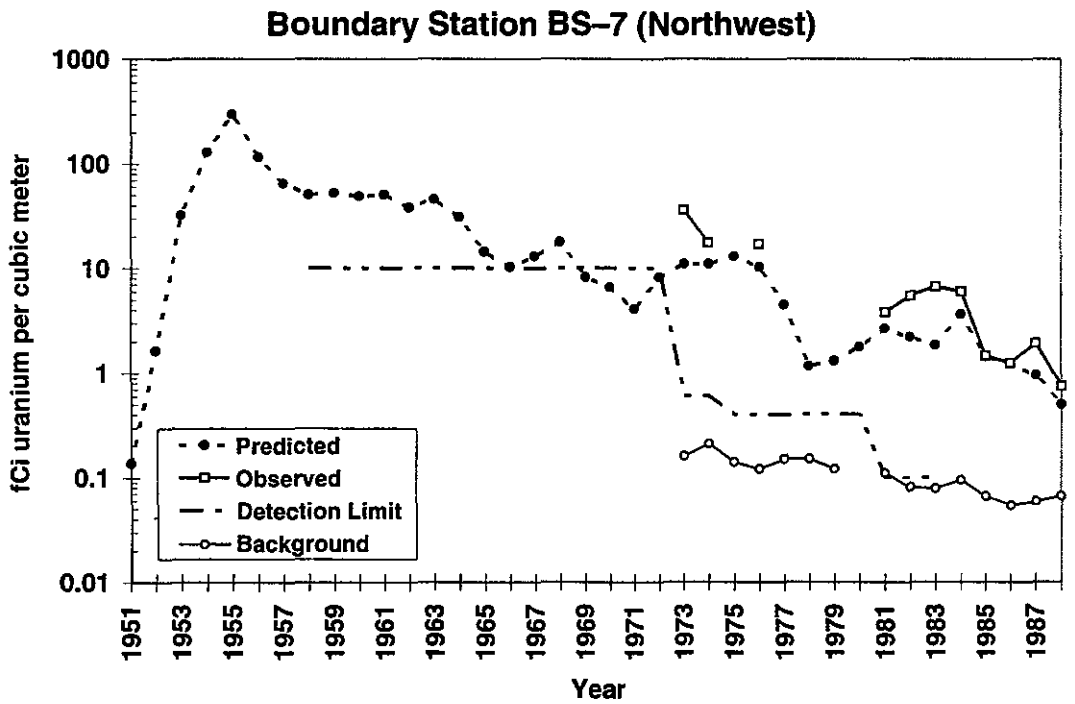

Figure N-19. Summary of observed and predicted concentrations of uranium in air at Boundary Station BS–7, northwest of the FMPC.

Table N-24. Temporal Trend in P/O for Air at Boundary Stations

Year	BS-1	BS-2	BS-3	BS-4	BS-5	BS-6	BS-7	All-station average
1972	1.54	3.10	2.78	2.55	1.71	1.34		**2.2**
1973	1.07	2.58	2.58	2.91	2.09	1.68	0.30	**1.9**
1974	1.01	2.61	3.69	3.79	2.08	2.50	0.62	**2.3**
1975	1.07	2.43	2.89	2.84	1.95	2.05		**2.2**
1976	1.01	3.36	3.55	3.24	2.38	2.75	0.60	**2.4**
1977	0.79	2.28	2.12	1.88	1.20	2.54		**1.8**
1978	0.33	0.59	0.43	0.40	0.17	0.54		**0.4**
1979	0.21	0.69	0.38	0.27	0.16	0.43		**0.4**
1980	0.94	2.17	2.32	0.88	0.84	1.43		**1.4**
1981	0.73	1.21	1.43	1.23	0.68	1.59	0.70	**1.1**
1982	0.30	1.04	0.91	0.88	0.42	0.85	0.40	**0.7**
1983	0.18	0.51	0.45	0.36	0.25	0.50	0.28	**0.4**
1984	0.47	1.22	1.02	1.39	0.78	1.12	0.60	**0.9**
1985	1.11	2.02	1.60	1.19	0.94	1.90	0.98	**1.4**
1986	0.98	1.78	1.16	1.24	1.08	2.37	0.98	**1.4**
1987	0.64	1.26	0.82	0.91	0.73	1.32	0.50	**0.9**
1988	0.44	0.71	0.72	1.01	0.77	1.98	0.67	**0.9**
1972–1988 average	**0.8**	**1.7**	**1.7**	**1.6**	**1.1**	**1.6**	**0.6**	

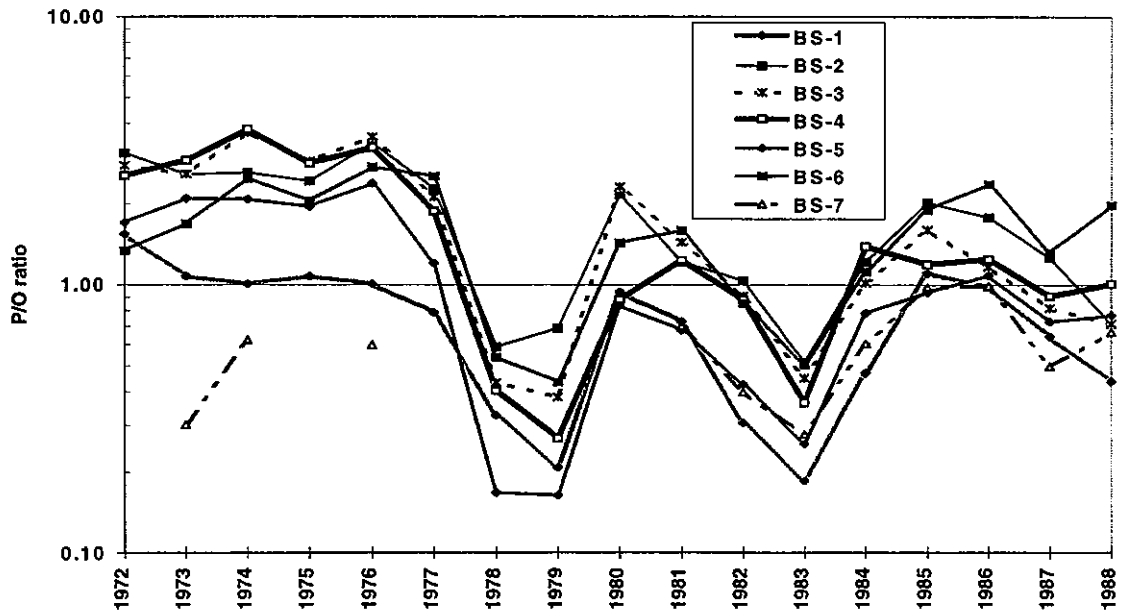

Figure N-20. Temporal trend in predicted-to-observed (P/O) ratios at boundary air monitoring stations. As Table N-24 shows, the long-term agreement is quite good; all boundary stations except BS–4 show agreement within a factor of 2 when averaged over the entire time interval. Individual years show more significant discrepancies. The dips in the P/O ratios for all stations in 1978, 1979, and 1983 suggest something other than systematic model bias, which would result in a similar P/O ratio for all years. For example, the source term could be underestimated in those years, or the actual meteorological conditions could have resulted in less dispersion than the generalized weather data set predicted.

Deposition of Uranium on Gummed-Film

Deposition of uranium around the FMPC was monitored using gummed-film between 1954 and 1964. Table N-25 illustrates the computation of correlation and bias for deposition rates of uranium at one gummed-film station, NE–1, which is on the northeast corner of the production area perimeter. The same computation was conducted for 25 locations within the boundary (see map in validation section of Volume I).

Table N-25. Computation of Correlation and Bias for Predicted and Observed Deposition Rates of Uranium at Gummed-Film Station NE–1[a]

	Observed ($mg\ m^{-2}\ y^{-1}$)	Predicted ($mg\ m^{-2}\ y^{-1}$)	ln(O)	ln(P)	P/O	ln(P/O)
1954	1207	3000	7.10E+00	8.01E+00	2.49	0.91
1955	11271	6900	9.33E+00	8.84E+00	0.61	-0.49
1956	4360	3100	8.38E+00	8.04E+00	0.71	-0.34
1957	1852	2100	7.52E+00	7.65E+00	1.13	0.13
1958	1853	1900	7.52E+00	7.55E+00	1.03	0.03
1959	1451	2100	7.28E+00	7.65E+00	1.45	0.37
1960	1830	2100	7.51E+00	7.65E+00	1.15	0.14
1961	1113	2300	7.01E+00	7.74E+00	2.07	0.73
1962	1804	1500	7.50E+00	7.31E+00	0.83	-0.18
1963	3839	1600	8.25E+00	7.38E+00	0.42	-0.88
1964	3157	1100	8.06E+00	7.00E+00	0.35	-1.05
sum	33,737	27,700				
				Average	1.11	-0.06
				Standard deviation	0.67	0.61

[a]Geometric bias = exp(-0.06) = 0.94; correlation between ln(O) and ln(P) = 0.49.

To use all the stations, which were monitored over a variety of different time periods, we compared the *cumulative* observed deposition to the cumulative predicted deposition over the same interval. These data are compiled in Table N-26. Overall, the predicted deposition is less than the adjusted gummed-film measurements (geometric bias of 0.41). Because of the primary importance of inhalation rather than exposure pathways following deposition, we preferred that our calibration preserve good agreement with historic air monitoring data. One possibility for the deposition bias is that the collection efficiency used to correct the gummed film observations is too low, but this cannot be confirmed with information available to us.

Additional general discussion and interpretation of the deposition measurements compared to predictions is presented in the validation section of Volume I.

Table N-26. Computation of Bias and Correlation for Predicted and Observed Cumulative Deposition of Uranium[a]

Station	Years compared	Distance from FMPC (km)	Cumulative observed deposition (mg U m^{-2})	Cumulative predicted deposition (mg U m^{-2})	P/O	ln(P/O)
N-1	1954–1964	0.34	41754	32400	0.78	-0.25
N-2	1957–1964	0.72	6645	3280	0.49	-0.71
N-3	1957–1964	1	4496	2390	0.53	-0.63
NE-1	1954–1964	0.51	33737	27700	0.82	-0.20
NE-2	1957–1964	0.99	8767	6440	0.73	-0.31
NE-3	1957–1964	1.2	5207	4080	0.78	-0.24
NE-4b	1961–1964	4.2	1239	720	0.58	-0.54
E-1	1954–1964	0.32	101362	77000	0.76	-0.27
E-2	1957–1964	0.73	16943	7310	0.43	-0.84
SE–1	1954–1964	0.51	41984	15910	0.38	-0.97
SE-2	1957–1964	0.98	7425	3800	0.51	-0.67
SE-3	1957–1964	1.6	4297	1750	0.41	-0.90
S-1	1954–1964	0.25	160350	28000	0.17	-1.75
S-2	1957–1964	0.87	8566	2050	0.24	-1.43
S-3	1957–1964	1.4	5411	1540	0.28	-1.26
SW-1	1954–1964	0.52	53133	9340	0.18	-1.74
SW-3	1957–1964	1.2	7993	1930	0.24	-1.42
W-1	1954–1964	0.33	48831	34800	0.71	-0.34
W-2	1957–1964	0.62	18347	4430	0.24	-1.42
W-3	1957–1964	1.1	5626	2710	0.48	-0.73
NW-1	1954–1964	0.51	15537	6550	0.42	-0.86
NW-3	1957–1964	1.6	4111	1019	0.25	-1.39
A	1957–1964	0.22	148254	48300	0.33	-1.12
B	1955–1964	0.1	221543	103400	0.47	-0.76
C	1955–1964	0.11	206971	42300	0.20	-1.59
				Average	0.46	-0.89

Geometric Bias = exp (-0.89) = 0.41

[a] Different locations were monitored during certain years (see column 2). Therefore, the absolute deposition amounts shown are not comparable among locations.

Uranium in Soil

The historical measurements of uranium in surface soil are reviewed in Shleien et al. (1995). One of the earliest sets of data on uranium in surface soil was presented in Ross (1959). The soil samples were taken to a depth of 2.5 cm (1 in.) near the gummed-film monitoring stations (total of 22 locations). Figure N-21 presents these data as a function of distance. It is clear that large amounts of uranium were deposited within the site perimeter (approximately 0.5 km from the FMPC center). The maximum concentration measured onsite is over 1000 times higher than natural background levels of around 2 pCi per gram of soil.

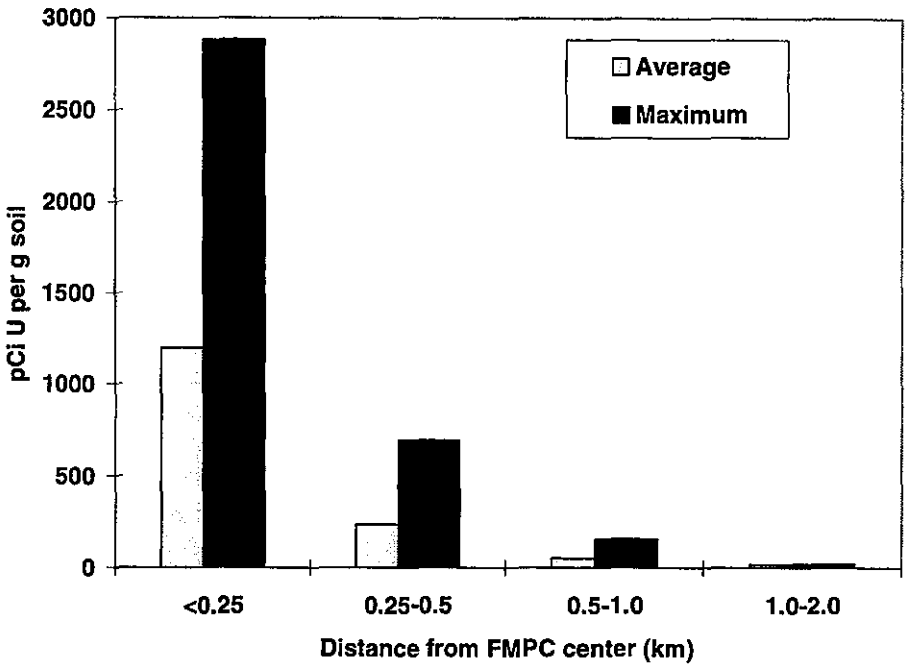

Figure N-21. Measured concentration of uranium in surface soil with distance from the FMPC in 1959 (Ross 1959). Background concentrations of natural uranium are around 2 picocuries (pCi) U per gram (g) of soil. Large concentrations of uranium were measured in soil within the FMPC perimeter (about 0.5 km from the FMPC center). The sample size in this early study was small. The number of samples in each group, beginning closest to the site, was 3, 4, 8, and 7.

Although soil samples were taken in conjunction with vegetation periodically throughout the 1960s, no information on sampling depth was located. A routine program for monitoring of uranium in soil at locations on the FMPC boundary was begun in 1971. This program and the associated data are discussed in Appendix C. These time-series data provided an opportunity for validation of predicted amounts of uranium in soil, based on our reconstructed source terms (Voillequé et al. 1995) and model of uranium dynamics in soil (Appendix B). Figure N-22 compares predicted concentrations of uranium in surface soil at the boundary stations with the measured values. Because of the importance of the earlier time period, the 1959 sampling data were also included, after adjusting them for the difference in sampling depth, based on a profile of uranium in soil from 1976 (Figure N-23).

The computation of geometric bias (P/O ratio) for uranium in soil is documented in Tables N-27 through N-33. The predicted soil concentrations in the plots and P/O tables are based on a surface soil compartment with a depth of 10 cm (4 in.). In addition to use in this validation, this soil compartment is further used in the model to calculate uptake of uranium by the roots of plants. Another shallower surface soil compartment of 0.5 cm (0.2 in.) is used to calculate the amount of uranium in air from resuspended particles (Appendix D).

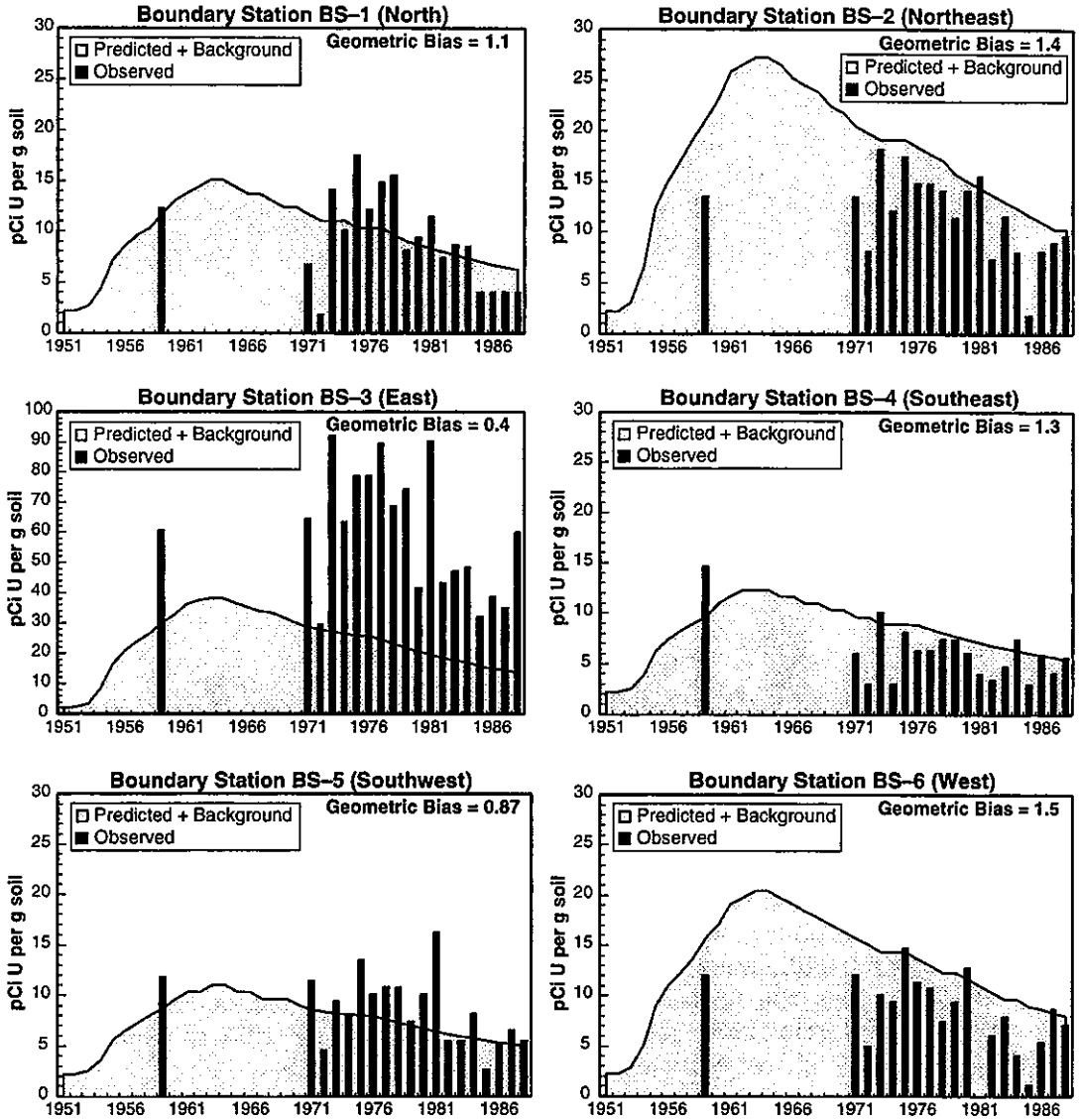

Figure N-22. Comparison of predicted and observed concentrations of uranium in soil [10-cm (4-in.) depth] at six locations on the FMPC boundary. A background (Bkgd) concentration of 2.2 pCi g^{-1} was added to the predicted values before comparison to observations. The BS–3 location is near the old solid waste incinerator and is known to be contaminated by ash residues. Routine monitoring at BS–7 did not begin until 1981 and is not shown here. The geometric bias at BS–7 was 1.4.

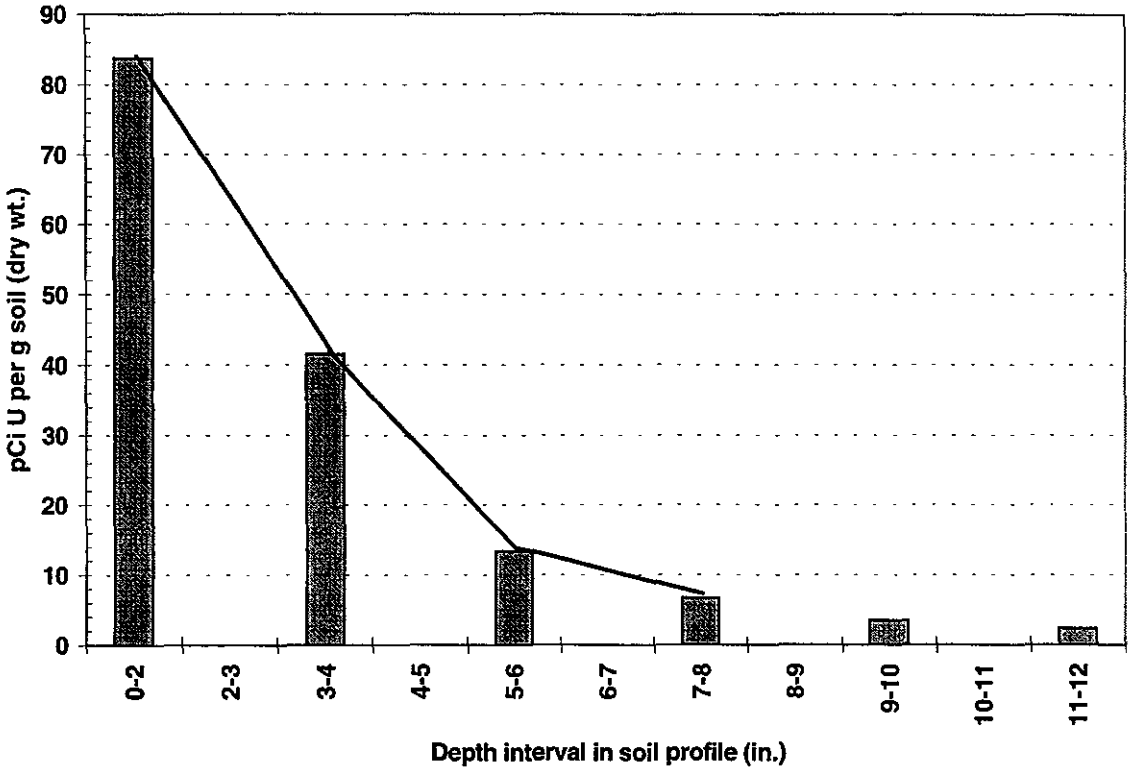

Figure N-23. Vertical profile of uranium in soil at a location near boundary station BS–3 in 1976 (Boback et al. 1977). The authors estimated vertical movement of uranium through the soil column at about 0.5 in. per year. Based on this profile, the concentration in a 1-in. sample is estimated to be about 1.24 times the concentration in a 10-cm (4-in.) sample. The soil sampling data from 1959 (1-in. depth) were divided by 1.24 to permit comparison with other concentrations based on a 10-cm depth.

Table N-27. Computation of Correlation and Bias for Predicted and Observed Concentrations of Uranium in Soil (pCi g^{-1}) at Boundary Station BS–1[a]

Year	Predicted	Predicted + background	Observed (O)	ln(Predicted + background)	ln (O)	P/O	ln P/O
1959	9.5	11.7	12.3	2.5	2.5	0.95	-0.05
1971	9.5	11.7	6.7	2.5	1.9	1.74	0.55
1972	8.8	11.0	1.8	2.4	0.6	6.10	1.81
1973	8.8	11.0	14.1	2.4	2.6	0.78	-0.25
1974	8.8	11.0	10.1	2.4	2.3	1.09	0.08
1975	8.1	10.3	17.5	2.3	2.9	0.59	-0.53
1976	8.1	10.3	12.1	2.3	2.5	0.85	-0.16
1977	8.1	10.3	14.8	2.3	2.7	0.70	-0.36
1978	7.4	9.6	15.5	2.3	2.7	0.62	-0.48
1979	6.8	9.0	8.1	2.2	2.1	1.11	0.10
1980	6.5	8.7	9.4	2.2	2.2	0.92	-0.08
1981	6.1	8.3	11.4	2.1	2.4	0.73	-0.32
1982	5.7	7.9	7.4	2.1	2.0	1.07	0.07
1983	5.4	7.6	8.7	2.0	2.2	0.87	-0.13
1984	5.1	7.3	8.5	2.0	2.1	0.86	-0.15
1985	4.8	7.0	4.0	1.9	1.4	1.75	0.56
1986	4.5	6.7	4.0	1.9	1.4	1.68	0.52
1987	4.3	6.5	4.0	1.9	1.4	1.61	0.48
1988	4.0	6.2	4.0	1.8	1.4	1.55	0.44
				Average		1.00	0.11

[a] Geometric bias = exp(0.11) = 1.1; correlation between ln(O) and ln(Predicted + background) = 0.45.

Table N-28. Computation of Correlation and Bias for Predicted and Observed Concentrations of Uranium in Soil (pCi g^{-1}) at Boundary Station BS–2 [a]

Year	Predicted	Predicted + background	Observed (O)	ln(Predicted + background)	ln (O)	P/O	ln P/O
1959	18.9	21.1	13.5	3.1	2.6	1.57	0.45
1971	18.3	20.5	13.5	3.0	2.6	1.51	0.42
1972	17.6	19.8	8.1	3.0	2.1	2.44	0.89
1973	16.9	19.1	18.2	2.9	2.9	1.05	0.05
1974	16.9	19.1	12.1	2.9	2.5	1.58	0.46
1975	16.9	19.1	17.5	2.9	2.9	1.09	0.09
1976	16.2	18.4	14.8	2.9	2.7	1.24	0.22
1977	15.5	17.7	14.8	2.9	2.7	1.20	0.18
1978	14.9	17.1	14.1	2.8	2.6	1.21	0.19
1979	13.5	15.7	11.4	2.8	2.4	1.38	0.32
1980	12.8	15.0	14.1	2.7	2.6	1.07	0.06
1981	12.2	14.4	15.5	2.7	2.7	0.93	-0.08
1982	11.5	13.7	7.4	2.6	2.0	1.85	0.62
1983	10.8	13.0	11.6	2.6	2.5	1.12	0.12
1984	10.1	12.3	8.0	2.5	2.1	1.54	0.43
1985	9.5	11.7	1.8	2.5	0.6	6.48	1.87
1986	8.8	11.0	8.1	2.4	2.1	1.36	0.30
1987	8.1	10.3	9.0	2.3	2.2	1.15	0.14
1988	8.1	10.3	9.7	2.3	2.3	1.06	0.06
				Average		1.23	0.36

[a] Geometric bias = exp(0.36) = 1.4; correlation between ln(O) and ln(Predicted + background) = 0.54.

Table N-29. Computation of Correlation and Bias for Predicted and Observed Concentrations of Uranium in Soil (pCi g^{-1}) at Boundary Station BS–3 [a]

Year	Predicted	Predicted + background	Observed (O)	ln(Predicted + background)	ln (O)	P/O	ln P/O
1959	27.7	29.9	60.5	3.4	4.1	0.49	-0.70
1971	26.4	28.6	64.6	3.4	4.2	0.44	-0.82
1972	25.7	27.9	29.6	3.3	3.4	0.94	-0.06
1973	25.0	27.2	92.2	3.3	4.5	0.30	-1.22
1974	24.3	26.5	63.3	3.3	4.1	0.42	-0.87
1975	23.7	25.9	78.8	3.3	4.4	0.33	-1.11
1976	23.7	25.9	78.8	3.3	4.4	0.33	-1.11
1977	22.3	24.5	89.5	3.2	4.5	0.27	-1.30
1978	21.0	23.2	68.7	3.1	4.2	0.34	-1.09
1979	19.6	21.8	74.1	3.1	4.3	0.29	-1.22
1980	18.3	20.5	41.7	3.0	3.7	0.49	-0.71
1981	17.6	19.8	90.2	3.0	4.5	0.22	-1.52
1982	16.2	18.4	43.1	2.9	3.8	0.43	-0.85
1983	15.5	17.7	47.2	2.9	3.9	0.38	-0.98
1984	14.9	17.1	48.3	2.8	3.9	0.35	-1.04
1985	13.5	15.7	32.0	2.8	3.5	0.49	-0.71
1986	12.8	15.0	38.8	2.7	3.7	0.39	-0.95
1987	12.2	14.4	35.0	2.7	3.6	0.41	-0.89
1988	11.5	13.7	60.0	2.6	4.1	0.23	-1.48
					Average	0.36	-0.98

[a] Geometric bias = exp(-0.98) = 0.38; correlation between ln(O) and ln(Predicted + background) = 0.48.

Table N-30. Computation of Correlation and Bias for Predicted and Observed Concentrations of Uranium in Soil (pCi g^{-1}) at Boundary Station BS–4 [a]

Year	Predicted	Predicted + background	Observed (O)	ln(Predicted + background)	ln (O)	P/O	ln P/O
1959	7.4	9.6	14.6	2.3	2.7	0.66	-0.42
1971	7.4	9.6	6.0	2.3	1.8	1.61	0.47
1972	7.4	9.6	3.0	2.3	1.1	3.21	1.17
1973	6.8	9.0	10.1	2.2	2.3	0.89	-0.12
1974	6.8	9.0	3.0	2.2	1.1	2.99	1.09
1975	6.8	9.0	8.1	2.2	2.1	1.11	0.10
1976	6.6	8.8	6.3	2.2	1.8	1.40	0.34
1977	6.3	8.5	6.3	2.1	1.8	1.35	0.30
1978	5.9	8.1	7.4	2.1	2.0	1.09	0.09
1979	5.5	7.7	7.4	2.0	2.0	1.05	0.05
1980	5.2	7.4	6.1	2.0	1.8	1.21	0.19
1981	4.9	7.1	4.0	2.0	1.4	1.77	0.57
1982	4.6	6.8	3.4	1.9	1.2	2.00	0.69
1983	4.3	6.5	4.7	1.9	1.5	1.39	0.33
1984	4.1	6.3	7.4	1.8	2.0	0.85	-0.16
1985	3.9	6.1	3.0	1.8	1.1	2.02	0.70
1986	3.7	5.9	5.9	1.8	1.8	0.99	-0.01
1987	3.4	5.6	4.1	1.7	1.4	1.38	0.32
1988	3.2	5.4	5.6	1.7	1.7	0.96	-0.04
				Average		1.36	0.30

[a] Geometric bias = exp(0.30) = 1.3; correlation between ln(O) and ln(Predicted + background) = 0.31.

Table N-31. Computation of Correlation and Bias for Predicted and Observed Concentrations of Uranium in Soil (pCi g^{-1}) at Boundary Station BS–5 [a]

Year	Predicted	Predicted + background	Observed (O)	ln(Predicted + background)	ln (O)	P/O	ln P/O
1959	6.6	8.8	11.8	2.2	2.5	0.74	-0.30
1971	6.4	8.6	11.4	2.2	2.4	0.76	-0.28
1972	6.2	8.4	4.6	2.1	1.5	1.82	0.60
1973	6.0	8.2	9.4	2.1	2.2	0.87	-0.13
1974	5.9	8.1	8.1	2.1	2.1	1.00	0.00
1975	5.8	8.0	13.5	2.1	2.6	0.59	-0.52
1976	5.7	7.9	10.1	2.1	2.3	0.78	-0.25
1977	5.4	7.6	10.8	2.0	2.4	0.70	-0.35
1978	5.1	7.3	10.8	2.0	2.4	0.67	-0.40
1979	4.8	7.0	7.4	1.9	2.0	0.95	-0.06
1980	4.5	6.7	10.1	1.9	2.3	0.66	-0.42
1981	4.2	6.4	16.2	1.9	2.8	0.39	-0.93
1982	3.9	6.1	5.4	1.8	1.7	1.13	0.13
1983	3.7	5.9	5.5	1.8	1.7	1.08	0.07
1984	3.5	5.7	8.2	1.7	2.1	0.70	-0.36
1985	3.3	5.5	2.6	1.7	1.0	2.12	0.75
1986	3.1	5.3	5.1	1.7	1.6	1.04	0.04
1987	3.0	5.2	6.5	1.6	1.9	0.80	-0.23
1988	2.8	5.0	5.5	1.6	1.7	0.90	-0.10
				Average		0.84	-0.14

[a] Geometric bias = exp(-0.14) = 0.87; correlation between ln(O) and ln(Predicted + background) = 0.55.

Table N-32. Computation of Correlation and Bias for Predicted and Observed Concentrations of Uranium in Soil (pCi g^{-1}) at Boundary Station BS–6 [a]

Year	Predicted	Predicted + background	Observed (O)	ln(Predicted + background)	ln (O)	P/O	ln P/O
1959	13.5	15.7	12.0	2.8	2.5	1.31	0.27
1971	13.5	15.7	12.1	2.8	2.5	1.30	0.26
1972	12.8	15.0	5.0	2.7	1.6	3.01	1.10
1973	12.2	14.4	10.1	2.7	2.3	1.42	0.35
1974	12.2	14.4	9.4	2.7	2.2	1.53	0.42
1975	12.2	14.4	14.8	2.7	2.7	0.97	-0.03
1976	11.5	13.7	11.4	2.6	2.4	1.20	0.18
1977	10.8	13.0	10.8	2.6	2.4	1.21	0.19
1978	10.1	12.3	7.4	2.5	2.0	1.67	0.51
1979	10.1	12.3	9.4	2.5	2.2	1.31	0.27
1980	9.5	11.7	12.8	2.5	2.5	0.91	-0.09
1981	8.8	11.0	no data	2.4			
1982	8.1	10.3	6.1	2.3	1.8	1.69	0.53
1983	7.4	9.6	7.9	2.3	2.1	1.22	0.20
1984	7.4	9.6	4.0	2.3	1.4	2.41	0.88
1985	6.8	9.0	1.1	2.2	0.1	8.15	2.10
1986	6.5	8.7	5.4	2.2	1.7	1.61	0.48
1987	6.1	8.3	8.7	2.1	2.2	0.95	-0.05
1988	5.7	7.9	7.1	2.1	2.0	1.12	0.11
				Average		1.31	0.43

[a] Geometric bias = exp(0.43) = 1.5; correlation between ln(O) and ln(Predicted + background) = 0.53.

Table N-33. Computation of Correlation and Bias for Predicted and Observed Concentrations of Uranium in Soil (pCi g^{-1}) at Boundary Station BS–7 [a]

Year	Predicted	Predicted + background	Observed (O)	ln(Predicted + background)	ln (O)	P/O	ln P/O
1959	3.1	5.3	10.2	1.7	2.3	0.52	-0.65
1981	1.9	4.1	2.0	1.4	0.7	2.05	0.72
1982	1.8	4.0	2.7	1.4	1.0	1.49	0.40
1983	1.7	3.9	2.5	1.4	0.9	1.56	0.44
1984	1.6	3.8	3.2	1.3	1.2	1.19	0.18
1985	1.6	3.8	0.4	1.3	-0.9	9.63	2.26
1986	1.4	3.6	2.9	1.3	1.1	1.25	0.22
1987	1.4	3.6	3.6	1.3	1.3	0.99	-0.01
1988	1.3	3.5	4.4	1.2	1.5	0.79	-0.23
					Average	2.16	0.37

[a]Geometric bias = exp(0.37) = 1.4; correlation between ln(O) and ln(Predicted + background) = 0.44.

The time trend in the P/O ratio for soil is illustrated in Figure N-24. Boundary station BS–3 is consistently under-predicted. We believe this is because of contamination of the soil areas around the old solid waste incinerator, from spills and wind dispersal of ash during handling of ash residues (see Appendix K of Voillequé et al. 1995). The location that is most over-predicted is to the west (BS–6). The high P/O for a majority of the stations in 1972 and 1985 suggests a systematic bias in the uranium analysis in soil for those years; in fact, the measured uranium concentrations in soil for three of the seven boundary stations in 1985 were so low as to be treated as outliers in the determination of weathering rate parameters for uranium in soil (Appendix C).

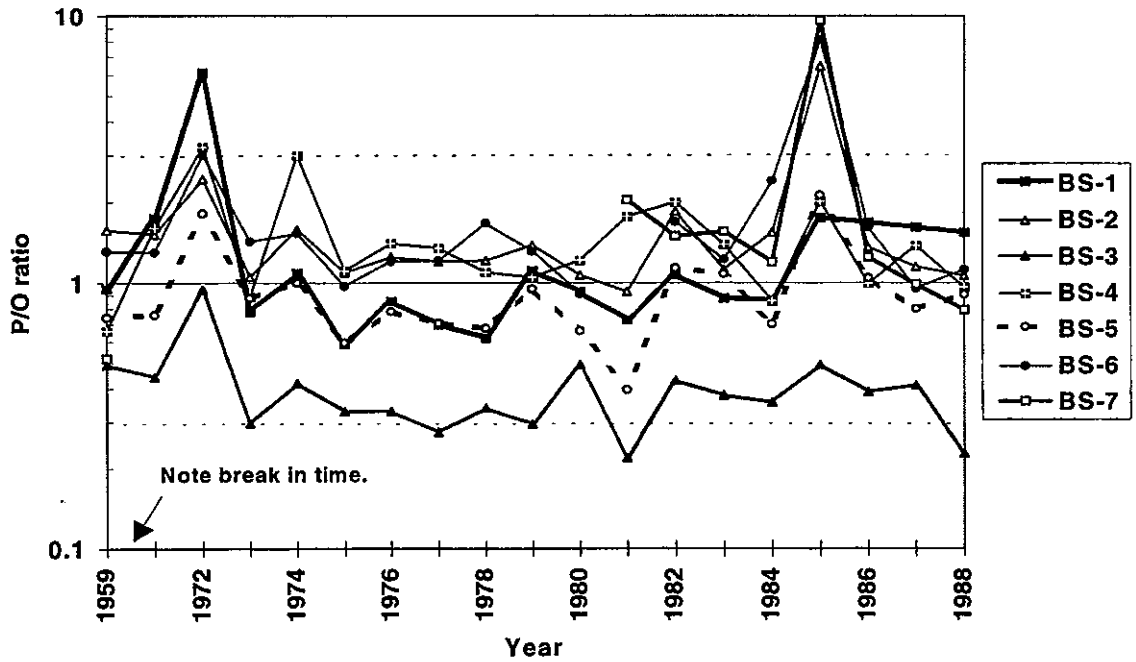

Figure N-24. Time trend in P/O ratio for uranium in soil at seven locations on the FMPC boundary. In the area between the dashed lines, there is agreement within a factor of three.

Summary of Validation Results for Uranium

Three major types of environmental media (air, gummed-film, and soil) were used to validate our predicted environmental concentrations throughout the FMPC operating history. No one medium was monitored over the entire time period of FMPC operations, but in total, these data cover a time interval from 1954 through 1988 (the end of this study's scope). Table N-34 summarizes the validation results for these three media. There were significant discrepancies between predicted and observed concentrations for particular places and years. This is not unexpected, given the myriad of uncertainties involved in the source term reconstruction, the environmental transport calculations, and the environmental sampling and analysis. However, when viewed in the aggregate, the agreement between predicted and observed concentrations in the environment is excellent. This gives us confidence that our predicted doses from past releases of uranium from the FMPC are reasonable, particularly over long periods of time.

Table N-34. Summary of Validation Results for Uranium Using Air, Soil, and Gummed-Film Monitoring Data

Medium and location	Number of stations (n)	Time interval	Geometric Bias (P/O)	Uncertainty in Bias [a]
Air (perimeter)	4	1958–1971	1.0	0.6–1.8
Air (boundary)	7	1972–1988	1.0	0.6–1.6
Gummed-film (perimeter to 4.2 km)	20	1954–1964	0.4	0.3–0.7
Soil (boundary)	7	1959, 1971–1988	1.1	0.7–1.7

[a] All-station geometric bias (P/O) × / ÷ geometric standard deviation of geometric bias for n stations.

REFERENCES

Aas C. A., S.J. Clement, G.L. Gels, and C.A. Lojek. 1987. *Feed Materials Production Center Environmental Monitoring Annual Report for 1986.* Report FMPC-2076. Westinghouse Materials Company of Ohio, Cincinnati, Ohio.

Boback M.W., K.N. Ross, and D.A. Fuchs. 1977. *Feed Materials Production Center Environmental Monitoring Annual Report for 1976.* Report NLCO-1142 Special. National Lead Company of Ohio, Cincinnati, Ohio.

Byrne J.M. 1992a. Letter and computer disks, to Duane W. Schmidt. Reference number WEMCO:EM:EMON:92-1274, dated August 31. Westinghouse Environmental Management Company of Ohio, Cincinnati, Ohio.

Byrne J.M. 1992b. Letter and computer disks, to Duane W. Schmidt. Reference number WEMCO:EM:MON:92-1344, dated September 15. Westinghouse Environmental Management Company of Ohio, Cincinnati, Ohio.

Byrne J. 1995. Letter and computer disk contaning spreadsheet files of air monitoring data, titled AIR86, AIR87, AIR88, OFFAIR87, and OFFAIR88, to S.K. Rope, August.

Gels G.L. and C.A. Lojek. 1988. *Feed Materials Production Center Environmental Monitoring Annual Report for 1987*. Report FMPC-2135. Westinghouse Materials Company of Ohio, Cincinnati, Ohio.

Gels G.L., M.A. Grib, and J.S. Oberjohn. 1989. *Feed Materials Production Center Environmental Monitoring Annual Report for 1988*. Report FMPC–2173. Westinghouse Materials Company of Ohio, Cincinnati, Ohio.

Grumski J.T. 1987. *Summary, K-65 Silo 1 Flange Changeout Operation*. Internal report, dated November 9. Westinghouse Materials Company of Ohio, Cincinnati, Ohio.

Grumski J.T. and P.A. Shanks. 1988. *Completion Report, K-65 Interim Stabilization Project, Exterior Foam Application/Radon Treatment System Operation*. Draft internal report, dated February 1988. Westinghouse Materials Company of Ohio, Cincinnati, Ohio.

Hagee G.R., P.H. Jenkins, P.J. Gephart, and C.R. Rudy. 1985. *Radon and Radon Flux Measurements at the Feed Materials Production Center, Fernald, Ohio*. Report MLM-MU-85-68-0001, Mound, Monsanto Research Corporation, Miamisburg, Ohio.

Killough G.G., M.J. Case, K.R. Meyer, R.E. Moore, J.F. Rogers, S.K. Rope, D.W. Schmidt, B. Shleien, J.E. Till, and P.G. Voillequé. 1993. *The Fernald Dosimetry Reconstruction Project, Task 4, Environmental Pathways — Models and Validation*. Draft. RAC Report CDC-3, Radiological Assessments Corporation, Neeses, South Carolina.

Ross K.N. 1959. "Uranium in Surface Dirt," Internal memo dated April 6, 1959, to A.O. Dodd. National Lead Company of Ohio, Cincinnati, Ohio.

Shleien B., S.K. Rope, M.J. Case, G.G. Killough, K.R. Meyer, R.E. Moore, D.W. Schmidt, J.E. Till, and P.G. Voillequé. 1995. *The Fernald Dosimetry Reconstruction Project. Task 5. Review of Historic Data and Assessments for the FMPC*. RAC Report CDC-4. Radiological Assessments Corporation, Neeses, South Carolina.

U.S. Department of Energy (DOE). 1986. *Investigation of April 25, 1986 Radon Gas Release from Feed Materials Production Center K-65 Silos*. Report DOE/OR-877, dated June 27. DOE Incident Investigation Board.

Voillequé P.G., K.R. Meyer, D.W. Schmidt, S.K. Rope, G.G. Killough, M. Case, R.E. Moore, B. Shleien, and J.E. Till. 1995. *The Fernald Dosimetry Reconstruction Project. Tasks 2 and 3. Radionuclide Source Terms and Uncertainties*. RAC Report CDC-5. Radiological Assessments Corporation, Neeses, South Carolina.

APPENDIX O

INVESTIGATION OF RELATIVELY HIGH BACKGROUND URANIUM MEASUREMENTS AT DISTANT ENVIRONMENTAL MONITORING STATIONS

PREFACE

This appendix documents an investigation that was conducted in the summer of 1994. The conclusion of the investigation was to use the early environmental monitoring data collected within 5 km of the Feed Materials Production Center (FMPC) in our validation exercises. Uranium deposition measurements made at more distant locations were of suspect quality, perhaps from cross-contamination of those relatively low-level samples.

The findings of this investigation were documented in a technical memorandum to the Centers for Disease Control and Prevention, dated September 15, 1994, which has the same title as this appendix. Later, it was decided that the background information compiled during the investigation should be made available to the public as an appendix to this final Task 6 report, which contains the validation comparisons (Appendix N). Consequently, this appendix contains the original technical memorandum of September 1994, with only minor formatting and editorial changes.

Because this investigation was conducted over 3 years ago, the language reflects that point in the dose reconstruction project. In addition, there are several places in the appendix that do not reflect the final results of the project. To avoid possible misinterpretation of this material, an occasional note to the reader is inserted at those locations.

INTRODUCTION

Historical environmental data collected around the FMPC provide an important piece of information for the Fernald Dosimetry Reconstruction Project. These data, which were compiled in our Task 5 report (Shleien et al. 1994) are being used in the final Task 6 report for comparison with predictions of past environmental concentrations. The predictions are based on source term reconstruction and environmental transport modeling.

Until the 1980s, most routine environmental monitoring conducted by the FMPC contractor was relatively close to the facility. One exception was monitoring of uranium deposition onto gummed-film at seven distant stations, between 4 and 19 km away (Figure O-1). Deposition to gummed-film at stations closer to the site began in 1954, but the distant station monitoring began in 1959. The entire gummed-film monitoring program was discontinued in the mid-1960s. These data are important to the project for two reasons: (1) they are one of the only sets of data collected during the time period of highest releases, and (2) they provide a way to check our environmental transport model performance in terms of drop-off in uranium deposition with distance from the facility.

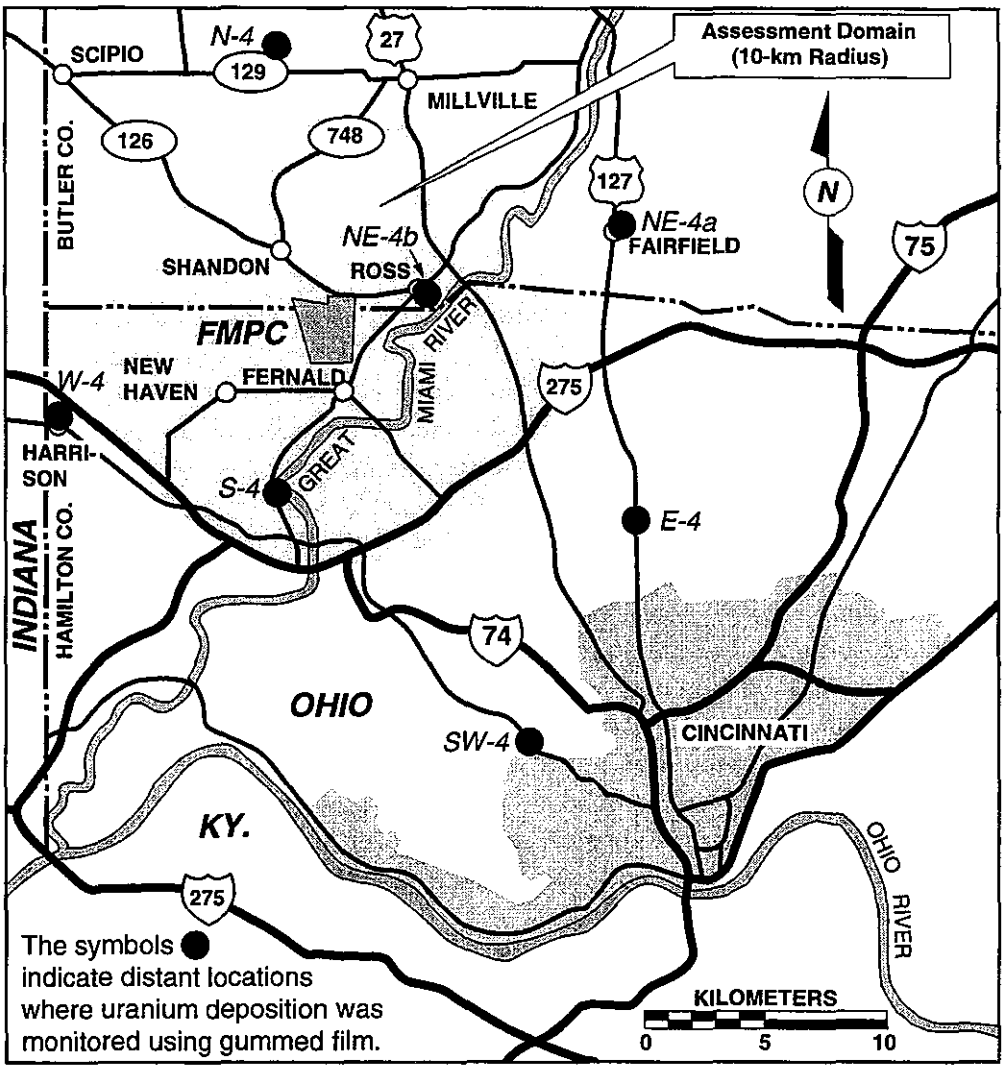

Figure O-1. Location of the FMPC. The assessment domain is the region around the site with which this study is principally concerned. Uranium deposition was monitored at most of these stations between 1959 and 1964.

SUMMARY OF THE PROBLEM

The measured uranium deposition to gummed-film as a function of distance from the FMPC shows a rapid decline within 2 km and a basically flat response beyond 5 km (Figure O-2). Uranium concentrations in vegetation samples, which were collected routinely at various distances from the FMPC, exhibit a similar pattern (Figure O-3). Uranium in soil samples taken in 1959 and 1965 also show a drop-off in the first few kilometers from the FMPC and a flat response beyond 4 km (Figure O-4).

Taken together, these environmental data indicate that the sphere of measurable influence of the FMPC on environmental uranium levels probably was within 5 km. The flattening off of the curves at greater distances suggests that samples from the more distant

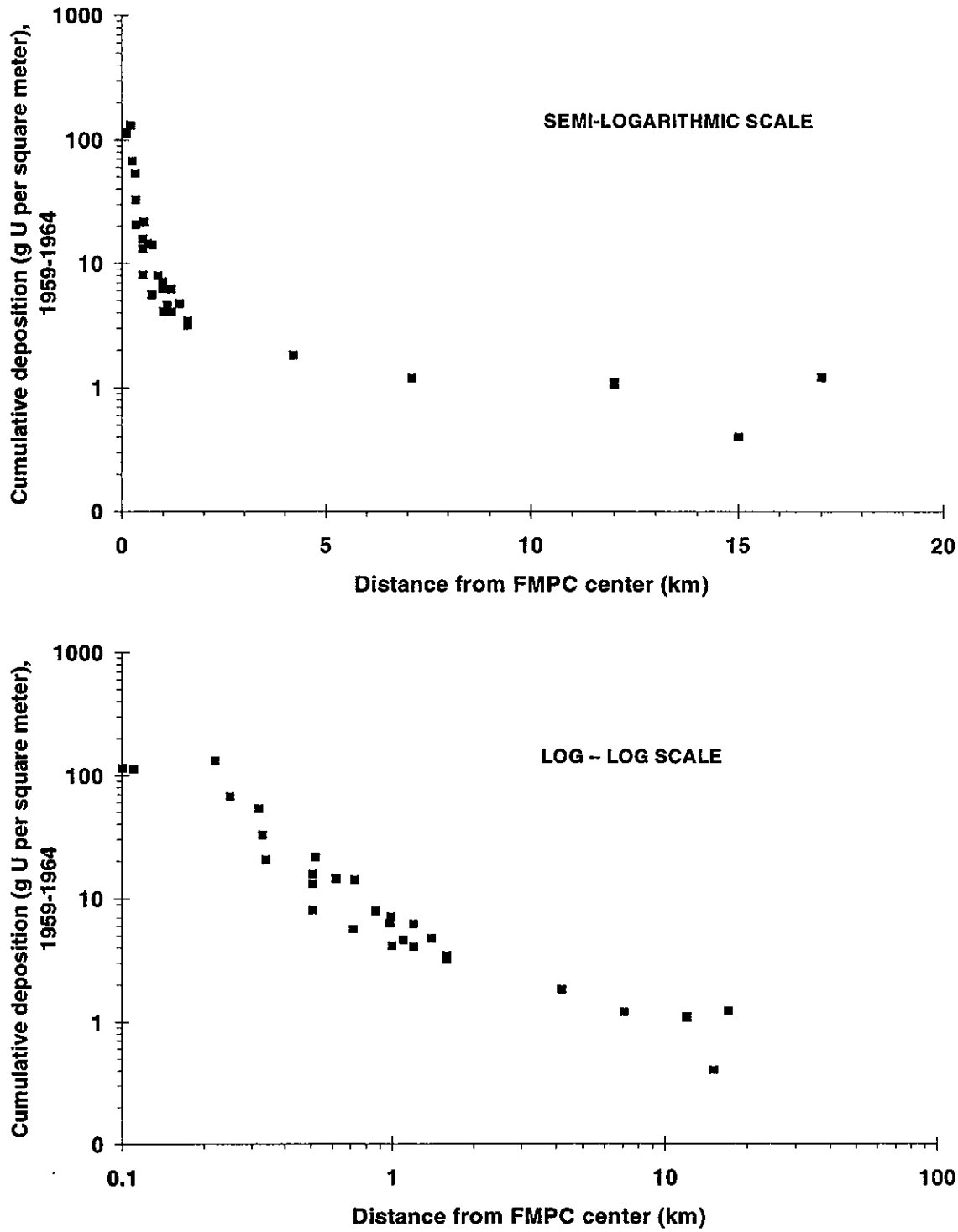

Figure O-2. Cumulative deposition of uranium as a function of distance from the site (same data plotted using two scales). All directions are pooled together in these plots. Depsotion was measured by gummed-film and was corrected by RAC using a 14% collection efficiency.

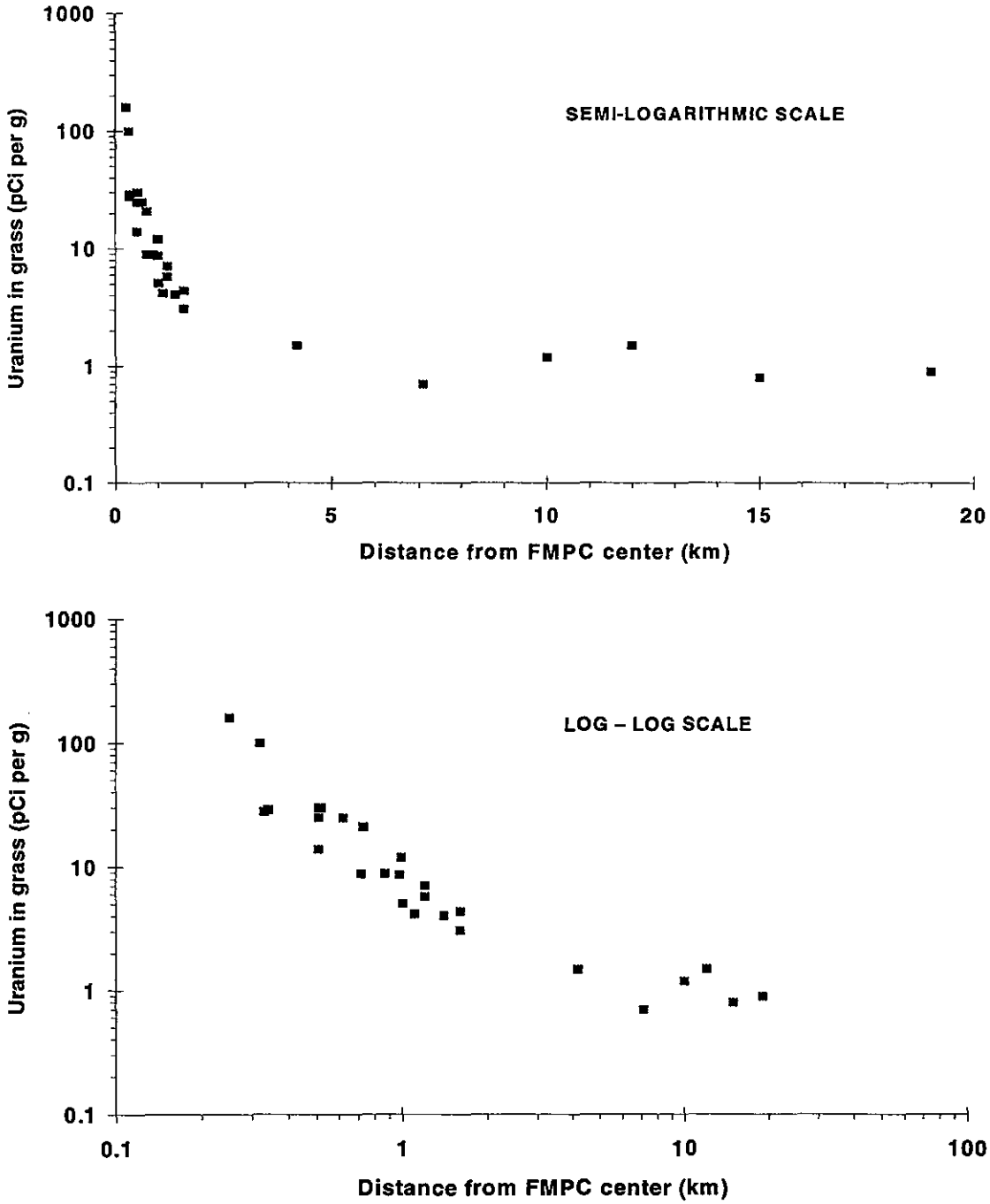

Figure O-3. Average concentrations of uranium in grass with distance from the FMPC (same data plotted using two scales). Values plotted are the grand average of annual averages for the years 1958–1968. All directions are pooled together in these plots. See Table B5S–3 of Shleien et al. (1994) for data. The samples were not washed. A background of 1 pCi U g^{-1} in grass is rather high, given that background soil is around 3 pCi U g^{-1}. Recent measurements of uranium in vegetation collected at offsite locations have averaged 0.1 pCi U g^{-1} or less (Shleien et al. 1994, Appendix B, Part 5).

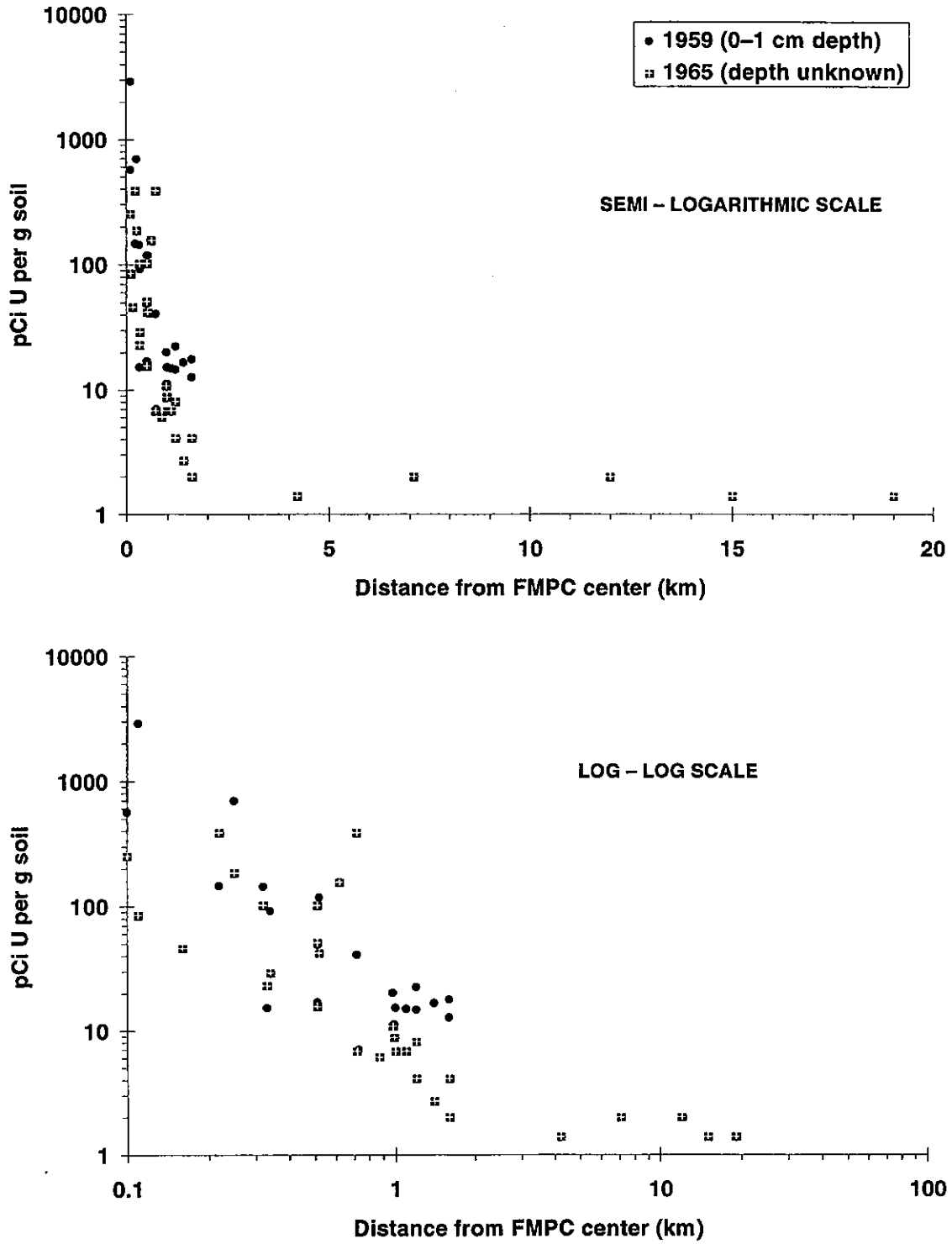

Figure O-4. Concentrations of uranium in soil with distance from the FMPC in 1959 and 1965 (same data plotted using two scales). Data were obtained from FMPC analytical data sheets. All directions are pooled together in these plots. Background uranium (total) in surface soil of this area averages about 2.8 pCi g^{-1} (Shleien et al. 1994, Appendix A).

stations were measuring some background level of uranium. (In this assessment, the term "background" is used to mean true *natural* background from uranium in surface soil plus any additional uranium from non-FMPC sources, such as fertilizers or coal ash.)

However, the amounts of uranium deposited on gummed-film (as well as on vegetation) at the distant stations were considerably higher than what would be expected from natural background. In addition, uranium concentrations (measured at the FMPC lab) in precipitation from the Abbe Observatory, 24 km south of the FMPC, were 5 to 11 times higher than those predicted from Fernald releases at 10 km south (Figure O-5).[1] The uranium concentrations in precipitation were within a factor of 10 of the FMPC detection limit, but they were well above background uranium in precipitation today (Figure O-5).

Five of the seven distant gummed-film monitoring stations were outside the 10-km domain established for the Fernald Dosimetry Reconstruction Project (Figure O-1). However, when comparing model predictions of deposition within 10 km to historic measurements using gummed-film, it was obvious that these measured concentrations would be higher than predictions at those distant locations. Vegetation and rainwater monitoring data showed the same relative drop-off with distance, i.e., they supported the gummed-film data.

Different deposition models were tried, and the impact of particle size was tested. It became apparent that the amount of uranium measured at these distant stations was too great, by at least a factor of 10, to be attributed to deposition from a once-through passage of the airborne plume of material released from the FMPC. In short, the problem is high measured background levels of uranium in the environment in the 1960s — apparently not from the FMPC, but whose source is unexplained.

An attempt to explain the high background levels involved identifying all possible sources of uranium as well as examining of the quality of the measurement data. The possible contributors to uranium deposition at the distant stations that were identified are listed below. These sources are in addition to the direct deposition from the airborne effluent released from the FMPC.

- natural background
- fertilizers
- coal fly ash
- resuspension and redistribution of uranium released from the FMPC before 1959 (i.e. surface soil contamination around the site)
- other government and commercial facilities that handled large amounts of uranium
- fallout from weapons testing.

In addition to other sources of uranium, two important issues affect our interpretation of the gummed-film data:

1. Collection efficiency of the gummed-film for airborne particulates
2. Analytical issues (e.g., detection limits; contamination of samples; computation of uranium concentrations from measurement results; and chemical interference with fluorimetric analysis).

[1] Subsequent modifications in the source term for uranium and the dispersion model would result in a different predicted uranium concentration at 10 km south than is shown in Figure O-5.

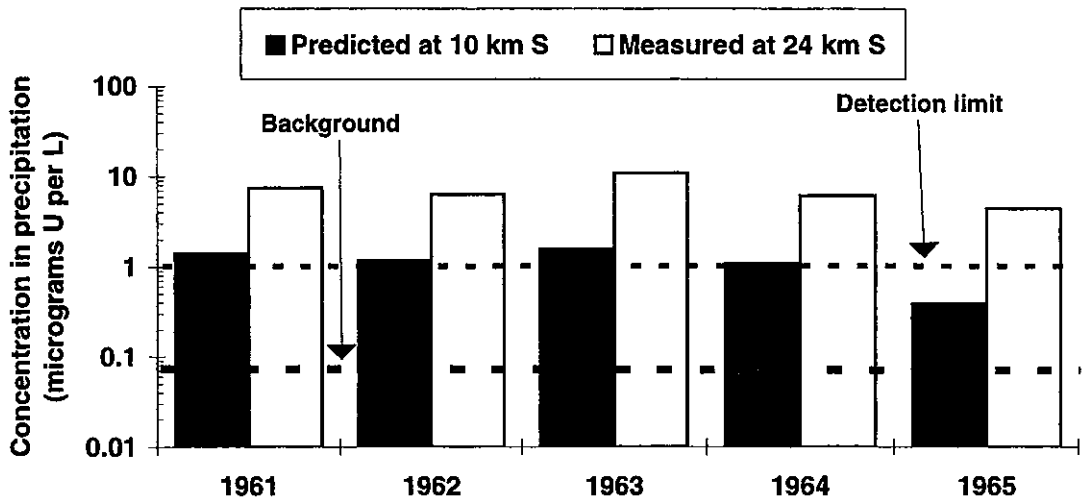

Figure O-5. Comparison of measured concentration of uranium in precipitation 24 km south of the FMPC in the 1960s with the predicted concentrations at 10 km south during the same time period. The background value shown is based on measurements in Columbus, Ohio, in the 1980s (see discussion in Shleien et al. 1994, Appendix B Part 3). *[Note to reader: subsequent modifications in the source term for uranium and the dispersion model would result in a different predicted uranium concentration at 10 km south than is shown here.]*

Figure O-2 illustrated the *cumulative* observed deposition to gummed-film with distance from the site over a 6-year period. In contrast, Figure O-6 shows the monthly average deposition *rate* at the distant stations over the same time interval. This deposition rate is more readily compared with other sources, which will be discussed later. Figure O-6 also demonstrates that except for two distant stations at 12 km ENE and 15 km ESE, the observed deposition rates at the other five distant stations are similar (i.e., there is not much difference between the locations that are between 4 and 19 km away from the site, in various directions). In general, the measured deposition rate ranges between 0.1 and 1 mg U m^{-2} d^{-1}.

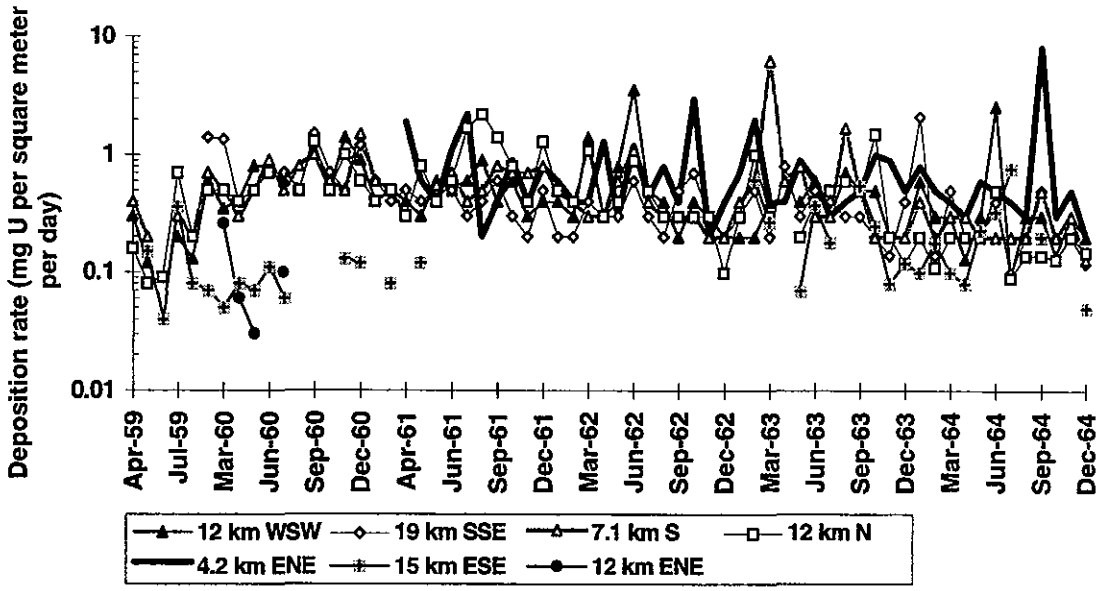

Figure O-6. Monthly average uranium deposition rates measured by gummed-film at distant stations. Measured values were corrected for a 14% collection efficiency (Killough et al. 1993, Appendix M). The collection efficiency applied to the gummed-film measurements could be too low, by at most a factor of four (60%/14%). If so, the corrected deposition rates would be too high. This issue is discussed further in a later section; however, this factor of four could only account for a small part of the difference between measured values and the estimated deposition from natural background, which is around 0.0003 mg m^{-2} d^{-1} (see next section).

SUMMARY OF APPROACH TO INVESTIGATION OF THE PROBLEM

Our information gathering and calculations were focused on answering the following questions:

1. Were the uranium concentrations in the environment as high as the measurements indicate, or was there some problem with the data?
2. If the concentrations were high, what was the source (or sources)?
3. If the concentrations were not as high as the measurements indicate, what are the implications, if any, for the use of the environmental data?

Our first examination of the FMPC data suggested that the techniques and detection limits should have been adequate to measure the concentrations seen at distant locations. For example, the uranium measurements for rain, vegetation, and gummed-film were almost never reported as "less-than-detectable," suggesting adequate sensitivity. The precision of the analysis for uranium in air was examined from paired field replicates taken and analyzed in 1963; half of the pairs differed by less than 18%, although about 20% of the pairs differed by more than a factor of 2 (Killough et al. 1993, Figure L-3).

Next, we looked for other sources of uranium in the environment, as well as background measurements over a wide period of time. Some other sources of uranium were generic (like coal ash), and some were specific (e.g., the Paducah Gaseous Diffusion Plant). Available monitoring data were examined, particularly any uranium-specific monitoring during the time period of interest. Because many of the obvious sources (facilities handing large quantities of uranium) did not have very sensitive monitoring methods and/or did not have monitoring stations very far away, we looked at other measurements of uranium in air at various places and times.

The bulk of this technical memo describes our assessments of the various other sources of uranium in the environment and resulting estimates of their contributions to the background deposition rate. The final section includes our conclusions and recommendations about this issue.

NON-FMPC SOURCES OF URANIUM AND INDEPENDENT MEASUREMENTS

Natural Background Uranium in Soil and Air

The conventional wisdom is that naturally occurring uranium in soil particles is the primary source of airborne uranium in the environment (UNSCEAR 1982). The airborne dust particles subsequently redeposit to the ground surface or, in the case of deposition monitoring, to the surface of the gummed-film. This natural background contribution to uranium deposition should be relatively constant over time in a given region.

To our knowledge, no current program monitors uranium in dry *deposition*. Therefore, to assess the magnitude of natural background uranium deposition, the background concentration of uranium in air was examined, and then a deposition velocity (Killough et al. 1993) was applied to that airborne concentration.

The U.S. Environmental Protection Agency (EPA) has been routinely measuring uranium in airborne particulates in a number of cities in the U.S., including several in Ohio. In our Task 5 report (Shleien et al. 1994, Appendix A), we compiled the data for Columbus, Ohio, between 1980 and 1987. For our deposition assessment, we used the range of these measurements (0.05–0.14 fCi U m^{-3}). A calculated estimate of uranium background in air, based on suspension of soil dust (0.07–0.1 fCi U m^{-3} air), is in good agreement with the measurements from Columbus (Shleien et al. 1994, Appendix A).

A wide distribution for the deposition velocity was assumed, based on particles ranging from 0.02 to 10 microns diameter (Killough et al. 1993, Table G-4). The most likely value was assumed to be 1 cm sec^{-1} with extremes of 0.02 to 8 cm sec^{-1}.The resulting median estimate of the background deposition rate is 0.0003 mg U m^{-2} d^{-1} (5th–95th percentile interval: 0.00007–0.0008). This estimated natural background deposition rate is over 100 times less than the observed rates at stations up to 19 km from the FMPC.

Initially, there was no reason to suspect that the natural background uranium concentration in air would not be constant during the operating history of the FMPC. However, as part of our additional information search to resolve this background issue, the concentrations of uranium in air from Columbus, Ohio, back to 1973 (beginning of this monitoring program) and up to 1991 were compiled. These measurements, plotted in Figure O-7, suggested a decrease of perhaps a factor of three between 1973 and 1991. Subsequent literature review indicated that this decrease could have been due to implementation of Clean Air Act legisla-

tion, which reduced uranium emissions to air from coal and oil-fired electrical generating plants. At any rate, a downward trend was suggested, so it was important for us to locate other accurate and sensitive measurements of background uranium in air before 1973.

Other measurements of uranium in air at various places and times are shown on Figure O-7. Most of the research studies were designed to measure low concentrations. McEachern et al. (1971) recognized that little information of background atmospheric levels of uranium could be found in the literature. Consequently, they measured uranium concentrations in surface air at six rural and urban locations within New York State in 1968–1969. Sensitive analytical techniques were used (mass spectrometry and fission track analysis). Daily average concentrations ranged from 0.1 to 1.47 nanograms U per m^{-3} (0.07 to 1.0 fCi total U m^{-3}), with an average of 0.35 fCi m^{-3}. A significant correlation existed between the uranium concentration and the mass concentration of total suspended particulates. Levels of uranium in the air in 1969 were attributed to naturally occurring sources and nonnuclear industrial activity.

Other data for uranium in air are also plotted on Figure O-7. Literature citations are given in the figure caption. Concentrations measured around sites handling large quantities of uranium are discussed in a later section. The highest concentrations not associated with a uranium facility were measured downwind of an older-design coal-fired plant in Alabama (Bedrosian et al. 1970).

In addition to the EPA data from Columbus, Ohio, and the miscellaneous literature values located, Figure O-7 illustrates uranium measurements in air close to the FMPC from 1958 through 1991. The annual average concentrations of uranium in air at the FMPC perimeter ranged from 339 to 39 fCi U m^{-3} between 1958 and 1971. Monthly average concentrations ranged up to 1300 fCi m^{-3} in February 1958. The location of the monitoring station was changed from the perimeter fence to a further location at the NE boundary, where annual average concentrations ranged from 3 to 22 fCi U m^{-3} between 1972 and 1988 (maximum individual month: 45 fCi U m^{-3} in August 1972). These data reported here are not corrected for air sampler efficiency; this correction would result in a value which is about 35% higher.[2]

The approximate detection limit (DL) for the analysis of uranium in air at the FMPC is shown on Figure O-7 as a broken line. For the earlier time period, the DL was determined from the analytical data sheets. Later, the DL was reported in the annual environmental reports. It is obvious that the DL in the 1960s was not adequate to detect concentrations considered background today (or perhaps even then). However, the method was adequate to determine compliance with the applicable Atomic Energy Commission (AEC) standard at the time of 2000 fCi m^{-3} for uncontrolled areas. The monitored concentrations were almost always above detection limits. The main reason for the improvement in the detection limit in the early 1970s was a change from non-continuous monitoring of air (about 56 hours per week) at the perimeter to continuous monitoring at the boundary. This resulted in a larger volume of air being sampled.

The relatively recent monitoring data at *offsite* air monitoring stations around the FMPC are consistent with background levels (annual averages of 0.04 to 0.12 fCi m^{-3} in 1989 and

[2] Final assessment of air sampler collection efficiency is discussed in Appendix L. Corrected concentrations would be 25-30% higher.

1990). Until very recently, concentrations of uranium in air at the boundary of the Fernald site have been well above current background levels (Figure O-7).

In general, independent measurements of uranium in air as early as the late 1960s did not indicate very high levels in the environment. At most, concentrations might have been a factor of three or four higher than today, whereas the FMPC-measured deposition rates to gummed-film at distant stations were over 100 times higher than estimated background.

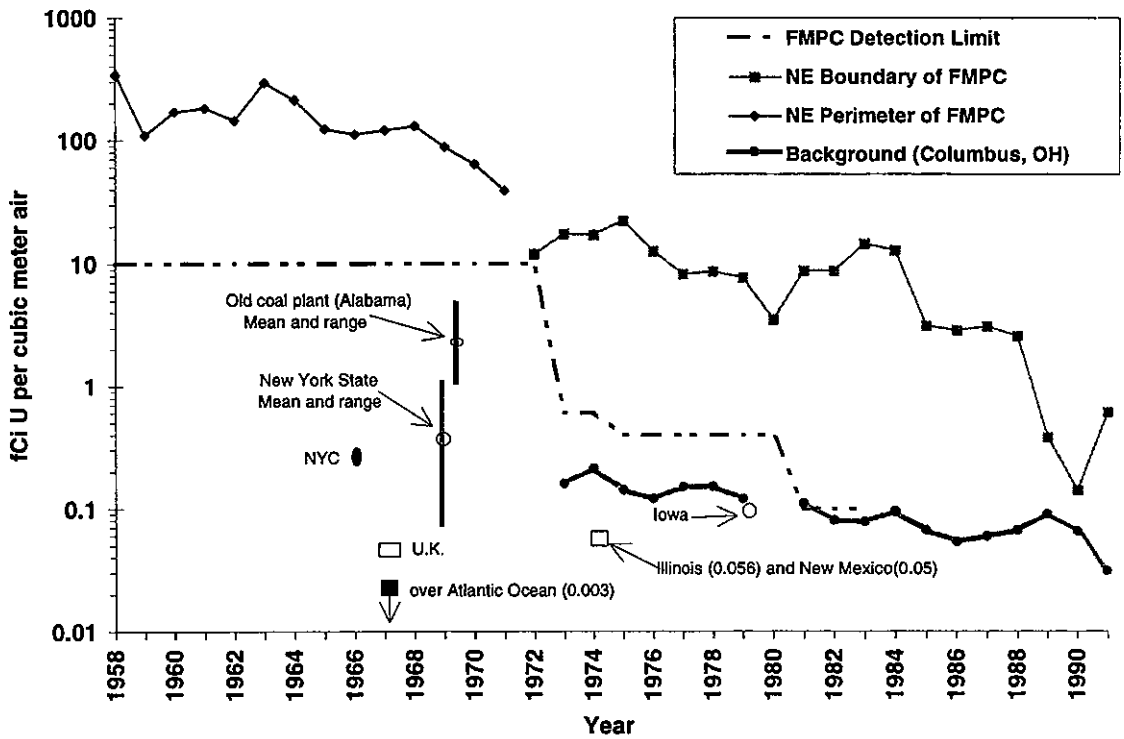

Figure O-7. Comparison of uranium in air around the FMPC (reconstructed annual averages, not corrected for sampler collection efficiency) with background measurements in Columbus, Ohio (EPA data), as well as other point estimates at various locations. The FMPC detection limit for uranium in air is shown as a broken line. The main reason for the improvement in the detection limit in the early 1970s was a change from noncontinuous monitoring of air (about 56 hours per week) at the perimeter to continuous monitoring at the boundary. This resulted in a larger volume of air being sampled. Literature citations for non-FMPC data are: NYC: (Welford and Baird 1967); Iowa: (Styron 1980); downwind of old coal-fired power plant in Alabama: (Bedrosian et al. 1970); New York State: (McEachern et al. 1971); United Kingdom and Atlantic Ocean: (Hamilton 1970); Illinois: (Sedlet et al. 1975); and New Mexico: (Apt and Lee 1975).

Coal Ash, Fertilizer, and Soil Contamination as Contributors to Measured Depositions

Coal ash and fertilizer are two common materials known to be enriched in uranium concentrations (UNSCEAR 1982). The Cincinnati/Hamilton area is industrial, so coal-fired boilers were probably common. Also, there was undoubtedly residential use of coal for heating. (Coal has a higher potential for contributing to uranium contamination than does oil.) UNSCEAR (1982) gives a concentration range of 100–300 Bq ^{238}U per kg in escaping fly ash from coal-fired power plants. Concentrations in phosphate fertilizers are given as 740 Bq per kg in superphosphate, 2000 Bq per kg monoammonium phosphate, 2100 Bq per kg in triple superphosphate, and 2300 Bq per kg in diammonium phosphate. Concentrations in coal ash and phosphate fertilizers are approximately 4 and 40 times the naturally occurring concentrations in soils, respectively.

Urban air usually averages around 30–150 μg of particulates m^{-3} of air. If we assume that the particulate concentration in air was 100 μg m^{-3}, and that coal ash contributed 50%, fertilizer dust 10%, and background soil 40% of the total particulate mass, the deposition rates shown in Table O-1 are obtained. For this calculation, uncertainties were propagated for the concentrations of uranium in the various materials and for the deposition velocity, which we allowed to range from 0.02 to 8 cm s^{-1}, with a most likely value of 1 cm s^{-1}.

Table O-1. Hypothetical Deposition Rates from Soil, Coal Ash, and Fertilizer in Air

Source	Deposition Rate (μg U m^{-2} d^{-1})	
	Median Estimate	5th–95th Percentile Range
Soil	0.3	0.06–1.0
Coal Ash	1.7	0.4–4.9
Fertilizer	2.8	0.6–7.9
Total	5.4	2.2–11

Even the upper bound on this background deposition rate (11 μg or 0.011 mg m^{-2} d^{-1}) does not approach the measured values, after they are corrected for 14% collection efficiency (Figure O-6). If the true collection efficiency were in fact 60% (a factor of four greater), all but a few of the measured concentrations would still be higher than the estimated background deposition range (Figure O-8).

Our conclusions about the relatively small possible contribution of coal ash to the deposition rate are consistent with studies of the impact of coal-burning facilities on the environment. Jaworowski et al. (1980) found a 34% increase in uranium in glacier ice dated at 1950–1977 compared to pre-industrial ice. Styron (1980) estimated that the maximum environmental deposition of radionuclides from stack emissions at a *modern* power plant burning western coal for 20 years would be only 0.1 to 1.0% of the background concentrations in soil. Bedrosian et al. (1970) detected increased levels of natural uranium in ground-level air of up to 4.4 fCi U m^{-3} downwind from the Widows Creek Power Plant in Alabama in 1969 (see Figure O-7 for perspective on this concentration). Bedrosian et al. (1970) was unable to detect increased concentrations of uranium in soil or plants, even though this coal plant was

one of the older and more poorly controlled operating plants in the U.S., releasing over 30% of its fly ash. Beck et al. (1980) estimated a deposition rate of uranium of 0.14–1.6 μg U m^{-2} d^{-1} from a model power plant in 1972 (range is based on a 52-m and 152-m stack height). This range overlaps our range of estimated deposition from coal ash (Table O-1).

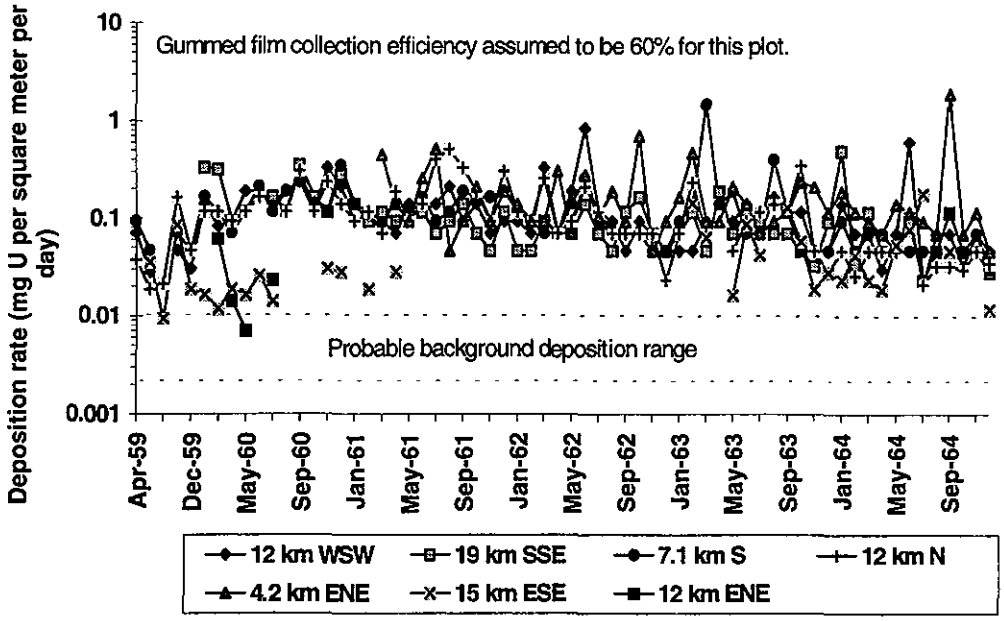

Figure O-8. Comparison of probable background deposition range from soil dust, coal ash, and fertilizer (between dashed lines) with monthly average deposition rates measured by the FMPC using gummed-film at distant locations. These measured deposition rates have been corrected for 60% collection efficiency, which was the estimated value at the time the monitoring was done (Harley et al. 1960). A collection efficiency of 14% is our best estimate based on recent knowledge (see Shleien et al. 1994, Appendix B, Part 1). Deposition rates using 14% collection efficiency were plotted in Figure O-6.

Resuspension and Redistribution of Uranium Released from the FMPC before 1959

Because natural background, coal ash, and fertilizer could not contribute as much as the measured uranium deposition rates, we speculated that uranium measured on films at the distant locations might be due to resuspension and redistribution of the large amount of uranium released from the FMPC in the 1950s. Figure O-9 illustrates that most of the uranium released from the FMPC to air was emitted before the distant gummed-film stations were established.[3] Thus, there was a large reservoir of contaminated material relatively close to the surface of the soil, which could have been available for resuspension and redistribution.

[3] Subsequent modifications were made in the source term for uranium and the soil model that would result in different values than illustrated in Figure O-9. However, the observations made in the context of this investigation are still valid. See Appendix N of this report for final time trends of reconstructed concentrations of uranium in surface soil.

The predicted concentrations of uranium in soil are highest during the period that the distant gummed-film stations were in use. Later, weathering processes removed uranium from the surface soil layer.

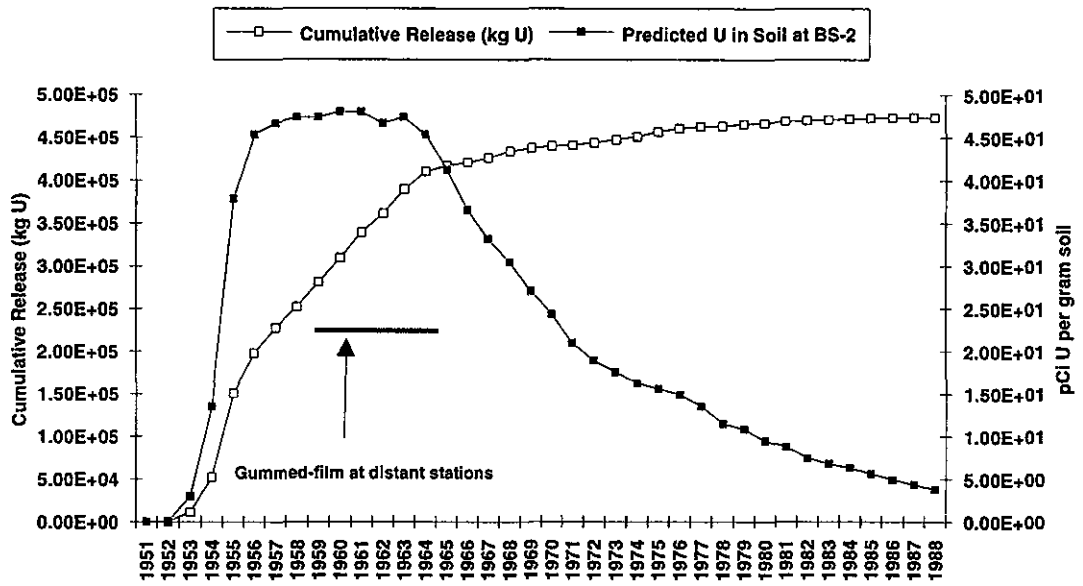

Figure O-9. Cumulative amount of uranium released to air from the FMPC as reconstructed in this study (Voillequé et al. 1993), and model prediction of resulting uranium concentration in surface soil at BS–2 (NE boundary). *[Note to reader: Subsequent modifications were made to the source term for uranium and the soil model after this figure was drafted. However, the general observations are still valid. See Appendix N for final reconstructed trends for uranium in surface soil.]*

An accurate model of the deposition, resuspension, and spatial redistribution of uranium from airborne uranium releases from the FMPC would be very difficult and time consuming to construct. A judgment was made earlier in this project that resuspension was likely to be less significant than inhalation of direct releases of uranium and radon from the plant. Consequently, a relatively simple empirical approach was taken to evaluate resuspension. In the Task 4 report (Killough et al. 1993), a method for evaluating resuspension *at the same point as deposition* was developed, based on a mass-loading approach, which used site-specific measurements of airborne particulates. *[Mass-loading approach to resuspension is discussed in Appendix D of this volume.]* However, no method was derived to account for resuspension and *redistribution* of material that had previously been deposited at another location.

A simple scoping calculation was made to evaluate whether previously released uranium might account for the observed deposition rates. Uncertainties were propagated through the calculation for the following parameters (which are followed by an asterisk). The scoping calculation assumed that the entire airborne release of uranium through 1962* was deposited within a distance of 2 km from the site. This uranium was distributed within a depth of 1 cm* of soil of bulk density of 1.5 g* cm^{-3}. The concentration of airborne particulate was 70 μg* m^{-3} air. The reduction in airborne contamination at 7 km (compared to the 2-km

radius circle) was a factor of 20*, and at 4 km it was a factor of 2.7*, based on air monitoring data from the 1980s. The deposition velocity for airborne particulates at the downwind location was assumed to be 1* cm s^{-1}. Table O-2 presents a summary of the results.

Table O-2. Plausible Deposition Rate at Two Distances from Resuspension and Redistribution of Previously Deposited Uranium

	Deposition Rate (μg U m^{-2} d^{-1})	
Distance (km)	Median estimate	5th–95th percentile range on estimate
4	108	19–560
7	14	2.6–75

These plausible deposition rates from resuspension and redistribution are higher than the background rates computed earlier; they could be in the range of measured values, at least closer to the site, particularly if the collection efficiency of the gummed-film were higher (Figures O-10a and 10b). However, an important factor that tends *not* to support redistribution as a significant contributing source is that there is not much difference between measurements at 4 and 7 km (or beyond, for that matter). Our screening calculation suggests that there would be an eight-fold decrease in the contribution from resuspension over this distance. The relative constancy of the concentrations over distances between 7 and 19 km from the FMPC suggests that resuspension from FMPC-released materials is unlikely to be the source of the measured depositions.

Other Government and Commercial Facilities Handling Large Amounts of Uranium

There were other industrial processing sites, including other Manhattan Engineer District and Atomic Energy Commission (AEC) facilities, in the midwestern U.S. that were likely sources of releases of uranium to the environment in the 1940s, 1950s, and 1960s (Table O-3). We identified some of these facilities through database searches and reviews of the technical literature. Another lead was a list of companies represented at a 1958 symposium on Occupational Health Experience and Practices in the Uranium Industry (see Weinstein 1958). Although it is unlikely that any one of these *alone* would have accounted for enough uranium to affect the background in the Cincinnati area, the cumulative contributions of these sources, and any others, might have contributed to an ambient background level that was higher than typically observed today.

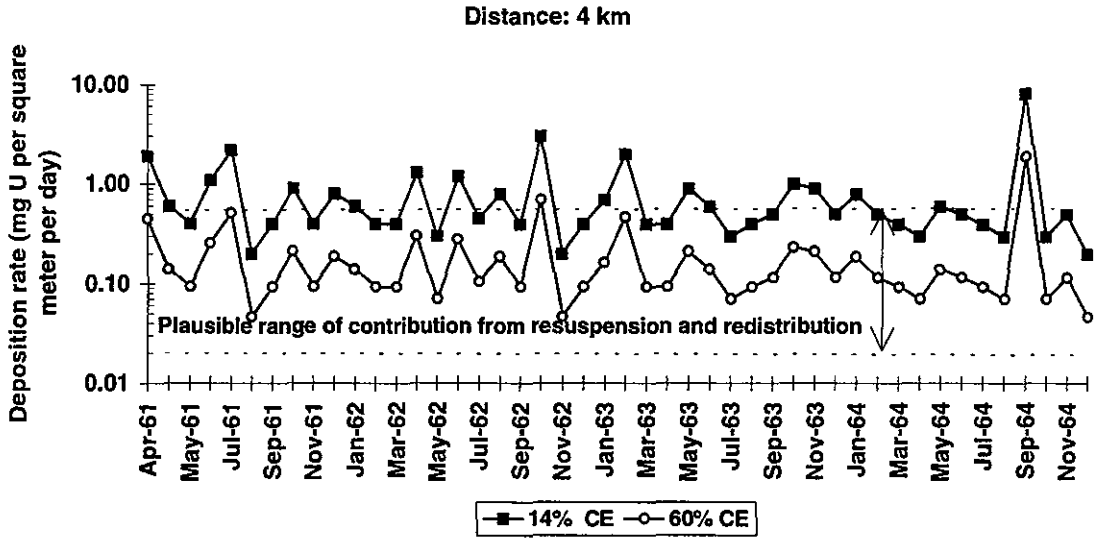

Figure O-10a. Plausible contribution of resuspension and redistribution of uranium (between dotted lines) to measured depositions at 4 km.

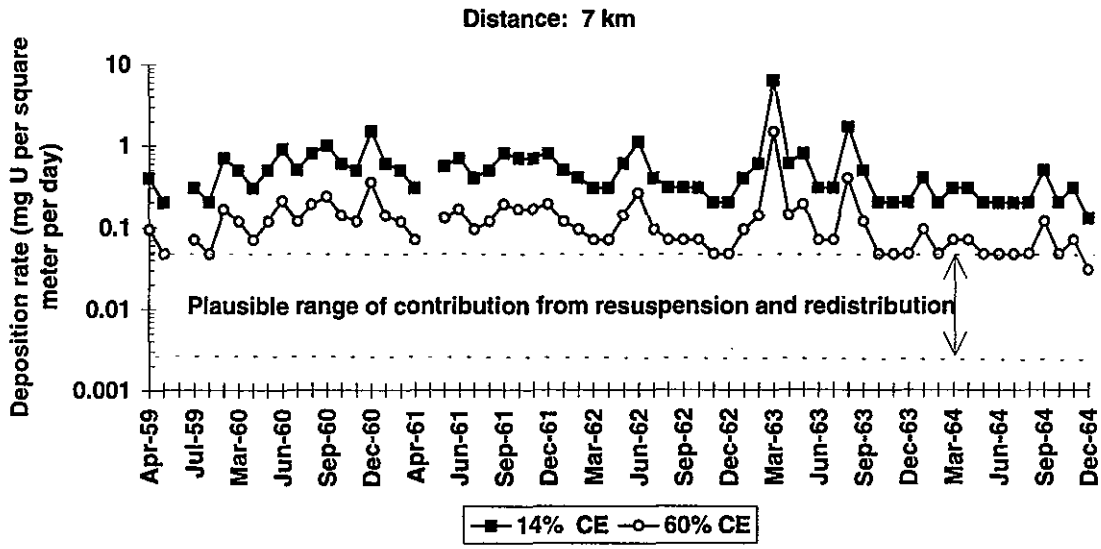

Figure O-10b. Plausible contribution of resuspension and redistribution of uranium (between dotted lines) to measured depositions at 7 km. Two values for collection efficiency (CE) are shown: 60% is believed to represent an upper bound, whereas 14% is the best estimate based on recent studies.

Some of the sites listed in Table O-3 had environmental monitoring programs, and uranium-specific data were located and examined. There were two purposes for examining these routine monitoring data from the facility contractors: (1) to determine if releases were high enough to suggest a major source of uranium for the region and (2) to see if any remote background data were obtained as part of their monitoring programs.

Table O-3. Other Facilities in the Midwestern and Eastern U.S. That Were Likely Sources of Uranium Releases to the Environment in the 1950s and 1960s

Facility	Location
Weldon Spring Plant, Mallinckrodt Chemical Works Uranium Division[a]	Weldon Spring, Missouri
Paducah Gaseous Diffusion Plant, Union Carbide Nuclear Company[a]	Paducah, Kentucky
Aircraft Nuclear Propulsion Department, General Electric, Co.[b]	Cincinnati, Ohio
Oak Ridge National Laboratory (particularly the Gaseous Diffusion Plant), Union Carbide Nuclear Company[a]	Oak Ridge, Tennessee
Harshaw Chemical Company[a]	Cleveland, Ohio
Bettis Atomic Power Laboratory, Westinghouse Electric Corporation (fuel fabrication)	Pittsburgh, Pennsylvania
Portsmouth Area Gaseous Diffusion Plant, Goodyear Atomic Corporation[c]	Piketon, Ohio
Uranium machining operations (e.g., Albaugh[d] Craft Corporation)	Oxford, Hamilton, Dayton, et al.

[a] Uranium-specific monitoring data obtained.
[b] No uranium specific monitoring data for air. Uranium released in liquid wastes.
[c] No uranium-specific monitoring data (gross counts only).
[d] Documents also use the spelling "Alba Craft."

No historical monitoring data on uranium deposition to gummed-film were located. However, there were measurements of gross radioactivity on gummed-film around the Oak Ridge Plant. These data are discussed in a later section that deals with weapons fallout. Only uranium-specific monitoring of air and water were reported in the contractor monitoring information that we found. Because we are interested in airborne pathways, the air monitoring data were more relevant, and those data are discussed here.

The 1958 Environmental Monitoring Summary for the Paducah Plant (Baker and Brown 1959) presented uranium-specific analyses (fluorometric method) for air samples collected on the perimeter of that facility. The results (mean, 88 fCi U m^{-3}; range 33–227) suggest that this facility was similar to the Fernald facility in terms of impacting uranium concentrations in offsite air (see Figure O-7). Subsequent monitoring reports for the Paducah facility were examined through 1970. These reports present *not* uranium-specific analysis, but rather total long-lived alpha, "interpreted as uranium." The detection limit was about 20 fCi m^{-3}, even higher than at the FMPC. Throughout the 1960s, reported average concentrations of "uranium-alpha" at the Paducah site perimeter ranged from 10 to 570 fCi m^{-3}. In 1964, average concentrations of uranium-alpha in offsite samples taken 5 miles away from the facility ranged from 11 to 24 fCi m^{-3} (very close to their detection capabilities at the time). In 1969, average concentrations 1 mile from the facility were in the range of 10 to 20 fCi m^{-3}.

There were only a few calendar quarters of monitoring around the Oak Ridge Gaseous Diffusion Plant (ORGDP) in the 1960s in which *uranium* concentrations in air were reported in the journal *Radiological Health Data*. No information was given on the method or the detection limits. A release of uranium from the ORGDP in the fourth quarter of 1960 resulted in high concentrations of 4000–31,000 fCi U m^{-3} air at 2 miles and 1000–17,000 fCi U m^{-3} air at 5 miles from the plant (averages in each of four directions) during a single sampling period. During the rest of the quarter, the uranium concentrations were 0–170 fCi m^{-3} at 2 miles and 160–700 fCi m^{-3} at 5 miles from the facility. (There is no discussion about why concentrations seem to be higher at 5 miles than at 2 miles from the facility.) In the first and second quarters of 1961, uranium concentrations 5 miles away were 103 and 130 fCi m^{-3}, respectively. Uranium-specific analyses were replaced with gross alpha analyses in the fourth quarter of 1961. Like the Paducah facility, the uranium concentrations measured around the ORGDP are similar to those around Fernald in this time period; they suggest either impact from the facility, a regionally high background, or a very insensitive analytical method, which resulted in an estimate of ambient concentrations that was well above true background.

Early air pollution surveys in 1949 at the Harshaw Chemical Company and the Mallinckrodt Chemical Works indicated that concentrations near those facilities were at least as high as those observed at the FMPC. A plot of air pollution survey results around the Mallincrodt Chemical Works obtained by the Health and Safety Laboratory (HASL) of the New York Operations Office of the AEC (Weinstein 1958) showed concentrations of uranium in air of approximately 3 μg U (2000 fCi) m^{-3} at 900 ft, decreasing to 200 fCi m^{-3} at 4000 ft from the plant.

Information on the uranium operations at the Harshaw Chemical Company was located (Keller 1951, Hammond 1954, Wynveen et al. 1984). During the Manhattan Engineer District/AEC era, work involving radioactive materials was performed at various sites throughout the continental U.S. Among these sites was the Harshaw Chemical Company Complex at 1000 Harvard Ave, Cleveland, Ohio. The Harshaw Chemical Company was used primarily for the refining of yellowcake into uranium orange oxide, although the plant was capable of reducing orange oxide (UO_3) to brown oxide (UO_2), fluorination of brown oxide to green salt (UF_4) and fluorination of green salt to hexafluoride (UF_6). The feed materials for this plant came from uranium mills throughout the U.S. and Canada. Orange oxide, produced batchwise in the thermal decomposition pots of Harshaw Chemical Co., was reduced, hydrofluorinated, and cast at the Mallinckrodt Chemical Works near St. Louis. In September 1952, the AEC asked Harshaw to make any necessary changes to increase the production between four and five times (Hammond 1954).

This facility was decontaminated by Harshaw and released from AEC control in 1960. A search of AEC records indicated insufficient documentation to assure adequate decontamination had taken place, so a radiological assessment of the site was begun in 1976 (Wynveen et al. 1984). The Radiological Survey Group of Argonne National Laboratory was assigned responsibility for the survey. Extensive surface contamination with normal uranium was found throughout the site, mainly in one building, but also in 16 others and at 32 exterior locations. Several soil samples indicated extensive contamination (ranging up to 1820 pCi U per g soil). Levels were significantly above guidelines for release of the site for unrestricted use.

A plot of data from an early air pollution survey conducted by the Health and Safety Laboratory of New York City (Weinstein 1958) around the Harshaw Chemical Company showed concentrations of uranium in air of approximately 3 μg U (2000 fCi) m^{-3} at 1500 ft from the facility, decreasing to 400 fCi m^{-3} at about 4000 ft from the plant. If this facility was decommissioned in 1960, it would not have been directly contributing to environmental levels measured by the FMPC gummed-film after that time.

Machining of uranium was done at several commercial sites in the area, under contract with the Fernald site. One business we identified was Albaugh Craft (or Alba Craft) Corporation, believed to have been doing this type of work between 1952 and 1957. Like the Harshaw facility, it has been identified as a Formerly Utilized Remedial Action Program site, and cleanup work is underway. Other potential regional sources identified in a document database from the National Lead Company of Ohio are Associate Aircraft Tool and Manufacturing Company (Hamilton), Carboloy Company (Detroit), General Electric Plant (Shelbyville, Indiana), Cincinnati Milling Machine Company, Dayton Metal Stamping Company (Dayton), Simonds Saw and Steel (location unknown), Magnus Brass Company (Cincinnati), and American Foundries (location unknown).

Other sites noted in Weinstein (1958) that handled large amounts of uranium and that we have *not* investigated are the Middlesex Sampling Plant, the Lake Ontario Ordnance Works, and milling plants in the Colorado plateau area.

Other regional sites that used or processed radioactive materials that were identified, but that are unlikely sources of significant releases of uranium, include

1. Mound Laboratory, Monsanto Chemical Company, Miamisburg, Ohio
2. Shippingport Atomic Power Station, Duquesne Light Company, Shippingport, Pennsylvania
3. Battelle Memorial Institute, Columbus, Ohio
4. Argonne National Laboratory, Argonne, Illinois
5. Plum Brook Reactor Facility, Lewis Research Center, NASA, Sandusky, Ohio.

It is beyond the scope of this project to generate estimates of historical environmental contamination from these various facilities. They are simply identified and listed as examples of possible contributors to higher historical concentrations of uranium in the environment.

Fallout of Uranium from Nuclear Weapons Testing

Uranium is not normally regarded as a significant component of fallout from nuclear weapons testing. UNSCEAR (1982) does not include uranium in its annex on exposure of the public from nuclear explosions. However, because other more obvious sources could not account for measured depositions, this source was also investigated as a possibility. We thought that perhaps even though uranium had relatively minor dose significance compared with other radionuclides (for example, strontium, cesium, and plutonium), it still may have been present as a component of weapons fallout.

A computer search of Nuclear Science Abstracts was performed for the words "uranium" and "fallout." Many articles dealt with the short lived isotope, ^{237}U, (half-life, ≅ 6 days),

which is formed by the neutron capture reaction: $^{238}U(n,2n)^{237}U$. Interest in this isotope is due to the fact that its production relative to other isotopes can indicate what kind of bomb was detonated (Mishra et al. 1975).

Freiling and Kay (1966) discuss radionuclide particles in debris from tests detonated in the air (as opposed to at or below ground level). They describe the chemical composition of the particles as usually a mixture of the oxides of iron, aluminum, *uranium*, and plutonium. The isotopes ^{239}Np, ^{237}U, and ^{240}U behaved similarly in terms of their volatility.

Sisefsky and Persson (1970) refer to particles of oxides of iron and/or aluminum that incorporate the less volatile nuclides:

> When the oxides of iron and aluminium have condensed almost entirely, a gaseous remainder is left which is thus enriched in the more volatile nuclides. On account of the expansion of the cloud, they will eventually form very small particles, which may consist mainly of the relatively volatile U_3O_8 and be readily soluble in precipitation water, on account of their small sizes.

Uranium-238 and ^{234}U were identified in fresh fallout from six nuclear explosions [conducted by China and the Union of Soviet Socialist Republics (U.S.S.R.)] during 1961–1966 (Matsunami and Mamuro 1968). The samples were collected on a roof at a laboratory in Japan. Hot fallout particles were separated from ambient dust particles by elaborate procedures (Mamuro et al. 1962) before chemical separation and analysis. The presence of uranium in the hot particles from four of the six samples (Chinese tests) was clearly detected. Uranium was not detected in samples from 1961 and 1962 (Soviet tests). The main origin of the uranium found in the hot particles was believed to be the tamper materials, in which uranium, natural or depleted in ^{235}U, is used.

Atom number ratios of $^{239}Pu/^{238}U$ ranged from 1.2×10^{-5} to 1.1×10^{-4} for the four samples. We calculated what the uranium deposition in the Midwestern U.S. might have been *if* the atom number ratio were the same there. However, that ratio is dependent on the bomb design, and we do not know the atom ratios for the number of large tests, conducted mainly by the U.S. and U.S.S.R., which had already injected nuclear debris into the atmosphere before 1960 (Holleman et al. 1987). When the plutonium-to-uranium ratio is applied to deposition measurements of ^{239}Pu in Pittsburgh, Pennsylvania during 1960–1963 (Holleman et al. 1987), a relatively low estimated deposition of uranium from weapons fallout was obtained. The median deposition rate was 0.11 $\mu g\ U\ m^{-2}\ d^{-1}$, with a 90% confidence range of 0.01 to 1.45 $\mu g\ U\ m^{-2}\ d^{-1}$. This estimate is comparable to the background deposition rate from naturally occurring uranium dust in the air and would not explain the measured deposition rates around Fernald.

A second way of estimating the potential magnitude of uranium in fallout was to scale the estimated excess uranium in air in 1973, which was assumed to be entirely from weapons fallout, back to the early 1960s, based on relative concentrations of plutonium and strontium that were measured throughout this time (Voillequé 1994a, 1994b). This approach is conservative (tending to overestimate) because some of the excess uranium in 1973 was probably from oil- and coal-fired facilities, whose effluents have been cleaned up in the past two decades following implementation of Clean Air Act legislation. Estimates based on this scaling approach were ≅ 0.3 to 0.9 $mg\ m^{-2}\ mo^{-1}$ (10 to 30 $\mu g\ U\ m^{-2}\ day^{-1}$) in 1963 (peak year)

based on scaling using ^{90}Sr (Voillequé 1994a) and 0.6 mg m^{-2} mo^{-1} (20 μg U m^{-2} day^{-1}) based on scaling using plutonium (Voillequé 1994b).

We have no uranium measurements in air in 1963 at areas remote from the FMPC to check whether this scaling method is reasonable. However, concentrations of uranium in air in 1966 in New York City (0.27 fCi U m^{-3}, Figure O-7) were over 10 times less than the back-projection for the peak year of 1963 (15 fCi U m^{-3}) using this scaling method (Voillequé 1994b). We believe this approach yields an overestimate for the contribution of weapons fallout to uranium deposition.

Therefore, the magnitude of uranium deposition from weapons fallout is broadly estimated to be in the range of 0.1 μg U m^{-2} day^{-1} (based on atom ratios measured in Japan) to 30 μg U m^{-2} day^{-1} (based on scaling to strontium concentrations). Thus, weapons fallout cannot account for the measured depositions of uranium to gummed-film at distant stations around the FMPC, if the collection efficiency is 14%, and only a small fraction of the measurements if the collection efficiency is 60%.

The measurements of gross radioactivity deposited on gummed-paper around the Oak Ridge National Laboratory can give some perspective on the background fallout deposition in this area of the U.S. There was little information on the analytical technique in the annual summary reports (e.g., Hart 1960). However, we could gather that the gummed-paper was analyzed for long-lived radioactive particulates using autoradiography. This produced an estimate of radioactive particles deposited per square foot. The number of particles in different activity ranges was then used to estimate the total long-lived activity in microcuries per square foot. All values were based on averages of weekly samples. The average weekly deposition rates for 1958 through 1964 are illustrated in Figure O-11.

The perimeter and remote monitoring locations were believed to be measuring mostly weapons fallout. When fallout was low, the impact of laboratory operations was evident by the greater deposition on the onsite samples. The authors of the Oak Ridge monitoring reports note that there was a drastic curtailment of laboratory operations in the first half of 1960. Also, the arrival of weapons test fallout in September 1961 was obvious from an abrupt increase in radioactivity in weekly air and gummed-paper samples.

These data give an indication of the temporal trend in fallout radioactivity in this area of the U.S. during the time interval of interest. The peak year, of these 7 years, in the Oak Ridge area appears to be 1962, with 1964 being considerably less. This general pattern is consistent with deposition rates of ^{90}Sr in New York City (Eisenbud 1973), which were low in 1960–1961, higher in 1958–1959, and higher still in 1962–1964. This temporal trend is not seen in the FMPC gummed-film data, where the measured uranium deposition rates are fairly constant over this time period (Figure O-6), indicating that fallout from weapons tests is not likely to be the major contributor to those measured depositions.

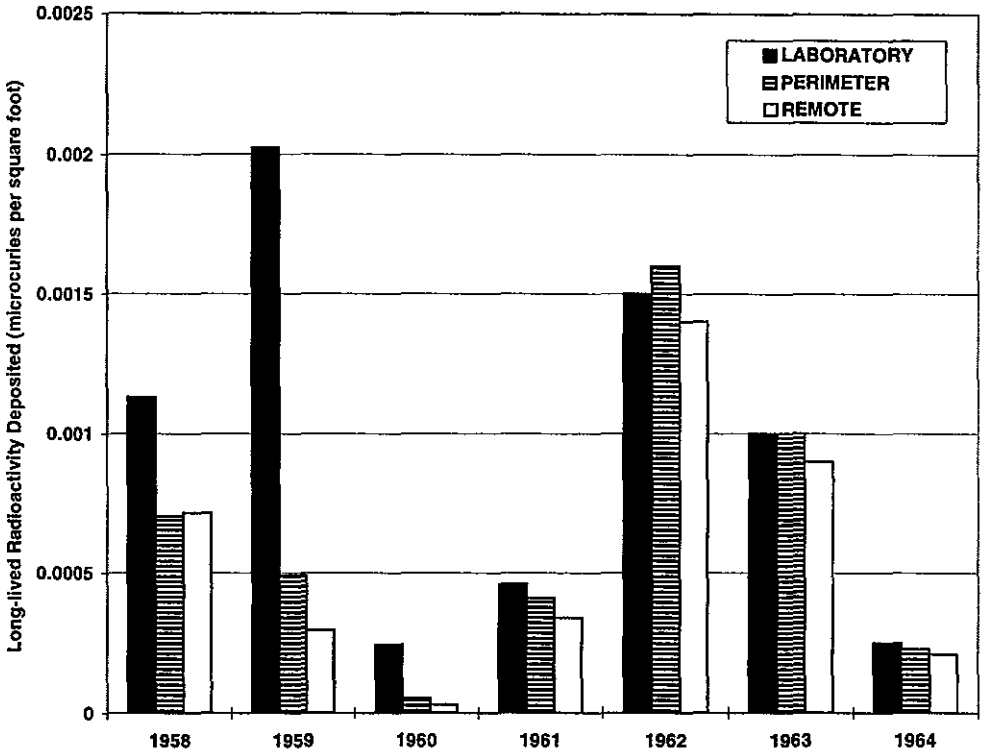

Figure O-11. Total long-lived radioactivity deposited to gummed-paper in the vicinity of the Oak Ridge National Laboratory between 1958 and 1964. The values are annual averages of weekly samples at onsite (laboratory), the laboratory perimeter, and remote locations.

Summary of Contributions from Various Sources

Figure O-12 summarizes the estimates of uranium deposition rates from various sources compared to measured deposition rates to gummed-film at distant stations around Fernald, assuming 14 and 60% collection efficiency for particulates. The contribution of other uranium processing sites in the U.S. was not estimated and, thus, is not plotted here. The total contributions of the sources identified can only account for a small number of the measured quantities if the collection efficiency is 14%. A summed total deposition rate at 7 km from the site is 34 μg U m^{-2} day^{-1} (high estimate 120), whereas the median of the measured values at the distant stations was 400 μg U m^{-2} day^{-1} if the CE were 14%. Thus, efficiency-corrected measured values were about 10 times higher than can be accounted for by the sources identified and illustrated in Figure O-12.

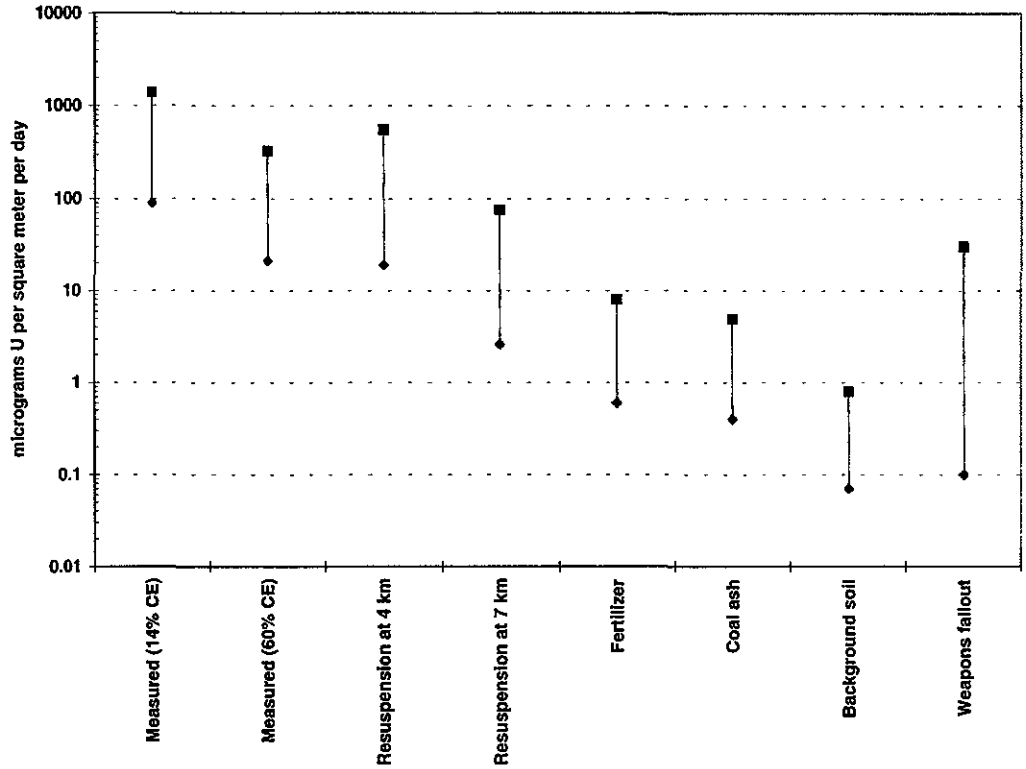

Figure O-12. Summary of estimates of uranium deposition rates from various sources compared to measured deposition rates to gummed-film at distant stations around Fernald, assuming 14 and 60% collection efficiency (CE) for particulates. The plot illustrates high and low estimates based on the methods outlined in this memo. The methods used to estimate contributions from resuspension, fertilizer, coal ash, and fallout are probably somewhat conservative (tending to overestimate deposition). However, the contribution from other uranium processing sites in the U.S. was not estimated. The total contributions of the sources illustrated here can only account for a small fraction of the measured quantities, if the collection efficiency is 14%.

DATA QUALITY AND INTERPRETATION ISSUES

Because no sources have been identified that can account for the measured uranium depositions at all of the distant stations, we must reexamine the validity of the measurements. Two data quality and interpretation issues have been identified:

1. Collection efficiency of the gummed-film for airborne particulates
2. Analytical laboratory problems with cross-contamination or other contributions.

The collection efficiency, although an important factor in use of these data, has been incorporated into our evaluations in the previous sections. A collection efficiency of 60%,

which was used by FMPC personnel at the time the measurements were taken, is believed to be an upper bound. The current state-of-the art knowledge in this area favors a collection efficiency of 14% (see discussions in Killough et al. 1993, Appendix M, and Shleien et al. 1994, Appendix B Part 1).

An early procedure for uranium analysis of a sample by the fluorometric method at the FMPC laboratory is described in Boback (1960). Uranyl salts will absorb energy from ultraviolet light and release the absorbed energy as a yellow-green fluorescence. When the uranium is fused with sodium fluoride, the amount of fluorescence is increased. The method involves a photoelectric measurement of the amount of fluorescence, which is proportional to the amount of uranium in the sample.

Boback (1960) includes a description of sample treatment, alternative extraction methods, preparation of stock solutions, blanks and cleaning of laboratory apparatus. If the procedure was followed, blanks and standards were run with each set of environmental samples. Each sample solution was analyzed in triplicate; if all three readings were not within acceptable agreement (see Boback 1960), the sample would be done over.

The fluorometric method allowed for quantitative determination of sub-microgram quantities of uranium (Boback 1960, Owens 1976, Shleien et al. 1994, Appendix B, Part 2). No values reported as less-than-detectable were found on the analytical data sheets for gummed-film. The lowest levels reported for gummed-film samples were between 10 and 20 μg.

Many of the analytical data sheets for gummed-film reported quantities of 100 to 300 μg U per film (1 ft^2) from the distant locations. This amount of uranium was measured before any collection efficiency estimate was applied to the data. We initially conducted a scoping analysis to evaluate how much of various uranium-containing materials would need to be on the gummed-film to contribute the measured amounts at the distant locations. Unreasonably large quantities were obtained (Table O-4). This analysis did not consider the collection efficiency of the gummed-film for these other materials. If the collection efficiency for these materials was also 14%, then about seven times more material would have had to be initially deposited than is shown in Table O-4.

Table O-4. Amounts of Various Materials Needed to Contribute 100–300 μg Uranium on a One Square-Foot Gummed-Film Sample

Material	Grams material per film (median estimate)	5th–95th percentile range
Background uranium in soil	52	21–140
Coal fly ash	13	6–26
Fertilizer	1	0.8–3.5

However, after examining the procedures, we were reminded that mass quantities reported on the analytical data sheets were *computed* based on the measured concentration in an aliquot of a diluted solution. The amount the sample was diluted depended on how much uranium was expected in the sample. For example, river water samples containing low concentrations of uranium could be analyzed without dilution, or might even require concentration (Dugan 1971), whereas the residue from an ashed solid sample containing a large amount of uranium might be diluted considerably before analysis. In the latter case, a

small amount of contamination might appear as a relatively large *computed* mass of uranium in the sample.

Another search for procedures describing the analysis of gummed-film was undertaken (Boback 1994). Although several procedures related to the fluorometric analysis were found, no specific procedure was found that described in detail how gumpapers were treated before analysis. M. Boback recalled that the gumpapers were ashed, dissolved in nitric acid, diluted with distilled water, and filtered before analysis by the fluorometric method (Boback 1994). A procedure describing counting procedures for beta activity confirms that gummed-film samples were ashed in a muffle furnace at 600–800 °C and counted for beta activity before they were put into solution for further analysis (Boback 1961).

Contamination of samples with uranium in the FMPC laboratory is a possible source of the high concentrations in samples taken at distant locations. Besides contamination from inadequately cleaned laboratory apparatus, Owens (1976) pointed out that if flux pellets are not completely dry before fusion, there will be splatter from dish to dish, causing cross-contamination of the samples. Boback (1960) also noted that the gas-air mixture and position of the dish must be carefully adjusted and controlled to avoid a splattered disk. If the samples from the more distant locations were run alongside those taken near the facility, this could have led to cross-contamination. Because we located no recorded quality assurance results of duplicates, blanks, or standards for gummed-film, we have been unable to quantify this potential problem.

Certain substances, such as chromium and iron, will cause low uranium results by quenching the fluorescence of the sodium fluoride-uranium flux (Dugan 1971, Owens 1976). Dugan (1971) states that the fluorescence of blanks carried through the FMPC procedure is equivalent to about 0.005 to 0.01 mg U L^{-1}; and that this background fluorescence limits the accuracy of the method in the concentration range of 0.001 to 0.01 mg L^{-1}. This is the concentration range (roughly within 10 times the detection limit) of the measurements of uranium in precipitation from the Abbe Observatory (Figure O-5).

CONCLUSIONS AND IMPLICATIONS FOR USE OF THE ENVIRONMENTAL DATA IN VALIDATION EXERCISES

The problem of unexplained high background measurements of uranium at distant locations around the Fernald facility in the 1960s has been taken seriously in the Fernald Dosimetry Reconstruction Project. We have thoroughly researched and analyzed this issue as well as can be done under the scope of this project. Because of lack of documented information in several key areas, no definitive conclusions can be made. Scientific judgment must be applied based on the weight-of-evidence. Our conclusions are highlighted here.

The flat concentration curves with distances beyond 5 km are the main argument that the Fernald site is not the primary contributor to the measured uranium concentrations at the distant locations. There is a small possibility that a combination of the Fernald site, other uranium processing facilities, weapons fallout, and resuspension of FMPC-released uranium could truly have resulted in environmental contamination with uranium at the measured levels. Contributions from coal ash, fertilizer, and background uranium in soil would have made very minor contributions to measured deposition rates.

However, all of the uranium measurements during this period were run in the FMPC analytical laboratory. There were no corroborating measurements by a laboratory using more sensitive methods or that did not have as much potential for contamination from high-level samples. No documentation was located that could verify reasonable results for laboratory blanks, for example, although procedures indicated that they should have been run. We feel that the weight-of-evidence indicates a larger probability that the FMPC laboratory in the late 1950s and early 1960s could not accurately measure uranium at the low concentrations truly present at the more distant locations. A likely reason is cross-contamination from apparatus and samples containing much higher uranium concentrations, but this is unproven.

It is our recommendation and intention to use the early environmental monitoring data collected within 5 km of the site in our validation exercises. These exercises will compare predicted environmental concentrations, based on source term reconstruction and environmental transport modeling, with the measured environmental concentrations. The results of the validation exercises will be presented in the final (Task 6) report of the dose reconstruction project. The concentrations measured close to the FMPC are 10 to 1000 times higher than those measured further away. It is our judgment that the laboratory should have been able to measure uranium with reasonable accuracy at these much higher levels. The environmental data provide important confirmation of the timing and dispersion of airborne releases and a check on model performance, and thus are too important to the project to discount entirely.

REFERENCES

Apt K.E. and V.J. Lee. 1975. *Environmental Surveillance at Los Alamos During 1974*. Rep. LA–5977–PR. In: *Environmental Monitoring at Major U.S. Energy Research and Development Administration Sites. Calendar Year 1974*. Report ERDA-54 (1974), National Technical Information Service, Springfield, Virginia.

Baker R.C. and E.G. Brown. 1959. *AEC Research and Development Report. Environmental Monitoring Summary for the Paducah Plant for 1958*. Report KY-273, Union Carbide Nuclear Company, Paducah, Kentucky.

Beck H.L., C.V. Gogolak, K.M. Miller, and W.M. Lowder. 1980. "Perturbations on the Natural Radiation Environment due to the Utilization of Coal as an Energy Source." pp. 1521–1558 in *Natural Radiation Environment III*, T.F. Gesell, W.M. Lowder, eds., Report CONF-780422(Vol. 2), Technical Information Center, U.S. Department of Energy.

Bedrosian P.H., D.G. Easterly, and S.L. Cummings. 1970. *Radiological Survey Around Power Plants Using Fossil Fuel*. Report EERL-71-3, U.S. Environmental Protection Agency, Rockville, Maryland.

Boback M.W. 1960. *Fluorometric Method of Analysis for Uranium*. Analytical Laboratory Department document dated April 1, 1960, National Lead Company of Ohio, Cincinnati, Ohio.

Boback M.W. 1961. *Counting Procedures, Beta Activity*. Analytical Laboratory Department document revised May 10, 1961, National Lead Company of Ohio, Cincinnati, Ohio.

Boback M.W. 1994. Memo 94-026 dated May 18, 1994, to Felix Rogers, Centers for Disease Control and Prevention. Subject: Procedure for Treatment & Analysis of Gumpapers. Westinghouse Environmental Management Company of Ohio, Cincinnati, Ohio.

Dugan T.A. *Fluorimetric Method of Analysis for Uranium.* 1971. National Lead Company of Ohio, Cincinnati, Ohio.

Eisenbud M. 1973. *Environmental Radioactivity*. Second Edition. Academic Press, New York, New York.

Freiling E.C. and M.A. Kay. 1966. "Radionuclide Fractionation in Air-Burst Debris." *Nature* **209**(5020):236–238.

Hamilton E.I. 1970. "The Concentration of Uranium in Air from Contrasted Natural Environments." *Health Physics* **19**:511-520.

Hammond D.A. 1954. *Technical Report on the Expanded Harshaw TBP Extraction Process.* Report NYO-1468 dated May 11, 1954. Declassified March 15, 1960. The Harshaw Chemical Company, Cleveland, Ohio.

Harley J.H., N.A. Hallden, and L.S.Y. Ong. 1960. *Summary of Gummed-Film Results Through December 1959*. Report HASL-93. National Technical Information Service, Springfield, Virginia.

Hart J.C. 1960. *Applied Health Physics Annual Report for 1958*. Oak Ridge National Laboratory Rep. ORNL-2777. National Technical Information Service, Springfield, Virginia.

Holleman J.W., P.A. Quiggins, B.D. Chilton, M.S. Uziel, H.A. Pfuderer, and J.A. Longmire. 1987. *Worldwide Fallout of Plutonium from Nuclear Weapons Tests*. Report ORNL-6315. National Technical Information Service, Springfield, Virginia.

Jaworowski Z., L. Kownacka, M. Bysiek. 1980. "Global Distribution and Sources of Uranium, Radium–226, and Lead–210." pp. 383–403 in *Natural Radiation Environment III*. T.F. Gesell, W.M. Lowder, eds., Report. CONF-780422(Vol. 2), Technical Information Center, U.S. Department of Energy.

Keller W.H. 1951. *Production of Uranium Metal from Uranium Tetrafluoride Made from Uranium Trioxide Produced at Harshaw Chemical Co.* Report NYO-1329 dated December 27, 1951. Declassified March 2, 1957. Mallinkrodt Chemical Co., St. Louis, Missouri.

Killough G.G., M.J. Case, K.R. Meyer, R.E. Moore, J.F. Rogers, S.K. Rope, D.W. Schmidt, B. Shleien, J.E. Till, and P.G. Voillequé. 1993. *The Fernald Dosimetry Reconstruction Project. Task 4. Environmental Pathways — Models and Validation*. Draft Report CDC-3. Radiological Assessments Corporation, Neeses, South Carolina.

Mamuro R., A. Fujita, T. Matsunami and K. Yoshikawa. 1962. "Microscopic Examination of Highly Radioactive Fall-Out Particles." *Nature* **196**(4854):529–531.

Matsunami T. and T. Mamuro. 1968. "Uranium in Fallout Particles." *Nature* **218**:556–557.

McEachern P., W.G. Myers, and F.A. White. 1971. "Uranium Concentrations in Surface Air at Rural and Urban Localities within New York State." *Envir. Sci. Tech.* **5**(8):700–703.

Mishra U.C., B.Y. Lalit, S.K. Sethi, V.K. Shukla, and R.V. Ramachandran. 1975. "Some Observations Based on the Measurements on Fresh Fallout From the Recent Chinese and French Nuclear Explosions." *J. Geophys. Res.* **80**(36):5045–5049.

Owens J.W. 1976. *Fluorometric Determination of Uranium in Environmental Materials.* Report LA-6338-MS. National Technical Information Service, Springfield, Virginia.

Sedlet J., N.W. Golchert, and T.L. Duffy. 1975. *Environmental Monitoring at Argonne National Laboratory Annual Report for 1974.* Rep. ANL-75-18. In: *Environmental Monitoring at Major U.S. Energy Research and Development Administration Sites. Calendar Year 1974.* Report ERDA-54 (1974). National Technical Information Service, Springfield, Virginia.

Shleien B., S.K. Rope, M.J. Case, G.G. Killough, K.R. Meyer, R.E. Moore, D.W. Schmidt, J.E. Till, and P.G. Voillequé. 1994. *The Fernald Dosimetry Reconstruction Project. Task 5. Review of Historic Data and Assessments for the FMPC.* Report CDC-4. Radiological Assessments Corporation, Neeses, South Carolina.[4]

Sisefsky J. and G. Persson. 1970. "Fractionation Properties of Nuclear Debris from the Chinese Test of 24 December 1967." *Health Physics* **18**:347–356.

Styron C.E. 1980. "An Assessment of Natural Radionuclides in the Coal Fuel Cycle." pp. 1511–1520 in *Natural Radiation Environment III.* T.F. Gesell, W.M. Lowder, eds., Report CONF-780422(Vol. 2), Technical Information Center, U.S. Department of Energy.

UNSCEAR (United Nations Scientific Committee on the Effects of Atomic Radiation). 1982. *Ionizing Radiation: Sources and Biological Effects.* 1982 Report to the General Assembly, with annexes. United Nations, New York.

Voillequé P.G., K.R. Meyer, D.W. Schmidt, S.K. Rope, G.G. Killough, M. Case, R.E. Moore, B. Shleien, and J.E. Till. 1993. *The Fernald Dosimetry Reconstruction Project. Tasks 2 and 3. Radionuclide Source Terms and Uncertainties.* Draft Report CDC-5. Radiological Assessments Corporation, Neeses, South Carolina.

Voillequé P.G. 1994a. "Fallout Contribution to Measured Uranium Deposition." Memo dated May 10, 1994, to S.K. Rope, Environmental Perspectives, Inc., Idaho Falls, Idaho.

Voillequé P.G. 1994b. "Global Fallout Contribution to Measured Uranium Deposition, Part 2." Memo dated May 23, 1994, to S.K. Rope, Environmental Perspectives, Inc., Idaho Falls, Idaho.

Weinstein M.S. 1958. "Environmental Contamination." pp. 180–184 in *Symposium on Occupational Health Experience and Practices in the Uranium Industry*, held in New York City, October 15–17, 1958. Report HASL-58, U.S. Atomic Energy Commission and the Health and Safety Laboratory, New York.

Welford G.A. and R. Baird. 1967. "Uranium Levels in Human Diet and Biological Materials." *Health Physics* **13**:1321-1324.

Wynveen R.A., W.H. Smith, C.M. Choleen, A.L. Justus, and K.F. Flynn. 1984. *Formerly Utilized MED/AEC Sites Remedial Action Program. Radiological Survey of the Harshaw Chemical Company, Cleveland, Ohio.* Report DOE/EV-0005/48. National Technical Information Service, Springfield, Virginia.

[4] *[Note to reader: the final date of the Shleien et al. report was March 1995 and the Voillequé et al. report was June 1995; however these versions were not available at the time this appendix was written (see preface to this appendix for explanation).]*

APPENDIX P

PREVIOUS STUDIES OF URANIUM AND RADON RELEASES

This appendix summarizes previous studies of uranium and radon releases from the Feed Materials Production Center (FMPC) in Fernald, Ohio, that were completed prior to the completion of the Fernald Dosimetry Reconstruction Project. These studies reported quantities of materials released and radiation doses to the population from these FMPC releases (Boback et al. 1985, Boback et al. 1986, Boback et al. 1987, IT 1989, Makhijani 1988, Makhijani and Franke 1989, Franke 1988, Moore 1984, Kennedy 1985). Uranium release estimates and previous studies of radon releases are reviewed separately. This analysis is limited to estimates of airborne releases of uranium and radon and radon decay products because the inhalation pathway has been shown to be the major contributor to dose to the offsite population and because it provides a useful basis for comparisons among the studies (Meyer et al. 1996, Voillequé et al. 1995). Other pathways and radionuclides did contribute to offsite doses; however, the extent of their contribution was generally less than for the inhalation pathway (see Appendix K).

PREVIOUS AIRBORNE URANIUM RELEASE ESTIMATES USED IN DOSE CALCULATIONS

In the studies reviewed here, the radiation dose estimates were based on release data for airborne uranium. Table P–1 presents annual airborne uranium release estimates reported in previous assessments of past releases.

Site-based Estimates

The source term estimates originating from the FMPC come from several reports. By 1985, the best source of uranium release data was Boback et al. (1985). In November 1986, a revision of this document listed new estimates for airborne uranium discharges for the early years prior to the initiation of continuous site stack sampling (Boback et al. 1986). The 1986 report increased the estimate of airborne uranium releases by just over 20% and identified additional release sources of airborne uranium such as the Plant 2/3 gulping operations.

The third historical release report (Boback et al. 1987) built upon the earlier estimates (Boback et al. 1986), but it included releases from incinerators and discharges from the Plant 8 wet scrubbers. This third report estimated airborne uranium releases from plant operations only. Other sources of airborne uranium releases were reported in 1988 (Dolan and Hill 1988, Semones and Sverdrup 1988) and 1989 (Clark et al. 1989) as addenda to Boback et al. (1987). The other sources of uranium emissions that were added to initial estimates were (a) gulping emissions, (b) other uranium process emissions, (c) emissions from building exhausts, (d) laboratory venting, (e) fugitive dusts from storage areas and waste pits, and (f) nonroutine events (accidents). These latter uranium release estimates are listed in Table P-1 as Clark et al. (1989) and IT (1989).

Table P-1. Summary of Airborne Uranium Release Estimates (kg)

Year	Source of Estimates				
	Boback et al. (1987)	Clark et al. (1989) IT (1989)	Moore (1984) Kennedy (1985)	Makhijani and Franke (1989) Alt #1	Alt #2
1951	123	125	NA	123	123
1952	499	543	NA	499	499
1953	2078	2183	21	2081	2081
1954	15119	15486	1350	16270	17081
1955	32976	33893	1414	37019	40383
1956	13595	15519	21043	20268	25988
1957	8045	11025	9577	16329	23474
1958	5513	9055	4472	14536	22364
1959	5127	9177	5956	16018	25596
1960	4873	9153	4693	17765	28955
1961	3516	7427	4066	15212	25376
1962	4568	6942	3740	14459	22886
1963	6036	6375	5390	13588	19603
1964	5253	5583	7004	14830	22765
1965	7045	7494	7846	9228	14232
1966	3049	3731	2813	7242	11350
1967	2925	3726	2786	8286	13045
1968	4655	5885	4357	10387	16492
1969	3898	4708	4228	5111	8123
1970	1488	1983	1434	3346	5116
1971	772	1092	775	1655	2625
1972	614	1601	351	1685	2858
1973	496	1739	528	1886	3212
1974	235	2697	236	2898	5262
1975	318	3138	118	3415	6211
1976	169	3539	225	4005	7354
1977	192	978	79	2427	4029
1978	222	261	139	756	1032
1979	155	200	56	874	1291
1980	267	317	257	734	1001
1981	587	677	198	557	685
1982	280	395	479	1446	2039
1983	181	376	180	1776	2723
1984	377	1014	174	2084	3105
1985	121	315	NA	1051	1562
1986	62	130	NA	NA	NA
1987	42	302	NA	NA	NA

Estimates by Independent Contractors

In response to concern from residents of the Fernald area, the Centers for Disease Control and Prevention (CDC) contracted with the International Technology Corporation (IT) in 1985 to assess the feasibility of conducting an epidemiological study of the possible health effects from exposure to radiation among the residents of communities near the FMPC. For their dose estimates, the IT Corporation used site-generated estimates of FMPC uranium emissions, essentially those in Boback et al. (1987) with revisions provided by Clark et al. (1989). The estimates used by IT are listed in Table P-1 as Clark et al. (1989) and IT (1989).

Estimates from Other Organizations

Moore (1984) and Kennedy (1985) provided FMPC source term estimates for the U. S. Environmental Protection Agency. Their estimates appear to be based loosely on the release estimates reported by the site in 1985 (Boback et al. 1985), but some of the values reported in the EPA documentation for the mid-1980s are lower.

The Radioactive Waste Campaign (Resnikoff 1989) and the Institute For Energy and Environmental Research (IEER) (Franke 1988, Makhijani and Franke 1989) both employed the uranium release data from an FMPC report (Boback et al. 1987). The Radioactive Waste Campaign document converted the uranium release values from kilograms of uranium to curies using a conversion factor of 6.67×10^{-7} Ci g^{-1} (Resnikoff 1989). Makhijani (1988) and Makhijani and Franke (1989) estimated airborne uranium releases for two alternative situations that were based on different efficiency factors for the Plant 8 scrubbers (Alternative #1 used 70% efficiency and Alternative #2 used 83% efficiency). They used Alternative #1 to make radiation dose estimates (Franke 1988, Makhijani and Franke 1989). They also based a uranium release estimate on soil sampling data (Makhijani 1988).

Table P–2 presents the total estimated airborne uranium releases from the FMPC for various periods during its operational history (1951–1988). These previous studies have yielded uranium release estimates that are less than our median, or 50th percentile, estimate of 310,000 kg uranium, with 5th and 95th uncertainty bounds of 270,000 to 360,000 kg. Our uncertainty ranges do not encompass these previous estimates except for those of Makhijani and Franke (1989) and Franke (1988).

Uranium release estimates from most other studies are less than our median, or 50th percentile, estimate of 310,000 kg uranium.

PREVIOUS RADIATION DOSE ESTIMATES TO THE PUBLIC FROM URANIUM RELEASED TO AIR FROM THE FMPC

Table P–3 summarizes the methodologies used in various studies for determining radiation doses to residents near the FMPC. The environmental transport, airborne radionuclide concentrations and radiation doses in most cases were determined with the AIRDOS–EPA computer code (Moore et al. 1979, ORNL 1986). Radiation doses are expressed as committed dose equivalent (70 year) to the lung or effective dose equivalent for individuals at different distances from the site and with different physical characteristics. To run atmospheric transport models, knowledge of various site-specific parameters is required, including the quantity and type of materials released, the particle size distributions of the

released materials, the meteorological conditions, and the effective stack height (physical stack height plus plume rise). These studies have differing approaches because of the variations in source term estimates, atmospheric modeling parameters, target population groups, and dosimetry. The dose estimates from these various studies are not directly comparable because of different approaches, assumptions and parameter values used in the studies.

Table P–2. Summary of Estimates of Total Airborne Releases of Uranium from the FMPC 1951–1987

Reference	Years (inclusive)	Uranium (kg)
Moore (1984) Kennedy (1985)	1953 – 1984	96,000
Boback et al. (1987)	1951 – 1985	135,000
Dolan & Hill (1988), Clark et al. (1989), IT (1989)	1951 – 1987	179,000
Makhijani and Franke (1989); Franke (1989)	1951 – 1985 Alternative #1 Alternative #2 Based on soil sampling	 270,000 391,000 273,000–1,400,000
Meyer et al. 1996; Voillequé et al. (1995) (Current study)	1951 – 1988	310,000 (270,000-360,000)[a]

[a] 5th to 95th percentile distribution

The IT (1989) study calculated doses using an EPA–AIRDOS code (ORNL 1986) for seven specific distances (1100 to 24,000 m) in 16 different directions from the FMPC. Meteorological data from the Cincinnati-Northern Kentucky Airport were used in the atmospheric model calculations. They assumed an area source (circle with a 337-m diameter) instead of a point source, a 20-m effective stack height, and a particle size of 1-μm average median aerodynamic diameter. They calculated 70-year committed effective dose equivalents to an individual on an annual basis for the years of operation (Table P-4), and computed the 70-year cumulative dose equivalent to the lung (Table P-5). The calculated 70-year committed dose equivalent to the lung of a maximally-exposed individual over the 34-year period of the study (1951–1984) was about 25 rem (for all sources except radon).

Previous studies, reviewed here, calculated the dose equivalent to the lung on an annual basis. The IT (1989) study calculated the effective dose equivalent.
The effective dose equivalent provides a measure of the dose to the whole body, taking into account the dose absorbed by each of the target organs and the sensitivity of those organs to radiation.

Table P-3. Summary of Methods Used in Previous Dose Calculations for Residents Near the FMPC

Study	Particle size (μ)[a]	Translocation class[b]	Effective stack height	Uranium source configuration	Meteorology	Distance from site center (m)	Direction	Target individual characteristics	Computer model
IT (1989)	1	Class D, Y or W	20	Area (89,200 m^2)	Cincinnati-airport (1951-1984)	Seven distances	All	ICRP 30	AIRDOS-EPA
Moore (1984)	1	NA[c]	10	Point	Cincinnati-airport (1981)	810	NE	ICRP 30	AIRDOS-EPA
Kennedy 1985	2	Class Y 90% Class W 10%	30	Point	Cincinnati-airport (1981)	1143	NNE	ICRP 30	AIRDOS-EPA
Franke (1988)	1	Class Y	10	Point	Dayton airport (1976)	Site boundary	All	ICRP 30 (avg. adult and 15-yr-old male, exercising)	NA
Resnikoff (1989)	1	NA	NA	NA	Dayton airport	1000	NE		EPA-AIRDOS

[a] Activity median aerodynamic diameter.
[b] Classification scheme for inhaled material according to its rate of clearance from the pulmonary region of the lung.
[c] NA=not available.

The methodology and assumptions used by the EPA (EPA 1984) are based on the International Commission on Radiation Protection (ICRP) 26 and ICRP 30 models (ICRP 1977, ICRP 1979). These models were employed for the estimates in Tables P–4 and P–5. Both Moore (1984) and Kennedy (1985) calculated committed dose equivalent (70 years) to a maximally-exposed individual based on the AIRDOS–EPA computer code (Moore et al. 1979). The meteorology for both studies was the 1981 Cincinnati airport data that were routinely used by the FMPC for dispersion calculations. Different source term estimates, particle size and translocation classes, plume rise, stack heights, and locations for the maximally-exposed individual were employed. These differences contribute to the different resultant doses (Tables P-4 and P-5). For 1953 through 1984, the committed dose equivalent to the lung for the maximum individual was 42.6 rem for the Moore (1984) estimate and 21.6 rem for the Kennedy (1986) estimate (Table P–5).

The IEER study (Makhijani and Franke 1989, Franke 1988) used the isotopic concentrations of measured airborne particulates in FMPC air for 1986 as the basis for calculating an average cumulative dose equivalent of 75 rem to the lung of an adult. If the target individual was a 15-year-old boy exercising for one-half hour during an accidental release of uranium, then the subject's lung dose would be 5.5 times higher than the average adult's dose, or 410 rem (Table P–5).

Resnikoff (1989) estimated radiation doses to the public using EPA's computer code AIRDOS (Moore et al. 1979) and Dayton airport meteorology. Using 1981 as the reference year, he calculated a lung dose of 365 mrem based on an estimated uranium release of 677 kg (Table P–4). The committed dose equivalent to the lungs for the maximum individual for the period of the study was estimated to be 84.3 rem (Table P–5).

Table P-4 presents the annual radiation dose estimates to a specific individual from these previous studies. These doses are expressed either as the committed dose equivalent to the lungs or effective dose equivalent. Table P–5 summarizes total radiation doses to the lungs from uranium releases to the individuals identified in each study for various years between 1951 and 1987.

Table P–4. Annual Dose Estimates Reported in Previous Studies[a] (rem)

Year	Dose equivalent to the lung				Effective dose equivalent
	Moore (1984)[b]	Kennedy 1985[c]	Resnikoff 1989[d]	Franke 1988[e]	IT 1989[f]
1951	none reported	none reported	0.007	none reported	0.002
1952	none reported	none reported	0.31	none reported	0.010
1953	0.009	0.004	0.18	0.40	0.045
1954	0.60	0.30	9.3	6.0	0.38
1955	0.63	0.30	20	9.0	0.73
1956	9.4	5.0	8.6	1.1	0.26
1957	4.3	2.0	5.0	1.3	0.16
1958	2.0	1.0	3.4	1.5	0.13
1959	2.6	1.0	3.2	1.4	0.14
1960	2.1	1.0	3.0	1.6	0.11
1961	1.8	0.90	2.2	1.3	0.083
1962	1.7	1.0	2.8	1.8	0.12
1963	2.4	1.0	3.7	1.7	0.20
1964	3.1	2.0	3.2	1.7	0.16
1965	3.6	2.0	4.4	2.6	0.22
1966	1.2	0.60	1.9	0.70	0.072
1967	1.2	0.60	1.8	1.1	0.078
1968	1.9	1.0	2.9	2.0	0.12
1969	1.9	1.0	2.4	1.6	0.11
1970	0.66	0.30	0.92	0.50	0.060
1971	0.34	0.20	0.48	0.25	0.029
1972	0.16	0.080	0.38	0.10	0.019
1973	0.23	0.10	0.31	0.25	0.018
1974	0.10	0.050	0.15	0.075	0.011
1975	0.052	0.030	0.19	0.12	0.011
1976	0.099	0.050	0.10	0.10	0.008
1977	0.035	0.020	0.12	0.10	0.014
1978	0.061	0.030	0.11	0.10	0.013
1979	0.024	0.010	0.093	0.10	0.012
1980	0.11	0.060	0.17	0.15	0.007
1981	0.088	0.040	0.37	0.20	0.008
1982	0.21	0.010	0.17	0.075	0.010
1983	0.079	0.040	0.11	0.10	0.005
1984	0.077	0.040	0.23	0.10	0.020
1985	none reported	none reported	0.047	none reported	none reported
1986	none reported	none reported	0.019	none reported	none reported
1987	none reported	none reported	0.019	none reported	none reported

[a] Table P–5 summarizes doses for entire period.
[b] Reported doses for individual located at 810 m northeast of the site.
[c] These reported values represent a "best estimate of the maximum individual lung dose for an individual" located at 1143 meters downwind in the north northeast sector.
[d] Reported doses for individual located at 1100 m north northeast of the site.
[e] Reported "maximum individual radiation doses to the lung of an average adult at the plant boundary due to non-accidental releases of uranium."
[f] Committed effective dose to the maximally exposed individual.

Table P-5. Summary of Total Lung Doses from Uranium[a]

Study	Years (inclusive)	Equivalent dose to lungs (rem)	Cumulative effective dose (rem)
Moore (1984)	1953-1984	43	
Kennedy (1985)	1953-1984	22	
Makhijani and Franke	worst case[b]	75[c]	
(1989), Franke (1988)		410[d]	
IT (1989)	1951-1984	25	2.7
RAC-current study			
Scenario 1	1951-1988	46 (14-140)	6.1 (2.1-18)
Scenario 2	1951-1988	15 (4.4-42)	2.1 (0.74-5.7)
Scenario 3	1951-1988	13 (4.6-36)	3.1 (1.9-6.1)
Scenario 4	1960-1978	4.8 (1.5-14)	0.93 (0.40-2.2)
Scenario 5	1951-1988	4.0 (1.2-11)	0.53 (0.17-1.4)
Scenario 6	1951-1988	24 (7.8-67)	3.3 (1.1-8.8)
Scenario 7	1951-1988	4.0 (1.2-9.6)	0.55 (0.21-1.2)
Scenario 8	1975-1988	0.7 (0.2-2)	0.096 (0.030-0.25)
Scenario 9	1951-1969	8.5 (2.5-24)	1.1 (0.35-3.0)

[a] These dose estimates are not directly comparable because of different approaches, assumptions and parameter values used in the various studies; these values represent doses from airborne uranium only, and radon has not been considered.
[b] Maximum lung dose from a single accidental release over a one-hour period, using weekly air concentrations.
[c] Average adult.
[d] Exercising 15-year-old male near fence.

EVALUATION OF PREVIOUS ESTIMATES OF RADON RELEASES FROM THE K-65 SILOS

The IT Corporation evaluated the source term for radon-222 emissions from the K-65 storage silos in their assessment of doses from historical releases from the FMPC (IT 1989). This assessment did not include original calculations; rather, it summarized and revised calculations from two other sources. Two pathways for emissions of radon from the silos were considered: (1) diffusion of radon from the K-65 residue into the silo air space and subsequent diffusion through the concrete domes into the surrounding air and (2) free air exchange between the silo air and surrounding air through cracks in the domes. The estimate of diffusion emissions was taken directly from the calculation of Borak (1985). The Boback et al. (1987) report estimated the radon emissions from only the diffusion pathway and incorporated the Borak report as Appendix A. In the IT report, the estimate of air exchange

emissions was taken from the Westinghouse Materials Company of Ohio feasibility investigation report, with minor modifications (Grumski 1987, IT 1989). Detailed descriptions of these previous assessments of radon releases from the K-65 silos are presented in Appendix J of the Task 2/3 source term report for this project (Voillequé et al. 1995).

These previous studies of Borak (1985) and the IT Corporation (1989) estimated radon releases from information about the silos and the K-65 material in them. A more recent study estimated the radon releases based on a back-calculation from measured radon concentrations around the FMPC and models of the atmospheric dispersion of the radon in transport to the monitoring locations (Hamilton et al. 1993). The result was an estimated release rate of 1150 Ci y^{-1} for 1989 and 1990. The uncertainty in this estimate was not provided. However, the range of estimated source terms when individual locations were considered was 575 to 4025 Ci y^{-1}.

Table P-6 compares our results with previous estimates of the emissions of radon from the K-65 silos. This comparison of release rates is only for a relatively short period and during the lowest releases. The other studies did not report uncertainties associated with the release estimates.

Table P-6. Comparisons of Current Estimates of Radon Release Rates (Ci y^{-1}) from K-65 Silos to Release Rates from Other Studies

	Percentiles of our estimates			Results of other studies	
Period, release pathway	5th	Median	95th	Value	Reference
1980–1987, diffusion	56	140	320	60 [a]	Borak 1985, IT 1989
1980–1987, air exchange	250	740	2000	1023 [a]	IT 1989
1980–1987, total	340	880	2400	1083 [a]	IT 1989
1988, total	36	220	1300	1150 [b]	Hamilton et al. 1993

[a] These results were considered by IT (1989) to apply to the complete period 1953–1984, but we believe that the conditions and parameters used to develop the estimates were only valid for the period July 1979–1987.

[b] This result was the average release rate calculated for 1989–1990. We compare it to our results for 1988 because we believe conditions of the silos were unchanged for 1988–1991.

Table P-7 summarizes estimates of radiation dose equivalent to the lung from radon releases from the K-65 silos from the current study and from the IT (1989) study. The IT study did not report uncertainties associated with the release rate estimates.

SUMMARY AND CONCLUSIONS

Estimates of releases of uranium and radon from the FMPC and their impact on the local residents have been reported previously. This appendix briefly assesses several of these studies and provides tables of release estimates and radiation dose estimates from these studies. The previous studies used a diversity of source term estimates, model assumptions, and site-specific parameters in calculating radiation doses to target individuals in the nearby community around the site. As a result, it is not possible to directly compare results among

the studies or compare the dosimetry results with this study. Nevertheless, the previous studies can be considered to contribute to an understanding of radiation doses to which the population around Fernald may have been exposed.

Our methodology involves estimating the 50th percentile, or median, estimate of the radiation doses to representative individuals described in nine scenarios in addition to conducting a formal uncertainty analysis of parameters associated with these dose estimates. This approach represents a significant improvement in the state-of-the-art of radiation dosimetry analysis that was not available in earlier studies.

Table P-7. Summary of Lung Equivalent Dose from Radon Releases

Study	Years (inclusive)	Equivalent dose to lungs (rem)	Effective dose (rem)
IT (1989)[a]	1951-1984		0.067
RAC[b]	1953-1984		
Scenario 1	1951-1988	360 (98–1400)	24
Scenario 2	1951-1988	360 (98–1300)	24
Scenario 3	1951-1988	260 (89–1000)	17
Scenario 4	1960-1978	120 (40–720)	10
Scenario 5	1951-1988	420 (10–200)	2.5
Scenario 6	1951-1988	220 (53–920)	16
Scenario 7	1951-1988	39 (12–150)	2.2
Scenario 8	1975-1988	44 (10–220)	3.0
Scenario 9	1951-1969	75 (17–480)	4.5

[a] Effective dose equivalent to the maximally exposed individual from radon only. The effective dose equivalent is the sum of the weighted dose equivalents for all irradiated tissues, using the weighting factors in ICRP Publication 26 (ICRP 1977).
[b] Dose equivalent to the lung from releases of radon and radon decay products from the FMPC; values are median estimates with 5th and 95th percentile values in parentheses.

REFERENCES

Boback M.W., D.A. Fleming, T.A. Dugan, R.W. Keys, and R.B. Grant. 1985. *History of FMPC Radionuclide Discharges.* Report NLCO–2039. Feed Materials Production Center. Westinghouse Materials Company of Ohio, Cincinnati, Ohio.

Boback M.W., D.A. Fleming, T.A. Dugan, R.W. Keys, and R.B. Grant. 1986. *History of FMPC Radionuclide Discharges.* Report FMPC–2058. Feed Materials Production Center. Westinghouse Materials Company of Ohio, Cincinnati, Ohio.

Boback M.W., D.A. Fleming, T.A. Dugan, R.W. Keys, and R.B. Grant. 1987. *History of FMPC Radionuclide Discharges.* Report FMPC–2082. Feed Materials Production Center. Westinghouse Materials Company of Ohio, Cincinnati, Ohio.

Borak T. B. 1985. "Calculation of radon emission, dispersion and dosimetry from K65 Storage Tanks at the Feed Materials Production Center." In: Boback, M. W., T.A. Dugan, D.A. Fleming, R.B. Grant, and R.W. Keys. 1987. *History of FMPC Radionuclide Discharges.* Report FMPC-2082. Westinghouse Materials Company of Ohio, Cincinnati, Ohio.

Clark T.R., L. Elikan, C.A. Hill, and B. L. Speicher. 1989. *History of FMPC Radionuclide Discharges, Revised Estimates of Uranium and Thorium Air Emissions from 1951–1987. Addendum to FMPC–2082.* Feed Materials Production Center. Westinghouse Materials Company of Ohio, Cincinnati, Ohio.

Dolan L.C. and C.A. Hill. 1988. *History of FMPC Radionuclide Discharges. Addendum to FMPC–2082.* Feed Material Production Center. Westinghouse Materials Company of Ohio, Cincinnati, Ohio.

Franke B. 1988. *Preliminary Assessment of Radiation Exposures Associated with Releases of Radioactive.* Institute for Energy and Environmental Research, Takoma Park, Maryland.

Grumski J.T. 1987. *Feasibility Investigation for Control of Radon Emission from the K-65 Silos.* Revision 1, July 30. Westinghouse Materials Company of Ohio, Cincinnati, Ohio.

Hamilton L.D., A.F. Meinhold, S.L. Baxter, S. Holtzman, S.C. Morris, R. Pardi, M.D. Rowe, C. Sun. 1993. *Pilot study of risk assessment for selected problems at the Fernald Environmental Management Project (FEMP).* Report BNL-48777, revised. Brookhaven National Laboratory, Upton, New York.

International Commission on Radiation Protection (ICRP). 1977. *Recommendations of the International Commission on Radiation Protection and Measurements.* ICRP Publication 26. Annals of the ICRP. Pergamon Press, New York.

International Commission on Radiation Protection (ICRP). 1979. *A Report of Committee 2, Publication 30,* Supplement to Part I, Annals of the ICRP. Pergamon Press, New York. Vol. 3, No. 1–4.

International Technology Corporation (IT). 1989. *Assessment of Radiation Dose and Cancer Risk For Emissions From 1951 Through 1984.* Report No. IT/NS–89–109.

Kennedy W.E. 1985. Ad Hoc Assistance—Lung Dose Estimates for FMPC from 1953 Through 1984, Radiological Experiment, Letter to Mr. S.P. Mather, Radiological Sciences Department, U.S. Department of Energy.

Makhijani A. 1988. *Release Estimates Of Radioactive and Non–Radioactive Materials To The Environment By The Feed Materials Distribution Center 1951–1985.* Institute for Energy and Environmental Research, Takoma Park, Maryland.

Makhijani A. and B. Franke. 1989. Addendum to the report *Releases Estimates of Radioactive and Non–Radioactive Materials to the Environment By The Feed Materials Distribution Center 1951–85.* Institute for Energy and Environmental Research, Takoma Park, Maryland.

Meyer K.R., P.G. Voillequé, G.G. Killough, D.S. Schmidt, S.K. Rope, B. Shleien, R.E. Moore, M.J. Case and J.E. Till. *Overview of the Fernald Dosimetry Reconstruction Project and Source Term Estimates for 1951–1988.* Health Physics 71(4): 425-437. October 1996.

Moore R.E., C.F. Baes, L.M. McDowell–Boyer, A.P. Watson, F.O. Hoffman, J.C. Pleasant, and C.W. Miller. 1979. AIRDOSE–EPA: *A Computerized Methodology for Estimating Environmental Concentrations and Dose to Man from Airborne Releases of Radionuclides,* EPA 520/1–79–009. Reprint of ORNL–5532.

Moore E.B. 1984. *Control Technology for Radioactive Emissions to the Atmosphere at U.S. Department of Energy Facilities.* PNL-4621. Pacific Northwest Laboratory, Richland, Washington.

Oak Ridge National Laboratory (ORNL). 1986. Code System for Implementation of Atmospheric Dispersion Assessment Required by the Clean Air Act. RSIC Computer Code Collection, CCC-476. Oak Ridge, Tennessee.

Resnikoff M. 1989. *Uranium Releases at Fernald. Radiation Doses To Nearby Residents.* Radioactive Waste Campaign, New York, New York.

Semones T.R. and E.F. Sverdrup. 1988. "Uranium Emissions From Gulping of Uranium Trioxide." *FMPC/SUB–019.* Westinghouse Materials Company of Ohio.

U.S. Environmental Protection Agency (EPA). 1984. *Background Information Document for Final Rules.* Radionuclide, 2;2.3: 1–3.

Voillequé P.G., K.R. Meyer, D.W. Schmidt, G.G. Killough, R.E. Moore, V.I. Ichimura, S.K. Rope, B. Shleien, and J.E. Till. 1995. *The Fernald Dosimetry Reconstruction Project Tasks 2 and 3—Radionuclide Source Terms and Uncertainties. RAC* Report CDC-5. Radiological Assessments Corporation, Neeses, South Carolina.

APPENDIX Q

FOLLOWUP OF ISSUES RELATED TO THE RADON SOURCE TERM

INTRODUCTION

Calculations of doses for the postulated nine exposure scenarios (see Appendix K of this report) show that radon releases are the most important contributor to cumulative lung dose and effective dose for all scenarios. In addition, the radon source term calculations have followed a non-traditional method that is less easily explained than the traditional approach. For these reasons, many radon-related aspects of the Project have been reevaluated. The Centers for Disease Control and Prevention (CDC) held a Radon Review Meeting in December 1995. Twelve peer reviewers, staff from the CDC, and representatives from the *RAC* Team attended and discussed radon source term and radon dispersion modeling aspects of the Project. As one result of the meeting, with the CDC's initiative, CDC and *RAC* staff performed additional document searches at the Fernald site to help ensure that all important data and documentation related to the radon source terms have been located and evaluated for use on the Project. The document searches located some data that had not been previously evaluated, and as a result some of the calculations related to the radon source term have been revised. In addition, since the release of the Task 2/3 report (Voillequé et al. 1995), an error in the calculation of the radon source term for 1988 was noticed.

The draft task 6 report addressed each of these items in its Appendix Q. The draft report was reviewed by the National Research Council (NRC) Committee on an Assessment of CDC Radiation Studies. Radiological Assessments Corporation pointed out numerous anomalies in the NRC committee's review and requested a meeting with the committee. The meeting took place in Washington, D.C., on March 31, 1997, where members of the *RAC* research team and CDC staff members presented additional material and answered questions posed by NRC committee members. Subsequently, the committee issued a letter to Dr. James M. Smith, chief of the CDC's Radiation Studies Branch, stating the committee's sense of that meeting. The committee acknowledged mistakes in its review of the draft task 6 report and requested that some additional material be incorporated into the final report. The letter is reproduced in Volume 1 of this report.

Much of the additional material sought in the NRC committee's letter is related to the release of radon from the K-65 silos, and details of *RAC*'s responses to those matters are discussed in this appendix, in addition to questions that were raised at the CDC's Atlanta meeting. Specifically, we consider the following topics:

- The additional document searches are described, and documents and data obtained are evaluated for usefulness to the Project (page Q-2).
- The calculations of the radon source term for 1988 are revised (page Q-14).
- The alternative source term calculations, which use a conventional method, are revised to reflect the additional data obtained, and analysis of the results is expanded (page Q-19).

- The estimate of radium-226 content in the K-65 silos is revised, also to reflect the additional data (page Q-7).
- A possible bias in calculations of the radon releases for 1959–1979 is removed (page Q-27).
- An algorithmic description of the radon release model is presented, with numeric values of the variables and calculated quantities to help the reader follow the steps (page Q-30).
- The equilibrium ratios of radon daughters at the point of release are reevaluated (page Q-36).
- Uncertainty distributions for parameters of the radon release model are expanded (page Q-37).
- Consistency of the gamma-field measurements with equilibrium ratios and rapid turnover during 1959–1979 is examined (page Q-40).

It should be noted that the numerous revisions of the model described in this appendix produce relatively minor changes in the estimates of radon dose to the subjects of the nine scenarios described in Appendix J. The dose estimates are presented in Volume 1 of this report and in Appendix K.

EVALUATION OF ADDITIONAL INFORMATION AND DOCUMENTS RELATED TO RADON SOURCE TERM

Since the appearance of the task 2/3 report (Voillequé et al. 1995), additional searches for historical documents related to the radon source terms from the K-65 silos have been performed. The purposes of these additional searches are generally as follows. Based on the dose calculations for the postulated nine exposure scenarios, the radon releases contribute more (relative to uranium releases) to the total doses than had been previously thought. In addition, the source term calculations have followed a non-traditional method that is less easily explained than the traditional approach. With the increased importance of doses from radon releases, it is reasonable to review aspects of the radon source term work. Thus, searches for additional documents were performed to help ensure that all important data and documentation related to the radon source terms have been located and evaluated for use.

Additional Document Searches

Searches for documents were performed at the Fernald Environmental Management Project's (FEMP) Records Center, in Forest Park, a suburb of Cincinnati, Ohio. The Records Center is now managed by Fernald Environmental Restoration Management Company (FERMCO). The Records Center has been significantly expanded since the early days of our dose reconstruction project, when we made numerous document searches at the site and at the (then) NLO records center. Documents from the Central Files of the site and documents gathered by NLO for the lawsuit are now combined in the current Records Center. Many boxes of historical documents have been inventoried, with key information entered into the document database; the database is now significantly expanded from the earlier NLO database developed for the lawsuit.

Two additional visits to the Fernald Records Center were made to search for documents related to the radon release pathway. Steve Adams, Felix Rogers, and Bob Whitcomb, of the Centers for Disease Control and Prevention (CDC), visited the Records Center in January 1996. The same CDC group, accompanied by Duane Schmidt of the *RAC* Team, visited the Records Center February 5–8, 1996. Document searches during these visits were primarily directed searches based on keyword searches of the document database and on recommendations of Brian Devir, manager of historical documents for the Records Center, who has extensive and detailed knowledge of the Records Center historical documents holdings. Also examined were a group of boxes that contained files from Don Fleming (who was involved in environmental monitoring activities at the site), from which some very useful radon monitoring data were previously obtained by *RAC* team members. In addition, some searches were completed by walking through rows of the spacesaver storage areas, and choosing boxes to examine based on information on the box labels.

For our alternative calculation for radon source terms, we had not previously obtained data on the radon diffusion coefficient, specific to the K-65 material, though this parameter is key to the calculation (the alternative calculation is discussed beginning on page Q-19). Because of the lack of specific data, we had relied on literature values, but the importance of the diffusion coefficient motivated us to search for additional documents that might provide information specific to the K-65 material. As a result of telephone inquiries by the CDC and *RAC* staff, we obtained copies of two reports related to vitrification of K-65 materials, that might include useful data (see page Q-10). It has turned out that while the reports are useful, there is insufficient data to estimate the radon diffusion coefficient for the K-65 material. To follow up, the CDC and *RAC* staff have talked with key personnel involved in the vitrification studies, from the testing contractor (Battelle, Pacific Northwest Laboratories) and the Fernald site. From these conversations, no additional documentation of radon diffusion coefficient measurements has been located.

Discussions with Personnel with Knowledge of K-65 Silos or Radon Monitoring at the Fernald Site

During the visits to the Fernald Records Center, discussions were held with a number of people who have knowledge of the K-65 silos or radon monitoring around the Fernald site. In searching for additional hourly radon concentration data, the CDC/*RAC* team talked to Stuart Hinnefeld, Tim Poff, and Larry Tomczak, who all work at the Fernald site and have been involved in radon monitoring, and to Phil Jenkins, who formerly worked at Mound Laboratories and performed radon monitoring at the Fernald site in the mid-1980s. For information about the K-65 silos and their ^{226}Ra content, the search team consulted Robert Vogel, who is an engineer on the FMPC operable unit 4 team (which is addressing cleanup of the silos area) and has much historical knowledge and documentation about the silos. Weldon Adams, former site manager of the Fernald site, was also consulted for information about the K-65 silos. Some of these discussions led to documents of potential use and interest; such documents are described in the next section.

During the February visit to the Fernald Records Center, the CDC/*RAC* team also talked with Mike Boback, who is now retired from the Fernald site. Boback worked at the site from

the mid-1950s through his recent retirement. He was involved in radon and other monitoring at the site for many years, and was responsible for the radon monitoring in the late 1970s that led to the routine radon monitoring program begun in 1980. Boback provided useful information about the radon monitoring, as well as names of additional people to contact for specific information.

The CDC/*RAC* team also discussed with Boback the radon monitoring performed in the silo head spaces in 1957 and the radon monitoring around the silos and around the site that began in 1978. After reviewing analytical datasheets that documented radon concentration measurements in the K-65 silo head spaces in 1957, Boback recalled that radon measurements in the 1950s were performed with a vibrating reed electrometer. He thought that the staff involved in the measurements had discovered a cracked chamber, which prompted them to discontinue use of the vibrating reed electrometer for radon measurements, probably around the late 1950s.

Regarding radon monitoring in the 1960s and 1970s, Boback thought that there had been very little, if any, radon monitoring performed between the time of the 1957 monitoring and the 1978 monitoring. This agrees with what *RAC* had found in its previous document searches, in that no significant radon monitoring information has been found for the period 1958–1977.

Boback also recalled a sampling technique that was often used to obtain samples of K-65 material from the K-65 silos. The technique involved swinging a bucket on a rope into the silo through one of the manholes in the dome, dragging the bucket across the surface of the material in the silo to scrape a sample into the bucket, and then retrieving the bucket containing the sample. Boback recalled that samples from the silos were needed occasionally, and this bucket sampling technique was usually employed. Of course, for the more thorough characterization efforts in the late 1980s and early 1990s, more sophisticated methods were used.

Evaluation of Additional Documents of Interest

A number of documents related to the K-65 silos and to radon monitoring around the Fernald site were obtained which had not been previously reviewed by the RAC Team. This was expected, as the document searches performed in the earlier stages of the project were never intended to be systematic searches of all documents at the site. In many cases, the documents not previously seen contained information similar to that in documents that had been obtained earlier in the project. Documents which appear to be most useful for the project, or are very interesting for other reasons, are described below. Note that we do not describe here documents that are the same as or similar to those obtained earlier, documents recently obtained that have no apparent use for the project, and documents of no special interest relative to radon releases.

Tests of radon emanation from K-65 material. A letter report was obtained that provides results of tests of radon emanation from samples of K-65 material (Boback 1979). This document had not been previously reviewed by the *RAC* Team.

This letter report (Boback 1979) indicates that samples of K-65 material were removed from Silo 2 (the northernmost of the two K-65 silos). A six-inch layer of dry K-65 material was

placed into a 55-gallon drum, and the radon "flux" (fluence rate) was measured at the top of the layer. Additional flux measurements were made after saturating the K-65 material with water, and then after additional water was applied to various depths above the K-65 material. The flux measurements for the watered conditions were made at the water surface. The purpose of the measurements was to determine the reduction in radon flux that would occur with different thicknesses of water applied.

At first, the results in this report look quite promising, as the dry measurements are of the quantity of radon released from the material into air above the material. Although only a six-inch-thick layer of K-65 material was used in the tests, it should be possible to use the results to estimate the release of radon from the K-65 material in the K-65 silos. This could then be used to improve our "alternative" calculation of radon source term (see Appendix J of the Task 2/3 report (Voillequé et al. 1995)).

However, it appears that the material sampled and used in these tests may not have been representative of the majority of the K-65 material in the silos. The report indicates that the ^{226}Ra concentration was measured to be 17,000 dpm g^{-1} (Boback 1979), which is equal to about 7700 pCi g^{-1}. However, measurements in the early 1990s indicated concentrations of ^{226}Ra in the K-65 material in Silo 2 range from 134,900 to 481,000 pCi g^{-1} (see results tabulated in our Task 2/3 report (Voillequé et al. 1995)). These recent measurements were for samples obtained from boreholes in the silo contents, at depths almost to the bottom of the silos. Thus there is a very large discrepancy in ^{226}Ra concentrations.

From earlier conversations with staff at the FMPC, there is information that indicates that materials other than K-65 material were added on top of the K-65 material in the K-65 silos, after all the K-65 material had been added. We assume that such other materials would have ^{226}Ra concentrations much lower than that of the K-65 material. As discussed earlier (see page Q-4), a typical technique used to obtain samples from the K-65 silos involved dragging a bucket across the surface of the material in the silo, which would result in a surface sample being obtained. If this method was used to obtain the samples for the emanation tests (which appears likely), the material obtained would have been from the surface layer of material in the silo.

From this information, there are two reasons that we think the material sampled for the emanation tests was likely not representative of the majority of the K-65 material in the K-65 silos: (1) the radium-226 concentration in the material sampled for the emanation tests was significantly different from measurements from the K-65 material, by an order of magnitude and more, and (2) it seems quite likely that the material sampled for the emanation tests was recovered from the surface layer in the silo, and thus may include significant quantities of materials that are not K-65 material. We have the additional concern that (3) materials sampled for the emanation tests had been removed from the silos and there may have been changes in physical characteristics between the *in situ* material and material moved to laboratory conditions.

The chemical and physical form of materials can be very important in determining the key parameters (related to calculations of radon emissions from a source material) of radon emanation fraction and radon diffusion coefficient through the material. With the concern that the material used in the tests may not be representative of the *in situ* K-65 material in

the silos, we feel that the data from the emanation tests are simply not appropriate for estimating parameters associated with releases of radon from the K-65 material in the silos. In conclusion, we do not use the results of these emanation tests for further calculations (including the refinement of our alternative calculation of radon source term).

Measurements of radon flux through K-65 silo domes. A document was obtained that provides results of measurements of the radon flux from the dome of K-65 Silo 2 (Green 1980b). This document had been previously obtained by the RAC Team, though the results had not been used in any RAC reports.

Green (1980b) reports results of radon flux measurements on the dome of K-65 Silo 2, and radon concentrations in air on and around the same Silo. The radon flux measurements are of potential interest, because they could provide data to estimate the rate of release of radon from the K-65 Silo domes. The flux measurements were made at four locations on the Silo 2 dome, of which two appeared to be on solid concrete, and two were above cracked concrete. A later study, by Mound Laboratory, involved flux measurements at 24 locations on each of the two K-65 silos (Hagee et al. 1984). Because the study by Green involved only four locations, the results are thought to be much less useful than those of the later Mound study, which are used in Appendix N of this report. We note that the results obtained by Green appear to be within the range obtained by Hagee et al (1984). However, there appears to be a systematic error in the results shown by Green, and thus the results of Green appear incorrect.

Weight of K-65 material in the K-65 silos. A number of documents were seen or obtained which indicate the total weight of material that was placed into the K-65 silos. One, which is certainly not the best example of original data, was a copy of a presentation overhead attached to a letter (Spenceley 1984). The overhead gives a total net weight of 19,385,126 lb of waste in the K-65 silos. Similar information had been obtained earlier by the *RAC* Team. An example is a summary table compiled by Lynch (1968), in the Nuclear Materials Control department of the FMPC, which gives the same value for total net weight of material in the K-65 silos. The information had not been used previously in any of our reports because its usefulness was not recognized.

In Appendix J of the Task 2/3 report (Voillequé et al. 1995), the bulk density of the K-65 material in the silos was used for two calculations: (1) a rough estimate of the total quantity of ^{226}Ra in the K-65 silos, for comparison with quantities of ^{226}Ra in the waste pits, and (2) an alternative calculation, using a conventional method, to estimate unconstrained (no silo domes) radon releases from the K-65 silos for comparison with results of our preferred method. For these calculations, the bulk density of the K-65 material was assumed to be represented by a uniform distribution with minimum 0.53 and maximum 1.179 g cm^{-3} (and average 0.85 g cm^{-3}) These bulk density values were based on measurement data obtained (Table J-4, Appendix J, Task 2/3 report).

The total weight of material in the K-65 silos could be used with the volume of material to develop another estimate of the bulk density of the K-65 material. This revised bulk density could be used to revise the results of the alternative calculation. From Appendix J (page J-21) of the Task 2/3 report (Voillequé et al. 1995), the total volume of material in the K-65 silos was estimated to be about 220,000 ft^3, which is 6.23×10^9 cm^3. The weight of 19,385,126 lb is

equal to 8.79×10^9 g. We assume that this weight, described as net weight, is the dry weight of silo contents. The bulk density can thus be estimated to be 1.4 g cm^{-3}.

We note that the documents obtained so far, that report the total weight of material in the K-65 silos, have been summary documents only; no documentation of or reference to the original source of the weight estimate has been located. Thus, the bulk density calculated from the weight of silo contents will be considered another estimate, which should be evaluated along with the measured bulk densities (reported in Table J-4, Appendix J of the Task 2/3 report, Voillequé et al. 1995) for determining the bulk density of the *in situ* K-65 material in the K-65 silos. The alternative calculation and the ^{226}Ra content calculation have been revised to account for the additional data on the bulk density of the K-65 material. These revisions are described later in this Appendix (page Q-19).

Measurements of ^{226}Ra concentration of K-65 material, at time of production. A group of documents was obtained that provides results of ^{226}Ra concentration measurements in K-65 materials, that were made at the time of the K-65 production. Most of these documents had been previously obtained by the *RAC* Team, though the results had not been used in any *RAC* reports.

The documents are of two types (1) tables and spreadsheets, some handwritten, that provide production information about the uranium ore processing campaigns at the FMPC, and (2) letter reports from the early 1950s, that tabulated comparisons of ^{226}Ra measurements results from three laboratories' analyses of split samples of K-65 material. The ^{226}Ra concentrations could be used to develop another estimate of the average ^{226}Ra concentration in the K-65 material in the silos. This estimated concentration could be used in refining the alternative calculation of radon released from the K-65 material (mentioned above). However, it is not entirely clear that the K-65 samples measured represent only those materials that were eventually placed into the K-65 silos at the FMPC. Some K-65 material was stored at other locations, and we do not have documentation to establish the final storage location for all K-65 material. It appears, though, that most of the K-65 material was eventually stored in the FMPC silos, so the measured concentrations are probably reasonably representative of the material at the FMPC.

Data on the weight and measured ^{226}Ra content of K-65 material produced during the ore processing at the FMPC have been compiled in Table Q-15 (at the end of this appendix) from the tables and spreadsheets obtained (Wolf 1955, Anonymous 1958, and Lynch circa 1958). One of the spreadsheets (Lynch circa 1958), which contains ^{226}Ra results for most of the FMPC processing, indicates that the ^{226}Ra results are from Evans, which refers to the laboratory of Robley Evans at the Massachusetts Institute of Technology. The units shown for ^{226}Ra concentration are as provided in the source documents.

The letter reports provide only the lot number and measured ^{226}Ra concentration of K-65 material which was produced at facilities other than the FMPC (prior to FMPC ore processing). Data on the measured ^{226}Ra content of K-65 material produced outside the FMPC have been compiled in Table Q-16 (at the end of this appendix) from the letter reports obtained (Morgan 1950, Morgan 1951a, Morgan 1951b, Morgan 1952, Smith 1952a, Smith 1952b, Smith 1952c, Smith 1952d, Smith 1952e, Huke 1953a, and Huke 1953b). The dates of

the letter reports presumably give some rough indication of the dates of the measurements and processing.

To estimate the ^{226}Ra concentration in the K-65 material in the silos, we assume that the measurements compiled in Tables Q-15 and Q-16 are representative of the materials that were placed into the silos. For the FMPC production of K-65 material, we have weights and corresponding ^{226}Ra concentrations; the mean ^{226}Ra concentration for K-65 material produced at the FMPC is the weighted average of the individual results (from Table Q-15). For the K-65 material produced at other facilities, we only have ^{226}Ra concentrations for individual lots of K-65 material. We assume that each lot of material would represent a similar weight, so the mean ^{226}Ra concentration for the K-65 material from non-FMPC production is just the mean of the individual measurements (from Table Q-16). To calculate the mean ^{226}Ra concentration in all K-65 material in the silos, we weight the means of FMPC-produced and non-FMPC-produced material by their respective weights. The weight of FMPC-produced material is taken from Table Q-15. The weight of non-FMPC-produced material is taken from another of the spreadsheets (Lynch 1968), which provides summary information about K-65 storage at the FMPC. Table Q-1 summarizes this estimation of the mean ^{226}Ra concentration of the K-65 material in the silos. The conversion of concentration units is straightforward.

Table Q-1. Summary of Calculated ^{226}Ra Concentration in K-65 Material Stored in the K-65 Silos at the FMPC

	Weight of K-65 material		^{226}Ra concentration	
Material	(pounds)	(% of total)	(mg ton^{-1})	(pCi g^{-1})
FMPC-produced	2,287,398	11.7	293	319,000
Non-FMPC-produced	17,265,573	88.3	402	438,000
All in silos	19,552,971		389	424,000

The estimated mean ^{226}Ra concentration in the K-65 material, based on the historical measurements made during uranium ore processing and K-65 production, is 424,000 pCi g^{-1}. This value is essentially the same as the mean concentration measured in sampling of the silos that occurred in 1991. This result will be used later in this appendix, in revisions to the alternative radon source term calculations (page Q-19).

Hourly and long-term measurements of radon in air near the K-65 silos in 1985–1987. From earlier in the project, we have known that hourly measurements of radon concentration in air had been performed near the K-65 silos, generally near or along the fence around the K-65 area. Some of these data, from 1986 and 1987, had been previously obtained, and are compiled in Appendix N of this report. However, during visits to the Fernald Records Center, information was found which indicated that such measurements had been performed starting in 1985, and that more measurements were made than had been located so far. A member of the CDC staff followed up on leads for this additional monitoring data. The contractors involved (Oak Ridge National Laboratory and Mound Laboratories) were consulted, but the additional data have not been found.

The hourly measurements were made very close to the K-65 silos, and show significantly elevated concentrations of radon. In Appendix N of this report, results are used to show that radon releases for 1980–1987 occurred primarily during daylight hours. In addition, it could be possible to use the measured concentrations with a radon dispersion model to develop an estimate of the radon source term. To perform this additional calculation, a model of radon dispersion very close to the silos must be developed, as the current transport model is thought not applicable at such close distances. We also note that because only a few locations were sampled, uncertainty in the estimated source term is likely to be quite large.

Data similar in usefulness, long-term measurements in 1980–1984 of radon concentrations in air at a single location midway between the two K-65 silos, were tabulated in our Task 5 report (Shleien et al. 1995). Again, back calculations of a source term could be performed with these data. Because of the need to develop a dispersion model, however, such work cannot be performed at this time. Also, with data from only one location, uncertainties would be large.

Date of sealing of K-65 silo dome penetrations. As determined in the Task 2/3 report (Voillequé et al. 1995), for radon releases from the K-65 silos, the most important change to the silos was the gasketing and sealing of silo dome openings, which included a 6-inch gooseneck vent pipe, influent and unloading manholes, and other penetrations. In the Task 2/3 report, we had not identified an exact date for this sealing, but had determined that it probably occurred at the end of June 1979 (see Table J-3 of Appendix J to the Task 2/3 report).

During the previously-mentioned searches at the Fernald Records Center, documents were obtained that provide an exact date. An FMPC internal memorandum report (Heatherton 1979) indicates that completion of the K-65 silo dome sealing was reported on June 29, 1979, the date that had been used. A handwritten spreadsheet compilation of radon concentration measurements (Anonymous circa 1980) indicates that the sealing was completed on June 25, 1979. This date agrees with the other information that has been reviewed, so we conclude that June 25, 1979, was the probable date that sealing of the K-65 silo dome penetrations was complete. This date has been used to revise the analysis of some of the environmental radon monitoring data from 1979 (see Appendix N). The radon source term calculations (Appendix J of the Task 2/3 report, Voillequé et al. 1995) are not affected by this difference of a few days.

Radon concentration measurements in the 1950s. Several analytical data sheets for radon measurements from the 1950s were obtained. Essentially all of these data sheets, along with a related memorandum, had been obtained previously by the *RAC* team. The most interesting measurements were of radon in air in the K-65 silos, in 1957 (NLCO 1957a and Ross 1957). Other radon in air measurements included radon in air in and around railcars of K-65 material being unloaded in 1952 (NLCO 1952), in Plants 2 and 3 during processing of Australian pitchblende in 1957 (NLCO 1957b), and a few others in Plant 2 and the K-65 area in 1953–1955 (NLCO 1953, NLCO 1954, and NLCO 1955).

The results of the measurements were reported on the data sheets in units of $\mu Ci\ L^{-1}$, $Ci\ L^{-1}$, and $Ci\ m^{-3}$. However, for many of the measurements (particularly those taken in the silos), when converted to units of $pCi\ L^{-1}$ it is clear that the results, as reported, were

significantly below established background concentrations. This does not make sense for samples that were taken in what are thought to be areas of very high radon concentrations. The analyses of these radon samples were made using the vibrating reed electrometer. As mentioned earlier (see page Q-4), discussions with FMPC staff indicate that there may have been problems with the vibrating reed electrometer. For these reasons, it appears that the reported results of these radon measurements in the 1950s may not be reliable, and we do not use them further.

Other characteristics of K-65 material, from vitrification reports. As a result of telephone inquiries by the CDC and *RAC* staff, we have obtained copies of two reports related to vitrification of K-65 materials (Janke and Chapman 1991 and DOE 1993). The plan for eventual disposal of the K-65 material involves vitrification of the material, and these reports provide results of testing of K-65 material for suitability for vitrification. Of most interest to the radon source term work are measurements of physical characteristics of the K-65 material and measurements of the rate of radon emanation from the K-65 material. We focus on the later report (DOE 1993) because of its greater quantity of measurement results, and because it is more recent, thus reflecting more current knowledge from the vitrification testing program.

For our alternative calculation for radon source terms, we had not previously obtained data on the radon diffusion coefficient through the K-65 material, though this parameter is key to the calculation (see also discussion of alternative calculation later in this appendix, beginning on page Q-19). Thus, we had hoped that information in these vitrification reports would be sufficient to allow estimation of the diffusion coefficient. However, because of the small sample size used in the emanation rate measurements, estimation of the diffusion coefficient is not feasible. This is shown by the following.

The usual equation for calculating radon flux above the surface of a ^{226}Ra-bearing material above an impervious layer is given by Collé et al. (1981) as:

$$j_D = \sqrt{\frac{D_e \varepsilon_w}{\lambda_{Rn}}} (\phi - C_a \lambda_{Rn}) \tanh\left(\frac{L_w}{l_w}\right) \qquad \text{(Q-1)}$$

where:

j_D = diffusion fluence rate of radon (radon flux) from the surface of the ^{226}Ra-bearing material, constrained by the radon above the surface of the material. The quantity of radon per unit time per unit area transported by diffusion from the source material (in this case the K-65 material) into the ambient air (pCi cm^{-2} s^{-1}, or similar).

D_e = effective diffusion coefficient of radon through the porous source material (cm^2 s^{-1}).

ε_w = porosity of the source material.

λ_{Rn} = the decay constant for radioactive decay of ^{222}Rn, = 2.10×10^{-6} s^{-1}.

ϕ = the pore space radon production rate. This is the quantity of radon produced in pore spaces of the source material per unit time per unit volume that is free to migrate through the pores of the material (pCi m^{-3} s^{-1}). Depends on characteristics of the source material, including ^{226}Ra concentration, radon emanation fraction, bulk density, and porosity, and on the radon decay constant.

C_a = concentration of radon above the surface of the material (pCi cm^{-3}).

L_w = thickness of the source material (cm).

l_w = diffusion length of radon in the source material (related to D_e) (cm).

The relationship between the diffusion length and the effective diffusion coefficient is given by (Collé et al. 1981):

$$l_w = \sqrt{\frac{D_e}{\varepsilon_w \lambda_{Rn}}} \tag{Q-2}$$

We make the substitution of Equation Q-2 into Equation Q-1, and then rearrange terms to obtain:

$$j_D = \varepsilon_w l_w (\phi - C_a \lambda_{Rn}) \tanh\left(\frac{L_w}{l_w}\right) \tag{Q-3}$$

For values of L_w significantly less than l_w, the approximate relationship holds:

$$\tanh\left(\frac{L_w}{l_w}\right) \approx \frac{L_w}{l_w}, \quad \text{for } L_w << l_w \tag{Q-4}$$

As we see later, the thicknesses (L_w) of the samples analyzed are roughly 1–1.5 cm. From the previous work on the alternative calculation, in Appendix J of the Task 2/3 report (Voillequé et al. 1995), our estimate of the 90% probability interval for the diffusion length (l_w) is 14–180 cm. Thus, a reasonably large value of (L_w/l_w) would be about 0.1. At this value, $\tanh(0.1) = 0.0997$, which illustrates the validity of Equation Q-4. With substitution of Equation Q-4 into Equation Q-3 we obtain

$$j_D = \varepsilon_w L_w (\phi - C_a \lambda_{Rn}), \quad \text{for } L_w << l_w . \tag{Q-5}$$

This last expression shows that for sample thicknesses that are significantly less than the radon diffusion length, the radon flux is independent of the diffusion length. For the samples analyzed by DOE (1993), it appears that the sample thicknesses *are* significantly less than the radon diffusion length. Thus, we can not use the radon emanation rates to reasonably estimate a radon diffusion length or diffusion coefficient. Another way of interpreting Equation Q-5 is that for small material thicknesses, essentially all of the radon produced in pore spaces escapes the material without being slowed down significantly; without some slowing of the escape of radon from a sample material, the diffusion coefficient can not be determined.

Although we can not estimate a radon diffusion coefficient, there are other useful data in the vitrification report (DOE 1993). The characterization of untreated (prior to vitrification) K-65 material samples included measurements of moisture content, bulk density, specific gravity, ^{226}Ra concentration, and radon emanation rate. With the data given we can also calculate the radon emanation fraction. Table Q-2 shows the measurement results given in DOE (1993). The ^{226}Ra concentrations measured are within the range seen in the 1991 sampling of the silos (135–891 nCi g^{-1}), as tabulated in Appendix J (Table J-5) of the Task 2/3

report (Voillequé et al. 1995). Thus, we feel confident that the samples analyzed should be reasonably representative of the K-65 material in the silos.

Table Q-2. Data on Characteristics of K-65 Material, from DOE (1993)

Sample	Radon emanation (pCi h^{-1})	Radon emanation (pCi cm^{-2} s^{-1})	Radon emanation (pCi g^{-1} h^{-1})	Moisture (wet weight fraction)	wet, compact bulk density (g cm^{-3})	specific gravity	^{226}Ra concentration (nCi g^{-1})
Silo 1A	78311	0.2683	525	0.269	1.81	2.79	368
Silo 1B	198126	0.6788	1457	0.353	1.67	2.77	414
Silo 1C	213466	0.7314	1711	0.359	1.70	2.74	441
Silo 2A	61360	0.2102	416	0.278	1.87	2.72	176
Silo 2B	171629	0.5880	1297	0.356	1.71	2.57	259
Silo 2C	57933	0.1985	533	0.297	1.92	2.81	242

From Table Q-2, the specific gravity data are directly useful for the alternative source term calculations (discussed later in this appendix, beginning on page Q-19). Other useful parameters are easily calculated. The vitrification report (DOE 1993) stated that the wet, compact bulk density (density of wet samples that were compacted) was probably the most representative of the *in situ* bulk density of the K-65 material in the silos. For the alternative calculation, we use dry bulk density. The dry density is calculated from the wet density and moisture content. The moisture content can be expressed as a fraction of the dry weight. For the calculation of emanation fraction, we need to know the sample thickness. The report (DOE 1993) did not provide values of the thickness, volume, or mass of the samples analyzed. However, these can be determined from the data provided. First, the cross-sectional area and dry mass of the samples can be determined from combinations of the radon emanation values (expressed with different units). The sample volume can then be determined using the dry mass and dry bulk density. The sample thickness is then determined from the sample cross-sectional area and volume.

The calculation of the emanation fraction depends on use of Equation Q-5. First, though, the pore space radon production rate (ϕ) can be expressed as a function of more basic parameters (Collé et al. 1981).

$$\phi = \frac{[\mathrm{Ra}] EF \rho_w \lambda_{Rn}}{\varepsilon_w} \qquad \text{(Q-6)}$$

where

[Ra] = concentration of ^{226}Ra in K-65 waste material (activity per mass).

EF = ^{222}Rn emanation fraction in K-65 material, which is the fraction of the radon formed (from the ^{226}Ra decay) that is in the pore spaces and is free to migrate.

ρ_w = dry bulk density of K-65 waste material (g cm^{-3}).

This expression can be substituted into Equation Q-5 to obtain the following equation:

$$j_D = \varepsilon_w L_w \left(\frac{[\mathrm{Ra}] EF \rho_w \lambda_{Rn}}{\varepsilon_w} - C_a \lambda_{Rn} \right) \qquad \text{(Q-7)}$$

For the radon flux measurements described in the vitrification report, the radon concentration above the K-65 sample (C_a) was expected to be around 3000 pCi L^{-1}, though measured values were not given (DOE 1993). With this concentration and reasonable estimates of the other parameters in Equation Q-7, the second term in the parentheses in Equation Q-7 is about five orders of magnitude smaller than the first term in the parentheses. Thus, the equation can be simplified further to:

$$j_D = L_w[Ra]EF\rho_w\lambda_{Rn} \quad \text{(Q-8)}$$

which can then be rearranged to obtain the radon emanation fraction:

$$EF = \frac{j_D}{L_w[Ra]\rho_w\lambda_{Rn}} \quad \text{(Q-9)}$$

Equation Q-9 is used to calculate radon emanation fraction values from the other parameters. Table Q-3 shows the parameters calculated from the basic data of the vitrification report. Of the parameters shown in Table Q-2 and Table Q-3, specific gravity, dry bulk density, moisture content, and radon emanation fraction will be evaluated for usefulness to the alternative source term calculations, later in this appendix (page Q-19).

Table Q-3. Calculated Characteristics of K-65 Material, Based on DOE (1993)

Sample	Dry, compact bulk density (g cm^{-3})	Moisture (fraction of dry weight)	Cross-sectional area (cm^2)	Mass (g)	Volume (cm^3)	Thickness (cm)	Radon emanation fraction
Silo 1A	1.32	0.368	81.1	149	113	1.39	0.19
Silo 1B	1.08	0.546	81.1	136	126	1.55	0.47
Silo 1C	1.09	0.560	81.1	125	114	1.41	0.51
Silo 2A	1.35	0.385	81.1	148	109	1.35	0.31
Silo 2B	1.10	0.553	81.1	132	120	1.48	0.66
Silo 2C	1.35	0.422	81.1	109	81	0.99	0.29

Conclusions

The additional document searches have identified documents related to the K-65 silos and radon monitoring around the Fernald site that were not previously obtained by the *RAC* Team. However, most of these documents provide information similar to that already obtained in other documents. As a result of the additional information, three changes in previous work are in order: (1) additional information has been obtained on bulk density, specific gravity, moisture content, ^{226}Ra concentration, and radon emanation fraction of the K-65 material. These data are evaluated later in this appendix (page Q-19) for revisions to parameter values used in the alternative calculation of radon source terms. (2) The additional information on bulk density and ^{226}Ra concentration of the K-65 material is also used in revising the rough estimate of the ^{226}Ra content of the K-65 silos (page Q-27). (3) Additional information has provided the exact date that the sealing of dome penetrations of the K-65

silos was completed; the exact date is used in a slight revision to the analysis of radon monitoring results from 1979 (Appendix N). Information in these additional documents has not lead to significant changes in the preferred method calculations of the radon source term from the K-65 silos or calculations of the dispersion of radon in air around the silos.

ADJUSTMENT OF RADON SOURCE TERM FOR 1988

The radon source terms were calculated and described in Appendix J of our Task 2/3 report (Voillequé et al. 1995). At the end of 1987, a layer of expanded foam was applied to the K-65 Silo domes, thus reducing the temperature cycling of the silo head space air and changing the release of radon. The radon release rate from the K-65 silos for 1988 was based on the release rate for 1980–1987 and the ratio of radon concentrations measured before and after installation of the foam layer. Radon concentrations in air had been measured at 16 locations on the fenceline immediately surrounding the K-65 silos. For these locations, we calculated average long-term concentrations and the ratio of the average for 1988–1991 to the average for 1987, which we called R_{mon}. Details are given on pages J-46 through J-53 of Appendix J of the Task 2/3 report. We calculated the release rate for 1988 using Equation J-46 of Appendix J of the Task 2/3 report:

$$Q_{1988} = Q_{post} R_{mon} \qquad \text{(Q-10)}$$

where Q_{1988} is the radon release rate for 1988 and Q_{post} is the radon release rate for 1980–1987.

Although we still feel that the general approach used to estimate the 1988 source term is valid, we neglected an important detail of the calculation in the Task 2/3 report. As calculated, the radon releases for 1980–1987 consist of two components: a daylight-only release, resulting from thermal pumping of the silo head spaces, and a 24-hour release, due to diffusion of radon from the head space through the silo domes into the atmosphere. For 1980–1987, the dominant release mechanism is thought to be thermal pumping; thus, most of the radon release occurs during daylight hours. For 1988, however, thermal pumping releases are much lower than in 1980–1987; thus, releases for 1988 are assumed to be relatively constant with the time of day. In Appendix N of this report, we describe hourly measurements of radon concentration in air near the K-65 silos, before and after the application of the foam layer, which support this partitioning of releases into daylight-only and 24-hour releases. In the 1988 source term calculation in Appendix J of the Task 2/3 report, we neglected to account for the different meteorological conditions that would apply to daylight-only releases and to 24-hour releases. The rest of this section discusses a revised calculation of the 1988 source term that accounts for the different meteorological conditions.

Revised Methodology for Radon Source Term for 1988

To account for different meteorological conditions for daylight-only releases and for 24-hour releases, we would like to apply the following equation to releases and measured concentrations for 1987 and 1988:

$$\chi = \sum_j Q_j (f_Q)_j \left(\frac{\chi}{Q}\right)_j \qquad \text{(Q-11)}$$

where

χ = radon concentration (pCi m^{-3})

j = an index for the different release types: day, night, or 24-hour

Q_j = the radon release rate for release type j, while release is occurring (pCi s^{-1})

$(f_Q)_j$ = the fraction of time that release type j occurs

$\left(\frac{\chi}{Q}\right)_j$ = dispersion factor (s m^{-3}) for release type j, (developed in Appendix M, this report).

There are also factors to account for uncertainties in dispersion estimates. These uncertainty factors are implicit in the dispersion factors as shown in Equation Q-11, but are described later in this section as the factors U and V_i.

Our idea is to apply Equation Q-11 to conditions of 1987 and 1988 and then determine the ratio of the two, which would be equal to R_{mon}. We apply Equation Q-11 to 1987 and 1988 and then form the ratio as follows:

$$\frac{\chi_{1988}}{\chi_{1987}} = \frac{Q_{88,24\text{-h}}(f_Q)_{88,24\text{-h}}\overline{\left(\frac{\chi}{Q}\right)}_{88,24\text{-h}}}{Q_{87,day}(f_Q)_{87,day}\overline{\left(\frac{\chi}{Q}\right)}_{87,day} + Q_{87,24\text{-h}}(f_Q)_{87,24\text{-h}}\overline{\left(\frac{\chi}{Q}\right)}_{87,24\text{-h}}} \qquad \text{(Q-12)}$$

where the subscripts represent the year of consideration (i) and the type of release (j).

The ratio on the left-hand side of Equation Q-12 is equivalent to R_{mon}, and substitution can be made. The radon concentration measurements were made at 16 locations along the fenceline of the K-65 area, as shown in Figure Q-1. We used average concentrations in defining R_{mon}, and so the dispersion factors used must also be averages (as indicated). We assume the average dispersion factor over all 16 compass directions is appropriate. The equation can be rearranged to calculate the source term for 1988:

$$Q_{88,24\text{-h}} = R_{mon} \cdot \frac{Q_{87,day}(f_Q)_{87,day}\overline{\left(\frac{\chi}{Q}\right)}_{87,day} + Q_{87,24\text{-h}}(f_Q)_{87,24\text{-h}}\overline{\left(\frac{\chi}{Q}\right)}_{87,24\text{-h}}}{(f_Q)_{88,24\text{-h}}\overline{\left(\frac{\chi}{Q}\right)}_{88,24\text{-h}}} \qquad \text{(Q-13)}$$

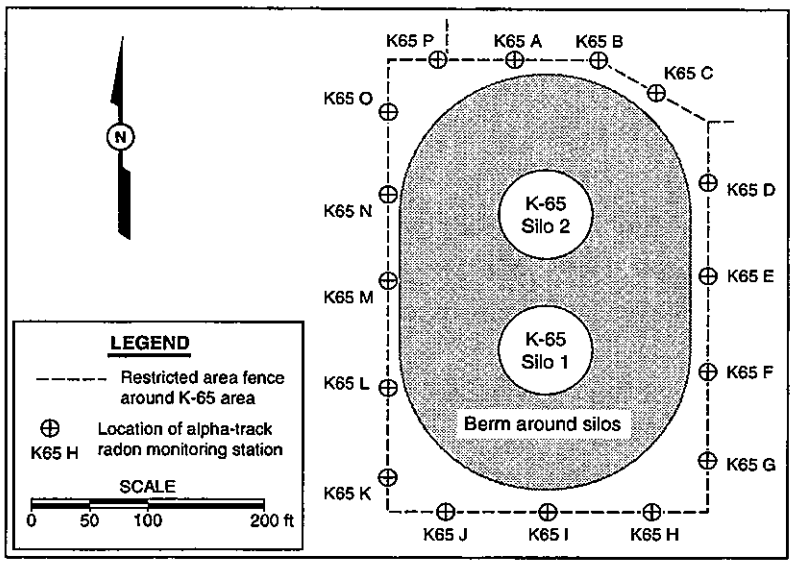

Figure Q-1. Locations of FMPC alpha-track radon monitoring on the K-65 area fenceline for 1987–1991. Locations of alpha-track monitoring were obtained from Byrne (1992).

The radon monitoring locations shown in Figure Q-1 are all roughly 40 m from the center of the silos. Thus, for the remainder of these calculations, we assume a distance from the source of 40 m. It is acknowledged that the empirical dispersion model may not be strictly applicable at such a small source to receptor distance. However, the exact form of the empirical dispersion factors is not critical to these calculations; rather, the relative differences in dispersion factors for the different types of release (daylight-only versus 24-hour) are more important. In addition, we note that the empirical model was developed based on measured radon concentrations as close as about 40 m from the source. Therefore, we believe that the empirical model is adequate for these calculations.

The dispersion factors can be written as:

$$\left(\frac{\chi}{Q}\right)_{i,j,\theta} = \left(\frac{\chi u}{Qf}\right)_j \left[\left(\frac{f}{u}\right)_{\text{eff}}\right]_{j,\theta} UV_i \qquad \text{(Q-14)}$$

where the subscripts i, j, and θ are indices representing the year, type of release, and wind direction, and

$\left(\frac{\chi u}{Qf}\right)_j$ = the diffusion factor applicable to release type j

$\left[\left(\frac{f}{u}\right)_{\text{eff}}\right]_{j,\theta}$ = the effective value of (f/u) for release type j and direction θ

U = a factor that accounts for uncertainty in the modeling of air dispersion

V_i = a factor that accounts for the year-to-year variability in the modeling of air dispersion

and f is the frequency occurrence of wind speed u, stability class l, and wind direction θ.

In the meteorological database that we employ, the joint frequencies have been normalized for each stability class l. Thus,

$$\left[\left(\frac{f}{u}\right)_{\text{eff}}\right]_{j,\theta} = \sum_l \left[\sum_k \left(\frac{f}{u}\right)_{k,l,j,\theta}\right] g_{l,j} \tag{Q-15}$$

where $g_{l,j}$ is the frequency of stability class l and release type j (daylight meteorology versus 24-hour meteorology).

Equation Q-14 can be used to calculate the dispersion factor for a single direction, whereas Equation Q-13 requires an average over all directions. If Equation Q-14 is averaged over direction θ, we obtain:

$$\begin{aligned}\overline{\left(\frac{\chi}{Q}\right)}_{i,j} &= \left(\frac{\chi u}{Qf}\right)_j \overline{\left[\left(\frac{f}{u}\right)_{\text{eff}}\right]}_j UV_i \\ &= \frac{1}{16}\left(\frac{\chi u}{Qf}\right)_j UV_i \sum_\theta \left[\left(\frac{f}{u}\right)_{\text{eff}}\right]_{j,\theta}\end{aligned} \tag{Q-16}$$

Equations Q-13 and Q-16 are used to estimate the 1988 source term. For Equation Q-16, the diffusion factors $(\chi u/(Qf))$ are based on the empirical model described in Appendix M of this report. The values of (f/u) are extracted from the composite meteorological data for the FMPC for 1987–1991, given in Appendix E of our Task 4 report (Killough et al. 1993). The calculated values of the dispersion factors $(\chi u/(Qf))$ and the values of (f/u) are shown in Table Q-4. The uncertainty parameter U cancels in Equation Q-13, as it is a factor in both numerator and denominator. The variability factor, V_i, is as used in the uncertainty analysis of Appendix M of this report, and is a lognormal distribution, with geometric mean 1 and geometric standard deviation 1.7.

The ratio of radon concentrations, R_{mon}, is as developed in Appendix J of our Task 2/3 report, a normal distribution with mean 0.612 and standard deviation 0.282 (Voillequé et al. 1995). The source terms for 1987, $Q_{87,\text{day}}$ and $Q_{87,24\text{-h}}$, are obtained from the source terms $Q_{\text{exch,post}}$ and $Q_{\text{diff,post}}$, described in Appendix J of the Task 2/3 report, with a correction (for the daylight-only release) to obtain a release rate during the actual release time:

$$Q_{87,\text{day}} = Q_{\text{exch,post}}\left(\frac{24 \text{ hours}}{12 \text{ hours of release}}\right) \tag{Q-17}$$

$$Q_{87,24\text{-h}} = Q_{\text{diff,post}} \tag{Q-18}$$

Table Q-4. Calculated Diffusion Factors and Meteorological Parameters Used in the Revised 1988 Radon Source Term Calculation

Parameter	Units	Type of release j	
		Daylight-only	24-hour
$\left(\frac{\chi u}{Qf}\right)_j$ (at 40 m)	m^{-2}	0.00512	0.0109
$\sum_\theta \left[\left(\frac{f}{u}\right)_{eff}\right]_{j,\theta}$	$s\ m^{-1}$	0.508	0.687

(the source term parameters, $Q_{exch,post}$ and $Q_{diff,post}$, used in calculations here, are the distributions of results calculated as in the Task 2/3 report). The values of f_Q are 0.5 for the 1987 daylight-only release and 1 for the other two cases.

Results

As for other source term calculations performed in the Task 2/3 report (Voillequé et al. 1995), the calculations of the revised radon source term for 1988 are implemented as Monte Carlo simulations. The Monte Carlo calculations for these analysis were performed using spreadsheet and forecasting software on an IBM-compatible microcomputer. Ten thousand iterations of the calculations were performed. The parameter distributions were generated using Crystal Ball®, version 3.0.1 for Windows (Decisioneering 1993). In Crystal Ball®, uniform distributions are generated using a multiplicative congruential generator, which has a period of length $2^{31} - 2$, and normal and lognormal distributions are generated using the Polar Marsaglia method (Decisioneering 1993).

Results of the revised calculations are summarized in Table Q-5. These can be compared to the previous results from the Task 2/3 report (Voillequé et al. 1995), which were a median of 540 Ci y^{-1} and 5th to 95th percentile range of 120–1300 Ci y^{-1}. The revised values are used in further calculations of scenario doses, elsewhere in this report. For the radon transport calculations, the releases are assumed to occur at a constant rate over each 24-hour period.

Table Q-5. Summary of Percentiles of Distribution of Revised Calculation of Radon Release Rate (Ci y^{-1}) for 1988

Percentiles	5th	25th	median	75th	95th
Release rate	36	110	220	440	1300

REVISITING THE ALTERNATIVE SOURCE TERM CALCULATIONS

In Volume I of this report we briefly discussed an alternative calculation for the radon source term from the K-65 silos, using a conventional method. The calculations were described in detail in Appendix J (pages J-73 through J-85) of the Task 2/3 report (Voillequé et al. 1995). In this section we discuss revisions to the alternative calculation and expand our analysis of the results. In order to reduce the large uncertainty in the results of the alternative calculation, we have attempted to locate additional supporting data. Earlier in this Appendix, we described recently obtained data that had not been previously evaluated. Some of these data are used in the alternative source term calculation, so we revise and update the calculations, below. In Appendix J of the Task 2/3 report (pages J-84 and J-85), we discussed a minimum radon production rate required to support the radon concentration in the K-65 silo head spaces. We revise and expand this discussion, below, to strengthen our analysis of the results of the alternative source term calculation.

Review of Equations Used for Alternative Source Term Calculations

Appendix J of the Task 2/3 report (Voillequé et al. 1995) contains a detailed description of the equations and assumptions used in the alternative source term calculations. This section provides a brief review, summarized from the Task 2/3 report. Since we present only a summary, references for the equations and details are not given here; they are provided in the Task 2/3 report. The alternative calculations use a conventional model to calculate radon emissions from a ^{226}Ra-bearing material. The conventional model is used to estimate radon releases from the K-65 material, but it does not address releases of the radon from the K-65 silos head spaces into the atmosphere. For this reason, we have chosen to calculate an unconstrained release rate, that would exist if the silos did not exist (their existence constrains, or slows, the release of radon to the atmosphere). We can calculate unconstrained release rates using our preferred method and the conventional method, and can thus compare results on an equivalent basis.

The primary equation used for the alternative method determination of the unconstrained radon release rate from the K-65 material is:

$$P_{Rn,0} = A_w \sqrt{\frac{D_e \varepsilon_w}{\lambda_{Rn}}} \cdot \phi \qquad \text{(Q-19)}$$

where

$P_{Rn,0}$ = unconstrained radon production rate. The quantity of radon per unit time transported by diffusion from the source material (the K-65 material) into the ambient air, assuming the silos do not cover the K-65 material (Ci y^{-1}).

A_w = surface area of the source material (the K-65 material) exposed to the air (m^2).

D_e = effective bulk diffusion coefficient of radon through the porous source material (cm^2 s^{-1}).

ε_w = porosity of the source material.

λ_{Rn} = the radioactive decay constant for ^{222}Rn (2.10×10^{-6} s^{-1}).

ϕ = the pore space radon production rate. Quantity of radon produced in pore spaces of the source material per unit time per unit volume that is free to migrate through the pores of the material (pCi cm^{-3} s^{-1}). Depends on characteristics of the source material, including ^{226}Ra concentration, radon emanation fraction, bulk density, and porosity, and on the radon decay constant.

The pore space radon production rate (ϕ) was previously expressed as a function of more basic parameters (Equation Q-6):

$$\phi = \frac{[Ra] EF \rho_w \lambda_{Rn}}{\varepsilon_w} \tag{Q-20}$$

where

[Ra] = concentration of ^{226}Ra in K-65 waste material (activity per mass).

EF = ^{222}Rn emanation fraction in K-65 material, which is the fraction of the radon formed (from the ^{226}Ra decay) that is in the pore spaces and is free to migrate.

ρ_w = dry bulk density of K-65 waste material (g cm^{-3}).

The porosity of the K-65 material is calculated from the density and specific gravity by:

$$\varepsilon_w = \frac{g_w - \rho_w}{g_w} \tag{Q-21}$$

where g_w is the specific gravity. The moisture saturation fraction, m_w, which is used in the estimation of the diffusion coefficient, is calculated from the moisture content (expressed as a fraction of dry weight), M_w, by:

$$m_w = \frac{M_w}{\frac{1}{\rho_w} - \frac{1}{g_w}} \tag{Q-22}$$

with the following constraint on M_w:

$$M_w \le \frac{1}{\rho_w} - \frac{1}{g_w} \tag{Q-23}$$

The pore space diffusion coefficient is estimated from an empirical correlation with moisture saturation fraction and porosity:

$$\hat{D} = (0.07 \text{ cm}^2 \text{ s}^{-1}) \exp\left(-4(m_w - m_w \varepsilon_w^2 + m_w^5)\right) \tag{Q-24}$$

where $\hat{D}$ is the empirically predicted pore space radon diffusion coefficient. Uncertainty in the diffusion coefficient, due to lack of material-specific measurements, in accounted for in the following:

$$D = U_D \hat{D} \tag{Q-25}$$

where U_D is an uncertainty factor. The effective diffusion coefficient is related to the pore space diffusion coefficient by the porosity:

$$D_e = D\varepsilon_w \quad \text{(Q-26)}$$

Equations Q-19 through Q-26 are used for the alternative calculation of the unconstrained radon release rate. To account for different units, we make use of the units conversion factors 3.156×10^7 s y^{-1} and 10^{-12} Ci pCi^{-1}.

Revisions to Parameter Distributions and Calculation Results

Bulk density of K-65 material. The distribution chosen in the Task 2/3 report (Voillequé et al. 1995) for the bulk density was a uniform distribution, with minimum 0.53 and maximum 1.179 g cm^{-3}. As mentioned above, another estimate of the bulk density of the K-65 material in the K-65 silos has been developed (see page Q-7). The additional estimate of bulk density is 1.4 g cm^{-3}. Because documentation supporting this additional estimate consisted of summary documents only, this estimate is not considered any stronger than the measured values that were compiled in the Task 2/3 report (reported in Table J-4). Values of dry bulk density measured in samples analyzed for the vitrification testing (see page Q-13) ranged from 1.08 to 1.35 g cm^{-3}.

These additional values are above the range assumed in the Task 2/3 report. Since we still have only a small number of estimates of the bulk density, so a uniform distribution is judged appropriate. Thus we now consider the bulk density of the K-65 material in the silos to have a uniform distribution with minimum 0.53 and maximum 1.4 g cm^{-3}.

Moisture content of K-65 material. The distribution chosen in the Task 2/3 report (Voillequé et al. 1995) for the moisture content (fractional dry weight basis) was a uniform distribution, with minimum 0.218 and maximum 0.90 or $(1/\rho_w - 1/g_w)$, whichever is smaller. Values of dry weight moisture content measured in samples analyzed for the vitrification testing (see page Q-13) ranged from 0.368–0.560. These additional values are within the range used earlier. We retain the distribution used in the Task 2/3 report.

Radium-226 concentration in K-65 material. In the assessment in the Task 2/3 report (Voillequé et al. 1995), the ^{226}Ra concentration in the K-65 material was assumed to have a uniform distribution, with minimum 134,900 and maximum 697,000 pCi g^{-1}. That distribution was based on analyses of samples taken in 1991 during characterization of the K-65 silo contents. We have evaluated additional data on measurements of the ^{226}Ra concentration that were made at the time of the K-65 production (see page Q-7). These additional measurements had a somewhat broader range than that assumed in the Task 2/3 report, though the standard deviation was similar (the broader range is expected as many more measurements were made). The mean ^{226}Ra concentration calculated from the additional data is 424,000 pCi g^{-1}, compared to 417,000 pCi g^{-1} from the results used in the Task 2/3 report.

As the two data sets have similar mean concentrations, it is appropriate to assume a distribution with central tendency. We thus now use a triangular distribution rather than a uniform distribution. The mean of the two mean concentrations is 420,000 pCi g^{-1}. Thus, we assume a triangular distribution with minimum 134,900, most likely value 420,000, and maximum 697,000 pCi g^{-1}.

Radon emanation fraction. For the Task 2/3 report (Voillequé et al. 1995), no emanation fraction measurements for K-65 material had been located, so we used values for uranium mill tailings, from the literature. The distribution chosen was uniform, with minimum 0.1 and maximum 0.4. However, we now have available calculated values based on measurements of samples of K-65 material performed for the vitrification study (see page Q-13). The additional data consist of six calculated values, which range from 0.19 to 0.66. This is a small number of samples, so we retain a uniform distribution, but now with minimum 0.19 and maximum 0.66.

Specific gravity. In the Task 2/3 report (Voillequé et al. 1995), the specific gravity of K-65 material was assumed to be represented by a normal distribution, with mean 2.98 and standard deviation 0.12. This was based on six measurements, with a range of 2.59–3.37, obtained from a Remedial Investigation Report (DOE 1990). Additional measurements of specific gravity were performed for the vitrification study, as described earlier (see page Q-12). For the additional six measurements, the range is 2.57–2.81. For the combined data set (all 12 measurements), the range is 2.57–3.37, and the mean value is 2.86. For the specific gravity of the K-65 material, we now assume a triangular distribution, with minimum 2.57, most likely value 2.86, and maximum 3.37.

Summary of parameters used. The other parameters required are the decay constant for ^{222}Rn, the surface area of the K-65 material, and the uncertainty factor for the radon diffusion. Because we have found no additional data on which these parameters should be reevaluated, we use the same values and distribution used in the Task 2/3 report (Voillequé et al. 1995). The distributions assigned to these parameters and those discussed above, for the alternative calculation, are summarized in Table Q-6.

Results. With the changes in distributions for parameters, described above, we have redone the alternative calculation using the Monte Carlo methods that have been described in the Task 2/3 report. Results of the calculated unconstrained radon release rate are summarized in Table Q-7. These values can be compared to the results given in the Task 2/3 report (Voillequé et al. 1995), which were a median value of 3500 Ci y^{-1} and 5th to 95th percentiles of 580–12,000 Ci y^{-1}. The revised results are generally higher than those in the Task 2/3 report. This is primarily due to the higher values of the distribution of the radon emanation fraction, which is now based on measurements of K-65 material and thus thought to be more appropriate than the previous reliance on literature values.

Minimum Radon Production to Support Radon Concentration in Head Spaces

In Appendix J of the Task 2/3 report (pages J-84 and J-85), we discussed the minimum radon production rate (release from the K-65 material) that would sustain the radon concentration, and thus total radon content, measured in the head spaces of the silos in 1987. Assuming, as we think is reasonable, that the radon concentration in the head spaces is approximately at equilibrium, the radon content, and thus there must be enough radon released into the head space air to make up for radon that is lost by decay and release. In this section, the calculations from the Task 2/3 report (page J-84) are revised and expanded to include an uncertainty analysis.

Table Q-6. Parameter Distributions for the Alternative Method Calculation of Unconstrained Radon Release Rate from the K-65 Silos

Parameter	Units	Distribution	Descriptive statistics
[Ra]	pCi g^{-1}	triangular	minimum = 134,900; most likely = 420,000; maximum = 697,000.
EF		uniform	minimum = 0.19; maximum = 0.66.
ρ_w	g cm^{-3}	uniform	minimum = 0.53; maximum = 1.4.
g_w		triangular	minimum = 2.57; most likely = 2.86; maximum = 3.37.
M_w	fraction, dry weight	uniform	minimum = 0.218; maximum = 0.90 or $(1/\rho_w - 1/g_w)$, whichever is smaller.
U_D		lognormal	geometric mean = 1; geometric standard deviation = 2^b.
A_w	cm^2	known [a]	value = 9.34×10^6 (for both silos combined).
λ_{Rn}	s^{-1}	known [a]	value = 2.10×10^{-6}.

[a] "Known" indicates that a single value is used in the calculation.

[b] Rogers et al. (1984) indicate that the variation among individual estimates of the diffusion coefficient for a particular soil at a given moisture content may be as much as an order of magnitude, especially at higher moisture saturation fractions. The geometric standard deviation (GSD) of 2 results in a 90% probability interval spanning approximately an order of magnitude (ratio of 95th to 5th percentile = 9.8). We consider this a reasonable representation of uncertainty, given the poor characterization of the K-65 material and how little is known about its similarity or dissimilarity to the soils measured by Rogers et al. (1984).

Table Q-7. Percentiles of Distribution of Unconstrained Radon Release Rate (Ci y^{-1}) from K-65 Silos—Alternative Calculation

Percentiles	5th	25th	median	75th	95th
Release rate	1,000	3,100	5,900	10,000	18,000

By minimum production rate we mean the production rate that would have to exist to support the radon in the head spaces *if there were no releases from the head spaces into the atmosphere*. To calculate the minimum production rate for the 1980–1987 period, we use Equation J-82 from the Task 2/3 report, with a slight change to the nomenclature:

$$P_{Rn,post:min} = C_{a,post}\lambda_{Rn}V_0 \qquad \text{(Q-27)}$$

where

$P_{Rn,post:min}$ = the minimum radon production rate that will sustain, at equilibrium, the head space radon concentration $C_{a,post}$ (pCi s^{-1}).

$C_{a,post}$ = concentration of ^{222}Rn in silo head space air (pCi cm^{-3}) for 1980–1987. This radon concentration was measured in 1987.

λ_{Rn} = the radioactive decay constant for ^{222}Rn (s^{-1}).

V_0 = volume of head space air in the silos (cm^3).

Equation Q-27 is used to calculate the minimum production rate for 1980–1987. This production rate is *constrained* by the radon concentration above the K-65 material, which is retained because of the existence of the silos above the K-65 material. An *unconstrained* production rate is the production rate that would exist if there were no silos. For comparison with the alternative calculation results, we need to calculate an unconstrained production rate, and here we wish to calculate a *minimum unconstrained* production rate, that would correspond to the calculated *minimum constrained* production rate $P_{Rn,post:min}$. The unconstrained production rate can be calculated from the constrained production rate by the form of Equation J-35 from the Task 2/3 report:

$$P_{Rn,0:\,min} = P_{Rn,post:\,min} \cdot \frac{(\phi/\lambda_{Rn})_{min}}{(\phi/\lambda_{Rn})_{min} - C_{a,post}} \qquad \text{(Q-28)}$$

where

$P_{Rn,\,0:\,min}$ = the unconstrained (the 0 refers to zero radon concentration above the source) radon production rate that would exist if the silos did not exist and that corresponds to the minimum constrained radon production rate of $P_{Rn,post:min}$.

ϕ = the pore space radon production rate in the K-65 material. Quantity of radon produced in pore spaces of the source material, per unit time per unit volume, that is free to migrate through the pores of the material (pCi m^{-3} s^{-1}). Depends on characteristics of the source material, including ^{226}Ra concentration, radon emanation fraction, bulk density, and porosity, and on the ^{222}Rn decay constant.

$(\phi/\lambda_{Rn})_{min}$ = the value of (ϕ/λ_{Rn}) that corresponds to our assumptions regarding the minimum production rate—namely that there are no releases from the silo head spaces to the atmosphere.

If there are no releases from the silos, the effective radon removal rate, λ_{eff}, is equal to the radon decay constant λ_{Rn}. We use this substitution in revising Equation J-34 of the Task 2/3 report to obtain:

$$(\phi/\lambda_{Rn})_{min} = C_{a,post} \cdot \frac{\varepsilon_w l_w + h}{\varepsilon_w l_w} \qquad \text{(Q-29)}$$

where

ε_w = porosity of the source material (the K-65 material).

l_w = diffusion length of radon in the source material, related to the diffusion coefficient (cm).

h = the effective height of the contained air space above the source material (cm) (see Figure Q-4).

To calculate the minimum unconstrained production rate, we use Equations Q-27, Q-28, and Q-29. We use a Monte Carlo procedure, as described in Appendix J of the Task 2/3 report, with the parameter distributions described there. (The distribution of the parameter $C_{a,\,post}$ has been modified since the draft report to have greater variance; this is discussed in a later section, beginning on page 37.) We note that in the absence of the silos, the unconstrained radon production is the same as an unconstrained release rate. Results of the calculation of the minimum unconstrained release rate that would support the measured radon concentration in the silo head spaces are summarized in Table Q-8.

Table Q-8. Percentiles of Distribution of Minimum Unconstrained Radon Release Rate (Ci y^{-1}) to Support Head Space Radon Concentration (Measured in 1987)

Percentiles	5th	25th	median	75th	95th
Release rate	2800	4400	5900	7900	12,000

Comparison of Results from Preferred Method and Alternative Method

We compare here the preferred method calculations and alternative method calculations of the unconstrained radon release rate from the K-65 silos, $P_{Rn,0}$. These results are also compared with the calculated minimum unconstrained radon release rate to support the measured radon concentration in the silo head spaces. First, we recall the results of the preferred method calculations; these are shown in Table Q-9.

Table Q-9. Percentiles of Distribution of Unconstrained Radon Release Rate (Ci y^{-1}) from K-65 Silos—Preferred Calculation

Percentiles	5th	25th	median	75th	95th
Release rate	4700	5900	6800	7900	9400

The unconstrained radon release rates are compared in Figure Q-2. Some observations are clear from this figure. The uncertainty range for results of the preferred method is much smaller than for results using the conventional method. In fact, the 90% probability interval (5th to 95th percentiles) of the preferred method results is contained within the 50% probability interval (25th to 75th percentiles) of the conventional method results. For convenience, we refer to the minimum unconstrained release rate to sustain the radon concentration in the silo head spaces as the "concentration-based minimum." Calculated unconstrained release rates that are lower than the 90% probability interval of the concentration-based minimum seem unreasonable. A troubling aspect of the conventional method calculation is that almost 20% of its distribution of results are below the 5th

percentile of the concentration-based minimum, for which the uncertainty variance is already conservatively large (see the discussion beginning on page 37). This indicates that some input parameter values used for the conventional calculation are probably not an accurate estimate of real values. This is not unexpected, because for the most important parameter, the radon diffusion coefficient, we used literature values rather than site-specific (for K-65 material) values.

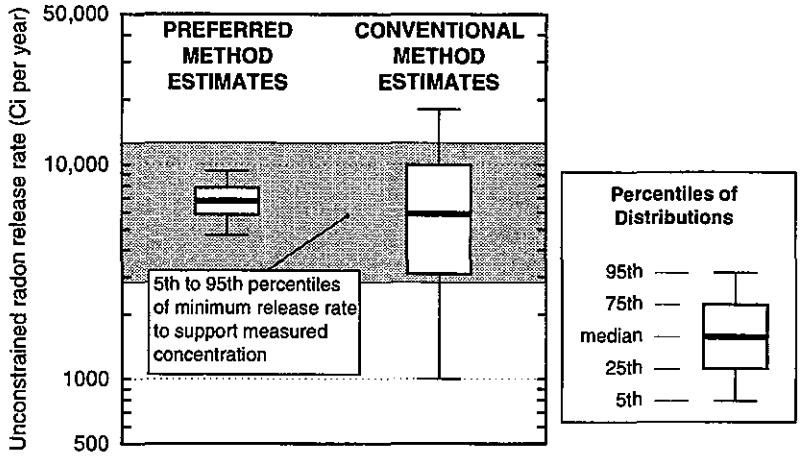

Figure Q-2. Comparison of estimated unconstrained radon releases from the K-65 silos using our preferred method and a conventional method (which we have also called the alternative method). The unconstrained radon release rate is the release rate estimated to occur if the K-65 material was open to the atmosphere. The band shown is the estimated 90% probability interval (5th to 95th percentile band) of the concentration-based minimum, which is the minimum required to sustain the radon concentration in the silo head spaces. The values of the conventional method results that lie below the concentration-based minimum band thus appear unreasonably low.

From this comparison of the conventional method results to the preferred method results and to the concentration-based minimum, we make the following conclusions: (1) Because the data available for input parameters for the conventional method are poor (as evidenced by how many results are lower than the 90% probability interval for the concentration-based minimum) the conventional method calculations should be considered rough, and the results should be considered less reliable than those from our preferred method (where we have more site-specific data for important parameters). This conclusion about the relative reliability of results from the two methods is also supported by the uncertainty in the conventional calculation results, which remains significantly greater than for the preferred method results. However, (2) the distribution of results of the preferred method calculation lies within the middle two quartiles of the distribution of results of the conventional method calculation. The general agreement of results of the two methods is encouraging, especially when the concentration-based minimum is considered. This provides some support for saying that (3) *the conventional method results provide some corroboration of the preferred method results.* This is perhaps the strongest statement we can make.

UPDATED ESTIMATE OF RADIUM-226 CONTENT OF THE K-65 SILOS

In Appendix J (page J-21) of the Task 2/3 report (Voillequé et al. 1995), we performed a rough calculation of the total quantity of ^{226}Ra in the K-65 silos. This value, 2200 Ci, was used for comparison with the quantity of ^{226}Ra estimated to be in the waste pits. As discussed earlier in this Appendix (see page Q-7), additional estimates of the bulk density of the K-65 material have been developed. The bulk density is now considered to be represented by a uniform distribution with range 0.53–1.4 g cm^{-3} (see page Q-21). We have also revised the distribution to be used for the ^{226}Ra concentration of the K-65 material, to a triangular distribution with minimum 134,900, modal value 420,000, and maximum 697,000 pCi g^{-1} (see page Q-21).

To update the estimate of the total quantity of ^{226}Ra in the K-65 silos, the revised distributions for bulk density and ^{226}Ra concentration are used in the following:

$$\text{Radium-226 content} = [\text{Ra}]\,\rho_w V_w \qquad \text{(Q-30)}$$

where [Ra] is the ^{226}Ra concentration of the K-65 material, ρ_w is the dry bulk density, and V_w is the volume of K-65 material in the two silos. Based on the range of depth of K-65 material in the silos (from Appendix J of the Task 2/3 report), V_w is assumed to have a uniform distribution with minimum 200,000 and maximum 240,000 ft^3. (5.7×10^9 to 6.8×10^9 cm^3).

A Monte Carlo simulation is used for this updated calculation. The updated results are a median value of 2400 Ci, and 5th to 95th percentile range of 1100–4300 Ci. We note that these results are intended primarily for general comparison with quantities of ^{226}Ra in other sources at the FMPC (e.g. the waste pits) and for validation exercises, such as estimation of the gamma exposure field above the silo domes, which is described in a subsequent section (page Q-40). The results are not intended for use in direct calculations related to the radon source terms.

ASSESSMENT OF A POSSIBLE BIAS IN PREFERRED-METHOD CALCULATIONS OF RADON RELEASES FOR 1959–1979

In response to comments from the Radon Review Meeting of December 1995, we have reevaluated the preferred-method calculations involving exposure rates on the K-65 Silo domes. According to the comments, our treatment, as described in Appendix J of the Task 2/3 report (Voillequé et al. 1995), of the exposure rates for background and for the 1959–1979 period would produce a small positive bias in the estimated head space radon concentration for 1959–1979. We note that this would then produce a small negative bias in the estimated radon release rate for 1959–1979. We point out in passing that the term *bias* technically refers to the difference between the expected value (mean) of an estimate and the true value of the parameter being estimated. In this case, the definition of this true value may be problematic.

In any case, the exposure ratio in question is

$$R_\gamma = \frac{X_{pre} - X_{bkg}}{X_{post} - X_{bkg}} \qquad \text{(Q-31)}$$

where, for the uncertainty analysis, uniform distributions are assumed for the background exposure rate, X_{bkg} (range 35.5–76 mR h^{-1}), the exposure rate for 1959–1979, X_{pre} (range 65–90 mR h^{-1}), and the exposure rate for 1980–1987, X_{post} (range 168–400 mR h^{-1}). The ranges used for the two parameters in the numerator overlap, and in our previous Monte Carlo source term calculations, for each iteration we reset the minimum of the distribution for X_{pre} to the greater of 65 mR h^{-1} and the sampled value for X_{bkg}. This procedure produces a larger sample mean than we would obtain if we sampled the uniform distributions without adjustment and computed the ratio, accepting negative values whenever they occur.

If we accept the mean value of the ratio, when it is sampled without the adjustment (i.e., if we do not reject the approximately 6% of negative values that occur during sampling) as an "unbiased" estimate of the quantity of interest, then we have a basis for a different strategy. However, the negative values produced by literal sampling of the ratio are unsuitable for further calculations required by the simulations. One must either reject the negative numbers that occur during sampling and accept the fact that one is increasing the sample mean, or else one must replace the sampling distribution with one that is associated with a positive-valued random variable. We have chosen the latter option.

Our procedure is to use the lognormal distribution that has the same mean and standard deviation as the distribution that would result from sampling the exposure ratio of equation Q-31 literally, with its component variables X_{pre}, X_{post}, and X_{bkg} represented by the independent uniform distributions described above. Using a sample of size 20,000 from the ratio R_γ (negative values included), we estimated the mean and standard deviation as α = 0.10 and β = 0.072, respectively. The formulas

$$GM = \frac{\alpha}{\sqrt{1+(\beta/\alpha)^2}}, \quad GSD = \exp\left(\sqrt{\ln\left(1+(\beta/\alpha)^2\right)}\right) \qquad \text{(Q-32)}$$

relate α and β to the geometric mean (GM) and geometric standard deviation (GSD) of the desired lognormal distribution. Thus we find GM = 0.081 and GSD = 1.9. Figure Q-3 shows a histogram of the sampled exposure ratio and the superimposed probability density function of this lognormal distribution. Each distribution is scaled to have an area of 100%.

Table Q-10 compares the radon releases predicted by the sampling method used in the task 6 draft report and sampling from the lognormal distribution just derived. Notice that the use of the lognormal distribution increased the indicated percentiles by 5% to 8% over those produced by the task 6 draft report method. In practice, the dose calculations were made with slightly different lognormal parameters, which added some conservatism to the uncertainty of the exposure ratio (GM = 0.084, GSD = 1.95, corresponding to a 95th to 50th percentile ratio of 3 in the R_γ uncertainty distribution). The effect of this change of the lognormal parameters decreases the 5th and 25th percentiles by about 100 Ci each; the remaining percentiles are the same as the ones in Table Q-10, to the precision shown. Even with the increased variance, the sensitivity of the pre-1970 release estimate to the gamma-exposure ratio is marginal, as is shown in a subsequent section (page Q-37; see Figure Q-6).

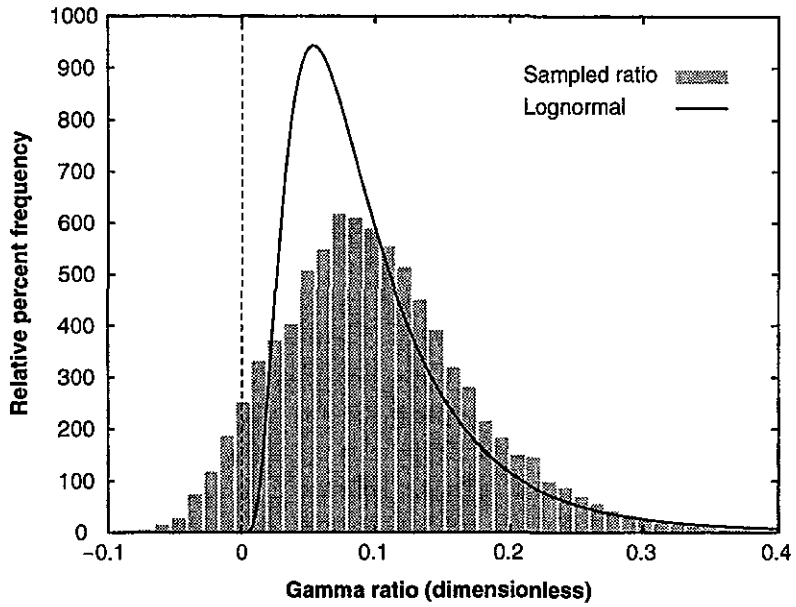

Figure Q-3. Representations of the uncertainty distribution of the gamma exposure ratio R_γ (equation Q-31). The grayscale histogram is the result of literal sampling of the ratio, with the variables X_{pre}, X_{post}, and X_{bkg} being represented by independent uniform distributions as described in the text, with no rejection of negative values. The curve is the graph of the probability density function of the lognormal distribution having the same mean (0.10) and standard deviation (0.072); its geometric parameters are GM = 0.081 and GSD = 1.9. Each distribution is scaled to a 100% area.

Table Q-10. Distributions of Annual Radon Releases 1959–1979 (Ci) Corresponding to Two Uncertainty Distributions for the Gamma Exposure Ratio R_γ[a]

	Percentiles				
	5%	25%	50%	75%	95%
Task 6 draft report[b]	2700	4300	5800	7900	12,000
Lognormal distribution[c]	2900	4600	6100	8300	13,000

[a] Equation Q-31. The percentiles shown are based on sample size 10,000 for each method.

[b] Uniform distributions for X_{pre}, X_{post}, and X_{bkg} as described in the text, with adjustment of sampling to avoid negative values of the exposure ratio.

[c] GM = 0.081 and GSD = 1.9, as derived in the text.

SUMMARY DESCRIPTION OF THE RELEASE MODEL FOR RADON IN THE K-65 SILOS

The K-65 silos are domed cylinders, 40 ft in radius. Each silo contains the residue of a slurry containing ^{226}Ra, which decays to ^{222}Rn. Because of its 1600-year half-life, any radiological depletion of the radium during the 40 years we are considering can be neglected. There is an air space (headspace) above the K-65 material in each silo. Some of the ^{222}Rn is free to migrate by diffusion through the interstices in the K-65 material; some of the diffusing radon is lost by radioactive decay (half-life 3.8 days), and some of the remainder enters the headspace. (For the time being, we ignore decay products and restrict attention to radon.) The headspaces are not of equal volume for the two silos, but it is reasonable to use an average volume, because we are interested in the total release of ^{222}Rn (and decay products) from both silos. It is also reasonable, for the calculations we are going to describe, to simplify the geometry of the headspace to that of a flat-head cylinder of the same volume (Figure Q-4).

From 1959 to mid-1979, each silo was ventilated through a vertical 6-inch-diameter gooseneck pipe that penetrated the highest part of the dome, and by other pipes and manholes that penetrated the dome. Radon-222 and its decay products escaped through the pipes and through cracks in the domes and walls. In mid-1979, the pipes were removed, the holes where they had penetrated were closed, and an effort was made to seal the cracks in the domes and walls. A series of measurements that began in April 1979 at station BS6, on the western site boundary, indicated that closing the silos reduced the radon concentrations at that location to essentially background levels (Volume 1, Figure 39). Subsequent monitoring near the silos indicated that the closure was not a completely effective seal, because air concentrations at some on-site monitoring locations exceeded background levels by detectable amounts. But at the site boundaries, the measured levels were near background.

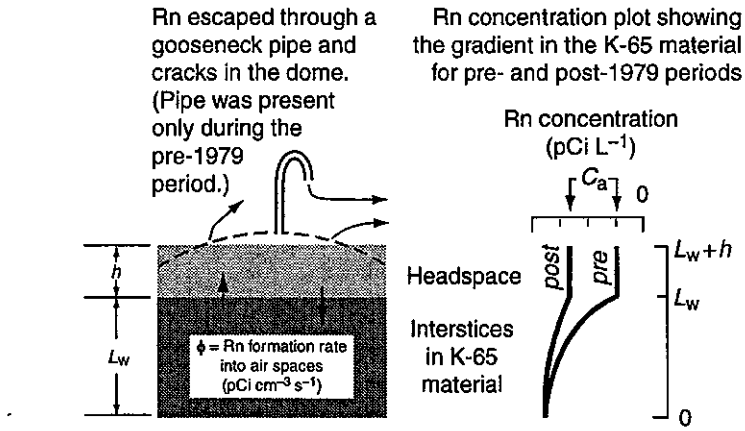

Figure Q-4. K-65 silos, with simplified geometry. Radon-222 forms from the decay of ^{226}Ra in the K-65 material and diffuses through interstitial air spaces and into the headspace. Concentrations in the K-65 interstitial air and in the headspace equilibrate, forming a gradient in the K-65 material (right-hand figure). The estimated headspace concentration is lower for the pre-1979 period, when the rate of loss through the gooseneck pipe and cracks in the dome was greater.

Thus we have two periods — before and after closure of the silos — requiring different parameterizations of a release model. In each period, there is an average concentration of ^{222}Rn in the headspace, C_a (pCi L^{-1}), which we treat as a steady-state quantity (i.e., time-invariant within each period). Before mid-1979, C_a would have been lower than afterward because of the greater exchange of air with the outside through the pipes and cracks, whereas the gross formation rate of ^{222}Rn in the K-65 material would have been the same for both periods, because the amount of ^{226}Ra remained essentially constant.

There is an initial temptation to use a one-box model for ^{222}Rn in the headspace, with a constant production rate P representing the infiltration of ^{222}Rn from the K-65 material. This is an acceptable approach, provided we take into account that P represents a *net* incursion rate, and that its value is different for the two periods. A more complete analysis is suggested by Figure Q-4, with two compartments that exchange ^{222}Rn (the K-65 interstices and the headspace). The concentration in the headspace represents a time average that is assumed to be uniform throughout the volume, because the headspace air is regularly mixed by expansion and convection currents set up by heat conducted through the silo walls and domes from the outside. The concentration in the network of interstices, however, is not uniform: it is maximum near the concrete floor of the silo and decreases to the headspace value C_a at the interface (Figure Q-4, plotted concentrations, labeled "pre" and "post"; the model tacitly assumes that the ^{226}Ra is uniformly distributed through the K-65 material). In this model, P (the net flow of ^{222}Rn across the interface) is a dynamic quantity that is proportional to the concentration gradient in the K-65 material. Since the gradients are different in the two periods, the values of P would also be different (Figure Q-4, pre and post curves: the gradients are equal to the slopes just below the interface).

The data and steps in the calculation are summarized below. Figure Q-5 is a schematic presentation of the relationships between the data and the steps. We give "nominal" numeric values to assist the reader in following the steps of the calculation, but one must remember that the estimation of releases for environmental transport and dose calculation involves Monte Carlo calculations.

First, we list the quantities that are directly related to measurements that have been made, and thus, in this sense, can be considered "known." We also list parameter values taken from the literature. We use the subscripts "pre" and "post" to indicate which period, both for data and calculated quantities.

A. The fractional loss rate of ^{222}Rn from the headspace to the outside during 1980–1987 that is attributable to temperature change: $\lambda_{v,\,post} = \Delta T / T_0 = 3.11 \times 10^{-7}\ s^{-1}$. The headspace volume: $V_0 = 51{,}000\ ft^3 = 1.44 \times 10^6$ L is the average for the two silos.
B. The 1987 measured concentration of ^{222}Rn in the headspace: $C_{a,\,post} = 2.59 \times 10^7$ pCi L^{-1}.
C. Parameters for diffusion through the dome (from the literature): porosity $\varepsilon_c = 0.215$ (dimensionless); radon diffusion length in concrete dome $l_c = 18.75$ cm; thickness of dome L = 3.5 in; surface area of dome $A_{dome} = 5300\ ft^2 = 4.92 \times 10^6\ cm^2$; and the radiological decay rate coefficient for ^{222}Rn: $\lambda_{Rn} = 0.181\ d^{-1} = 2.10 \times 10^{-6}\ s^{-1}$.

D. Measured gamma exposure rates at the surfaces of the domes, and estimated background, which includes gamma rays from the ^{226}Ra in the K-65 material and the radon decay products in the interstices:
   - 1959–1979: $X_{pre} = 77.5$ mR h^{-1}
   - 1980–1987: $X_{post} = 284$ mR h^{-1}
   - background: $X_{bkg} = 55.8$ mR h^{-1}.

   The ratio $(X_{pre} - X_{bkg})/(X_{post} - X_{bkg}) = 0.095$ from the given values, but our uncertainty analysis leads to a lognormal distribution for the ratio with geometric mean 0.084 (page Q-27). We use this latter number as the deterministic value of the ratio in the calculations that follow.

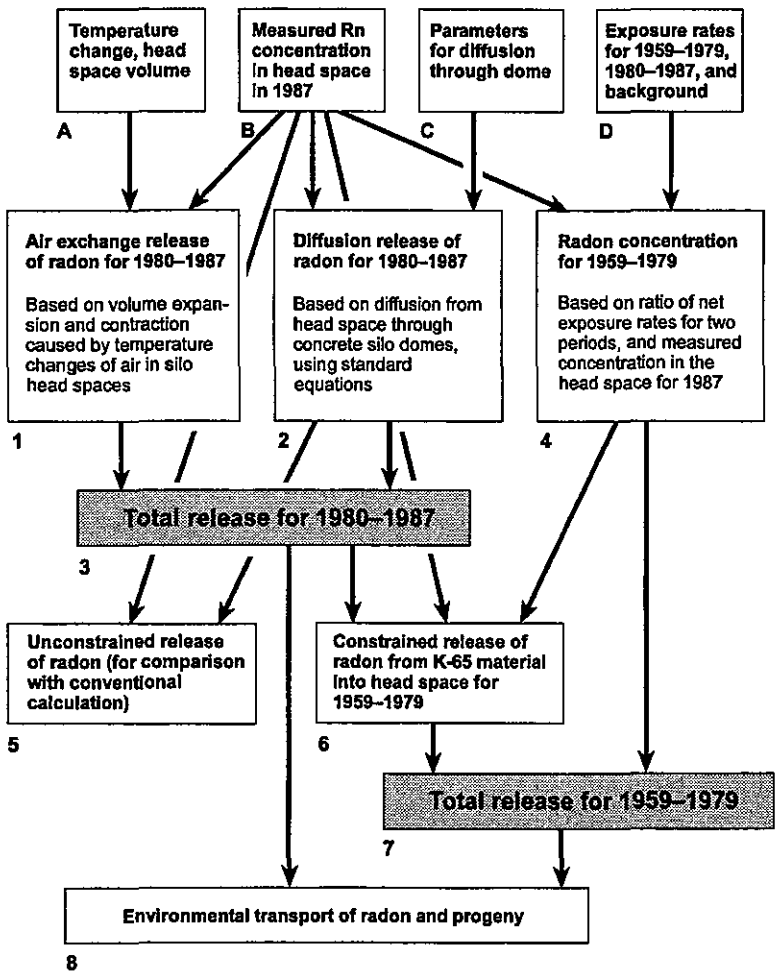

Figure Q-5. Flow sheet for the estimation of the primary radon releases from the K-65 silos. The letters and numerals below the boxes correspond to the data and computational steps outlined in the text.

It is also worthwhile, at this point, to remember what is not "known" from measurements:

a. The headspace concentration of ^{222}Rn for the earlier period: $C_{a,\,pre}$.

b. The fractional release rate for the earlier period: $\lambda_{v,\,pre}$.
c. The net production rates $P_{Rn,\,pre}$ and $P_{Rn,\,post}$ (net flux of Rn from the K-65 material to the headspace).
d. The quantity of ^{226}Ra in the K-65 material and the formation rate, ϕ, of ^{222}Rn that migrates into the interstitial airspaces (this does not include ^{222}Rn that is trapped in the K-65 material and unable to migrate).
e. The diffusion coefficient D_e for ^{222}Rn in the interstitial air spaces of the K-65 material, the porosity ε_w of the material, and the diffusion length of radon l_w in the material.
f. External air concentrations of ^{222}Rn before mid-1979, except for a single two-month data series at station BS6, located 300 m west of the silos.

Items a through e (and related quantities) are estimated from the data in items A through D, which are known with varying degrees of uncertainty. Prediction of external air concentrations of ^{222}Rn (item f) and decay products is, of course, the goal of the release model, coupled with an atmospheric transport model. But as we have noted, the data needed for a satisfactory validation of the predictions of air concentrations for the earlier period do not appear to exist.

The calculations follow:

1. Calculate air exchange release of Rn for 1980–1987. Use data A and B and $Q_{exch,post} = C_{a,post}\,\lambda_{v,post}V_0 = 2.59\times10^{7}$ pCi $L^{-1}\times 3.11\times10^{-7}$ $s^{-1}\times 1.44\times10^{6}$ L $= 1.16\times10^{7}$ pCi s^{-1}.
2. Calculate diffusion releases of Rn for 1980–1987. Use data B and C and the equations
$$Q_{diff,\,post} = JA_{dome}, \text{ where } J = \varepsilon_c\lambda_{Rn}l_c C_{a,\,post}/\sinh(L/l_c).$$
The loss rate coefficient for diffusion is $\lambda_{diff,\,post} = Q_{diff,\,post}/(C_{a,\,post}V_0)$. We have $J = 0.215\times2.10\times10^{-6}$ $s^{-1}\times 18.75$ cm $\times 2.59\times10^{7}$ pCi $L^{-1}\times 0.001$ L cm^{-3} / sinh(18.89 cm / 18.75 cm) = 0.446 pCi cm^{-2} s^{-1}. Then $Q_{diff,\,post}$ = 0.446 pCi cm^{-2} $s^{-1}\times 4.92\times10^{6}$ cm^2 = 2.19×10^{6} pCi s^{-1}. Finally, $\lambda_{diff,\,post} = 2.19\times10^{6}$ pCi s^{-1} / (2.59×10^{7} pCi $L^{-1}\times 1.44\times10^{6}$ L) = 5.87×10^{-8} s^{-1}.
3. Calculate total Rn releases for 1980–1987. Use results of steps 1–2 and $Q_{post} = Q_{exch,post} + Q_{diff,post} = 1.16\times10^{7}$ pCi $s^{-1} + 2.19\times10^{6}$ pCi $s^{-1} = 1.38\times10^{7}$ pCi s^{-1}.
4. Estimate the Rn concentration in the head space for 1959–1979. Use data B and D and $C_{a,pre} = C_{a,post}\,(X_{pre} - X_{bkg})\,(X_{post} - X_{bkg})^{-1}$. As indicated in item D, our nominal value for the X-ratio is 0.084. Therefore $C_{a,\,pre} = 2.59\times10^{7}$ pCi $L^{-1}\times 0.084 = 2.18\times10^{6}$ pCi L^{-1}.
5. Calculate the production rate (net rate of release from K-65 material into airspace) for unconstrained conditions. This is the unconstrained release rate. Use data A and B, results of step 2, and the equations
$$P_{Rn,\,0} = P_{Rn,\,post}\cdot\frac{\phi/\lambda_{Rn}}{\phi/\lambda_{Rn} - C_{a,\,post}}, \text{ where } P_{Rn,\,post} = C_{a,\,post}V_0\lambda_{eff,\,post}$$
$$\text{and } \phi/\lambda_{Rn} = C_{a,\,post}\cdot\frac{\lambda_{eff,\,post}}{\lambda_{Rn}}\cdot\frac{\varepsilon_w l_w + h}{\varepsilon_w l_w}.$$
The total rate coefficient $\lambda_{eff,\,post} = \lambda_{v,\,post} + \lambda_{diff,\,post} + \lambda_{Rn}$; h is the effective height of the airspace in the silos, ε_w is the porosity of the K-65 material, and l_w is the diffusion length of the K-65 material. The factor $(\varepsilon_w l_w + h)/(\varepsilon_w l_w)$ is treated as a constant with the value 6.35. First, $\lambda_{eff,\,post} = 3.11\times10^{-7}$ $s^{-1} + 5.87\times10^{-8}$ $s^{-1} + 2.10\times10^{-6}$ $s^{-1} = 2.47\times10^{-6}$ s^{-1}. Then $P_{Rn,\,post} = 2.59\times10^{7}$ pCi $L^{-1}\times 1.44\times10^{6}$ L $\times 2.47\times10^{-6}$ $s^{-1} = 9.21\times10^{7}$

pCi s^{-1}. Next, $\phi / \lambda_{Rn} = 2.59 \times 10^7$ pCi $L^{-1} \times (2.47 \times 10^{-6}\ s^{-1} / 2.10 \times 10^{-6}\ s^{-1}) \times 6.35 = 1.93 \times 10^8$ pCi L^{-1}. Finally, $P_{Rn,\,0} = 9.21 \times 10^7$ pCi $s^{-1} \times 1.93 \times 10^8$ pCi L^{-1} / $(1.93 \times 10^8$ pCi $L^{-1} - 2.59 \times 10^7$ pCi $L^{-1}) = 1.06 \times 10^8$ pCi s^{-1}.

6. Calculate production rate (net rate of release from K-65 material into airspace) for constrained conditions during 1959–1979. Use data B and results of step 5 and the equation

$$P_{Rn,\,pre} = P_{Rn,\,post} \cdot \frac{\phi / \lambda_{Rn} - C_{a,\,pre}}{\phi / \lambda_{Rn} - C_{a,\,post}},$$

where ϕ / λ_{Rn} is given in step 5. We have $P_{Rn,\,pre} = 9.21 \times 10^7$ pCi $s^{-1} \times (1.93 \times 10^8$ pCi $L^{-1} - 2.18 \times 10^6$ pCi $L^{-1}) / (1.93 \times 10^8$ pCi $L^{-1} - 2.59 \times 10^7$ pCi $L^{-1}) = 1.05 \times 10^8$ pCi s^{-1}.

7. Calculate total Rn releases for 1959–1979. Use the results of steps 4 and 6 and the equation $Q_{pre} = P_{Rn,\,pre} - C_{a,\,pre} \lambda_{Rn} V_0$ per silo. Total $Q_{pre} = (1.05 \times 10^8$ pCi $s^{-1} - 2.18 \times 10^6$ pCi $L^{-1} \times 2.10 \times 10^{-6}\ s^{-1} \times 1.44 \times 10^6$ L) $\times 2$ silos $= 1.97 \times 10^8$ pCi $s^{-1} = 6.2 \times 10^3$ Ci $year^{-1}$. The release rate coefficient can be calculated as $\lambda_{v,\,pre} = 0.5 \times 1.97 \times 10^8$ pCi $s^{-1} / (2.18 \times 10^6$ pCi $L^{-1} \times 1.44 \times 10^6$ L) $= 3.14 \times 10^{-5}\ s^{-1}$. This corresponds to 2.7 headspace volumes per day.

8. Compute the release of Rn for transport calculations. Use the result of step 3 or step 7 according to the year.

The foregoing calculations imply kinetics consistent with steady-state levels of radon decay products in the silo headspaces (^{218}Po, ^{214}Pb, ^{214}Bi, and ^{214}Po, of which the last two may always be assumed to be in secular equilibrium; therefore, we will mention only ^{214}Bi rather than ^{214}Bi and ^{214}Po).

If plateout of the decay products on the interior surfaces of the silos is neglected, the total activity of each decay product in a silo's headspace (Ci) may be calculated from the equations

$$\begin{aligned} A_1 &= V_0 C_a \\ A_i &= \lambda_i A_{i-1} / (\lambda_i + \lambda), \quad i = 2, 3, 4 \end{aligned} \tag{Q-32}$$

where i = 1, 2, 3, and 4 correspond, respectively, to ^{222}Rn, ^{218}Po, ^{214}Pb, and ^{214}Bi. The rate coefficients λ_i (s^{-1}) represent radioactive decay (λ_1 is equal to λ_{Rn} used previously), and λ accounts for loss from the headspace to the outside. In the columns labeled "uncorrected," Table Q-11 shows the levels of ^{222}Rn and each decay product for the two periods, based on equations Q-32 and values calculated in steps 1 through 7.

Step 4 is based on an approximation that substantially simplifies the calculation, namely the assumption that the outside gamma-field ratio (pre/post) would estimate the corresponding ratio of ^{222}Rn concentrations ($C_{a,\,pre} / C_{a,\,post}$). In fact, the gamma field above the silo domes is influenced principally by the decay products ^{214}Pb and ^{214}Bi (primarily the latter), and a ratio based on one or both of these nuclides would be preferred on physical grounds. In fact, it is possible to make a correction to the calculation that accomplishes this purpose. We illustrate the procedure by using the ^{214}Bi ratio, $A_{4,\,pre} / A_{4,\,post}$. From Table Q-11, we calculate that this ^{214}Bi ratio is 2.76 / 37.4 = 0.074, whereas the desired gamma ratio, based on analysis of the measurements, is 0.084. We observe from equations Q-32 that if $C_{a,\,pre}$ were higher by the factor 0.084 / 0.074 = 1.14 and all parameters in the equations remained the same, the ^{214}Bi ratio would be 0.084 as desired. Thus in step 4, we adjust the calculated value of $C_{a,\,pre}$ by this factor and recalculate the remaining quantities from that

point onward. We must recognize, however, that the recalculation does change a parameter in equations Q-32, namely a term in the pre-1979 release rate coefficient, λ, and thus we may expect that the resulting ratio may not be exactly on target. However, fine-tuning of the correction factor shows that the value 1.12 gives the desired ^{214}Bi ratio. The corrected levels of ^{222}Rn and decay products are shown in Table Q-11, with the ^{214}Bi ratio equal to 0.084 as desired. The reduction in the estimated annual release is only about 1%. We have included one iteration of the correction, without fine tuning, in the dose calculations.

Table Q-11. Estimated Levels of ^{222}Rn (Ci) and Decay Products in the Headspaces of the K-65 Silos

		No plateout			Plateout	
		Pre-1979		Post-1979	Pre-1979	Post-1979
	λ_i (s^{-1})	Uncorrected[a]	Corrected[a]			
Rn-222	2.10×10^{-6}	3.14	3.52	37.4	3.58	37.4
Po-218	3.79×10^{-3}	3.12	3.49	37.4	3.46	36.4
Pb-214	4.31×10^{-4}	2.90	3.28	37.4	3.07	34.2
Bi-214	5.86×10^{-4}	2.76	3.13	37.4	2.81	32.6

[a] Uncorrected refers to using the ^{222}Rn ratio $C_{a,\,pre} / C_{a,\,post}$ in the headspaces for calibration with the corresponding ratio gamma field measurements on the silo domes. Corrected means an adjustment has been made to approximate the use of the pre/post ratio of ^{214}Bi. The pre-1979 concentrations shown under "Plateout" have been corrected in this sense.

Equations Q-32 are appropriate for considering external gamma fields related to radon decay products, because plateout on the internal silo surfaces, which these equations neglect, does not remove the affected fraction of each decay product from the silos. Thus, in estimating the gamma exposure ratio in these calculations, we use the ^{214}Bi values given by equations Q-32. However, when we estimate equilibrium fractions of radon and decay products that escape to the outside air, we proceed differently, taking into account that plateout of decay products on the inner surfaces of the silos alters the equilibrium ratios of the escaping nuclides. Only attachment of ^{218}Po to suspended particles (condensation nuclei) is considered, because unattached fractions of subsequent decay products are negligible (NCRP 1984).

The calculation is somewhat more complicated than the one described by equations Q-32, but it is similar to the one for plateout of radon decay products inside buildings, which was explained in Appendix I. We consider the attachment of ^{218}Po (RaA) to very fine airborne particles, because the nuclide in the free ion (unattached) state in which it is formed from the decay of ^{222}Rn has enhanced potential for plateout.

The attachment process is governed by a rate coefficient

$$\lambda_S = \frac{S\bar{v}}{4} \quad s^{-1}, \tag{Q-33}$$

(NCRP 1984) where

S = $n\pi\overline{D}^2$ = surface area per unit volume ($cm^2\ cm^{-3}$) of condensation nuclei

$\overline{D}$ = diameter corresponding to the mean surface area of condensation nuclei (cm); the value 0.125×10^{-4} cm (0.125 μm) has been considered a typical average value for environmental atmospheres (NCRP 1984)

n = number concentration of condensation nuclei (cm^{-3}); outdoor counts measured in Socorro, NM, range from 9,000 to 50,000 condensation nuclei per cm^3 (George and Breslin 1980); for the K-65 silo interiors, we used a near-midrange value of 30,000 cm^{-3}

4 = ratio of spherical surface area to area of plane circular projection

$\overline{v}$ = average velocity of unattached ^{218}Po (RaA) ions = 1.38×10^4 cm s^{-1}.

Plateout is quantified by two deposition velocity parameters (cm s^{-1}), one for each state: v_{unatt} for unattached ^{218}Po and v_{att} for attached ^{218}Po and the other decay products. For the attached species, we use the nominal value of 0.2 m h^{-1} = 0.056 cm s^{-1}; for unattached species, we use 8 m h^{-1} = 0.22 cm s^{-1} (Knutson 1988). In order to convert these deposition velocities to deposition rate coefficients, with units s^{-1}, we multiply them by the surface-to-volume ratio of the silo headspace:

$$\rho_{S/V} = \frac{2\pi Rh + \pi R^2}{\pi R^2 h} = \frac{2}{R} + \frac{1}{h}, \qquad \text{(Q-34)}$$

where the radius R = 40 ft = 1219 cm, and the effective height h = 10 ft = 305 cm, giving $\rho_{S/V}$ = 0.005 cm^{-1} (the surface of the K-65 material, which the model treats as permeable, was not included in the surface area of the headspace). The equations for the ^{222}Rn and decay-product activities are

$$\begin{aligned}
&\text{Rn-222} && A_1 = P/(\lambda_1 + \lambda) \\
&\text{Po-218} && A_2^* = \lambda_2 A_1/(\lambda_2 + \lambda + \lambda_S + \rho_{S/V} \cdot v_{unatt}) \\
& && A_{\bar{2}} = \lambda_S A_2^*/(\lambda_2 + \lambda + \rho_{S/V} \cdot v_{att}) \\
& && A_2 = A_2^* + A_{\bar{2}} \\
&\text{Pb-214} && A_3 = \lambda_3 A_2/(\lambda_3 + \lambda + \rho_{S/V} \cdot v_{att}) \\
&\text{Bi-214} && A_4 = \lambda_4 A_3/(\lambda_4 + \lambda + \rho_{S/V} \cdot v_{att})
\end{aligned} \qquad \text{(Q-35)}$$

where the three equations for ^{218}Po give, respectively, the activities for unattached, attached, and total ^{218}Po (RaA). With the appropriate substitutions for the net production P and λ, equations Q-35 are suitable for both the pre-1979 and the post-1979 periods (for the post-1979 period, $\lambda = \lambda_{diff} + \Delta T/T_0$, where the first term refers to diffusion through the cracks in the concrete and the temperature ratio term represents loss to the outside by thermal expansion of the headspace gases).

REVISION OF EQUILIBRIUM RATIOS OF RADON DECAY PRODUCTS AT THE RELEASE POINT

Equations Q-35 are now the basis for calculation of the equilibrium ratios of radon decay products released during the pre-1979 period. This represents a change from the approach used for the draft report, in which ratios from the literature designated as "environmentally typical" (1 : 0.9 : 0.7 : 0.7) were assumed for the releases. These ratios were adopted from

NCRP 1984. Table Q-11 implies pre-1979 ratios of 1 : 0.96 : 0.86 : 0.78, and these numbers are typical of the values that are generated for the dose estimation (they vary, of course, from one Monte Carlo iteration to the next in response to parametric uncertainties in the release model; see the next section). However, the "environmentally typical" ratios were retained for the post-1979 releases, because the ratios computed in Table Q-11 for the sealed headspaces were likely atypical of the effluent gas that diffused through the concrete walls and domes, where plateout of the decay products would be high.

The very limited environmental radon daughter data tend to corroborate radon daughter releases at relatively large fractions of equilibrium (see Appendix N). The importance of the initial concentrations of decay products and the dynamics of formation and decay during downwind transport in the plume is evaluated further in Appendix I of this report.

EXPANSION OF THE UNCERTAINTY FOR RADON RELEASES DURING 1959–1979

So far, we have not gone into the question of parametric uncertainty of the reconstructed radon releases for the period before 1979. In the work done for the draft task 6 report, the annual pre-1979 release of ^{222}Rn from the K-65 silos was estimated as 6160 Ci year^{-1}, with 5th and 95th percentiles of 4200 and 8660 Ci year^{-1}, respectively (Table Q-10, "preferred methodology"). The NRC review committee objected to this uncertainty distribution as an implausibly narrow estimate of precision for the backcast releases.

Figure Q-6 shows an analysis of the parameters used in the calculation of the ^{222}Rn releases from the silos during the two periods 1959–1979 (pre) and 1980–1987 (post). The bar graph in the figure shows an estimate of the percent contribution of each parameter to uncertainty in the pre-1979 release. The analysis was performed with Crystal Ball® (Decisioneering 1993). Each parameter is assigned a probability distribution as a measure of uncertainty of its values, and we use Monte Carlo methods to propagate the parametric uncertainty distributions through the model to the resulting release estimates. Figure Q-6 readily identifies the post-1979 headspace radon concentration $C_{a,\,post}$ as the dominant parameter with 55.8% of the release variance. The headspace volume V_0, at 32.8%, is second. Uncertainty assumptions about the volume are already quite conservative, and increasing the variance of this parameter would not be physically reasonable. There is little to be gained from manipulating the distributions of the gamma ratio (to which, as explained in an earlier section, some variance was added) or λ_{post}, and the remaining parameters contribute negligibly to uncertainty. This process of elimination leaves only the distribution of $C_{a,\,post}$ for further consideration.

The distribution of $C_{a,\,post}$ in the draft report was based on samples of the gas in the headspaces of the silos, which were taken in a series of measurements during a single day (November 4, 1987). Following an analysis of these data, the task 2/3 report (Voillequé et al. 1995) assigned a normal distribution with mean = 2.62×10^7 pCi L^{-1} and standard deviation 4.1×10^6 pCi L^{-1} for this parameter. Subsequently, we assigned a lognormal distribution with the same mean and standard deviation; this distribution has geometric mean 2.59×10^7 pCi L^{-1} and geometric standard deviation 1.17. Thus, the 95th percentile exceeds the median by about 30% ($1.17^{1.65} \approx 1.30$). It is reasonable to ask whether the dispersion of this distribution should be increased, and if so, by how much.

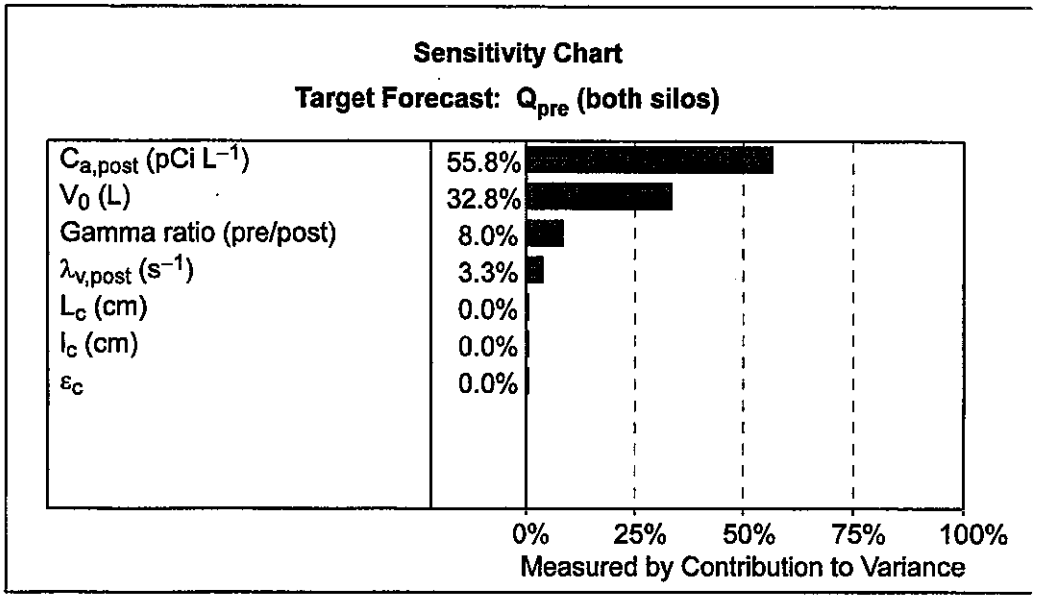

Figure Q-6. Sensitivity analysis of simulated release of radon from the K-65 silos 1959–1979. The bar graph indicates the approximate fractional contribution of each model parameter to the total variance in the predicted release.

The sampling of the headspace gas is discussed in the task 2/3 report (Voillequé et al. 1995) in Appendix J (pages J-8 and J-9). Samples were collected in sampling bags and in glass flasks, and analyses were performed by both Fernald (Westinghouse Materials Company of Ohio, or WMCO) and Mound Laboratory (WMCO analyzed only the glass flask samples). Differences in the results from the two sampling containers and opinions expressed by the experimenters led us to conclude that the glass flask results should be presumed more reliable, and these were used exclusively in our estimates. Analyzing these data led, as previously indicated, to a normal distribution and subsequently to the lognormal distribution described above. However, it is plausible that (1) the ^{222}Rn concentration in the headspaces might have varied daily or seasonally, responding to changing thermal influences, and the samples drawn on one day in November 1987 might not be representative of a long-term average. It could also be argued that (2) the ^{222}Rn concentration in the headspaces might have been spatially nonuniform within the containing volume, and thus samples drawn from access ports through the domes might not be representative of an average over the entire volume.

We have addressed these uncertainties by increasing the geometric standard deviation of the lognormal distribution given above from 1.17 to 1.52, which gives a 95th-to-50th percentile ratio of 2 for the ^{222}Rn concentration during the 1980s. We believe this is a conservative assumption. Temporal bias would be our first concern, and it seems unlikely that tracer concentrations in this essentially closed system could vary by as much as a factor of two when daily air exchanges were at most a few percent of the headspace air volume. Diffusion and convective movement within the enclosed gas would also tend to homogenize

the radon concentration within the headspace volume, reducing spatial bias in the sampling (however, in November, when the samples were taken, these effects would be less than, say, in August).

We performed some simulations to study the temporal trend of the headpace radon concentration, using a model that would tend to exaggerate fluctuations. The simulations were based on hourly data from the Cincinnati airport for the year 1987 and on a correlation of measured daily headspace gas expansion (inferred from fractional change in absolute temperature of the gas) with corresponding differences of maximum and minimum daily temperatures at the Cincinnati airport. The correlation reported in the task 2/3 report (Voillequé et al. 1995) is given by the equation

$$\Delta T / T_0\ (\mathrm{d}^{-1}) = (0.00179\ ^\circ\mathrm{F}^{-1}\ \mathrm{d}^{-1}) \times (T_{\max} - T_{\min}\ (^\circ\mathrm{F})) - 0.00516\ \mathrm{d}^{-1}. \qquad \text{(Q-36)}$$

The model integrates the gains and losses of concentration from one day to the next:

$$C_1 = C_0\, e^{-\lambda \cdot (1\ \mathrm{day})} + \frac{P}{V_0 \lambda}\left(1 - e^{-\lambda \cdot (1\ \mathrm{day})}\right), \qquad \text{(Q-37)}$$

where C_0 and C_1 are headspace concentrations for two successive days, the rate coefficient $\lambda = \lambda_{\mathrm{Rn}} + \lambda_{\mathrm{diff}} + \Delta T / T_0$, P is the net rate of movement of radon from the K-65 material into the headspace, and V_0 is the headspace volume. The subscripts Rn and diff refer, respectively, to radioactive decay of ^{222}Rn and loss from the headspace by diffusion through the concrete dome. Loss through penetrations that resulted from imperfect sealing of the silos (ventilation) is identified with the temperature ratio $\Delta T / T_0$, which is estimated by equation Q-36. The value of λ_{diff} was calculated in the previous section as $5.87 \times 10^{-8}\ \mathrm{s}^{-1} = 5.07 \times 10^{-4}$ day^{-1}. The value of λ_{Rn} is 0.181 d^{-1}, and the headspace volume V_0 is 1.44×10^6 L.

For each of the 365 days of the year 1987, we used Cincinnati airport records to obtain the temperature difference $T_{\max} - T_{\min}$ for equation Q-36. Proceding through the days in order, we evaluated equation Q-37 (beginning with an average value for C_0) and computed and recorded C_1. For the next day, the value of C_0 was replaced by the previous day's computed value of C_1. The value of λ changed daily according to its dependence on equation Q-36.

The result of the year's simulation was a mean concentration of 2.60×10^7 pCi L^{-1}, with maximum and minimum values 2.82×10^7 and 2.38×10^7 pCi L^{-1}, respectively. These extremes correspond to fluctuations above and below the mean value of about 9%, far less than the factor of two that we have postulated for uncertainty, thus allowing a generous margin for any spatial variations within the headspace. Table Q-12 indicates the radon release distributions for the K-65 silos for 1952 through 1988, as they were calculated from the factor-of-two uncertainty for the parameter $C_{\mathrm{a,\,post}}$, with distributions for other parameters as previously described.

The radon dose percentiles in Table K-5 (Appendix K) reflect the increased variance in the radon releases from the K-65 silos as indicated in Table Q-12. Even with this substantial increase of the parameter variance, the 95th/50th-percentile ratio of the scenario 1 dose distribution increases by only about 17% above its value given in the task 6 draft report. Other components of uncertainty, predominantly the air transport model calibration and the

back-extrapolation of recent meteorological data, dominate the composite uncertainty distribution of the radon dose estimates.

Table Q-12. Annual Release (Ci) of ^{222}Rn from K-65 Silos with Increased Uncertainty

Period	5%	25%	50%	75%	95%
1952–1953	160	810	1700	2900	5300
1954–1958	2200	3600	4900	6600	10,000
1959–1979	2800	4500	6100	8300	13,000
1980–1987	340	590	880	1400	2400
1988	36	110	220	440	1300

EFFECT OF RAPID TURNOVER DURING 1959–1979 ON DECAY-PRODUCT EQUILIBRIUM AND GAMMA-FIELD MEASUREMENTS ON THE SILO DOMES

Lacking adequate sampling of radon concentrations in either the K-65 silo headspaces or ambient outside air during the period before the silos were sealed, the *RAC* methodology relied partly on measurements of the gamma field near the silo domes taken before and after sealing to calibrate the release model. The calibration depended only on the ratio of the gamma-field components due to the headspace radioactivity before and after the silos were sealed. The ratio was estimated from gamma exposure rate measurements taken on the silo domes at various times before and after the silos were sealed. In order to remove the component of the gamma field that resulted from radioactivity in the K-65 material, we used gamma exposure rate measurements that were made in November of 1987, when radioactivity had been evacuated from the silo headspaces during the operation of the Radon Treatment System (RTS). These measurements presumably would directly estimate the field component due to the radioactivity in the K-65 material.

Since the calibration of the radon release model depended on the *ratio* of the gamma exposure rates from headspace radioactivity measured before and after the sealing of the silos (i.e., the ratio rather than the absolute magnitudes), it is conceivable that the inferred equilibrium state of radon decay products in the silo headspaces, together with radioactivity in the K-65 material, might predict a gamma field with absolute magnitude that is inconsistent with the measurements. If such were the case, it would cast doubt on the model's calibration and thus on its predictions of release. To rule out such a possibility, we have performed gamma exposure calculations based on the geometry and material composition of the silos and the K-65 material, using the levels of ^{222}Rn and the equilibrium ratios of decay products in the silo headspace that were calculated by the release model before and after the silos were sealed. Radium-226 in the K-65 material was discussed previously in this appendix; radon decay products in the K-65 material were assumed to be in equilibrium with the ^{226}Ra. Other radionuclides in the K-65 material were listed with estimated magnitudes in Table J-47 of Voillequé et al. 1995, but these radionuclides contributed negligibly to the

gamma field outside the domes. As a practical matter, the gamma field is dominated by the emissions of ^{214}Bi and ^{214}Pb, principally the former.

The gamma exposure calculations were carried out by integrating a gamma point-kernel model over each source region (headspace and K-65 material) and using mass attenuation coefficients and exposure buildup factors appropriate to emitted energy spectra and elemental compositions of the shielding media (K-65 material, air, and concrete dome). The results, expressed in units of exposure rate (mR h^{-1}), are summarized by the gray areas in Figure Q-7. Numeric values of the calculations and measurements are shown in Table Q-13. For this comparison, we have considered only the measurements made with detectors in contact with the concrete domes; the simulations assumed that the receptor points were situated on the surface of the dome.

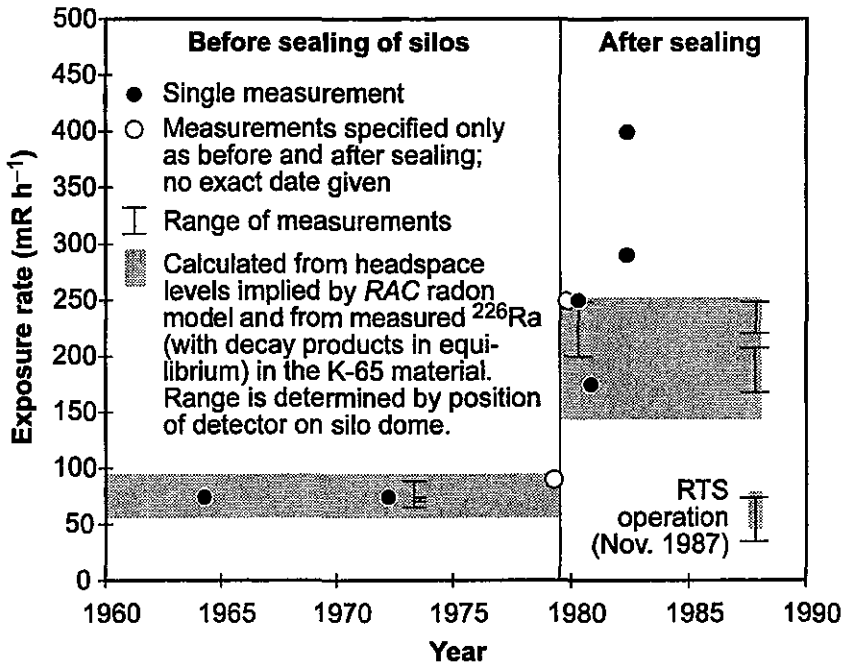

Figure Q-7. Gamma exposure field above the K-65 silo domes. Shaded areas indicate *RAC* calculations of the gamma exposure field based on headspace concentrations of ^{222}Rn gamma-emitting decay products (primarily ^{214}Pb and ^{214}Bi) and on gamma-emitting radioactivity in the K-65 material. The ranges of the calculations show variations resulting from the placement of the detector on the dome. Most measured values lie within the calculated ranges. The two outlier points for 1982 might have resulted from placement of the detector near a point of leakage or other experimental difficulties.

The point kernel method is based on the formula for the exposure rate ξ_γ (mR h^{-1}) at a receptor point due to a gamma-emitting source of activity A (Bq) and energy E (MeV) of intensity I (fraction per nuclear transformation):

$$\xi_\gamma = \frac{B(E, x_{\text{eff}}(E))\, K(E)\, AEI \exp\left(-\sum_i x_i(E)\right)}{4\pi r^2} . \qquad \text{(Q-38)}$$

Table Q-13. Calculated Values and Measurements of Exposure Rate (mR h^{-1}) on Domes of K-65 Silos Before and After Sealing

Calculated					Measured			
Distance (ft) from center:					Date of		Exposure	
0	10	20	30	40	measurement	Silo	rate	Reference
					Before sealing openings			
92.4	93.9	94.9	87.3	56.1	April 1964	1	75	Starkey (1964)
					March 1972	ns[a]	75	Nelson (1972)
					May 1973	1	65–90	Boback (1973)
					May 1973	2	70–75	Boback (1973)
					ns[a]	ns[a]	90	Boback (1980)
					After sealing openings			
251	251	235	215	146	April 1980	1	250	Green (1980c)
					April 1980	2	200–250	Green (1980c)
					ns[a]	ns[a]	250	Boback (1980)
					November 1980	1	175	Green (1980a)
					November 1980	2	85–175	Green (1980a)
					May 1982	1	290	Grant and Stevens (1982)
					May 1982	2	400	Grant and Stevens (1982)
					November 1987	1	168–208	Grumski and Shanks (1988)
					November 1987	2	221–250	Grumski and Shanks (1988)
					During RTS operation			
77.6	79.3	81.8	75.4	47.7	November 1987	1	35.5–68	Grumski and Shanks (1988)
					November 1987	2	60–76	Grumski and Shanks (1988)

[a] Not specified in the reference document.

The distance from the source to the receptor point is r (cm). The product AEI computes the rate of emission (MeV s^{-1}). The quantities $x_i(E)$ are mean free paths for gamma rays in shielding media indexed by i; they are the product of a medium- and energy-specific linear attenuation coefficient μ (cm^{-1}) and the linear distance (cm) a gamma ray traverses in medium i. The exponential factor accounts for attenuation of the beam at distance r from the source. The coefficient $K(E)$ converts energy flux units MeV cm^{-2} s^{-1} to the desired exposure units mR h^{-1} (HEW 1970, p. 132). The dimensionless buildup factor B is a function of the energy E and an effective mean free path parameter x_{eff}, which in turn depends on energy and the one or more media through which the gamma rays pass. The buildup factor accounts for the backscattering of gamma rays from outside the beam to the receptor.

The linear attenuation coefficients were tabulated in the database as a function of photon energy and element in the form of mass attenuation coefficients, μ/ρ (cm^2 g^{-1}), where ρ is the partial density of the element in the shielding medium. For each element in the shielding material, the mass attenuation coefficient is multiplied by the partial density of the element,

and the sum of products is multiplied by the path distance through the medium; the product gives the mean free paths for the medium. In this calculation, multiple media were involved (K-65 material, air in the headspace, and concrete dome), and three mean free path values, $x_i(E)$, are required for each source-receptor path, element, and photon energy E. For the elemental composition of the K-65 material, we used compounds typical of a sedimentary soil (Leet et al. 1978). Table Q-14 gives the mass breakdown by compound of this material, from which elemental partial densities were calculated. It was assumed that the K-65 material contained 37% water by mass. We used exposure buildup factors $B(E,x)$ that were tabulated for a concrete medium. Elemental composition of concrete, which was used generically for the silo domes, was taken from Patterson and Thomas (1973).

Table Q-14. Sedimentary Soil as Surrogate for K-65 Material

Compound	Percent (mass)
SiO_2	44.5
Al_2O_3	10.9
Fe_2O_3	4.0
MgO	2.6
CaO	19.7
Na_2O	1.1
K_2O	1.9
CO_2	13.4
MnO	0.3
FeO	0.9
TiO_2	0.6

Equation Q-38 is summed over all energy lines E of the source radionuclide and integrated over all points of the source region. Energies and intensities of photon emissions for the radionuclides in the headspace and the K-65 material were taken from Kocher (1981). In practice, the integration is accomplished by summing the formula over a large number of discrete point sources distributed uniformly over the source volume.

The database for the calculation was obtained from the Radiation Shielding Information Center (RSIC, now RSICC) of Oak Ridge National Laboratory in conjunction with the shielding code QAD-CGGP (the code itself was not used for this calculation). The relevant report is Trubey and Cain (1987), which cites Harima et al. (1986) for background information on the buildup factors. The database was compiled by Y. Harima, Tokyo Institute of Technology, and Y. Sakamoto, Japan Atomic Energy Research Institute (JAERI) from buildup factor data supplied by American Nuclear Society Standards Working Group ANS-6.4.3. The code and data were made available to RSIC by JAERI.

The results of these calculations closely approximate the primary ranges of the measurements, including those taken during the RTS operation in 1987. The good agreement with the RTS data suggests that the calculation accurately represents the component of the

gamma field due to the radioactivity in the K-65 material. Figure Q-7 shows the computed ranges and the measurements.

Two measurements taken in May 1982 exceed the calculated range. We think it likely that these two measurements may have been taken with detectors placed (possibly unintentionally) near points of leakage. It is also possible that temporal variations in the thermal pumping mechanism that partially drives the release of headspace gases might have permitted a temporary buildup in the headspace concentration of ^{222}Rn and decay products, although our estimates of temporal variation in the headspace concentration of ^{222}Rn make this explanation less plausible. Other possibilities include an uncalibrated instrument or local uranium contamination on top of the silo. In any case, these two data points are not typical of other measurements made since the silos were sealed.

We consider the results of these gamma exposure rate calculations a further validation of the release model. The calculation is another demonstration of consistency of the release model and its implied levels of radon and decay products in the silos with those measurements that are available. In the absence of contradictory information, it seems difficult to avoid the conclusion that the preferred radon release model is a reasonable interpretation of existing data, and that its estimates of the releases are reasonable and credible.

REFERENCES

Anonymous. 1958. Handwritten spreadsheet of data on ore processing and K-65 material production at the FMPC.

Anonymous. Circa 1980. Handwritten spreadsheet of radon concentrations measured from May 1978 through April 1980, at FMPC boundary stations.

Boback M.W. 1980. *K-65 storage tanks*. Internal memoradum to J.H. Cavendish. National Lead Company of Ohio, Cincinnati, Ohio.

——. 1979. *Radon Emanation Tests*. Internal memorandum to R.C. Heatherton, dated August 3, 1979. National Lead Company of Ohio, Cincinnati, Ohio.

——. 1973. *Survey of K-65 silos*. Handwritten radiation survey schematic. National Lead Company of Ohio, Cincinnati, Ohio.

Byrne, J. M. 1992. Letter to Duane W. Schmidt, with enclosed computer disk and drawings of Rn monitoring locations. Reference number WEMCO:EM:EMON:92-1344, dated September 15, 1992. Westinghouse Environmental Management Company of Ohio, Cincinnati, Ohio.

Collé R., R.J. Rubin, L.I. Knab, and J.M.R. Hutchinson. 1981. *Radon Transport Through and Exhalation from Building Materials: a Review and Assessment*. NBS Technical Note 1139, National Bureau of Standards, U.S. Department of Commerce, Washington, D.C.

Decisioneering. 1993. *Crystal Ball®,Version 3.0*. Software user's manual. Decisioneering, Inc., 1380 Lawrence Street, Suite 520, Denver, Colorado 80204-9849.

DOE (U.S. Department of Energy). *Remedial Investigation Report for Operable Unit 4, Task 6 Report, Feed Materials Production Center, Fernald, Ohio, Remedial Investigation and*

Feasibility Study. Draft final report, dated October 1990. Oak Ridge Operations Office, DOE, Oak Ridge, Tennessee.

DOE (U.S. Department of Energy). 1993. *Operable Unit 4 Treatability Study Report for the Vitrification of Residues from Silos 1, 2, and 3, Fernald Environmental Management Project, Fernald, Ohio*. Fernald Office, DOE.

George A.C. and A.J. Breslin. 1980. "The Distribution of Ambient Radon and Radon Daughters in Residential Building in the New Jersey–New York Area." In *The Natural Radiation Environment III*, T.F. Gesell and W.M. Lowder, eds. U.S. Department of Energy, Technical Information Center, Oak Ridge, Tennessee.

Grant R. and G. Stevens. 1982. *Gamma Survey of K-65 Tanks*. Handwritten note of radiation survey, dated May 19, 1982. National Lead Company of Ohio, Cincinnati, Ohio.

Green L.E. 1980a. Handwritten note of radiation survey, dated November 26, 1980.

——. 1980b. *K-65 Radon Emanation, Summary of Preliminary Data*. Internal memorandum to M.W. Boback, dated August 18, 1980. National Lead Company of Ohio, Cincinnati, Ohio.

——. 1980c. *Gamma Survey of K-65 Waste Storage Tanks*. Internal memorandum to M.W. Boback, dated April 25, 1980. National Lead Company of Ohio, Cincinnati, Ohio.

Grumski J.T. and P.A. Shanks. 1988. *Completion Report, K-65 Interim Stabilization Project, Exterior Foam Application/Radon Treatment System Operation*. Draft report. Westinghouse Materials Company of Ohio, Cincinnati, Ohio.

Hagee G.R., P.H. Jenkins, P.J. Gephart, and C.R. Rudy. 1985. *Radon and Radon Flux Measurements at the Feed Materials Production Center, Fernald, Ohio*. Rep. MLM-MU-85-68-0001, Mound, Monsanto Research Corporation, Miamisburg, Ohio.

Harima Y., Y. Sakamoto, S. Tanaka, and M. Kawai. 1986. "Validity of the Geometrical Progression Formula in Approximating Gamma-Ray Buildup Factors." Nucl. Sci. Eng. **94**:24–35.

Heatherton R.C. 1979. *Achievement Report - Health and Safety Division - June 1979*. Internal memorandum report, dated July 2, 1979. National Lead Company of Ohio, Cincinnati, Ohio.

Huke F.B. 1953a. *K-65 Sludge Radium Assays*. Letter to Robley Evans, Massachusetts Institute of Technology, dated March 26, 1953. Production Division, U.S. Atomic Energy Commission.

Huke F.B. 1953b. *K-65 Sludge Radium Assays*. Letter to Robley Evans, Massachusetts Institute of Technology, dated July 6, 1953. Production Division, U.S. Atomic Energy Commission.

Janke D.S. and C.C. Chapman. 1991. *Characteristics of Fernald's K-65 Residue Before, During and After Vitrification*.

Killough G.G., M.J. Case, K.R. Meyer, R.E. Moore, J.F. Rogers, S.K. Rope, D.W. Schmidt, B. Shleien, J.E. Till, and P.G. Voillequé. 1993. *The Fernald Dosimetry Reconstruction Project, Task 4, Environmental Pathways — Models and Validation*. Draft report for comment, dated March 1993. RAC Report CDC-3, Radiological Assessments Corporation, Neeses, South Carolina.

Knutson E.O. 1988. "Modeling Indoor Concentrations of Radon's Decay Products." Chapter 5 in *Radon and Its Decay Products in Indoor Air*, W.W. Nazaroff and A.V. Nero, Jr., eds. John Wiley and Sons, New York.

Kocher D.C. 1981. *Radioactive Decay Tables. A Handbook of Decay Data for Application to Radiation Dosimetry and Radiological Assessments.* U.S. Department of Energy, Technical Information Center, Oak Ridge, Tennessee.

Leet L.D., S. Judson, and M.E. Kauffman. 1978. *Physical Geology.* Prentice-Hall, Englewood Cliffs, New Jersey.

Lynch J.R. Circa 1958. *Q-11 Campaigns.* Handwritten spreadsheets. Feed Materials Production Center, Cincinnati, Ohio.

Lynch J.R. 1968. *Data on Raffinate Materials in Long-Term Storage Tanks.* Handwritten table and notes, dated May 15, 1968. Nuclear Materials Control, National Lead Company of Ohio, Cincinnati, Ohio.

Morgan J.P. 1950. *K-65 Sludge Radium Assays.* Letter to Robley D. Evans, Massachusetts Institute of Technology, dated December 21, 1950. Metal Branch, Production Division, U.S. Atomic Energy Commission.

Morgan J.P. 1951a. *K-65 Sludge Radium Assays.* Letter to Robley D. Evans, Massachusetts Institute of Technology, dated March 7, 1951. Metal Branch, U.S. Atomic Energy Commission.

Morgan J.P. 1951b. *K-65 Sludge Radium Assays.* Letter to Robley D. Evans, Massachusetts Institute of Technology, dated May 3, 1951. Metal Branch, Production Division, U.S. Atomic Energy Commission.

Morgan J.P. 1952. *K-65 Sludge Radium Assays.* Letter to Robley D. Evans, Massachusetts Institute of Technology, dated March 4, 1952. Staff Technical Branch, Production Division, U.S. Atomic Energy Commission.

NCRP (National Council on Radiation Protection and Measurements). 1984. *Evaluation of Occupational and Environmental Exposures to Radon and Radon Daughters in the United States.* NCRP Report No. 78, NCRP, Bethesda, Maryland.

Nelson M.S. 1972. *K-65 area survey results and actions.* Letter to C.L. Karl, U.S. Atomic Energy Commission, Cincinnati, Ohio. National Lead Company of Ohio, Cincinnati, Ohio.

NLCO (National Lead Company of Ohio). 1957a. Five analytical data sheets related to radon measurements in K-65 and metal oxide storage silos: (1) IH# 483, date reported May 28, 1957; (2) IH# 484, reported date May 31, 1957; (3) IH# 492, reported date May 31, 1957; (4) IH# 814, reported date September 5, 1957; and (5) No. 15594, reported date September 12, 1957. Analytical Department, Health and Safety Division, NLCO, Cincinnati, Ohio.

NLCO (National Lead Company of Ohio). 1957b. Four analytical data sheets related to radon measurements in Plants 2 and 3: (1) IH# 442, date reported May 20, 1957; (2) IH# 443, reported date May 17, 1957; (3) IH# 444, reported date May 17, 1957; and (4) IH# 461, reported date May 21, 1957. Analytical Department, Health and Safety Division, NLCO, Cincinnati, Ohio.

NLCO (National Lead Company of Ohio). 1952. Six analytical data sheets for air radon samples collected in train cars of drummed K-65 material: (1) Industrial Hygiene No. 1, dated August 11, 1952; (2) Industrial Hygiene No. 2, dated August 12, 1952; (3) Industrial Hygiene No. 3, dated August 13, 1952; (4) dated September 2, 1952; (5)

September 3, 1952; and (6) dated September 8, 1952. Health and Safety Division, NLCO, Cincinnati, Ohio.

NLCO (National Lead Company of Ohio). 1953. One analytical data sheet for radon in air sampled in K-65 area during K-65 drum dumping operations. Industrial Hygiene No. 249, dated October 29, 1953. Health and Safety Division, NLCO, Cincinnati, Ohio.

NLCO (National Lead Company of Ohio). 1954. One analytical data sheet for radon in air sampled in Plant 2. Industrial Hygiene No. 477, reported date February 3, 1954. Health and Safety Division, NLCO, Cincinnati, Ohio.

NLCO (National Lead Company of Ohio). 1955. One analytical data sheet for radon in air sampled in K-65 area. Industrial Hygiene No. 510, reported date March 18, 1955. Health and Safety Division, NLCO, Cincinnati, Ohio.

Patterson H.W. and R.H. Thomas. 1973. *Accelerator Health Physics*. Academic Press, New York, New York, and London, U.K..

Public Health Service. 1970. *Radiological Health Handbook, Revised Edition*. Public Health Service Publication No. 2016, U.S. Department of Health, Education, and Welfare.

Rogers V.C., K.K Nielson, and D.R. Kalkwarf. 1984. *Radon Attenuation Handbook for Uranium Mill Tailings Cover Design*. Report NUREG/CR-3533, PNL-4878, RAE-18-5, Rogers and Associates Engineering Corporation, Salt Lake City, Utah.

Ross K.N. 1957. *Health & Safety Information Report, Radon in K-65 Storage Tanks*. Internal memorandum to J.W. McKelvey, dated July 17, 1957. National Lead Company of Ohio, Cincinnati, Ohio.

Shleien B., S.K. Rope, M.J. Case, G.G. Killough, K.R. Meyer, R.E. Moore, D.W. Schmidt, J.E. Till, and P.G. Voillequé. 1995. *The Fernald Dosimetry Reconstruction Project, Task 5. Review of Historic Data and Assessments for the FMPC*. Rep. CDC-4, Radiological Assessments Corporation, Neeses, South Carolina.

Smith R.J. 1952a. *K-65 Sludge Radium Assays*. Letter to Robley D. Evans, Massachusetts Institute of Technology, dated June 11, 1952. Production Division, U.S. Atomic Energy Commission.

Smith R.J. 1952b. *K-65 Sludge Radium Assays*. Letter to Robley D. Evans, Massachusetts Institute of Technology, dated June 24, 1952. Production Division, U.S. Atomic Energy Commission.

Smith R.J. 1952c. *K-65 Sludge Radium Assays*. Letter to Robley Evans, Massachusetts Institute of Technology, dated August 12, 1952. Production Division, U.S. Atomic Energy Commission.

Smith R.J. 1952d. *K-65 Sludge Radium Assays*. Letter to Robley Evans, Massachusetts Institute of Technology, dated September 19, 1952. Production Division, U.S. Atomic Energy Commission.

Smith. R.J. 1952e. *K-65 Sludge Radium Assays*. Letter to Robley Evans, Massachusetts Institute of Technology, dated November 20, 1952. Production Division, U.S. Atomic Energy Commission.

Starkey R.H. 1964. *IH&R Department Monthly Report for April, 1964*. Internal memorandum to J.A. Quigley, dated May 8, 1964. National Lead Company of Ohio, Cincinnati, Ohio.

Trubey D.K. and V.R. Cain. 1987. *QAD-CGGP. A Combinatorial Geometry Version of QAD-P5A, a Point Kernel Code System for Neutron and Gamma-Ray Shielding Calculations*

Using the GP Buildup Factor. Report CCC-493, Oak Ridge National Laboratory, Oak Ridge, Tennessee.

Voillequé P.G., K.R. Meyer, D.W. Schmidt, S.K. Rope, G.G. Killough, M. Case, R.E. Moore, B. Shleien, and J.E. Till. 1995. *The Fernald Dosimetry Reconstruction Project, Tasks 2 and 3, Radionuclide Source Terms And Uncertainties*. RAC Report CDC-5, Radiological Assessments Corporation, Neeses, South Carolina.

Wolf R. 1955. Interoffice routing slip, dated January 31, 1955, with attached tables of Q-11 and K-65 material balances for ore processing campaigns. National Lead Company of Ohio.

Table Q-15. Radium-226 Concentration (mg ton^{-1}) in K-65 Material Produced in the FMPC Uranium Ore Processing, Measured During Production Campaigns [a]

Campaign, dates	Lot number	Weight (lb)	^{226}Ra	Lot number	Weight (lb)	^{226}Ra
Pilot 1, 3/54	1	14315	201	8	13048	120
	2	14741	177	9	11464	130
	3	13642	126	10	15058	105
	4	13031	73	11	13161	81
	5	13589	167	12	11078	78
	6	13692	92	13	10010	47
	7	4805	93	14	7968	5.1
Pilot 2, 6/54	15	11039	220	21	8573	279
	16	12882	166	22	13939	258
	17	9707	240	23	12882	245
	18	10136	203	24	14027	230
	19	9459	219	25	4352	123
	20	8888	179			
One, 10/55–1/56	B1–B42	315800	312			
Two, 8/56–10/56	C1–4	34400	398	C33–36	33000	237
	C5–8	30600	239	C37–40	38600	184
	C9–12	27800	151	C41–44	38400	268
	C13–16	30200	212	C45–48	35000	329
	C17–20	37400	215	C49–52	42000	336
	C21–24	53000	432	C53–56	38200	233
	C25–28	33200	423	C57–62	53200	229
	C29–32	36800	265			
Three, 3/57–4/57	D1–4	42000	283	D12–14	33000	357
	D5–7	39200	360	D15–16	23400	368
	D8–11	34800	252	D17–18	17600	90.4
Four, 5/57–6/57	E1–3	33800	439	E6–8	37200	282.7
	E4–5	32400	398			
Australian ore, 5/57–6/57	2G8650001	11600	491	2G8650003	12200	635
	2G8650002	12200	680			
Five, 9/57–10/57	F1–3	38600	380	F10–12	41600	464
	F4–6	42200	338	F13–14	24400	355
	F7–9	21000	162			
Six, 12/57	G1–3	43800	557	G7–9	30800	466
	G4–6	30800	360	G10–13	28800	130
Seven, 3/58	H1–3	35400	378	H4–7	32200	240
Australian ore, 3/58	H8–12	39664	176.3	H13–17	32448	182.1
Eight, 6/58–8/58	J1–31	353200	289 [b]			

[a] Data compiled from Wolf 1955, Anonymous 1958, and Lynch circa 1958.
[b] Concentration was calculated, in this present work, from the total quantity of ^{226}Ra and total weight of K-65 material.

Table Q-16. Radium-226 Concentration (mg ton^{-1}) in K-65 Material Produced at Facilities Other than the FMPC, Measured During Production

Reference	Lot #	^{226}Ra	Lot #	^{226}Ra	Lot #	^{226}Ra	Lot #	^{226}Ra	Lot #	^{226}Ra
Morgan 1950, dated 12/21/50	1	718	26	758	51	647	76	804.5	101	707
	2	560	27	765	52	777	77	750	102	646
	3	497	28	740	53	825	78	662	103	496
	4	514	29	796	54	851	79	677	104	428
	5	497	30	699	55	898	80	703	105	580
	6	527	31	732	56	740	81	621	106	621
	7	554.5	32	734	57	737	82	710	107	563
	8	532	33	788	58	752	83	685	108	580
	9	550	34	760	59	687	84	751	109	553
	10	744	35	827	60	660	85	802	110	636
	11	791	36	814	61	628	86	828	111	638
	12	927	37	706	62	671	87	651	112	672
	13	841	38	823	63	727.5	88	709	113	665.5
	14	785	39	825	64	643	89	597	114	750
	15	857	40	909	65	732	90	545.5	115	617
	16	960	41	966	66	740	91	518	116	666
	17	1023	42	933	67	748	92	519	117	758
	18	769	43	890	68	741	93	610	118	718
	19	760	44	834	69	679	94	563	119	736
	20	802	45	876	70	751	95	644.5	120	801.5
	21	960	46	822	71	718	96	592	121	720
	22	862	47	750	72	820.5	97	604		
	23	862	48	755.5	73	773	98	539		
	24	876	49	779	74	716	99	542		
	25	839	50	713	75	802	100	602		
Morgan 1951a, dated 3/7/51	122	757	127	794	132	458	137	644	142	519.5
	123	674	128	764	133	405.5	138	469		
	124	576	129	702	134	441	139	529		
	125	632	130	626	135	520	140	556		
	126	731	131	604	136	571	141	590		
Morgan 1951b, dated 5/3/51	143	524	147	343	151	371	155	266	159	316
	144	481	148	382	152	313	156	248	161	306
	145	404	149	275	153	263	157	255	162	263.5
	146	391	150	385	154	326.5	158	272		
Morgan 1952, dated 3/4/52	160	283.5	165	281	168	261.5	172	203	175	173
	163	283	166	244	170	231	173	216	176	194.5
	164	269	167	190	171	172.5	174	168	177	194
Smith 1952a, dated 6/11/52	169	208	181	233	185	268	189	322		
	178	281	182	249	186	328	190	285		
	179	268	183	287	187	297	191	293		
	180	250	184	304	188	298	193	312		
Smith 1952b, dated 6/24/52	192	310	198	260	204	287	210	266	215	271
	194	277	199	294	205	283.5	211	249		
	195	297	201	298	206	284	212	229		
	196	325	202	272	208	302	213	236		
	197	274	203	304	209	282	214	271		

Table Q-16. Radium-226 Concentration (mg ton^{-1}) in K-65 Material Produced at Facilities Other than the FMPC, Measured During Production (Continued)

Reference	Lot #	^{226}Ra	Lot #	^{226}Ra	Lot #	^{226}Ra	Lot #	^{226}Ra	Lot #	^{226}Ra
Smith 1952c, dated 8/12/52	200	306	224	336	234	218	245	306.5	48	291
	207	324	225	258	235	261.5	24	329	51	256
	216	278	226	284	236	316	28	375	53	257.5
	217	310	227	299	237	278	30	428.5	58	296
	218	268	228	286	238	297	32	378	60	264
	219	307	229	213	239	329	33	294.5	66	277
	220	300	230	256	240	324	38	291.5	69	272
	221	304	231	271	241	308	39	299.5		
	222	310	232	259	242	300	42	291.5		
	223	310	233	264	243	356	43	324.5		
Smith 1952d, dated 9/19/52	244	342	2	386	9	353	16	354	23	318
	246	337	3	345	10	305	17	367	25	338
	247	329	4	382	11	333	18	376	29	425
	248	304	5	322	12	360	19	402	31	371
	249	347	6	344	13	338	20	384	34	338
	250	366	7	431	14	286	21	349	35	328
	1	347	8	365	15	333	22	330		
Smith 1952e, dated 11/20/52	36	294	52	283	67	290	78	239	90	209
	37	288	54	222	68	285	79	226	91	206
	40	320	55	236	70	304	80	224	94	195.5
	41	270	56	270	71	276	81	233	98	216.5
	44	308	57	271	72	287	82	233	99	223
	45	306	59	286	73	264	83	235	100	227.5
	46	338	61	290	74	269	84	231.5	104	220
	47	300	63	298	75	268	85	215	106	214.5
	49	310	64	296	76	270	87	198		
	50	277	65	275	77	220	89	224.5		
Huke 1953a, dated 3/26/53	26	330	108	228	A-14	186	A-29	256	A-44	204
	27	344	109	215	A-15	204	A-30	236	A-45	197
	62	288	A-01	218	A-16	207	A-31	208	A-46	190
	86	226	A-02	196	A-17	196	A-32	212	A-47	200
	88	222	A-03	214	A-18	226	A-33	226	A-48	202
	92	225	A-04	198	A-19	238	A-34	194	A-49	162.5
	93	195	A-05	210	A-20	257	A-35	178	A-50	202
	95	189	A-06	213	A-21	220	A-36	214	A-51	176
	96	232	A-07	172	A-22	250	A-37	197	A-54	181.5
	97	202	A-08	198	A-23	254	A-38	200	A-58	202.5
	101	220	A-09	188	A-24	206	A-39	195	A-63	216
	102	204	A-10	199	A-25	230	A-40	218	A-65	224
	103	208	A-11	212	A-26	247	A-41	225	A-70	235
	105	222	A-12	232	A-27	242	A-42	216		
	107	243	A-13	203	A-28	222	A-43	207		
Huke 1953b, dated 7/6/53	A-52	171	A-61	211	A-71	228	A-78	160	A-85	194
	A-53	155	A-62	206	A-72	244	A-79	169	A-86	216
	A-55	175	A-64	221	A-73	197	A-80	179	A-87	182
	A-56	186	A-66	228	A-74	210	A-81	176	A-88	214
	A-57	206	A-67	234	A-75	190	A-82	171	A-89	216
	A-59	226	A-68	228	A-76	172	A-83	228	A-90	223
	A-60	186	A-69	221	A-77	188	A-84	190		

APPENDIX R

TOXICITY TO THE KIDNEYS FROM NATURAL URANIUM

URANIUM CONCENTRATIONS IN THE KIDNEYS

Introduction

This appendix reports details of calculations made to estimate maximum levels of uranium concentration (μg of uranium per gram of kidney tissue) in the kidneys of the subjects of nine exposure scenarios, defined in Appendix J, during and subsequent to their periods of exposure. Threshold concentration levels that are associated with biological effects in animals and humans are reviewed and compared with the estimated levels for the nine scenarios.

The calculation applies the ICRP Publication 69 (ICRP 1995) retention function for uranium in the kidneys to simulate a dynamic level (μg g^{-1}) over time. The simulation is driven by the estimated annual intake by ingestion and inhalation as functions of time for the period of the subject's exposure. The calculation takes into account the variation of kidney metabolism, mass, breathing rate, water consumption, and dietary intakes with age and (where the data support the distinction) sex.

Retention Function for Uranium in the Kidneys

The dynamic models of uranium retention in the kidneys used for toxicity estimates have the form

$$R_k(t) = \sum_{i=1}^{M} c_{ki} \exp(-t \cdot \ln 2 / T_{ki}), \qquad \text{(R-1)}$$

where

$R_k(t)$ = fraction of an acute uptake of uranium to the transfer compartment (i.e., blood) that remains in the kidneys t days later

k = index to indicate age category of subject at time of exposure (i.e., infant, 10-year-old child, adult)

M = number of terms in the sum

c_{ki} = fractional uptake coefficients for age category k (dimensionless)

T_{ki} = biological half-time of the uranium in the kidney compartment specified by term i. It is usual to replace the expressions involving half-times by removal rate coefficients:

$$\lambda_{ki} = \ln 2 / T_{ki}. \qquad \text{(R-2)}$$

The units of λ_{ki} are converted to reciprocal years for convenience with the annual time scale used in the calculation. The radiological decay rate coefficient has been omitted because of the long half-life of uranium relative to the processes considered here.

The kidney model of Equation R-1 has been adapted from the systemic uranium model presented in ICRP Publication 69 (ICRP 1995). We obtained the coefficients c_{ki} and the half-times T_{ki} by fitting three-term functions of the form given by Equation R-1 to retention curves generated by the ICRP model. Table R-1 shows the values of the fitted parameters for three age categories. For comparison, the table also shows parameters for the two-term kidney model of ICRP Publication 30 (ICRP 1979), which was used for the radiation dose calculations reported in Appendix K of this document. Figure R-1 compares the corresponding retention curves (the single curve for ICRP Publication 30 and the three age categories based

on ICRP Publication 69). Figure R-2 is a schematic summary of the exposure environment and metabolic models of the respiratory passages, gastrointestinal tract, and kidneys with which the estimates of kidney burden have been computed.

Table R-1. Parameters for ICRP Models of Kidney Metabolism

	Coefficient (dimensionless)			Half-time (days)			Gastrointestinal uptake fractions (dimensionless)	
Age group	c_1	c_2	c_3	T_1	T_2	T_3	Soluble	Insoluble
ICRP-69[a]								
Adult	.119	.00133	.000546	8.34	98.4	2310	.02	.002
Child (10 y)	.093	.00137	.000625	9.24	142	2060	.02	.002
Infant	.0766	.002	.000428	9.71	239	3080	.04	.004
ICRP-30[b]								
All ages	.12	.00052	—	6	1500	—	.05	.002

[a] Used for the kidney toxicity estimates in this appendix.
[b] Used for radiation dose estimates in Appendix K and elsewhere in this report.

The ICRP systemic model moves radioactivity taken into the body by inhalation or ingestion from a dynamic model of the respiratory passages or the gastrointestinal tract, respectively, into a transfer compartment (TC), which essentially represents the blood. Material is moved rapidly from this compartment to systemic organs (e.g., the kidneys) and excretion, the half-time being T_{TC} = 0.25 days. After uptake of uranium by the kidneys, removal over time is modeled by Equation R-1 using ICRP-69 parameters from Table R-1. Intakes from FMPC-related exposures (inhalation and ingestion) vary from year to year, and for any given year, the amount of uranium in the kidneys is based on the retention model applied to the intake for that year, and to each previous year's intake in order to account for residual retention. A table of kidney burden for each year is computed, and the maximum burden for the entire period of exposure is determined.

The calculation takes into account a subject's locations (with times spent at each one), dietary habits, and age progression throughout the period of simulation. Age-specific modeling is applied to physiological parameters such as breathing rate (relative to activity levels), water consumption, and kidney mass and metabolism. In other respects, the models of the lungs and gastrointestinal tract are not age specific. The inhaled and ingested uranium are partitioned into soluble and insoluble components, and the parameters for the lungs (corresponding to clearance classes D, W, and Y, as discussed in Appendix I) and the absorption fraction f_1 for the small intestine are set accordingly. The compartment models (Figure R-2) are represented by a moderately large system of coupled ordinary differential equations, which are solved with inputs from the environmental models that predict uranium concentrations in air, water, soil, and food products. The predicted environmental levels depend ultimately on the reconstructed source terms for effluents from the FMPC. Kidney levels for the subject of scenario 3 were strongly influenced by an assumed schedule of drinking water from a well contaminated by ground water, which received uranium released to Paddy's Run.

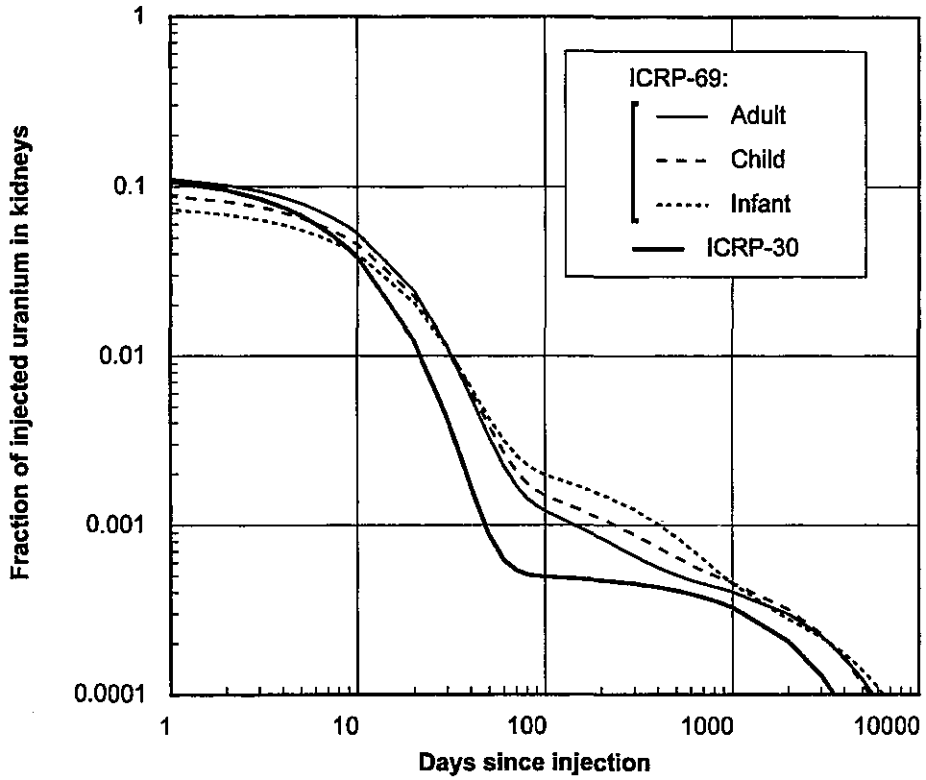

Figure R-1. Retention functions of uranium in the kidneys following an acute uptake to the blood. The age-specific curves based on ICRP Publication 69 (ICRP 1995) were used for estimating uranium burdens in the kidneys of the subjects of scenarios 1–9 (Appendix J). Radiation doses to the kidneys of the scenario subjects were based on the retention model of ICRP Publication 30, which is shown for comparison. Calculations with the two sets of models do not differ by as much as the figure might suggest, because of differences in the transfer fractions from the small intestine to blood f_1 (see Tables R-1 and R-2).

Age dependence for the ICRP Publication 69 model is handled by linear interpolation among the results of the three age representations shown in Figure R-1 (infant, child, adult). We interpret the curves to incorporate aging of the individual following exposure at the indicated age. Age-dependent breathing rates are shown in Table I-4, assumed drinking water consumption rates by age are given in Table I-5, and dietary information by sex and age is presented in Table I-6. These age-specific quantities are incorporated into the calculations of intakes and resultant kidney burdens of uranium for toxicity estimation, just as they are for radiation dose estimates. Age and sex dependence of the kidney mass also enter the calculations when the kidney burden is converted to micrograms of uranium per gram of kidney tissue ($\mu g\ g^{-1}$). The kidney masses are based on data taken from the Reference Man document, ICRP Publication 23 (ICRP 1975), and are shown plotted against age in Figure R-3. A moving average method was used to smooth the data.

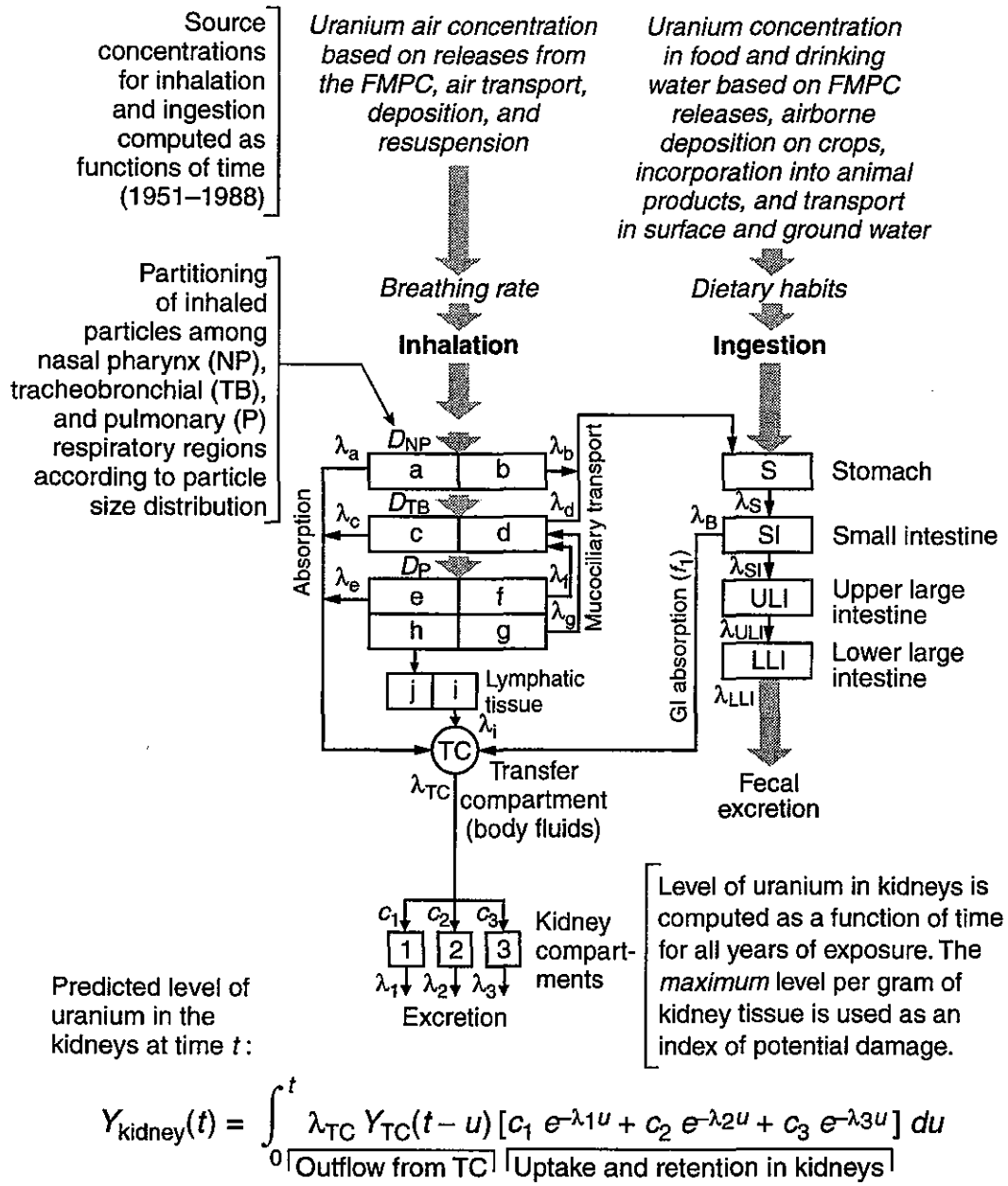

$$Y_{\text{kidney}}(t) = \int_0^t \lambda_{TC}\, Y_{TC}(t-u)\,[c_1\, e^{-\lambda_1 u} + c_2\, e^{-\lambda_2 u} + c_3\, e^{-\lambda_3 u}]\, du$$

Figure R-2. Schematic presentation of the exposure environment and metabolic models used to estimate maximum levels of uranium in the kidneys. Refer to Appendix I, Figures I-3 and I-7, for additional information about the model parameters for the respiratory passages and gastrointestinal tract, respectively. Parameters for the kidney compartments are given in Table R-1.

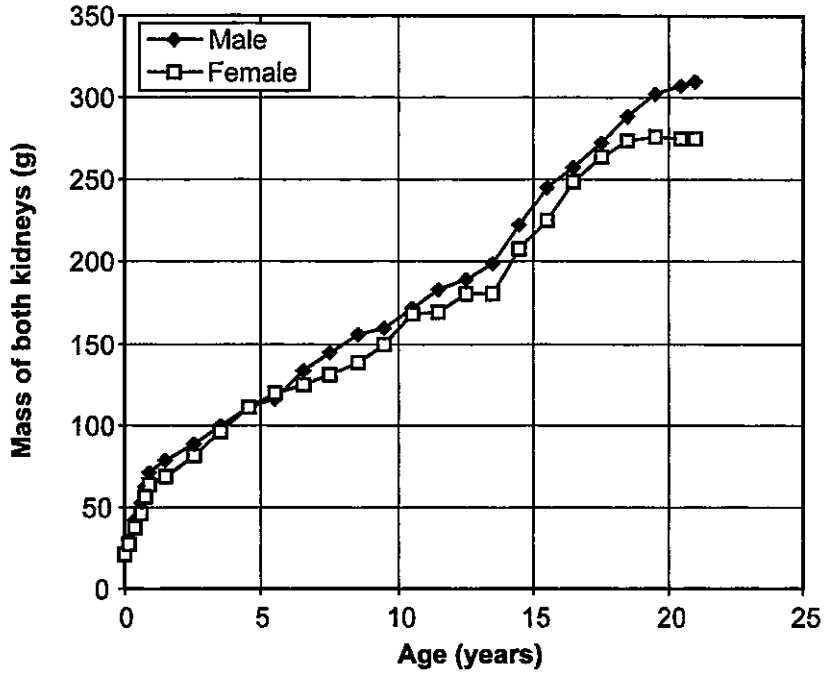

Figure R-3. Mass of both kidneys as a function of age and sex. These curves are based on data from ICRP Publication 23 (ICRP 1975), which were smoothed with a moving average technique.

Intake and Retention Estimates

Figure R-4 illustrates the simulation by showing, for the subject of scenario 1, a time tabulation of age, kidney mass, intakes of uranium by inhalation and ingestion, and the kidney burden of uranium, broken down by inhalation, ingestion, and total. The inhaled component is principally class Y (insoluble), but a high proportion of the ingested uranium is considered soluble, because it occurs in milk, meat, and eggs. Uranium that is deposited on the surfaces of produce is considered insoluble, but the component that is absorbed through the roots is treated as soluble after intake. The subject of scenario 1 was assumed to have taken 100% of her milk and eggs from animals kept on her land just northeast of the FMPC site and 50% of her remaining diet from her garden and from beef cows raised on her land. The maximum kidney burden occurred at the end of 1955, the year when the highest releases of airborne uranium occurred.

We need to point out that this pattern of exposure does not correspond to that of any known individual. Such exposure is conceivable, but the likelihood that any real individual's experience approximated it cannot be assessed at the time of this writing. Scenario 1 was invented to suggest ways in which an individual's lifestyle might tend to maximize most (not all) aspects of exposure to radioactive materials released from the FMPC. The scenario emphasized food produced on land that was near the FMPC site and located in the downwind direction for the prevailing winds.

Uranium in the kidneys (microgram/g kidney)

Year	Age	Mass(g)	Annual intake (microgram) Inhal D	Inhal W	Inhal Y	Inges Sol.	Inges Insol.	Kidney burden (microgram/g) Inhal	Inges	Total
1951	5	115.2	0.00E+00	0.00E+00	3.70E+00	6.30E+01	3.40E+01	1.60E-06	7.90E-05	8.10E-05
1952	6	122.2	0.00E+00	3.80E+01	2.30E+01	1.40E+03	1.20E+02	2.00E-04	1.60E-03	1.80E-03
1953	7	128	0.00E+00	2.50E+02	1.10E+03	1.60E+04	5.10E+03	1.70E-03	1.80E-02	2.00E-02
1954	8	134.6	0.00E+00	2.60E+03	6.00E+03	7.30E+04	1.90E+04	1.50E-02	8.00E-02	9.50E-02
1955	9	144.1	0.00E+00	9.40E+03	1.00E+04	1.80E+05	3.40E+04	4.70E-02	1.90E-01	**2.40E-01**
1956	10	158.9	0.00E+00	2.00E+03	5.70E+03	7.50E+04	2.40E+04	2.10E-02	1.00E-01	1.20E-01
1957	11	168.6	0.00E+00	5.00E+02	4.10E+03	4.60E+04	2.40E+04	1.40E-02	7.20E-02	8.60E-02
1958	12	175.1	0.00E+00	1.60E+02	4.00E+03	4.00E+04	2.30E+04	1.20E-02	6.30E-02	7.50E-02
1959	13	180.7	0.00E+00	3.50E+02	3.90E+03	4.50E+04	2.50E+04	1.20E-02	6.50E-02	7.70E-02
1960	14	194.1	0.00E+00	4.20E+02	3.60E+03	4.80E+04	2.50E+04	1.20E-02	6.40E-02	7.50E-02
1961	15	216.3	0.00E+00	1.70E+02	4.70E+03	4.10E+04	2.40E+04	1.00E-02	5.40E-02	6.40E-02
1962	16	236.8	0.00E+00	2.90E+02	3.50E+03	2.80E+04	1.60E+04	9.30E-03	4.10E-02	5.10E-02
1963	17	256.1	0.00E+00	4.30E+02	4.20E+03	3.00E+04	1.60E+04	9.10E-03	3.80E-02	4.70E-02
1964	18	268.6	0.00E+00	1.60E+02	3.20E+03	2.20E+04	1.10E+04	8.00E-03	3.20E-02	4.00E-02
1965	19	275.2	0.00E+00	2.90E+01	1.60E+03	9.60E+03	4.70E+03	7.10E-03	2.30E-02	3.10E-02
1966	20	276.2	0.00E+00	6.80E+01	1.10E+03	5.90E+03	3.80E+03	6.70E-03	2.00E-02	2.70E-02
1967	21	275.4	0.00E+00	8.30E+01	1.40E+03	6.70E+03	5.30E+03	6.40E-03	1.90E-02	2.50E-02
1968	22	275.4	0.00E+00	7.00E+01	2.00E+03	8.30E+03	7.10E+03	6.10E-03	1.90E-02	2.50E-02
1969	23	275.4	0.00E+00	3.10E+01	8.90E+02	4.70E+03	3.40E+03	5.60E-03	1.60E-02	2.10E-02
1970	24	275.4	0.00E+00	1.50E+01	7.50E+02	3.70E+03	2.60E+03	5.20E-03	1.40E-02	1.90E-02
1971	25	275.4	0.00E+00	5.40E+00	4.60E+02	3.60E+03	2.40E+03	4.70E-03	1.30E-02	1.80E-02
1972	26	275.4	0.00E+00	1.20E+01	9.70E+02	4.60E+03	4.10E+03	4.50E-03	1.30E-02	1.70E-02
1973	27	275.4	0.00E+00	4.00E+01	1.20E+03	5.90E+03	5.50E+03	4.30E-03	1.30E-02	1.70E-02
1974	28	275.4	0.00E+00	2.00E+01	1.20E+03	6.10E+03	6.00E+03	4.10E-03	1.30E-02	1.70E-02
1975	29	275.4	0.00E+00	8.30E+01	1.40E+03	7.10E+03	6.90E+03	4.00E-03	1.30E-02	1.70E-02
1976	30	275.4	0.00E+00	2.00E+01	1.20E+03	6.00E+03	5.80E+03	3.80E-03	1.20E-02	1.60E-02
1977	31	275.4	0.00E+00	1.10E+01	5.10E+02	3.30E+03	2.80E+03	3.50E-03	9.80E-03	1.30E-02
1978	32	275.4	0.00E+00	1.20E+01	1.20E+02	1.50E+03	7.20E+02	3.20E-03	8.20E-03	1.10E-02
1979	33	275.4	0.00E+00	3.30E+01	1.10E+02	1.60E+03	8.90E+02	2.90E-03	7.60E-03	1.10E-02
1980	34	275.4	0.00E+00	6.40E+01	1.40E+02	1.60E+03	7.30E+02	2.80E-03	7.00E-03	9.80E-03
1981	35	275.4	0.00E+00	1.40E+02	1.60E+02	1.90E+03	8.20E+02	2.70E-03	6.70E-03	9.50E-03
1982	36	275.4	0.00E+00	1.10E+01	2.40E+02	1.60E+03	9.50E+02	2.30E-03	6.10E-03	8.40E-03
1983	37	275.4	0.00E+00	2.40E+01	1.80E+02	1.60E+03	9.80E+02	2.10E-03	5.80E-03	7.90E-03
1984	38	275.4	0.00E+00	1.90E+01	4.00E+02	2.00E+03	1.60E+03	2.00E-03	5.70E-03	7.70E-03
1985	39	275.4	0.00E+00	1.10E+01	1.50E+02	1.30E+03	7.10E+02	1.80E-03	5.00E-03	6.80E-03
1986	40	275.4	0.00E+00	5.10E+00	1.30E+02	1.20E+03	7.90E+02	1.60E-03	4.60E-03	6.30E-03
1987	41	275.4	0.00E+00	3.30E+00	1.00E+02	1.30E+03	6.50E+02	1.50E-03	4.40E-03	5.90E-03
1988	42	275.4	0.00E+00	2.50E-01	5.20E+01	1.20E+03	5.00E+02	1.40E-03	4.10E-03	5.40E-03
Total intakes:			0.00E+00	1.80E+04	7.10E+04	7.40E+05	3.20E+05			

Maximum burden of uranium in the kidneys: 0.236333 microgram/g kidney

Figure R-4. Annual tabulation of the exposure of the subject of scenario 1 by inhalation and ingestion of uranium from the FMPC, and consequent burden of uranium in the kidneys. The figure is a reproduction of a computer spreadsheet, which tabulates year, subject's age, mass of the kidneys, intake of uranium by inhalation, intake of uranium by ingestion, and kidney burden of uranium, given as microgram per gram of kidney. Intakes are broken down according to solubility. Kidney burden of uranium shows, in addition to the total, the proportions that resulted from inhalation and ingestion.

Table R-2 shows the maximum kidney burden of uranium ($\mu g\ g^{-1}$) for each of the nine scenarios, where the maximum is taken over all annual kidney burdens from 1951 through

1988. We performed the calculation for both models (ICRP Publication 30 and ICRP Publication 69) to provide a comparison, because some reviewers expressed concern about the adequacy of the older model for this purpose. In fact, the differences are minor. The dominance of the retention curves for the ICRP-69 model (Figure R-1) is offset by the reduction of some of the gastrointestinal uptake factors f_1 (Table R-1).

Table R-2. Maximum Burden of Uranium in the Kidneys of Scenario 1–9 Subjects as Calculated with the Retention Models of ICRP Publications 30 and 69

Scenario	ICRP-30 ($\mu g\ g^{-1}$)	ICRP-69 ($\mu g\ g^{-1}$)
1	0.26	0.24
2	0.060	0.070
3	0.65	0.75
4	0.016	0.028
5	1.5×10^{-3}	2.2×10^{-3}
6	0.13	0.12
7	5.4×10^{-3}	6.6×10^{-3}
8	7.9×10^{-4}	7.6×10^{-4}
9	3.4×10^{-3}	4.9×10^{-3}

The results for scenario 3 shown in Table R-2 require special comment. The intent of developing this scenario was to examine possible effects of drinking water from a well located in the south plume migration field (Voillequé et al. 1995, Appendix M). Concentrations in the wells differed according to location relative to the plume migration. For scenario 3 simulations, we chose Well 15, which had the highest measured concentrations of any private well (Voillequé et al. 1995, Table M-1). The monitoring period (1982 and subsequently) does not include the entire time when above-background levels could have occurred, and we were obliged to extrapolate the observations backward in time to the 1960s, when the groundwater plume is believed to have crossed the southern site boundary. The reconstructed values used for 1968–1981 are based on Table M-8 of Voillequé et al. (1995). For the simulations described in this report, the measurements in Well 15 were used for 1982 through 1988. Figure R-5 shows two curves for the level of uranium in the kidneys of the subject of scenario 3 as a function of time, where the concentration is broken down according to ingestion and inhalation. The two kidney concentration curves show a similar trend until after 1968, when the plume reached the well according to the reconstruction. Concentrations plotted in Figure R-5 are associated with the end of each indicated year.

In order to distinguish carefully between what is real and what is hypothetical, we emphasize the following points:

(1) For purposes of scenario 3, the measurements of uranium in the well are assumed to be accurate. Although the reconstructed contamination history is required to approximate these recent measurements in Well 15 for the period after 1982, it may overestimate or underestimate the contamination in that well for the earlier period when no measurements are available. In the next section, we describe an approach to estimating uncertainties in this time series.

(2) Although there are some indications that water from Well 15 might have been used for human consumption during the period of contamination, the correspondence between any real person's use of this water and the exposure assumed for scenario 3 is unknown at this time. The scenario assumes that the well was the principal source of the subject's drinking water throughout the period of contamination. Real individuals may or may not have utilized the water from this well in accordance with the assumptions for scenario 3.

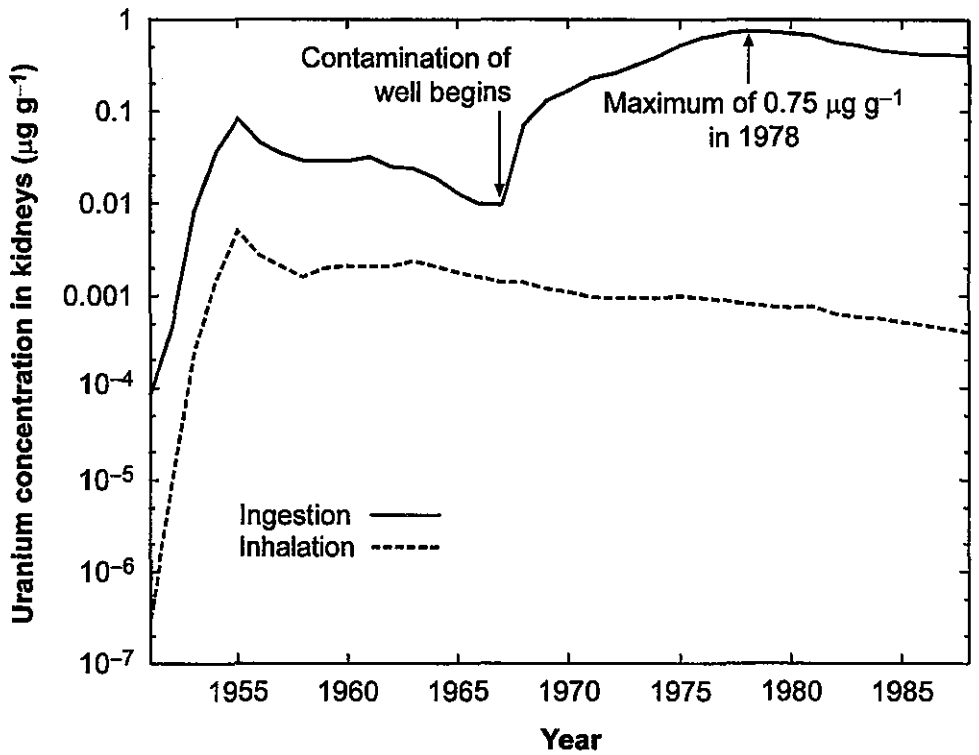

Figure R-5. Uranium concentrations in the kidneys of the subject of scenario 3 (μg g^{-1} kidney) for ingestion and inhalation. The ingestion history shows the effect of drinking uranium-contaminated water from Well 15, according to the reconstruction for that well described in Appendix M of the task 2/3 report (Voillequé et al. 1995). The maximum kidney concentration for this subject, estimated as 0.75 μg g^{-1}, occurred in 1978. This history of exposure is based on the assumption that the subject of scenario 3 obtained essentially all of his drinking water from Well 15 during the indicated period. Whether a similar exposure history to Well 15 occurred for any real individual is unknown at this time.

Uncertainty Distributions for Maximum Concentrations

The estimates of uranium concentrations in the kidneys given so far are based on deterministic assumptions and simulations. But the history of releases of uranium to the atmosphere and the environmental transport of this material have been treated stochastically in the estimation of radiation doses (Appendix K). The same uncertainties propagate into the estimates of maximum uranium levels in the kidneys. Figure R-6 shows the cumulative distribution of uncertainty in these estimates for each scenario. Each stochastic simulation used 250 Monte Carlo trials.

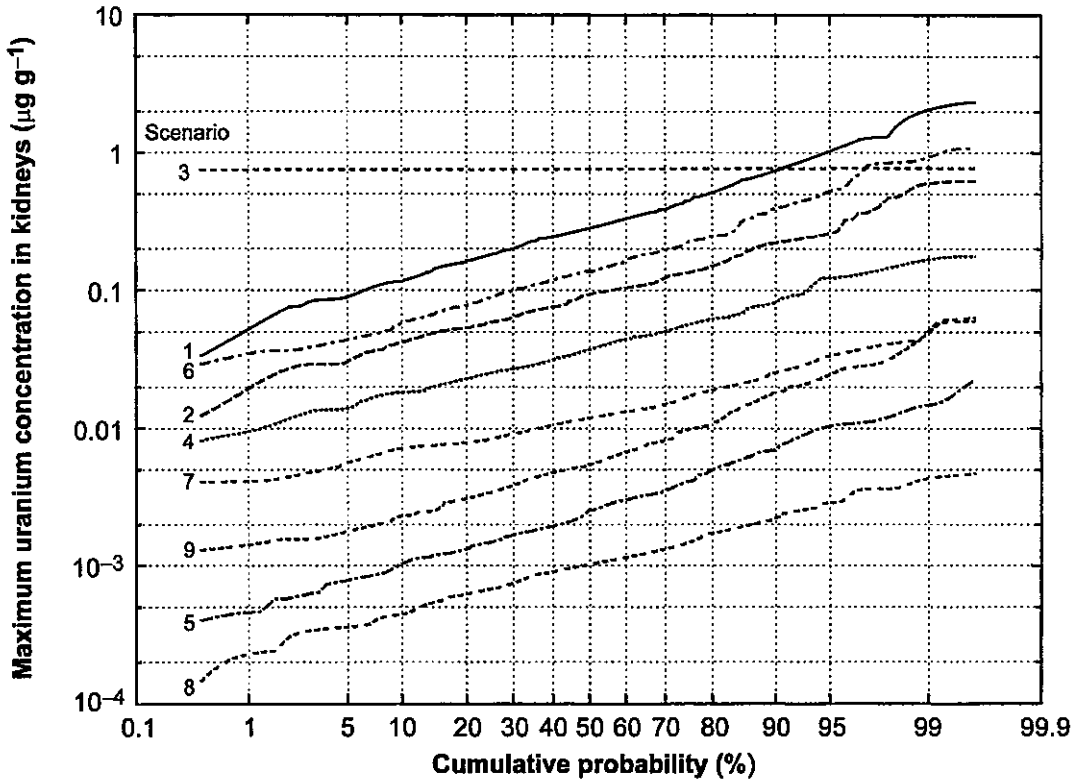

Figure R-6. Uncertainty distributions of maximum uranium concentration in the kidneys for scenarios 1–9. Scenario 3 is essentially unaffected (approximately the constant value 0.75 μg g^{-1}), because its dominant source of uranium in the kidneys for this scenario is water from Well 15, for which no uncertainty was assumed for the calculation depicted in this figure. This question is dealt with in a subsequent section. All other scenarios show shapes that would be reasonably represented by lognormal distributions.

The distributions plotted in Figure R-6 pertain only to uncertainties in release and environmental transport of uranium. They include uncertainties in such parameters as removal rate from surface soil and soil-to-plant transfer ratios. They do not contain uncertainties associated with the hypothetical subjects of the scenarios, either physiological or behavioral. Uncertainties of these latter types can be properly assessed only in relation to real individuals and populations. When such considerations are introduced, one expects that the slopes of the plotted distributions will increase.

Scenario 3, as calculated above, is practically unaffected by propagated uncertainties, because the dominant component of uranium in the kidneys for that scenario is from the contaminated water of Well 15, which greatly exceeds the contamination in this subject's inhalation and diet (Figure R-5). However, an uncertainty hypothesis based on reconstruction of histories of concentration in Well 15 is discussed below, and the results are applied to estimate a range of uncertainties for the subject of scenario 3. All other scenarios clearly show the propagated uncertainties from uranium release and transport; their 95th/50th-percentile ratios range from 2.8 to 4.3. Table R-3 gives the principal percentiles for all nine scenarios (the distribution for scenario 3 is based on uncertainty estimates for Well-15 contamination

that are developed in the next subsection). It is noted that the 50th percentiles often exceed their deterministic counterparts in amounts that show no clear pattern. This effect was discussed at the end of Appendix M. It does not indicate an error in the calculations. We consider the distributions in Table R-3 to be definitive for our estimates of potential risk; the deterministic quantities were meant to be used for breakdowns into components (Figure R-5) and comparisons of metabolic models (Table R-2).

Table R-3. Percentiles of Uranium Concentrations ($\mu g\ g^{-1}$) in the Kidneys of Subjects of the Nine Scenarios

	Percentile				
Scenario	5th	25th	50th	75th	95th
1	0.091	0.18	0.28	0.44	1.0
2	0.031	0.059	0.092	0.14	0.26
3	0.40	0.58	0.75	0.97	1.4
4	0.014	0.025	0.038	0.056	0.12
5	7.8×10^{-4}	0.0015	0.0025	0.004	0.010
6	0.044	0.090	0.14	0.22	0.52
7	0.0057	0.0084	0.012	0.017	0.033
8	3.6×10^{-4}	6.9×10^{-4}	0.001	0.0015	0.0029
9	0.0018	0.0035	0.0055	0.0097	0.024

A Method for Estimating Uncertainty for Scenario 3

As we noted above, the uncertainty distribution for the maximum uranium level in the kidneys of the scenario 3 subject is determined almost exclusively by uncertainty associated with reconstruction of the history of uranium concentrations in Well 15. In this section, we describe the process used to make this uncertainty estimate. The estimate is based on model histories of uranium concentrations in Well 15 and the range of their maximum values obtained by varying the source-to-well transit time over what is believed to be its largest plausible range. As Figure R-5 shows, the maximum concentration in the kidneys corresponds temporally with the maximum exposure level, and we assume a proportionality as well (i.e., doubling the maximum exposure level would approximately double the resulting maximum concentration in the kidneys). This relationship is not exact, but we believe it is reasonable for the present purpose.

The uranium entered Paddy's Run at a point about 2100 ft north of Well 15, where the storm sewer outfall ditch emptied into the creek. We use a simple one-dimensional model of ground water advection and diffusion in a narrow and shallow channel (transverse and vertical distributions are assumed uniform):

$$C_p(x,t) = \frac{\alpha}{\sqrt{2\pi}\sigma} \exp\left(-\frac{(x-ut)^2}{2\sigma^2}\right), \quad \sigma = \sqrt{2Kt} \tag{R-3}$$

where $C_p(x,t)$ (pCi L^{-1}) is the concentration in the well after the release of 1 kg of uranium into Paddy's Run, x is the distance (ft) from the point of release to the well, t is the time since the uranium left the source (travel time), u (ft $year^{-1}$) is the velocity of the moving pulse in the aquifer, K (ft^2 $year^{-1}$) is the dispersion coefficient (a measure of the rate of longitudinal spreading about the moving center), and α is a parameter that accounts for units conversion and initial dilution.

Equation R-3 applies to a pulse release (one that is instantaneous). To account for the release of uranium into Paddy's Run over many years, it is necessary to incorporate the pulse function C_p into a convolution integral with the source function S (kg year^{-1}), giving the resulting concentration at the well at time t:

$$C(x,t) = \int_0^t S(t-\tau) \cdot C_p(x,t)\, d\tau \,. \qquad \text{(R-4)}$$

Equation R-4 combines the contributions of all releases $S(t-\tau)$ for years before the time t at which the concentration in the well is estimated. The function S gives the rate at which uranium is entering the aquifer after percolation through layers of soil. Thus it includes a lag time T with respect to the actual release into Paddy's Run, $Q(t)$:

$$S(t) = Q(t-T) \,. \qquad \text{(R-5)}$$

The releases are shown by year in the top panel of Figure R-7, and in the bottom panel Equation R-4 is plotted for fixed x (2140 ft) and for three values of the total travel time $T + t$ = 10.7, 16, and 21.3 years. With $u = x / t$, the parameters K and α were chosen in each case to give the best fit (in the sense of least squares) to the well data for 1982–1992. The release data are plotted in Figure R-7 along with the fitted response curves in the bottom panel.

Voillequé et al. (1995) chose 10.7–21.3 years as being a plausible range of possible travel times for uranium released to Paddy's Run to reach an offsite well. This range was based on two previous hydrologic studies of the plume (GeoTrans 1985 and ASI-IT 1990). Table R-4 summarizes these travel-time estimates. Although the target well was nearer the point of release than Well 15, the analysis in the following paragraph suggests that this range is reasonable for Well 15.

The maximum release to Paddy's Run (Figure R-7, upper panel) occurred in 1964 and was followed by an abrupt decline. If we assume that the time series of concentrations in Well 15 reproduces large trends in the release curve, we conclude (noting that the well data decline from 1982 onward) that the longest travel time from release to well would be about 1982 minus 1964 or 18 years. Dispersive transport processes, both real and modeled, would distort the response curve to some extent, but the 21.3-year curve in the lower panel of Figure R-7 is consistent with this view, having its maximum after 1982. The minimum total travel time in Table R-4 (10.7 years) corresponds to a curve in the bottom panel of Figure R-7 that diverges from the well data after 1987; the shape of this curve precludes a better fit to the data. The best account shown in the figure is rendered by a curve corresponding to a 16-year total travel time, with interpolated vertical and horizontal components. This curve is similar to the one, from Voillequé et al. (1995, Table M-7), that was used for scenario 3 for well exposure in both the radiological and chemical estimates of kidney exposure to uranium. We take the maximum of the 16-year curve (703 pCi L^{-1}) as the 50th percentile of an uncertainty distribution, and we assign the maximum of the 10.7-year curve (1320 pCi L^{-1}) as the 95th percentile. This assignment is somewhat arbitrary but not unreasonable in the context of the relationship of the curves to the well data. To avoid imposing a specific upper bound on the concentrations, we choose a lognormal representation, determined by the two percentiles just given. The geometric mean is 703 pCi L^{-1}, and the geometric standard deviation is given by $(1320 / 703)^{1/1.65}$ = 1.46. The percentiles of this uncertainty distribution are shown in the lower panel of Figure R-7.

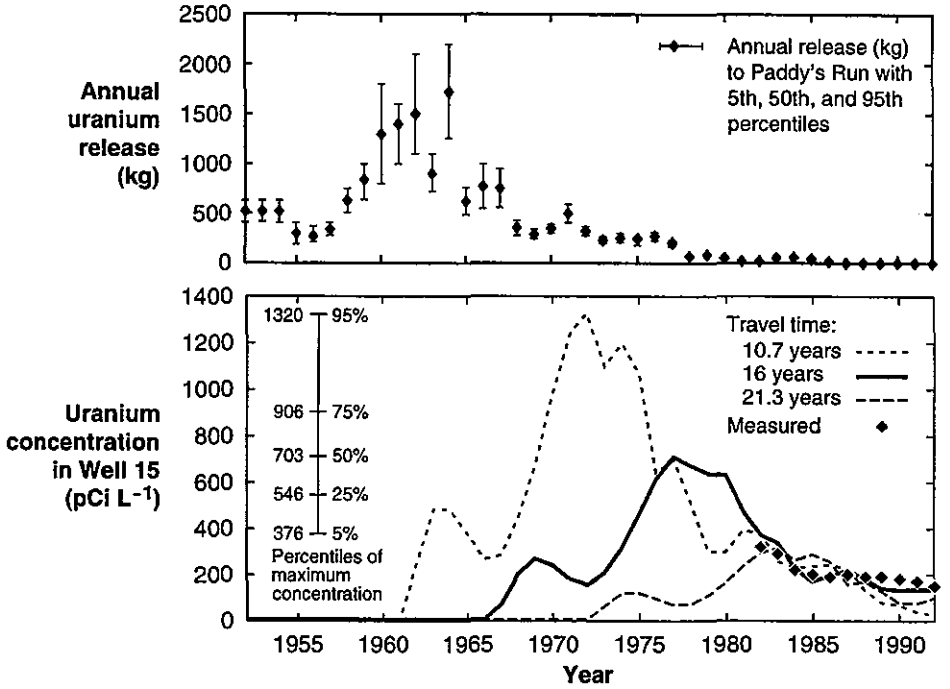

Figure R-7. Reconstructions of uranium concentration history in Well 15 based on measurements, release data, and source-to-well transit times estimated in studies of the aquifer. The top panel shows the history of releases of uranium to Paddy's Run (Appendix L of Voillequé et al. 1995). Points after 1988, for which the reference gave no data, were plotted equal to 1988. In the bottom panel, three deterministic estimates of concentration in the well are plotted, corresponding to the indicated total travel times (time for percolation through soil plus time in the aquifer). Each plot is based on the 50th percentiles of the annual releases shown in the top panel. The uncertainty distribution for the maximum concentration in the well is shown on the left side of the bottom panel; the derivation is discussed in the text.

Table R-4. Travel Times for Uranium Released to Paddy's Run to Reach Offsite Wells

	Estimated travel time (years)		
	Vertical to aquifer	Horizontal to offsite well	Total
GeoTrans[a]	7	3.7	10.7
Interpolated	13	3.0	16
ASI-IT[b]	19	2.3	21.3

[a] GeoTrans (1985). Cited by Voillequé et al. (1995).

[b] ASI-IT (1990). Cited by Voillequé et al. (1995).

We extend this distribution to the estimate of 0.75 μg g^{-1} in the kidneys of the subject of scenario 3 by assuming, for the maximum kidney concentration, a lognormal distribution with the same geometric standard deviation (1.46). This assumption is consistent with the proportionality assumption stated previously. The percentiles are recorded in the scenario 3

line of Table R-3. The maximum concentration in Well 15, of course, cannot have been less than the 1982 measurement (320 pCi L^{-1}). The lognormal uncertainty distribution permits smaller values (although with low probability), which have to be ruled out on empirical grounds. A similar observation technically holds for the maximum kidney concentrations for scenario 3 in Table R-3, but we believe the distribution as given by Table R-3 is a reasonable expression of uncertainty deriving from uranium concentrations in Well 15.

THE CHEMICAL TOXICITY OF NATURAL URANIUM

Uranium is a naturally occurring highly soluble radionuclide that is widely distributed in soil and in some minerals in the earth's crust. It is taken up in crops and is ingested by people mainly from the food chain. Inhalation of airborne particulate uranium occurs to a much lesser extent. Most of the natural uranium taken up by humans rapidly enters the blood stream and is cleared from the body through the kidneys (60% of U(VI) ion and 20% of U(IV) ion) within 24 hours (NCRP 1980). A small proportion of the intake is retained in the body. Normal levels in the human body are in the range 2–62 μg mostly stored in the skeleton. At much higher levels, uranium is chemically toxic, the principal target organ being the kidney.

The nephrotoxicity of natural uranium has a long history dating from 1853. It is discussed in some detail in the BEIR IV report (NAS/NRC 1988). Renal damage appears to be definite after concentrations of about 3 μg g^{-1} in kidney tissue for a number of different animal species, but renal damage may also occur after 1 μg g^{-1} in some species (dogs and female Wistar rats). While comparable exposures of humans to uranium are lacking, lower level exposures in man have shown similar metabolic and other properties for uranium to those in animals. Biokinetic models for uranium metabolism and deposition in the human, based on both animal and human data, are described in ICRP publication 30 (ICRP 1979), by Leggett (1994), and in ICRP publication 69 (ICRP 1995).

The concentration of 3 μg g^{-1} of uranium in the kidney has been widely used as a threshold level and as a limit for workers (Spoor and Hursh 1973) for many years. Confidence in this level as a limit has been based on the absence of chemical effects on the kidney within the scope of the endpoints studied among groups of exposed workers (Alexander 1988). However, these workers probably received kidney burdens of uranium only substantially below this level. Alexander (1988) also drew attention to studies showing effects in animals at levels as low as 0.5 μg g^{-1}.

Since the publication of the BEIR IV report a number of papers have discussed effects (not always involving the same endpoints) at levels lower than the 3 μg g^{-1} nominal threshold. A comprehensive review by Leggett (1989), covering all phases of recent knowledge on uranium effects and possible mechanisms of biological action in the kidney, notes also that the kidney may develop an acquired tolerance to uranium after repeated doses. This "acquired tolerance" nevertheless involves detectable histological and biochemical changes. These include histological changes in proximal kidney tubule cells which, upon regeneration after damage by uranium, become simple flattened cells with no microvilli on their luminal surfaces and reduced numbers of mitochondria in which few cristae are seen (Yuile 1973, Porte et al. 1963). Biochemical changes include diminished activity of alkaline phosphatase persisting for several months (Yuile 1973). The long term clinical significance of these cellular and biochemical changes is not known. Nevertheless, on the basis of this tolerance earlier

workers Neuman (1953) and Hodge (1953) considered that 2–3 μg g^{-1} of uranium could be tolerated without "serious tissue damage." However, it was clear from the work of Morrow and others that concentrations of 0.3 to 1.0 μg g^{-1} of uranium may cause renal abnormalities in dogs (Morrow et al. 1982a, 1982b, Morrow 1984). In humans injected with uranium for experimental purposes or occupationally exposed, 3 μg g^{-1} uranium in the kidney appears to be tolerated but not without mild renal dysfunction. However, the results of long term follow up studies of uranium workers (discussed in Appendix S), some of whom were at risk of exposure to relatively high levels of uranium dust, have not identified increased risks of death due to nonmalignant renal or kidney cancer among the exposed groups (Polednak and Frome 1981; Dupree et al. 1987; Checkoway et al. 1988; Dupree et al. 1995) or that could be attributed to their past exposure to uranium (Waxweiler et al. 1983) when compared with the general population.

Nevertheless, direct information on the effects of prolonged exposure to lower levels of uranium in humans is lacking and, in view of this, Leggett recommended that it may be prudent to lower the long standing guidance level (of 3 μg g^{-1} uranium in kidney tissue) by roughly an order of magnitude, i.e., to about 0.3 μg g^{-1} until more is known about the subtle physiological effects of small quantities of uranium in the kidneys. Kocher (1989), who assumed a lower level of 1 μg g^{-1} uranium in the kidney as the threshold for chemical toxicity, recommended using a safety factor of 10 for protection of the public, resulting in a nominal limit value of 0.1 μg g^{-1} uranium in kidney tissue. He pointed out that chemical toxicity rather than radiation dose would be limiting.

At about the same time Diamond (1989), in reviewing the effects of uranium in animals and the possible biological mechanisms of uranium toxicity, concluded that proteinuria and certain tubular effects in the kidney can begin at uranium concentrations of 0.1 to 0.2 μg g^{-1}. But such effects are often transitory and perhaps naturally reversible. He emphasized that it is not clear how directly these effects and levels can be extrapolated to man.

Shortly thereafter, Lu and Zhao (1990) reported a case of a Chinese man exposed to uranium for several years when an accident occurred which resulted in a concentration of 2.6 μg g^{-1} in the kidney. Abnormalities of kidney function resulted; however, the kidney function gradually returned to normal. The paper recommended that even though the effects were mild, a ten fold safety margin should be applied, and the limit should not exceed 0.26 μg g^{-1} uranium in the kidney.

Another recent comprehensive paper examines the effects of uranium on the kidney (Morris and Meinhold 1995). These authors note that no effect was observed in thousands of people occupationally exposed below the then limit of 3 μg g^{-1} in the kidney (Kathren and Weber 1988), although the actual exposures were not known. They point out also that the reserve capacity of the kidney (which is large) may have been affected even though direct effects were not observed. They state that some authors conclude that kidney damage can occur in virtually all species of animals at levels below 1 μg g^{-1} (Diamond 1989) and perhaps as low as 0.5 μg g^{-1}. They note, as is also noted above, that Wrenn et al. (1985) suggested a threshold level of 1 μg g^{-1} to which Kocher (1989) applied a safety factor of 10, thus, deriving 0.1 μg g^{-1} as a proposed limit for the public. Morris and Meinhold suggest a probability distribution of threshold values ranging from 0.1 μg g^{-1} to 1 μg g^{-1} with a peak at about 0.7 μg g^{-1} (Figure R–8). There is clearly a severity factor involved in this distribution also, i.e., effects at the lowest concentration are evidently very minor, and perhaps detectable only by sensitive tests. Effects between 0.5 μg g^{-1} and 1 μg g^{-1} in animals are still mild. A reasonable

interpretation of the Morris and Meinhold probability distribution is that there are no effects below 0.1 μg g^{-1} and virtually none under 0.2 μg g^{-1}, possibly modest (or "mild") effects on the kidney at 0.5 μg g^{-1}, and more severe effects begin at about 1.0 μg g^{-1} and are more likely after about 3 μg g^{-1}. It is worth noting that at least one recent text on the effects of uranium (Brodsky 1996) still considers the former limit of 3 μg g^{-1} uranium in kidney as unlikely to cause kidney damage even if present over a lifetime.

A recent paper (Russell et al. 1996) from the U.S. Transuranium and Uranium Registries, reports kidney autopsy sections of seven cases of low-level occupational exposure to uranium compared with six control cases. The pathologist involved in this blind study was not able to identify the uranium workers or any uranium-specific nephropathy. This suggests that the chronic low level of uranium experienced by these workers, which was probably an order of magnitude lower than the one-time permissible level of 3 μg g^{-1} but within the range considered by Morris and Meinhold, did not induce any identifiable permanent tissue damage. Obviously transient effects in the kidney, which may have occurred, would not have been detected in this study. The results of the study, nevertheless, are consistent with the Morris and Meinhold approach.

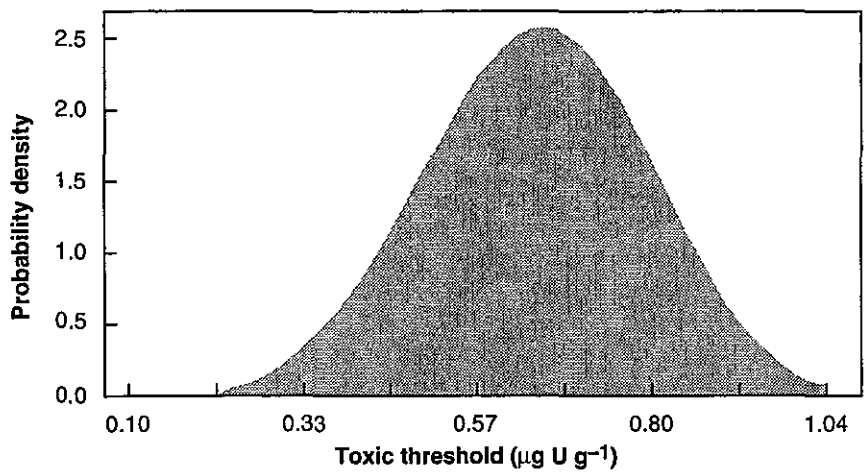

Figure R-8. Probability distribution of toxic thresholds for uranium in the kidney (redrawn from Morris and Meinhold, 1995, with permission). The numbers added to the vertical axis establish a coordinate scale in which the total area under the distribution curve is unity.

Considering all the above, it seems reasonable to adopt the approach of Morris and Meinhold as it has been interpreted here, namely, no effects below 0.1 μg g^{-1} to 0.2 μg g^{-1}, possibly mild effects on the human kidney at about 0.5 μg g^{-1} or so, with more severe effects just beginning at about 1 μg g^{-1}, and setting in more definitely at 3 μg g^{-1} and above.

Mild effects in the kidney can be detected by tests of kidney function, but these effects are transient in nature and are not expected to result in permanent damage to the kidney. More severe effects involve greater damage to the kidney that is likely to be clinically manifest and longer lasting, although the kidney has surprising amounts of reserve capacity and can recover after even quite pronounced clinical symptoms.

THE NEPHROTOXICITY OF URANIUM FOR THE NINE EXPOSURE SCENARIOS

The maximum kidney burdens of uranium and their uncertainties for the nine scenarios were given in Table R-3 earlier. Among these the 5th and 95th percentiles are about equally likely, but we are concerned mainly with the 50th percentile, i.e., the median value and with the 95th percentile representing close to the maximum value at low probability for each scenario. These 50th and 95th percentile values are reproduced in Table R-5.

DISCUSSION OF URANIUM TOXICITY

It is apparent from the final two columns of Table R–5 that in four of the exposure scenarios (5, 7, 8, and 9) neither the 50th or 95th percentile concentrations of uranium ever exceed 0.1 μg g^{-1} and, therefore, there are no nephrotoxic effects of any kind to be expected in representative individuals in these scenarios in any circumstance. Two additional scenarios (4 and 2) have 50th percentile values at 0.038 μg g^{-1} and 0.092 μg g^{-1} respectively and 95th percentile values at 0.12 μg g^{-1} and 0.26 μg g^{-1} and there is virtually no chance of even mild effects in the kidney in these two scenarios.

Table R-5. 50th and 95th Percentiles of Uranium Concentration (μg g^{-1}) in the Kidneys of Subjects of the Nine Scenarios

	Percentile	
Scenario	50th	95th
1	0.28	1.0
2	0.092	0.26
3	0.75	1.4
4	0.038	0.12
5	0.0025	0.010
6	0.14	0.52
7	0.012	0.033
8	0.001	0.0029
9	0.0055	0.024

Scenarios 6, 1, and 3 are more problematic. Scenario 6 has a 50th percentile of 0.14 μg^{-1} and a 95th percentile of 0.52 μg g^{-1}. The latter is just into the range where mild effects are possible but with a low likelihood. Scenario 1 has a 50th percentile value of 0.28 μg g^{-1} and a 95th percentile value of 1.0 μg g^{-1}. In this scenario mild effects are quite likely and there is a small chance of more severe effects. Scenario 3 has the greatest uncertainties with 0.75 μg g^{-1} at the 50th percentile and 1.4 μg g^{-1} at the 95th percentile. Thus, mild effects are likely and there is a small chance of more severe effects. However, it should be pointed out that severe effects beginning at 1 μg g^{-1} are inferred rather than directly known from experience.

CONCLUSION

Overall it would seem that no chemical toxicity effects are to be expected for human subjects in scenarios 2, 4, 5, 7, 8 and 9. There is a small chance of mild effects in human subjects in scenario 6. In scenarios 1 and 3 mild effects in human subjects are likely and there is a small chance of more severe effects in the kidney of those subjects.

REFERENCES

Alexander R. 1988. Introductory Remarks pp. 73–75. Concluding Remarks pp. 147–155. In: Proceedings of a Public Meeting, December 4, 1988, *Ultrasensitive Techniques for Measurement of Uranium in Biological Samples and the Nephrotoxicity of Uranium*. Kathren, R.L, Weber, J.R., eds. NUREG/CP-0093. United States Nuclear Regulatory Commission. Washington, D.C.

ASI-IT (Advanced Sciences, Incorporated, and International Technology Corporation). 1990. *Engineering Evaluation/Cost Analysis South Plume, Feed Materials Production Center, Fernald, Ohio*. Advanced Sciences Inc. and International Technology Corp., Cincinnati, Ohio, USA.

Brodsky A. 1996. *Radiation Risks and Uranium Toxicity*. RSA Publications. Hebron, Connecticut.

Checkoway H., N. Pearce, D.J. Crawford-Brown, and D.L. Cragle. 1988. "Radiation Doses and Cause-Specific Mortality Among Workers at a Nuclear Materials Fabrication Plant." *Am. J. Epidemiol.* **127**:255–266.

Diamond G.L. 1989. "Biological Consequences of Exposure to Soluble Forms of Natural Uranium." *Radiation Protection Dosimetry* **26**:23–33.

Dupree E.A., D.L. Cragle, R.W. McLain, D.J. Crawford-Brown, and M.J. Teta. 1987. "Mortality Among Workers at the Uranium Processing Facility, the Linde Air Products Company Ceramics Plant 1943–49." *Scand. J. Work Environ. Health* **13**:100–107.

Dupree E.A., J.P. Watking, J.N. Ingle, P.W. Wallace, C.M. West, and W.G. Tankersley. 1995. "Uranium Dust Exposure and Lung Cancer Risk in Four Uranium Processing Operations." *Epidemiology* **6**:370–375.

GeoTrans. 1985. *Preliminary Characterization of the Groundwater Flow System Near the Feed Materials Production Center, Great Miami River Valley-Fill Aquifer, Fernald, Ohio*. Report prepared for Ohio Environmental Protection Agency. GeoTrans, Inc., Columbus, Ohio.

Hodge H.C. 1953. Resume of Chapters 18 to 28: *Pharmacology and Toxicology of Uranium Compounds*. Voegtlin, C. and Hodge, H.C. eds. National Nuclear Energy Series Division VI, Volume 1, Part IV, pp. 2335–2423. McGraw Hill, New York.

International Commission on Radiological Protection (ICRP). 1975. *Report of the Task Group on Reference Man*. ICRP Publication 23. Pergamon Press, Oxford.

International Commission on Radiological Protection (ICRP). 1979. *Limits for Intakes of Radionuclides by Workers*. ICRP Publication 30 Part 1, *Annals of the ICRP* **2**(3/4). Pergamon Press, Oxford.

International Commission on Radiological Protection (ICRP). 1995. *Age Dependent Doses to Members of the Public from Intake of Radionuclides: Part 3 Ingestion Dose Coefficients*. ICRP Publication 69. *Annals of the ICRP* **25**(1). Pergamon Press, Oxford.

Kathren R.L., and J.R. Weber. 1988. Proceedings of a Public Meeting December 3–4, 1988 on *Ultrasensitive Techniques for Measurement of Uranium in Biological Samples and the Nephrotoxicity of Uranium*. NUREG/CP-0093. U.S. Nuclear Regulatory Commission, Washington, DC.

Kocher D.C. 1989. "Relationship Between Kidney Burden and Radiation Dose from Chronic Ingestion of U: Implications for Radiation Standards for the Public." *Health Phys.* **57**, 9–15.

Leggett R.W. 1989. "The Behavior and Chemical Toxicity of U in the Kidney: A Reassessment." *Health Phys.* **57**, 365–383.

Leggett R.W. 1994. "Basis for the ICRP's Age-Specific Biokinetic Model for Uranium." *Health Phys.* **67**, 589–601.

Lu S. and S.F. Zhao. 1990. "Nephrotoxic Limit and Annual Limit on Intake for Natural U." *Health Phys.* **58**, 619–623.

Morris S.C. and A.F. Meinhold. 1995. "Probabilistic Risk Assessment of Nephrotoxic Effect of Uranium in Drinking Water." *Health Phys.* **69**, 897–908.

Morrow P.E., R.M. Gelein, H.D. Beiter, J.B. Scott, J.J. Picano, and C.L. Yuile. 1982a. "Inhalation and Intravenous Studies of UF_6/UO_2F_2 in Dogs." *Health Phys.* **43**, 859–873.

Morrow P.E., L.J. Leach, F.A. Smith, R.M. Gelein, J.B. Scott, H.D. Beiter, F.J. Amato, J.J. Picano, and C.L. Yuile. 1982b. *Metabolic Fate and Evaluation of Injury in Rats and Dogs Following Exposure to the Hydrolysis Products of Uranium Hexafluoride*. NUREG/CR-2268. U.S. Nuclear Regulatory Commission, Washington, DC.

Morrow, P.E. 1984. "Biokinetics and Toxicology of Uranium." in: *Biokinetics and Analysis of Uranium in Man*. Moore, R.H., ed. U.S. Uranium Registry; USUR-05, HEHF-47. E1-E27. National Technical Information Service, Springfield, Virginia.

National Academy of Sciences/National Research Council (NAS/NRC). 1988. *Health Risks of Radon and Other Internally Deposited Alpha-Emitters*. BEIR IV Report. National Academy Press, Washington, DC.

National Council on Radiation Protection and Measurements (NCRP). 1980. *Management of Persons Accidentally Contaminated with Radionuclides*. NCRP Report No. 65. National Council on Radiation Protection and Measurements, Bethesda, Maryland.

Neuman W.F. 1953. "Urinary Uranium as a Measure of Exposure Hazard." in: *Pharmacology and Toxicology of Uranium Compounds*. Voegtlin C. and Hodge, H.C. eds. National

Nuclear Energy Series, Division VI. Volume 1 Part IV. 2241–2256. McGraw Hill, New York.

Polednak A.P. and E.L. Frome. 1981. "Mortality Among Men Employed Between 1943 and 1947 at a Uranium Processing Plant." *J. Occup. Med.* **23**:169–178.

Porte A., Y. Cussac, P. Stoebner, and J.P. Zahnd. 1963. "Sur la formation et l'ultrastructure des cellules de régénération dans les tubules rénaux de souris intoxiquées par le nitrate d'uranyle." *C.R. Soc. Biol.* (Paris) **157**:2079–2081.

Russell J.J., R.L. Kathren and S.E. Dietert. 1996. "A Histological Kidney Study of Uranium and Non-Uranium Workers." *Health Phys.* **70**(4): 466–472.

Spoor N.L. and J.B. Hursh. 1973. "Protection Criteria." in: *Uranium, Plutonium, Transplutonic Elements*. H.C. Hodge, J.N. Stannard and J.B. Hursh, eds. pp. 241–270. Springer Verlag, New York.

Voillequé P.G., K.R. Meyer, D.W. Schmidt, S.K. Rope, G.G. Killough, M. Case, R.E. Moore, B. Shleien, and J.E. Till. 1995. *The Fernald Dosimetry Reconstruction Projection Tasks 2 and 3 — Radionuclide Source Terms and Uncertainties*. RAC Report No. CDC-5, Radiological Assessments Corporation, Neeses, South Carolina.

Waxweiler R.J., V.E. Archer, R.J. Roscoe, A. Watanabe, and M.J. Thun. 1983. "Mortality Patterns Among a Retrospective Cohort of Uranium Mill Workers." In *Epidemiology Applied to Health Physics*. CONF-830101, pp. 428–435. *[need publisher, city]*

Wrenn M.E., P.W. Durbin, B. Howard, J. Lipsztein, J. Rundo, E.T. Still, and D.L. Willis. 1985. "Metabolism of Ingested U and Ra." *Health Phys.* **48**:601–633.

Yuile C.L. 1973. "Animal Experiments." In *Uranium, Plutonium, Transplutonic Elements: Handbook of Experimental Pharmacology*. Hodge H.C., J.N. Stannard, J.B. Hursh, eds. Vol. 36, 165–196. Springer-Verlag, New York.

APPENDIX S

LIFETIME RISKS OF FATAL CANCER FOR INDIVIDUAL SCENARIOS AT THE FEED MATERIALS PRODUCTION CENTER

INTRODUCTION

Radiation-induced cancer is a late effect of radiation exposure. The exposure may be due to external radiation or to intakes of radionuclides by inhalation or ingestion. The effect is called late because an induced cancer will not be manifest for at least 2–10 years after exposure and may still occur in the case of solid tumors after 40 years or more. The effect is also known as stochastic or random because when a population is exposed to radiation only a few of the exposed individuals will actually get a latent induced cancer. The great majority of exposed individuals will not get such a cancer. The frequency or likelihood of a cancer occurring depends on the dose. For radiation protection purposes it is assumed that after low doses, the frequency is proportional to the dose (i.e., the response is linear). Thus, the larger the dose, the greater the frequency. Even at very low doses, therefore, there is a small possibility of a cancer being induced.

Radiation-induced cancers may be induced in many organs or tissues in the body but are more likely to be induced in some tissues and organs than others. Leukemia, resulting from exposure of the bone marrow, is a relatively early manifestation of exposure that begins to occur after a latency of only 2 years. Stomach, lung, colon, esophagus, liver, bladder, breast, skin, and thyroid are organs in which cancer is comparatively readily induced by radiation but only after a long initial latent period of 5–10 years or more. In general, the type of cancer induced by radiation is not distinguishable from the cancers that arise naturally or from other causes. Their presence is known from epidemiological studies of irradiated populations that show an increase in the number of excess cancers with increasing radiation dose.

Cancers arising spontaneously without any known cause are responsible for more than 20% of deaths in a population such as that in the U.S. (However, the causes of some cancers are known, e.g., smoking can cause lung cancer.) Populations in other countries have similar spontaneous rates of cancer, but the type of cancer that is most frequent varies. For example, stomach cancer has a high incidence in Japan and a low incidence in the U.S. Conversely, colon cancer has a high incidence in the U.S. and a low incidence in Japan. These differences may be due to diet or other aspects of environment or lifestyle as well as to genetics. They give rise to problems in understanding how radiation-induced cancer risks estimated in an exposed Japanese population can be transferred to other populations.

Another problem arises because exposed populations have only been observed over limited periods even though these may be quite lengthy (e.g., the A-bomb survivors considered in our analysis were observed from 1950 to 1985, 35 years). We want to estimate the impact of the radiation exposure over the whole of the lifetime of an individual or population, i.e., the lifetime risk. Consequently, it is necessary to project the risk from the observed period to the expected risk in a complete lifetime using projection methods that depend on past experience. Obviously, these are uncertain because they are projections. In the case of the A-bomb survivor population, 39% of the original study population had died by 1985 and

could be evaluated for mortality; the effects on the remaining 61% have to be projected to obtain a lifetime risk.

There is also the problem that exposure of the population being studied is often over in a short period of time, i.e., it is at high dose rate, as encountered in the A-bomb explosions or medical therapy. However, we want to know the rate of cancer induction after exposure for long periods of time, i.e., at low dose rate, more often encountered by radiation workers or by the public. We know well from studies in animals and other biological organisms that low dose rate is invariably less effective biologically than high dose rate (NCRP 1980, UNSCEAR 1993), usually between 2 and 10 times. Thus, a correction to the estimate of risk for dose rate, known as a dose and dose rate effectiveness factor (DDREF), must be made. The magnitude of this correction involves a large uncertainty that may be different for cancers in different organ or tissue sites. Nevertheless, for radiation protection, an average value is used.

Finally, there is statistical uncertainty in the estimates of the number of cancers in the population studied as well as possible biases such as underreporting of cancer on death certificates. In addition, the doses to which people were exposed have to be reconstructed after the event and involve attendant uncertainties, which can, in some cases, be quantified. Both these parameters have been carefully studied in the Lifespan Study (LSS) of the A-bomb survivors, the most important source of human risk estimation (Shimizu et al. 1988, 1990).

EVALUATIONS OF THE RISK OF RADIATION-INDUCED CANCER

This section treats the most recent evaluations of the A-bomb survivor data together with evaluations of medically exposed and occupationally exposed populations. It also deals specifically with the risk of kidney cancer and the risk of lung cancers due to radon, and it discusses direct epidemiological data for uranium.

Lifetime Risk Estimates

In the period 1988–1993, the United Nations Scientific Committee on the Effects of Atomic Radiation (UNSCEAR 1988), the Biological Effects of Ionizing Radiation (BEIR) Committee of the National Academy of Sciences in the U.S. (NAS/NRC 1990), the International Commission on Radiological Protection (ICRP) (ICRP 1991), and the National Council on Radiation Protection and Measurements (NCRP) (NCRP 1993a, 1993b) evaluated the risk of cancer from the study of all known exposed human populations. The A-bomb survivors were evaluated for the period 1950–1985. A later UNSCEAR (1994) report listed the 41 known epidemiological studies of exposed persons that can contribute to estimates of the risk of cancer. Principal among these is the study of mortality data in the A-bomb survivors in Japan, initially for the period 1950–1985 but extended to 1987 as new incidence data from the tumor registries became available for the period 1958–1987 (Thompson et al. 1994). However, the results of the 1988 evaluation of the 1950–1985 mortality data in terms of overall lifetime risk were not altered substantially by the extension of the data to 1987.

The A-bomb mortality data were recently updated further to include the period 1950-1990, (Pierce et al. 1996). Again, although a wealth of new detail became available the risk estimates were not essentially different from those derived by UNSCEAR in 1988. The A-bomb survivor study (Shimizu et al. 1988, 1990; Pierce et al. 1996) is so superior in its wealth of detail to all other studies, including the medical and occupational studies, that it is used

almost exclusively for radiation risk estimation. The other studies, particularly medical, provide supporting information both on total cancer risk and on many tumor sites (such as breast, thyroid, and lung). Some studies provide unique information to supplement the A-bomb data especially in selected tumor sites. For a few sites, such as breast and thyroid, there have been many different studies that contribute to risk estimation (UNSCEAR 1994). Occupational studies of U.K., U.S. and Russian workers give low dose information that is of relatively low precision but is generally supportive of the results from the A-bomb survivor studies (UNSCEAR 1994).

The risk estimates used today for radiation protection of workers and the public are those derived by the ICRP (ICRP 1991) and supported by the studies and opinions of the NCRP (NCRP 1993a, 1993b). They are based mainly on mortality data in the A-bomb survivor population for the period 1950–1985 supplemented, for some organs, by medical studies.

Evaluations by ICRP took into account the separate evaluations of the 1950–1985 data for the A-bomb survivors by UNSCEAR (UNSCEAR 1988) and BEIR V (NAS/NRC 1990). The ICRP also did their own evaluations and considered a variety of populations. ICRP transferred the risk information in the Japanese population to four other populations (U.S., U.K., China and Puerto Rico) by two different transfer methods (absolute and relative) and averaged the result because evidence is not clear on which method is preferable. Averaging two methods of transfer reduces the uncertainty (Land and Sinclair 1991, ICRP 1991). ICRP projected in time from the risk estimate for the observed population to lifetime risk in the entire population using a constant relative risk model. They divided the risk estimate for the acute high dose exposures from the A-bombs by an average dose and dose rate effectiveness factor of 2 considering radiobiological data and human experience, including the shape of the dose response curve for the A-bomb survivor data itself. (See ICRP 1991 para B62). This correction applies to low linear energy transfer (LET) radiations[1] such as x and gamma rays but not to high LET radiations, such as alpha particles.

The net result is that for our purposes in radiation protection, risk estimates for all fatal cancers are recommended by ICRP and NCRP as follows:

Table S–1. Recommended Lifetime Risk Estimates for Radiation-induced Fatal Cancer

Population	Risk estimate (Sv^{-1})	Source
Population of all ages	5×10^{-2}	ICRP (1991)
		NCRP (1993a)
Adult workers	4×10^{-2}	ICRP (1991)
		NCRP (1993a)
Elderly adults (>65)	1×10^{-2}	Sinclair (1992)
Children (<20)	10×10^{-2}	Sinclair (1992)
		NCRP (1993a)

[1] LET (linear energy transfer) refers to the manner in which radiations deposit energy in tissue; high LET radiations deposit energy more densely, low LET radiations deposit energy more sparsely; consequently, low LET radiations are less effective biologically.

In addition to the risk of all cancers following radiation exposure, the risk associated with cancer in the individual organs and tissues that play a major part in the total cancer risk can also be assessed. Again, most of the information comes from the study of the A-bomb survivors, but for some organs (liver, bone, thyroid, and skin), medical exposures were until recently the principal source. Very recently, estimates of risk for liver and thyroid cancer have been derived also from the A-bomb data, mainly from the incidence data (UNSCEAR 1994).

Table S–2 presents the risk factors (average probabilities of fatal cancer) recommended by ICRP and NCRP for the principal organs and tissues.

Table S–2. Probability of Fatal Cancer in Organ and Tissue Sites for Different Age Groups

	Average probabilities of fatal cancer $\times 10^{-2}$ Sv^{-1} [a]			
Tissue or organ	Population of all ages[b, c]	Adult workers[b, c]	Elderly adults (>65)[d]	Children[c, d]
Bladder	0.30	0.24	0.06	0.60
Bone marrow (Leukemia)	0.50	0.40	0.10	1.00
Bone	0.05	0.04	0.01	0.10
Breast	0.20	0.16	0.04	0.40
Colon	0.85	0.68	0.17	1.70
Liver	0.15	0.12	0.03	0.30
Lung	0.85	0.68	0.17	1.70
Esophagus	0.30	0.24	0.06	0.60
Ovary	0.10	0.08	0.01	0.20
Skin	0.02	0.02	0.01	0.04
Stomach	1.10	0.88	0.22	2.20
Thyroid	0.08	0.06	0.02	0.16
Remainder	0.50	0.40	0.10	1.00
Total (Whole body)	5.00	4.00	1.00	10.00

[a] Numbers are averages for both sexes.
[b] ICRP (1991).
[c] NCRP (1993a).
[d] Sinclair (1992).

Risk to the Kidney

The kidney presents a special problem because it is a target organ for uranium exposure (see later) and because its risk of cancer is not separately defined by ICRP and NCRP; thus, it is not given in Table S–2. Formally, in the ICRP/NCRP protection system used for compliance with radiation protection standards, the kidney could be treated as part of the remainder. However, for risk purposes there is another more appropriate approach. Among the risks of

fatal cancer estimated for the A-bomb survivors in the period 1950–1987, the risk of fatal cancer in urinary organs (including kidney) is 0.67×10^{-4} person year sievert $(PYSv)^{(-1)}$[2] and for the urinary bladder alone it is 0.49×10^{-4} $(PYSv)^{-1}$ (Ron et al. 1994, Table VII). Of the difference between these two 0.18×10^{-4} $(PYSv)^{-4}$, 85% is due to the kidney (39 of 46 deaths) (Ron et al. 1994, Table II). Thus, the risk of fatal cancer during the observation period in kidney alone is 0.18×10^{-4} $(PYSv)^{-1} \times 85\% = 0.15 \times 10^{-4}$ $(PYSv)^{-1}$ versus 0.49×10^{-4} $(PYSv)^{-1}$ for the urinary bladder alone, i.e., the risk of a fatal kidney tumor is about 0.31 of the risk of a fatal bladder tumor. The U.S. Environmental Protection Agency (EPA), in a modification of the ICRP evaluation of risks (Puskin and Nelson 1995), stated a lifetime risk for kidney of 5.9×10^{-4} Sv^{-1} compared to bladder 24.9×10^{-4} Sv^{-1}, i.e., the lifetime risk for the kidney is about 0.24 of the lifetime risk for the bladder. Considering these two sources, the lifetime risk of a fatal kidney tumor is taken to be 0.27 of the lifetime risk of a fatal bladder tumor, which is listed in Table S–2 as 0.30×10^{-2} Sv^{-1} or 0.30% per Sv. Thus, the lifetime risk for the kidney is 0.08×10^{-2} Sv^{-1} or 0.08% per Sv, a little higher than the EPA value. This value is used throughout our analysis.

Radon Dosimetry and Risk

The equivalent doses to the lungs from radon in the various scenarios are estimated in the following way. The dose conversion procedure outlined in NCRP Report No. 78 page 47 (NCRP 1984) assesses the contributions of radon daughters, Radium A, Radium B, and Radium C, separately in the case of males, females, and children and for both light activity and resting. This procedure was used to obtain the absorbed dose to the bronchial epithelium in units of rads for given concentrations of radon daughters in picocuries per cubic meter (pCi m^{-3}). These estimates of absorbed dose in rad were converted to units of gray (divide by 100) and multiplied by a W_R[3] of 20 to obtain the equivalent dose in sievert. (See Appendix I for details.)

The risks associated with these equivalent doses are estimated as follows. The BEIR IV estimate of radon risk gives 350 excess deaths per 10^6 people per working level month (WLM[4]) in a lifetime (NAS/NRC 1988, page 8). This estimate is the most widely accepted estimate at this time. It is intermediate between other values found by assessment bodies over the years, Table S–3.

This estimate is also supported by a subsequent analysis (Lubin et al. 1994) of many more cohort studies of miners than those considered in BEIR IV (11 compared to 4, and a

[2] $PYSv^{-1}$ = (person year $sievert^{-1}$, is a measure of the number of people exposed, the length of the period of observation, and the equivalent dose.

[3] W_R is the radiation weighting factor (ICRP 1991). It is a recommended average value of the relative biological effectiveness (RBE), i.e., the ratio of the biological effectiveness of alpha particles to that of x-rays and gamma rays. Values of RBE may vary with biological endpoint or exposure circumstances such as dose rate. ICRP recommends a single average value for W_R of 20 for alpha particles.

[4] WLM = Working Level Month, is a unit of exposure to radon. A Working Level (WL) is a defined concentration of alpha particles in air (1.3×10^5 MeV in 1 liter of air), and the WLM is exposure to 1 WL for one working month of 170 hours.

total of 2700 lung cancer deaths). A recent comparable ICRP estimate is 280 per 10^6 per WLM (ICRP 1993), which is only a little less (20%) than the BEIR IV value.

Table S–3. Estimates of Lifetime Risk of Lung Cancer Mortality Due to Lifetime Exposure to Radon Progeny (from Table 9-1, NCRP 1993a)

Source	Excess lifetime lung cancer mortality (deaths per 10^6 person-WLM)
UNSCEAR (1977)	200-450
UNSCEAR (1988)	150-450
BEIR III (NAS/NRC 1980)	730
NCRP (1984)	130
ICRP (1987)	170-230[a] 360[b]
Puskin and Yang (1988)	115-400
BEIR IV (NAS/NRC 1988)	350

[a] Relative risk with ICRP (1987) reference population.

[b] Relative risk with the 1980 United States population used by BEIR IV (NAS/NRC 1988).

In some instances, e.g., Puskin (1992), a factor of 0.7 (variously given as 0.6 to 0.9 by NAS/NRC 1991) is used to convert from the exposure circumstances in mines to those in homes (to account for differences in breathing rates, attached and unattached fractions, and other factors), i.e., the BEIR IV number is modified from 350 excess deaths per 10^6 per WLM to 220 excess deaths per 10^6 per WLM. Because part of this difference is already accounted for by using the conversion factor from WLM to rads or gray for domestic exposure (next paragraph) the BEIR IV value will be used in our analysis. Other factors not accounted for will be considered to be within the range of uncertainties discussed later.

NCRP Report No. 78 gives values for the dose to bronchial epithelium per unit exposure of 0.5 rad/WLM for miners, but 0.7 rad/WLM for men and 0.6 rad/WLM for women in domestic or environmental exposures (NCRP 1984). If we average the values for men and women, namely 0.65 rad/WLM, we have effectively corrected the risk for miners by a factor of 0.5/0.65 = 0.77 for domestic exposures, which is within the range given by NAS/NRC (1991) for environmental circumstances. Then a lifetime risk of radon of $350/10^6$/WLM becomes $540/10^6$/rad to the bronchial epithelium. This is $54000/10^6$/gray or $2700/10^6$/sievert (RBE = 20), i.e., $0.27 \times 10^{-2}\text{Sv}^{-1}$. This figure is only about 40% of the value that would be obtained for adults from the exposure of the A-bomb survivors to external gamma radiation. This is a well known discrepancy that has been widely discussed but not yet resolved. The estimate derived from radon studies is a more direct measure of radon risk; therefore, it will be used throughout our analysis. The range of uncertainties discussed later will include the values that would be derived from the A-bomb studies in the 90% confidence interval, i.e., between the 5^{th} and 95^{th} percentile values.

Epidemiological Experience with Uranium

Risk estimates derived from the A-bomb survivor studies may be the best procedure available but they are an indirect approach to determining the risks from uranium. We need to consider whether specific epidemiological information is available from the exposure of individuals to uranium sources that could provide a more direct estimate of the risks from uranium. No previous environmental situations in which exposures to uranium in the atmosphere or via ingestion pathways have been documented; therefore, there is no direct information on health effects of these exposures in the general public. However, nuclear energy workers in certain phases of the nuclear energy cycle have been exposed to uranium in various forms. Recent reviews of epidemiological experience appear in the BEIR IV report (NAS/NRC 1988) and in the UNSCEAR report for 1994, Annex A. Because UNSCEAR (1994) is more recent, the following is quoted on the subject of uranium from its review of Epidemiological Studies of Radiation Carcinogenesis.

> para 319 Miners of uranium and other ores are exposed to high concentrations of radon gas and its progeny, and they are considered separately as workers exposed to measured concentrations of radon (UNSCEAR 1994, Annex A, Section III C). Among those working above ground in the processing of uranium, exposures to radon gas and its progeny are low, but there may be exposure to alpha, beta and gamma-radiation from uranium compounds and progeny. A number of cohort studies have been carried out of the health of men exposed to uranium mainly in the form of UCl_4 and UO_3 in the nuclear energy industry (Checkoway et al. 1988; Polednak and Frome 1981). These studies have been considered together with other studies of nuclear energy workers (UNSCEAR 1994, Annex B, Section IIB.1). No hazards specific to uranium were identified in the cohort studies, apart from a suggestion in the study of workers employed at a uranium processing plant in Tennessee during the Second World War that men first exposed to uranium dust at the age of 45 years or older might be at increased risk of developing lung cancer (Polednak and Frome 1981). A case-control study of men who had worked at the plant and subsequently died of lung cancer was performed, in which cumulative radiation lung doses were evaluated in detail and smoking status, x-ray examinations received during employment, history of lung diseases and potential for diagnostic radiation were determined from employee medical records (Cookfair et al. 1983). The study included 330 cases and 641 controls. When all the men in the study were included in the analysis, there was no suggestion of an increase in risk with increasing exposure. However, among those aged over 45 years when first exposed, the relative risk of lung cancer was found to increase with increasing level of exposure after controlling for age and smoking status. Among men with high exposures to the lung (0.20–0.75 Gy), for which a quality factor of 10 was suggested in the paper (mean equivalent dose: 2.75 Sv) (Beck et al.

> 1983), there was a fourfold increase in lung cancer risk (based on 11 cases and 6 controls), and this increase was statistically significant. It is possible that the increase is a chance finding based on subset analysis or inadequate control for smoking.

This finding among the more highly exposed is based on a small number of cases and is only a subset of the overall data. It tends to be dismissed by UNSCEAR (1994), perhaps justifiably. Nevertheless it is interesting to compare the risk derived from this subset with the risk of lung cancers derived from the A-bomb data. Taking the statement here at face value, a four-fold increase in lung cancer risk means an excess relative risk (ERR) of 4 – 1 = 3. This resulted from an average dose of 2.75 Sv using an RBE of 10 (Beck et al. 1983). It would have been 5.5 Sv if a more currently accepted RBE of 20 were used. In any case, the ERR Sv^{-1} becomes either 1.1 or 0.55. Either value compares well with the ERR Sv^{-1} values for the A-bomb data of 0.80 for incidence and 0.63 for mortality (Ron et al. 1994), i.e., they are broadly similar. The quotation from UNSCEAR (1994) continues:

> Uranium millers are also exposed to airborne dust containing ^{234}U, ^{238}U and ^{230th}. Two studies of uranium millers have been carried out (Archer et al. 1973; Waxweiler et al. 1983). In both studies the number of deaths observed from lung cancer was less than expected, and neither study reported an excess of bone cancer. However, both studies reported an excess of cancers of lymphocytic and haematopoietic tissue other than leukemia (4 observed, 1 expected in the entire period) (Archer et al. 1973); 6 observed, 2.6 expected in the period more than 20 years after commencement of employment (Waxweiler et al. 1983). The observed deaths comprised giant follicular lymphoma (two), multiple myeloma (two), lymphosarcoma (three) and Hodgkin's disease (three).

The Waxweiler et al. study was prompted by the observations of Archer et al. 1973 although in a different cohort of workers. Although neither result was significant Waxweiler et al. thought these effects may have an occupational etiology. However the fact that the effects were not related to length of employment mitigates against that hypothesis. In any event, more importantly, it should be noted that in both studies the number of deaths from lung cancer was less than expected.

A further paper (Dupree et al. 1995) on the subject of workers exposed to uranium has appeared since the UNSCEAR review in 1994. This paper notes that four previous studies (Polednak and Frome 1981, Cookfair et al. 1983, Dupree et al. 1987, Checkoway et al. 1988) had examined workers at four uranium processing plants. These studies (except Dupree et al. 1987) found an excess of lung cancer in subgroups of workers but no excess in the group overall. In the latest paper (Dupree et al. 1995), the fate of these same workers is reexamined in more detail over a longer follow-up period, in a matched case control study. The abstract of the paper, which indicates the findings, follows:

> We examined the relation between uranium dust exposure and lung cancer mortality among workers employed in four uranium processing or fabrication operations located in Missouri, Ohio, and Tennessee. Among

> workers who had at least 30 years of potential follow-up, we identified 787 lung cancer cases from death certificates and matched one control to each case. Health physicists estimated individual annual lung doses from occupational exposure primarily to insoluble uranium compounds, using contemporary monitoring data. With a 10 year lag, cumulative lung doses ranged from 0 to 137 centigrays (cGy) for cases and from 0 to 80 cGy for controls. Health physicists assigned annual external radiation doses to workers having personal monitor records. Archivists collected smoking information from occupational medical records. Odds ratios for lung cancer mortality for seven cumulative internal dose groups did not demonstrate increasing risk with increasing dose. We found an odds ratio of 2.0 for those exposed to 25 cGy and higher, but the 95% confidence interval of 0.20 to 20 showed great uncertainty in this estimate. There was a suggestion of an exposure effect for workers hired at age 45 years or older. Further analyses for cumulative external doses and exposures to thorium, radium and radon did not reveal any clear association between exposure and increased risk, nor did dichotomizing workers by facility.

Not given in the abstract above are the relative risks for total dose, 1.00 (0.86-1.09) or for internal irradiation only 1.01 (0.98-1.04), neither of which indicate an increased risk.

Thus, in common with the earlier assessments, this latest study does not find any clear association between increasing internal dose and lung cancer risk. Among these various assessments of worker exposure to uranium, whenever an estimate of risk is possible, e.g., in a small subset of the data, as noted above, the result is similar to that to be expected on the basis of the A-bomb survivor data. Consequently, while no sound estimate of risk can be derived from the limited epidemiological data available, there is no reason to assume that for exposure to uranium the risks derived from the A-bomb survivor study are not broadly applicable.

EXPOSURES AND DOSIMETRY AT FERNALD

Individual Exposure Scenarios

Nine different exposure scenarios involving different locations at Fernald and different specific representative individuals have been considered in this report. Scenarios 1, 2, and 3 feature primary locations within about 2 km from the center of the FMPC production area; scenarios 5, 7, and 9 are based on primary locations that are 8–10 km from the site; and scenarios 4, 6, and 8 are intermediate with respect to location, 3–4 km from the site. See Appendix J for details of all scenarios. (Note: Scenario dose information used for uranium, other radionuclides, and for radon is from Table K–2.)

Exposure and Dosimetry

Individuals in the scenarios listed above close to the Feed Materials Production Center (FMPC) at Fernald, Ohio, were exposed to a range of uranium, thorium, and radium radio-

nuclides (Appendix K, Figure K–1) by a variety of different pathways on the one hand, and to radon gas from the K–65 silos on the other hand. These two components are treated quite separately.

For the radionuclides of uranium, thorium and radium for each exposure situation (Appendix J), the absorbed dose (Gy) to each relevant organ from each radionuclide is estimated for each of the exposure pathways using dose conversion factors (Appendix K). The radiation components are categorized according to two distinct groups: (1) high LET radiations such as alpha particles and (2) low LET radiations such as beta particles, x-rays, and gamma rays. High LET radiations are more effective biologically (approximately 20 times) than low LET radiations. The equivalent dose (sievert) for each organ for each inhalation and ingestion pathway is determined by multiplying the high LET component of the absorbed dose by 20 and adding the low LET component of the absorbed dose to it. The total equivalent dose (sievert) for each organ is the sum of the equivalent doses (sievert) for all of the pathways for that organ.

Radon doses are calculated for each scenario as described in Appendix K. Because the alpha radiation is high LET the number of sieverts (equivalent dose) resulting from the number of grays (absorbed dose) is 20 times greater (ICRP 1991). The doses described so far are known as nominal doses, i.e., they are calculated without regard to the uncertainties involved. In Appendix K the uncertainties in dose conversion coefficients and other sources of error are discussed. For each scenario an uncertainty distribution is developed for the equivalent doses from both the uranium, thorium and radium radionuclides and the radon exposures.

For the lung the nominal, 5th, 50th and 95th percentile equivalent doses for the uranium, thorium and radium radionuclides are given in Table S–4 (taken from Table K–4) and for radon in Table S–9 (taken from Table K–5). Corresponding doses for the other relevant organs (bone Table S–5, kidney Table S–6, liver Table S–7, bone marrow Table S–8) for uranium, thorium and radium radionuclides are also taken from Table K-4.

Table S–4. Nominal and 5th, 50th and 95th Percentile Equivalent Doses to the Lungs from Uranium, Thorium and Radium Radionuclides

	Nominal equivalent	Percentiles of cumulative dose (Sv)		
Scenario	Dose (Sv)	5th	50th	95th
1	0.36	0.14	0.41	0.99
2	0.10	0.049	0.14	0.43
3	0.092	0.042	0.13	0.31
4	0.036	0.017	0.05	0.13
5	0.030	0.011	0.041	0.11
6	0.18	0.08	0.22	0.55
7	0.028	0.012	0.039	0.092
8	0.005	0.003	0.008	0.019
9	0.059	0.025	0.076	0.22

Table S–5. Nominal and 5th, 50th and 95th Percentile Equivalent Doses to the Bone from Uranium, Thorium and Radium Radionuclides

	Nominal equivalent	Percentiles of cumulative dose (Sv)		
Scenario	Dose (Sv)	5th	50th	95th
1	0.11	0.079	0.17	0.36
2	0.035	0.025	0.056	0.13
3	0.23	0.13	0.26	0.78
4	0.048	0.034	0.074	0.17
5	0.006	0.003	0.0095	0.026
6	0.058	0.043	0.097	0.22
7	0.012	0.009	0.016	0.030
8	0.001	0.0005	0.0011	0.0027
9	0.011	0.006	0.016	0.043

Table S–6. Nominal and 5th, 50th and 95th Percentile Equivalent Doses to the Kidney from Uranium, Thorium and Radium Radionuclides

	Nominal equivalent	Percentiles of cumulative dose (Sv)		
Scenario	Dose (Sv)	5th	50th	95th
1	0.012	0.007	0.017	0.039
2	0.005	0.003	0.007	0.015
3	0.042	0.023	0.045	0.14
4	0.0025	0.002	0.004	0.008
5	0.0003	0.0002	0.0005	0.0016
6	0.006	0.004	0.010	0.017
7	0.0009	0.001	0.0013	0.0023
8	0.0002	0.0001	0.00025	0.0007
9	0.0006	0.0003	0.0008	0.0024

Table S–7. Nominal and 5th, 50th and 95th Percentile Equivalent Doses to the Liver from Uranium, Thorium and Radium Radionuclides

	Nominal equivalent	Percentiles of cumulative dose (Sv)		
Scenario	dose (Sv)	5th	50th	95th
1	0.0019	0.0008	0.0022	0.0069
2	0.0013	0.0006	0.0016	0.0044
3	0.002	0.0011	0.0022	0.0066
4	0.0008	0.0004	0.0010	0.0030
5	0.0002	0.0001	0.0003	0.0012
6	0.001	0.0004	0.0012	0.0034
7	0.0002	0.0001	0.0003	0.0009
8	0.0001	0.00005	0.00017	0.00055
9	0.0003	0.0001	0.0004	0.002

Table S–8. Nominal and 5th, 50th and 95th Percentile Equivalent Doses to the Bone Marrow from Uranium, Thorium and Radium Radionuclides

Scenario	Nominal equivalent dose (Sv)	Percentiles of cumulative dose (Sv)		
		5th	50th	95th
1	0.013	0.008	0.020	0.044
2	0.0048	0.0035	0.008	0.018
3	0.040	0.023	0.044	0.13
4	0.0084	0.006	0.013	0.031
5	0.0009	0.0006	0.0015	0.0043
6	0.0068	0.0048	0.011	0.026
7	0.0016	0.0014	0.0022	0.0042
8	0.0003	0.0002	0.0004	0.001
9	0.0015	0.0009	0.0023	0.0064

Table S–9. Nominal and 5th, 50th and 95th Percentile Equivalent Doses to the Lung from Radon

Scenario	Nominal equivalent dose (Sv)	Percentiles of cumulative dose (Sv)		
		5th	50th	95th
1	3.0	0.98	3.6	14
2	3.0	0.98	3.6	13
3	2.1	0.89	2.6	9.8
4	1.2	0.4	1.5	7.2
5	0.32	0.11	0.42	1.9
6	2.0	0.53	2.2	9.2
7	0.27	0.12	0.38	1.5
8	0.38	0.095	0.42	2.2
9	0.57	0.18	0.84	4.8

Later, these distributions of uncertainties in equivalent dose will be combined with distributions of uncertainty in risk per unit dose to provide the uncertainties in overall risk for all nine scenarios.

The Most Important Organs Exposed to the Releases at Fernald

When the whole body is uniformly exposed to ionizing radiation, all the organs and tissues listed in Table S–2 are exposed equally (i.e., to the same nominal dose). However, it is more usual with radionuclide releases that some organs and tissues will be exposed more than others and indeed some, perhaps many, organs and tissues will receive essentially no exposure. In the case of the releases at Fernald, which are due mainly to radon and to isotopes of uranium and thorium (Appendix K, Figure K–1) relatively few organs and tissues are exposed. The seven most important exposed organs to consider are the lungs, bone surface, kidney, liver, bone marrow, testes, and ovaries. Exposures to other organs and

tissues by both inhalation and ingestion are minimal and they need not be considered for the purposes of this study (Table K–2). As we see later in this appendix, the risk of lung cancer dominates the risks as compared with other organs.

The choice of the most important organs to consider depends on several factors: (1) the organs with weighting factors (especially the highest weighting factors) in the ICRP system (ICRP 1991). When exposed, these organs will have the greatest fraction of the total cancer risk (namely bone marrow, colon, lung, and stomach). Exposure of the gonads (the ovaries and testes) determines the genetic risk. (2) the organs receiving the highest dose for a given intake via the inhalation route (for uranium) are the lungs, followed by kidney about 50 times less. Other organs are 100 times less or lower (ICRP 1995b). (3) the organs receiving the highest dose for a given intake via the ingestion route (for uranium) are bone, kidneys (about 3 times less), liver (about 8 times less), and bone marrow about (10 times less). Other organs are less still. For thorium, bone is highest, followed by kidney and liver almost 100 times less and all other organs lower doses still (ICRP 1995a). (4) any organ with a selectively high concentration for an incoming radionuclide in that organ. Kidney is such an organ when uranium exposure is involved, and uranium toxicity in the kidney must be considered (see Appendix R) as well as the radiological risk. For radon the lung is the principal organ irradiated; the exposure of all other organs is minimal (UNSCEAR 1994).

Among the seven organs selected for consideration, doses less than 10^{-4} Sv (0.1 mSv) will not be listed in this appendix, and risks will not be calculated for them. The doses are available in Appendix K, however. A dose of 10^{-4} Sv is chosen as a cut-off because among the organs most likely to get cancer, the highest risk (stomach) for a population of all ages is about 1×10^{-2} Sv^{-1} (Table S-2). Other organs have smaller risks. Thus, a dose of 10^{-4} Sv cannot produce a risk in any organ of more than about 1 in 1 million. This small risk is regarded by many authorities as negligible (for example, Food and Drug Administration (FDA 1979), EPA (1979), Travis et al. 1989).

The 50th percentile doses to the testes and the ovaries are at most about $1–2 \times 10^{-3}$ Sv in the nine scenarios (Table K–4). The risk of cancer in the ovaries is about 0.1×10^{-2} Sv^{-1} (Table S–2) and for the testes it is much lower. This means that the maximum risk of cancer in ovaries or testes after a dose of 10^{-3} Sv is 1.0×10^{-6}, i.e., 1 chance in 1 million. Consequently, as far as cancer induction is concerned, testes and ovary will not be considered further. However, the irradiation of the ovaries and testes in the young (less than age 30 on average) can give rise to hereditary (genetic) effects. The risk of such effects is 2.4×10^{-2} Sv^{-1} in young people [1.0×10^{-2} Sv^{-1} averaged over all generations, ICRP (1991)]. The risk of such hereditary effects after a dose of 10^{-3} Sv is 2.4×10^{-5} or about 2½ chances in 100,000, much smaller than all the other risks to be described later. Consequently, the testes and the ovaries will not be considered further for either cancer or genetic risk and will not be listed in Tables S–13A to S-21B.

Among the remaining organs, the doses to the lungs from the inhalation route and to the bone surfaces for the ingestion route are the largest. Nevertheless, doses and risks to the other three organs are included in the scenario evaluation in Tables S–13A to S–21B, provided the doses are above 10^{-4} Sv (0.1 mSv) as described above. Risks less than 10^{-5} will not be recorded in the tables for clarity in presentation.

The contributions to the total dose from the external gamma rays is small from all pathways except air (< 10^{-4} Sv, Table K–2). Only the air source of gamma rays is included in

the scenario evaluation Tables S–13A to S–21B. Median (50th percentile) doses for uranium and thorium, and for radon are used throughout these tables. Uncertainties in dose estimates and 50th percentile values are treated in Tables S–4 through S–9 and in more detail later.

The risks estimated as described above will be applied to determine the risks of cancer for hypothetical individuals in the exposure scenarios. First, however, it is necessary to consider whether adjustments for age and sex need to be made in order to obtain a better estimate of the true risk to individuals of known age and sex.

ADJUSTMENTS TO THE RISK FOR AGE AND SEX OF THE REPRESENTATIVE INDIVIDUALS IN THE NINE SCENARIOS

The scenarios refer to hypothetical individuals, all young at the start of exposure, who had different lengths and modes of exposure according to the assumptions made about their locations, lifestyles, and residence time. The risk of total cancer induction for an individual is known to depend on both age and sex. As can be seen from the data presented in Table S–2, risks for total cancer can vary with age by a factor of 10 from the youngest to the oldest. At young ages, males and females also differ for total cancer induction by about 50%. These features can be seen in Table S–10 from Sinclair 1992, based on the analysis of Land and Sinclair (1991).

Table S–10. Fatal Cancer Risk for Different Ages and Sex After Low Dose or Low Dose Rate Exposure[a] ($\times 10^{-2}$ Sv^{-1})

Age (years)	Male	Female	Average
0-19	8.1	12.8	10.4
20-64	3.2	4.2	3.7
65-90	0.8	0.9	0.9
0-90	4.2	5.8	5.0

[a] U.S. population, average of multiplicative and National Institutes of Health models (see text).

Similar age and sex dependencies have since been reported for the A-bomb data on total cancer updated to 1987 by UNSCEAR 1994, (Table 28) and for the A-bomb data updated to 1990 by Pierce et al. (1996). While it seems appropriate to consider applying age and sex corrections when the age and sex are known, it would be misleading to make these of too high precision because the data are not known in sufficient detail. For example, referring to Table S–10, males under 20 (8.1 x 10^{-2} Sv^{-1}) have 1.6 times the average risk for both sexes and all ages (5.0 x 10^{-2}), which are the numbers in the first column of Table S–2. Males over 20 should be considered to have a risk of 0.6 times (3.2 vs. 5.0 x 10^{-2} Sv^{-1}) the average risk. Females under 20 would have a risk of 2.5 times the average risk (12.8 vs. 5.0 x 10^{-2} Sv^{-1}) and over 20, 0.8 times the average risk (4.2 vs. 5.0 x 10^{-2} Sv^{-1}). The female to male risk for these ratios is about 1.5. Using these ratios for under 20 and over 20, male and female, is about as fine as it seems reasonable to refine the age and sex corrections.

Table S–10 and the discussion so far refer to total cancer induction. For individual tumors the age and sex response could be different and must be considered for each tumor

site, especially since some tumors are at sites which are unique to one or other sex. In the absence of specific information it will be assumed that the form of the response is similar to that for total cancer induction. The age and sex response for individual tumors is considered as follows.

Lung Cancer Risk

Dependence on age. The available evidence for lung cancer, especially recently in the LSS, i.e., for low-LET radiation, seems to describe a pattern quite different from that of all cancers taken together. First it is useful to note that in Land and Sinclair (1991, Table 9) there is little difference in the percentage weights of lung cancer in the three age groups 0–19, 20–60, and 65–90 (19%, 13%, 16% respectively) implying that the frequency of lung cancer is about the same fraction of the total risk in each age group. Therefore, at that point in time lung cancer appeared to have an age pattern similar to all cancers. Later information from the LSS shows a different picture. In an extensive discussion of the incidence of attributable lung cancers in the LSS, Thompson et al. (1994) find little dependence on age of exposure for lung cancers overall. For one histological type, squamous cell carcinoma, the risk is even found to increase with increasing age at exposure.

Following this evaluation of the incidence data, the 1994 UNSCEAR report (Annex A, Table 8, Part V) gives an absolute risk over the observation period for those less than 20y that is many times less than the risk for those over 20. The BEIR V Committee (NAS/NRC 1990) used a model that showed a similar difference. Even allowing for a much longer period of expression for the younger ages this implies a lifetime risk for young ages less than that at older ages. In the most recent LSS report (Pierce et al. 1996) this conclusion is reinforced, as the authors derive a negative coefficient with age at exposure for breast tumors and for all cancers, but a positive coefficient with age at exposure for lung tumors. The impact of this on the age dependence of the lifetime risk is less certain.

Until recently, corrections involving greater risk at younger ages were frequently recommended (e.g. 3:1, ICRP 1987) and according to Scott, Gilbert and Boecker (1993) were implicit in the BEIR IV (NAS/NRC 1988) model for constant relative risk. However the BEIR IV report states firmly (p. 49 & 50) that age at exposure did not affect the risk from radon exposure. In the more recent ICRP evaluation (ICRP 1993, p12) no distinction between the risks for children and for adults is made. In the most comprehensive recent evaluation of eleven studies of miners (Lubin et al. 1994) also found no clear relationship between age at first exposure and risk. This conclusion was reached despite the fact that in the Chinese study, 75% of the fatal cancers resulted from those exposed initially at less than 20 years.

It must be emphasized that information and data on radiation-induced lung cancer in young persons is scant for both low-LET and high-LET radiations. Consequently, whether or not those at younger ages are more or less susceptible to the risk of lung cancer must at present remain one of the largest uncertainties. It is compounded further by the influence of smoking which is difficult to separate out and clearly has a risk that inclines toward those at older ages and longer smoking histories. However, on the basis of current information, it seems appropriate to consider lung as an exception among the organs, with either very little effect of age at exposure on the lifetime risk or an age response that leans toward higher risk at older ages. In any event, in the case of either uranium and thorium or radon exposure and

lung cancer it seems inappropriate to apply a correction to the risk in favor of greater risks in the young. No correction on the basis of age at exposure will therefore be made either for uranium and thorium or for radon exposure.

Dependence on Sex. The lifetime risk for males and females for fatal lung tumors differ by less than a factor of 2 (1.8×10^{-2} Sv^{-1} vs 3.1×10^{-2} Sv^{-1}) according to UNSCEAR 1994 (Table 32). In the most recent report of the LSS (Pierce et al. 1996) the differences are still in favor of a greater risk for females but much smaller. The EAR per 10^4 PYSv is 1.61 (0.28, 3.16) for males and 1.79 (0.88, 2.85) for females so the difference is well within the confidence limits. The lifetime risks for those at age 30 are given as 1.6×10^{-2} Sv^{-1} for males and 1.9×10^{-2} Sv^{-1} for females.

Evidently, these differences are small and well within the uncertainties involved. They do not suggest that a correction needs to be made. Correspondingly, very limited evidence for female lung cancer after exposure to radon suggests at most minor differences from the male lung cancer risk (BEIR IV, NAS/NRC 1988, ICRP 1993, Lubin et al. 1994). Consequently, in the case of the Fernald scenarios no adjustment for sex will be made to the risk of lung cancer from exposures to uranium and thorium or to radon.

Bone Cancer Risk

Dependence on age. UNSCEAR 1994 (Annex A, Table 8, Part VI) gives an observed risk from the LSS (for low-LET radiation) for both incidence and mortality of 3 times for those under 20 vs. those over 20 and, therefore, an even larger ratio could be expected for the lifetime risk.

For high-LET radiation the principal information comes from exposure to the alpha particles of injected ^{224}Ra for the treatment of bone tuberculosis and ankylosing spondylitis. In one of the earliest analyses of the bone sarcomas induced by this radionuclide (Spiess and Mays 1970 and see also BEIR IV (NAS/NRC 1988) p207) juveniles and adults were analyzed separately; juveniles were found to have twice the risk of adults. In many subsequent analyses juveniles and adults were merged together but in a later analysis by Mays and Spiess 1983, they were once again separated. Mays and Spiess found the risk for juveniles to be 1.4 times those of adults [see Figure 4-6, BEIR IV (NAS/NRC 1988)] but BEIR IV comments that if dose protraction were taken into account in the life table analysis the difference between juveniles and adults would vanish. In yet another analysis that corrects for competing risks using a proportional hazards model (Chmelevsky et al. 1986) juveniles or adults were separated into different dose groups. Now, no difference was found for juveniles or adults (see Figure 4-7 BEIR IV NAS/NRC 1988). The BEIR IV Committee concludes that most, if not all, of the former differences between juveniles and adults was due to failure to take into account competing risk, loss to follow up and dose protraction. In the case of radium dial painters, the victims were all young women and the age range was not broad enough to make any conclusion about an age dependence of bone tumor induction.

The ^{224}Ra exposures described above are likely to be the best source of comparison for uranium in bone because they both expose the endosteal surface, and these show little age effect. Nonetheless, with the low-LET exposures showing an effect greater than 3 times for young vs. older it seems reasonable to apply a modest factor of 2 to the adult risk value, to obtain the risk in those under 20, i.e., the average risk for fatal bone tumors will be

multiplied by 1.41 for years exposed at under age 20 and by 0.71 for years exposed over age 20.

Dependence on Sex. For bone, the excess absolute risk after low-LET radiation over the observation period for males is about 3 times that of females (UNSCEAR 1994 Table 8 part VI) for both incidence and mortality. More recent data from the LSS (Pierce et al. 1996a) suggests a ratio of 0.12/0.05 or 2.4. In view of the fact that the period of expression in females is longer than in males the induced lifetime risk will be somewhat less different, perhaps down to about a factor of 2. For high-LET exposures (^{224}Ra) the data are less specific and show little dependence on the sex of the exposed person. In view of the relatively high risk ratio for males after low-LET radiation, a correction factor for the males of 1.41 times the average risk and for females 0.71 times the average risk is recommended.

Corrections for age and sex in the case of bone tumor risk could be regarded as quite definite for low LET radiation but more controversial for high LET radiation where the evidence of age and sex effects is much less clear.

On the assumption that the high LET information is scant and if it were more prolific it would show a similar age and sex effect to low LET radiation, corrections for age and sex are recommended. Thus, we will apply a factor of 1.41 x 1.41 (= 2.00) for males under 20, 1.00 (1.41 x 0.71) for males over 20 and for females under 20 and 0.50 (0.71 x 0.71) for females over 20. As it turns out, the bone tumor risk in the Fernald scenarios is small but applying the correction is believed to come closer to the true risk than not applying it, i.e., the uncertainty is reduced.

Liver Tumor Risk

Although corrections for both age and sex are recommended for the liver tumor risk in another context, exposure to plutonium (RAC 1997), the liver tumor risks in all scenarios at Fernald turn out to be too small to record. Consequently, no age or sex corrections will be applied.

Bone Marrow Risk

Dependence on age. In the exposure of bone marrow the age pattern for the excess absolute risk of leukemia after low-LET radiation (Pierce et al. 1996) is well known and different from some other cancers in that it is broadly U shaped. The sensitivity is high in the young, about 3 times that of the young adult and in the old is about 1½–2 times the young adult. UNSCEAR 1994 (Annex A, Table 8, Part XII) gives an observed risk (over the whole period of expression) of about 0.75 times for those under 20 vs those over 20.

For high-LET radiation the most important source of radiation induced leukemia is thorotrast (e.g., Andersson et al. 1993). The types of leukemia generated differ somewhat from the distribution of leukemias after low LET (e.g., there are more erythro-leukemias) and there are more induced cases of Hodgkin's lymphoma. The authors did not find any dependence on age at injection among the cases induced. Note that although liver tumors are induced in greater number (5 times or more) the risk of leukemia is actually higher because the dose to the bone marrow is much lower than to the liver.

In view of these sources of information, no age correction will be applied for the risk of leukemia induced by uranium and thorium in the bone marrow.

Dependence on sex. In the case of the bone marrow, the lifetime risks for leukemia in males after low-LET radiation, 1.3% Sv^{-1} (UNSCEAR 1994), is only 1.4 times that for females, 0.9% Sv^{-1}, and about the same in the latest report on the LSS (Pierce et al. 1996a). For high-LET radiation no sex difference was observed in the induction of leukemia by thorotrast. Given the uncertainties involved in all these estimates it is not considered appropriate to apply a sex correction factor for the risks in bone marrow.

Kidney Tumor Risk

Information on kidney risk is quite limited and no details of age dependence and sex dependence are directly available. A possible comparison with other urinary organs such as the bladder may be relevant. Information on the age and sex dependence of risk of a bladder tumor is also limited but some detail is provided in UNSCEAR 1994, Table 8, Part IX. The incidence data shows only a very small sex difference and a relatively large age effect in which the risk at age greater than 20 is greater than at age less than 20. For mortality data the sex difference is larger but the age difference smaller. Since the age data is in a direction different from that of all cancers the information cannot be regarded as definitive. In view of this state of affairs no age and sex corrections are recommended for kidney tumor risk. Fortunately, only 2 scenarios, 1 and 3, have a small identifiable risk of a kidney tumor.

Summary of Age and Sex Corrections for Different Tumor Sites

The corrections proposed are as in the following table. Only for bone tumor risk are corrections recommended. These adjustments in the case of bone apply only to the portion of the risk engendered by doses from uranium and thorium and not from radon.

Table S–11. Summary of Age and Sex Correction

Site	Age	Sex
Lung tumor risk	None	None
Bone tumor risk	<20, x 1.41	male x 1.41
	>20, x 0.71	female x 0.71
Liver tumor risk	None	None
Bone marrow (leukemia) risk	None	None
Kidney tumor risk	None	None

Procedure for Correction of Bone Tumor Risks for Age and Sex

For each scenario the birth date of the individual and the sex are the starting point. Exposures occurred between 1951 and 1988. The information on annual exposures to uranium and thorium during this period (from tables like Table K–3 for scenario 1) was divided into two parts, those while the individual was under age 20 and those over age 20. The fraction of the dose at under age 20 was multiplied by the relevant risk factor for the sex of the

individual, Table S–11 and added to the fraction of the dose received at over age 20, times its risk factor (Table S–11) to obtain the final net risk factor. The results of this procedure for the risk correction factors to be applied to bone tumor risk only are shown in Table S–12.

Table S–12. Summary of Age and Sex Corrections for Bone Tumor Risk in the Fernald Scenarios

Scenario	Birth date	Sex	Risk correction factor
1	1946	F	0.83
2	1951	M	1.65
3	1951	M	1.60
4	1960	F	0.96
5	1951	M	1.64
6	1946	F	0.84
7	1951	M	1.66
8	1970	M	1.77
9	1951	M	1.71

LIFETIME RISKS FOR THE INDIVIDUAL EXPOSURE SCENARIOS

The lifetime risks associated with a given equivalent dose to an organ resulting from exposure to uranium and radionuclides other than radon are taken from Table S–2 using the figures for a population of all ages for four of the seven most important organs: lungs, bone, liver, and bone marrow. For kidney the risk is not given in Table S–2, but it is determined separately from the A-bomb data as 0.08×10^{-2} Sv^{-1} (0.08% per sievert) as described earlier. Testes and ovaries are not included because the doses to them are less than $1^{-2} \times 10^{-3}$ Sv for all scenarios and both the cancer and genetic risks are very small. Doses less than 10^{-4} Sv cannot contribute a risk greater than 10^{-6} and are, therefore, not included. The uncertainties in any dose or risk estimate in this study are much greater than 10^{-4} Sv or 10^{-5} risk as will be seen later.

The risk of lung cancer for radon is taken to be 0.27×10^{-2} Sv^{-1} based on direct epidemiological data, i.e., the BEIR IV (NAS/NRC 1988) assessment of the epidemiological data and conversion factor to dose used by NCRP (NCRP 1984) (see text on page S5). The lifetime risks corresponding to the doses determined from the releases for each of scenarios 1–9 are determined in the same way. Adjustments have been made to the risk for sex and for age during exposure for the bone tumor risk only as explained in the previous section.

The complete method is outlined for scenario 1 as follows. The first step in evaluating the risk to individuals in scenario 1 is to add the equivalent doses for each pathway and obtain a total equivalent dose for each organ or tissue resulting from radionuclides other than radon. These additions are listed in Table K–2 as nominal values. Uncertainties in the doses are shown in Table K–4. They have been reproduced in this current report as Tables S–4 to S–8. These include the 5th, 50th, and 95th percentile values of the uncertainty distribution of doses for each organ and each scenario (from Table K–4). From these tables the 50th percentile values are entered in Tables S–13A to S–21A for the appropriate scenario of the appropriate organ. Radon is treated separately throughout. The equivalent dose from radon is

shown as the nominal values in Table S–9 obtained from Table K–2. The 5th, 50th, and 95th percentile values of the uncertainty distribution shown in Table S–9 were obtained from Table K–5. The 50th percentile values are entered in Tables 13–B to 21–B. Doses less than 10^{-4} Sv (10^{-1} mSv) are not included, but if needed they can be found in Appendix K, Table K–2. Table S–13B shows that the exposure of the lung from airborne particulates and from radon is the most important exposure component for this scenario.

In Table S–13A, the second column lists the relevant risk factors (from Table S–2 or for kidney from the text) for an average member of the public. These risk factors are used to multiply the 50th percentile equivalent doses given in column 3 (from Tables S–4 to S–8) to give the risk for that organ in the fourth column. The adjustment factor to the risk for age and sex in the case of bone tumors is given in the fifth column, and the adjusted values of the risk in the final, sixth column. The risks can now be added for each organ to obtain the total risk for the whole body.

In Table S–13B, the second column lists the risk factor for radon, viz. 0.27×10^{-2} Sv^{-1}, the 50th percentile radon equivalent dose is listed in the third column, and the average risk associated with it is listed in the fourth column. The adjustment factor to the risk for age or sex is 1.00 so no column is required for it. The fifth column repeats the risk from uranium and thorium from Table S–13A. The last (sixth) column gives the total risk of lung cancer, of other tissues and of all cancers.

In scenario 1, the total probability of any fatal cancer is found to be 1.34×10^{-2} (1.34%) for all sources. Most of this risk is to the lung (1.32×10^{-2} or 1.32%). Only 0.02×10^{-2} (0.02%) is due to risk in organs other than the lung. Radon is the most important radiation source contributing 0.97×10^{-2} or 74% of the risk to the lung for this scenario.

The calculations for scenarios 2–9 are conducted in exactly the same way as for scenario 1, as shown in detail in Tables S–14A through S–21B.

Table S–13A. Scenario 1: Lifetime Risks for Each Organ and for Total Cancer (U + Th)

	Sources other than radon				
Organ or tissue	Probability of fatal cancer x 10^{-2} Sv^{-1} (Table S-2)	50th percentile equivalent dose (Sv) (Tables S-4 to S-8)	Lifetime risk of fatal cancer x 10^{-2}	Adjustment factor for age and sex	Adjusted lifetime risk x 10^{-2}
Lungs	0.85	0.41	0.3490	1.0	0.3490
Bone	0.05	0.17	0.0085	0.83	0.0070
Kidney	0.08	0.017	0.0014	1.0	0.0014
Liver	0.15	0.0022	0.0003	1.0	0.0003
Bone marrow	0.50	0.020	0.0100	1.0	0.0100
Total	-	-	-	-	0.3677

Table S–13B. Scenario 1: Lifetime Risks from Radon and All Sources

	Radon			Other	All Sources
Organ or tissue	Probability of fatal cancer x 10^{-2} Sv^{-1}	50th percentile equivalent dose (Sv) (Table S-9)	Lifetime risk x 10^{-2}	(U+Th) risk x 10^{-2}	Total risk x 10^{-2}
Lungs	0.27	3.6	0.972	0.349	1.321
Other tissues	-	-	-	0.019	0.019
All cancer	-	-	0.972	0.368	1.34

Table S–14A. Scenario 2: Lifetime Risks for Each Organ and for Total Cancer (U + Th)

	Sources other than radon				
Organ or tissue	Probability of fatal cancer x 10^{-2} Sv^{-1} (Table S-2)	50th percentile equivalent dose (Sv) (Tables S-4 to S-8)	Lifetime risk of fatal cancer x 10^{-2}	Adjustment factor for age and sex	Adjusted lifetime risk x 10^{-2}
Lungs	0.85	0.14	0.1190	1.00	0.1190
Bone	0.05	0.056	0.0028	1.65	0.0046
Kidney	0.08	0.007	0.0006	1.00	0.0006
Liver	0.15	0.0016	0.0002	1.00	0.0002
Bone marrow	0.50	0.008	0.0040	1.00	0.0040
Total	-	-	-	-	0.1284

Table S–14B. Scenario 2: Lifetime Risks from Radon and All Sources

	Radon			Other	All Sources
Organ or tissue	Probability of fatal cancer x 10^{-2} Sv^{-1}	50th percentile equivalent dose Sv (Table S-9)	Lifetime risk x 10^{-2}	(U+Th) risk x 10^{-2}	Total risk x 10^{-2}
Lungs	0.27	3.6	0.972	0.119	1.091
Other tissues	-	-	-	0.009	0.009
All cancer	-	-	-	0.128	1.100

Table S–15A Scenario 3: Lifetime Risks for Each Organ and for Total Cancer (U + Th)

	Sources other than radon				
Organ or tissue	Probability of fatal cancer x 10^{-2} Sv^{-1} (Table S-2)	50th percentile equivalent dose (Sv) (Tables S-4 to S-8)	Lifetime risk of fatal cancer x 10^{-2}	Adjustment factor for age and sex	Adjusted lifetime risk x 10^{-2}
Lungs	0.85	0.13	0.1105	1.0	0.1105
Bone	0.05	0.26	0.0130	1.60	0.0208
Kidney	0.08	0.045	0.0036	1.0	0.0036
Liver	0.15	0.0022	0.0003	1.0	0.0003
Bone marrow	0.50	0.044	0.0220	1.0	0.0220
Total	-	-	-	-	0.1572

Table S–15B. Scenario 3: Lifetime Risks from Radon and All Sources

	Radon			Other	All Sources
Organ or tissue	Probability of fatal cancer x 10^{-2} Sv^{-1}	50th percentile equivalent dose Sv (Table S-9)	Lifetime risk x 10^{-2}	(U+Th) risk x 10^{-2}	Total risk x 10^{-2}
Lungs	0.27	0.26	0.702	0.1105	0.813
Other tissues	-	-	-	0.047	0.047
All cancer	-	-	-	0.157	0.860

Table S–16A. Scenario 4: Lifetime Risks for Each Organ and for Total Cancer (U + Th)

	Sources other than radon				
Organ or tissue	Probability of fatal cancer x 10^{-2} Sv^{-1} (Table S-2)	50th percentile equivalent dose (Sv) (Tables S-4 to S-8)	Lifetime risk of fatal cancer x 10^{-2}	Adjustment factor for age and sex	Adjusted lifetime risk x 10^{-2}
Lungs	0.85	0.05	0.0425	1.0	0.0425
Bone surface	0.05	0.074	0.0037	0.96	0.0036
Kidney	0.08	0.004	0.0003	1.0	0.0003
Liver	0.15	0.001	0.0002	1.0	0.0002
Bone marrow	0.50	0.013	0.0065	1.0	0.0065
Total	-	-	-	-	0.0531

Table S–16B. Scenario 4: Lifetime Risks from Radon and All Sources

	Radon			Other	All Sources
Organ or tissue	Probability of fatal cancer x 10^{-2} Sv^{-1}	50th percentile equivalent dose Sv (Table S-9)	Lifetime risk x 10^{-2}	(U+Th) risk x 10^{-2}	Total risk x 10^{-2}
Lungs	0.27	1.5	0.405	0.043	0.448
Other tissues	-	-	-	0.011	0.011
All cancer	-	-	0.405	0.054	0.459

Table S–17A Scenario 5: Lifetime Risks for Each Organ and for Total Cancer (U + Th)

	Sources other than radon				
Organ or tissue	Probability of fatal cancer x 10^{-2} Sv^{-1} (Table S-2)	50th percentile equivalent dose (Sv) (Tables S-4 to S-8)	Lifetime risk of fatal cancer x 10^{-2}	Adjustment factor for age and sex	Adjusted lifetime risk x 10^{-2}
Lungs	0.85	0.041	0.0349	1.0	0.0349
Bone surface	0.05	0.0095	0.0005	1.64	0.0008
Kidney	0.08	0.0005	-	1.0	-
Liver	0.15	0.0003	-	1.0	-
Bone marrow	0.50	0.0015	0.0008	1.0	0.0008
Total	-	-	-	-	0.0365

Table S–17B. Scenario 5: Lifetime Risks from Radon and All Sources

	Radon			Other	All Sources
Organ or tissue	Probability of fatal cancer x 10^{-2} Sv^{-1}	50th percentile equivalent dose Sv (Table S-9)	Lifetime risk x 10^{-2}	(U+Th) risk x 10^{-2}	Total risk x 10^{-2}
Lungs	0.27	0.42	0.113	0.035	0.148
Other tissues	-	-	-	-	-
All cancer	-	-	0.113	0.035	0.148

Table S–18A. Scenario 6: Lifetime Risks for Each Organ and for Total Cancer (U + Th)

	Sources other than radon				
Organ or tissue	Probability of fatal cancer x 10^{-2} Sv^{-1} (Table S-2)	50th percentile equivalent dose (Sv) (Tables S-4 to S-8)	Lifetime risk of fatal cancer x 10^{-2}	Adjustment factor for age and sex	Adjusted lifetime risk x 10^{-2}
Lungs	0.85	0.22	0.1870	1.0	0.1870
Bone surface	0.05	0.097	0.0049	0.84	0.0041
Kidney	0.08	0.010	0.0008	1.0	0.0008
Liver	0.15	0.0012	0.0002	1.0	0.0002
Bone marrow	0.50	0.0110	0.0055	1.0	0.0055
Total	-	-	-	-	0.1976

Table S–18B. Scenario 6: Lifetime Risks from Radon and All Sources

	Radon			Other	All Sources
Organ or tissue	Probability of fatal cancer x 10^{-2} Sv^{-1}	50th percentile equivalent dose Sv (Table S-9)	Lifetime risk x 10^{-2}	(U+Th) risk x 10^{-2}	Total risk x 10^{-2}
Lungs	0.27	2.2	0.594	0.187	0.781
Other tissues	-	-	-	0.011	0.011
All cancer	-	-	0.594	0.198	0.792

Table S–19A. Scenario 7: Lifetime Risks for Each Organ and for Total Cancer (U + Th)

	Sources other than radon				
Organ or tissue	Probability of fatal cancer x 10^{-2} Sv^{-1} (Table S-2)	50th percentile equivalent dose (Sv) (Tables S-4 to S-8)	Lifetime risk of fatal cancer x 10^{-2}	Adjustment factor for age and sex	Adjusted lifetime risk x 10^{-2}
Lungs	0.85	0.039	0.0332	1.0	0.0332
Bone surface	0.05	0.016	0.0008	1.66	0.0013
Kidney	0.08	0.0013	0.0001	1.0	0.0001
Liver	0.15	0.0003	-	-	-
Bone marrow	0.50	0.0022	0.0001	1.0	0.0011
Total	-	-	-	-	0.0357

Table S–19B. Scenario 7: Lifetime Risks from Radon and All Sources

	Radon			Other	All Sources
Organ or tissue	Probability of fatal cancer x 10^{-2} Sv^{-a}	50th percentile equivalent dose Sv (Table S-9)	Lifetime risk x 10^{-2}	(U+Th) risk x 10^{-2}	Total risk x 10^{-2}
Lungs	0.27	0.38	0.103	0.033	0.136
Other tissues	-	-	-	0.003	0.003
All cancer	-	0.38	0.103	0.036	0.139

Table S–20A. Scenario 8: Lifetime Risks for Each Organ and for Total Cancer (U + Th)

	Sources other than radon				
Organ or tissue	Probability of fatal cancer x 10^{-2} Sv^{-1} (Table S-2)	50th percentile equivalent dose (Sv) (Tables S-4 to S-8)	Lifetime risk of fatal cancer x 10^{-2}	Adjustment factor for age and sex	Adjusted lifetime risk x 10^{-2}
Lungs	0.85	0.0080	0.0068	1.0	0.0068
Bone surface	0.05	0.0011	0.0001	1.77	0.0002
Kidney	0.08	0.0003	-	-	-
Liver	0.15	0.0002	-	-	-
Bone marrow	0.50	0.0004	0.0002	1.0	0.0002
Total	-	-	-	-	0.0072

Table S–20B. Scenario 8: Lifetime Risks from Radon and All Sources

	Radon			Other	All Sources
Organ or tissue	Probability of fatal cancer x 10^{-2} Sv^{-1}	50th percentile equivalent dose Sv (Table S-9)	Lifetime risk x 10^{-2}	(U+Th) risk x 10^{-2}	Total risk x 10^{-2}
Lungs	0.27	0.42	0.113	0.007	0.120
Other tissues	-	-	-	-	-
All cancer	-	0.42	0.113	0.007	0.120

Table S–21A. Scenario 9: Lifetime Risks for Each Organ and for Total Cancer (U + Th)

	Sources other than radon				
Organ or tissue	Probability of fatal cancer x 10^{-2} Sv^{-1} (Table S-2)	50th percentile equivalent dose (Sv) (Tables S-4 to S-8)	Lifetime risk of fatal cancer x 10^{-2}	Adjustment factor for age and sex	Adjusted lifetime risk x 10^{-2}
Lungs	0.85	0.076	0.0646	1.0	0.0646
Bone surface	0.05	0.016	0.0008	1.71	0.0014
Kidney	0.08	0.0008	0.0001	-	0.0001
Liver	0.15	0.0004	0.0001	-	0.0001
Bone marrow	0.50	0.0023	0.0012	-	0.0012
Total	-	-	-	-	0.0674

Table S–21B. Scenario 9: Lifetime Risks from Radon and All Sources

	Radon			Other	All Sources
Organ or tissue	Probability of fatal cancer x 10^{-2} Sv^{-1}	50th percentile equivalent dose Sv (Table S-9)	Lifetime risk x 10^{-2}	(U+Th) risk x 10^{-2}	Total risk x 10^{-2}
Lungs	0.27	0.84	0.227	0.065	0.292
Other tissues	-	-	-	0.003	0.003
All cancer	-	0.84	0.227	0.068	0.295

Summary of Risks of Cancer Derived for Each Scenario

Table S–22 summarizes results for lung cancer and total cancer for all nine scenarios. The risk for all cancers is shown in the last column and ranges from 0.12 × 10^{-2}, i.e., 0.12%, to 1.34 × 10^{-2} or 1.34%. The risk of cancer of the lung dominates all other risks. Risks in organs other than lung do not exceed 5% of the total risk and mostly are 2% or less. For the lung, radon is always the principal source; other sources contribute about 6%–32% of the total lung cancer risk, depending on the scenario.

Table S–22. Risk of Fatal Cancer Estimated for Each Scenario Based on 50th Percentile Doses

	Risk of lung cancer (x 10^{-2})			Risk of cancer in other organs (x 10^{-2})	Total
Scenario	Sources[a] other than radon	Radon	Total	Sources other than radon	cancer risk (x 10^{-2})
1	0.349	0.972	1.321	0.019	1.340
2	0.119	0.972	1.091	0.009	1.100
3	0.111	0.702	0.813	0.047	0.860
4	0.043	0.405	0.448	0.011	0.459
5	0.035	0.113	0.148	-	0.148
6	0.187	0.594	0.781	0.011	0.792
7	0.033	0.103	0.136	0.003	0.139
8	0.007	0.113	0.120	-	0.120
9	0.065	0.227	0.292	0.003	0.295

[a] Radionuclides, especially uranium and thorium, see Appendix K, Figure K-1.

UNCERTAINTIES IN ESTIMATES OF FATAL CANCER RISKS FOR THE EXPOSURE SCENARIOS AT FERNALD

The estimation of risks involves uncertainties in each of the parameters involved in the estimation. When the risk estimates come from a single source it is usually possible to analyze the steps in the derivation of the risk estimate and assign uncertainty values (e.g., 5 to 95% confidence limits) to each of the parameters involved.

In the evaluation of doses and risks to hypothetical individuals in the various exposure scenarios at Fernald, it is evident that two distinctly different sources are responsible for the exposures. One source is the mainly uranium and thorium radionuclides (and their decay products) released from the site to the air, water, and soil in the vicinity of Fernald (Figure K–1). The other is due to radon released or escaping from the K–65 silos. With regard to uncertainties these two sources will be treated separately because it is apparent that entirely different considerations enter into the uncertainties concerned with the risk per unit dose in each case. Thus, we will in each case discuss each source of uncertainty and combine them to obtain the uncertainty distributions for risk per unit dose for each scenario. Then we will combine the resulting distributions for each scenario with the uncertainty distributions for dose (Tables S–4 and S–9 and Tables K–4 and K–5). These combinations become the uncertainty distributions for risk in the two cases.

Finally, the risk distribution for U + Th and for radon are combined to yield a final distribution of uncertainties for all exposure scenarios at Fernald. In these uncertainties, the only endpoint addressed is cancer of the lung. Since it makes up 98% of the risk in most cases the matter of uncertainties in the contribution of the risk in the other tissues can essentially be ignored.

Uranium and Thorium Radionuclides

A list of the radionuclides comprising this source of exposure is given in Appendix K, Figure K–1. The doses to selected organs of individuals in the risk scenarios are given in Table K–2. The methodology for obtaining these doses is described in Appendices I and K. The uncertainties in these dose estimates are also calculated and 5th, 50th, and 95th percentile values of the possible dose given for each of the organs in each of the scenarios given in Table K–4 and in Tables S–4 to S–8. In the case of the lung (Table S–4), the doses for which dominate all other organ doses, the 5%–95% values range from about 0.33 to 3 times the median value but are scenario dependent. In the following section, the actual uncertainty values for the lung dose are combined with uncertainties in risk per unit dose. One important factor is not included, so far, in this estimate of uncertainty in the equivalent dose. This is the uncertainty in the RBE value used to account for the high LET component of the dose. For most of the scenarios, this high LET component accounts for 90–95% of the total equivalent dose to the lung when a RBE of 20 is used. The RBE almost certainly depends on which organ is involved in the effect and for some organs like bone marrow the RBE for leukemia induction may be quite low, in the range of 1–3 rather than 20 (e.g., Andersson et al. 1993).

There may also be quite high RBE values for induced cancer in the lung in some animal studies, with an RBE of 30 or so (NCRP 1990, NRPB 1993). The average of many studies summarized in NRPB (1993) is about 20, and for the lung a broad range for all species of animal of 6 to 40 is given. Recent Russian studies of plutonium workers (Hohryakov and Romanov 1994) are within a factor of two of the ICRP estimated risks for lung cancer, suggesting that the RBE of 20 is probably quite good for lung cancer in humans given other important uncertainties such as the dose and dose rate effectiveness factor. For cancer induction in the lung, the RBE value of 20 is probably uncertain from at least 10 to 40, i.e., from 0.5 to 2.0 times the nominal value. This uncertainty is included in the risk per unit dose group (Table S-23).

The risk per unit dose for the lung from uranium and thorium radionuclides is determined from the data on the A-bomb survivors, i.e., the LSS (Shimizu et al. 1988, 1990). For uncertainties in the risk of all fatal cancer in the LSS, an analysis is available by the NCRP (NCRP 1997). This analysis considers (a) uncertainties and biases in the epidemiological data, (b) various sources of potential error in the dosimetry, including uncertainties in the magnitude and RBE of the neutron component, (c) uncertainty in the transfer between populations, (d) uncertainty in the projection to lifetime risk, and (e) uncertainty in the correction for dose and dose rate effectiveness. When combined, these uncertainties yield an uncertainty distribution with 5th and 95th percentiles at about a factor of 3 below and above the 50th percentile value of the risk. Thus, the 90% confidence interval for the nominal value 5×10^{-2} Sv^{-1} (5% per Sv) ranges from about 1.2×10^{-2} Sv^{-2} (1.2% per Sv) to 8.8×10^{-2} Sv^{-1} (8.8% per Sv). The uncertainty in the risk for individual tumor sites (Table S–2) are likely to be considerably greater, especially for some sites, but they have not been separately evaluated and published as yet.

To use this NCRP analysis we need to consider the extent to which the various factors used in the derivation for uncertainties in total cancer are applicable to lung cancer specifically. Obviously, the epidemiological results are less certain for a single organ such as lung than for total cancer. The excess absolute risk for lung is given by Shimizu et al. (1988, 1990) as 1.68 (0.97-2.49) i.e., a multiplicative range of (0.58 to 1.48) about the central value,

which is broader than the range (0.75-1.25) for total cancer. [Note: more recently a similar range for lung is given by Ron et al. (1994) for data to 1987 namely 1.9 (1.0-2.9), i.e., a range of 0.52-1.52 about the central value]. The other factors involved in the NCRP derivation of uncertainties (dosimetry, transfer, projection, and dose rate correction factors) are probably not very different for lung than for total cancer and constitute the third entry in Table S–23.

Table S–23 summarizes the features of these last three uncertainty distributions. To evaluate the overall uncertainty distribution (the product of these three distributions) Monte Carlo calculations were performed using the Crystal Ball® computer program (Decisioneering 1993). The last column of Table S–23 shows the assumed forms of distributions for these calculations. Each distribution was modeled by a lognormal distribution with the values for the geometric mean (GM) and geometric standard deviation (GSD) shown. The results of the calculations involving these three uncertainties are summarized at the bottom of Table S–23. The product distribution was found to have a median of 1.0 with 5th and 95th percentile values of 0.33 and 2.6, respectively.

Table S–23. Components of Uncertainties in Risks (per 50th percentile dose) from Uranium and Thorium Radionuclides

Source of uncertainty	5th percentile	95th percentile	Parameters of distribution
Uncertainty in RBE	0.5	2.0	Lognormal GM = 1.0, GSD = 1.52
Uncertainty in epidemiological statistics	0.5	1.5	Lognormal GM = 1.0, GSD = 1.28
Uncertainty in other components of risk derivation	0.5	2	Lognormal GM = 1.0, GSD = 1.52
Combined	0.33	2.6	50th percentile 1.0

Because the lung cancer risk totally dominates and the other cancers have similar uncertainties in dose (Table K-4), we will treat all cancer induced by uranium and thorium alike and the same as lung cancer.

The next step in the estimation of risk and its uncertainties for the uranium and thorium radionuclides involves combining the results of risks for the 50th percentile doses for each scenario (Table S–23) with the dose values for lung and their uncertainties in Table S-4 and Table K-4. (The nominal values and 50th percentile values are quite similar, varying only a little from scenario to scenario.) The combined results for risk and uncertainty (from all sources) for each scenario for uranium and thorium radionuclides are given in Table S–24.

Table S–24. Risks and Uncertainties from all Sources for Lung Cancer from Uranium and Thorium Radionuclides

	Lung cancer risks from uranium and thorium x 10^{-2}					
	Nominal values of	Percentiles				
Scenario	risk	5th	25th	50th	75th	95th
1	0.3	0.079	0.2	0.37	0.69	1.8
2	0.085	0.025	0.065	0.11	0.22	0.48
3	0.076	0.025	0.053	0.11	0.21	0.44
4	0.03	0.0067	0.018	0.038	0.078	0.17
5	0.025	0.0068	0.016	0.03	0.061	0.15
6	0.15	0.042	0.1	0.19	0.37	0.83
7	0.023	0.0067	0.016	0.032	0.06	0.13
8	0.0043	0.0012	0.0027	0.0058	0.012	0.025
9	0.49	0.012	0.036	0.065	0.13	0.27

The distribution of Table S–24 has an average 50th percentile value 1.02 times the nominal value. For scenario 1, the 50th percentile value of risk is 0.37×10^{-2}, the 5th percentile is 0.079×10^{-2}, and the 95th percentile is 1.8×10^{-2}, for uranium and thorium radionuclides.

Radon

The consideration of uncertainties in radon risk are quite different because radon risks are derived directly from human exposure to radon in uranium and other mines. The BEIR IV Committee gives an extensive discussion of the many factors that produce uncertainty in radon risk estimates but not all the factors are quantitated. A more comprehensive list is given by Lubin et al. (1994), see page 109; however, very few quantitative assignments are made for each of these uncertainties and no overall derivation is made, or possible from the information supplied. Puskin (1992) considers a more limited range of factors, but these are analyzed quantitatively. He concludes that the range of 5%–95% values is about 0.5 to 4 times the median value. However, he also states very clearly those uncertainties that he has not been able to quantitate.

In this analysis we have considered the BEIR IV discussion in detail to try to estimate from it reasonable values of the uncertainties in their risk/exposure conversion factor for the major components because it is the BEIR IV risk per unit exposure that is are used in this text. First, the statistical uncertainties in the analysis of the four main studies of miners are considered. These give a 5%–95% range of 0.59 times to 1.7 times (BEIR IV, page 41). They also discussed the dosimetry involved in the determination of risk per unit exposure but did not assign a figure to uncertainty. Partly by analogy with the detailed work done on dosimetry for the A-bomb survivors (NCRP 1997), a range of 0.71 times to 1.4 times the central value was assigned by us for dosimetry in relation to the calibration factor. The BEIR IV report then discusses modeling especially in relation to smoking and concludes that between the 5%–95% level there is a factor of 4 uncertainty (BEIR IV, page 47), which is

interpreted to mean 0.5 times to 2 times the central value. Temporal uncertainties might also be included. Other sources of uncertainty include sex and age (the population of miners were all males), conversion factors, exposure (WLM) to dose (Sv), correcting for the mining environment to the home environment, breathing rates, equilibrium factors, etc. another range of 0.5 times to 2 times the central value. Thus, we have the following group of factors in Table S–25.

Table S–25. Components of Uncertainty in the Risks Per Unit Exposure from Radon[a]

Source of uncertainty	5th percentile	95th percentile	Parameters of distribution
Uncertainty in statistics	0.59	1.7	Lognormal GM = 1.0, GSD = 1.38
Uncertainty in dosimetry of the dose per unit exposure	0.71	1.4	Lognormal GM = 1.0, GSD = 1.23
Uncertainty in modeling and smoking	0.5	2	Lognormal GM = 1.0, GSD = 1.52
Uncertainty in other factors (including age, sex, home environment, conversion factors)	0.5	2	Lognormal GM = 1.0, GSD = 1.52
Combined	0.33	3.3	50th percentile 1.0

[a] That is, the uncertainties in the BEIR IV conversion factor for risk per unit exposure *viz.* 350 excess lung cancer deaths per 10^6 people per WLM in a lifetime.

To determine the overall uncertainty distribution of the product of these factors, Monte Carlo calculations were performed using the Crystal Ball computer program (Decisioneering 1993). Because all four distributions were asymmetric, all were treated as lognormal distributions with the parameters shown in the last column of Table S–25.

It is useful to note that the range for the risk of radon-induced cancer (0.33 to 3.3) is from about 100 cancers per 10^6 people per WLM to 1200 cancers for 10^6 people per WLM about a nominal central BEIR IV value of 350 cancers per 10^6 per WLM. All the known assessments, from NCRP (130 cancers per 10^6 per WLM) to UNSCEAR, ICRP, and BEIR III (730 cancers per 10^6 per WLM) fit within this range (see Table S–3). The estimate of lung cancer risk from the LSS of the A-bomb survivors would correspond to about 1100 cancer deaths per 10^6 people per WLM and also fits within the range of uncertainty. Puskin's range is 0.5 times to 4 times the central value, even broader on the high side.

The combined uncertainty in these factors and risks must now be combined with the estimates of uncertainty in radon dose. These are somewhat greater for radon than for uranium and thorium and are given in Table S–9 and in Appendix K, Table K–5 in more detail. Examination of this table shows that the 5th–95th percentile values are about 0.33 to 3 times the median value and somewhat scenario dependent, but the 50th percentile values are always 20%–30% higher than the nominal values. The resulting combined distributions for the risk from radon for each scenario are shown in Table S–26.

Table S–26. Risks and Uncertainties from all Sources for Lung Cancer from Radon

	Risks from radon x 10^{-2}					
	Nominal	Percentiles				
Scenarios	values of risk	5th	25th	50th	75th	95th
1	0.81	0.096	0.41	0.87	1.9	8.3
2	0.81	0.11	0.4	0.94	1	6.4
3	0.57	0.1	0.33	0.67	1.2	4.7
4	0.32	0.055	0.17	0.35	1	2.7
5	0.086	0.015	0.05	0.099	0.27	0.78
6	0.54	0.078	0.21	0.54	1.3	3.7
7	0.073	0.015	0.048	0.1	0.22	0.86
8	0.1	0.018	0.043	0.1	0.24	1.1
9	0.15	0.022	0.093	0.2	0.48	2.3

Risk and Uncertainty for All Radiation Sources at Fernald

The risks and uncertainties from uranium and thorium (Table S–24) are combined with those from radon (Table S–26) to obtain final uncertainty values in the total risk as in Table S–27 using the Monte Carlo calculations by Crystal Ball. The largest risks are for scenario 1. The 50th percentile is 1.3 x 10^{-2} (1.3%), the 95th percentile is 9.6 x 10^{-2} (9.6%) and the 5th percentile 0.24 x 10^{-th} (0.24%), lifetime. The range of risk in most of the scenarios is a factor of 30-50 for the 5th to the 95th percentile.

Table S–27. Risks of Lung Cancer and Uncertainties in Risks from All Radiation Sources at Fernald

	Risks x 10^{-2}					
	Nominal	Percentiles				
Scenarios	values of risk	5th	25th	50th	75th	95th
1	1.1	0.24	0.7	1.3	2.5	9.6
2	0.9	0.18	0.51	1	2.2	6.8
3	0.65	0.15	0.41	0.8	1.4	4.9
4	0.35	0.08	0.23	0.41	1.1	2.9
5	0.11	0.025	0.075	0.16	0.32	0.9
6	0.69	0.15	0.38	0.75	1.6	4.2
7	0.096	0.026	0.072	0.15	0.28	1
8	0.1	0.02	0.047	0.11	0.26	1.1
9	0.2	0.046	0.14	0.31	0.59	2.5

The Effect of Smoking on Radiation Risk to the Lung

Radon. The largest component of the exposures at Fernald was from radon. Smoking and radon as separate causes of lung cancer may also interact to make smokers more likely to be at risk of lung cancer from radon exposure. The BEIR IV Committee (NAS/NRC 1988) recognized that smoking and radon exposure combine multiplicatively (or nearly so) on a relative risk scale. However, in order to make an adjustment in the absolute risk because of smoking vs nonsmoking it is necessary to have an absolute risk comparison. Lubin et al. (1994) note that smoking may not modify the effect of exposure to radon to the extent previously thought (Summary pXVI). They believe that current risk estimates for lung cancer caused by indoor radon assume a multiplicative interaction with smoking which may overestimate the risk for smokers and underestimate the risk for nonsmokers (p5). The relative risks of radon induced lung cancer in never smokers is found to be of the order of 3 times that for smokers, 1.03% (0.2%, 5.7%) for nonsmokers vs 0.34% (0.1%, 1.5%) for smokers. (Lubin et al. p103). The absolute risks, however, are clearly greater in smokers. Lubin et al. (1994, Table 28, p105) give two estimates of the absolute risk per WLM for smokers vs nonsmokers using first a joint multiplicative relationship for Rn progeny and smoking and second by applying a smoking adjustment to the risk models, multiplying the baseline ERR/WLM by 0.9 for smokers and 3.0 for never smokers. The latter procedure, which is preferred, gives 9800 lung cancer deaths attributable to radon in smokers in a total of 104,300 lung cancer deaths and 4700 lung cancer deaths attributable to radon in nonsmokers. This is a ratio of 2.1 to 1, or about a factor of 2, for the ratio between the absolute risk of radon-induced cancer in smokers vs. nonsmokers. (Note also that evaluations of the contribution of smoking to radon-induced cancer in miners are confounded by the presence of potentially carcinogenic agents such as arsenic, silica and diesel fumes, since the contribution of these sources may be very difficult to ascertain).

Uranium, Thorium and Radium Radionuclides. Our estimate of lung cancer risk is derived from the Lifespan Study of the A-bomb survivors and based on a population of all ages, including smokers and nonsmokers. An RBE of 20 is used to account for the effectiveness of alpha particle doses. There is no reason to suppose that the effects of smoking would be different (for these particles) from those for radon, i.e., smokers having about twice the absolute risk of nonsmokers for the same radon concentration.

In the Fernald scenarios 1–9 no smoking status was assigned. All of the nominal subjects chosen were young and may have experienced much of their exposure as nonsmokers. However, to obtain a maximum possible risk for smokers the lung cancer risks (of Table S–27) can be multiplied by 1.41. To obtain a minimum possible risk for nonsmokers the lung cancer risks of Table S–27 can be multiplied by 0.71. This increases the maximum lung cancer risk in a smoker in scenario 1 at the 95th percentile to 13.5% while for a nonsmoker the scenario 1 risk at the 95th percentile is 6.8%. At the 5th percentile the risk for a smoker is 0.34% and for a nonsmoker it is 0.17%. The 50th percentile values of risk are 1.8% for a smoker and 0.92% for a non-smoker. The procedure to obtain separate risks for smokers and nonsmokers for other scenarios is exactly the same.

RISK ESTIMATES FOR CANCER AND COMPARISONS WITH HUMAN EXPERIENCE

Natural Background Radiation

Natural (background) radiation has been present on and about the earth since it began (indeed, radioactivity levels were much greater at the earth's beginning), and man has been exposed to natural radiation since he evolved on earth. The radiation comes from both terrestrial and cosmic sources. On earth, among all the 92 natural elements that form the substances of the earth, most are stable but some, especially those in the higher atomic numbers above lead (number 82), are unstable. These unstable elements emit radiations (alpha, beta, and gamma) at a defined rate in order to reach stability. Those with long half-lives like uranium-238 ($T_{1/2} = 4.5 \times 10^9$ years, approximately equal to the age of the earth) persist for very long times and give rise to a series of radioactive daughter elements, some more active than the parent, with shorter half-lives, like radium ($T_{1/2}$ = 1600 years) and radon ($T_{1/2}$ = 3.82 days) before eventually becoming stable. These natural radioactive parents and their daughters are found everywhere on earth in the soil, water, and air to a greater or lesser extent. They expose human beings externally from the ground and building materials and, also, internally because they are in virtually everything we eat and drink. Because radon is a gas and constantly escaping from the earth, we are also all exposed to it by inhalation. In addition to these earthly sources, radiation is present throughout the universe, including in the outer spaces of the solar system.

To some degree, we on earth are protected from exposure to this cosmic radiation by our atmosphere, which tends to shield much of it out, and by the magnetic field of the earth, which retains many of the radiation particles in belts outside the earth. Nevertheless, some cosmic radiation reaches earth and exposes us to a degree even at sea level. At higher altitudes the levels increase and frequent fliers and crew in airplanes are exposed to substantially more cosmic radiation than those living at sea level. Astronauts and others venturing into space must face even higher exposures, but their stay in space is of limited duration.

We can, of course, evaluate the exposure of humans on earth and the impact it has on them. The exposure varies somewhat according to factors such as the terrain, the type of soil, and the altitude. Table S–28 shows the effective dose per year from the average natural background radiation estimated for the U.S. (NCRP 1987a), together with the average exposure from manmade sources.

Table S–28. Average Exposure of Members of the U.S. Population
Effective Dose - mSv per year (NCRP 1987)

Natural background radiation	
Cosmic	0.28
Terrestrial	0.28
Internal	0.39
Radon	2.00
Manmade exposure, including medical	0.60
Total	3.6

These are average numbers. In individual locations, sources like radon can vary greatly and alter the average exposure by factors of 2 or much more.

On the assumption that all doses can cause stochastic effects in proportion to the dose, this natural radiation can be expected to cause some cancer. In a lifetime of 70 years, an individual at sea level will have received about 250 mSv with a corresponding risk of cancer, using the nominal value of 5×10^{-2} Sv^{-1}, of about 1.25%. (In the Denver area, with about twice the cosmic ray component and twice the terrestrial component (NCRP 1987b), the lifetime effective dose is a little more, ~ 290 mSv or 1.45% risk). Thus, of the natural risk of fatal cancer of about 20% lifetime, background radiation may be responsible for approximately 1.25%. In other words, background radiation may contribute about 6% of the total natural risk of cancer. Among natural radiation background sources, radon contributes 55% of the total exposure and is responsible for a lifetime risk of about 0.7%, all of which is in the form of lung cancer (Table S–28 and Table S–29).

Scenarios for Radiation Exposure from Fernald Sources

As shown in Table S–27, the scenarios considered at Fernald indicate 50th percentile values of the total lung cancer risks for the entire exposure period from 0.11×10^{-2} to 1.3×10^{-2} i.e., 0.11% to 1.3%. The latter, the highest exposure, is for scenario 1, and the total risk for scenario 1 is about the same as the estimate of risk for natural background sources. Thus, the exposure in scenario 1 is equivalent to about a doubling of the risk of background radiation in a lifetime. If the individual in scenario 1 was a smoker and received most of her exposure while a smoker, her risk would have been higher, about 1.8%. On the other hand, if she were a nonsmoker, her risk would have been less or about 0.9%. The scenarios with the lowest exposures (scenarios 5, 7, and 8) are about one-tenth of this exposure and increase the risk of natural background by only about 10%.

Another way of stating the risk is that if the average individual has a 20% likelihood of dying of a fatal cancer naturally, then individuals at scenario 1 would have their risk of 20% increased (at the 50th percentile) by 1.3% to 21.3%. This represents an increase in the natural risk of cancer of about 7%. Another comparison that can be made is that the individual represented by scenario 1 has a lung cancer risk greater than that of a nonsmoker but less than one-sixth that of a smoker. These risks are summarized in Table S–29.

These comparisons are based on the 50th percentile values of risk but in the case of Fernald, the 5th and 95th percentiles are also given. As already noted, the uncertainties in these estimates range for the 95th percentile up to a factor of about 7 times the 50th percentile value and down to about 5 times less than it. Thus, the highest (95th percentile) risk for scenario 1 could be 9.6% (Table S–27), which is about 50% of the natural risk of dying of cancer. Additionally, because the 9.6% is virtually all lung cancer risk, it is comparable with the risk for a smoker (Table S–29). Ninety-fifth percentile risks for the other scenarios range down to about 5% of the natural risk of dying of cancer. These higher risks are, of course, not very likely, perhaps no more likely than the much lower risks at the 5th percentile, which for the nine scenarios (Table S–27) range from 0.02% to 0.24%, i.e. from 0.1% to 1% of the natural risk of dying of cancer.

Table S–29. Comparison of Lifetime Risks in the U.S.

	Natural Risk (%)	Natural radon risk (average) (%)	Natural radiation background risk (other than radon) (%)	Natural radiation background risk (average) (%)	Highest exposure in Fernald scenario (%) Percentiles 5th	50th	95th
Lung cancer							
Smoker[a,b]	9	1.0	0.1	1.1	0.34	1.8	13.5
Nonsmoker[c]	0.9	0.5	0.1	0.6	0.17	0.9	6.8
All cancer[d]	~20	0.7	0.55	1.25	0.24	1.3	9.6

[a] NAS/NRC (1988).
[b] Male ~12%, female ~6%.
[c] Male 1.1%, female 0.6%.
[d] Smokers and nonsmokers.

Another comparison can be made in relation to natural radon exposure. The average concentration of radon in homes in the United States is about 1 pCi L^{-1} (NCRP 1984). The risk associated with exposure to this concentration is about 0.5% lifetime. [NCRP Report 78 p5 gives a risk of 2.1 x 10^{-6} risk per pCi per m^3 based on a lifetime risk of 150 per 10^6 per WLM. Based on the BEIR IV value of $350/10^6$ /WLM, which has been used throughout this text, this would yield 4.9 x 10^{-3} or 0.5% per pCi L^{-1} (NCRP 1984)]. EPA also has an action level for the concentration of radon in homes of 4 pCi L^{-1} (EPA 1986) with an associated risk of about 2% lifetime. Consequently, for scenario 1, the 50th percentile value is about 2-3 times the risk of the average radon concentration in the U.S. but only a little more than half the EPA's action level. The 95th percentile value is about 5 times the EPA action level and the 5th percentile is only about $1/8^{th}$ of the EPA action level.

Taken as a whole, the additional risks of scenarios like 1, 2, 3 and 6 are not negligible but they are comparable with the risk of natural background sources and smaller (at the 50th percentile) than EPA action levels for household radon exposure. There is a small chance (95th percentile) that these risks will be several times the EPA action levels and also a small chance (5th percentile) that they will only be a small fraction of the action levels.

Finally it should be noted that the risks developed in this report do not take account of special sensitivities or resistances to radiation carcinogenesis that may result from a given person's hereditary characteristics, lifestyle or other factors that may influence individual risk.

DETERMINISTIC EFFECTS

It is also necessary to consider whether deterministic effects are possible after the exposures estimated for the various scenarios. Deterministic effects are direct effects of exposure that usually manifest themselves within days or weeks of an acute exposure. They include effects such as visible erythema (reddening) on the skin, cataracts, epilation (hair loss), sterility, bone marrow depression, and so on. Such effects do not occur unless two conditions are met: (1) the dose exceeds a dose threshold for the effect, and (2) the dose is received in a comparatively short time, perhaps an hour or less. Thresholds for these acute

effects are well known. The most sensitive are in the range 0.1 to 0.5 Sv, but most tissues have thresholds much higher than this, perhaps several to many sievert (NCRP 1991).

In the scenarios considered, the greatest organ exposures by far are to the lungs (mainly from radon), and the exposures are all received over a long period of time. The highest exposures to the lung are in scenario 1 with 50th percentile value 3.6 Sv from radon and 0.41 Sv from other sources (both received over a very long period). Deterministic effects in the lung have thresholds, the lowest of which is about 4 Sv (acute exposure) (NCRP 1991) for pneumonitis. Pneumonitis is an acute reaction. Chronic exposures spread over many years, even if doses were several times the threshold, would not be expected to cause pneumonitis. In this case, for scenario 1, the 50th percentile doses are at about the acute dose threshold, but the doses are received over a very long time. Even the less likely but possible larger doses at the 95th percentile (about 14 Sv) due to uncertainties (Table K–5 for radon, Table K–4 for uranium and thorium) would be unlikely to produce these acute effects nor are they likely to produce other late effects such as fibrosis. Consequently, no risk of deterministic effects would be expected to result from the slowly received FMPC exposures.

REFERENCES

Andersson M., B. Carstensen, and J. Visfeld. 1993. "Leukemia and Other Related Hematological Disorders Among Danish Patients Exposed to Thorotrast." *Radiat. Res.* **134**:224–233.

Archer V.E., J.K. Wagoner, and F.E. Lundin. 1973. "Cancer Mortality Among Uranium Mill Workers." *J. Occup. Med.* **15**:11–14.

Beck W.L., D.L. Cookfair, C.L. Sowder et al. 1983. "Radiation Dosimetry for Epidemiologic Lung Cancer Study." In *Epidemiology Applied to Health Physics.* CONF-830101. pp. 436–443. National Technical Information Service, Springfield, Virginia.

Checkoway H., N. Pearce, D.J. Crawford-Brown and D.L. Cragle. 1988. "Radiation Doses and Cause-Specific Mortality Among Workers at a Nuclear Materials Fabrication Plant." *Am. J. Epidemiol.* **127**:255–266.

Chmelevsky D., A.M. Kellerer, H. Spiess and C.W. Mays. 1986. "A Proportional Hazards Analysis of Bone Sarcoma Rates in German Radium-224 Patients". pp 32-37 in the *Radiobiology of Radium and Thorotrast.* W. Gössner, G.B. Gerber, U. Hagen, and A. Luz, Eds. Munich, West Germany.

Cookfair D.L., W.L. Beck, C. Shy et al. 1983. "Lung Cancer Among Workers at a Uranium Processing Plant." In *Epidemiology Applied to Health Physics.* CONF-830101, p. 398–406. [Publisher, city]

Decisioneering. 1993. Crystal Ball Version 3.0. *User Manual Forecasting and Risk Analysis for Spreadsheet Users.* Decisioneering, Inc., Denver, Colorado.

Dupree E.A., D.L. Cragle, R.W. McLain, D.J. Crawford-Brown, and M.J. Teta. 1987. "Mortality Among Workers at the Uranium Processing Facility, the Linde Air Products Company Ceramics Plant 1943–49." *Scand. J. Work Environ. Health* 13:100–107.

Dupree E.A., J.P. Watkins, J.N. Ingle, P.W. Wallace, C.M. West, and W.G. Tankersley. 1995. "Uranium Dust Exposure and Lung Cancer Risk in Four Uranium Processing Operations. " *Epidemiology* **6**: 370–375.

Environmental Protection Agency (EPA). 1979. "National Emissions Standards for Hazardous Air Pollutants: Benzene". Fed. Register **49**: 23558.

Environmental Protection Agency (EPA). 1986. *A Citizen's Guide to Radon*. US EPA Report OPA-86-004, Environmental Protection Agency. Washington, D.C.

Food and Drug Administration (FDA). 1979. "Chemical Compounds in Food Producing Animals". Fed. Register **44**: 17070.

Hohryakov V.F. and S.A. Romanov. 1994. "Lung Cancer in Radiochemical Industry Workers." *The Science of the Total Environment* **142**:25–28.

International Commission on Radiological Protection (ICRP). 1987. *Lung Cancer Risk from Indoor Exposures to Radon Daughters,* ICRP Publication 50. *Annals of the ICRP* **17**(1). Pergamon Press, Oxford.

International Commission on Radiological Protection (ICRP). 1991. *The 1990 Recommendations of the ICRP,* ICRP Publication 60. *Annals of the ICRP* **21**(1–3). Pergamon Press, Oxford.

International Commission on Radiological Protection (ICRP). 1993. *Protection Against Radon-222 at Home and at Work.* ICRP Publication 65. *Annals of the ICRP* **23**(2). Pergamon Press, Oxford.

International Commission on Radiological Protection (ICRP). 1995a. *Age-Dependent Doses to Members of the Public from Intake of Radionuclides: Part 3: Ingestion Dose Coefficients.* ICRP Publication 69. *Annals of the ICRP* **25**(1): 1–74. Pergamon Press, Oxford.

International Commission on Radiological Protection (ICRP). 1995b. *Age-Dependent Doses to Members of the Public from Intake of Radionuclides: Part 4: Inhalation Dose Coefficients.* ICRP Publication 71. *Annals of the ICRP* **25**(3-4). Pergamon Press, Oxford.

Land C.E. and W.K. Sinclair. 1991. "The Relative Contribution of the Different Organ Sites to the Total Cancer Mortality Associated with Low Dose Radiation Exposure." *Annals of the ICRP* **22**: (1) pp. 31–57. Pergamon Press, New York.

Lubin J., J.D. Boice, Jr., C. Edling, R.W. Hornung, G. Howe, E. Kunz, R.A. Kusiak, H.I. Morrison, E.P. Radford, J.M. Samet, and M. Tirmarche. 1994. "Radon and Lung Cancer Risk," NIH Publication 94-3644. National Institutes of Health, Washington, DC.

Mays C.W. and H. Spiess. 1983. "Epidemiological Studies of Patients Injected with ^{224}Ra." In *Epidemiology Applied to Health Physics*. Proceedings of the 16th Mid Year Topical Meeting of the Health Physics Society. CONF-830101. National Technical Information Service, Springfield, Virginia. pp. 159-163.

National Academy of Sciences/National Research Council (NAS/NRC). 1980. *The Effects on Populations of Exposure to Low Levels of Ionizing Radiation: 1980,* BEIR III report. National Academy of Sciences, Washington, DC.

National Academy of Sciences/National Research Council (NAS/NRC). 1988. *Health Risks of Radon and Other Internally Deposited Alpha-Emitters.* BEIR IV Report. National Academy Press, Washington, DC.

National Academy of Sciences/National Research Council (NAS/NRC). 1990. *Health Effects of Exposure to Low Levels of Ionizing Radiation,* BEIR V report. National Academy of Sciences, Washington, DC.

National Academy of Sciences/National Research Council (NAS/NRC). 1991. *Comparative Dosimetry of Radon in Mines and Homes.* Companion to BEIR IV. National Academy of Sciences, Washington, DC.

National Council on Radiation Protection and Measurements (NCRP). 1980. *Influence of Dose and its Distribution in Time on Dose–Response Relationships for Low LET Radiations.* NCRP Report No. 64. National Council on Radiation Protection and Measurements, Bethesda, Maryland.

National Council on Radiation Protection and Measurements (NCRP). 1984. *Evaluation of Occupational and Environmental Exposures to Radon and Radon Daughters in the United States.* NCRP Report No. 78. National Council on Radiation Protection and Measurements, Bethesda, Maryland.

National Council on Radiation Protection and Measurements (NCRP). 1987a. *Ionizing Radiation Exposure of the Population of the United States.* NCRP Report No. 93. National Council on Radiation Protection and Measurements, Bethesda, Maryland.

National Council on Radiation Protection and Measurements (NCRP). 1987b. *Exposure of the Population in the United States and Canada from Natural Background Radiation.* NCRP Report No. 94. National Council on Radiation Protection and Measurements, Bethesda, Maryland.

National Council on Radiation Protection and Measurements (NCRP). 1990. *The Relative Biological Effectiveness of Radiations of Different Quality.* NCRP Report No. 104. National Council on Radiation Protection and Measurements, Bethesda, Maryland.

National Council on Radiation Protection and Measurements (NCRP). 1991. *Misadministration of Radioactive Material in Medicine – Scientific Background.* NCRP Commentary No. 7. National Council on Radiation Protection and Measurements, Bethesda, Maryland.

National Council on Radiation Protection and Measurements (NCRP). 1993a. *Risk Estimates for Radiation Protection.* NCRP Report No. 115. National Council on Radiation Protection and Measurements, Bethesda, Maryland.

National Council on Radiation Protection and Measurements (NCRP). 1993b. *Limitation of Exposure to Ionizing Radiation,* NCRP Report No. 116. National Council on Radiation Protection and Measurements, Bethesda, Maryland.

National Council on Radiation Protection and Measurements (NCRP). 1997. *Uncertainties in Fatal Cancer Risk Estimates used in Radiation Protection.* NCRP Report No. 126. National Council on Radiation Protection and Measurements, Bethesda, Maryland.

National Radiological Protection Board (NRPB). 1993. *Estimates of Late Radiation Risks to the U.K. Population.* Documents of the NRPB 4, no. 4. National Radiological Protection Board, Chilton, Oxon, U.K.

Pierce D.A., Y. Shimizu, D.L. Preston, M. Vaeth and K. Mabuchi. 1996. "Studies of the Mortality of Atomic Bomb Survivors. Report 12, Part I. Cancer: 1950-1990." *Radiat. Res.* **146**:1-27.

Polednak A.P. and E.L. Frome. 1981. "Mortality Among Men employed Between 1943 and 1947 at a Uranium Processing Plant." *J. Occup. Med.* **23**:169–178.

Puskin J.S. 1992. "Analysis of the Uncertainties in Estimates of Radon-Induced Lung Cancer." *Risk Analysis* **12**:277–285.

Puskin J.S. and Y.Yang. 1988. "A Retrospective Look at Rn-induced Lung Cancer Mortality from the Viewpoint of a Relative Risk Model." *Health Phys.* **54**:635-643.

Puskin J.S. and C.B. Nelson. 1995. "Estimates of Radiogenic Cancer Risks." *Health Phys.* **69**:93–101.

Radiological Assessments Corporation (RAC). 1997. *Assessing Risks of Exposure to Plutonium.* Rocky Flats Report Task 3. Neeses, South Carolina.

Ron E., D.L. Preston, K. Mabuchi, D.E. Thompson, and M. Soda. 1994. "Cancer Incidence in Atomic Bomb Survivors. Part IV Comparison of Cancer Incidence and Mortality." *Radiat. Res.* **137** Supplement, S 98–112.

Scott B.R., E.S. Gilbert and B.B. Boecker. 1993. "Health Effects Models for Nuclear Power Plant Accident Consequent Analyses." Chapter 3, *Late Somatic Effects.* In NUREG/CR-4214 Rev. 1 Part II Addendum 2, LMF-136. U.S. Nuclear Regulatory Commission, Washington, D.C.

Shimizu Y., H. Kato, and W.J. Schull. 1988, 1990. Lifespan Study Report 11. Part 2. Cancer Mortality in the Years 1950–85. Based on Recently Revised Doses (DS86). Technical Report RERF TR-5-88. Radiation Effects Research Foundation, Hiroshima, Japan and in *Radiat. Res.* **121**:120–141.

Sinclair W.K. 1992. "Radiation Induced Cancer Risk Estimates, Today and Tomorrow." In Proceedings No. 13 of the National Council on Radiation Protection and Measurements. *Genes, Cancer and Radiation Protection.* pp. 3–13. National Council on Radiation Protection and Measurements, Bethesda, Maryland.

Spiess H. and C.W. Mays. 1970. "Bone Cancers Induced by ^{224}Ra (ThX) in Children and Adults." *Health Phys.* **19**:713-729.

Thompson D.E., K. Mabuchi, E. Ron, M. Soda, M. Tokunaga, S. Ochikubo, S. Sugimoto, T. Ikeda, M. Terasaik, S. Izumi, and D.L. Preston, 1994. "Cancer incidence in atomic bomb survivors. Part II: Solid tumors, 1958–1987." *Radiat. Res.* **137**:S17–S67.

Travis C.C., S.R. Pack, and H.A. Hattemer-Frey. 1989. "Is Ionizing Radiation Regulated More Stringently Than Chemical Carcinogens?" *Health Phys.* **56**:527–531.

United Nations Scientific Committee on the Effects of Atomic Radiation (UNSCEAR). 1977. *Sources and Effects of Ionizing Radiation*. Report to the General Assembly. United Nations, New York.

United Nations Scientific Committee on the Effects of Atomic Radiation (UNSCEAR). 1988. *Sources, Effects and Risks of Ionizing Radiation*. Sales No. E.88.IX.7. United Nations, New York.

United Nations Scientific Committee on the Effects of Atomic Radiation (UNSCEAR). 1993. Annex F. *Influence of dose and dose rate on stochastic effects of radiation*. Sales No. E.94.IX.2. United Nations, New York.

United Nations Scientific Committee on the Effects of Atomic Radiation (UNSCEAR). 1994. Annex A. *Epidemiological Studies of Radiation Carcinogenesis*. Sales No. E.94.1X.11. United Nations, New York.

Waxweiler R.J., V.E. Archer, R.J. Roscoe, A. Watanabe and M.J. Thun. 1983. "Mortality Patterns Among a Retrospective Cohort of Uranium Mill Workers." *In Epidemiology Applied to Health Physics*. CONF-830101. pp. 428–435. National Technical Information Service, Springfield, Virginia.

APPENDIX T

EPISODIC RELEASES

INTRODUCTION

In this project the term "episodic releases" refers to actual accidental releases from Feed Materials Production Center (FMPC) operations that were large enough to be given special treatment for environmental transport and dose assessment. The largest contributor to radiation dose to the public from past FMPC operations was routine release of radon and decay products from the K-65 waste storage silos (see Volume I). The releases from these silos were relatively uniform throughout a year; only one known accidental release in 1986 warranted special consideration as an episodic release. Similarly, the reconstruction of historic releases of uranium, thorium, and decay products from the FMPC production area has established that routine releases dominate the total releases. Some types of accidental releases of uranium, for example failures of a type of particulate collection system called "dust bags" (Adams 1985), were so common that they could be considered routine in terms of reconstruction of past releases. Therefore these release amounts were included in our routine release estimates. However, six episodic releases of uranium to the atmosphere were identified (Voillequé et al. 1995). This appendix assesses the dose consequences of those six uranium episodic releases and the one radon release.

CRITERIA FOR TREATMENT AS EPISODIC RELEASE

Early in the dose reconstruction project, it became clear that large amounts of uranium had been frequently discharged to the atmosphere and to the Great Miami River. As many as 10 facilities contributed to the total uranium discharges from the FMPC. The largest releases were not always from the same facilities, although some facilities were clearly more important sources of effluents than others. The magnitudes of the total discharges decreased substantially over the years, with the time period before 1965 being most important for releases of uranium from the production area and the time period before 1980 being most important for radon releases from the K-65 silos. (See Volume I for an overview of the time trends in historical releases of uranium and radon from the FMPC.)

These factors required that the criteria for special dose assessment procedures must consider the magnitude of the release in the context of the releases from all of the facilities at the FMPC and the relative importance of the release to the total discharge at the time it occurred. Releases in recent years that were large enough to cause significant changes to the overall plant effluent and result in an official inquiry (e.g., Investigation Board 1988) would have had a relatively minor effect on the total releases during most earlier years of operation.

In consideration of this historical context, the following criteria were used for this project to determine whether special evaluation of a release from an event was warranted (Voillequé et al. 1995):

- The event under consideration caused the composite release rate of the FMPC to increase by a factor of 10 or more above the value that would otherwise have been observed
- The duration of the high release rate caused by the particular event was less than 10 days.

The second criterion considers the fact that natural dispersion phenomena also play a significant role in the dosimetric analysis. For releases of long duration, the variability in dispersion conditions, including wind direction, will spread the effect over a wider area and reduce the magnitude of the increased dose to individuals. The criteria for episodic releases were developed at a time in the reconstruction project when it was believed that the reconstruction of uranium releases could be achieved on a monthly time scale. Although it was later determined that an annual time resolution was the best that was achievable, the episodic release criteria were not reevaluated.

SUMMARY OF EPISODIC RELEASES

In Appendix K of our final source term report (Voillequé et al. 1995), potential episodic releases to air over the entire operating history of the FMPC were thoroughly reviewed. Only six incidents involving releases of uranium were identified that met our criteria for special treatment as episodic releases (Table T-1). One of those six, the November 1960 dust loss from the Pilot Plant, actually did not meet the criteria for an episodic release after a re-evaluation of the loss of particle mass in the effluent sampling lines. That release was consequently included in the routine dust collector source term for 1960 for the dose calculations in this final report. It should be emphasized that *all* known releases were included in the total source term estimates, but only a small number are truly episodic releases, by our definition.

In addition to actual known episodic events, historic releases from "non-routine events," such as fires, spills, and leaks, were estimated generically based on the frequency of occurrence of these events in the FMPC operating history and their consequences. The median source term from these non-routine events was estimated to be a total of 1300 kg uranium between 1952–1988. Thus, the total accidental releases of uranium, whether episodic or non-routine, are minor compared with the total atmospheric source term of 81,000 kg of uranium from the Plant 8 scrubbers, 66,000 kg from the Plant 2/3 scrubbers, and 140,000 kg from exhaust serviced by dust collectors.

For the purposes of this dose reconstruction, the majority of releases of uranium from the FMPC were routine, not episodic. The five episodic releases were evaluated separately on a case-by-case basis depending on the available information.

Table T-1. Summary of Six Episodic Releases of Uranium That Were Identified from Incident Reports and Environmental Air Monitoring (Voillequé et al. 1995)

Start date of release	Description of release	Amount released (kg U)	Duration of release	Episodic release rate (g U min^{-1})	Routine release (kg U y^{-1})[a]	Routine release rate (g U min^{-1})
11/7/53	Release of UF_6 from defective cylinder in Pilot Plant	45	15 min	3000	5747	11
11/12/60	Dust loss from dust collector bags in Pilot Plant and replacement of bags	780	< 8 days	68[c]	15780	30
2/14/66	Release of UF_6 from cylinder in Pilot Plant from operator error	750	1 hr	12,500	2316	4.4
9/21/78	Unknown source	20–370[b]	< 7 days	2.0–37	225	0.43
2/1/79	Unknown source	60–680[b]	< 7 days	6.0–67	372	0.71
9/13/83	Unknown source	290–360[b]	< 7 days	29–36	525	1.0

[a] Median estimate of annual release from dust collectors and scrubbers (Table 5, Volume I).
[b] Range of estimated release amounts is based on measurements of uranium in air from several different ambient air monitoring stations and back-calculation to amount released using a preliminary dispersion model (see Table K-30 of Voillequé et al. 1995). In this Task 6 report, the air monitoring data are used directly to estimate potential dose from inhalation during these 3 weeks. A revised estimate of the release quantity has not been generated using the final atmospheric model.
[c] Our final assessment did not result in classification of this accident as an episodic release, because the episodic release rate is less than ten times the routine release rate. The amount of uranium released was included in the routine dust collector source term for 1960.

One incident involving radon release, which met our criteria for treatment as an episodic release, was identified. A release of radon occurred in the middle of the day on April 25, 1986, from unauthorized venting of the K-65 silos (DOE 1986). In Appendix K of our final source term report (Voillequé et al. 1995), we estimated an upper bound on the quantity of radon released. The median estimate (from an uncertainty distribution) of this upper bound was about 30 Ci of radon. The release occurred over a period of about 3¾ hours. Thus, a nominal estimate of the upper bound on the release rate is about 8 Ci h^{-1}. In Appendix J of our final source term report (Voillequé et al. 1995), we calculated the annual quantities of radon *routinely* released from the K-65 silos for 1980–1987. The median estimates of routine releases are equivalent to a rate of about 0.2 Ci h^{-1} during daylight hours for this period. Therefore, based on the estimated upper bound for the episodic release, the release of April 25, 1986, qualifies for special treatment as episodic rather than routine.

EVALUATION OF DOSE CONSEQUENCES OF EPISODIC RELEASES

The five episodic releases of uranium to air can be divided into two categories in terms of how dose consequences are evaluated: (1) uranium hexafluoride gas releases from the Pilot

Plant (in 1953 and 1966) and (2) possible releases identified from ambient air sampling data. The radon release is evaluated separately, using information specific to that source.

Uranium Hexafluoride Gas Releases from Pilot Plant (11/7/53 and 2/14/66)

The 1966 release is addressed first, because it is much more significant. This episodic release occurred from the Pilot Plant on Monday, February 14, 1966. A description of the uranium hexafluoride (UF_6) release was obtained from NLO (1966) and Boback and Heatherton (1966) and is reviewed in Appendix K of our source term report (Voillequé et al. 1995). Aspects relevant to the treatment of offsite dose consequences of the release are also presented here.

The starting time of the release was about 8:40 a.m. and the duration was about 1 hour. An estimated 750 kg (as U) of gaseous UF_6 was released to the atmosphere and 910 kg was released to the Great Miami River via Manhole 175 (NLO 1966). The estimated release to the atmosphere is based on the weight lost from the original cylinder containing the UF_6 and the amounts of uranium identified in the liquid waste streams. The UF_6 was enriched in ^{235}U to 2.1%—higher than typically used in most processes at the FMPC. Using this enrichment percentage, the 750 kg U release can be apportioned into about 16 kg (0.034 Ci) ^{235}U and 734 kg (0.25 Ci) ^{238}U.

The UF_6 gas escaped from a 10-ton steel cylinder, which contained the feed material for this part of the FMPC process, in which conversion of UF_6 to UF_4 took place. When used in the chemical reduction process, the steel cylinders were cradled in a movable vaporizer chest. The gas in the cylinder was under a pressure of about 50 psig. When an operator attempted to open a valve of the cylinder, the valve unscrewed from the cylinder, and the pressurized gas was expelled from the container. [For this to happen, a copper pigtail attached to the valve had to be damaged. The investigation report (NLO 1966) theorizes how this may have happened.] The gas was vented to the atmosphere through a removable hood positioned over the vaporizer chest. Pilot Plant personnel began to spray the cylinder with a water hose and were quickly joined by the fire brigade (time = 8:47 a.m.), who connected fire hoses and began to direct the spray into the cloud near the place where it was leaving the vaporizer chest. The hood was then raised, and a direct water stream was applied to the end of the chest so that it rebounded against the cylinder at the valve opening. Continued application of water for about 1 hour finally cooled the cylinder and reduced its pressure sufficiently to permit a wooden plug to be driven in the valve opening.

A majority of the UF_6 that escaped from the cylinder was absorbed in spray from fire hoses that were kept trained on the escaping gas (Boback and Heatherton 1966). Use of water to control the leak resulted in an estimated 2000 pounds (910 kg) of uranium lost to the Great Miami River via Manhole 175 (NLO 1966).

The escaping gas released to air was carried by wind in a southeasterly direction over the Laboratory Building and the Administration Building, which were evacuated. Airborne UF_6 hydrolyzes quickly on contact with moisture in air to form uranyl fluoride (UO_2F_2) and hydrogen fluoride (HF). Boback and Heatherton (1966) states that there was a "light fog of steam and hydrolyzed UF_6 which drifted near the lab and Administration buildings." The wind was estimated to be from the west and northwest at 0–4 mph (NLO 1966), or 0–1.8 m s^{-1}. There was no onsite meteorological monitoring at this time. Security police were posted at access roads, prohibiting anyone from entering during the time of the incident.

Personnel involved in the emergency actions or who had any reason to believe that they may have inhaled some of the material were asked to submit urine samples. These data are summarized in NLO (1966). In our judgment, these worker bioassay data did not provide useful information for assessing the offsite consequences of this release.

Monitoring of the Pilot Plant environment following the 1966 episodic release indicated that most of the contamination occurred in the immediate area of the incident, i.e., the Pilot Plant itself and the pad north of the Pilot Plant. Offsite areas just south of the FMPC were monitored for alpha contamination with hand-held instruments and showed no contamination above instrument background. Milk samples collected offsite were analyzed on February 15, 1966, and were found to have uranium concentrations that were the same as those found in samples taken during the last 4 months of 1965. Soil, vegetation, and water samples collected within the FMPC boundary at varying distances south of the production area did not contain any significant concentrations of uranium.

Consequently, the environmental data were not useful for establishing the possible exposure of the public to uranium from the 1966 UF_6 release. Therefore, we used an atmospheric dispersion model to estimate the offsite concentrations of uranium hydrolysis products in air using the estimated release amount, duration, and general information on wind speed and direction. With the security personnel postings, the nearest downwind location that a member of the public likely could have been was along Route 128, about 1.3 km southeast of the Pilot Plant. (See Figure 4 of Volume I for location map.)

Routine releases of uranium from the production area are modeled as ground-level area sources, because of the many release points and the likely entrapment of the plumes in the wake of buildings (see Appendix M). The routine release model could not be used for the episodic releases of UF_6 because these releases occurred from a single release point (the Pilot Plant) and over a short period of time. The dispersion of the episodic gas releases was modeled as a Gaussian plume, in which the downwind air concentration at ground-level and plume centerline (directly downwind) can be described as (Hanna et al. 1982):

$$\chi / Q = (\pi \sigma_y \sigma_z u)^{-1} \exp\left(-h^2/(2\sigma_z^2)\right) \qquad \text{(T-1)}$$

where

χ/Q = dispersion factor in s m^{-3}, which is the ratio of the downwind air concentration, χ, in Ci m^{-3} to release rate, Q, in Ci s^{-1}

σ_y, σ_z = diffusion coefficients in the horizontal and vertical directions, respectively (m)

u = wind speed (m s^{-1})

h = release height (m).

In our calculation, the release height, h, was allowed to vary between 0 m (ground level) and 20 m. As described previously, the gas was seen escaping from openings in the building and drifting near adjacent buildings. The stack height from this part of the Pilot Plant was 16 m. The chemical reactions of the UF_6 with atmospheric constituents are exothermic, releasing heat and producing some plume rise. We selected 20 m as an upper bound on the release height. The uncertainty in the release height has very little effect on the assessment of public exposure. Even an effective release height of 50 m would result in only a 3–5%

smaller predicted air concentration at the receptor distance (1.3 km), depending on the stability class.

The equations for σ_y and σ_z depend on atmospheric conditions, often categorized as Pasquill types. Gifford (1976), cited in Hanna et al. (1982), tabulates Pasquill turbulence types based on meteorological conditions of wind speed and daytime insolation (or nighttime). According to the observations of wind speed and time of day of the 1966 release, we would choose "slightly to moderately unstable" atmospheric stability conditions (Pasquill type B or C) to describe the dispersion of this release. However, examination of the FMPC meteorological data (1987–1991) indicates that Class D stability class (neutral condition) is much more probable than class B or C in February. From the FMPC data, a frequency for class A, B, C, and D was determined to be 0, 0.022, 0.054 and 0.924, respectively, for daytime conditions in February and a wind speed of 0–2 m s^{-1}. Our assessment considered all three of these stability classes at the noted frequencies.

The formulas for σ_y and σ_z for the different stability classes were taken from Table 4.5 of Hanna et al. (1982), which are recommended by Briggs (1973) for distances of 0.1 to 10 km. The equations for urban conditions, rather than open-country conditions, were used, because of the number and proximity of buildings in the FMPC production area. For the 1966 episodic release, our nominal estimate of the dispersion factor, χ / Q, at 1300 m was 9.4×10^{-6} s m^{-3}.

Miller and Hively (1987) addresses the uncertainty of the Gaussian plume model, by reviewing a number of validation studies in which predicted concentrations of a material in air are compared with measurements. In this review, the authors cite Pasquill (1974), which estimated an uncertainty in the Gaussian model of 10 to 20% for short downwind distances (<10 km), steady winds, and ground-level releases. This author indicates that an error of 30 to 35% may be more appropriate for elevated releases. Miller and Hively (1987) maintains that this is the best accuracy that can be expected by present Gaussian plume atmospheric dispersion models. The authors conclude that the annual average air concentration over flat terrain can be predicted within a factor of 2 to 4 using the Gaussian plume model.

In our assessment of the possible consequences of the episodic UF_6 releases, the exact location of the receptor is not specified; rather, the person is assumed to be at the plume centerline for the entire duration of the plume passage. This flexibility in the precise location of the receptor favors a smaller model uncertainty than if a precise location had been specified. For our assessment, we used a model uncertainty factor that incorporated a factor-of-two uncertainty because of inaccuracy of the Gaussian plume model.

The particle-size characteristics of the aerosol were considered. Bostick et al. (1985) used a variety of physical and chemical techniques to examine the products from the atmospheric hydrolysis of UF_6. Of all the properties of the aerosol, the report states: "the most salient is the small size of the UO_2F_2 particles which are produced." Both the particulate uranyl fluoride and the hydrofluoric acid (HF) gas produced from the hydrolysis are hygroscopic, tending to pick up additional water molecules. The particulate UO_2F_2 is readily visible as a white aerosol cloud or "smoke" that may rise and be dispersed into the environment. Figure 4 of Bostick et al. (1985) plots measurements of the median aerodynamic particle size for airborne uranyl fluoride, as a function of time elapsed (range 0 to 400 minutes) from the release of UF_6 into environments of 35 and 100% relative humidity. Over this interval of time and conditions, the median particle size ranged from 0.25 to 0.5 μm. For our nearest receptor, at about 1.3 km, with a wind speed of 1.1 m s^{-1}, the plume transit time to the individual would

have been about 20 minutes. From the experimental data plotted in Figure 4 of Bostick et al. (1985), an aerosol with a median aerodynamic diameter of about 0.35 μm can be expected, and was used in our calculations.

Intake of uranium by inhalation was calculated for a maximally-exposed adult at 1.3 km directly downwind (at plume centerline) for the duration of the plume passage. Uranium compounds such as UF_6 and UO_2F_2 are rapidly absorbed from the lung and have been assigned to inhalation class D (ICRP 1979) for the purposes of determining radiation dose (see Appendix I for dose factor tables). In contrast to class W and Y compounds, class D uranium is cleared more quickly from the lungs, resulting in a considerably lower effective dose per unit intake than for class W or class Y. However, class D chemical forms do result in a larger chemical and radiological dose to the kidney than the less soluble chemical forms. Chemical toxicity considerations are discussed in a later section of this appendix after the radiation doses are presented.

To compare the radiation doses from episodic releases with those for routine releases, which are a variety of chemical forms, the *effective dose* has been computed and presented here. The internal dose conversion factors for a 1-μm particle size, from Table I-1S (^{238}U) and Table I-2S (^{235}U) in Appendix I were adjusted to correspond to a 0.35-μm particle size using the correction factor outlined in Appendix I (Equation I-3). The parameter values necessary to compute that correction are shown in Table T-2. The correction factor obtained using Equation I-3 was 1.15, or a 15% higher effective dose for the smaller particle size (0.35 μm) as compared to the nominal values for 1-μm particles.

Table T-2. Parameter Values for Correction of Inhalation Dose Factor for Particle Size of Uranyl Fluoride from Hydrolysis of Uranium Hexafluoride Releases

	Aerodynamic diameter	
Parameter	1 μm	0.35 μm
D_{NP}	0.30[a]	0.10[b]
D_{TB}	0.08[a]	0.08[b]
D_P	0.25[a]	0.40[b]
d_{NP}	0.29[c]	not applicable
d_{TB}	0.14[c]	not applicable
d_P	0.57[c]	not applicable

[a] From Figure I-3.
[b] Estimated from Figure I-4.
[c] From Table I-1S.

Table T-3 presents parameter values which were treated as uncertain quantities in the exposure assessment of the 1966 UF_6 release. Dose results from this accident are presented in Table T-4. The intake amount [milligram (mg) of uranium inhaled] is presented to permit assessment of chemical toxicity effects from the uranium.

Table T-3. Uncertainty Distributions Used to Assess Offsite Inhalation Dose from the 1966 Episodic Release of Uranium Hexafluoride

Parameter [a]	Nominal value	Distribution type and uncertainty (if applicable)
Release quantity (Ci)	16 kg (0.034 Ci) ^{235}U 734 kg (0.25 Ci) ^{238}U	Normal, standard deviation of 20%
Wind speed (m s^{-1})	1.2	Triangular, range 0.5–2
Release height (m)	10	Uniform, range 0–20
Model uncertainty factor	1.0	Log-triangular, range 0.5–2.0
Inhalation rate (m^3 d^{-1})	52	Uniform, range 30.2 to 73.4[b]

[a] Atmospheric stability class was also treated as an uncertain parameter by considering all possible stability classes observed in the composite FMPC meteorological data set for 1987–1991. Stability classes B, C, and D were weighted according to their probability of occurrence in the month of February under the wind speed conditions of the accident.

[b] See Appendix I. Lower inhalation rate represents a female under conditions of light activity and upper rate represents a male under conditions of vigorous activity.

Table T-4. Radiation Dose and Uranium Intake to Hypothetical Adult Receptor from February 1966 Episodic Release of Uranium Hexafluoride[a]

Receptor location	Intake (mg U inhaled)	Effective dose (μSv)
1.3 km downwind of release	4.2 (1.8, 9.5)	15 (6.7, 34)

[a]Values in table are median estimate (50th percentile) followed by 5th and 95th percentiles in parentheses.

A similar approach was used to assess the UF_6 release that occurred in the Pilot Plant on November 7, 1953, when a cylinder containing UF_6 was breached releasing approximately 100 pounds (45 kg U) of the gas. The magnitude of that release is very small relative to routine releases that followed in the next several years. It is characterized as an episodic release because the release time was short and the baseline release rate from the entire facility in 1953 was relatively low. According to production records, this material was most likely to have been natural uranium, rather than enriched uranium, as was the case for the 1966 release. Therefore, the nominal release quantity is estimated at 0.32 kg ^{235}U (0.68 mCi) and 44.7 kg ^{238}U (15 mCi). A standard deviation of 20% for the release quantity was used in the uncertainty analysis.

This accident occurred in the morning of November 7, 1953. Davis (1953) notes that the duration of the release was 15 minutes and that there was a strong northerly wind blowing at the time. The dispersion of this release was modeled assuming a wind speed of 10 mph (4.5 m s^{-1}) with a range of 5–15 mph (2.2–6.7 m s^{-1}). Based on the time of day and wind speed, we might choose slightly unstable (Pasquill type C) atmospheric conditions to describe this release. However, recent FMPC meteorological data show a probability frequency for stability

classes A, B, C, and D of 0.095, 0.090, 0.068 and 0.747, respectively, for daytime conditions in November and a wind speed of 4–6 m s^{-1}. Our assessment included all four of these classes at the noted frequencies. The uncertainties in the model accuracy, release height, and inhalation rate were incorporated into the calculation as described previously for the 1966 episodic release (Table T-3). The nearest distance to the site boundary in a downwind direction (south) is about 1 km, so a potential dose was calculated for that distance. The receptor was assumed to be at the maximum (plume-centerline) concentration for the duration of plume passage. The nominal estimate of χ / Q at that distance is 3.2×10^{-6} s m^{-3}. Dose estimates are presented in Table T-5.

Table T-5. Radiation Dose and Uranium Intake for a Hypothetical Adult Receptor from the 1953 Episodic Release of Uranium Hexafluoride[a]

Receptor location	Intake (mg U inhaled)	Effective dose (μSv)
1 km downwind of release	0.08 (0.04, 0.18)	0.29 (0.13,0.62)

[a]Values in table are median estimate (50th percentile), followed by 5th and 95th percentiles in parentheses.

Episodic Releases Identified Using Ambient Air Monitoring Data

In addition to reviewing accident reports and investigation documents, environmental monitoring data for air and deposition (gummed film) from 1958 through 1984 were evaluated to identify potential episodic releases. An initial screening assessment of air monitoring data indicated that 14 undocumented episodic releases may have occurred during this time period (see Appendix B–Part 2 of Shleien et al. 1995). Further analyses of these data were performed to determine if the apparent releases met the criteria for implementing special dose assessment procedures.

First, a baseline concentration of airborne uranium was estimated for each location and time period of concern. The baseline concentration was defined as the average uranium concentration during the 3-week period before and the 3-week period after the elevated concentration was observed. If the elevated concentration was determined to be at least 10 times greater than the baseline concentration, the result was considered for further evaluation. Concentrations for 8 of the 14 cases exceeded this criterion.

In our source term report (Voillequé et al. 1995), the airborne uranium concentrations during these periods were used to estimate a possible release amount from the unidentified episodic releases, to compare those possible releases with amounts released from other production area souces. A release amount (kg U), shown in Table T-1, was estimated using the following approach and assumptions:

1. It was assumed that the release point was the center of the FMPC. Distances to each air monitoring location were presented in Table K-29 of Voillequé et al. (1995).
2. Average meteorological conditions for the month of the potential episodic release were assumed.

3. A building wake model (Killough et al. 1993) was used to calculate dispersion parameters (χ/Q, s m^{-3}) for each air monitoring location.
4. For each time period and location of concern, the measured uranium concentration in air was used, along with the estimated χ/Q, to calculate the release rate. (All locations during the time period of concern that showed elevated airborne uranium concentrations were used to obtain a range of possible source term values.)

Results of the calculations are shown in Table K–30 of Voillequé et al. (1995). Based on the upper range of estimated source term values, three episodic releases were apparent. They occurred during the weeks ending on September 28, 1978, February 8, 1979, and September 20, 1983. The range of release rate values estimated for each of these weeks were 6–56 kg d^{-1}, 12–100 kg d^{-1}, and 47–57 kg d^{-1}, respectively. The sources of these episodic releases are unknown, because supporting documentation could not be found. Vaaler and Nuhfer (1989) identified the vacuum transfer ("gulping") of UO_3 in Plant 2/3 as a significant unmonitored source of uranium emissions to the atmosphere. However, Semones and Sverdrup (1988) indicates that this process was not in operation during the years 1978 and 1979. It estimated a total loss of 130 kg of uranium for the year 1983, which represents an average daily loss over 100 times less than the episodic release calculated here. Other possible unmonitored sources include the old solid waste incinerator (through 1979) and the Plant 8 scrubbers.

In contrast to our earlier reports, the objective of this Task 6 report is to evaluate the radiation doses received by the public from past FMPC releases. The most direct method for evaluating dose for the three episodic releases that were identified from the ambient air monitoring samplers is to work directly from the measured concentrations in air at the site boundary. An estimate of the potential dose during each of these three weeks was made using the equation:

$$H = \chi\, I\, R\, t\, DF \qquad \text{(T-2)}$$

where

H = Effective dose (mSv)

χ = Highest uranium concentration in air measured at a boundary station, corrected for routine baseline concentration (fCi U m^{-3})

I = Inhalation rate (m^3 h^{-1})

R = Receptor reduction factor, to account for receptor distances farther from the boundary (unitless)

t = Exposure time (168 h)

DF = Effective dose conversion factor (1.18×10^{-6} mSv fCi^{-1}), which is equivalent to 3.19×10^{-5} Sv Bq^{-1}, Table I-1s).

Because the air samplers were collected weekly, it is impossible to discern over what time period the releases occurred. It is conceivable that a member of the public could have been near the boundary at the time of a relatively short-term release. In our uncertainty analysis, we allowed the receptor reduction factor, R, to range from 0.5, which would be consistent with a distance of about 1 km away (see Appendix M), to 1.0, which would be appropriate for a receptor at the boundary. The inhalation rate was allowed to vary between 0.45 m^3 h^{-1} (resting) to 3 m^3 h^{-1} (vigorous activity), with a most probable value of 1.1 m^3 h^{-1}. Because the

source of the uranium is unknown, it was also assumed that the chemical form of the released material was inhalation class Y, which results in the largest dose factor, *DF*, for uranium. No correction was applied for reducing the concentration indoors, because the release could have occurred over a relatively short time period when the receptor was outdoors. Dose results from the assessment of these three unknown sources are presented in Table T-6.

Table T-6. Radiation Doses to Hypothetical Adult Receptors from Potential Episodic Releases Identified by Examination of Air Monitoring Data

Beginning date of week	Receptor location[a]	Air concentration (fCi U m^{-3})	Effective dose (mSv)[b]
September 1, 1978	Boundary station 6 (west)	88	0.017 (0.0082,0.033)
February 1, 1979	Boundary station 3 (east)	440	0.086 (0.041,0.16)
September 13, 1983	Boundary station 1 (north)	114	0.022 (0.011,0.043)

[a] Location of highest measured uranium concentration among boundary air monitors.
[b] Median estimate followed by 5th and 95th percentiles in parentheses.

Table T-7 summarizes the median estimate of radiation dose to a maximally exposed offsite individual from the five episodic releases contrasted with the dose from routine releases of uranium received by the scenario 1 individual during the same year. The scenarios used in this study, which describe a variety of possible exposure conditions, are described in Appendix J. The scenario 1 individual resided 1.7 km northeast of center of the FMPC, and would have been 20 years old in 1966. Scenario 1 resulted in the highest cumulative radiation dose of the nine scenarios developed.

Chemical form is an important consideration in uranium compound dosimetry. The insoluble (class Y) compounds produce an effective dose per unit intake of over 100 times that of the most soluble (class D) forms. Although the 1966 UF_6 release represented the largest mass, the soluble chemical forms of that release decreased the effective dose relative to the three unknown source releases, which were assigned to the most insoluble inhalation class (Y).

Table T-7 illustrates the small contribution of episodic releases of uranium compared with releases included in the routine source term. All episodic releases produce an effective dose that is less than 0.2% of the cumulative effective dose to the scenario 1 individual. These cumulative doses are used to estimate risk from radiation exposures (see Appendix S). When viewed as a percentage of the *annual* effective dose from uranium, the episodic releases could contribute as much as 12% (in 1979). The dosimetric impacts of the episodic releases of uranium are even less significant when compared to the dose from past releases of radon and decay products.

Table T-7. Summary of Estimated Effective Dose from Episodic Releases and Comparison with Dose from Routine Releases of Uranium

	Estimate of annual effective dose (mSv)			% of total dose due to episodic releases	
Episodic release	Episodic	Routine[a] (scenario 1)	Total	% annual dose	% cumulative dose[b]
Nov. 1953 UF_6 release	0.00029	0.10	0.10	0.3	<0.1
Feb. 1966 UF_6 release	0.015	2.0	2.0	0.7	<0.1
Sept. 1978 Unknown source[c]	0.017	0.72	0.74	2.3	<0.1
Feb. 1979 Unknown source[c]	0.086	0.64	0.73	12	0.18
Sept. 1983 Unknown source[c]	0.022	0.40	0.42	5.2	<0.1

[a] See Appendix K for dose results for all scenarios. Values here do not include dose from radon and decay products and represent direct inhalation only (not ingestion or external pathways).
[b] The cumulative effective dose to the scenario 1 individual (excluding dose from radon and decay products) from all pathways is 47 mSv (nominal estimate).
[c] Inhalation class Y (most conservative) was assumed for these unknown sources.

Chemical Toxicity Considerations for Uranium Episodic Releases

The scope of this project is reconstruction of past releases of radioactive materials and *radiation* doses to the public from those releases. Releases of non-radioactive chemicals and their effects are outside the scope of this project. However, natural uranium, a radioactive material that was handled in large quantities at the FMPC, is chemically toxic; in fact, chemical toxicity considerations often dominate exposures to natural uranium, especially for more soluble forms (PHS 1990, McGuire 1990). For this reason, the chemical toxicity of uranium was addressed in this study (Appendix R).

With respect to the two episodic releases of UF_6, other chemical toxic effects are briefly reviewed here. When UF_6 is released in air, concentrated aerosols of chemicals are formed that can be grouped into three categories according to their toxic effects: (1) uranyl fluoride (UO_2F_2), a relatively soluble uranium compound in which the uranium ions act as a heavy-metal poison that can affect the kidneys, (2) HF, which can cause burns on the lungs, skin, eyes, and gastrointestinal tract, and (3) fluorides (uranyl fluoride and hydrogen fluoride), which can cause fluoride poisoning. These chemical effects of the hydrolysis products can be more important than the radiological effects of uranium. Two deaths have resulted from massive accidental releases of UF_6 at nuclear facilities (Kathren and Moore 1986, Moore and Kathren 1985). The cause of death for these workers, who were close to the accident, was acute toxic effects of HF.

Because of the concern for the toxic effects of HF, the offsite air concentration of this compound was estimated for the 1966 episodic release of UF_6. One kilogram of UF_6 contains 0.68 kg of uranium and 0.32 kg of fluoride. The 750 kg U released thus corresponds to 1100 kg UF_6. The reaction of one kilogram of UF_6 with water in air produces 0.23 kg of HF (McGuire 1990). Thus, the estimated amount of HF released in this accident is 250 kg over one hour, or a release rate of 69 grams of HF per hour. Using the dispersion factor developed for uranium, at a distance of 1.3 km, the median concentration of HF in air is estimated to be 0.6 mg m^{-3}; with a 95th percentile estimate of 1.5 mg m^{-3}. The National Institute for Occupational Safety and Health (1994) recommended exposure limit (REL) for HF is 2.5 mg m^{-3}.

The REL is a concentration to which workers may be exposed and represents a time-weighted concentration for up to a 10-hour workday during a 40-hour workweek. Thus, it would seem unlikely that a member of the public suffered severe effects from this HF release, although a person with other respiratory complications might have been affected.

At first glance, the relatively small radiation doses from the episodic releases (Table T-7) suggest that the uranium toxicity evaluations done for the cumulative exposure scenarios would be more conservative (i.e. result in a larger amount of uranium exposure to the kidney) than any of the episodic releases. However, because of the soluble chemical form and short timing of the UF_6 releases, a chemical toxicity assessment must be made specially for these two episodic releases.

The cumulative exposure scenarios (Appendix J) represent chronic exposure over many years. The dynamics of annual intakes and retention of uranium in the body were used to estimate the uranium concentration in the kidney of various receptors for each year of exposure. The maximum uranium concentration in any year was compared with concentrations associated with health effects (Appendix R).

In contrast, the episodic releases represent an acute exposure situation. The possible toxic effects of uranium in these releases were assessed differently than the routine exposure scenarios, but using the same ICRP-30 metabolic models for the lung and the kidney (Appendices I and R). The impact of a newer metabolic model of the kidney (ICRP-69) was investigated in Appendix R; differences between that and the older ICRP-30 model were found to be minor.

Table T-8 lists the fractional deposition of 0.35 μm particles of Class D materials in the lungs. All lung compartments except b and d transfer the deposited class D material rapidly (in less than one day) to body fluids. The <6% cleared from compartments b and d to the gastrointestinal tract are expected to contribute only an additional 0.0025 to the fraction cleared directly from lung to blood. Thus, a fraction of 0.53 of the amount inhaled is transferred rapidly to body fluids. From this transfer compartment, a fraction of 0.12 is translocated to the kidney where it is retained with a biological half-time of 6 days (Appendix R, Table R-1).

Table T-8. Fractional Deposition Following Inhalation of Class D Particles (0.35 μm)[a]

Total Exhaled	**0.42**
lung compartment a	0.05
lung compartment b	0.05
lung compartment c	0.08
lung compartment d	<0.01
lung compartment e	0.32
lung compartment h	0.08
Total Deposited	**0.58**

[a]See Figure I-3 for illustration of lung compartments.

The maximum concentration of uranium in the kidney following the inhalation of uranium from the episodic releases is computed by

$$C_{max} = I f_{TC} f_{kidney} / m \qquad \text{(T-3)}$$

where

C_{max}	=	maximum concentration in the kidney (μg U per gram kidney)
I	=	total amount of uranium inhaled during passage of plume (μg U)
f_{TC}	=	fraction of inhaled uranium reaching transfer compartment (0.53)
f_{kidney}	=	fraction of uranium transferred from body fluids to kidney (0.12)
m	=	mass of kidney (310 g for adult male, ICRP 1975).

The estimated consequences of the uranium hexafluoride release depend strongly on the atmospheric stability conditions. If the recent FMPC meterological data for February are used, which are strongly weighted toward class D stability, a considerably higher impact (larger concentration of uranium in the kidney) is predicted than if the actual stability were Class C or Class B. These latter two stability classes are certainly possible based on the sketchy onsite weather observations (time of day, wind speed, and wind direction). Distance from the release also affects the predicted concentration in the kidney of the receptor (Figure T-1). Although a person might not have been as close as 1.3 km, it is likely that at least some individuals were exposed at a distance of around 3.5 km (the New Baltimore area).

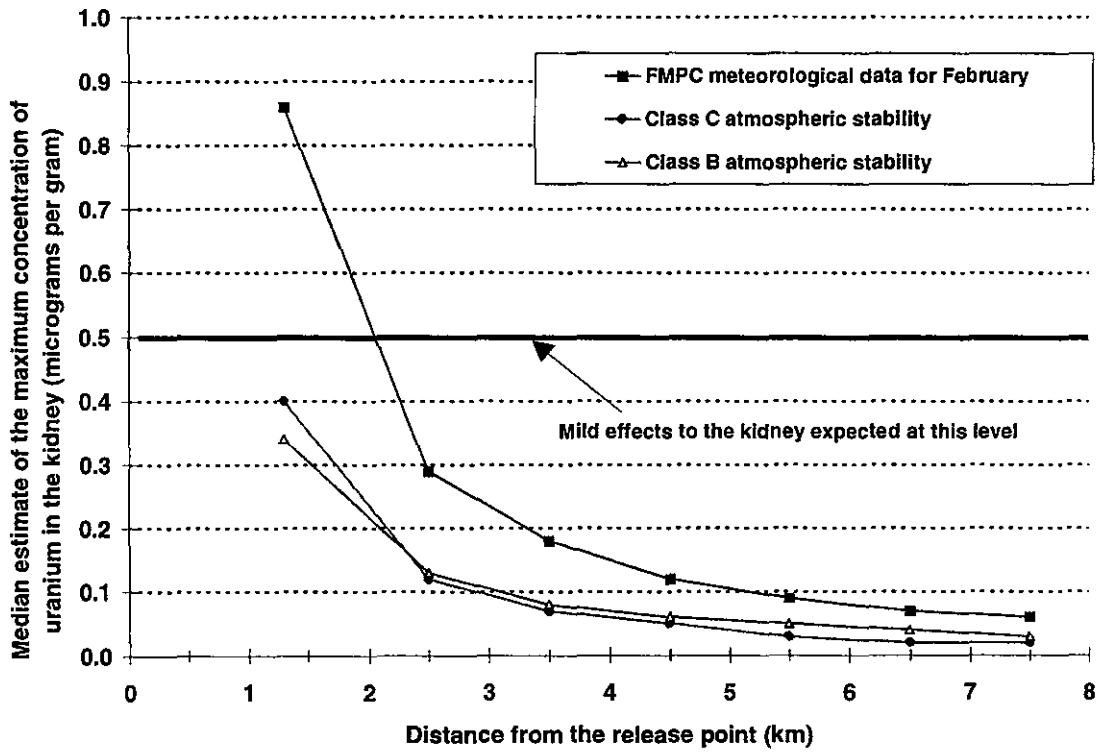

Figure T-1. Effect of distance and atmospheric stability on predicted maximum concentration of uranium in the kidney from the February 1966 episodic release of uranium hexafluoride. The points plotted are medians of an uncertainty distribution. The uncertainty about the maximally-exposed individual's kidney concentration is plotted in Figure T-2.

The median estimate of the maximum concentration of uranium in the kidneys of an adult who was 1.3 km downwind during the entire passage of the contaminated plume from

the 1966 release is 0.86 μg U g^{-1} kidney with 5th and 95th percentile estimates of 0.37 and 2.0 μg U g^{-1}. Because this was an acute (short-term) exposure, the concentrations in the kidney would decrease following the exposure (Figure T-2).

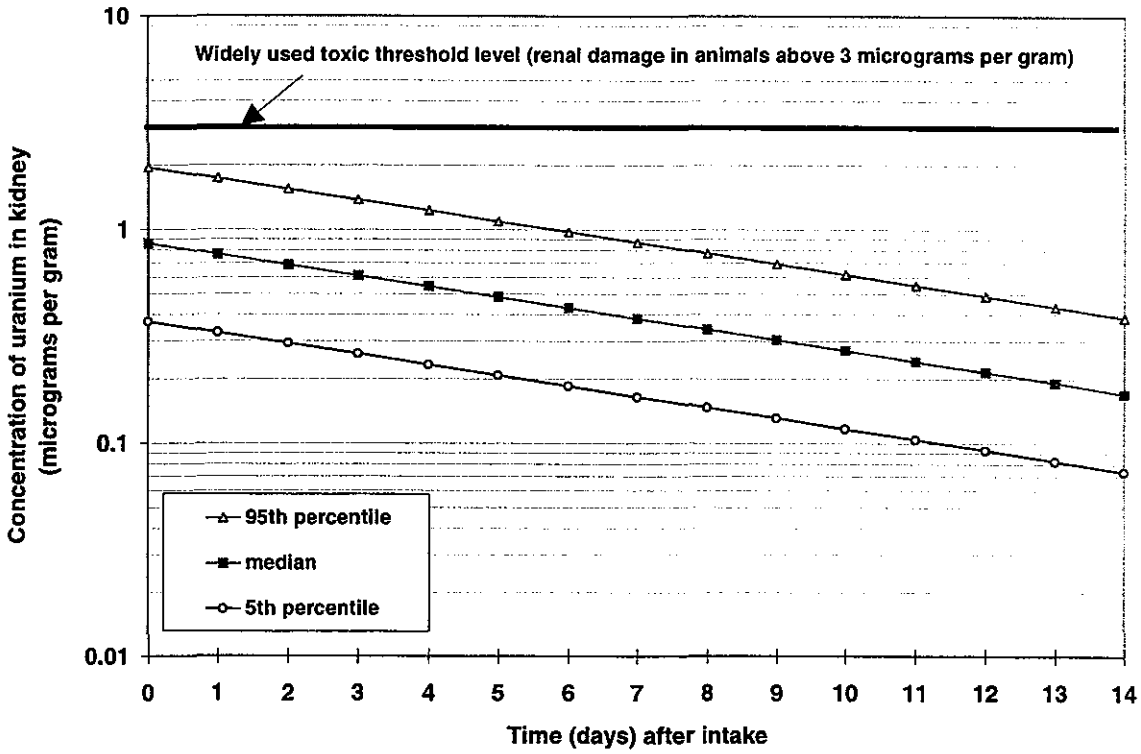

Figure T-2. Concentration of uranium in the kidney with time after intake for a maximally-exposed adult who was 1.3 km directly downwind of the 1966 episodic release. The biological half-time of the majority of uranium translocated to the kidneys is 6 days (Appendix R), and that retention is plotted here. A concentration of 3 μg U g^{-1} has been widely used as a toxic threshold; however some studies show mild toxic effects in the range of 0.1 to 0.5 μg U g^{-1} and more severe effects above 0.5 μg U g^{-1} (see Appendix R). A 95th percentile estimate for this maximally exposed individual results in a concentration of uranium in the kidney above 0.5 μg U g^{-1} for about 12 days, and the median estimate was above this level for about 5 days. The 5th percentile estimate never exceeds 0.5 μg U g^{-1}.

Recent scientific literature on uranium toxicity was reviewed in Appendix R. A concentration of 3 μg U g^{-1} has been widely used as a toxic threshold, as renal damage has been observed above this level in a number of animal species. However some studies show mild toxic effects to the kidney in the range of 0.1 to 0.5 μg U g^{-1} and more severe effects above 0.5 μg U g^{-1}. Our 95th percentile estimate for the maximally exposed individual from the 1966 uranium hexafluoride release results in a concentration of uranium in the kidney above 0.5 μg U g^{-1} for about 12 days, and the median estimate was above this level for about 5 days. The 5th percentile estimate never exceeds 0.5 μg U g^{-1}.

The maximum kidney concentrations presented here for the 1966 episodic release are roughly comparable to those estimated for the scenario 3 individual from routine releases

(mainly from consumption of contaminated well water). The median estimate of the highest annual concentration in the kidney for that scenario was 0.75 μg U g^{-1} and the 95th percentile estimate was 1.4 μg U g^{-1} (Table R-3). The cumulative exposure scenarios represent a much larger intake of uranium spread out over a longer period of time, during which time the material was being cleared from the body. The uranium concentrations in the kidney from the routine releases would have been sustained for a longer period of time compared with uranium burdens from an episodic release. In addition, the number of people possibly exposed to the episodic release would have been less than from routine releases.

The intake of uranium from the 1953 UF_6 episodic release was over 50 times less than the intake from the 1966 release. The maximum concentration in the kidney (median 0.02 μg U g^{-1}, 95th percentile, 0.04 μg U g^{-1}) is below a "no effect" level for toxic effects (0.1 μg U g^{-1}), discussed in Appendix R.

Radon Release (April 25, 1986)

Description of release. Two reports describing the April 25, 1986, radon release have been located. The first was a preliminary letter report, issued by the DOE (Reafsnyder 1986). The second was the formal report of the DOE Incident Investigation Board (DOE 1986). The following description of the incident and radon release is taken from DOE (1986).

On April 14, 1986, a subcontractor began applying the weatherproof coating to the K-65 silo domes. The coating material was a neoprene hapalon, applied as a fluid. This work was stopped on April 17, 1986, because of radiation safety concerns. Work resumed on April 18, but only for part of the day. On the afternoon of April 18, work was again stopped, after it was discovered that air from the silos was escaping through the protective coating and apparently causing high radiation levels above the dome areas. It was then noticed that bubbles were present in the coating on Silo 2, and cracks and holes were also visible on Silo 2.

On Friday, April 25, 1986, the K-65 silos were vented, without authorization, by FMPC staff. The venting was apparently performed to reduce the pressure in the silos and the high radiation above the silo domes, so coating the domes could proceed. The silos were vented by removing one of the blank flanges on the domes and installing a new 2-in. flange, an elbow, a quick release coupling, and lengths of flexible, schedule 80, plastic pipe. The blank flange was removed from Silo 2 at about 10:15 a.m., and the blank flange from Silo 1 was removed immediately after. Between 10:30 and 10:40 a.m., two 50-ft sections of the pipe were attached to the new flange on Silo 2. Between 10:50 and 11:00 a.m., one 50-ft section of the pipe was attached to the new flange on Silo 1. At 1:00 p.m., it was agreed that the blank flanges were to be reinstalled. At 2:00 p.m., it was reported that the blank flanges had been reinstalled on the K-65 silos. Thus, the venting took place from about 10:15 a.m. to 2:00 p.m., a total of about 3¾ hours.

Environmental monitoring results. At the time of this episodic release, a few radon monitoring programs were in place at the FMPC (Reafsnyder 1986, DOE 1986). These included (1) onsite measurements at 17 locations and offsite measurements at three locations within 2 mi of the site, performed by Mound Laboratories, (2) measurements at the boundary air monitoring stations, onsite locations, and some offsite locations, using alpha-track monitors for 3-month-long measurements, performed by the FMPC, and (3) continuous

measurements (which actually provided hourly results) with a radon gas monitoring instrument, very near the K-65 silos.

Regarding results of the Mound Laboratories measurements, DOE (1986) indicates that average measured concentrations, for onsite and offsite locations, for the 2-week period that included April 25, 1986, were higher than similar averages for the preceding 1½-year period. We have compiled results of the Mound measurements in Appendix M of this report. Based on our compilation, the averages for this 2-week period were generally higher than the long-term averages, but they were not higher than the range of results for other 1- or 2-week periods measured by Mound. Thus, estimations of increases in concentrations (if any) that were due to the episodic release would be quite uncertain using the Mound monitoring data.

Because of the accidental radon gas release from the silos, the alpha-track detectors maintained by the FMPC were retrieved and analyzed earlier than scheduled. For the period March 18–April 29, 1986, concentrations at two offsite locations appeared higher (both at 1.29 pCi L^{-1}) than average offsite concentrations for 1985 (at 0.59 and 0.37 pCi L^{-1} for the two locations) (DOE 1986). However, from the 1986 annual environmental monitoring report (WMCO 1987), it appears that the two offsite locations, called OS1 and OS2, were in opposite directions from the K-65 silos at distances of 10 and 6 km, respectively. Though possible, it seems unlikely that the short-term episodic release would have caused the higher concentrations at both locations. It thus seems reasonable to assume that the episodic radon release is not the only reason for the higher concentrations.

The third category of environmental measurements, the hourly radon concentrations, was made within about 35 ft of where the radon was discharged from the flexible pipes (DOE 1986). Measurement results for April 23 and 24, 1986, were markedly different from those of April 25, the day of the release. For April 23 and 24, peak hourly concentrations, occurring from mid-morning to mid-afternoon, were about 10 and 40 pCi L^{-1}, respectively. On April 25, the peak hourly concentration was 694 pCi L^{-1} at 2:00 p.m. This significant difference seems to indicate that radon releases on April 25 were substantially greater than on April 23 and 24.

Quantitative use of the hourly data for assessment of the release is problematic for several reasons. On April 23 and 24, the releases can be assumed to be from the domes of the silos, while on April 25, the releases were from the domes and the flexible pipes that had been attached. The exact locations of the release points in relation to the measurement point are not clearly described in documents obtained, although an illegible drawing attached to a dose assessment report (Hinnefeld 1986) seems to indicate that the release points were roughly north or northwest and south or southwest from the monitor. In addition, although weather observations from the Cincinnati airport were recorded, wind directions around the silos on these days are not known.

In summary, the hourly measurements made close to the K-65 silos provide the best corroboration (though only qualitative) that an episodic release occurred on April 25, 1986. However, it appears that comparisons of concentrations measured during the release time with concentrations measured at other times are not useful for a quantitative assessment of the release.

Potential dose from the radon release. A preliminary dose assessment was performed shortly after the episodic radon release (Hinnefeld 1986). However, we do not agree with an important assumption that was made in that assessment. The silo venting was

accomplished through two assemblies of pipe and hose, one attached to each silo. The investigation report (DOE 1986) indicates that the hoses extended down the east side of the berms around the silos. In the preliminary dose assessment, a point midway between the two release points was selected as the "average emission point," and this was assumed to be the emission point for the further calculations (Hinnefeld 1986). Based on the wind direction from the Cincinnati airport, the preliminary dose assessment assumed that the hourly radon monitoring instrument was downwind from the average emission point. However, it appears to us that if the radon monitor was downwind from the average emission point, the monitor would not be downwind from the actual locations of the two individual release points. Thus, we believe the conclusions made in the preliminary assessment regarding the source term and estimated doses are invalid because the conclusions were based on an invalid assumption of a downwind monitor location.

Because of the lack of detailed information about conditions of the episodic radon release, we developed estimated doses based on our upper bound estimate of the source term and assumptions of an individual who might have been exposed along the site boundary (a reasonable estimate of a maximally exposed individual). The preliminary dose assessment report (Hinnefeld 1986) indicates that meteorological data were not being printed at the FMPC guardhouse. [As described in our Task 4 report (Killough et al. 1993), the data set obtained from the site shows routine collection of meteorological data at the site started in August 1986.] The data used in the preliminary assessment are from the Cincinnati airport, which is about 29 km from the FMPC (Table T-9). For lack of site-specific meteorological data, the Cincinnati data are used in our dose estimates, with modifications as discussed below.

Table T-9. Meteorological Data from Cincinnati Airport, April 25, 1986

Time of day	Wind direction (°)	Wind speed (knots)
1000	240	10
1100	250	10
1200	280	6
1300	250	5
1400	240	8
1500	210	11
1600	240	10
Average, 1000–1400	250	7.8

For the estimated time of the release, the wind direction at the Cincinnati airport was from the west and west-southwest. These are predominant directions for the airport and for the FMPC, and so we assume that one potential receptor location is on the eastern boundary of the site at the closest point to the K-65 silos, which is approximately east from the K-65 silos at air monitoring station AMS–3. The distance from the silos to AMS–3 is about 1470 m. Because the wind directions at the FMPC during the release are not known, we also evaluated a "worst case," with a receptor at the point on the site boundary closest to the K-65

silos. This second potential receptor location is approximately at air monitoring station AMS-6, on the western boundary. The distance from the silos to AMS–6 is about 330 m.

For exposure to radon and its decay products, the dose rate factor (dose per unit radon concentration) is the greatest for a child (see Appendix I). Thus, we assume that the potentially-exposed individuals at the two locations are 10-year-old children. The exposure times are assumed to be 3¾ hours, with the plume blowing toward the receptor for the entire exposure time (i.e., the wind frequency $f = 1$). The activity level of the exposed individuals is assumed to be light activity.

The estimate of the upper bound on the source term for the release was developed in Appendix K of the final source term report (Voillequé et al. 1995). The 5th, 50th, and 95th percentile values of the upper bound of radon released are 8, 30, and 100 Ci, respectively. The source term is represented by a lognormal distribution with geometric mean 30 Ci and geometric standard deviation 2.2. The rate of radon release is calculated from the release quantity and the length of the release, 3¾ hours. For the wind speed, we use the data from the Cincinnati airport, with modification. The average wind speed during the time of the release was 7.8 knots (Table T-9), or 4.0 m s^{-1}. In Appendix E of the Task 4 report (Killough et al. 1993) it was seen that the ratio of mean wind speed at the FMPC to mean wind speed at the airport was 2.1 m s^{-1} : 4.5 m s^{-1}. We use this ratio to estimate that the mean wind speed at the FMPC during the release might have been about 1.9 m s^{-1}.

For performing the dose calculations, we use the empirical radon dispersion model developed for the routine releases from the K-65 silos (in Appendix M). The composite diffusion parameter, $\chi u / (Qf)$, is shown in Table T-10 for each of the daytime atmospheric stability classes A–D. The probabilities of occurrence of each class are also listed; our calculation assumed stability-related uncertainty distributions for this parameter based on Table T-10.

Table T-10. Radon Diffusion as a Function of Stability Class and Distance

		Diffusion $\chi u / (Qf)$ (m^{-2}) at Two Distances	
Stability	Probability	330 m	1470 m
A	0.1347	5.91×10^{-5}	4.50×10^{-6}
B	0.0565	1.28×10^{-4}	1.03×10^{-5}
C	0.0942	2.59×10^{-4}	2.53×10^{-5}
D	0.7056	4.80×10^{-4}	7.22×10^{-5}

For each distance, there is a composite lognormal calibration and residual uncertainty factor for the dispersion model: GSD 1.72 for a distance of 330 m and 1.98 for a distance of 1470 m. Uncertainty in the source term (GSD 2.2) was the second major component of overall uncertainty for evaluation of this episodic release.

The relative activity concentrations of decay products (Rn : RaA : RaB : RaC) at the source were 1 : 0.97 : 0.91 : 0.87, on the basis of estimates for the silo headspaces after sealing. This includes the effects of plateout on the silo walls (see Appendix Q). Decay kinetics were taken into account according to the distance the plume traveled for each scenario.

Median results for a 10-year-old child engaged in light activity outdoors were 0.023 Sv at 330 m and 0.0032 Sv at 1470 m. The percentiles of the uncertainty in these doses are presented in Table T-11.

Table T-11. Summary of Distribution of Estimated Lung Dose from Upper-Bound Source Term of Episodic Radon Release

	Estimated dose to the lung (Sv) [a]		
Receptor location	5th percentile	Median	95th percentile
Western site boundary, at AMS–6	0.0026	0.023	0.14
Eastern site boundary, at AMS–3	0.00018	0.0032	0.024

[a] Lung doses tabulated here are dose equivalent to the tracheobronchial epithelium of the lung.

Our upper-bound source term estimate of 30 Ci radon, which was used for this episodic release assessment, is less than 4% of the routine release quantity of 880 Ci radon for 1986. However, the release rate is 80 times higher (8 Ci h^{-1} versus 0.1 Ci h^{-1}). Because of the short duration of the release, the radon and decay products are assumed to blow toward a receptor who could have been at the FMPC boundary during the entire time. Consequently, the median dose to a member of the public from the episodic release at the worst possible exposure location (0.023 Sv, Table T-11) is roughly twice the annual lung dose for the scenario 2 individual in 1986 (0.011 Sv). The more likely possible exposure location along the FMPC boundary (AMS-3, based on a westerly wind) would have resulted in a lung dose of 0.0032 Sv from the episodic release, or roughly 3 times less than the lung dose to the scenario 2 individual from routine releases in that year. In addition, the lung doses estimated from this episodic release are considerably smaller than annual doses from routine releases before the silos were sealed. They are insignificant compared to the *cumulative* lung doses to the individuals of scenarios 1 and 2 (3.0 Sv). These cumulative lung doses are used to estimate risk to residents of the area from historical radon releases from the FMPC (see Appendix S).

REFERENCES

Adams W. J. 1985. "Listing of Major Dust Collector Uranium Releases." Attachment to letter to M. R. Theisen, DOE-ORO, January 3. National Lead Company of Ohio, Cincinnati, Ohio.

Boback M. W. and R. C. Heatherton. 1966. *Bioassay Aspects of a UF_6 Fume Release.* Presentation at 12th annual Bioassay and Analytical Chemistry Meeting, Gatlinburg, Tennessee, October 13–14, 1966. Report NLCO-986, November 1. National Lead Company of Ohio, Cincinnati, Ohio.

Bostick W.D., W.H. McCulla, and P. W. Pickrell. 1985. "Sampling, Characterization, and Remote Sensing of Aerosols Formed in the Atmospheric Hydrolysis of Uranium Hexafluoride." *J. Environ. Sci. Health* **A20**(3): 369–393.

Briggs G.A. 1973. *Diffusion Estimation for Small Emissions*. ATDL Contribution File No. 79, Atmospheric Turbulence and Diffusion Laboratory.

Davis J. O. 1953. "Hex Leak." Internal memorandum to F. L. Cuthbert, November 7. National Lead Company of Ohio, Cincinnati, Ohio.

Gifford F.A. 1976. "Turbulent Diffusion Typing Schemes—A Review." *Nucl. Safety* **17**:68–86.

Hanna S.R., G.A. Briggs and R.P. Hosker, Jr. 1982. *Handbook on Atmospheric Dispersion.* Report DOE/TIC–11223. National Technical Information Service, Springfield, Virginia.

Hinnefeld S.L. 1986. *Preliminary Evaluation of Radiological Impact of K-65 Tank Venting on April 25, 1986.* Internal memorandum to H.D. Christiansen, April 29. WMCO:EH(HP):86:0094, Westinghouse Materials Company of Ohio, Cincinnati, Ohio.

International Commission on Radiological Protection (ICRP) 1975. *Report of the Task Group on Reference Man.* ICRP Publication 23. Pergamon Press, Oxford.

International Commission on Radiological Protection (ICRP) 1979. *Limits for Intakes of Radionuclides by Workers.* ICRP Publication 30 Part 1. *Ann ICRP* **2**(3/4). Pergamon Press, Oxford.

Investigation Board. 1988. *Investigation Report on Plant 2/3 Gulping Emission at the Feed Materials Production Center, June 1988.* Report DOE-ORO-897, November. U.S. Department of Energy, Oak Ridge, Tennessee.

Kathren R.L. and R.H. Moore. 1986. "Acute Accidental Inhalation of Uranium: A 38-year Follow-up." *Health Phys.* **51**:609:620.

Killough G.G., M.J. Case, K.R. Meyer, R.E. Moore, J.F. Rogers, S.K. Rope, D.W. Schmidt, B. Shleien, J.E. Till, and P.G. Voillequé. 1993. *The Fernald Dosimetry Reconstruction Project. Task 4. Environmental Pathways — Models and Validation.* RAC Report CDC–3. Radiological Assessments Corporation, Neeses, South Carolina.

McGuire S.A. 1990. *Chemical Toxicity of Uranium Hexafluoride Related to Radiation Doses.* NUREG–1391. National Technical Information Service, Springfield, Virginia.

Miller C.W. and L.M. Hively. 1987. "A Review of Validation Studies for the Gaussian Plume Atmospheric Dispersion Model." *Nuclear Safety* **28**(4): 522–531.

Moore R.H. and R.L. Kathren. 1985. "A World War II Uranium Hexafluoride Inhalation Event with Pulmonary Implications for Today." *J. Occup. Med.* **27**:753–756.

National Institute for Occupational Safety and Health (NIOSH). 1994. *NIOSH Pocket Guide to Chemical Hazards.* Publication 94–116. National Technical Information Service, Springfield, Virginia.

National Lead Company of Ohio (NLO). 1966. *Uranium Hexafluoride Gas Release, Feed Materials Production Center, Fernald, Ohio.* Report of investigating team, March 16. National Lead Company of Ohio, Cincinnati, Ohio.

Pasquill F. 1974. *Atmospheric Diffusion.* 2nd edition, John Wiley and Sons, New York.

Reafsnyder J.A. 1986. *Report on the Venting of Radon Gas at Fernald, Ohio.* Letter to various, with attached report. May 29. U.S. Department of Energy, Oak Ridge Operations, Oak Ridge, Tennessee.

Semones T.R. and E.F. Sverdrup. 1988. *Uranium Emissions from Gulping of Uranium Trioxide*. Report FMPC/SUB–019. Westinghouse Materials Company of Ohio, Cincinnati, Ohio.

Shleien B., S.K. Rope, M.J. Case, G.G. Killough, K.R. Meyer, R.E. Moore, D.W. Schmidt, J.E. Till, and P.G. Voillequé. 1995. *The Fernald Dosimetry Reconstruction Project. Task 5. Review of Historic Data and Assessments for the FMPC.* RAC Report CDC–4. Radiological Assessments Corporation, Neeses, South Carolina.

U.S. Department of Energy (DOE). 1986. *Investigation of April 25, 1986 Radon Gas Release from Feed Materials Production Center K-65 Silos*. DOE Incident Investigation Board. Report DOE/OR-877, June 27. U.S. Department of Energy, Oak Ridge, Tennessee.

U.S. Public Health Service (PHS). 1990. *Toxicological Profile for Uranium*. PB91–180471. National Technical Information Service, Springfield, Virginia.

Vaaler S.C and K.R. Nuhfer. 1989. "Airborne Emission from Historical Non-routine Events." Internal memorandum to B.L. Speicher, March 9. Westinghouse Materials Company of Ohio, Cincinnati, Ohio.

Voillequé P.G., K.R. Meyer, D.W. Schmidt, S.K. Rope, G.G. Killough, M. Case, R.E. Moore, B. Shleien, and J.E. Till. 1995. *The Fernald Dosimetry Reconstruction Project. Tasks 2 and 3. Radionuclide Source Terms and Uncertainties.* RAC Report CDC–5. Radiological Assessments Corporation, Neeses, South Carolina.

Westinghouse Materials Company of Ohio (WMCO). 1987. *Feed Materials Production Center Environmental Monitoring Annual Report for 1986*. Report FMPC-2076, WMCO Cincinnati, Ohio.